

Strathclyde Institute of Pharmacy and Biomedical Sciences
and
GlaxoSmithKline

New Dose Estimation Methods and their Application in Early
Drug Discovery using Intravenous, Oral and Inhaled Routes
of Administration for New Chemical Entities

Thesis submitted to the University of Strathclyde in the
fulfilment of the requirements for the degree of
Doctor of Philosophy

By

Simon Peter Teague

2019

Declaration of Authenticity and Author's Rights

This thesis is the result of the author's original research. It has been composed by the author and has not been previously submitted for examination which has led to the award of a degree.

The copyright of this thesis belongs to the author under the terms of the United Kingdom Copyright Acts as qualified by University of Strathclyde Regulation 3.50. Due acknowledgement must always be made of the use of any material contained in, or derived from, this thesis.

Signed:

Date:

A special thank you to my wife

Claire

and my children

Joseph, Oliver and Ellery

Acknowledgements

I would like to thank my industrial supervisor Dr Peter Eddershaw and academic supervisors Professor Simon MacKay and Dr Blair Johnston for their help and support throughout the duration of this project. I would like to thank Peter for the numerous scientific debates and general discussions we have had over the years, Peters council has been invaluable throughout my PhD and GSK career.

I would like to thank Dr Klara Valko who has been a friend, mentor and colleague for several years whilst at GSK and following Klara's subsequent retirement. I would like to thank Klara for her support, encouragement and unwavering belief in me. Klara's passion for science continues to inspire.

I would like to thank Shenaz Bunally and the Physicochemical Profiling Group for generating the HPLC HSA, AGP and IAM data.

I would like to thank the *in vivo* biology group Douglas Ball, Joanne Morley, Heather Read and Finlay McNab for running the target engagement and efficacy PD studies for the JAK program. I would also like to thank the team for engaging in discussion and adapting the study designs to help adapt classic PD models to PKPD models.

I would also like to acknowledge Emma Sherriff who worked with me for several years within the Respiratory DMPK group where we worked on multiple lead optimisation programs, including some of those referenced in this thesis and also assisted in some of the logistical aspects in this report.

Finally, I would like to thank my wife Claire for giving me the love and support that has enabled me to complete this thesis.

Michael Richard Teague

15th January 1946 – 18th June 2016

Abbreviations

ACAT	Advanced compartmental absorption and transit
ACN	Acetonitrile
ADME	Absorption, distribution, metabolism and excretion
ADMET	Absorption, distribution, metabolism, excretion and toxicity
AE	Adverse Event
AGP	α -1-acid glycoprotein
ALI	Acute lung injury
AO	Aldehyde oxidase
AP	Absorption potential
API	Active pharmaceutical ingredient
ARDS	Acquired respiratory distress syndrome
AUC	Area under the curve
AUMC	Area under the first moment curve
BCS	Biopharmaceutical classification system
BDDCS	Biopharmaceutical drug-drug interactions classifications system
BEI	Binding Efficiency Index
B:P	Blood-to-plasma ratio
C	Concentration
C_0	Concentration at time zero
CAT	Compartmental absorption and transit
CBAG	Capsule based aerosol generator
C_e	Effect compartment concentration
CEDD	Centre of Excellence for Drug Discovery
<i>CHI</i>	Chromatographic hydrophobicity index
<i>CHIN</i>	Chromatographic hydrophobicity index of the neutral species
CI	Confidence interval
CL_b	Total systemic clearance in blood
CL_{bu}	Unbound clearance in blood
CL_{int}	Intrinsic clearance
CLND	Chemi-Luminescent Nitrogen Detector
CL_p	Total systemic clearance in plasma
CL_u	Unbound clearance

cLogP	Calculated logarithm of the octanol water partition coefficient
C_{\max}	Concentration maximum
CNS	Central nervous system
COPD	Chronic obstructive pulmonary disorder
CYP450	Cytochrome P450 enzyme e.g. 3A4
Da	Dalton
DE	Drug efficiency
DE_{\max}	Maximum drug efficiency
DE-DP	Drug efficiency dose prediction
$DRUG_{\text{eff}}$	Drug efficiency (<i>in vitro</i> or <i>in vivo</i>)
$DRUG_{\text{eff max}}$	Maximum Drug efficiency
DP	Dose prediction
dR/dt	Change in response with time
DDI	Drug-drug interaction
DMPK	Drug Metabolism and Pharmacokinetics
DMSO	dimethyl sulfoxide
E_{\max}	Maximum effect
EC_{50}	The drug concentration which produces 50% of the maximum stimulation
ER	Extraction ratio
E_{\max}	The maximum effect attributed to the drug
F_a	Fraction absorbed
F_{abs}	Fraction of a dose absorbed
FMO	Flavin-containing monooxygenase
FD_p	Fraction of dose reaching the portal vein
F_g	Fraction of drug escaping gut metabolism
F_h	Fraction of drug that escapes hepatic extraction
F	Bioavailability
FDA	U.S. Food and Drug Agency
F_{non}	The unionized fraction of the drug at pH 6.5
f_{ub}	Fraction unbound in blood
f_{up}	Fraction unbound in plasma
f_{ut}	Fraction unbound in tissue
GI	Gastrointestinal
GSK	GlaxoSmithKline
Hct	Haematocrit

hERG	Human ether-a-go-go related gene
HDM	House dustmite
HTS	High throughput screen
HPLC	High performance liquid chromatography
HSA	Human serum albumin
IC ₅₀	Half maximal inhibitory concentration
IC ₉₀	90% inhibition concentration
IAM	Immobilised artificial membrane
ICH	International Conference on Harmonisation
ID	Identification
IgE	Immunoglobulin E
IH	Inhaled
IL	Interleukin
I _{max}	Maximum inhibition
IN	Intra nasal
IS	Internal standard
IV	Intravenous
JAK	Janus kinase
<i>k</i>	Retention factor
K _e	Elimination rate constant
K _{el}	Elimination rate constant
K _{eo}	Effect compartment rate constant
K _i	Inhibition constant
K _{in}	Turnover rate
K _m	Michaelis–Menten constant
K _p	Partition coefficient
K _{out}	Fractional turnover rate
LogD	Logarithm of the octanol water partition coefficient at pH7.4
Log <i>k</i>	Logarithm of the retention factor
LogK	Logarithm of the retention factor on linear scale
LogP	Logarithm of the octanol water partition coefficient
LBF	Liver blood flow
LC	Liquid Chromatography
LE	Ligand Efficiency
LLE	Lipophilic Ligand Efficiency Index

LLoQ	Lower limit of quantification
MDI	Metered dose inhaler
MDCK	Madin-Darby canine kidney cell
MEC	Minimal effective concentration
MMD	Mixed multiple dose
MLogP	Moriguchi LogP
MOA	Monoamine oxidase
MRM	Multiple reaction monitoring
MRT	Mean residence time
MS	Mass spectrometry
MS/MS	Tandem mass spectrometry
MW	Molecular Weight
m/z	Mass to charge ratio
N-PCAT model	Nasal-Pulmonary compartmental absorption & transit model
NCA	Non-compartmental analysis
NCE	New Chemical Entity
NDA	New drug application
P _{aq}	Aqueous permeability
PPB	Plasma protein binding
PBPK	Physiologically-based Pharmacokinetics
PBS	Phosphate buffered saline
PD	Pharmacodynamic
PFI	Property Forecast Index
P-gp	P-glycoprotein
pH	Logarithmic scale used to specify the acidity or basicity of an aqueous solution
ϕ_o	Organic phase concentration
pIC ₅₀	Logarithmic value of the half maximal inhibitory concentration measured
PI3K γ	Phosphatidylinositol-4,5-bisphosphate 3-kinase gamma
PI3K δ	Phosphatidylinositol-4,5-bisphosphate 3-kinase delta
PK	Pharmacokinetics
pK _a	Logarithm of the dissociation constant
pK _i	Logarithmic value of the inhibition constant
PKPD	Pharmacokinetic / Pharmacodynamic

PO	Oral administration
PPB	Plasma protein binding
P_w	Permeability of the gut wall
pXC_{50}	Logarithmic value of the half maximal inhibitory or excitatory concentration measured
QP	Quantitative pharmacology
QSAR	Quantitative Structural Activity Relationship
RA	Rheumatoid arthritis
RED	Rapid Equilibrium Dialysis
S_0	Intrinsic aqueous solubility of the neutral form of the drug
SC	Subcutaneous
SDev	Standard deviation
SEM	Standard error of the mean
SLF	Simulated lung fluid
STAT	Signal Transducer and Activator of Transcription
τ	Dosing interval
t_0	Dead time
t_R	Retention time
$t_{1/2}$	Terminal half-life
T cell	Immune cell
Th cell	Immune response helper cell
TPP	Target product profile
T_{max}	Time to maximum concentration or effect
uHPLC	Ultra high performance liquid chromatography
ULoQ	Upper limit of quantification
USAN	United States Adopted Name
V_d	Volume of distribution
V_{dc}	Volume of the central compartment
$V_{d\beta}$	Volume of distribution area
V_{dss}	Volume of distribution at steady-state
V_p	Volume in the plasma compartment
V_L	Volume of the luminal content
V_m	Volume of mobile phase
V_s	Volume of stationary phase
V_t	Volume in the tissue compartment

WBB	Whole blood binding
WDF	Wrights dust feeder

Contents

1	Abstract	17
2	Introduction	19
2.1	The Drug Discovery Process and the Importance of Effective Early Discovery 19	
2.2	Biopharmaceutical Classification System (BCS).....	21
2.2.1	Property-Based Design and Properties Influential to Developability of Oral Products	23
3	A Brief Description of the Project	31
3.1.1	Property-Based Design of Selected Intravenous, Oral and Inhaled Programs a Brief Description.....	35
3.1.2	Pi3K γ IV Program.....	35
3.1.3	Pi3K δ Oral Program	35
3.1.4	JAK Inhaled Program	35
4	ADME - Absorption, Distribution, Metabolism and Excretion in Dose Prediction....	36
4.1.1	Absorption	37
4.1.2	Distribution	42
4.1.3	Metabolism and Elimination - Clearance	49
4.2	Important Physicochemical Properties	54
4.2.1	Lipophilicity – Octanol/Water Partition (LogP) and Property Forecast Index (PFI)	54
4.2.1	Biomimetic Properties (<i>HSA</i> , <i>AGP</i> and <i>IAM</i> binding).....	62
4.2.2	Biomimetic Properties and Tissue Distribution.....	69
4.2.3	Estimating the absorption potential from solubility and artificial membrane permeability.....	74
4.2.4	What is Drug Efficiency?.....	78
4.3	Approaches for Early Dose Estimation	84
5	Project Context, Design and Objectives.....	88
5.1	Analysis of Drug Efficiency with Marketed Drugs	90

5.2	Using the Intravenous (IV) Route for Dose Estimation: The Pi3K γ Project	91
5.3	Using the Oral Route for Dose Estimation: The Pi3K δ Project	92
5.4	Using the Pulmonary Route for Dose Estimation: The JAK Project.....	94
5.4.1	Balancing Drug Retention and Systemic Distribution Requirements in Respiratory Medicines Development.	98
6	Experimental and Computational Methods	102
6.1	<i>In Vivo</i> Studies performed at GSK.....	102
6.2	Experimental Conditions of Physicochemical and Biomimetic Measurements 102	
6.2.1	Measurements of Human Serum Albumin Binding	103
6.2.2	Measurements of Phospholipid Binding using Immobilized Artificial Membrane HPLC Column	106
6.2.3	Measurements of Chromatographic Lipophilicity	108
6.2.4	Measurements of High Throughput Solubility and Artificial Membrane Permeability	112
6.3	Experimental Methods for the Measurement of <i>In vitro</i> Clearance.....	114
6.3.1	Measurement of <i>In vitro</i> Clearance in Liver Microsomes.....	115
6.3.2	Measurement of <i>In vitro</i> Clearance in Hepatocytes	116
6.4	Experimental Methods to Measure Aldehyde Oxidase Metabolism from Cytosol and Lung Tissue.....	119
6.4.1	Aldehyde Oxidase Mouse and Human Lung Homogenate.....	120
6.4.2	Data analysis, interpretation and reporting.....	121
6.5	Experimental Methods to Measure Solubility in Simulated Lung Fluid (SLF) and Cell Permeability using MDCK Cells.....	122
6.5.1	SLF Solubility	122
6.5.2	Cell Permeability	123
6.6	Experimental Methods for Determining <i>In Vivo</i> IV Pharmacokinetics and Lung Retention.	123
6.6.1	Determining IV Pharmacokinetics in Mice.....	123

6.6.2	Determining IV Pharmacokinetics in Rats	125
6.6.3	Determining IV Pharmacokinetics in Minipig	126
6.6.4	Determining Lung Exposure in Mice	127
6.6.5	Details of the Intra-Nasal Dose Technique.....	129
6.6.6	Inhalation Studies in Rodents	130
6.7	<i>In Vitro</i> Enzyme and Cellular Potency Measurements of PAN JAK 1/2/3 Inhibitors	133
6.8	Assessment of Unbound Drug Fraction in Blood and Lung Homogenate by Rapid Equilibrium Dialysis (RED)	134
6.9	Computational and Visualization Tools Applied in the Data Analysis and Evaluation of the Reliability of Various Dose Prediction Methods.....	135
6.9.1	<i>In silico</i> Volume of Distribution Model (Model not published)	136
6.9.2	<i>In silico</i> Clearance Model (Model not published)	139
6.10	Physiologically Based Pharmacokinetic Modelling	141
6.10.1	The Advanced CAT (ACAT) model.....	143
6.10.2	Physiologically Based Pharmacokinetic Modelling using GastroPlus using an Early Lead JAK Inhibitor to Establish Mouse Physiological Settings	150
7	Results and Discussion	155
7.1	Evaluation of Methods for Dose Prediction at the Early Stages of Lead Optimisation: A Comparison using the Data of Known Drug Molecules	155
7.2	Dose Estimation Analysis used for the Pi3Ky Program.....	180
7.2.1	Comparison of Various Dose Estimation Methods used in the Pi3Ky Program for Intravenous Administration in Acute Lung Injury	180
7.2.2	Sensitivity analysis, the effect of the potency measured in enzyme assay or in whole blood	184
7.2.3	Sensitivity Analysis of the Effect of the Errors on Early Estimation of the Volume of distribution and Intrinsic Clearance of the Compounds.....	186
7.2.4	Sensitivity Analysis of the Effect of Errors in the Estimation of Intrinsic Clearance.....	188
7.3	Aldehyde Oxidase: A Special Case	191

7.3.1	The Importance of Considering Unbound Clearance.....	195
7.4	Investigation of the Estimated Dose using Various Methods for the Pi3Kδ Program for Oral Administration in Asthma	203
7.4.1	Absorption Rate	204
7.4.2	Elimination Rate	204
7.4.3	Estimating Clinical Dose from DE _{max} (HLPC DE-DP).....	205
7.5	Do the Properties of Inhaled/Pulmonary Drugs Differ from Oral Non-CNS and Oral CNS Drugs?.....	221
7.6	Investigating Lung Retention and Dose in the JAKi Program for Inhaled Administration in Asthma	237
7.7	JAK Pharmacology in Asthma and COPD.....	238
7.7.1	JAK Program Target Product Profile	239
7.7.2	Aldehyde Oxidase Metabolism in the Lung?	248
7.7.3	Understanding the Pharmacodynamic and Pharmacokinetic (PKPD) Relationship in the JAKi Drug Discovery Project	258
7.7.4	Confirming Lung Duration is Required for Target Engagement and Cytokine Induced pSTAT5 Inhibition.	275
7.8	PBPK and PBPKPD Analysis of JAK Inhibitors.....	278
7.8.1	Building a PBPK Model Using the Tool Molecule GSK3532706	280
7.8.2	Linking PBPK to PKPD to Build an Integrated PBPKPD Model	286
7.8.3	Developing More Complex 8-Day Cytokine Mouse Model	291
7.8.4	House Dust-Mite (HDM) Mouse <i>In Vivo</i> Efficacy Model	293
7.8.5	PBPK Enables us to Dig Deeper into other Compartments of Interest ..	300
8	Concluding Discussion	303
8.1	Drug Attrition.....	303
8.2	Lipophilicity	308
8.3	Drug Efficiency	309
8.4	Dose Estimation of Systemically Delivered Compounds.....	310
8.4.1	Potency	311

8.4.2	Volume of Distribution.....	311
8.4.3	Clearance.....	312
8.4.4	Absorption.....	313
8.4.5	Aldehyde Oxidase and Unbound Clearance.....	314
8.5	DE _{max} and Inhaled Delivery Compounds.....	315
8.5.1	Aldehyde Oxidase in the Lung – Implications for Drug Discovery in Inhaled Delivery Programs.....	317
8.5.2	PKPD and PBPKPD Modelling and Simulation in the Inhaled Delivery Project	318
8.6	Summary of key findings of this work within the GSK Respiratory Therapeutic Area	325
9	Future Work.....	327
10	Appendix.....	328
10.1	List of Tables.....	328
10.2	List of Figures.....	330
10.3	List of Equations and Reference Number.....	337
11	Appendix II.....	344
12	Reference.....	389
13	Published Work.....	409
13.1	How to identify and eliminate compounds with a risk of high clinical dose during the early phase of lead optimisation in drug discovery.....	409
13.2	<i>In vitro</i> membrane binding and protein binding (IAM MB/PB technology) to estimate <i>in vivo</i> distribution: applications in early drug discovery.....	410
13.3	Physicochemical and biomimetic properties of molecules that affect lung retention after inhaled administration.....	411

1 Abstract

The pharmaceutical industry continues to face mounting fiscal, political and regulatory challenges developing the next generation of innovative medicines. Drug discovery scientists are directly challenged with the task of trying to overcome the challenge of poor R&D productivity by improving the quality of new chemical entities progressing into drug development to reduce drug attrition. This project focusses on early drug discovery and investigates the potential of a concept called Drug Efficiency (DE). DE was originally introduced by the Psychiatry CEDD (Centre of Excellence for Drug Discovery at GlaxoSmithKline) as an *in vivo* pharmacokinetic (PK) and PK-pharmacodynamic (PD) parameter to try and improve the quality of compounds progressing into *in vivo* PKPD models.

The aim was to select compounds which would achieve higher free concentrations in the CNS, and therefore increase target engagement and improve efficacy. The focus of this project was to show how DE (and it's *in vitro* biomimetic derived equivalent HPLC DE_{max}) can be used for projects involving intravenous (IV), oral and pulmonary routes of administration to select compounds with improved physicochemical properties (low MW, lipophilicity and solubility) and therefore more likely to have a low efficacious clinical dose during early lead optimisation.

The combination of HPLC DE_{max} and *in vitro* potency makes it possible to estimate a clinical dose that would result in an efficacious steady-state free concentration at the site of action. The influence of the potential discrepancies between the *in vitro* and a later stage *in vivo* DE_{max}, the whole blood potency, volume of distribution and clearance on the dose estimation has been investigated using data from a GSK programme profiled during lead optimisation. It was found that drug potency had the greatest influence on estimating the clinical dose. When the estimated dose was low, the impact of small changes in PK parameters such as the volume of distribution and clearance had less effect and typically did not affect compound ranking.

For inhaled pulmonary drugs, the physicochemical and PK properties are often considered to be the opposite of drugs administered by the IV and oral routes. The biggest challenge in the design of inhaled drugs is achieving the optimum balance of lung

retention and pharmacological duration of action without causing lung toxicity. Unlike extravascular drugs, where there have been multiple physicochemical analyses and concepts proposed to help select the right balance of properties for successful drug design, there are very few drug design concepts beyond solubility and permeability for inhaled drug design. This project shows how HPLC DE_{max} can be used as a third critical parameter alongside solubility and permeability to help design inhaled small molecules which have “intrinsic” lung retention, pharmacological duration of action and improved lung safety.

Lung retention was measured for a set of small molecule JAK inhibitors, which all had similar solubility and permeability, but different intrinsic lung retention. It was found that compounds with drug efficiencies (DE_{max}) of around 1% had extended lung exposure. Introducing DE_{max} as an additional parameter has shown that biomimetic binding can provide further information to help identify compounds with the improved potential to become drug candidates with the desired lung residency when administered via the pulmonary route.

2 Introduction

2.1 The Drug Discovery Process and the Importance of Effective Early Discovery

Starting in the late 1980's through to the 2000's, pharmaceutical companies have relied heavily on high throughput screening technologies (HTS), to identify new chemical entities (NCE) for therapeutic targets of interest. HTS approaches have helped identify templates with acceptable baseline target affinities which could then be optimised further to achieve the desired target product profile (TPP), with potency being a key component/focus of the TPP, closely followed by an appropriate ADME (Absorption, Distribution, Metabolism & Elimination) and safety profile.

After discovering and validating potential targets, the drug discovery process usually continued by screening large compound libraries against a target receptor, enzyme or protein to identify potential lead molecules or chemical templates, which can then be further optimised towards the desired TPP [1]. Pharmaceutical companies have typically established large compound libraries (ca. 0.5-4 million compounds) to increase the likelihood of identifying potential leads [1]. Compound libraries or collections are typically based on commercially available compounds and active in-house lead optimisation programs of work, including both present and past. These are compounds selected from optimised lead series templates which will have reached certain milestones e.g. a candidate selection, a new drug application (NDA), or more often of no further interest to specific programs due to a suboptimal profile based on the TPP. This may be due to a lack of affinity or selectivity to the target of interest, or suboptimal ADME properties. Compound libraries are normally carefully managed to ensure only drug-like templates are present and broad chemical space is represented. This is to ensure target relevant hits represent appropriate drug like chemical space for lead optimisation. Compounds in an HTS library would usually be considered as "fragments" or "small molecules" if they are in the molecular weight (MW) range of 200-600Da, with potency/affinity in the low micromolar – high nanomolar range. If compounds fall within this parameter range they would often be considered as hits or compounds of further interest [2]. However, compounds often come from existing lead optimisation programs and these molecules may be on the upper end of small molecule space for initial hits, as a result of parameter

optimisation for previous targets. Ideally, early leads or hits would be <300Da as the process of lead optimisation often increases molecular size by 100-120Da's whilst addressing target affinity and ADME issues [2][3]. Compound libraries expand over time as newer compounds are synthesised and submitted to respective libraries to generate compound diversity and novelty.

Combinatorial chemistry is also a technique which can generate large numbers of compounds but often with similar properties to the leads they were based upon. The disadvantage here is that large numbers of compounds with very little molecular diversity become part of the compound library. The advantage of combinatorial chemistry is the rapid and efficient synthesis of many NCEs, some of which are structural analogues of existing compounds and some which are novel [4].

The process by which compounds are filtered and then selected to become part of the compound library is fundamental to maintaining chemical diversity. Careful management of compound libraries is a fundamental requirement to maximise the chances of a successful HTS campaign against new targets. This should increase the chance of identifying and selecting several relevant and diverse chemical templates for lead optimisation, which then have greater potential of meeting a program team's TPP.

Large scale chemical syntheses using combinatorial chemistry in conjunction with HTS have been used since their widespread adoption in the 1990's, to enable medicinal chemists to rapidly scan through many compounds for "hit like" structures or templates against an *in vitro* target [4]. The size and nature of an HTS depends upon the program of work being employed, with the larger pharmaceutical companies committing to as many as thirty screening campaigns per year, across several therapeutic areas. Fundamentally, the industrialisation of drug discovery using the HTS approach works in two ways [3]:

- Previously developed compounds are scanned against many targets to find a previously unknown affinity.
- Previously developed compounds are scanned against many specific targets that are known to have an affinity for specific functional groups.

The number of NCEs identified through HTS and progressed as lead compounds were reported to be substantially less than 1% (around 1 in 100,000) in 2003, but by 2006 had increased to over 50% [5][6]. The growth of success was mapped in a study of 58 HTS laboratories, in which it was shown that 18 had a combined total of 46 candidate compounds undergoing clinical trials in 2000, and in 2004 this had increased to a total of 104 candidates from 26 laboratories [5]. This represents a 226% increase over a four-year period and shows that the increased use of HTS in early stage compound identification has been successfully implemented into research. However, the quality of those hits may be questioned with the quantity of candidates being delivered becoming the metric of success rather than the quality. This is demonstrated by the number of NDA's remaining low, or even reducing proportionally to R&D expenditure, with the reasons for failure continuing along familiar themes; lack of efficacy and toxicity [7][8]. Or to express in more general terms, a lack of compound quality with respect to the balance of physicochemical properties, ADME and pharmacology [8,9].

2.2 Biopharmaceutical Classification System (BCS)

The BCS was developed as a framework correlating *in vitro* drug dissolution, solubility and gastrointestinal (GI) permeability to *in vivo* bioavailability which was first proposed by Amidon *et al.* in the early 1990's [10]. The principle of the BCS is to recognise that drug dissolution, solubility and GI permeability are fundamental parameters for human drug absorption. The original purpose of the system was part of the Food and Drug Administration (FDA) guidance designed to aid in the regulation of post-approval changes and generic drugs to give potential biowaivers for *in vivo* bioequivalence studies [11] based on *in vitro* data.

The BCS model places oral drugs into four categories or classes: 1) high solubility and high permeability; 2) low solubility and high permeability; 3) high solubility and low permeability and 4) low solubility and low permeability as shown in Figure 2.2-1.

Figure 2.2-1 The Biopharmaceutical Classification System Model [11].

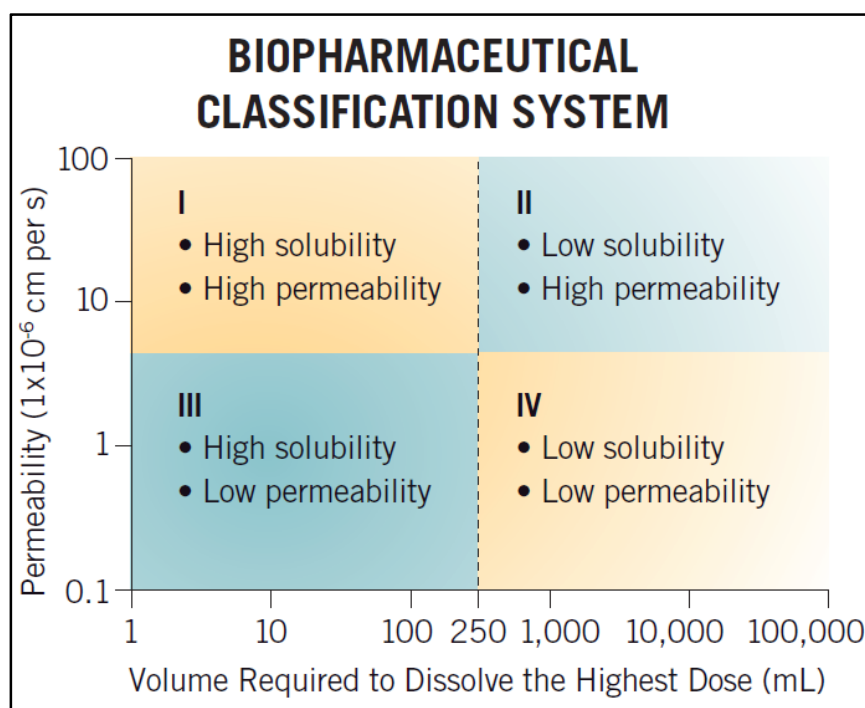


Figure 2.2-1 shows the BCS Model as defined by the FDA for solubility and permeability, Classes I-IV [11]. A compound must completely dissolve at its highest dose in 250 mL water over a pH range of 1-7.5 at 37°C to be classed as highly soluble.

Although the original purpose of the BCS model was as a tool for the FDA, it has helped drug discovery teams to improve the efficiency of drug development by identifying compounds/chemical series with inherent oral absorption characteristics (class I) or with good permeability that require formulation enhancement to achieved *in vivo* absorption (class II). The model can also be used to direct project teams away from areas of chemical space which have poor absorption characteristics (low solubility and permeability, class IV) that are more difficult to develop and have a higher probability of failure.

A complimentary system to the BCS is the biopharmaceutics drug disposition classification system (BDDCS) which was proposed by Wu and Benet [12]. Both models utilise solubility and permeability as their primary parameters, but the major difference is BCS focuses on predicting oral absorption potential, whilst the BDDCS predicts drug

disposition and potential drug-drug interactions in the liver and intestine. This complementary model was developed because Wu and Benet recognised that drugs which have high intestinal permeability are typically eliminated via metabolism, whereas drugs which have low intestinal permeability are eliminated as unchanged drug in the urine or faeces, Figure 2.2-2 shows each class for the BDDCS [12,13].

Figure 2.2-2 Metabolism and Transporter Effects of Solubility and Permeability

	High Solubility	Low Solubility
High Permeability/ Metabolism	<p>Class 1 Transporter effects minimal in gut and liver</p>	<p>Class 2 Efflux transporter effects predominate in gut, but both uptake & efflux transporters can affect liver</p>
Low Permeability/ Metabolism	<p>Class 3 Absorptive transporter effects predominate (but can be modulated by efflux transporters)</p>	<p>Class 4 Absorptive and efflux transporter effects could be important</p>

Figure 2.2-2 shows drug transporter and metabolism predictions based on the BDDCS proposed by Wu and Benet [12,13]

2.2.1 Property-Based Design and Properties Influential to Developability of Oral Products

The seminal work by Lipinski *et al.* 1997 [4,14] highlighted the importance of physicochemical properties of putative drug molecules that have an effect on their ADME properties, specifically oral absorption. Despite the “Rule of 5” being over 20 years old it still has importance in today’s drug discovery environment. Since then, there has been

multiple analysis focussing on the importance of “drug-like” chemical space, which include Astex “Rule of 3” [2], Pfizer’s 3-75 [15], “Three Pillars” analysis [16], and Gleeson’s “ADMET Rules of Thumb” [17], to mention but a few. Despite the compelling evidence put forward by Lipinski *et al.* for controlling physicochemical properties, many pharmaceutical companies and drug discovery groups have continued to progress candidate molecules which occupy suboptimal or chemical space outside of what is considered to be desirable for oral absorption [9,18].

In developing the “Rule of 5”, Lipinski [4] focused attention on the calculated properties of the United States Adopted Name (USAN) database to define what were the preferred physicochemical properties of compounds to achieve successful progression into clinical trials based on ADME properties. It was assumed that most compounds with suboptimal properties would have been filtered out during preclinical safety testing and phase I studies as a result of safety alerts such as hERG or sub-optimal human exposure [4].

Lipinski’s analysis identified solubility and permeability as essential requirements to oral absorption. He acknowledged that the change in the properties of drug discovery compounds between the 1970’s through to the 1990’s was largely due to the industrialisation of the pharmaceutical industry, since it had become feasible to quickly synthesise and screen large chemical libraries as a result of technological advances. One of Lipinski’s observations was that “the physicochemical profile of current leads no longer depends on compound solubility sufficient for *in vivo* activity” [4], but instead depends on:

1. The medicinal chemistry principles of relating SAR to *in vitro* activity
2. The nature of the HTS screen
3. The physicochemical profile of the screening set
4. “Human decision making, both overt and hidden for defining compound acceptability as a starting point for medicinal chemistry.”

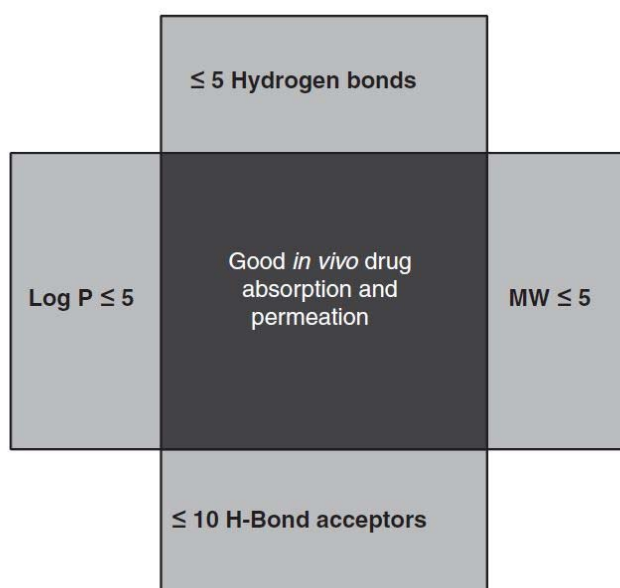
One of the most reliable ways for a medicinal chemist to improve *in vitro* potency is to incorporate a properly positioned lipophilic group. For example, a methyl group can add 0.7kcal/mol to the binding energy [4] if orientated in a way that occupies a receptor pocket. By contrast, manipulation of polar groups involved in ionic interactions has little impact on increasing potency unless you can accurately target an ionic interaction within the target receptor [4]. By focussing lead template optimisation in this way, it is little

surprise that the process of improving affinity/potency alone by the addition of lipophilic groups results in a diametrically opposing relationship with ADME properties [17][19].

The “Rule of 5” states that poor absorption and permeation are more likely when:

1. There are more than 5-H bond donors (expressed as the sum of OH and NH's)
2. The molecular weight is over 500
3. The LogP is over 5 (or MLogP is over 4.15)
4. There are more than 10 H-bond acceptors (expressed as the sum of N and O's)

Figure 2.2-3 Lipinski’s Rule of 5 Highlighting the Importance of Lipophilicity [4]



The naming of the rule derives from each of the four parameters being close to, or a multiple of, 5, not the common misconception that there are 5 rules! Almost 90% of orally active drugs achieving a phase II milestone meet the rule of 5 criteria [4].

Lipinski *et al* subsequently performed a retrospective analysis of the Pfizer compound collection pre- and post the HTS revolution in drug discovery of 1989. Table 2-1 highlights

the percentage of compounds being synthesised pre- and post-1989, where molecular obesity [29] really started to become apparent when compared to commercial or marketed compounds.

Table 2-1 Percentage of Compounds with MWT (Inc. Salt) above 500 [4]

Year registered	Synthetic compounds	Commercial compounds
Pre-1984	16.0	5.4
1984	18.9	14.7
1985	12.1	15.5
1986	12.6	5.5
1987	13.4	5.8
1988	14.6	8.2
1989	23.4	4.1
1990	21.1	3.3
1991	25.4	1.8
1992	34.2	6.8
1993	33.2	8.4
1994	32.7	7.9

Table 2-1 C A Lipinski *et al* Advanced Drug Delivery Reviews 46 (2001) [4]

In the drug discovery environment, the majority of program teams' lead optimisation strategies have traditionally been for medicinal chemists to assume that maximising *in vitro* potency will translate into low dose clinically efficacious therapies [19][21]. This has led to a primary screening cascade approach where *in vitro* potency sits as the primary filter for newly synthesised compounds. The net result of this is often a lead optimisation strategy which results in a diametrically opposed relationship between physicochemical properties associated with high *in vitro* potency and ADMET properties [22].

Given the acceptance of the rule of 5 and the substantial empirical evidence that control of fundamental physical properties, especially lipophilicity, are important for eventual success, it is perhaps a surprise to see that much of the chemistry from the patent literature occupies the upper ranges of the rule of 5 drug-like spectrum [9]. The average oral drug marketed since 1983 has a cLogP of 2.7 and Mol Wt of 358, whereas the average patented compound from four large pharmaceutical companies in the period 2003—2007 has cLogP of 4.1, and Mol Wt of 450 [23] (Figure 2.3-2). By analysing the

trend in lipophilicity and molecular weight throughout the pharmaceutical sector over a decade (1996-2006), Leeson and co-workers concluded that companies such as AstraZeneca and Pfizer have actively targeted “drug like space” by focusing attention on reducing lipophilicity and molecular weight, but others appeared to have remained static or failed to make progress in optimising these properties. This included companies such as GSK, Johnson & Johnson and Wyeth [23], (Figure 2.2-4).

Figure 2.2-4 Trends in Molecular Mass and cLogP in Approved Compounds [9]

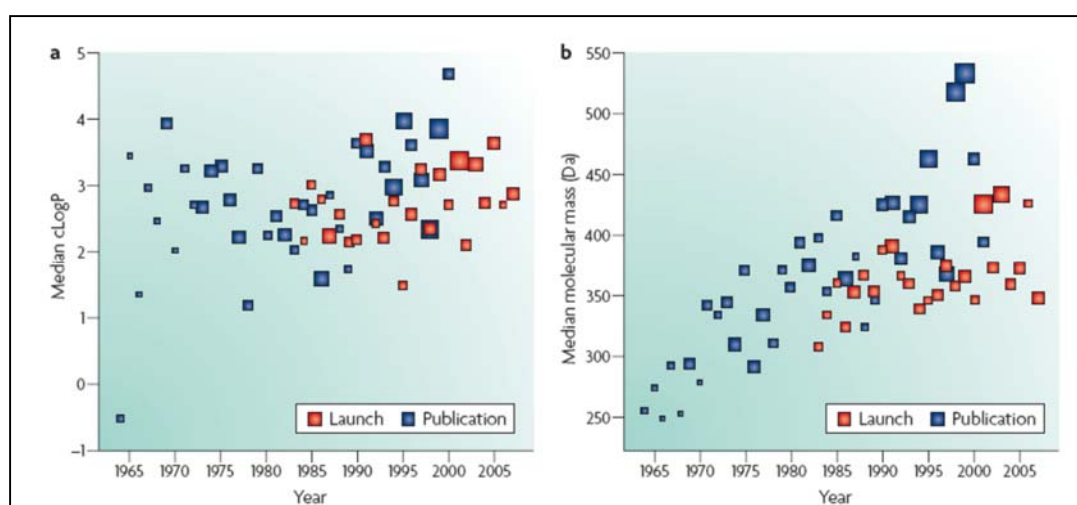


Figure 2.2-4 Show the trend in molecular mass and cLogP for approved compounds over a 20-year period

Figure 2.2-5 Changes in Physical Properties of Patented Compounds by Target Over Time [14].

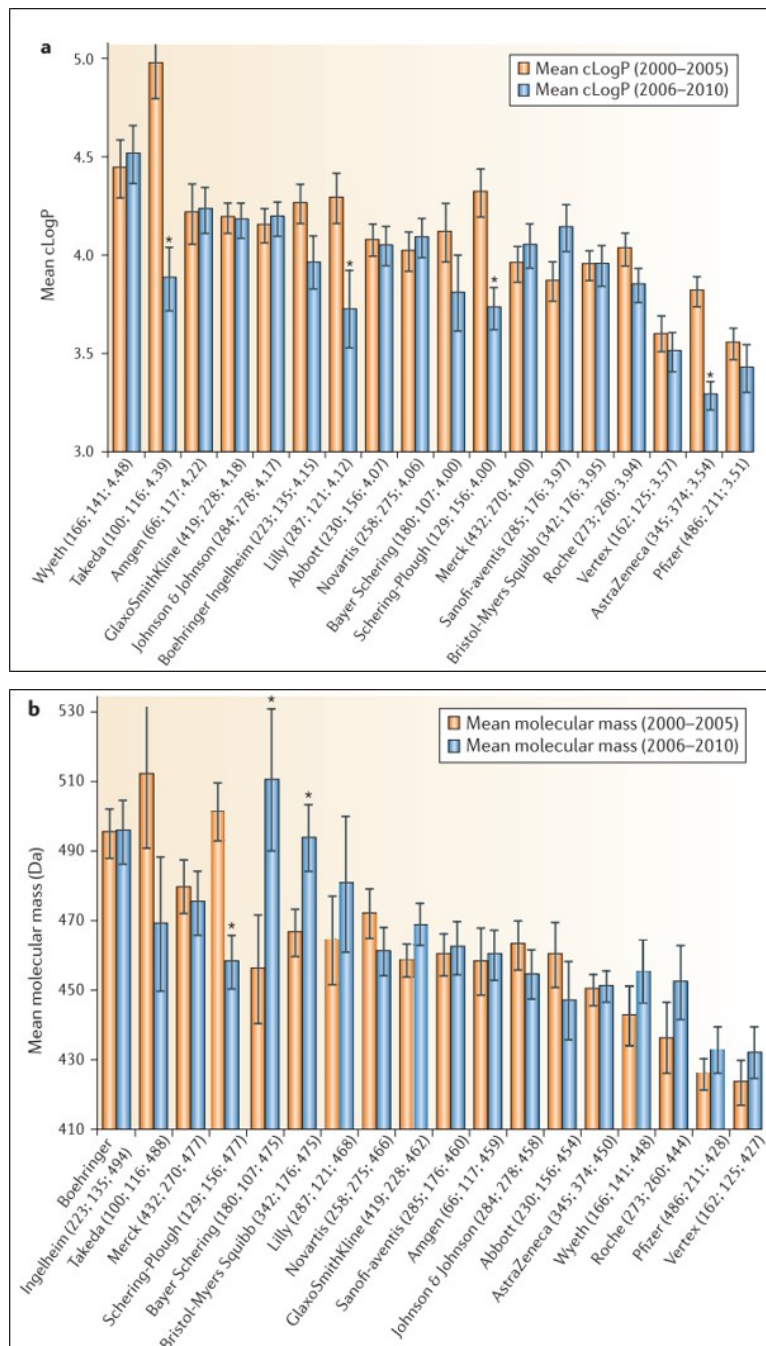


Figure 2.2-5 Shows the trend in molecular mass and cLogP for patented compounds by the major pharmaceutical companies 2000-2010.

As indicated already, the main causes of attrition have been identified as a lack of preclinical safety or clinical efficacy. Pfizer published data they acquired from internal sources on 44 Phase II programs that reached a decision point between 2005 and 2009 [16]. Their aim was to identify the reasons for high levels of Phase II drug attrition across the pharmaceutical sector from their previous experience of failed programs, in order to improve strategic project management and secure a higher chance of success for their current and future assets. They developed the concept that there were three main elements required to increase the chance of successful progression to Phase III, which they termed the 'Three Pillars of Survival' [16]:

1. Suitable compound exposure over a desired period of time at the target.
2. Sufficient compound-target binding to cause the desired effect.
3. Sufficient target modulation to cause a pharmacological effect.

The study was aimed more at improving the chances of compound survival and improving the risk management of their assets, rather than focusing directly on compound quality in lead optimisation. However, it is clear that there is a need to identify compounds with optimal physicochemical properties to ensure that the Three Pillars paradigm can be met and should be a central strategy in any lead optimisation program. This is because the concept effectively links the optimisation of target binding, potency, and compound exposure, which are all vital elements of developing clinically efficacious drugs.

The 'Three Pillars' confidence matrix shows the importance of establishing an understanding of target engagement to maximise project success rates and drive down compound attrition. Having confidence in all Three Pillars equates to optimising the properties of the molecule such that they give the desired exposure and binding at the target site, which amounts to a pragmatic and logical approach to drug discovery (Figure 2.2-6).

Figure 2.2-6 Three Pillars Concept as a Confidence Matrix [12]

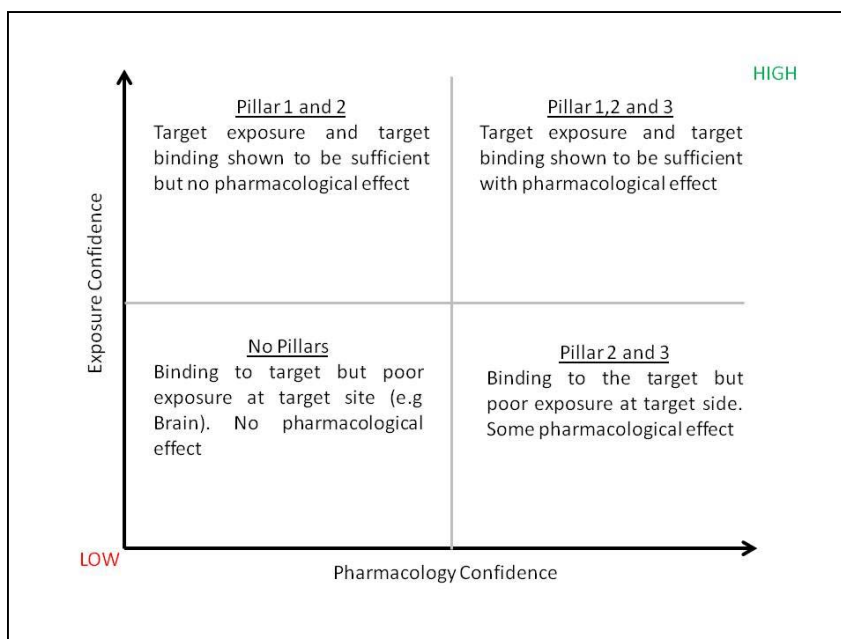


Figure 2.2-6 Three Pillars confidence matrix as described by Morgan *et al.* [16]

An assessment of the Three Pillars Concept is now incorporated into many lead optimisation programs (see Figure 2.2-7) within GSK to encourage program teams to focus on the relationship of pharmacokinetics and pharmacodynamics (PKPD) in pre-clinical space all the way through to clinical development. By adopting this approach, the hope is that there will be an increase in productivity and success in programs developing low dose (<100mg) drugs, which have the intended efficacy and safety in the clinic.

Figure 2.2-7 PKPD and Human Clinical Dose Estimation Matrix Used at GSK

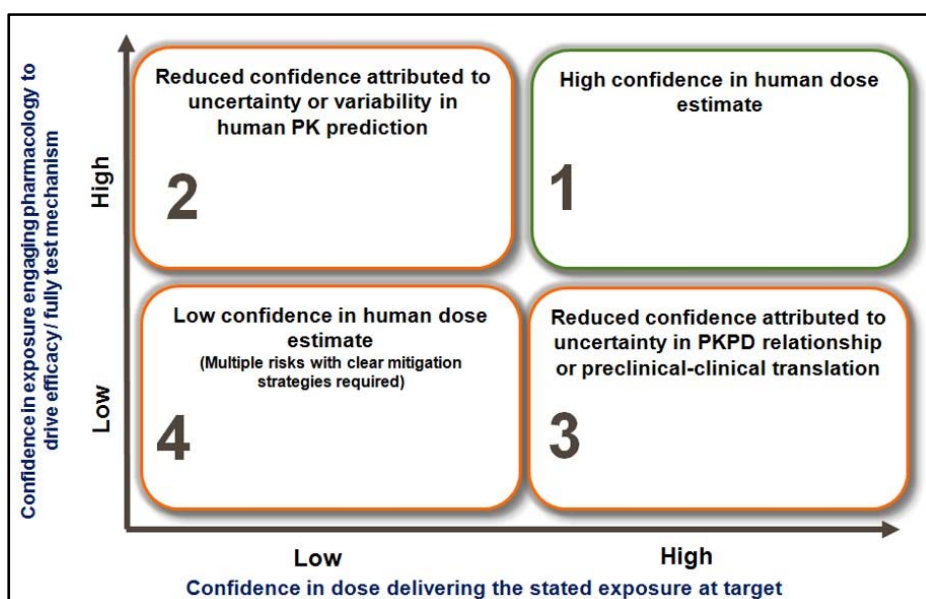


Figure 2.2-7 the GSK human dose prediction confidence matrix

3 A Brief Description of the Project

The most influential properties of compounds or chemical templates for developability are lipophilicity, solubility, permeability, protein binding and acid/base character. In this work, the aims are to investigate how these properties:

- Influence drug efficiency and dose estimation based on measured and calculated physicochemical and biomimetic properties that are available to early drug discovery program teams for lead optimisation.
- Can drug efficiency and dose prediction be used to rank compounds for further studies to improve the efficiency of the lead optimisation process.

Early clinical dose prediction [24][25] is an accepted but relatively new approach in drug discovery, for increasing the chance of selecting optimal molecules which have the greatest chance of engaging the target of interest in the clinic. We would like to understand if the concept of drug efficiency has the potential to direct lead chemical

series development, and aid selection of molecules which are likely to have a low clinical dose.

A low clinical dose (<100mg) is central to GSK and the wider pharmaceutical industry's vision of candidate quality because high clinical dose (>100mg) has consistently been associated with poor drug developability or toxicity. It is therefore expected that focusing on lowering clinical dose would enhance the developability prospect of candidate drugs through the reduction of toxicity and idiosyncratic adverse reactions, see Table 3-1 [26].

Table 3-1 Drug Withdrawals in the United States between 1980-2006 [26]

Primary Pharmacology		Secondary Pharmacology		Direct Organ(s) Toxicity	
Drug	Daily Dose (mg)	Drug	Daily Dose (mg)	Drug	Daily Dose (mg)
Alosetron	1.0	Astemizole	10	Benoxaprofen	600
Cerivastatin	0.3	Cisapride	40	Bromfenac	100
Encainide	150	Dexfenfluramide	15	Nomifensine	125
Flosequinan	100	Fenfluramide	15	Remoxiprine	300
Rofecoxib	25	Grepafloxacin	400	Suprofen	800
		Mibefradil	100	Temafloxacin	600
		Rapacuronium	100	Ticrynafen	400
		Terfenadine	120	Tolcapone	300
				Troglitazone	400
				Trovafloxacin	200
				Zomepirac	400

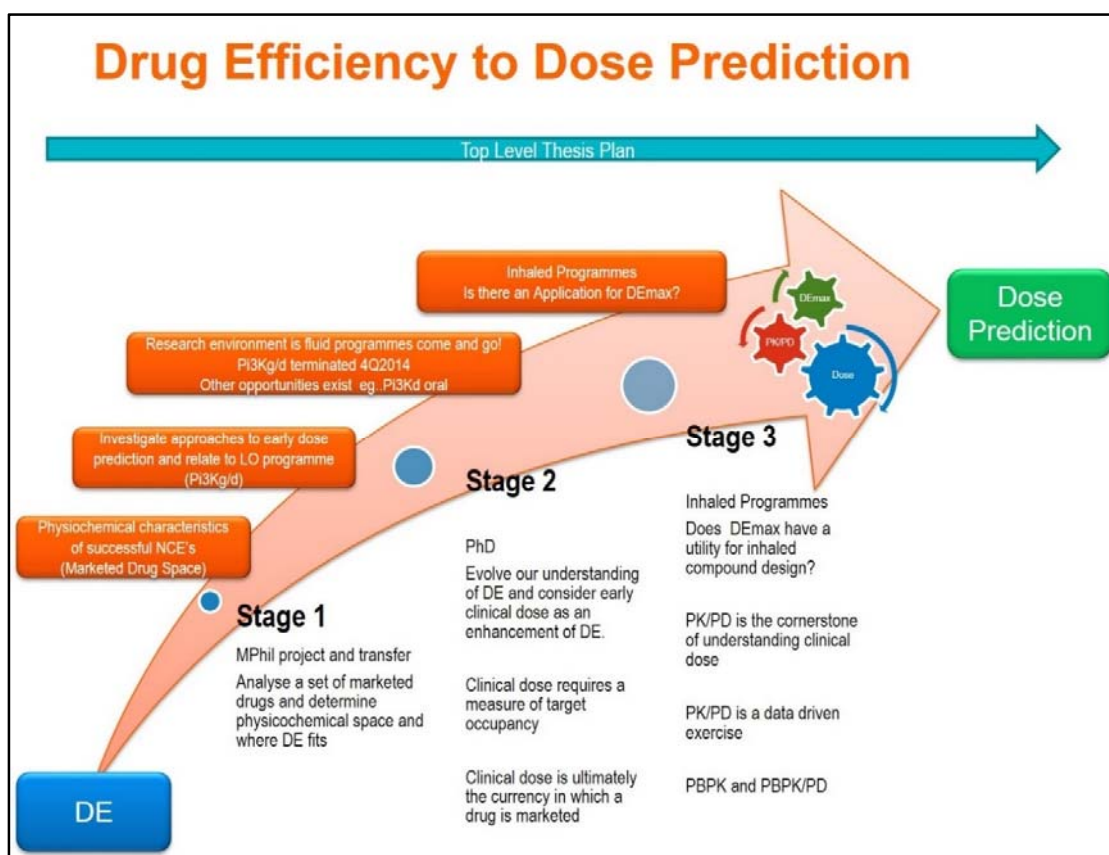
Table 3-1 Highlights drug withdrawn from the market in the US between 1980-2006. The clinical dose and reason for drug withdrawal is given. The risk of toxicity increases as the clinical dose increases, typically >100mg's.

Early dose prediction has the potential to help lead optimisation teams to design lead series and select molecules with desired physicochemical properties and PK profiles, which are likely to translate to good clinical PK, and therefore be selected as candidate molecules. At the early stages of drug discovery, we usually know the *in vitro* enzyme or cellular potency of compounds, which is then used to build SAR along with some simple physicochemical parameters to enable decision making. This project will aim to evaluate whether bio-mimetic based drug efficiency ($Drug_{eff}$) in combination with clinical dose

estimation techniques, increases the drug discoverer's potential to identify high quality candidates with increased potential of become efficacious medicines.

The concept of drug efficiency was introduced by Braggio *et al.* [27] in 2010. Drug efficiency is a pharmacokinetic term which is defined as the percentage of the dose administered that is in the bio-phase of interest *in vivo* which is freely available to exert a pharmacological effect. A more complete definition of drug efficiency will be detailed in Section 4.2.4.

Figure 2.2-1 PhD Project Plan



To explore the relationship between drug efficiency and dose prediction, three drug discovery programs were selected that were differentiated by their routes of administration design paradigms: IV, oral and inhalation. This was to explore whether the concept was more suitable to specific types of drug discovery projects

3.1.1 Property-Based Design of Selected Intravenous, Oral and Inhaled Programs a Brief Description

A more detailed description of each program will be given on Section 5.

3.1.2 Pi3K γ IV Program

The PI3K γ program was chosen for the design of good pharmacodynamic properties for compounds administered intravenously. In this program compounds are designed for acute lung injuries for hospitalised patients where the intravenous administration is advantageous.

3.1.3 Pi3K δ Oral Program

A set of marketed drugs and the PI3K δ oral program were selected to investigate the design principles for low dose orally administered compounds.

3.1.4 JAK Inhaled Program

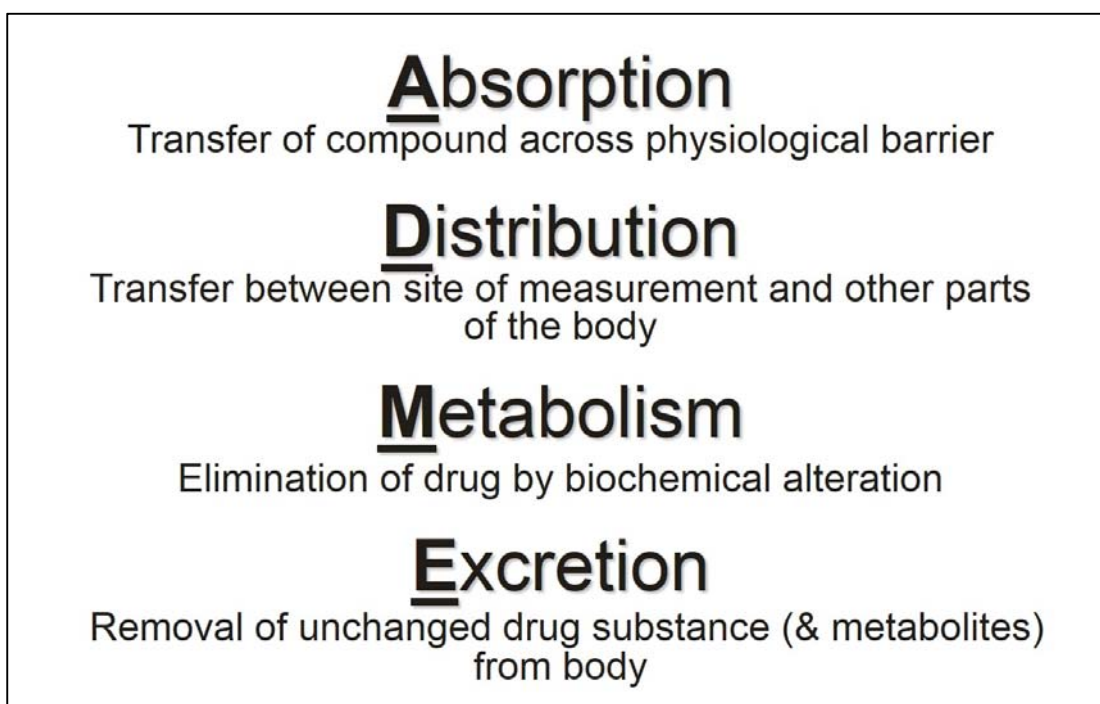
The pan JAKi (1/2/3) program compounds have been studied as an example for the design of inhaled drugs with long lung retention for treatment of chronic inflammation in asthma.

A more detailed description of project objectives and each of the above targets is presented in chapter 5.

4 ADME - Absorption, Distribution, Metabolism and Excretion in Dose Prediction.

A simple description of ADME and a definition of each term is described in Figure 2.2-1.

Figure 2.2-1 Basic Definition of ADME



The clinical dose depends on several pharmacokinetic parameters and to potency or minimum effective concentration (MEC) against the target, this is described by the dose calculation equations: Equation 38 and Equation 39 detailed later in Section 4.3. The potency or MEC is one of the most influential parameters in achieving a low clinical dose. The *in vitro* affinity of a compound is typically expressed as an EC_{50} for agonists or pIC_{50} but ideally a pK_i value should be determined for antagonists. From these data, the free concentration of the drug molecule that would be needed at the site of action in order to exert half of the maximum biological activity can be estimated. However, there are several ADME parameters that affect the free concentration at the site of action, particularly the intrinsic clearance, absorption and the distribution of the compound in the body. Drugs can be administered in various ways that produce different pharmacokinetic profiles. In

this project, different dose estimation approaches have been investigated after intravenous, oral and inhaled (intranasal) administration. After administering a drug, it is either absorbed from an extravascular site of administration (e.g. gastrointestinal tract, lung etc...) or is directly administered to the systemic circulation (IV). Upon reaching the general circulation, the drug is distributed into the tissues and other compartments in the body. It will also begin to be cleared from the body by various pathways (metabolic, hepatic and renal clearance) with different elimination rates. The basic terms that are generally used in describing the ADME profile of a compound are now defined.

4.1.1 Absorption

There are several ways by which a drug can be administered, such as intravenous, subcutaneous, topical, inhaled, intranasal, and most commonly the oral route. We typically think of absorption with respect to orally delivered small molecules and their absorption from the gastrointestinal tract (GI). GI absorption is the process that a drug undergoes following oral administration resulting in its appearance in the central compartment (systemic blood). The fraction of drug that was dosed and appears in the central compartment is referred to as oral bioavailability (F) and normally expressed as percentage bioavailability (%F).

Figure 2.2-2 Process of Absorption of a Drug from the GI Tract

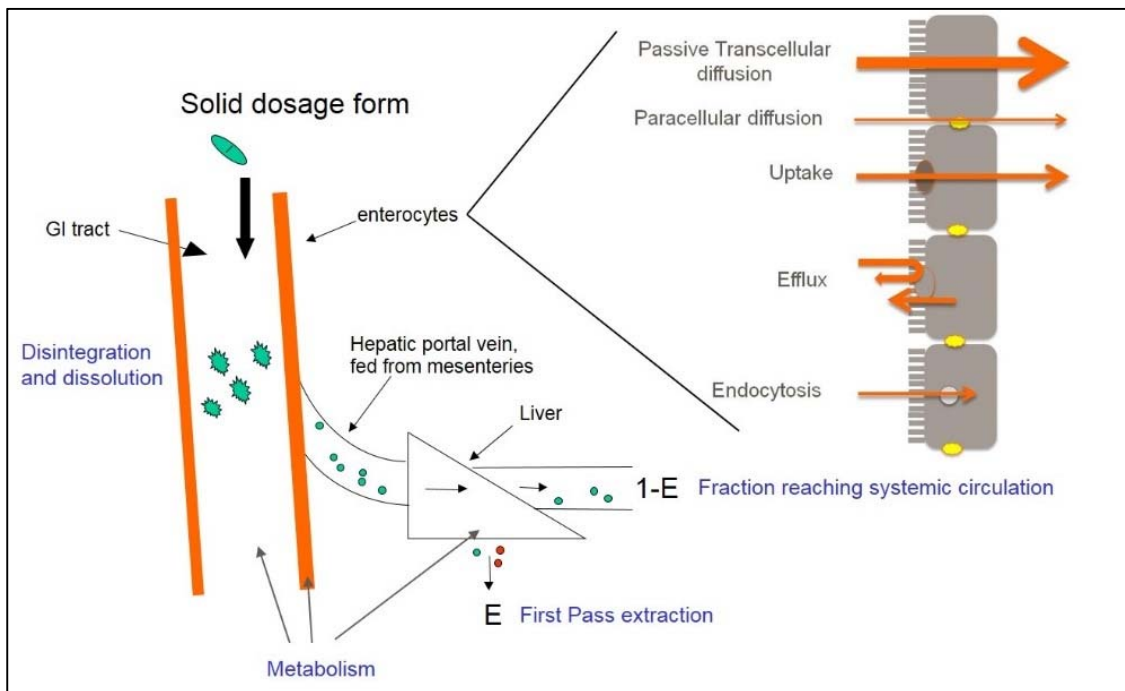


Figure 2.2-2 Shows a simple schematic of the processes involved in a drug reaching the systemic circulation following oral administration

For orally administered drugs, if taken in a solid form such as a tablet, dissolution must precede the release of the active pharmaceutical ingredient (API) that will then dissolve in the GI fluid, in accordance with its solubility. Following gastric emptying, the drug will pass through the duodenum, jejunum and ileum where most of the absorption through the GI wall will occur. The fraction absorbed (F_a) is the proportion of the administered dose which permeates the GI wall/reaches the enterocytes before entering the hepatic portal vein.

Following absorption, the drug will pass through to the portal vein, where it will then be presented to the liver. The liver is the principle organ in the body responsible for the metabolism of the vast majority of small molecules/drugs, due to the high expression of metabolising enzymes such as the cytochrome P450's. Any parent drug which then enters the central compartment is referred to as the fraction which escapes hepatic extraction (F_h) or often referred to as first pass extraction. The fraction of drug which then reaches the central compartment following oral delivery, is referred to as the oral

bioavailability (F) (see Equation 1). The oral bioavailability is an important pharmacokinetic term for a drug, as this is this fraction of administered drug which reaches the systemic circulation in order to bind to its target (e.g. receptor or enzyme) and elicit a pharmacological effect. Bioavailability will be 100% when a drug is administered intravenously, whereas oral bioavailability is typically below 100%, as its physicochemical properties and first pass metabolism through the liver (Equation 1) normally reduces the amount of parent compound appearing in the central compartment. Metabolism may start in the gut as enzymes and efflux transporters are expressed in the GI wall. Oral bioavailability may approach 100% due to complete absorption ($F_a = 1$), and low hepatic extraction ($F_h \leq 1$). Clearance and Metabolism will be discussed later in Section 4.1.3.

Equation 1

$$F = F_g \cdot F_a \cdot F_h$$

F=Bioavailability, F_g =Fraction of drug escaping gut metabolism, F_a =Fraction of drug absorbed from the GI Tract, F_h =Fraction of drug that escapes hepatic extraction

Equation 2

$$F_h = 1 - ER$$

$$\text{where } ER = \frac{CL}{Q}$$

F_h =Fraction of drug that escapes hepatic extraction, ER=Extraction Ratio, CL=Clearance, Q=Organ Blood Flow

The underlying physicochemical processes of absorption are an area of significant importance to pharmaceutical development and DMPK scientists and can be investigated in several ways using *in silico*, *in vitro* and *in vivo* systems. If a drug is administered as a solid such as in a standard compressed tablet, the tablet has to disintegrate, and the drug becomes solubilised before it is able to permeate the intestinal wall; this is determined by the dissolution rate and solubility. From the stomach to the large intestine, the pH of the gut lumen has a large pH range and can change from being very acidic (pH 1.5), to very alkaline (pH 10). This means that ionization plays a significant role in the solubility and absorption of small molecules. Small molecules can be in different ionization states in different parts of the GI tract. Importantly the ionized species are more soluble than the

non-ionized species. Therefore, acidic molecules with pK_a 's which result in unionized species at low pH are less soluble in the stomach than basic compounds that are readily ionized at low or physiological pH.

There are several other endogenous phospholipids such as micelles and enzymes in the intestinal lumen that may aid solubility. The most important micelles are taurocholate and phosphatidyl choline. Lipophilic drug molecules can partition into micelles, which can help to accelerate the dissolution rate.

When the drug molecule is in solution, there is a high probability that it will permeate through the intestinal wall. The passive absorption process is governed by the rate of permeation that follows Fick's law of diffusion (see Equation 3), which describes the flux of molecules from higher concentration to the lower concentration. The major physicochemical driving force of absorption is the concentration difference between the intestinal lumen (apical) and the other side (basolateral) of the intestinal wall. The intestinal wall is densely networked with blood vessels. The continuous blood flow creates a concentration gradient which reduces the drug concentration and drives the permeability through the intestinal wall. Very small molecules can also be absorbed paracellularly through small gap junctions between the intestinal cells, whereas most drug molecules diffuse through the cells, which means they have to go through several phospholipid bilayers, which reduces their absorption rate.

Equation 3

$$J = -D \frac{d\phi}{dx}$$

J is the diffusion flux with the dimension amount per unit time, D is the diffusion coefficient with the dimension of area per unit time, ϕ is the concentration with the dimension amount per unit volume, x is position with dimension length.

There are also active transport processes that can carry molecules through the intestinal wall to enhance absorption rates and active efflux processes which can significantly limit absorption. A well-known and important example is P-glycoprotein (P-gp), which can limit absorption from the intestine as well as other organs throughout the body (e.g. CNS uptake). These efflux transporters have evolved to protect the body from potentially

harmful xenobiotics. There are metabolising enzymes present in the GI tract and cells, which can directly metabolise drug molecules to reduce the fraction of drug reaching the portal vein and therefore limiting bioavailability.

Besides the physicochemical aspects of absorption, there are also several other important physiological factors. For example, the effect of food can influence the GI pH, enzyme expression and gut motility. There are large individual variations in the size of the absorption surface in the gut, depending on age, gender, and disease state. The usual way to estimate absorption *in vivo* during the drug discovery and development process is to measure the systemic blood or plasma concentrations of a drug over time, and then construct a concentration-time profile. From these curves it is possible to calculate parameters such as, maximum concentration (C_{max}), elimination rate (K_{el}) and the Area Under the Curve (AUC). The AUC is the basis for non-compartmental pharmacokinetic (NCA) evaluation, which is one of the most frequently used methods of determining pharmacokinetic parameters such as clearance. The bioavailability of the drug can be calculated by comparing the AUC values after oral and intravenous administration and expressed as a percentage (%F). The first pass metabolism or extraction ratio can be estimated from the IV clearance. The absorption can then be estimated from the bioavailability and extraction ratio using Equation 1 and Equation 2 described earlier in this section.

As the absorption process involves complex physicochemical and biological processes, it is very difficult to predict absorption solely from chemical structure. However, there are now some effective computational Physiological Based Pharmacokinetic (PBPK) models such as GastroPlus™, which can help predict absorption from the GI tract. This will be discussed further in Section 6.10.

When compounds are absorbed from the GI tract they enter the circulating blood via the hepatic portal vein, before entering the liver. The purpose of the liver is to protect the body and act as a barrier to xenobiotics reaching the systemic circulation, which may be harmful/toxic. The liver metabolises xenobiotics to less toxic or inactive metabolites, which are generally more polar and can be easily excreted via the renal system or back to the GI tract via the bile where they can be excreted.

It is generally much easier to directly measure bioavailability than absorption in pre-clinical studies, bioavailability is also generally more relevant parameter when assessing systemic exposure of an oral drug. However, absorption can be directly measured *in vivo* if required by sampling from the portal vein and systemic circulation in rodents. These models are generally more complex and require more invasive surgical techniques to cannulate blood vessels to enable repeated blood sampling.

4.1.2 Distribution

Distribution is defined as the reversible transfer of a drug between one compartment to another and in pharmacokinetic terms referred to as volume of distribution. Volume of distribution (V_d) represents one of the most important pharmacokinetic parameters of a drug, and often one of the most misunderstood and is defined as, the fluid volume that would be required to contain the amount of drug present in the body at the same concentration as in the plasma. Both V_d and clearance (CL) are the predominant factors which affect the duration of action and dosing frequency of a drug due to their relationship to half-life and are related by Equation 4 [28].

Equation 4

$$CL = V_d \cdot K_{el}$$

CL=Systemic clearance, V_d = Volume of distribution, K_{el} =Elimination rate constant

Once the absorption process has occurred and the parent drug has escaped first pass metabolism ($F \leq 1$), the compound reaches the systemic blood circulation and distributes around the body. The circulating blood volume allows the drug to be transported around the body and partition into the different tissues and organs. Clearance continues via the liver and/or kidneys as the compound is recirculated through these organs. Various pharmacokinetic models can describe the distribution of the drug as a function of time, often using a non-compartment method (NCA) or linear regression of a log linear concentration-time profile to determine CL (blood or plasma), V_d and half-life ($T_{1/2}$). However, in reality the body is made up of many tissues which can be represented as several compartments. The simplest compartmental model involves one compartment, although two compartment models are probably more consistent with most concentration-time profiles and are more representative of a physiological system, using a central

compartment (blood/plasma) and a tissue compartment (rest of the body). Concentration-time curves using compartmental models are more complex to analyse and require differential equations to describe the body as a multi-compartment system. As compounds often distribute more slowly to tissues that have a low blood supply, such as adipose, muscle or skin, then multi-compartment models are required to accurately describe the concentration-time curve obtained from *in vivo* experiments. One of the better approaches to modelling this type of complex data and which has emerged in recent years is PBPK modelling, which will be described in more detail in Section 6.10.

V_d is a proportionality factor between the total amount of drug administered to the body and the concentration measured in the blood or plasma. Blood or plasma represents the reference space where the drug concentration is measured. Therefore, the V_d is the calculated theoretical volume that would be necessary to contain the amount of administered drug at the same concentration as it is in the blood or plasma.

There are three simultaneous processes which govern V_d following IV bolus administration: the initial intravascular distribution of the drug throughout the blood/plasma pool; the distribution of the drug by diffusion into tissues; and the irreversible elimination of the drug from the body.

Although only a theoretical parameter, the V_d of small molecules is typically related to tissue volumes as a helpful means to contextualise how a molecule distributes throughout the body. DMPK scientists typically rank compounds into low (0.6 L/kg), moderate (0.6-5 L/kg) and high (>5 L/kg) volumes. Figure 2.2-3 shows how the physiological body fluid volumes for human V_d is normally divided and provides drug discovery scientists with a general indication of where a compound is likely to distribute based on its measured V_d .

Figure 2.2-3 Physiological Body Fluid Volumes for Human [28]

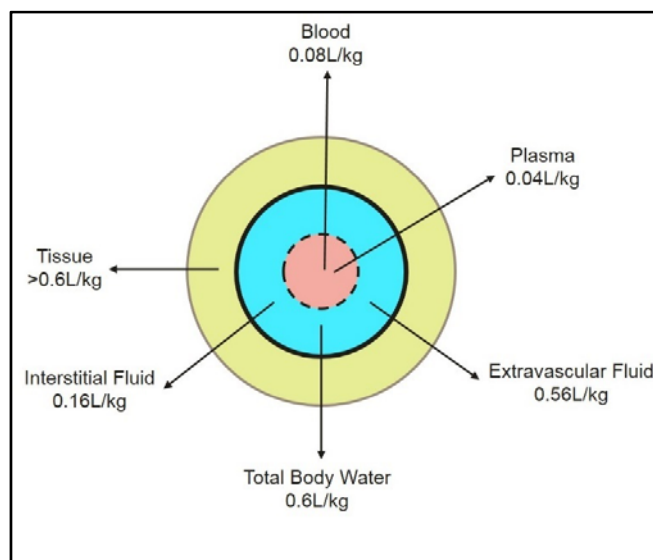


Figure 2.2-3 Physiological volumes of body fluids in human. Adapted from reference [28]

How a drug/molecule distributes into tissues is driven by several physicochemical properties and physiological processes, but one of the most significant factors is its acid/base classification. Basic molecules tend to have affinity for binding to α 1-acid-glycoprotein and albumin in plasma, and this affinity is often related to lipophilicity (see section 4.2.1) [28], and have moderate to large volumes in the order of 1-25 L/kg. Basic molecules also tend to partition into the phospholipids as they bind to the negatively charged phospholipid head groups of these proteins: phosphatidylcholine and phosphatidylserine are the major phospholipids in plasma and tissues, respectively. Concentrations of phosphatidylserine reflect closely the ranking of the tissue partition coefficients (K_p) of many basic drugs in tissues (lung > kidney > liver > muscle and heart > brain), which are ionized at physiological pH [28]. Figure 2.2-4 and Figure 2.2-5 help to visualise the process of distribution between the blood/plasma and tissues compartments.

Figure 2.2-4 The Schematic Illustration Free Drug Partitioning Between the Plasma and Tissue Compartments.

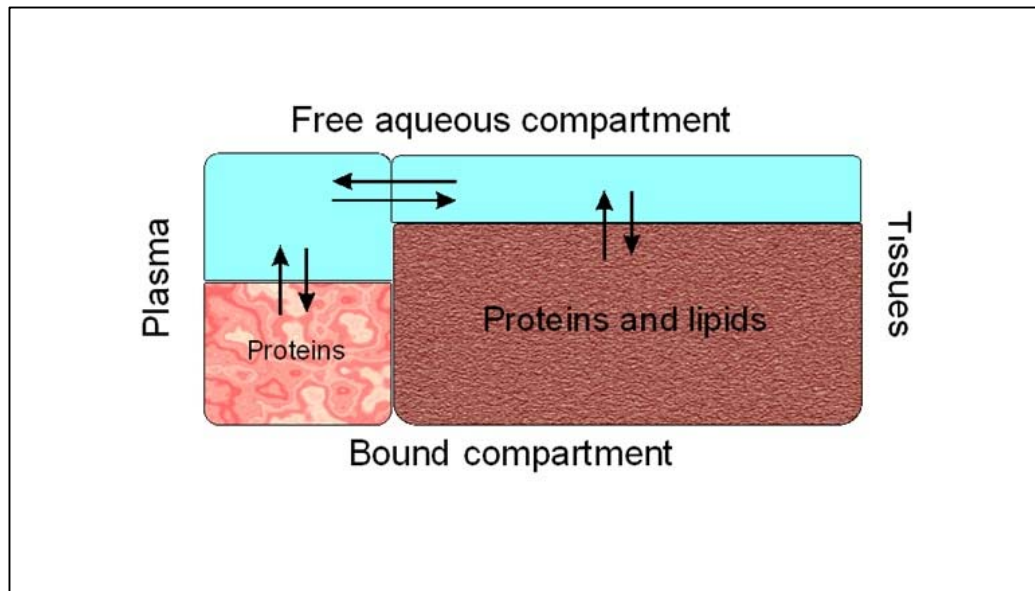


Figure 2.2-4 Shows how the unbound/free compound distributes between the plasma and tissue compartments

Neutral molecules have no charge related interaction and their V_d 's tend to be directly related to lipophilicity and are in the moderate range (0.6 – 5 L/kg). Lipophilicity is also important for acids; however, the dominant interaction of these molecules tends to be their high affinity for albumin resulting in a very low free fraction in plasma (f_{up}). This, along with their negative charge at physiological pH that is responsible for low affinity for phospholipid head groups and low tissue binding (high f_{ut}) results in acidic compounds having low V_d 's that are similar to plasma protein or total body water (0.04 – 0.6 L/kg). This is illustrated in Figure 2.2-5.

Figure 2.2-5 A Physiological Schematic Describing Volume of Distribution Illustration of a Drug's Partitioning Between the Plasma and Tissue Compartments

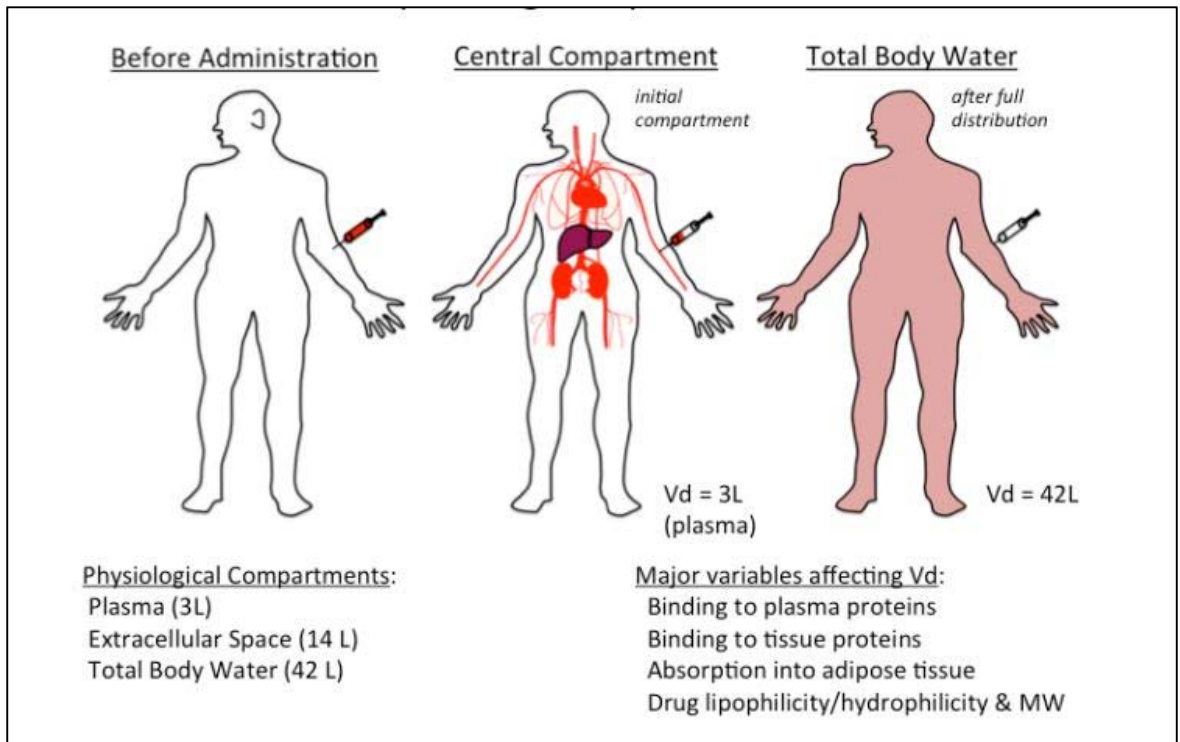


Image downloaded on April 20th 2018 from

http://tmedweb.tulane.edu/pharmwiki/doku.php/introduction_to_pharmacokinetics

There are typically three volume terms which can be calculated and used to describe the V_d : the volume of the central compartment (V_{dc}), the volume at steady state (V_{dss}) and the volume of distribution area ($V_{d\beta}$). Each volume term is defined by different points of a concentration-time curve following bolus intravenous administration of a drug (Figure 2.2-6).

Figure 2.2-6 Description of Volume Terms from Concentration-Time Curve

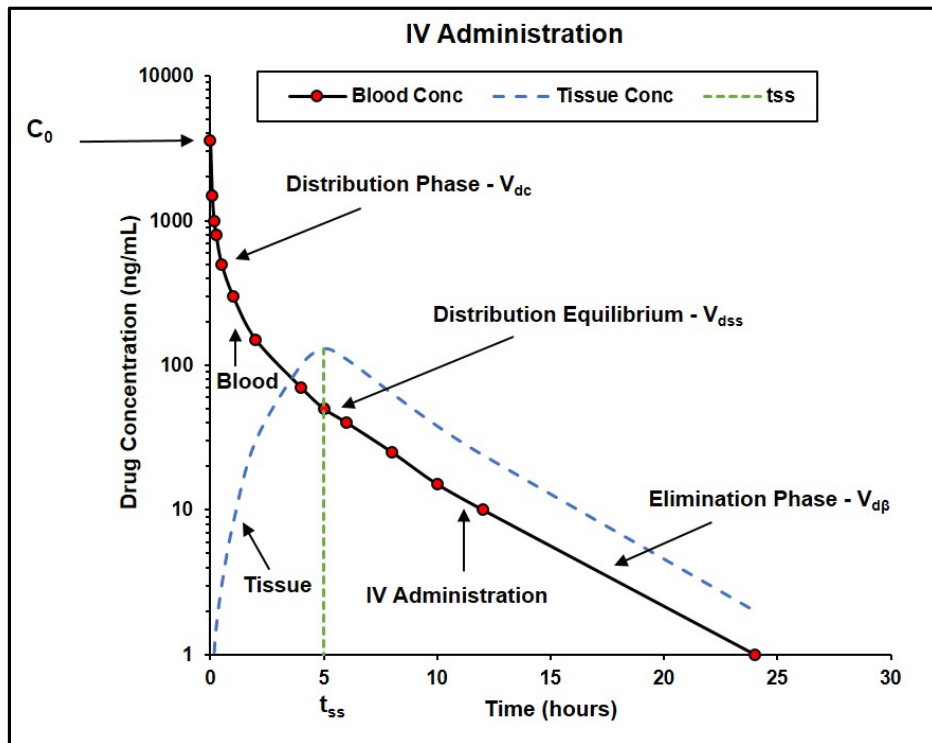


Figure 2.2-6 describes the different volume of distribution terms which are derived from a concentration time curve, [28].

The different V_d terms can be described by Equation 5, Equation 6 and Equation 7.

Equation 5

$$V_{dc} = \frac{\text{Dose}}{C_0}$$

V_{dc} is the volume of the central compartment, dose is the amount of drug administered, C_0 is the concentration at time zero.

Equation 6

$$V_{dss} = \text{Dose} \cdot \frac{\text{AUMC}}{(\text{AUC})^2} = \text{CL} \cdot \text{MRT}$$

V_{dss} is the volume of distribution at steady state, dose is the amount of drug administered, AUC is the area under the time concentration curve, AUMC is the area under the first moment time concentration curve, MRT is the mean residence time, CL is the systemic clearance.

Equation 7

$$V_{d\beta} = \frac{\text{CL}}{K_{el}}$$

$V_{d\beta}$ is the volume of distribution area, CL is the systemic clearance, K_{el} is the elimination rate constant

V_{dc} is the apparent volume immediately after a bolus IV dose. This volume is generally lower than the V_{dss} as it assumes instantaneous distribution, and therefore does not give a good estimate of apparent volume when distribution for a compound is slow, for example when it perfuses slowly into tissues such as adipose and muscle. V_{dss} is the most widely quoted value for V_d in drug discovery, as it represents the apparent volume under steady state conditions, which is the dosing conditions for most compounds being developed. $V_{d\beta}$ is derived from the terminal phase, but is often confounded by a poorly profiled terminal phase of the concentration-time curve and/or low analytical sensitivity. This volume term is also a function of clearance and will therefore change with time and is not considered to be a pure measure of V_d .

Equation 8 is another useful way to describe V_{dss} , as it is based on physiological descriptors of V_d . This relationship follows the principles of Fick's Law, which describes the process of passive diffusion of unbound drug as a determinant of V_d and is illustrated by Figure 2.2-4.

Equation 8

$$V_{dss} = V_p + V_t \cdot \left(\frac{f_{u_p}}{f_{u_t}} \right)$$

V_{dss} is the volume of distribution at steady state, V_p is the volume in the plasma compartment, V_t is the volume in the tissue compartment, f_{u_p} is the fraction unbound in plasma, f_{u_t} is the fraction unbound in tissue

Equation 8 can be also be expressed as Equation 9, where K_p is the partition coefficient between plasma and tissue compartments.

Equation 9

$$V_{dss} = V_p + V_t \cdot K_p$$

V_{dss} is the volume of distribution at steady state, V_p is the volume in the plasma compartment, V_t is the volume in the tissue compartment, K_p is the plasma tissue partition coefficient.

It can be seen how the biomimetic measurements of phospholipid and albumin binding described in Section 4.2.1 relate to volume of distribution because of the physiological importance of these lipids and proteins. As a result, these measurements can be used to model V_{dss} to help with decision making in the early stages of drug discovery. An advantage of the biomimetic approach is the ability to generate data for large number of compounds relatively cheaply in early discovery, unlike *in vivo* V_{dss} , which can only be measured for a relatively small number of compounds for both practical and ethical reasons.

4.1.3 Metabolism and Elimination - Clearance

Metabolism and excretion are the processes by which a drug or molecule is cleared from the body. These two processes are often collectively referred to as clearance. The important role or consequence of metabolism is to deactivate or reduce the pharmacological activity of the parent molecule.

Metabolism and transporter processes are defense mechanisms to protect the body from xenobiotics. Metabolism occurs in most tissues in the body, although the liver is the

primary organ for metabolism due to the high expression of metabolising enzymes. The extent of metabolism differs widely across other organs and tissues such as the gut wall, kidney, skin, lung and blood/plasma. Metabolism is the process by which molecules are catalytically changed / bio-transformed to a metabolite. Small molecules are typically metabolised by one or two general processes known as Phase I and Phase II metabolism. The most common Phase I process involves redox reactions in the liver catalyzed by a family of proteins call the Cytochrome P450 enzymes. Cytochrome P450s (CYPs) are the major drug metabolising enzymes, responsible for ~75% of human drug metabolism, with the main CYPs of interest being 3A4, 2D6, 2C19, 2C9 and 1A2. CYP 3A4 and 2D6 are responsible for the metabolism of approximately 50% of all small molecules. Other Phase I processes include hydrolysis of esters and amides by esterases and amidases and oxidation of aldehydes and alcohols by oxidases and dehydrogenases to name a few. These processes generally produce metabolites with increased polarity and solubility, which can be excreted directly through the hepatobiliary or renal systems, or undergo further Phase II metabolism by conjugation with endogenous polar molecules before they are excreted via the bile or renal systems. Table 4-1 provides a list of the most common Phase I and II reactions.

Table 4-1 The Most Common Phase I and II Reactions

Examples of the main Phase I and II Reactions	
Phase I	Phase II
<p>Oxidation CYP P450 >50% of drugs MAO's, FMO, Aldehyde Oxidase Xanthine Oxidase</p> <p>Reduction Carbonyl reductases using (P450) reductase</p> <p>Hydrolysis Amides, ethers, esters</p>	<p>Glucuronidation Addition of glucuronic acid to: OH, CO₂H, NH, NH₂, NOH</p> <p>Sulphation Addition of sulphate to: OH, CO₂H, SH</p> <p>Amino acid conjugation Via aa transferases – glycine, taurine to: OH, NH₂</p> <p>Conjugation Via glutathione-S-transferases to electrophilic atoms: C, O, N & S</p>

Small molecules and their metabolites can be excreted from the body via the hepatobiliary (Figure 2.2-7) or renal systems (Figure 2.2-8), with the route often dependent on their physicochemical properties and functional groups. The lung is also a site of excretion for specific drug types such as volatile anaesthetics.

Figure 2.2-7 Physiological Schematic of the Hepatobiliary System and Upper GI Tract

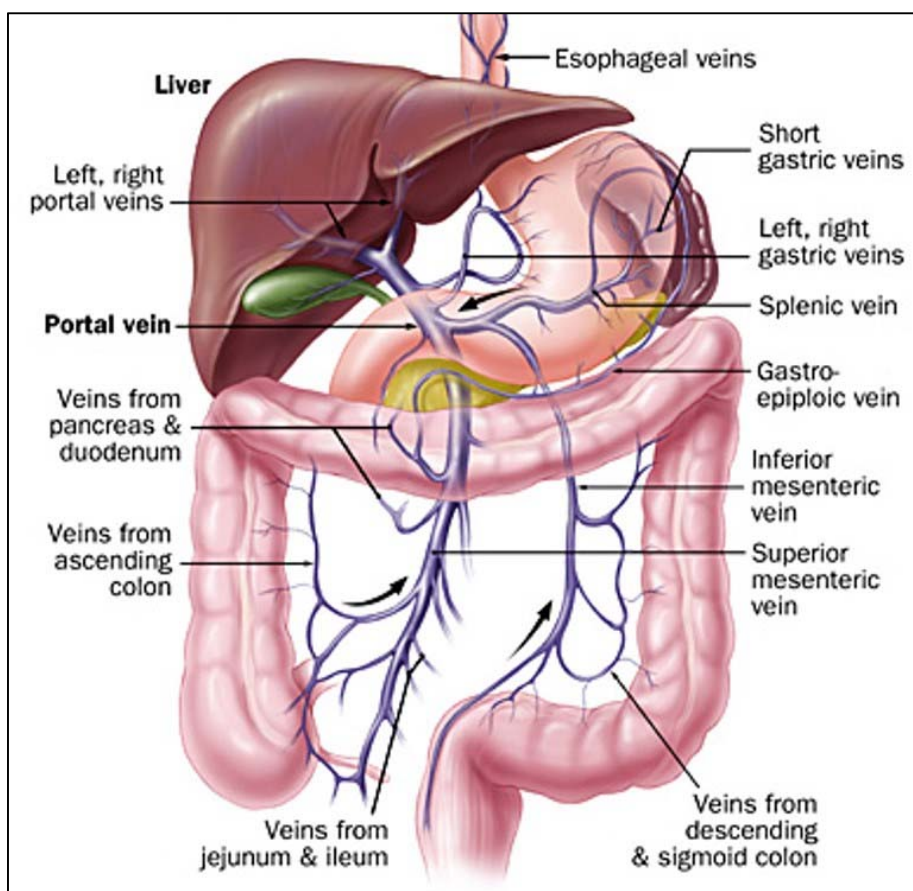


Figure 2.2-7 Shows the major features of the hepatobiliary system and GI tract. Reproduced from [29]

Figure 2.2-8 Physiological Schematic of the Renal System

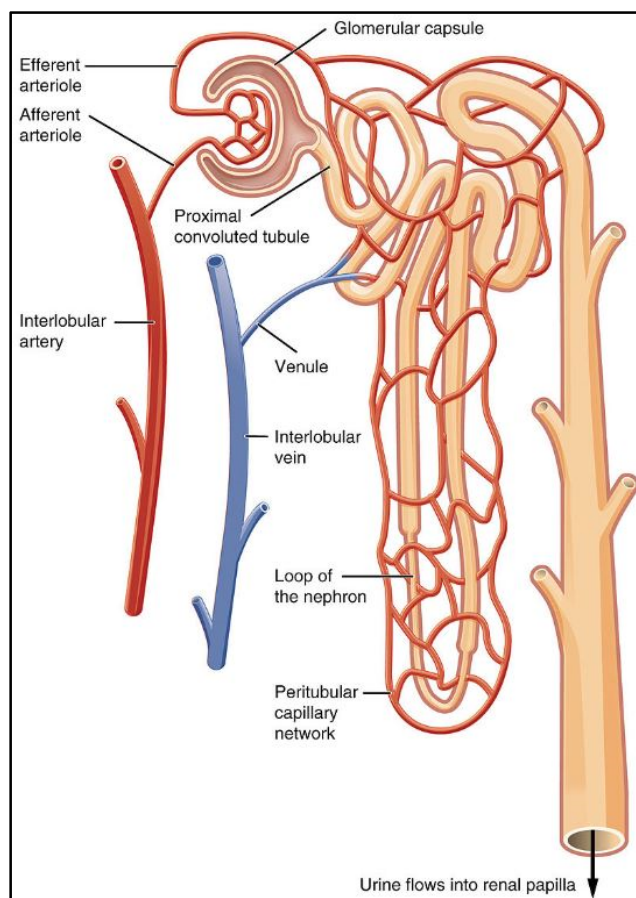


Figure 2.2-8 Shows a nephron which is the microscopic structural and function unit of the kidney (glomerular filtration system - GFR). Reproduced from [30].

Excretion of small molecules can occur via the hepatobiliary system via active uptake, metabolism (Phase I, II or a combination) or biliary transport as shown below in Figure 2.2-9. Understanding the mechanism of biliary elimination is important in drug development but the rate of elimination is difficult to scale from pre-clinical species to human. Currently there are very few options to characterise this process with confidence *in vitro*.

Figure 2.2-9 Hepatobiliary Uptake

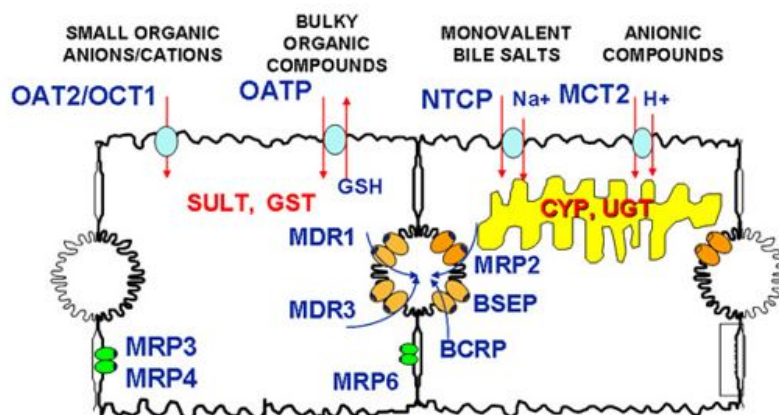


Figure 2.2-9 Shows a schematic of the main transporters present in hepatocytes. BCRP-Breast Cancer Resistance Protein, BSEP-Bile Salt Export Pump, CYP-Cytochrome P450, GSH-Glutathione, GST-Glutathione S-Transferases, MCTR-Monocarboxylic Acid Transporter, MDR-Multi Drug Resistance Protein, MRP-Multidrug Resistance Associated Protein, NTCP-Sodium Dependent Taurocholate Co-transporting Polypeptide, OATP-Organic Anion Transporting Polypeptides, OCT-Organic Cation Transporters, UGT-UDP-Glucuronosyltransferases [31]

Metabolism and excretion are collectively described by the pharmacokinetic term clearance. Clearance reflects the ability of the body or an organ to eliminate a drug molecule from the systemic circulation. Clearance is a rate term with units of L/h and is normally expressed in terms of the blood flow rate of the liver, as this is the major organ responsible for clearance of the majority of small molecules.

At the early stages of drug discovery, it is not economically viable or ethical to generate *in vivo* clearance data for large numbers of compounds, many of which would not represent potential drug candidates. *In vitro* methods are used to help screen out the majority of compounds prior to *in vivo* testing. These *in vitro* systems of clearance include microsomes, S9, cytosol and hepatocytes that can be used to measure a compound's metabolic stability in pre-clinical species of interest and human. The data generated from these systems can then be used to estimate the *in vivo* clearance and help justify the progression of a compound into an animal model.

4.2 Important Physicochemical Properties

It is a common misconception by drug discovery teams that high *in vitro* potency at the biological target or targets of interest will result in low clinical dose therapeutics. As a result of this hypothesis, many pharmaceutical companies have developed industrialised screening cascades to enable high throughput *in vitro* potency screening as an early filter for medicinal chemists to screen large numbers of synthesised NCE's [19]. However, it has become apparent over the past two decades that this approach has introduced a physicochemical bias into many chemical lead series and individual NCE's, which has almost inevitably resulted in many compounds being developed with exquisite *in vitro* potency, as a result high molecular weight and lipophilicity, which then leads to a diametrically opposing relationship between target potency and achieving the desired ADMET properties for a successful NCE [19].

However, when physicochemical properties are taken into consideration early in the drug discovery process, there is a higher probability of producing more drug-like candidate molecules during drug development for clinical use. The impact of key physicochemical properties are considered in the following sections.

4.2.1 Lipophilicity – Octanol/Water Partition (LogP) and Property Forecast Index (PFI)

Lipophilicity has been recognised as one of the most important physicochemical parameters in drug discovery and design for many years [20]. Almost all of the rules that have been proposed and most discovery teams have lipophilicity as a primary parameter, or it is in some way implicit in these drug design rules. The reason lipophilicity is fundamental to drug design is that it contributes to both the PD and ADMET characteristics of a drug, where it influences solubility and permeability through membranes, potency, selectivity (and therefore promiscuity), metabolism, PK and toxicological characteristics [4][15][19–28].

The biological distribution of a compound is most often characterised by a measure of its lipophilicity, usually the logarithm of the octanol/water partition coefficient (LogP) [33]. It describes the compound's affinity for the lipophilic solvent relative to the aqueous buffer and it is equal to the ratio of the equilibrium concentrations in the two immiscible solvents

and has traditionally involved the 'shake-flask' method. The octanol/water partition coefficient (LogP) for the neutral form and distribution coefficient at a particular pH (LogD), which differs from the LogP for ionizable compounds, have been measured for hundreds of thousands of compounds over several decades of pharmaceutical research. Based on compiled data, numerous *in silico* software packages are now commercially available for the *in silico* calculation of LogP values (e.g. cLogP). In order to calculate the distribution coefficient (LogD) at a particular pH of ionizable compounds, the pK_a values need to be determined/calculated. Using the Henderson Hasselbalch equation (shown by Equation 10) the percentage of the ionized form can be calculated and LogD values determined.

Equation 10

$$\text{LogD}_{\text{pH}} = \text{Log}\left(P \cdot 10^{\text{ch}(\text{pK}_a - \text{pH})} + D_{\text{fully ionised form}} \right) - \text{Log}\left(1 + 10^{\text{ch}(\text{pK}_a - \text{pH})} \right)$$

where *ch* is the charge which is -1 for acids and +1 for bases.

The octanol/water lipophilicity has been shown to correlate with pharmacological activity data. According to the Hansch approach [33], the logarithmic value of the octanol/water partition coefficient can describe the movement of a drug to its site of action. As described above, Lipinski's Rule of Five [4] includes the lipophilicity, stating that there should be a LogP less than 5, in order to expect oral absorption. Arguably a LogP of <5 is a very high number and should be considerably lower for high quality drug candidates. With the evolution of combinatorial chemistry and the hunt for more potent compounds the drug discovery library of compounds has become more lipophilic. Lipophilic compounds do not favour an aqueous environment, and bind to any available non-polar biological surfaces, such as proteins causing non-specific and promiscuous binding. For these reasons, experimental measurement and *in silico* calculation of octanol/water lipophilicity are now wide-spread in drug discovery. Several ligand efficiency parameters were also introduced [34] such as BEI (Binding Efficiency Index), LE (Ligand Efficiency Index), LLE (Lipophilic Ligand Efficiency Index), which all relate the potency of a molecule at its target to some sort of lipophilicity parameter. This focus on lipophilicity has resulted in a shift by medicinal chemistry teams to design less lipophilic molecules but which still retain potency for their targets.

Techniques to measure octanol/water partition coefficients have been designed to achieve higher throughput by reducing the volume of the solvents in which the partition takes place in a 96-well plate format. However, this approach increased the ratio between the solvent interface and volume and distorted the results for amphiphilic molecules (having both hydrophilic and hydrophobic parts). A sensitive and robust analytical technique using chromatographic lipophilicity measurements is now commonly employed to determine partition coefficients.

In reversed-phase chromatography, retention is the result of the dynamic equilibrium constant of the compounds between the aqueous mobile and the non-polar C-18 stationary phase. The chromatographic method has numerous advantages over the traditional method for measuring liquid/liquid partition coefficients. A much smaller amount of compound is required for the reversed-phase retention measurements, and small impurities do not alter the results as they are separated from the main components. Furthermore, chromatographic measurements can be easily automated, and retention time measurements are inherently more precise than the concentration determination process for the shake-flask method. As a consequence of automation, higher throughput can be achieved (over 100 compounds per day per instrument can be measured).

The chromatographic partitioning equilibrium of the compound between the mobile phase and the stationary phase occurs on a very large surface, which is similar to a physiological system where the partitioning of compounds is between the circulating blood and tissues. There has been a large numbers of publications since the early 1980's describing the methods and applications of reversed phase chromatographic retention and the correlation with lipophilicity expressed by partition coefficients [34–37]. The main principles of the most often used approaches will be discussed here to give enough background information and context into how these methods are used to generate *in vitro* drug efficiency and other matrix binding measurement in early drug discovery.

Most of these methodologies have been based on isocratic measurements of reversed-phase retention, which is then normalised by the dead time of the system and expressed as a retention factor shown by Equation 11.

Equation 11

$$k = \frac{t_R - t_0}{t_0}$$

where k is the retention factor, t_R is the retention time and t_0 is the dead time [38].

The retention factor (k) is equal to the proportion of the average number of molecules in the stationary and mobile phases and can be directly related to the logarithmic distribution coefficient ($\text{Log}K$) of the compound. The concentration of the compound in the two phases (to get the partition coefficient) is expressed by introducing the volume ratio of the stationary and mobile phases, V_s and V_m [38], respectively, which is a constant in a given chromatographic system (see Equation 12):

Equation 12

$$\text{Log} K = \text{Log} k + \text{Log} \left(\frac{V_s}{V_m} \right)$$

Where $\text{Log}K$ – logarithm distribution coefficient, $\text{Log}k$ – logarithm of the retention factor, V_s and V_m - volume of the stationary and mobile phases

One of the main disadvantages of using isocratic measurements is that compounds with a wide range of lipophilicities would need to be measured using different mobile phase compositions, which is time consuming for large numbers of compounds. In these cases, it would be necessary to change the mobile phase composition and mix the aqueous buffer with various concentrations of miscible organic solvents (usually acetonitrile or methanol). Higher organic phase concentrations in the mobile phase will reduce the retention of more lipophilic compounds. The measured retention factor ($\text{Log}k$) needs to be extrapolated to the same mobile phase composition, usually to pure aqueous mobile phase. To be able to measure the relationship between reversed-phase retention and the concentration of the organic phase, the mobile phase compositions have been analysed and described in detail by Valko *et al* [39]. Equation 13 describes the linear relationship between the retention factor and the organic phase concentration as volume percentage (ϕ) in the mobile phase and may provide a solution for such extrapolation.

Equation 13

$$\text{Log } k = a\varphi + b$$

Log k - retention factor, φ - hydrophobicity index, a & b are the gradient and intercept
There is a linear relationship between Log k and the % organic in the mobile phase (φ), constants for the equation of the line a and b can be determined by carrying out the Log k measurements using 3 to 5 different organic phase concentrations (φ) in the mobile phase. The a constant is the gradient, and the b constant is the extrapolated Log k (intercept) value to a zero-organic phase concentration, i.e. neat water (buffer) often referred to as Log k_0 . The Organisation for Economic Co-operation and Development (OECD) [40] suggested the extrapolated logarithmic retention factor (Log k_0) for the determination of lipophilicity. A set of standard compounds can be used to calibrate the system to the octanol/water scale by plotting the logarithm of the octanol/water partition coefficients (Log P) as a function of Log k_0 values. A straight line should be obtained with slope and intercept values used to convert the Log k_0 values to Log P values.

As discussed above, the isocratic retention measurements have to be carried out using different organic phase concentrations, plotting the obtained Log k values as a function of the organic phase concentration and, by fitting a straight line, extrapolating the Log k values to zero organic phase concentration to get Log k_0 . This is a time-consuming procedure even where the process has been automated.

A study by Valko *et al* [41] has shown that the organic phase concentration (φ_0) which gives the Log k_0 , showed a good correlation with the octanol/water partition coefficients (Log P) for more than 500 diverse compounds [41]. This organic phase concentration that is a characteristic for the compound is called the chromatographic hydrophobicity index (CHI). The φ_0 values are in the measurable range and express the composition of the mobile phase when the compound has an equal distribution between the stationary and the mobile phases. It was later found to have a good linear correlation with the gradient retention times (t_R) for a wide variety of compounds [38][42]. Thus, by a simple calibration, the gradient retention times can be converted to the CHI , which showed a linear correlation to the Log k_0 values. The CHI can be calculated using Equation 14 and is equivalent to the isocratic hydrophobicity index (φ) [38,43].

Equation 14

$$\varphi = CHI = at_R + b$$

φ - hydrophobicity index, CHI - chromatographic hydrophobicity index, t_R - gradient retention time, a & b are the gradient and intercept of the line

The introduction of generic gradient reversed phase methods for the analysis of a wide variety of drug discovery research compounds for quality analysis has had a huge impact on the measurement of gradient retention times for lipophilicity determination. This means that compounds with a wide range of lipophilicities could be analysed by a single fast gradient method without the loss of resolution. To achieve a fast gradient reversed phase analysis, high flow rate, fast gradient and short column length should be used: this enables the achievement of the same separation efficiency as with a slow gradient [44]

To get lipophilicity data that is comparable when obtained in different laboratories that use different instruments or reversed phase columns, it is always advisable to use a calibration set of compounds (see section 6.2.3 Measurements of Chromatographic Lipophilicity), with fixed *CHI* values at three different mobile phase pH's to standardise the gradient retention times [45].

On the *CHI* scale, the lipophilicity ranges from 0 to 100. As the octanol/water partition coefficient (LogP) is widely used and preferred by drug discovery scientists and medicinal chemists, the *CHI* scale of lipophilicity has been converted to a more familiar *CHI*LogD scale using Equation 15, based on the fitted data of 76 known drug molecules with measured *CHI* and LogP values [29]. The LogP can also be estimated by using the *CHI* of the neutral species (*CHIN*). The parameters for expressing *CHI* lipophilicity based on calculated LogP data for more than 20K compounds is shown by Equation 16 and called *Chrom*LogD [30].

Equation 15

$$CHI\text{LogD} = 0.054CHI - 1.467$$

Equation 16

$$\text{ChromLogD} = 0.0857\text{CHI} - 2$$

GSK have over half a million compounds with measured *ChromLogD* values that have provided the input for the in-house *in silico ChromLogD* calculations, which had a very good correlation with the measured values (Figure 4.2-1).

Relatively recently, Young *et al* [8] introduced the Property Forecast Index (PFI) which is the sum of *ChromLogD* and the number of aromatic rings in the molecule (Equation 17).

Equation 17

$$\text{PFI} = \text{ChromlogD} + \text{Number of Aromatic Rings}$$

where PFI is - Property Forecast Index

Aromaticity has been shown to increase crystal lattice energy, to reduce solubility in general and should be avoided or reduced to improve developability of candidate molecules [46]. The PFI concept means that there should be scope to optimise the lipophilicity of the molecule if necessary, as long as we do not increase aromaticity.

Figure 4.2-1 Plot of Measured and Calculated ChromLogD Values for Mixed Project Compounds. Source Data Downloaded from GSK Corporate Database April 2018

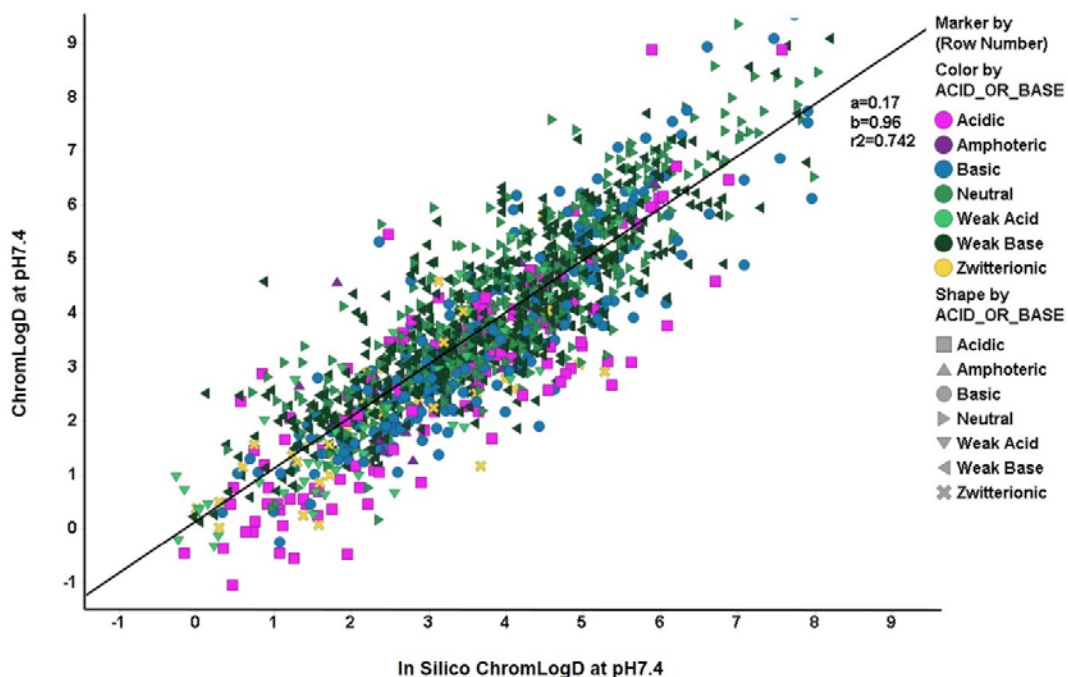


Figure 4.2-1 shows the measured and calculated ChromLogD Values for Mixed Project Compounds of the different molecule classes for a selection of cross project GSK small molecules

Table 4-2 shows how the binned PFI values can be related to other properties of the molecules, such as solubility, albumin binding, p450 inhibition, clearance, hERG inhibition, and promiscuity.

The HPLC platform provides a high throughput for measuring a compound's lipophilicity expressed as *CHI*LogD or ChromLogD. Combining this parameter with the number of aromatic rings in the molecules provides a general property forecast index that can be used as a general guideline for the medicinal chemist. It is suggested that PFI values should be less than 6 for a candidate molecule. It should also be mentioned that very low PFI values (less than 3) are not necessarily advantageous as the permeability of very polar compounds are compromised [8].

Table 4-2 Percentages of Compounds Achieving Defined Target Values in Various Developability Assays Categorised by PFI or iPFI Bins [8].

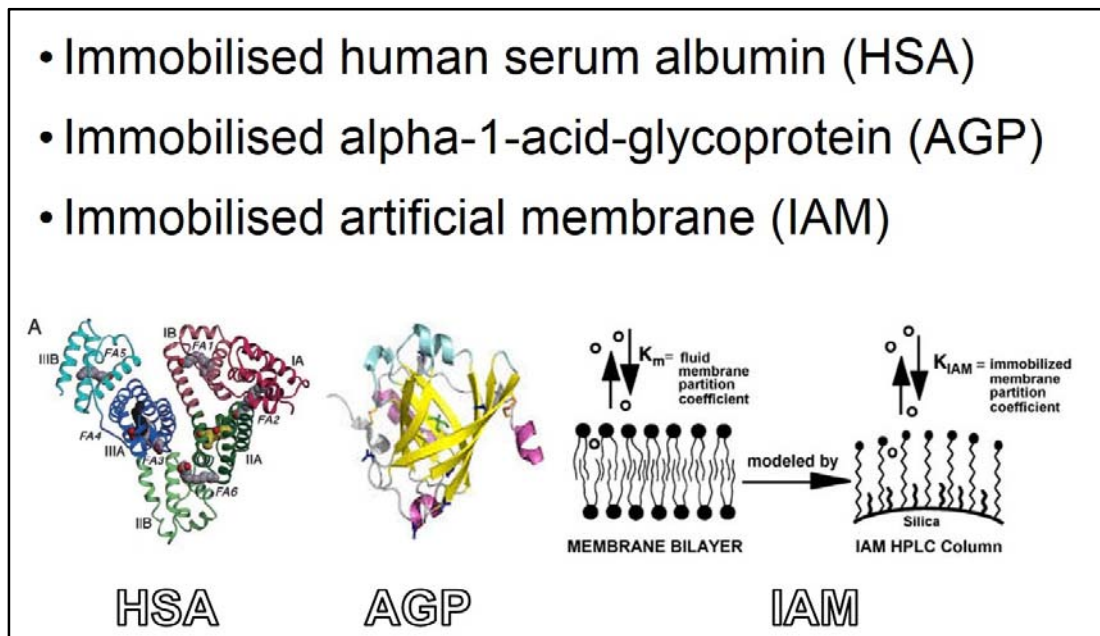
Assay / target value	PFI = mChrom log $D_{pH7.4}$ + #Ar								
	<3	3-4	4-5	5-6	6-7	7-8	8-9	9-10	>10
Solubility >200 μ M	89	83	72	58	33	13	5	3	2
%HSA <95%	88	80	74	64	50	30	17	8	4
2C9 pIC ₅₀ <5	97	90	83	68	48	32	23	22	38
2C19 pIC ₅₀ <5	97	95	91	82	67	52	42	42	56
3A4 pIC ₅₀ <5	92	83	80	75	67	60	58	61	66
Cl _{int} <3 ml/min/kg	79	76	68	61	54	42	41	39	52
Papp >200 nm/s	20	30	46	65	74	77	65	50	33
	iPFI = mChrom log P + #Ar								
hERG pIC ₅₀ <5 (+1 charge)	86	93	88	70	54	36	29	21	11
Promiscuity <5 hits with pIC ₅₀ >5	85	78	74	65	49	30	20	13	7

Neither the octanol/water, nor the C-18 reversed phase chromatographic systems are the same as the biological partition system. We can, however, use chemically bonded proteins and immobilized phosphatidylcholine stationary phases in chromatography to better model biological partitions.

4.2.1 Biomimetic Properties (HSA, AGP and IAM binding)

The development of chemically bonded columns with physiologically relevant proteins the same as the components of *in vivo* proteins has become a useful tool for measuring the physicochemical characteristics of compounds. Figure 4.2-2 shows the common stationary phase proteins which are commercially available for determining protein binding to physiologically relevant proteins.

Figure 4.2-2 Common Stationary Phase Proteins which are Commercially Available



Plasma protein binding has been recognised [32] as an important property of drug molecules that effects distribution and may alter the pharmacodynamic effects of potential drugs under certain conditions. Chromatography can be used to provide higher throughput measurements of protein binding compared to traditional plasma protein binding measurements by equilibrium dialysis [48] or by ultrafiltration methods [49].

The predominant plasma protein of interest is human serum albumin (HSA) which is normally present in the systemic circulation at a concentration of 40 to 75 g/L. Based on the definition of the isocratic retention factor that approximates the proportion of the average number of molecules in the stationary phase and the mobile phase, the percentage binding can be calculated from Equation 18.

Equation 18

$$\%HSA \text{ bound} = 100 \left(\frac{k}{1+k} \right)$$

Where k is the retention factor and HSA is Human Serum Albumin

In this equation, we consider all of the specific and non-specific binding of the compound to the *HSA* stationary phase. Moreover, the binding is considered as a partition equilibrium between the free-flowing aqueous mobile phase and the albumin stationary phase that also contains adsorbed water molecules which do not move with the mobile phase.

The principal characteristic of the partition process is that the partition coefficient is independent of the amount of the partitioning compound, while the stoichiometric binding constant depends on the concentration of the ligand and the protein. When using HPLC protein phases, the protein concentration is much higher than the ligand concentration, as it will occupy only a very small part of the column at any point throughout the gradient time. To express the binding constant from the % *HSA* data, Equation 19 can be used [45]:

Equation 19

$$\text{Log } k(\text{HSA}) = \text{Log} \frac{\% \text{HSA bound}}{100 - \% \text{HSA bound}} - \text{Log}[\text{HSA}]$$

Where *HSA* is Human Serum Albumin and $\text{Log } k(\text{HSA})$ is the binding constant

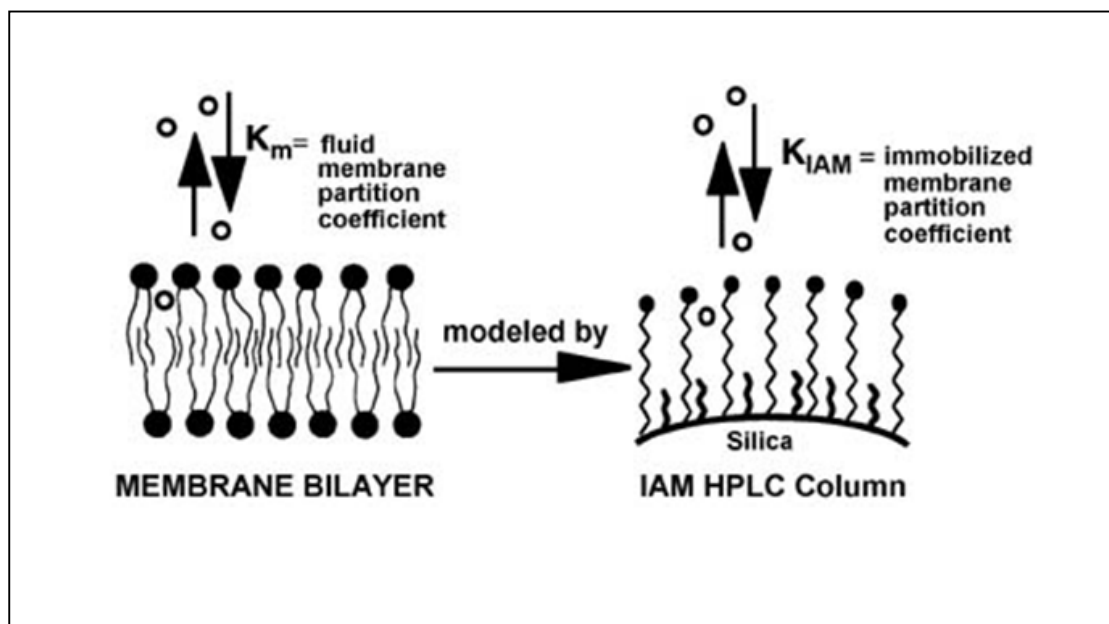
Another important protein type is the glycoprotein family. Alpha-1-acid glycoprotein (*AGP*) can be found in the plasma at 1.5% (0.7 g/L) of the total plasma protein concentration. Although the role of this protein is poorly understood, strong binding of drugs to *AGP* can cause variable efficacy in clinical studies [50][51]. The main reason for this is that the *AGP* concentration can vary in a disease state, and with gender, age, and pregnancy, etc. Inflammation, cancer, cardiovascular disease, infections, and injuries may cause an increase in *AGP* concentration in plasma [50], which may affect a drug's plasma protein binding [52] and distribution. *AGP* contains 46% carbohydrate and sialic acid moiety with a negative charge and therefore can be expected to bind positively charged basic drug molecules, which can be very important for how a compound is distributed and retained by a tissue, e.g. lung. The variability of *AGP* type and level in patients means it is important to know the *AGP* binding of putative drug molecules before candidate selection is made to avoid progressing compounds with strong binding affinities that can lead to later problems in clinical efficacy.

The logarithmic retention times from the *AGP* column can be plotted against the literature Log *k* values that can be obtained from % binding values analogous to Equation 19 with *AGP* replacing the *HSA* term.

These biomimetic HPLC measurements provide information about the compound's interaction with the actual protein. As the chromatographic retention factor depends on the experimental conditions, it is important to calibrate the chromatographic system by measuring the retention data for a set of compounds for which the binding data is also available from other methodologies such as equilibrium dialysis, ultrafiltration or capillary electrophoresis frontal analysis [53]. In this way, the obtained data would be comparable between laboratories and reproducibility improved.

Phospholipids as well as proteins are also important components in the body and in tissues. Drug molecules may partition into phospholipids and as a result, their distribution will be altered. Pidgeon *et al.* [54] designed and patented stationary phases that model the lipid bilayer of the cells by immobilizing phosphatidylcholine on the silica surface. Various commercially available Immobilised Artificial Membrane (*IAM*) phases are manufactured by Regis Technologies Inc (Morton Grove, IL USA). The stationary phase has a phosphatidylcholine head group but only a single chain hydrocarbon connects it to the silica surface. The free silanol groups are treated to avoid secondary interactions with the compounds being analysed. The similarity between the lipid bilayer and the *IAM* stationary phase is shown in Figure 4.2-3. The principle of determining compound partitioning into *IAM* is the same previously described for C18, *HSA* and *AGP* uHPLC reversed phase chromatography.

Figure 4.2-3 The Similarity of the Phosphatidylcholine Membrane Bilayer and the Immobilized Artificial Membrane (IAM) Stationary Phase.



As previously described for *HSA* and *AGP* experiments, the gradient retention times can be converted to *CHI IAM* values using a standard calibration mixture of compounds. For inter-laboratory comparison of the results, it is essential to use the same set of compounds and their *CHI IAM* values that have been established isocratically; this is described in Section 6.2.2 [55].

The correlation between chromatographic partition and a biological partition is not always aligned. However, it has been shown that it is possible to convert one to the other by introducing additional variables to achieve a better correlation [45]. This can be achieved by including the H-bond donor count or H-bond acidity parameter with the *CHI*, which has been measured using an acetonitrile gradient to achieve a better correlation with the octanol/water LogP values [56]. Equation 20 and Equation 21 describe the relationship between the *CHI* values of the neutral form of the compounds, and the LogP values that were measured for a set of 86 diverse drug molecules [45][56].

Equation 20

$$CHI \text{Log} P = 0.047CHI + 0.36HBC - 1.10$$

n=86 $r^2=0.89$ s=0.39 F=336

Equation 21

$$CHI \text{Log} P = 0.054CHI + 1.32A - 1.88$$

n=86 $r^2=0.94$ s=0.29 F=655

where n refers to the number of compounds used to calculate the equation, r^2 is the multiple regression coefficient, s is the root mean square error and F is the Fischer-test value

where n refers to the number of compounds, r^2 is the multiple regression coefficients, s is the root mean square error and F is the Fischer-test value, CHI refers to the CHI obtained by acetonitrile gradient on C-18 reversed phase column, HBC stands for the count of H-bond donor groups on the molecules, while A is the Abraham H-bond acidity parameter. Equation 20 and Equation 21 were reported to give the best correlation between the chromatographic lipophilicity and the octanol/water partition ($\text{Log}P$) for neutral compounds only [45].

The chromatographic lipophilicity can also be measured using the IAM stationary phase in the same way as the C-18, HSA and AGP stationary phases to generate a CHI , which can then be compared to the octanol/water partition ($\text{Log}P$). The CHI IAM values can be converted to the octanol/water scale using Equation 22 and Equation 23 [45][57].

Equation 22

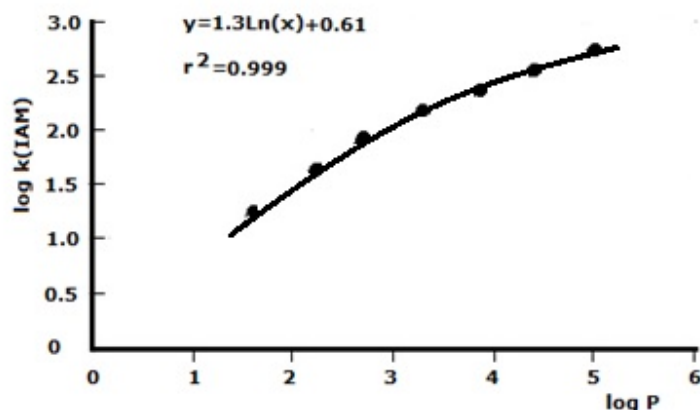
$$\text{Log} k \text{ IAM} = 0.046CHI \text{ IAM} + 0.42$$

Equation 23

$$\text{Log} K \text{ IAM} = 0.29e^{\text{Log} k \text{ IAM}} + 0.7$$

Equation 23 was obtained by plotting the $\text{Log} k$ (IAM) values for the acetophenone homologue series as a function of the octanol/water partition ($\text{Log}P$) [45][57]. Figure 4.2-4 shows the plot used to obtain Equation 23 where $\text{Log} k$ (IAM) is transformed to $\text{Log} K$ (IAM) by an exponential function to produce a linear relationship [57].

Figure 4.2-4 The Logk (*IAM*) Values of the Acetophenone Homologues up to Octanophenone as a Function of their LogP Values [45].



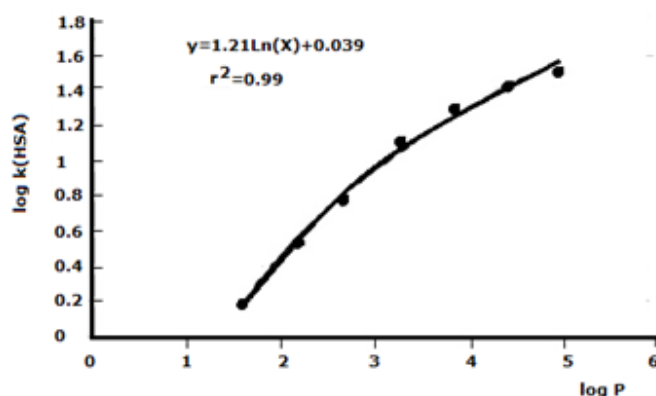
According to Valko [45], the acetophenone homologue series was selected for the scale conversion as these were all neutral molecules with only one H-bond acceptor group and one aromatic ring. A similar curvature as the one seen for Logk *IAM* was reported by Valko [45] and Hollosy [57] when the Logk values obtained from a *HSA* column for the acetophenone series were plotted as a function of octanol/water partition coefficients (see Figure 4.2-5).

Equation 24 shows how Logk (*HSA*) is converted to LogK (*HSA*) using an exponential function to produce a linear relationship [57].

Equation 24

$$\text{Log K (HSA)} = e^{\text{Log k HSA}}$$

Figure 4.2-5 The Plot of the Log_k (HSA) Values for the Acetophenone Homologues as a Function their LogP Values [45].



4.2.2 Biomimetic Properties and Tissue Distribution

Biomimetic binding properties, such as human serum albumin and phospholipid binding have similar selectivity towards the molecular descriptors as the octanol/water partition system. However, there is a significant difference when charged compounds are investigated. Barbato [94] has reviewed published *IAM* partition data and compared it with the octanol/water partition, liposome partition and other biological partition data for neutral and charged compounds. It has been demonstrated that the octanol/water partition fails to model biological partition for positively charged compounds [9][59–61][82]. The octanol/water and other liquid/liquid partition systems are very sensitive to the presence of charge, and charged molecules do not partition into octanol. However, positively charged compounds are attracted to the negatively charged surface of the *IAM* stationary phase, and therefore positively charged basic drugs are retained by the negatively charged phosphate groups.

Ottiger and Wunderli-Allenspach [62] systematically investigated the effect of pH on *IAM* retention and compared it with the liposomal partition. In general, they found good agreement between the two, although there were some exceptions at pH's 5 to 8. Barbato *et al.* [59] reported that protonated β -blockers were retained more strongly than lipophilic neutral compounds. As a general approximation, it can be assumed that the electrostatic interaction between the opposite charges compensates for the effect of reduced

lipophilicity by the charge and the *IAM* retention is proportional to the LogP octanol/water instead of the LogD octanol/water despite the pH being of around 7. Li *et al.* [60][63] amended the solvation equation with an ionization parameter that can be calculated from the pK_a values of basic compounds. This improved the statistical parameters of the solvation equation; moreover, they could model the *IAM* retention data of 55 diverse drug molecules by using the calculated LogP values and the charge descriptors. However, negatively charged compounds have shown less retention on *IAM* stationary phase than one would expect from their LogD at pH 7.4 [64].

It is interesting to note that *HSA* binding is much stronger for negatively charged compounds than would be expected from their LogD values at pH 7.4 as shown in Figure 4.2-6. This is because albumin has positively charged binding sites for fatty acids and it repels positively charged compounds. So, we can conclude that although the octanol/water partition system seems to be a good model for *IAM* and *HSA* binding of compounds, this is true only for neutral compounds that have no charge at physiological pH. When the two types of binding (*IAM* and *HSA*) are plotted is shown in Figure 4.2-6, strong differentiation between the positively and negatively charged drug molecules can be seen.

Figure 4.2-6 shows the plot of the *HSA* and *IAM* binding of ca. 2000 cross project GSK molecules. The colour shows the presence of a positive or negative charge on the molecules at physiological pH. Positively charged compounds bind with higher affinity to phospholipids (*IAM*), while negatively charged compounds bind with higher affinity to albumin. The weak acids, weak bases and neutral compounds tend to have a similar affinity for both *HSA* and *IAM*. This would explain the observed large volume of distribution values often associated with basic drugs compared to the very low values seen with acidic drugs, which tend to bind strongly to plasma proteins. The octanol/water partition system is not sensitive to the charge of a compound unlike the biomimetic partitioning which is arguably more physiologically relevant for assessing the partition of compounds through its greater charge sensitivity. Charged molecules simply do not partition into the octanol and the LogD drops regardless whether it is a positive or a negative charge. The volume of distribution model determined from biomimetic binding data that was published by Hollosy *et al* [65] revealed that the difference between the *IAM* and *HSA* binding correlated very well the human clinical volume of distribution data

of over 150 known drug molecules. It can be seen from Figure 4.2-6 that the same trend is evident with 2000 cross project molecules from the GSK corporate database.

Figure 4.2-6 The Plot of the *HSA* and *IAM* Binding of 2000 Cross Project Compounds. This Data was Downloaded from the GSK Database in March 2018

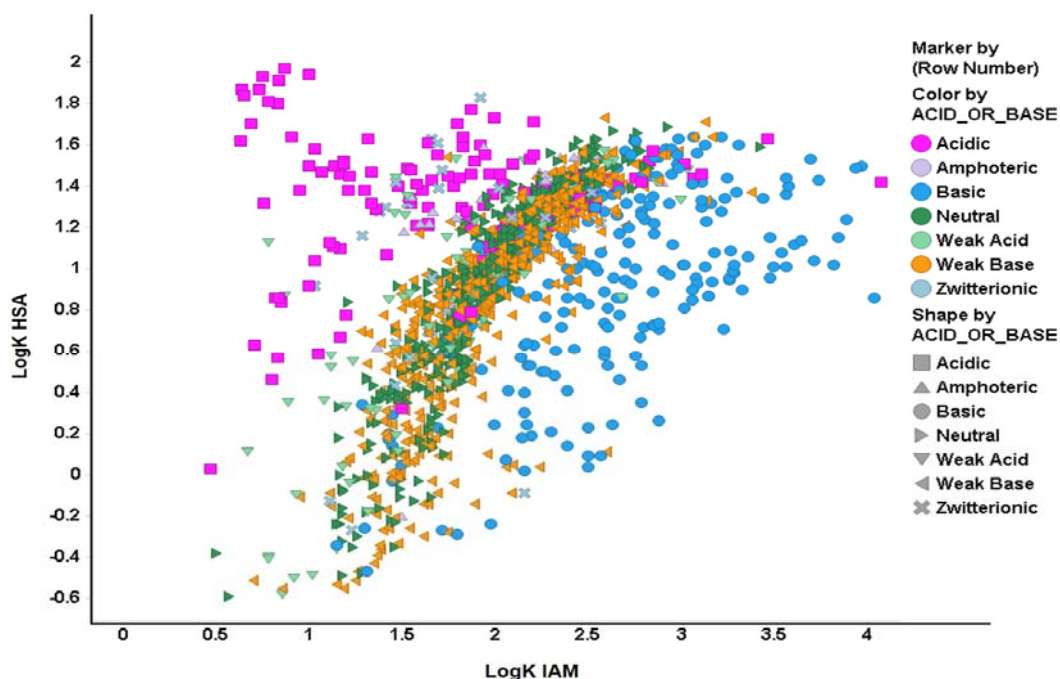


Figure 4.2-6 shows the *HSA* and *IAM* stationary phase biodistribution of different acid/bases classes for a selection of cross project GSK small molecules

The volume of distribution at steady state is one of the most important pharmacokinetic parameters that can be obtained only by *in vivo* experiment after the administration of a known amount of compound (dose) intravenously and then measuring the steady state plasma concentration by repeated dose. The volume of distribution is then calculated as the dose divided by the steady state plasma concentration and it is essentially proportional to the compound distribution between the moving plasma and the stationary tissue compartments. Lombardo *et al.* [66][67], published a model for estimating the volume of distribution of neutral and basic drugs using chromatographically determined ELogD values [67], the plasma protein binding data and the fraction of ionized molecules at pH 7.4 calculated from the pK_a of the compounds at physiological pH's. The model did

not work for acids, as the parameter for the fraction of ionized molecules in the equation referred only to the positively charged compounds. In principle, the measured ELogD was too low for describing the tissue distribution of the acidic compounds. Later, in 2006 Hollosy et al. [57] published an improved volume of distribution model using biomimetic *IAM* and *HSA* binding data using acidic, basic and neutral drug molecules. It was found that the difference between the *IAM* and *HSA* binding resulted in a good model of *in vivo* human volume of distribution for over 150 known drugs, which is shown by Equation 25.

Equation 25

$$\text{Log } V_{dss} (\text{HUMAN}) = 0.44 \text{ Log K (IAM)} - 0.22 \text{ Log K (HSA)} - 0.66$$

$$n=179, r^2=0.76, s=0.33, F=272$$

where n refers to the number of compounds used to calculate the equation, r^2 is the multiple regression coefficient, s is the root mean square error and F is the Fischer-test value

where n refers to the number of compounds used to calculate the equation, r^2 is the multiple regression coefficient, s is the root mean square error and F is the Fischer-test value. $\text{Log } V_{dss}$ is the logarithm of the steady state volume of distribution obtained from human clinical studies after intravenous administration; LogK (IAM) is the measured *IAM* binding using the gradient method and the *CHI (IAM)* values scaled to the octanol/water LogP scale as described earlier by Equation 22 and Equation 23, while the LogK (HSA) is also the measured albumin binding on immobilised *HSA* stationary phase and scaled to the octanol/water scale by using Equation 24. The coefficients of the two biomimetic parameters were obtained by using regression analysis of 176 known drug data. As both variables are scaled to the same octanol/water LogP scale, the regression coefficients were comparable and more meaningful [57].

The mechanistic model shows that compound partitioning into tissues from the plasma compartment depends on the difference between the two types of binding (*IAM* and *HSA*). The *IAM* binding represents the tissue affinity, while the *HSA* binding represents the plasma protein binding of the compounds. It can be seen in Figure 4.2-6 that the major difference between the two types of binding is due to their different sensitivities to charge. Positively charged molecules tend to partition into the tissues, whereas the negatively charged molecules stay in the plasma compartment. It is more difficult to estimate the binding differences of neutral compounds. *IAM* and *HSA* binding is

dependent on the shape of the molecules. Interestingly a similar model that was generated for rat volume of distribution [57] had slightly different regression coefficients as shown in Equation 26.

Equation 26

$$\text{Log } V_{dss} (\text{RAT}) = 0.27 \cdot \text{Log } K (\text{IAM}) - 0.29 \text{ Log } K (\text{HSA}) - 0.30$$

n=247 r²=0.66 s=0.35 F=234

where n refers to the number of compounds used to calculate the equation, r^2 is the multiple regression coefficient, s is the root mean square error and F is the Fischer-test value

It seems that the rat has less fatty tissue than human, therefore containing less phospholipid relative to the plasma, resulting in a smaller regression coefficient of LogK (*IAM*). This is because most rat PK studies are run in young lean animals, which is much different to a diverse clinical population. Obviously, these models are very crude as they include only the two major binding types in the body. Some drug molecules may bind strongly to other proteins or lipids that are present in smaller quantities. Also, the model is not dynamic and therefore excludes the effect of active transport, which can be an important factor in distribution [68]. The root means square error of the above mechanistic models is 0.35, which may represent the variation that is due to active the transport of some compounds along with non-specific binding to other components in the body. In addition, when a compound is very lipophilic it prefers to bind to hydrophobic components and this may also influence how a compound is distributed.

The unbound volume of distribution (V_{du}) is becoming a more widely used term. A simple definition is the dose divided by the free plasma/blood concentration. The V_{du} will always be high when the free fraction of a compound is low. Based on the free drug hypothesis [69][70], the free concentration of the compounds should be the same in all compartments in the body, assuming there is no active transport. Therefore, the unbound volume of distribution can be used to estimate the unbound concentration of the compounds in the tissue [71]. The biomimetic model for unbound volume of distribution [72] showed that the sum of the *IAM* and *HSA* binding data correlated to the measured V_{du} for a diverse set of 70 drugs [72]; this model is shown below by Equation 27.

Equation 27

$$\text{Log Vdu} = 0.43 \text{Log K (IAM)} + 0.23 \text{Log K (HSA)} - 0.72$$

n=70 $r^2=0.84$ s=0.32 F=129

where n refers to the number of compounds used to calculate the equation, r^2 is the multiple regression coefficient, s is the root mean square error and F is the Fischer-test value.

The unbound fraction in tissues inversely correlates with the sum of the two types of binding as described by Equation 28 [72]:

Equation 28

$$\text{Log } f_{\text{ut}} = -0.52 \text{Log K(IAM)} - 0.66 \text{Log K (HSA)} + 0.55$$

n=70 $r^2=0.85$ s=0.58 F=182

where n refers to the number of compounds used to calculate the equation, r^2 is the multiple regression coefficient, s is the root mean square error and F is the Fischer-test value.

These models are simple mechanistic models that take into account the major binding components in the body, namely the phospholipid and albumin protein binding and therefore intuitively should be a solid foundation for a model of distribution. A big advantage of the biomimetic approach over traditional octanol/water partition is the system is able to show the effect of charge, which gives a more physiological representation of lipophilicity.

4.2.3 Estimating the absorption potential from solubility and artificial membrane permeability

To estimate the dose of orally administered compounds it is important to assess the absorption rate. The relationship between *in vivo* absorption and physicochemical properties of drugs is dependent on a wide range of factors, which include drug related properties and the physiological conditions of the system. The physicochemical properties of the drug which affect absorption include solubility, dissolution rate of the solid drug substance, particle size, crystal form of the solid drug substance and ionization properties. The physiological variables which will affect absorption include the volume of

the fluid in the GI tract or specifically stomach, composition of the intestinal fluids (fed or fasted state) and pH, gut motility, the permeability and surface area of the intestinal wall, and blood flow. It is very difficult to include all of these parameters into a single model to estimate absorption of NCE's. Dressman *et al.* [73] have tried to include as many variables as possible into one single dimensionless number which they have classified as the absorption potential (AP). Excluding the effect of the first-pass metabolism and metabolism in the gut, the fraction of a dose absorbed (F_{abs}) is a function of the permeability of the gut wall (P_w), the aqueous permeability of the drug (P_{aq}), the intrinsic aqueous solubility of the neutral form of the drug (S_0), the dose (X), the unionized fraction of the drug at pH 6.5 (F_{non}) and the volume of the luminal content (V_L). This is shown in Equation 29 [73].

Equation 29

$$F_{abs} = f(P_w, P_{aq}, S_0, X, F_{non}, V_L)$$

Where F_{abs} is the fraction absorbed, P_w permeability of the gut wall, P_{aq} is the aqueous permeability, F_{non} is the unionized fraction, S_0 is the intrinsic aqueous solubility, V_L is the volume of the luminal content and X is the dose

By further simplifying the conditions of absorption, such as only considering the neutral form of the drug will be permeable, and the average pH of the small intestinal lumen (inc. duodenum, jejunum, and ileum where most of the absorption takes place) is pH 6.5, the primary parameters of interest can be arranged into a dimensionless number, called absorption potential (AP) as described by Equation 30 [73].

Equation 30

$$AP = \text{Log} \left(P * F_{non} * \frac{S_0 * V_L}{X} \right)$$

Where AP is the absorption potential, P is the aqueous permeability, F_{non} is the unionized fraction, S_0 is the intrinsic aqueous solubility, V_L is the volume of the luminal content and X is the dose

The authors have shown data for a few known drugs, where the AP followed a sigmoid relationship with the fraction absorbed. In principle, the absorption potential is proportional to the product terms of intrinsic solubility, permeability and the fraction of the

non-ionized form of the molecule at pH 6.5 [73]. It means that if any of the product terms are close to zero, (i.e. either the solubility or the permeability is poor) the absorption will be poor. The V_L parameter can be considered constant using the average volume of the intestinal fluid in the lumen. For a given series of drug discovery compounds, a given dose (X) can also be considered constant. Therefore, the product terms of solubility, permeability and the fraction of non-ionized form can be used for assessing and ranking drug discovery compounds with regards to their absorption potential. Measured data exists for solubility and permeability both at pH 7.4. Ni *et al.* [74] have demonstrated that when the solubility and the partition coefficient were measured at the same pH, the product term remains constant. The explanation for this is that ionization affects solubility in an opposite way to lipophilicity. Ionization decreases lipophilicity while it increases solubility as shown in Figure 4.2-7, which is an example of a basic drug [74].

Measured solubility (μM) and permeability (nm/sec) data generated for project compounds GSK can be multiplied with the logarithm of the product term used calculate a version of the absorption potential. Based on the obtained data, the compounds were put into a low absorption category if the calculated absorption potential ($\text{Log}(\text{DMSO solubility } [\mu\text{M}] \times \text{AMP permeability } [\text{nm}/\text{s}])$) was below 4, because if one of the parameters (solubility or permeability) is low, the absorption should be low and the absorption potential cannot be higher than 4. High absorption compounds should have both high permeability and high solubility. Solubility is considered high when the DMSO precipitative solubility in phosphate buffer saline at pH 7.4 is higher than $200 \mu\text{M}$. High permeability is considered when the compound's AMP permeability is greater than $200 \text{ nm}/\text{s}$. The absorption potential would be high for such compounds $\text{Log}(200 \times 200)$, i.e. 4.78. So, compounds with an absorption potential greater than 5 were considered to be high.

Figure 4.2-7 A Theoretical Plot Showing the Independence of the Product Term of Lipophilicity and Solubility (LogD^*S) from pH. Adapted from Reference [74].

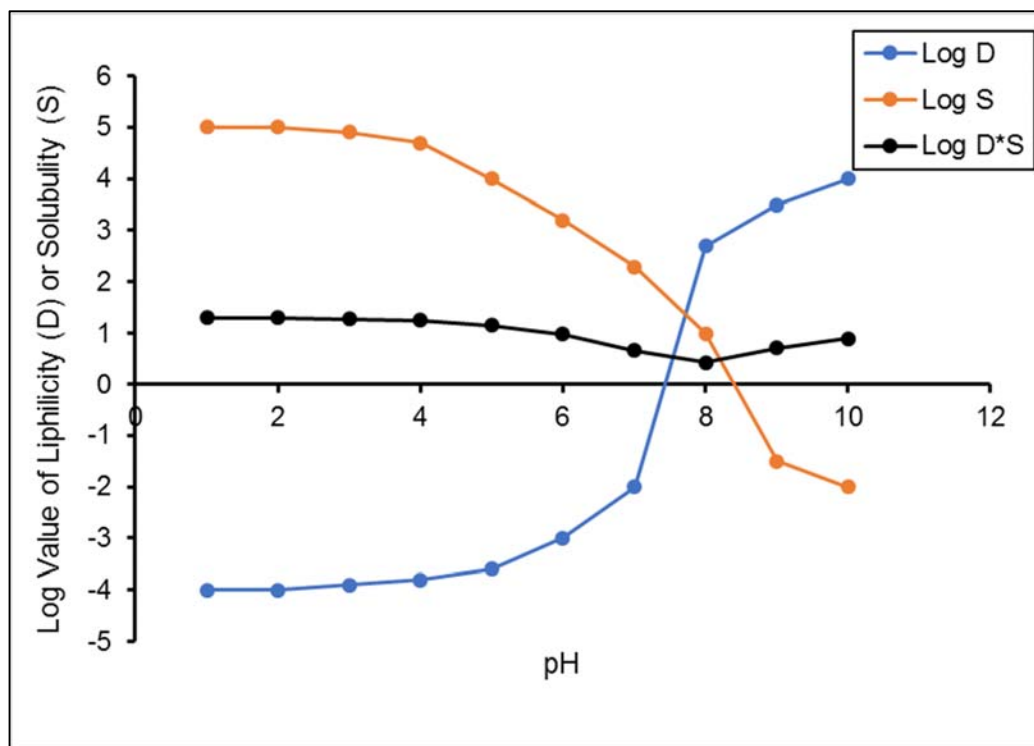


Figure 4.2-7 Shows a plot for a theoretical base of Lipophilicity – LogD ; Aq Solubility – LogS ; Product term Lipophilicity x Solubility – Log (D.S) with respect to pH. [74].

Table 4-3 Example Solubility and Lipophilicity for a Theoretical Base Showing the Independence of the Product Term from pH. See Data Plot in Figure 4.2-7

Solubility (mg/mL)		Lipohilicity (o/w)		Product Term	
S	Log S	D	Log D	Log D*S	pH
100000	5	0.0001	-4	1.30	1
100000	5	0.0001	-4	1.30	2
79432.82347	4.9	0.0001	-3.9	1.28	3
50118.72336	4.7	0.0002	-3.8	1.25	4
10000.00000	4	0.0003	-3.6	1.16	5
1584.89319	3.2	0.0010	-3	0.98	6
199.52623	2.3	0.0100	-2	0.66	7
10.00000	1.00	501.1872	2.7	0.43	8
0.03162	-1.5	3162.2777	3.5	0.72	9
0.01000	-2	10000.0000	4	0.90	10

4.2.4 What is Drug Efficiency?

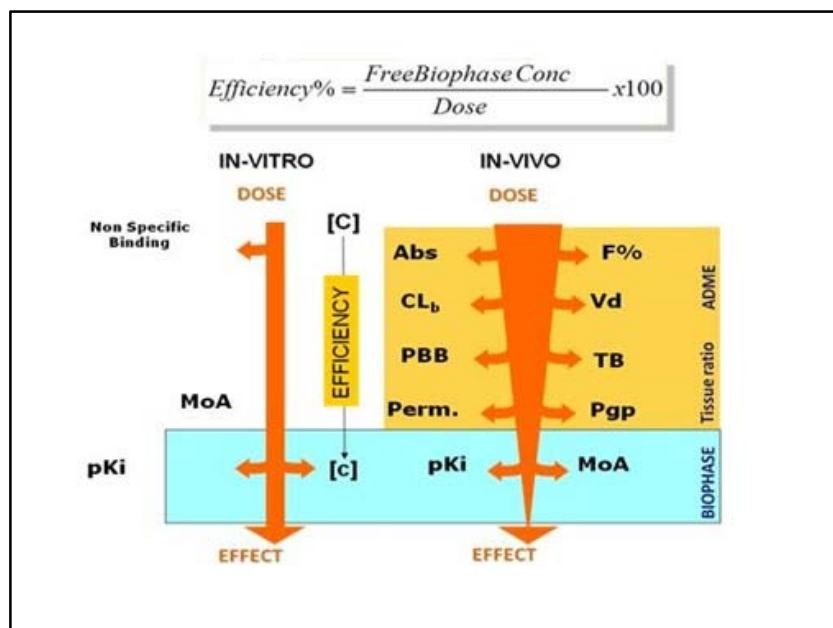
In 2010 Braggio *et al* [27] introduced the concept of drug efficiency ($DRUG_{eff}$) as an efficient tool for optimising the structure of a lead molecule into a successful drug. Instead of focussing on individual ADME properties, drug efficiency combines them into a single parameter. The authors defined drug efficiency as the percentage of the dose that is available in the bio-phase concentration *in vivo* to exert the pharmacological activity, as shown in Equation 31.

Equation 31

$$\% DRUG_{eff} = \frac{\text{Free Bio – phase Concentration}}{\text{Dose}} \cdot 100$$

An illustration of what drug efficiency is and means from an *in vitro* and *in vivo* perspective is shown in Figure 4.2-8.

Figure 4.2-8 The DRUG_{eff} Definition – Dose and Effect (PKPD)



Abs= absorption, CL_b= clearance, V_d= volume of distribution, TB= tissue binding, P-gp = P-glycoprotein efflux, Perm.= permeability, MoA= mode of action, pK_i is the negative logarithm of the dissociation constant of the drug and receptor.

For antibacterial targets, GPCR receptors and ion channel blockers, it is generally accepted that following oral administration it is the free concentration of the compound in the blood, that is proportional to the actual clinical efficacy [75][76]. Therefore, in these cases, drug efficiency is essentially the reciprocal value of the unbound volume of distribution (V_{du}), which is proportional to the dose divided by the free blood/plasma concentration, see Equation 32 and Equation 33.

Equation 32

$$V_{du} = \frac{Dose}{Unbound\ Concentration}$$

Where V_{du} is the unbound volume of distribution

Equation 33

$$\% \text{ DRUG}_{\text{eff}} = \frac{100}{V_{du}}$$

Valko *et al.* have used the unbound volume of distribution model [72] they developed from *HSA* and *IAM* biomimetic binding data, to estimate the clinical drug efficiency of 115 known drug molecules [77]. The *in vitro* Drug_{eff max} model is shown by Equation 34, which is the biomimetic description of Equation 33

Equation 34

$$\text{Log (in vitro DRUG}_{\text{eff max}}) = 2 - (0.23\text{LogK(HSA)} + 0.43 \text{Log K (IAM)} - 0.72)$$

The Drug_{eff max} is defined as the maximum drug efficiency that can be achieved assuming 100% absorption (bioavailability) when there is no permeability barrier for the compound. There are some broad assumptions and limitations to drug efficiency because of the static nature of the model which will be discussed later. A plot of the measured *in vitro* DRUG_{eff max} and the *in vivo* DRUG_{eff max} of 115 drugs obtained from the clinical PK studies can be seen in Figure 4.2-9.

Figure 4.2-9 The Plot of *In Vivo* and *In Vitro* Log DRUG_{eff max} for 115 Known Drug Molecules. Shape and Colour are According to the Target Class the Drugs Belong [77]

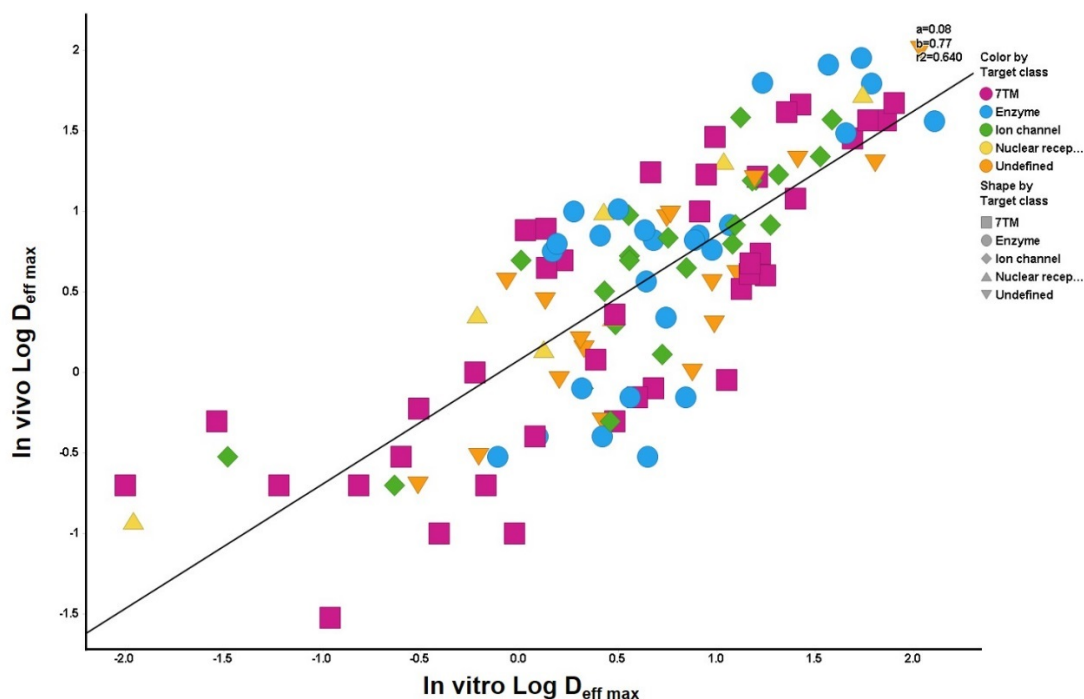


Figure 4.2-9 Shows a plot of *in vivo* DRUG_{eff max} versus *in vitro* DRUG_{eff max}. Colours represent different target classes Pink – 7TM (7-Trans Membrane), Blue – Enzyme, Green – Ion channel, Yellow – Nuclear receptors, Orange – Not classified, Grey – Unknown.

Although the correlation coefficient is much lower ($r^2 = 0.64$) than was obtained for the 70 drug molecules measured using the unbound volume of distribution model ($r^2=0.84$) as described by Equation 27, this should still be considered as a reasonably good correlation between the *in vitro* and *in vivo* human DRUG_{eff max} when the fact that this is a diverse set of drugs from multiple therapeutic areas is taken into consideration. A correlation coefficient of greater than ≥ 0.6 would typically be considered as a reasonable correlation when building QSAR models.

DRUG_{eff max} should not be considered as a prediction tool, but rather a ranking tool for the early drug discovery stage of compound progression. The *in vivo* property can be estimated by using the biomimetic binding data from only two major components of the

body, albumin type proteins, and phosphatidylcholine phospholipid. From this simple *in vitro* model the correlation to the complex *in vivo* system is remarkably good, underlying the fact that these are the two major non-specific binding sites in the body and are important factors in the distribution of a drug to its target enzyme or receptor. The *in vitro* drug efficiency concept incorporates several drug-like properties (physical properties) and the pharmacodynamic profile of the compound (target concentration).

Optimising compounds using drug efficiency intrinsically includes a number of physicochemical properties that improve the chance of finding a successful molecule that can be turned into a drug. The drug efficiency can be estimated *in vitro* in the early stages of lead identification or lead optimisation, and when compounds are selected for further progression to *in vivo* studies, the *in vivo* DRUG_{eff max} can be confirmed, although *in vivo* DRUG_{eff} will always be lower than the *in vitro* derived value, which is due to minimal non-specific binding in an *in vitro* system as described by Figure 4.2-8. When significant deviation in the general trend is observed between the *in vitro* and *in vivo* data, it could indicate a possible active transporter effect, poor absorption or the existence of a permeability barrier between the body compartments. As the drug efficiency is inversely proportional to the sum of the albumin and phospholipid binding, this in principle should show a good correlation with LogP and would support the use of LogP for characterising the proportion of the dose that has the potential to reach the target. In this respect, LogP is more important than LogD as it describes the intrinsic lipophilicity of a drug molecule and is not affected by ionisation.

An evolution of the DRUG_{eff max} concept which was subsequently introduced was the drug efficiency index (DEI) [78]. DEI was defined as the sum of potency (expressed as K_d or IC_{50}) and the logarithm of drug efficiency (Equation 35). DEI combines two important properties of putative drug molecules, namely the *in vitro* potency and the drug efficiency. It has also been shown [77] that the *in vitro* DEI_{max} had an excellent inverse correlation with the ligand lipophilicity efficiency (LLE) proposed by Leeson *et al.* [9] (Figure 4.2-11). The agreement is superficially good as both parameters contain the pXC_{50} values, and it has been shown that cLogP and the *in vitro* DRUG_{eff max} have a good inverse correlation [77].

Equation 35

$$DEI = pIC_{50} + \text{Log}(\%DE_{\text{max}})$$

DEI is the drug efficiency index

Equation 36

$$LLE = pIC_{50} - \text{LogP}$$

LLE is the ligand lipophilicity efficiency

Figure 4.2-10 Agreement Between *In Vitro* DEI_{max} (pXC50+Log DRUG_{eff} max) and LLE (pXC50 – cLogP) [77]

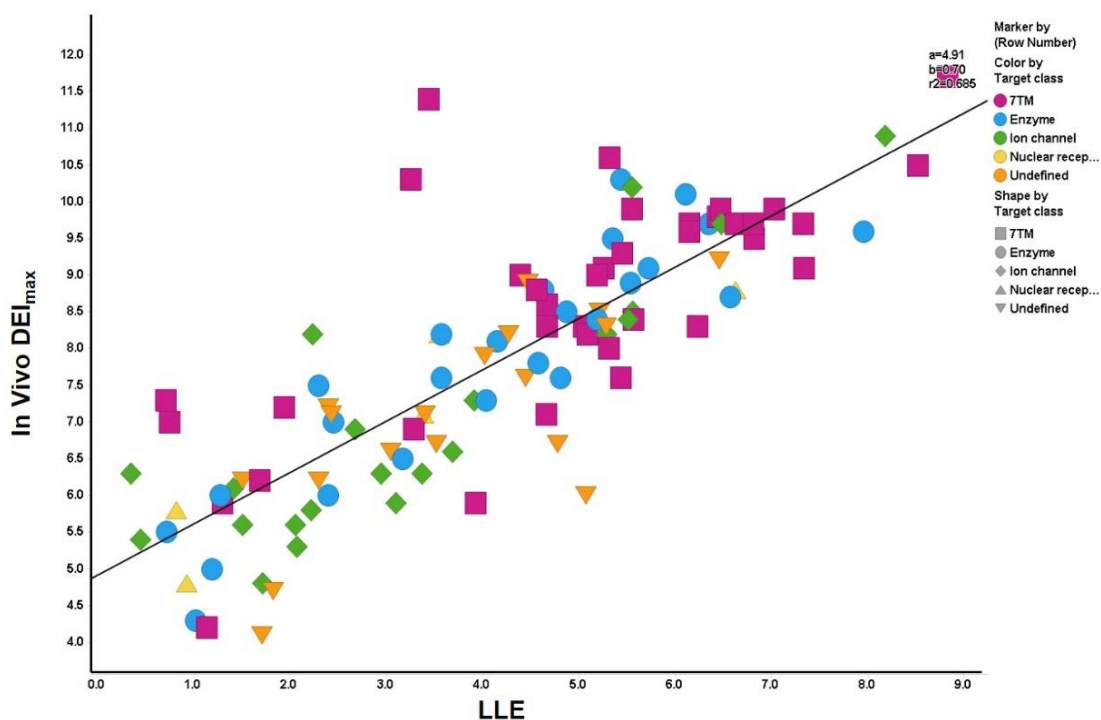


Figure 4.2-10 Shows a plot of in vivo DEI_{max} verses LLE. Colours represent different target classes Pink – 7TM (7-Trans Membrane), Blue – Enzyme, Green – Ion channel, Yellow – Nuclear receptors, Orange – Not classified, Grey – Unknown.

The drug efficiency ($DRUG_{eff}$) concept introduced by Braggio *et al.* [27], was proposed as a new tool to guide drug discovery program teams, as it relates the free drug concentration in the target bio-phase relative to the administered dose (Figure 4.2-9 and Equation 31).

The efficacious concentration of a compound that is high enough to sufficiently engage a biological target and produce a certain response can be estimated from *in vitro* potency measurements. Under *in vitro* assay conditions, $DRUG_{eff}$ is typically >99%, with any non-specific binding having only a marginal impact on the free concentration. However, at this stage, it is very difficult to estimate the dose that will be required to produce an equivalent efficacious free bio-phase concentration *in vivo* when minimal measured data, particularly pharmacokinetic data, is available.

The drug efficiency equation previously quoted (Equation 31) includes the dose as one of the parameters, so by re-arranging the equation we can express the dose as the ratio of the unbound bio-phase concentration and the $DRUG_{eff}$ (Equation 37).

Equation 37

$$\text{Dose} = \frac{\text{Free bio-phase concentration}}{DRUG_{eff}}$$

The required free (or unbound) bio-phase concentration of drug is the concentration which would be sufficient to engage the target and produce the desired pharmacological effects. The unbound bio-phase concentration would normally refer to a steady state concentration. This might appear to limit the utility of the drug efficiency approach since $DRUG_{eff}$ assumes steady state conditions as there is not drug elimination accounted for in the equation.

4.3 Approaches for Early Dose Estimation

For a high-quality drug candidate, we are aiming for low dose (below 100 mg) in order to reduce the probability of failure during drug development [26]. Therefore, it is essential to estimate the efficacious dose as early as possible. If we know the required dose, we can set up other physicochemical requirements, such as the solubility required for final formulation.

The essence of the dose estimation procedures is to estimate the minimum effective concentration of the compound at the site of action using the *in vitro* potency data. The available free concentration of the drug can be estimated using the drug efficiency concept or using bioavailability, volume of distribution and clearance data. Thus, the dose includes all important properties such as potency, physicochemical properties, bioavailability, clearance, etc. in one parameter.

An early prediction of clinical dose at the hit to lead phase or lead optimisation enables program teams to rank compounds within a chemical template or across chemical templates at early discovery phases. An improved understanding of the physicochemical characteristics and their relationship to ADME properties can then be translated to target engagement and the PKPD relationship, thus helping to identify and progress higher quality molecules to fully explore the clinical concentration response curve for a given biological target. The importance of having the potential to explore the complete dynamic range of the concentrations curve enables a full evaluation of a drug's clinical relevance in the disease(s) of interest.

At high doses, drugs are more likely to show toxicity [15][79][80], which generally speaking is due to the high exposure burden. Targeting a low dose and exposure is important to avoid adverse effects. The study of Wager *et al.* [81] showed that the occurrence of *in vivo* toxicity correlated with the exposure. They found that if the total human efficacious plasma concentration was less than 250 nM and the free drug concentration was less than 40 nM, the failure rate of exploratory compounds due to animal toxicity was reduced significantly.

The clinical dose depends on the absorption rate, elimination rate and volume of distribution as has been described by McGinnity *et al.* [24], and shown by Equation 38.

Equation 38

$$\text{Dose} \left(\frac{\text{mg}}{\text{kg}} \right) = \frac{\frac{24}{\tau} \text{MEC} \cdot V_{dss} \cdot (k_a - k_{el})}{F \cdot k_a \left(\frac{1}{1 - \exp(-k_{el} \cdot \tau)} - \frac{1}{1 - \exp(-k_a \cdot \tau)} \right)}$$

Where τ is the dosing interval, MEC is the minimum effective concentration (which can be estimated from e.g. $\text{pIC}_{50/90}$ or K_i), V_{dss} is the volume of distribution at steady state, k_a is the first order absorption rate constant, k_{el} is the elimination rate constant, and F is the bioavailability expressed as the fraction of orally administered drug dose-normalised area under the curve relative to that following IV administration. Multiplying the result by 70 expresses the actual daily human dose in mg/day for an average 70 kg human.

A simplified version of Equation 38 can be used where the absorption rates are removed and is shown in Equation 39, which can be used as an alternative when predicting doses for intravenous administration where absorption rates (k_a) are not relevant.

Equation 39

$$\text{Dose} \left(\frac{\text{mg}}{\text{kg}} \right) = \frac{\frac{24}{\tau} \text{MEC} \cdot V_{dss} \cdot (\exp(k_{el} \cdot \tau) - 1)}{F}$$

where τ is the dosing interval, MEC is the minimum effective concentration, V_{dss} is the volume of distribution at steady state, k_{el} is the elimination rate constant, and F is the bioavailability expressed as the fraction. Multiplying the result by 70 expresses the actual daily human dose in mg/day for an average 70 kg human

The equations are based on a simple empirical one-compartment pharmacokinetic model including a first order absorption rate constant. McGinnity *et al.* [24] have shown that the equation could be used to successfully predict the clinical dose of 28 known drugs when they used an MEC value obtained from clinical data, following administration of the efficacious dose as described on the product label. They also highlighted the difficulties of predicting the human steady-state volume of distribution (V_{dss}) without *in vivo* experiments, and the elimination rate (k_{el}) using *in vitro* intrinsic clearance.

Decisions based on predictions of human PK and clinical dose have a significant impact on drug candidate selection, as well as on the number of animal studies that are likely to be required to support it. Other methods for PK predictions using allometric scaling

[82][83][84] or physiologically based pharmacokinetic (PBPK) modelling [85][86] also require measured or *in silico* calculated parameters as inputs.

In summary, there is no single method which gives a definitive prediction of the human PK parameters listed above, and ultimately the effective clinical dose. However, by using a combination of these established methods it is possible to predict a realistic range within which these parameters are most likely to fall. This can help with the decision-making process of selecting compounds that are most likely to meet the anticipated requirements for progress to clinical development [9]. At very early stages, prior to synthesis, only *in silico* estimates of the volume of distribution, clearance, and $DRUG_{eff\ max}$ are possible, while as the lead optimisation process develops, *in vitro* and then *in vivo* measurements can be made on a small selection of compounds.

In this project, I have evaluated the utility of the $DRUG_{eff\ max}$ concept as an alternative method to predict clinical dose in early drug discovery. This was initially done using a set of known marketed drug molecules. Using the data of the marketed set of compounds, the estimated dose has been compared when using various methods and compared to the actual clinical dose. Since HPLC DE_{max} values can be generated early in a compound screening cascade using HPLC-based measurements before any more in-depth *in vitro* / *in vivo* drug metabolism and pharmacokinetic screening is carried out, the two different approaches to dose prediction are represented in Figure 4.3-1 as DMPK-DP using the one compartment approach described by McGinnity [24], or the DE-DP which utilises the $DRUG_{eff\ max}$ concept and is the focus of this project. The potential utility of this parameter has been investigated as an early indication of compound quality using real project compounds from three drug discovery programs which will be described in Section 5: Objectives.

Figure 4.3-1 DMPK Dose Prediction (DMPK-DP) and DE_{max} Dose Prediction (DE-DP) Schematic

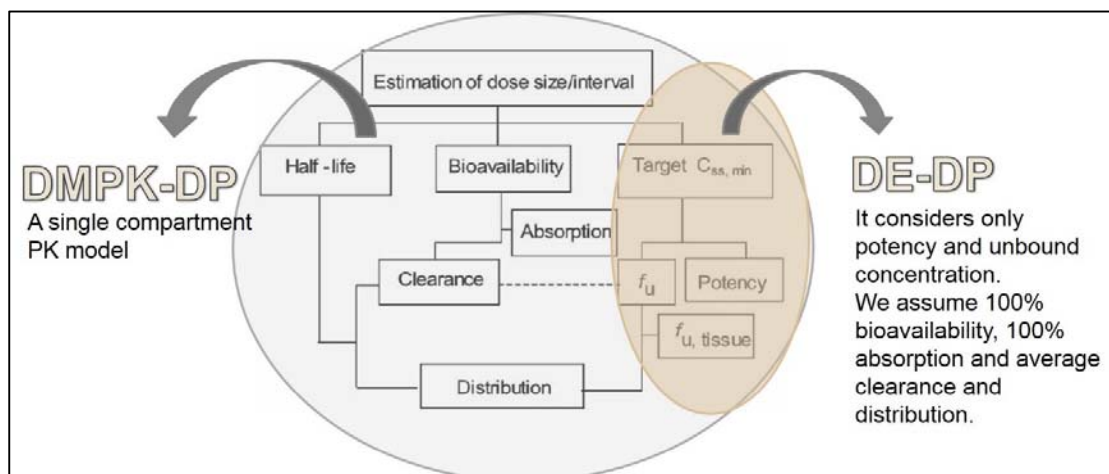


Figure 4.3-1 shows the pharmacokinetic parameters required for predicting clinical dose using a single compartment method (DMPK-DP) and the DE_{max} method (DE-DP). Adapted from McGinnity et al. [24]

5 Project Context, Design and Objectives

The Respiratory Therapeutic Area represents an important area of pharmaceutical research within GSK's R&D organisation due to the success of several blockbuster asthma and COPD treatments over the past 50 years. These include Ventolin, a fast acting β agonist (salbutamol) delivered using as a metered dose inhaler (MDI), Seretide a steroid (fluticasone propionate, FP) and long acting β agonist (salmeterol) combination, delivered as an inhaled dry powder via the Diskus® Device, and more recently a portfolio of 2nd generation of inhaled steroid, long acting β agonist (fluticasone furoate, FF and vilanterol) and muscarinic antagonist (umeclidinium) medicines, all delivered as dry powders using the latest Ellipta® Device. These medicines can be delivered as individual components or as various combinations of steroid, β agonist, β agonist & muscarinic antagonist, depending on the symptoms or condition being treated. The very latest product to be approved by the FDA and EMA is a triple combination product delivering all three classes of drug in a single inhaler device.

With a continued vested interest to identify the next generation of inhaled respiratory medicines to remain at the forefront of these conditions, GSK maintains multiple discovery and development research programs. I have worked within the Respiratory therapeutic area for the last 8 years, so it was a natural extension of my work to investigate how the physicochemical and biomimetic properties of drugs being developed can be utilised to improve the development process, aid dose prediction via different routes of administration and explore parameters that affect lung retention.

The project seeks to address the following objectives:

- a. Develop new dose estimation models based on the drug efficiency concept and the required free concentration at the site of action. Search for methodology with available high throughput properties at GSK that can be used to streamline the early drug discovery/lead optimisation process
- b. Compare the new models with the traditional models used at later stages in the drug discovery process. Evaluate how the new models perform by comparison with the traditional dose estimation models based on one compartmental pharmacokinetics.
- c. Explore *in vitro* methodology that can be introduced and applied in dose estimation models. Search for new *in vitro* methodology that can be applied for early compound characterization with a predictive potential for later stage *in vivo* properties.
- d. Investigate the effects of potential variability of the estimated parameters (potency, volume of distribution, clearance, drug efficiency) on the early dose prediction, monitor the possible error and confidence of the predictions and check the statistical characteristics of the model at every stage of the lead optimization process.
- e. Apply and evaluate the new approaches in the following drug discovery programs that involve three different levels of complexity:
 - i. PI3K Gamma/Delta program (IV administration)
 - ii. PI3K Delta program (oral administration)
 - iii. Pan JAKi program (inhaled delivery)

To address these objectives, the following approaches were adopted:

1. Analysis of drug efficiency with marketed compounds – can the clinical dose be retrospectively predicted for these marketed compounds?
2. Development of a simple model to evaluate dose estimation using compounds that are administered via the intravenous (IV) route to establish conceptually whether the drug efficiency method of dose prediction works in a lead optimisation setting to filter and identify “higher quality”. A GSK compound database for the Pi3Kgamma / delta program was used for this analysis.
3. Development of a more complex model that introduces oral pharmacokinetic parameters. A different GSK compound database for the oral Pi3K delta program was used for this analysis
4. Finally, develop a very complex model targeting the lung where inhaled delivery of small molecules is the focus. A third GSK database for the JAK inhaled (JAKi) program was used for this analysis.

5.1 Analysis of Drug Efficiency with Marketed Drugs

A set of marketed drugs was selected from various target classes for which the majority of data was available for early dose estimation. Thus, the *in vitro* potency (pIC_{50}), the *in vivo* human volume of distribution, clearance and absorption, as well as the actual clinical dose and the frequency of the administration were known parameters. The aim of the study was to investigate how the various dose estimation approaches work and to compare the results with the actual clinical dose. The analysis of the marketed drugs data would provide a benchmark for the dose estimation approaches and would reveal expected discrepancies between the predicted and actual dose. Though the set had the advantage that clinical data were available it had a disadvantage that drugs from various target classes from different therapeutic areas were mixed together. Any significant conclusions from this set however can be considered as generally valid for a diverse set of compounds (drugs).

5.2 Using the Intravenous (IV) Route for Dose Estimation: The Pi3Ky Project

This target was selected as a recent example of a lead optimisation program aiming to treat Acute Lung Injury (ALI) and the acute respiratory distress syndrome (ARDS), both clinical syndromes of acute respiratory failure that results in substantial morbidity and mortality. My role in this program was as the DMPK/QP lead scientist, with responsibility for DMPK strategy, PK analysis and modelling, and clinical dose predictions.

The program team's aim was to identify selective phosphoinositide 3-kinase gamma (PI3Ky) inhibitors which were expected to impact on neutrophils in several ways. The release of NFkB-dependent pro-inflammatory cytokines (e.g. TNF α , IL-1 β) will be suppressed through inhibition of the PI3K/Akt/NFkB pathway along with neutrophil respiratory burst (reduction of tissue-damaging ROS and MMPs) [87][88][89]. Secondly, chemotaxis of neutrophils to the lung is governed by several chemo-attractants such as interleukin-8 (IL-8), GM-CSF, C5a, and the formulated peptide fMLP and will be attenuated through inhibition of Pi3Ky [90]. Thirdly, the Pi3K/Akt pathway has been reported to be an important survival pathway for neutrophils and therefore inhibition of PI3Ky should be a powerful means of evoking neutrophil apoptosis [91]. A drug candidate developed to target the Pi3Ky enzyme would be indicated in the treatment of acute lung injury in hospitalised patients. Acute lung injury (ALI) is a syndrome of hypoxemic respiratory failure with acute and persistent lung inflammation and increased vascular permeability caused by direct or indirect lung injury. There are no effective pharmacologic therapies for the treatment or prophylaxis of ALI.

The pathogenic mechanisms of ALI include changes in alveolocapillary permeability, inflammation, extracellular matrix remodeling and abnormal alveolar micromechanics [92] [93]. Neutrophils are believed to be the major cell type contributing to lung damage in ALI. Studies have shown that circulating neutrophils are activated in ALI/ARDS and it has also been shown that after developing ALI the severity of lung injury correlates with the extent of neutrophil influx into the air spaces of the lung [93]. In some patients, the persistence of neutrophilia is associated with higher mortality [94]. Despite the clinical association, it should be borne in mind that this does not necessarily mean that neutrophils are responsible for lung damage in ALI. As ALI patients are generally hospitalized, a medicine administered intravenously has the advantage of a rapid onset

of action in very seriously injured patients who might not be able to swallow any medication. The intravenous administration route has different pharmacokinetic and pharmacodynamic profiles from the oral and inhaled routes and therefore the dose estimation approaches for this scenario will focus on parameters that do not involve absorption.

Figure 5.2-1 Neutrophil Fate and Function in ALI (ARDS)

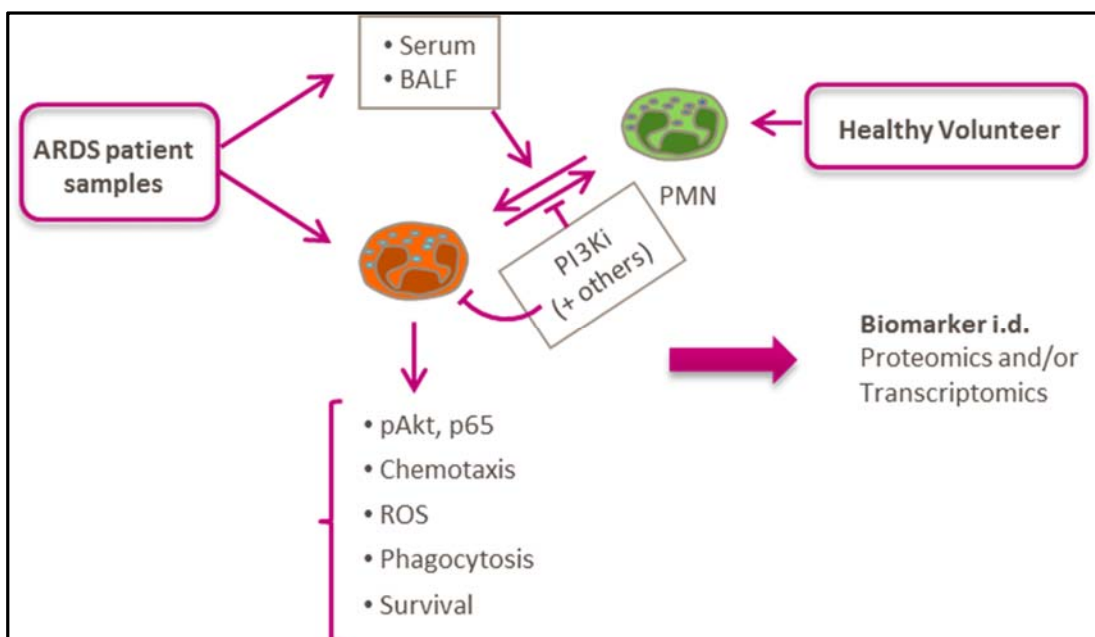


Figure 5.2-1 Shows the some of the functional effects of Pi3Ky inhibition on neutrophils from ARDS samples

5.3 Using the Oral Route for Dose Estimation: The Pi3K δ Project

To study an active project at GSK that introduced a higher level of complexity through oral administration, compounds that have been developed to inhibit the phosphoinositide 3-kinase delta (Pi3K δ) enzyme has been selected. My involvement in this program was to perform the complex pre- clinical PKPD analysis of a functional *in vivo* model of lung inflammation.

PI3K δ is a lipid kinase expressed predominantly in leucocytes, where it regulates activation, proliferation and the function of multiple cell types, thereby modulating immune

responses [95]. PI3K δ inhibition will prevent recruitment of inflammatory cells, including T lymphocytes or eosinophils. It also inhibits the release of pro-inflammatory mediators from neutrophils such as cytokines, chemokines, reactive oxygen species, and proteolytic enzymes [96]. In addition, targeting the PI3K δ pathway improves innate immune responses to infections by promoting neutrophil and T cell mediated host defense. Inhibition of PI3K δ may restore steroid effectiveness under conditions of oxidative stress. There are a number of immune cell types which contribute to allergen-induced asthma, including T-cells, eosinophils, B-cells and mast cells. In allergic asthma, the pre-dominant subset of effector T-cells, Th2 cells, produce IL (interleukin)-4, IL-5, IL-9 and IL-13. IL-4 promotes the secretion of allergen specific IgE, which activates mast cells to release mediators such as histamines, prostaglandins and leukotrienes, leading to tissue inflammation [97]. Additionally, IL-5 stimulates B-cell growth and immunoglobulin (Ig) secretion as well as being a key mediator of eosinophil activation [97].

A selective PI3K δ inhibitor is predicted to block T-cell activation in the lung, reducing the production of pro-inflammatory Th2 cytokines. PI3K δ is also involved in B-cell and mast cell activation which are key contributors to asthma pathogenesis. Therefore, the inhibition of PI3K δ should dampen down the inflammatory cascade involved in the asthmatic response through a wide breadth of pharmacology. PI3K δ blockade may prevent Th2, Th17, B-cell and mast cell activation. Unlike current medicines, PI3K δ inhibitors may affect a broad spectrum of cell types [97][98]. In addition, PI3K δ inhibitors may have anti-viral properties as seen in Influenza infection models [99].

The PI3K δ program offered GSK the opportunity to develop an oral medicine for the treatment of asthma following a successful program to develop an inhaled PI3K δ . An oral program was based on the growing evidence of a systemic effect of PI3K δ in asthma and safety information generated from the inhaled program. In addition, the commercial opportunity for an oral treatment of asthma is very high: with the exception of Montelukast there are currently no effect commercially successful oral treatments of asthma.

The analysis of the PI3K δ oral program provided the opportunity to apply the approaches directly to a real drug discovery program and provide a proof-of-concept for the proposed dose estimation methodologies.

Figure 5.3-1 Cells Involved in Atopic Asthma which are Targets of Current Therapies.

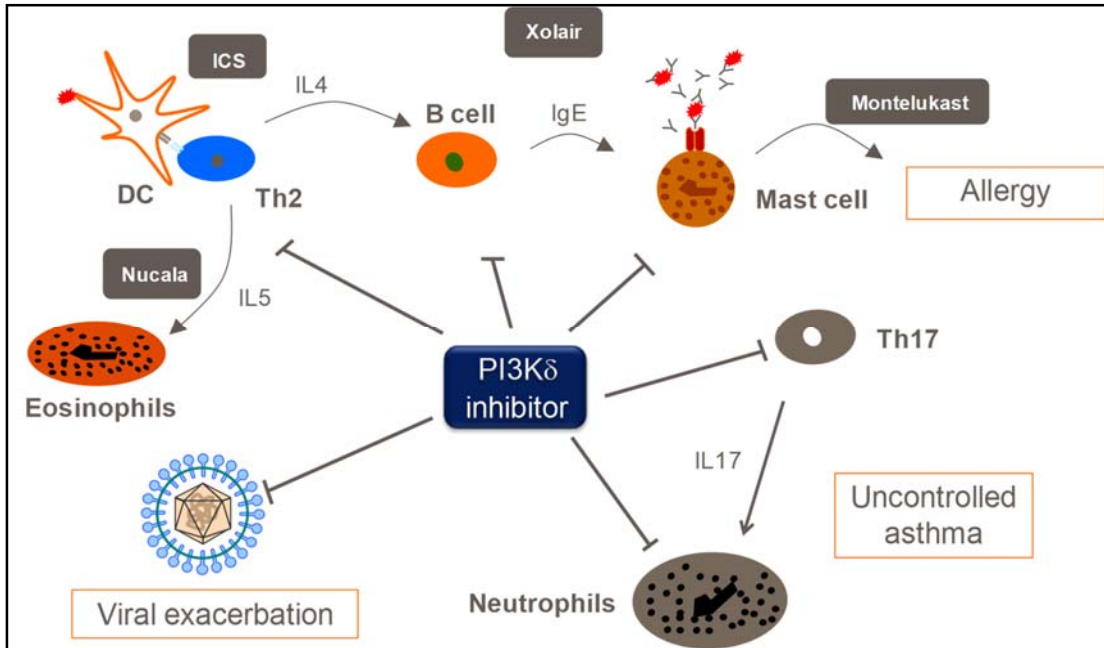


Figure 5.3-1 Shows some of the major functional effects of PI3K δ inhibition on key inflammatory cells

5.4 Using the Pulmonary Route for Dose Estimation: The JAK Project

For the most complex model for dose prediction, an active inhaled lead optimisation program has been selected, where compounds were developed as pan-JAK inhibitors for the treatment of moderate to severe asthma. There are four members of the JAK family (JAK1, JAK2, JAK3, TYK2) which control the signalling of numerous cytokines, which have been implicated in the pathogenesis of inflammatory diseases [100][101]. As described previously, there are a number of immune cell types which contribute to allergen-induced asthma, including T-cells, eosinophils, B-cells and mast cells. In allergic asthma, the pre-dominant subset of effector T-cells, Th2 cells, produce IL4, IL-5, IL-9 and IL-13. IL-4 and IL-13 promote the secretion of allergen specific IgE, which activates mast cells to release pro-inflammatory mediators. More specifically to JAK, upon binding to its receptor, signalling via the JAK-STAT pathway is initiated (Signal Transducer and Activator of Transcription). The JAK-STAT signal transduction pathway is utilised by

cytokines with a wide variety of differing functions including both pro- and anti-inflammatory activities. Therefore targeting JAK 1/2/3 in the lung is attractive therapeutically in order to reduce the chronic inflammation that is associated with asthma [101], as shown in Figure 5.4-1, Figure 5.4-2 and Figure 5.4-3.

The inhaled route of administration was selected for the JAK program based on the safety profile of other commercially available JAK inhibitors. Tofacitinib is an oral JAK inhibitor marketed for the treatment of rheumatoid arthritis (RA) and prescribed where patients have an inadequate response to, or who are intolerant of, methotrexate which is the standard of care for RA. Tofacitinib has a black box warning limiting its use and dose level due to immune suppression. Therefore, the GSK strategy was to develop an inhaled JAK inhibitor which would potentially have an improved therapeutic index. This would be achieved by restricting its primary pharmacological effect to the lung by minimising systemic exposure and reduce the risk of immune suppression.

Figure 5.4-1 Cytokine Binding and JAK Signalling

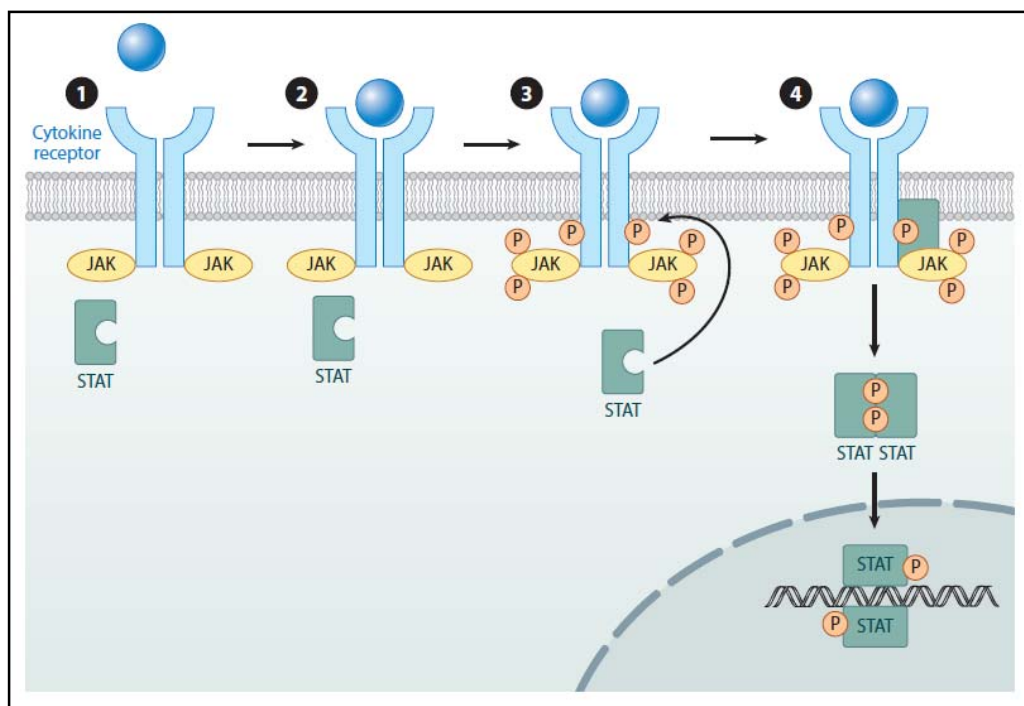


Figure 5.4-1 Shows the JAK-STAT signal transduction pathway following cytokine receptor binding

Figure 5.4-2 Consequences of JAK Activation

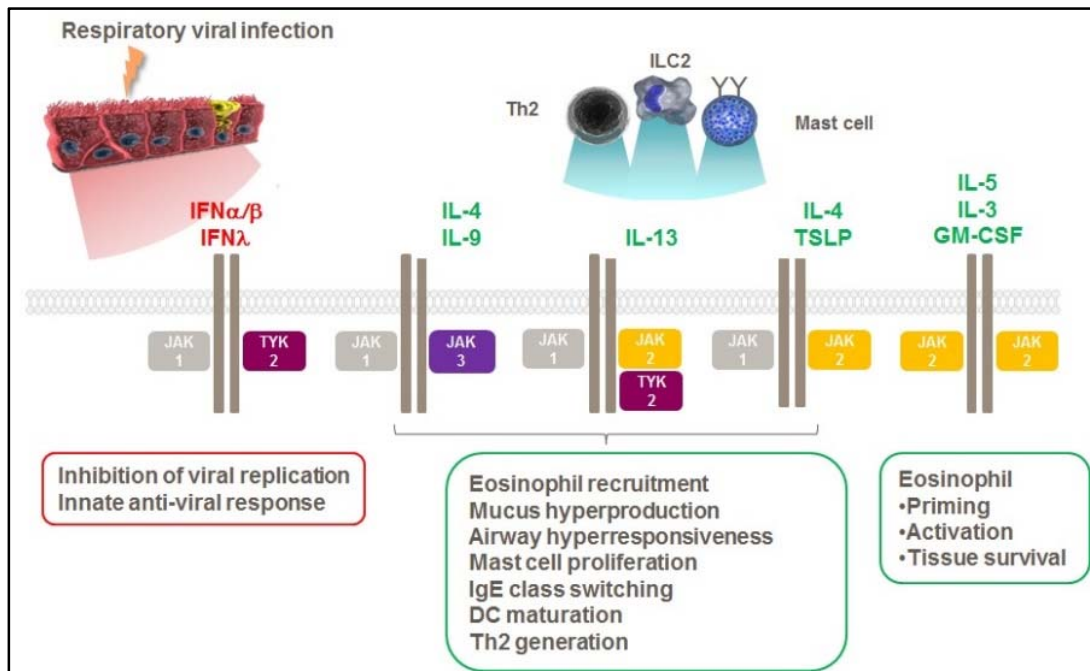


Figure 5.4-2 Shows some of the functional inflammatory effects of JAK 1/2/3 activation suggesting the potential benefit of a JAK inhibitor in inflammatory airway disease

Figure 5.4-3 Mechanisms of Allergic Inflammation in Asthma (adapted from [102])

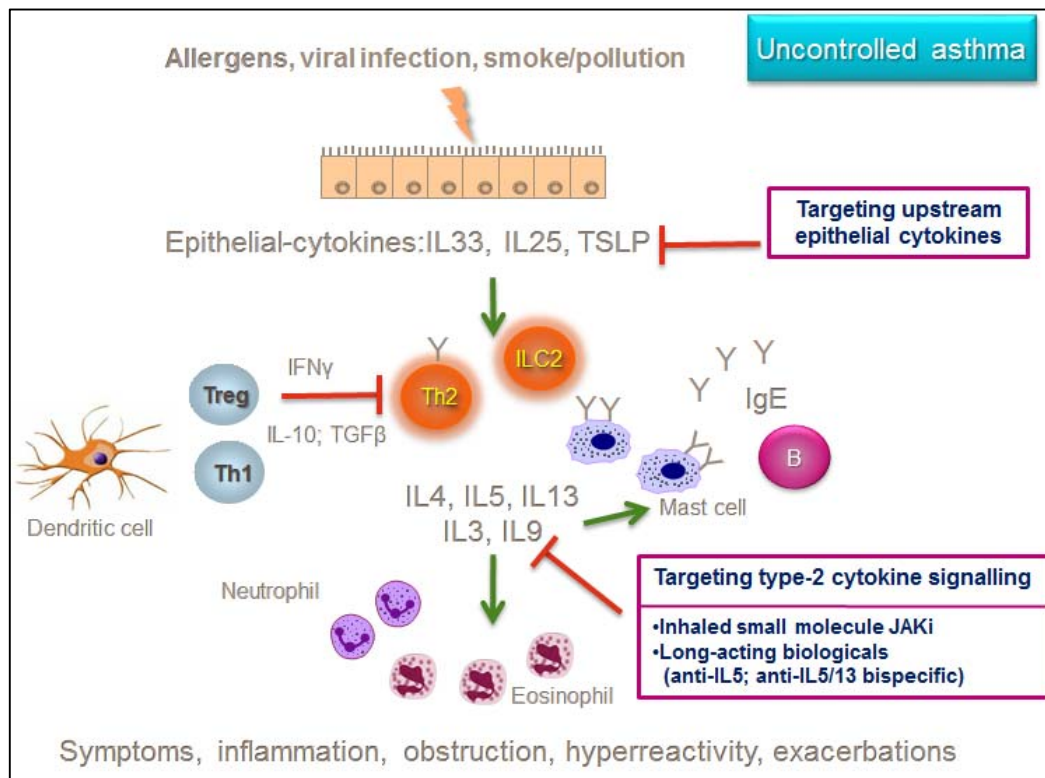


Figure 5.4-3 Shows some of the inflammatory processes involved in asthma

The analysis of the JAK inhaled delivery program provided the opportunity to raise the level of complexity of the model under development and apply the methodologies directly to an active drug discovery program and assess its performance as a further proof-of-concept for the approach. Whether there are specific physicochemical and biomimetic properties that affect lung retention that can be focussed on and optimised an inhaled delivery program was also assessed. The unique challenges associated with drugs delivered by the pulmonary route are summarised in the following section.

5.4.1 Balancing Drug Retention and Systemic Distribution Requirements in Respiratory Medicines Development.

Inhaled administration is especially advantageous for local treatment of various lung diseases, particularly when treating inflammatory lung disorders such as asthma and Chronic Obstructive Pulmonary Disease (COPD). From a drug development perspective, for a once daily dosage regime to succeed via pulmonary delivery, it is now recognised that to ensure sustained engagement of small molecules to their targets in the lung, good or prolonged “intrinsic” lung retention is a desirable property.

Despite reports of substance inhalation from early history, it is only technological advances in the second half of the 20th century that have made inhaled drug administration a viable, effective and preferred method to treat lung disorders. Although isoprenaline was introduced as an inhaled medicine for the treatment of asthma in 1951, the pulmonary delivery of drugs was initially considered impractical, inefficient and unreliable to accurately deliver a defined dose of an inhaled drug due to limitations in the technology available. Devices that accurately administer metered inhaled doses to the lung have now been developed (e.g. Ventolin[®], Seratide[®]), and in recent years, the FDA has also approved inhaled drugs that do not directly target the pulmonary system. For example, in 2006 an inhaled version of human-derived insulin to treat diabetes was developed and approved, although this was subsequently withdrawn due to toxicological reasons. Despite this set-back, inhalation is still recognised as a rapid and efficient systemic delivery method for small-molecule therapeutics via the large surface area presented by the epithelial cells in the trachea and in the alveoli.

From a DMPK perspective, pulmonary drug delivery offers several advantages. Pre-systemic drug metabolism is reduced because metabolising enzymes have low expression levels in the lungs [103][104], and absorption correlates well with CaCo2 and MDCK cell permeability [105]. Furthermore, polar drugs with large polar surface areas and H-bond potential can also permeate through the epithelial lung cells. The pulmonary epithelial barrier is more permeable than the intestinal mucosa and the blood brain barrier [106], and compounds that are substrates for P-gp efflux transporters [107] are also often absorbed well through the lungs. Therefore, for molecules that are poorly absorbed from the GI tract, inhaled administration potentially offers an alternative route to the systemic circulation. However, the rapid absorption associated with this route also poses

enormous challenges for drug discovery teams developing small molecules against targets in lung tissues or cells [104], where retention is a primary requirement, rather than systemic distribution.

In order to investigate the parameters that affect the absorption and pharmacodynamic profiles of drug molecules via inhaled administration, it is necessary to consider the anatomical parameters of the lungs, the formulation of the active material and the inherent properties of the active molecules. While the surface area of the upper airways is only a few square metres in humans, for the alveoli it is more than 100 m² [108]. The airways are mainly lined with mucus-secreting goblet cells, which are pseudostratified ciliated columnar cells that help to quickly remove any solid particles which are deposited. Insoluble particles that are inhaled and deposit in these airways are therefore quickly and efficiently evicted by the mucus-ciliary escalator [109]. Solid particles that reach deeper into the airways can remain for as long as 24 hours [110]. The air-side surface of each of the 500 million alveoli in the human lungs is protected by 12-14 of alveolar macrophages [111][112] that can digest insoluble particles that are deposited, although there are insoluble, non-digestible particles that can deposit deep in the alveoli and remain for years [111]. For example, coal dust remains trapped for a lifetime and can result in silicosis [111]. Using insoluble drug to increase lung retention is therefore not necessarily the best approach to adopt, primarily because slow dissolution rates are not compatible with the high concentrations required for efficient target engagement, but also because of an increased risk of lung irritancy and toxicity [113]. Figure 5.4-4 is adapted from reference [111] and shows a schematic illustration of the lung epithelial cells in different parts of the lung that cover a large surface area promoting permeability. Depending on the position of the target (in the lung, in the epithelial cells), we may want to design compounds that are retained in the lung and not reach the general circulation. Alternatively, if the lung is to be the route for systemic delivery against a target which is not in the lung, we may want the drug to reach the general circulation rapidly. Ideally, compounds that target the lungs for the treatment of asthma or lung infections should avoid the general circulation either by being poorly absorbed or rapidly cleared in order to avoid potential side effects. To develop drugs with reasonably long lung retention profiles, it is important to have access to methods that can measure the compound concentration time profile not only in the systemic circulation, but also in the lung itself.

Figure 5.4-4 The Illustration of Epithelial Cells in Different Parts of the Lung

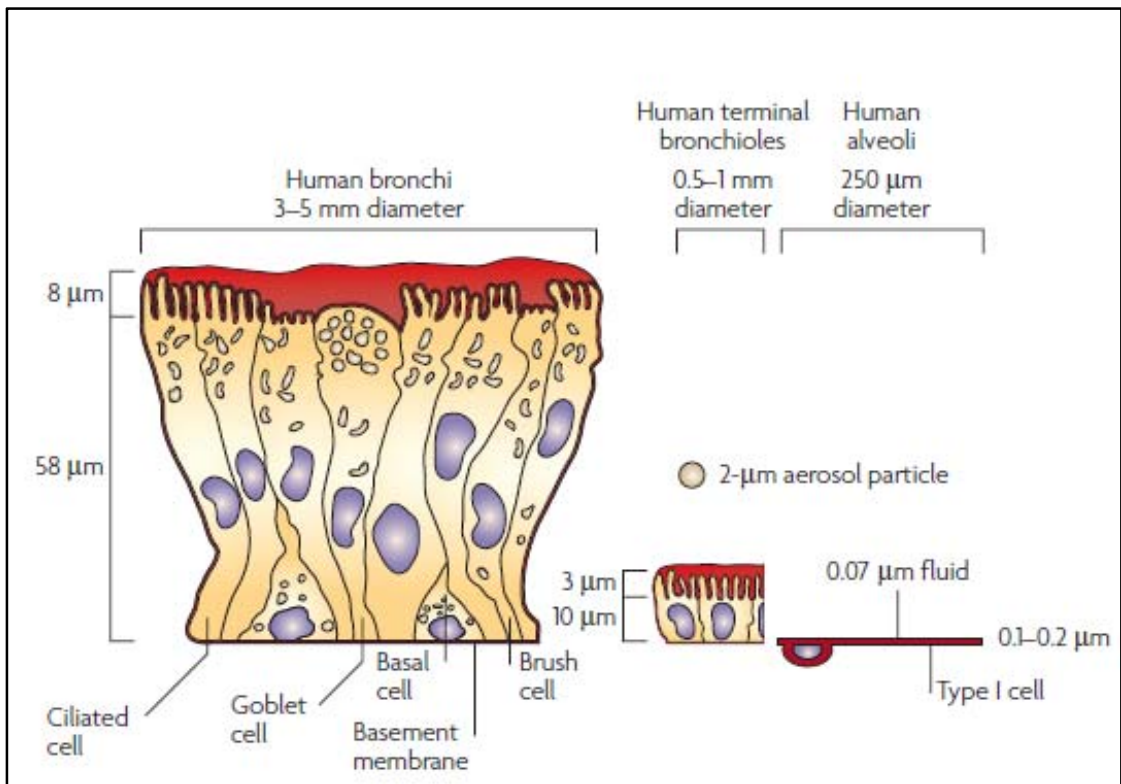


Figure 5.4-4 Shows a schematic of main cell types and dimensions of the lung [111]

Inhaled particulates can cause adverse pathology in the lungs, which is characterised by the formation of foamy macrophages in the alveolar [113][114][115]. Where specifically in the lungs it is best to deposit a drug to achieve optimum absorption has not been yet identified and probably target specific, but several hypotheses are emerging which are dependent on a number of factors [111][116]. Firstly, the nature of the therapeutic intervention needs to be considered: is a local pharmacological response to the drug required (such as treating asthma) or is the aim to achieve rapid systemic absorption i.e. is the aim to use the pulmonary/inhaled route to overcome poor oral ADME properties? Due to differences in surface area, morphology and permeability in the epithelial cells of the trachea and the alveoli, the particle size of the inhaled active ingredient (Active Pharmaceutical Ingredient – API) can be modulated to reach different regions of the lung and airways. Aerosol particles with an average aerodynamic diameter of about 1 to 2 μM , if slowly and deeply inhaled, can reach deep into the lungs with an efficiency of up to 90% in the peripheral regions, which are rich in alveoli [111].

Besides the formulation developed to deliver the drug, its inherent physicochemical properties, primarily solubility, lipophilicity and permeability, will also play a key role in determining lung retention times and bioavailability: for example, small molecules with moderate lipophilicity can have extremely rapid absorption kinetics from the lungs [106]. In 2003 Tronde *et al* [117] published a comprehensive analysis of the structure – lung absorption relationship for 34 inhaled drugs based on rat *in vivo* pharmacokinetics, although the set cannot be considered to be particularly diverse, comprising mostly steroids or β 2-agonists. Generally, rapid absorption was observed through the lungs for drugs that were more polar and therefore less lipophilic than associated with optimal oral absorption. Moreover, retained good absorption from the lung was evident with drugs with low permeability when measured *in vitro*. Drug absorption rate correlated with the molecular polar surface area, H-bonding potential and apparent permeability measured in CaCo-2 cell monolayers. They also noted high lung absorption rates for Talinolol and losartan, both of which are substrates for P-gp efflux in the gastrointestinal tract, and suggests that these transporters have a less important role in the lungs. One possible explanation for this are the high local concentrations associated with dry powder dissipation that perhaps saturate potential P-gp transporters in the lung [118].

In a study by Ritchie *et al* [119][120] involving 81 marketed respiratory drugs, they also demonstrated that this class was associated with higher polar surface area, a greater number of hydrogen bonds and higher molecular weight than the majority of oral drugs. In addition, while the lipophilicity of the inhaled drugs was generally lower than that of the oral drugs, other properties such as total ring count were similar for both classes. Edwards *et al* [105] studied the lung retention expressed as Lung $T_{1/2}$ (min) of 17 marketed inhaled drugs using an isolated perfused ventilated rat lung (IPRLu) model, which was also used to assess the lung retention of 82 drug discovery compounds at GlaxoSmithKline. They developed a partial least square QSAR model to estimate the log % solubilized dose in the lung perfusate. Based on this model, the most significant variables that positively influenced lung absorption were *in silico* permeability, bioavailability P-gp score and MDCK cell permeability, while the number of positively chargeable groups, rotatable bonds, and H-bond donors negatively influenced the lung absorption.

These previous studies identify that for drugs to be safely administered via the pulmonary route and achieve longer lung retention to maximise duration of the pharmacological effect, they should have moderate solubility, permeability and lipophilicity in order to minimise the formation of foamy macrophage and prevent systemic distribution.

I will further investigate physicochemical and biomimetic properties that may affect lung retention and the estimated dose for inhaled compounds using the PAN JAK inhibitor project compounds as a case study.

6 Experimental and Computational Methods

At GSK, there are various organisational units with unique expertise in *in silico* model building and calculations. The Computational Chemistry Unit helps the program teams to identify the relevant *in silico* properties to use during lead optimization and ensures that the models are available for the chemist in a user-friendly way. Similarly, the various *in vitro* and physicochemical measurements are performed by separate expert groups. Experimental details of physicochemical measurements and *in silico/in vitro* methods providing data for the project are described below.

6.1 In Vivo Studies performed at GSK

All animal studies were ethically reviewed and carried out in accordance with Animals (Scientific Procedures) Act 1986 and the GSK Policy on the Care, Welfare and Treatment of Animals.

6.2 Experimental Conditions of Physicochemical and Biomimetic Measurements

As described in the introduction, the maximum drug efficiency can be calculated from the measured albumin and phospholipid binding data [77]. These measurements are run by the Physicochemical Characterisation Group and the data are deposited in the company database where it is then available via an excel search tool called Helium.

6.2.1 Measurements of Human Serum Albumin Binding

The measurements were run on a ChiralPak-HSA column with dimensions of 50 x 3 mm using Agilent 1200 HPLC equipment with plate based auto sampler and diode array detector. The ChiralPak-HSA columns were obtained from Chiral Technologies Inc. The mobile phase A is 50 mM ammonium acetate buffer adjusted to pH 7.4 in order to be similar to physiological pH conditions. 100% HPLC grade iso-propanol was used as mobile phase B. The 6 min gradient run was timed as: 0 to 3.0 min 0 to 30% iso-propanol 3 to 5 min at 30% isopropanol; 5 to 5.2 min then back to 100% pH 7.4 ammonium acetate buffer and the column re-equilibrated in a 6 min run time. The mobile phase flow rate was 1.8 mL/min and the separation took place at an elevated temperature of 40°C (in order to reduce column back pressure and imitate physiological conditions). Before the assay plates were run, the retention times were calibrated using a set of known drug molecules as listed in Table 6-1. Using the plasma protein binding % data from the literature they were converted to $\text{Log}k$ data using Equation 19. The logarithm of the gradient retention time was plotted against the linearised $\text{Log}k$ HSA data from the literature. The slope and intercept values of the obtained straight lines were used to convert a new compound's retention data to HSA binding data. Typical calibration data are shown in Table 6-1 [55].

Table 6-1 Typical calibration data for the HSA binding measurements using an HSA column

Compound	Literature Plasma protein binding (%PPB)	Linearised PPB (Logk)	gt _R (min)	Log(gt _R)
Nizatidine	35.00	-0.28	0.94	-0.03
Bromazepam	60.00	0.17	1.20	0.08
Carbamazepine	75.00	0.46	1.63	0.21
Budenoside	88.00	0.83	1.84	0.26
Nicardipine	95.00	1.20	3.01	0.48
Indometacine	99.00	1.69	3.84	0.58
Piroxicam	94.50	1.16	2.82	0.45
Diclofenac	99.80	1.92	4.20	0.62
Flurbiprofen	99.96	1.98	4.30	0.63

A typical HPLC chromatogram for the standard calibration mixture is shown in Figure 6.2-1.

Figure 6.2-1 An Example Chromatogram of Known Drugs using Immobilized Human Serum Albumin (ChiralPak-HSA) HPLC Column.

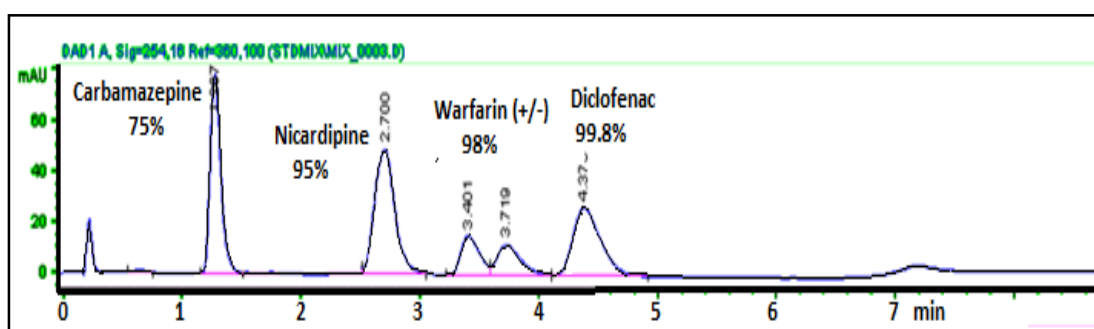
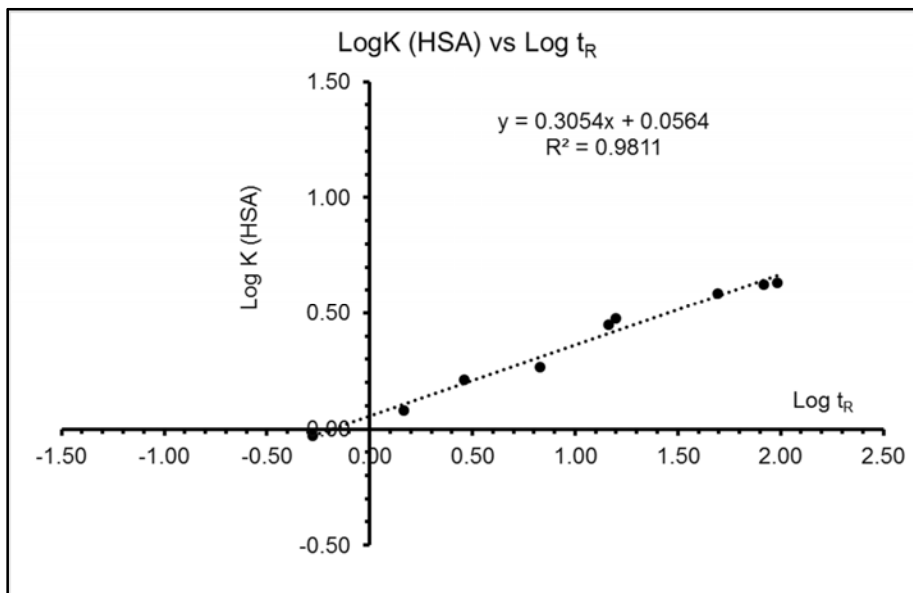


Figure 6.2-2 shows a typical calibration line for the gradient retention times.

Figure 6.2-2 Calibration Plot for the Gradient Retention Times and HSA Binding for the Calibration Set of Compounds (GSK data).



Using the slope and intercept of the straight line, the unknown HSA binding can be calculated using an excel template where $\text{Logk (HSA)} = \text{slope} \times \text{Log } t_R(\text{HSA}) + \text{intercept}$. Table 6-2 shows GSK NCE program compound values calculated from the HSA calibration plot Figure 6.6-2

Table 6-2 Excel Calculations for the HSA Binding from the Gradient Retention Time Obtained on the ChiralPak-HSA Column.

GSK Number	$t_R(\text{HSA})$	Slope	0.3054
		Intercept	0.0564
		%HSA	Logk (HSA)
GSK700917A	1.2	73.31	0.42
GSK703971A	3.5	93.96	1.13
GSK703972A	2.5	87.72	0.82
GSK700143A	3.1	91.88	1.00
GSK700142A	2.6	88.51	0.85

The HPLC column integrity can also be checked by injecting the racemic mixture of warfarin. When two peaks were observed, it indicated that the major binding site (warfarin binding site) remained intact on the immobilised albumin (Figure 6.2-1).

6.2.2 Measurements of Phospholipid Binding using Immobilized Artificial Membrane HPLC Column

Commercially available Immobilized Artificial Membrane HPLC columns were obtained from Regis Technologies (Morton Grove IL, USA). An IAMPC.DD2 100 x 4.6 mm column with an acetonitrile gradient was used. The run time was 6 min and the buffer contained 50 mM ammonium acetate at pH 7.4. The gradient profile was: 0 to 2.5 min 0 to 80% acetonitrile then kept at 80% acetonitrile for 3 min; then from 3 to 3.2 min back to 100% buffer and re-equilibration of the column by the end of the 6-min run. The gradient retention times were calibrated using a set of compounds for which the chromatographic hydrophobicity indices (*CHI*) had been measured isocratically according to reference [64]. The calibration set of compounds are listed in Table 6-3 A typical chromatogram is shown in Figure 6.2-6.

Table 6-3 The Calibration set of Compounds used for Obtaining the *IAM* Binding Parameter *CHI* (*IAM*)

Compound	t_R 7.4	CHI (IAM)
Octanophenone	5.296	49.4
Heptanophenone	5.069	45.7
hexanophenone	4.813	41.8
Valerophenone	4.518	37.3
Butyrophenone	4.175	32
Propiophenone	3.767	25.9
Acetophenone	3.169	17.2
Acetanilide	2.776	11.5
Paracetamol	2.201	2.9

Figure 6.2-3 A Typical Chromatogram of the IAM Calibration Set of Compounds (Paracetamol, Acetanilide Acetophenone, Propiophenone, Butyrophenone, Valerophenone, Hexanophenone, Heptanophenone and Octanophenone)

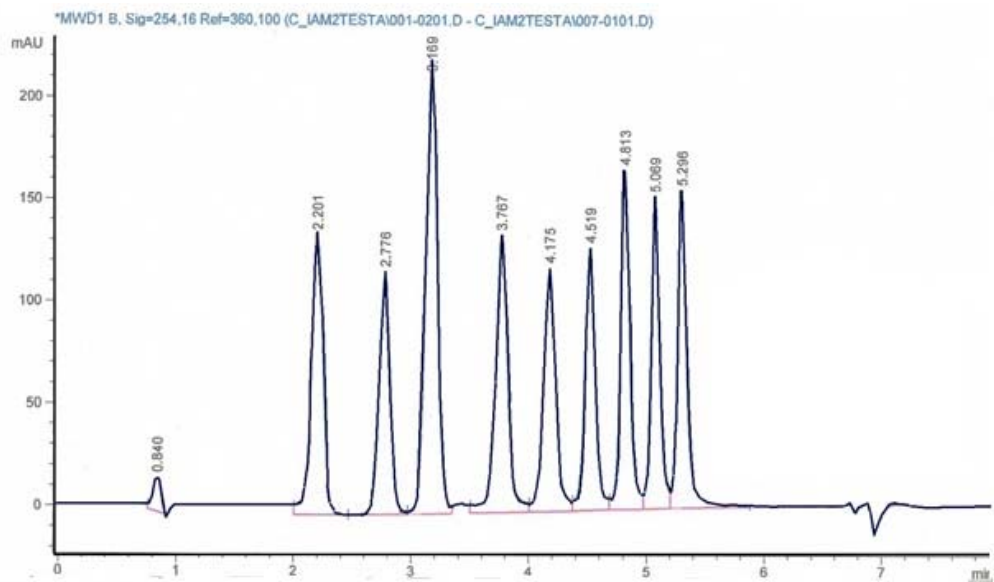
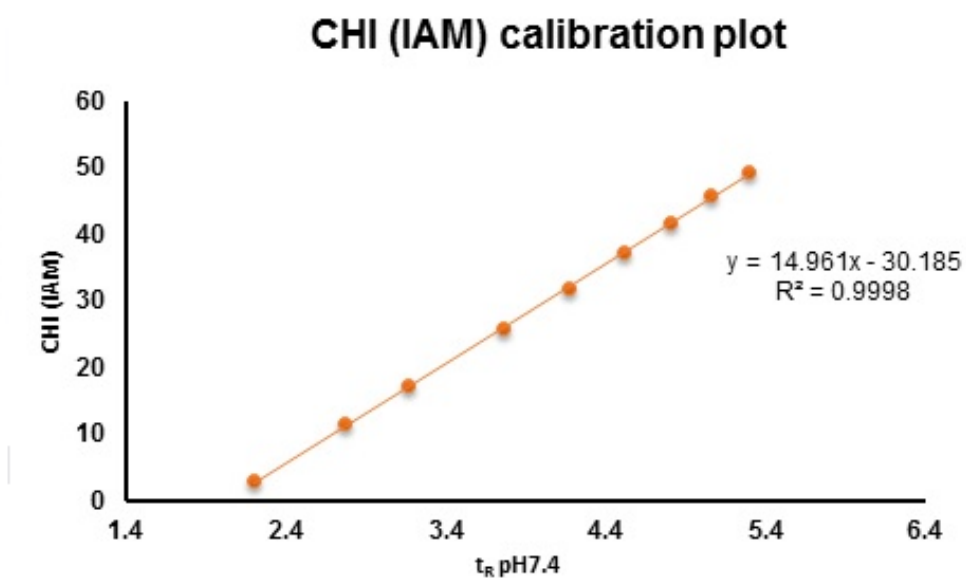


Figure 6.2-3 shows a typical calibration chromatogram; each peak is in order of the compounds in the figure title and that of Table 6-3.

Figure 6.2-4 A Typical Calibration Plot used to Calculate CHI IAM Values from the Measured Gradient Retention Times of Drug Discovery Compounds.



6.2.3 Measurements of Chromatographic Lipophilicity

The lipophilicity of the drug discovery compounds was determined by HPLC using C-18 reversed phase columns. A fast acetonitrile gradient was used, starting with a 100% aqueous mobile phase. Three measurements of the gradient retention times were made using pH 2 0.01M phosphoric acid, pH 7.4 50 mM ammonium acetate and pH 10.5 50 mM ammonium acetate buffer as starting mobile phases.

Table 6.4 shows a calibration set of compounds with fixed CHI values at three different mobile phase pH's that can be used to standardise of the gradient retention times. The CHI data for the test mix shown in Table 6-4 has been suggested for the calibration of the gradient retention times at pH 2.6, pH 7.4, and pH 10.5 [45].

Figure 6.2-5 shows a typical chromatogram of the test mix at pH 7.4. As previously discussed, the use of the same CHI values for calibration of the actual gradient retention times should enable the CHI values then obtained to show good inter-laboratory agreement even if they were obtained with slightly different reversed phase column

dimensions and conditions. Some of the compounds of the calibration set have retention times which are sensitive to slight variation in the mobile phase pH. Thus, low correlation coefficients (r^2 below 0.99) indicate differences in mobile phase pH or non-linearity of the gradient and the calibration is a useful guide for system suitability and changes to experimental conditions.

Table 6-4 The Chromatographic Hydrophobicity Index Values for the Calibration [45]

Compound	CHI at pH 2.6	CHI at pH 7.4	CHI at pH 10.5
Theophylline	19.9	18.4	5.0
Phenyltetrazole	42.2	23.6	16.0
Benzimidazole	6.3	34.3	30.6
Colchicine	43.9	42.0	43.9
Phenyltheophylline	51.7	51.2	51.3
Acetophenone	64.1	65.1	64.1
Indole	72.1	71.5	72.1
Propiophenone	77.4	77.4	77.4
Butyrophenone	87.3	87.5	87.3
Valerophenone	96.4	96.2	96.4

Figure 6.2-5 shows typical calibration plots obtained at three pH's on C-18 column for the determination of the Chromatographic Hydrophobicity Index (*CHI*) values. Chromatogram peaks in Figure 6.2-5 are in the order listed in Table 6-4

Figure 6.2-5 A Typical uHPLC Chromatogram

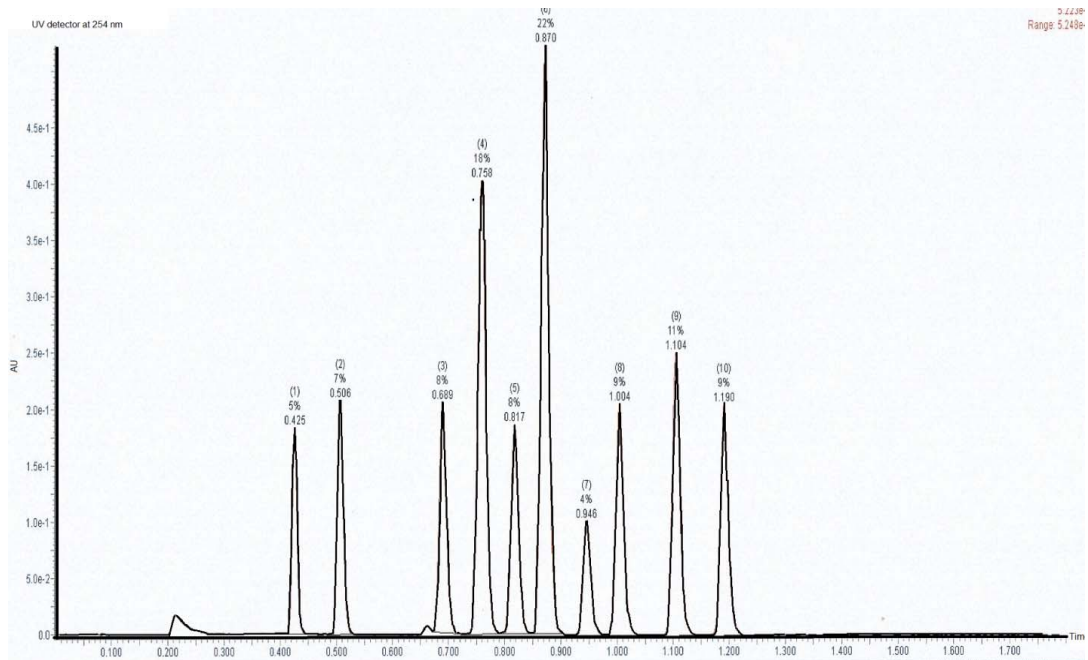
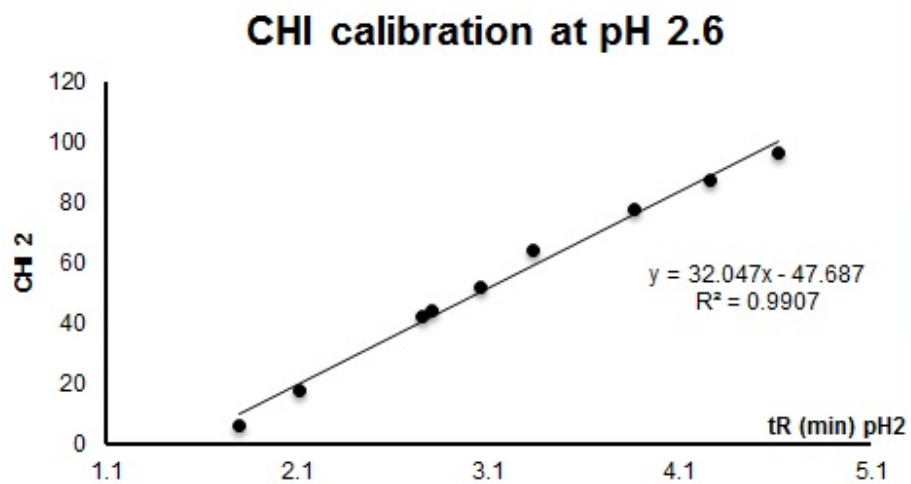


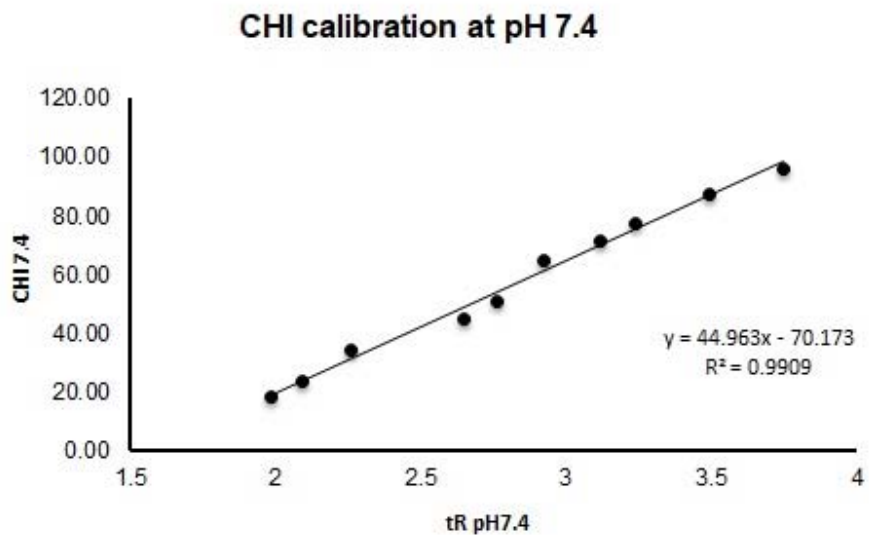
Figure 6.2-5 shows a typical uHPLC chromatogram of the standard test mix in Table 6-4 run at pH 7.4. Each chromatogram peak is in order of the compounds listed in Table 6-4.

Figure 6.2-6 Calibration Plots for the CHI Determination on C-18 Reversed Phase Columns at Three Different Starting Mobile Phase pH: a) pH2.6; b) pH7.4; c) pH10.5

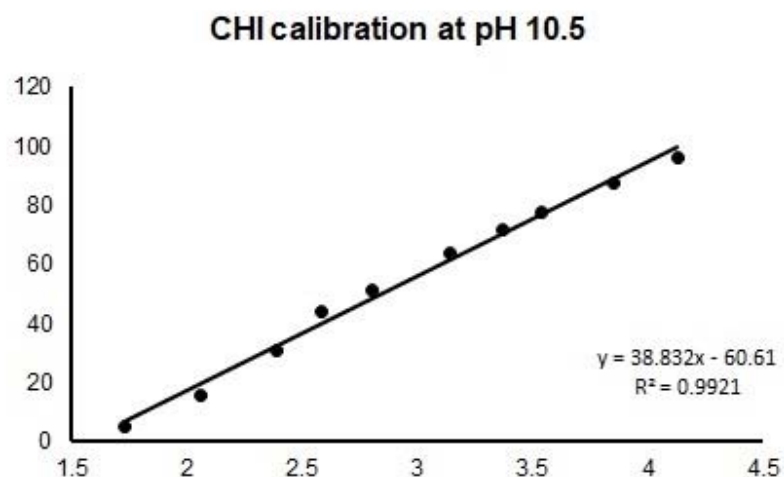
a.



b.



C.



6.2.4 Measurements of High Throughput Solubility and Artificial Membrane Permeability

6.2.4.1 The Kinetic Solubility Assay Developed at GSK

A 5 μ L of 10mM DMSO stock solution of test compound was diluted in 100 μ L (0.5mM) in pH7.4 phosphate buffered saline, equilibrated for 1 hour at room temperature, filtered through Millipore Multiscreen_{HTS}-PCF filter plates (MSSL BPC). The filtrate was then quantified by suitably calibrated flow injection using a Chemi-Luminescent Nitrogen Detector (CLND) [121]. The maximum solubility in phosphate buffer saline under the assay condition was equivalent to the amount of compound that was diluted in the buffer. If the compound's DMSO solution provided for the assay was 10 mM, it was equivalent to 500 μ M. If no compound had precipitated during the 1 h equilibration time with the buffer, then the solubility was reported to be higher than 500 μ M. When no compound was detected in the buffer filtrate, then the solubility was reported to be less than 1 μ M, which was the detection limit. Compounds that had no nitrogen atoms in their structure could not be detected by CLND. The detector signal was calibrated using various concentration of caffeine that has 4 nitrogen atoms. The detector signal was proportional

to the number of nitrogen atoms per mole. A correction factor was used when the molecules contained adjacent nitrogen atoms. The standard error of the CLND solubility determination was $\pm 30 \mu\text{M}$, the upper limit of the solubility was $500 \mu\text{M}$ when working from 10 mM DMSO stock solution. Compounds that had less than $50 \mu\text{M}$ solubility were considered low solubility, while solubility was high when greater than $200 \mu\text{M}$. As the concentration was expressed in weight of the active material, the μM solubility values were often converted to $\mu\text{g/mL}$ concentration. However, larger molecular weight compounds seemingly have higher $\mu\text{g/mL}$ solubility so when comparing discovery compounds solubility, the molar concentration should be used.

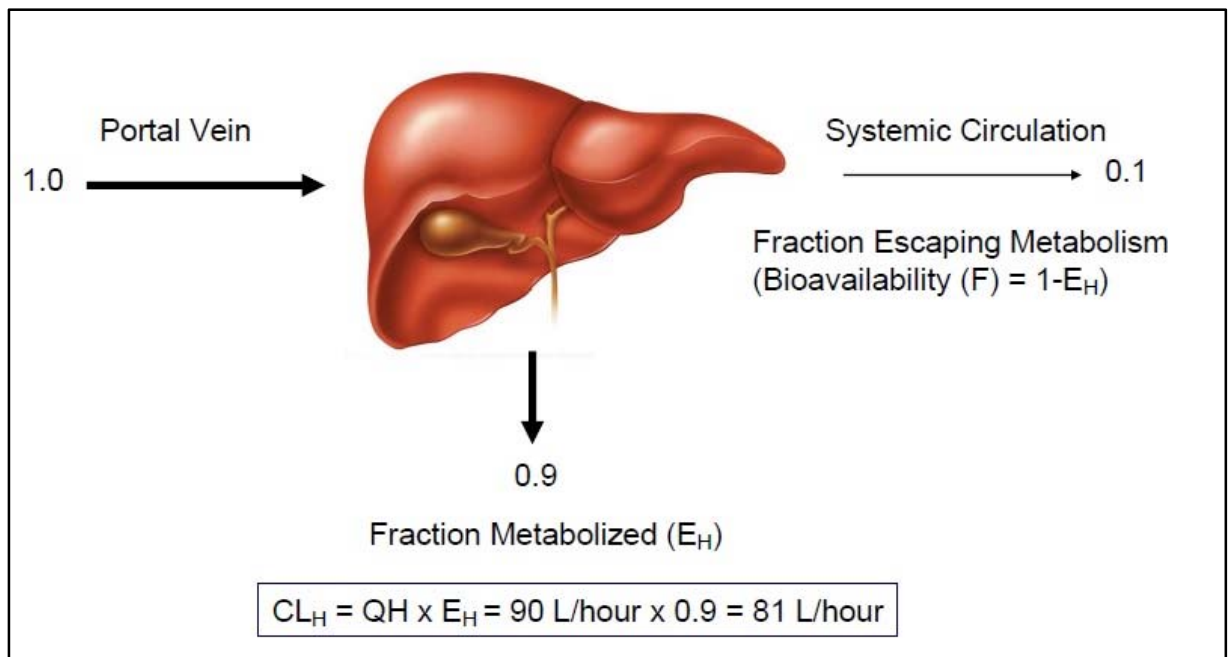
6.2.4.2 Artificial Membrane Permeability Assay

An artificial membrane permeability assay has been developed internally at GSK. This assay was based on the application of black lipid membrane between two buffer compartments (donor and acceptor compartments). $2.5 \mu\text{L}$ of a 10 mM sample solution in pH 7.4 phosphate buffer was added to the donor compartment. To enhance solubility, 0.5% hydroxypropyl-cyclodextrin (encapsin) was added to the buffer. The artificial black lipid membrane was prepared from 1.8% phosphatidyl choline and 1% cholesterol in decane solution and applied to the porous filter between the donor and acceptor compartments. The application of the membrane and buffer solutions were made by a Tecan robot. To improve efficiency, the membrane had to be solvated by the buffer within a short period of time in order to retain the natural bi-layer form. The sample concentration in both the donor and acceptor compartment was determined by LC-MS after a 3 h incubation and gentle shaking at room temperature [122]. The permeability (LogP_{app}) measuring how fast molecules passed through the black lipid membrane was expressed in nm/s . The average standard error of the assay was around $\pm 30 \text{ nm/s}$ that can be higher at the low permeability range. The usual permeability values that are measured by this methodology ranged between 3 to 600 nm/s . When the permeability was less than 50 nm/s , it was considered to be low. When the permeability was greater than 300 nm/s , it was considered to be high. The absorption potential of the oral PI3K δ compounds was estimated by using the product term of the measured CLND solubility and the artificial membrane permeability values as described in section 4.2.3. The cut-off values were determined in order to consider if any of the values were low then absorption potential would also be low.

6.3 Experimental Methods for the Measurement of *In vitro* Clearance

The liver is the most important site of drug metabolism in the body. Approximately 60% of marketed drugs are cleared by hepatic CYP enzyme mediated metabolism. The Intrinsic clearance is the ability of the liver to remove the drug in the absence of flow limitations and binding to cells or proteins in the blood. Figure 6.3-1 illustrates the hepatic extractions and the calculation of the hepatic extraction ratio.

Figure 6.3-1 The Schematic Illustration and Calculation of Hepatic Extraction Ratio.



Previously referred to Equations 1 and 2

Equation 1

$$F = F_g \cdot F_a \cdot F_h$$

F – Bioavailability, F_g – Fraction escaping gut metabolism, F_a – Fraction absorbed, F_h – Fraction escaping metabolism by the liver

Equation 2

$$F_h = (1 - E)$$

F_h – Fraction escaping first pass metabolism by the liver, E -Extraction ratio

6.3.1 Measurement of *In vitro* Clearance in Liver Microsomes

Liver microsomes are subcellular fractions which contain membrane bound drug metabolising enzymes, notably CYP450s and MOA's (Table 4-1). To measure the *in vitro* intrinsic clearance a pool of human liver microsomes was used. In order to understand the species differences rat and minipig microsomes were also used. The metabolic activity of P450 enzyme was checked using standard methodology [123], appropriate control compounds were included with each species.

Compounds were incubated at a concentration of 0.5 μ M in 0.5 mg liver microsomes, 0.1M phosphate buffer (pH7.4) and NADPH at 37 °C for a maximum of 1 h (incubation volume 25 μ L). At each time point, typically 0, 5, 15, 30 and 45 min the reaction was terminated by adding 50 μ L of protein precipitation solvent with an internal standard at an assay well. The samples were centrifuged, and a volume of supernatant combined as a cassette of up to 4 compounds before being analysed by LC-MS/MS analysis. For each compound a single exponential decay equation was calculated from a time response plot.

The equation for a single exponential decay is:

Equation 40

$$y = A_0 \cdot e^{-kt}$$

Where A_0 = initial value, k = Elimination rate constant, t = time, e = exponential. This equation should be applicable for most datasets.

Equation 41

$$CL_{int} \left(\frac{\mu L}{min} \text{ protein} \right) = \frac{\frac{Ln2}{k}}{\text{Assay Protein Concentration}}$$

Equation 42

$$CL_{int} \text{ (mL/min)/g liver) = } CL_{int} \text{ (\mu L/min/mg). SF} \left(\frac{\text{g}}{\text{kg}} \right)$$

CL_{int} = Intrinsic clearance, k = Elimination rate constant, SF = Scaling factor

6.3.2 Measurement of *In vitro* Clearance in Hepatocytes

Hepatocytes are liver cells with intact membranes and physiological concentrations of Phase I and II metabolising enzymes and cofactors, notably CYP450s, MOA's, glucuronidation and conjugation reactions (Table 4-1), which are believed to be a model close to the whole liver for drug clearance measurements [124]. In order to understand the species differences rat, minipig and human hepatocytes were used.

Suspensions of cryopreserved hepatocytes were used. Incubations were performed at a test or control compound concentration of 0.5 μ M at 37°C. The cell density is 0.5x10⁶ viable cells/mL. Control incubations were also performed in lysed cells to reveal any non-enzymatic degradation. Appropriate control compounds were included with each species.

Samples (50 μ L) are removed from the incubation mixture at 0, 5, 10, 20, 40 and 60min (control sample at 60min only) and added to methanol, containing internal standard, (100 μ L) to stop the reaction. The samples were centrifuged, a volume of supernatant combined as a cassette of up to 4 compounds before being analysed by LC-MS/MS analysis.

The results of the intrinsic *in vitro* clearance were expressed as μ L/min/million cells or mL/min/g of liver. For each compound a single exponential decay equation was calculated from a time response plot Equation 40.

Equation 43

$$CL_{int} \left(\frac{\frac{\mu\text{L}}{\text{min}}}{\text{million}} \text{ cells} \right) = \frac{\frac{\text{Ln}2}{k}}{\text{Assay Cell Density}}$$

Equation 44

$$CL_{\text{int}} (\text{mL}/\text{min})/\text{g liver} = Cl_{\text{int}} (\mu\text{L}/\text{min}/\text{million cells}) \cdot SF \left(\text{million} \frac{\text{cells}}{\text{g}} \right)$$

CL_{int} = Intrinsic clearance, k = Elimination rate constant, SF= Scaling factor

The hepatocyte clearance was converted to the whole liver intrinsic clearance using an appropriate scaling method described below [83] (also see Figure 6.3-2 for examples of scaling methods).

Data from either the microsomal or hepatocyte assays were used to calculate the *in vivo* metabolic clearance with the following listed assumptions:

1. Distribution into the liver is perfusion rate limited and no diffusional barrier exists.
2. Only unbound drug crosses the cell membrane and occupies the enzyme site.
3. The hepatic enzymes have a homogenous distribution in the liver.

When these assumptions are considered, three models can be used: the well-stirred model; the parallel-tube model and the dispersion model (Figure 6.3-2). The well-stirred model is by far the simplest and most widely used, although variants are also used depending on the available data. Non-restrictive and restrictive versions of the equation are frequently used. The non-restrictive model is where protein and matrix binding are not taken into account, and the restrictive model is where protein binding as a minimum, and matrix binding can both be taken into account. The well-stirred model assumes homogeneous distribution of the drug in the liver, and that the drug concentration coming out of the liver is the same as the intracellular drug concentration.

Figure 6.3-2 The Schematic Illustration of Various Liver Models used to Estimate the *In Vivo* Hepatic Clearance from *In Vitro* Microsomal Stability Data [31].

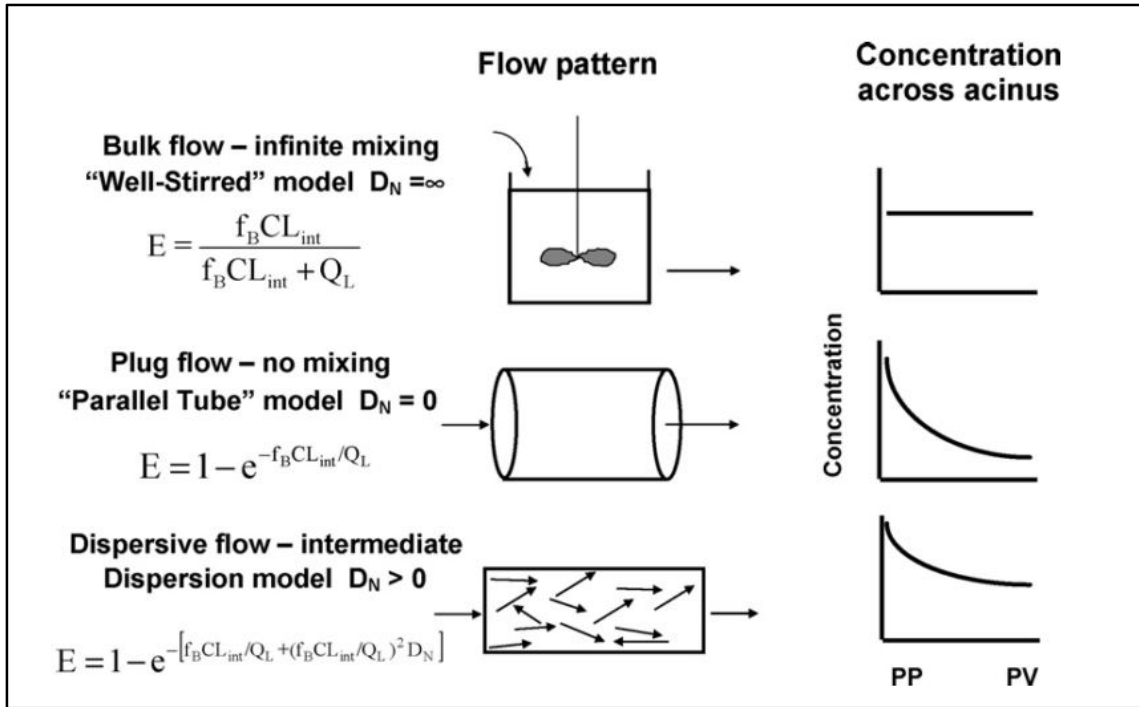


Figure 6.3-2 shows the different liver models used to estimate the *in vivo* hepatic clearance from *in vitro* stability data. D_N -system mixing rate, f_B – fraction unbound in blood, CL_{int} – intrinsic clearance, Q_L – liver blood flow.

D_N denotes the dispersion number and indicated that in the well stirred model the concentration throughout the liver was identical, whereas the parallel tube model represented the other end of the spectrum where there is no flow and therefore a concentration gradient across the liver. The Dispersion model is somewhere in between the two. There are other more complex zonal models of clearance, but these have not been considered and will not be referred to.

The well-stirred model was used here to calculate the estimated *in vivo* hepatic clearance from *in silico* or *in vitro* CL_i data, which was assumed to be the same as total clearance but did not account to any extra hepatic clearance that may have occurred *in vivo*.

Equation 45

$$CL_h \text{ (WSM non res)} = \frac{(CL_{int} \cdot SF) \cdot Q_h}{(CL_{int} \cdot SF) + Q_h}$$

Equation 46

$$CL_h \text{ (WSM res)} = \frac{\left(\frac{CL_{int}}{f_{uinc}} \cdot SF \cdot f_{ub}\right) \cdot Q_h}{\left(\frac{CL_{int}}{f_{uinc}} \cdot SF \cdot f_{ub}\right) + Q_h}$$

Where CL_{int} = *in vitro* clearance, f_{ub} = fraction unbound in blood, SF = scaling factor, f_{uinc} = fraction unbound in the matrix and Q_h = liver blood flow.

6.4 Experimental Methods to Measure Aldehyde Oxidase Metabolism from Cytosol and Lung Tissue

Aldehyde oxidase (AO) is an enzyme that is predominantly expressed in liver, however it is also known to be expressed in other tissues such as the respiratory, digestive and endocrine [125], but typically at much lower levels. AO is not related to Cytochrome P450, but is known to catalyse the oxidation of a wide range of endogenous and exogenous *N*-heterocycles and aldehydes, AO metabolism was first described by Beedham *et al* [126]. A standard metabolic stability screening strategy using microsomes (CL_{int}) would not detect whether a compound is a substrate for aldehyde oxidase. The method below was used as an *in vitro* procedure to determine if a chemical entity was a substrate for AO biotransformation, using liver cytosol or lung homogenate and LC-MS/MS for parent molecule or AO metabolite detection. Aldehyde Oxidase Liver Cytosol Multiple Species

In these liver cytosol studies, each test compound and a positive control from the GSK library was prepared as a 5 mM DMSO stock solution. A specific AO inhibitor isovanillin was also prepared at starting concentration of 11.1 mM. Liver Cytosol was purchased frozen in 1mL vials at a protein concentration of 10 or 20 mg/mL. For each assay, vials of cytosol for the relevant species being tested were thawed rapidly in a water bath at 37°C and pooled. The Cytosol was diluted with 50mM potassium phosphate buffer in order to obtain a 2.2 mg/mL protein concentration.

The AO inhibitor isovanillin was diluted to 1.1 mM with 50 mM potassium phosphate buffer. This solution was then incubated at 37°C, along with a separate aliquot of 50 mM

potassium phosphate buffer. Each test compound (potential AO substrate) was diluted to 50 μM with 10% DMSO (v/v aq).

For each compound and species duplicate wells containing 450 μL of 2.2 mg/mL cytosol and 45 μL either AO inhibitor (isovanillin at 1.1 mM in 50 mM potassium phosphate buffer) or buffer (50 mM potassium phosphate buffer) were prepared. This plate was maintained at 37°C in a heated water bath and referred to as the incubation plate.

An aliquot of 95:5 (v/v) acetonitrile:ethanol (extraction buffer), containing a suitable internal standard was added to each sample well of a 96 deep well plate in accordance with a pre prepared sample reference plate map. This plate was referred to as the extraction Plate.

To start the assay a 5 μL aliquot of test compound was added to allocated test wells of the Incubation plate (total incubation volume 500 μL - 2mg/mL cytosol, 0.5 μM test compound and were appropriate 100 μM on isovanillin). Immediately after compound was added, a 0 min sample aliquot (50 μL) from each incubation well was taken and dispensed into the allocated wells of the extraction plate. Further samples were taken from the incubation plate at pre-defined times e.g. 3, 6, 9, 15, 30, 45, 60 min and dispensed into the extraction plate. After the last sample was taken, the extraction plate was then centrifuged at 3500 rpm for 10 min. A volume of each supernatant was placed into a fresh 96 well plate and diluted with water. Each well was then assayed for test compound and internal standard in using LC-MS/MS.

6.4.1 Aldehyde Oxidase Mouse and Human Lung Homogenate

Lung tissue was weighed and transferred into Precellys™ homogenising tubes each containing ceramic beads. A volume of buffer (PBS -100 mM sodium phosphate + 150 mM sodium chloride pH 6.9 -7.2) was added to each tube before being homogenised in a Precellys 24 for 2 x 20 sec at 5500 rpm. The resulting lung homogenate was pooled into a single sterilin pot. An additional dilution step was performed to produce a 1:6 diluted lung homogenate.

For each compound and species duplicate vials containing 450 μL of lung homogenate and 45 μL either AO inhibitor (isovanillin at 1.1 mM in 50 mM potassium phosphate buffer)

or buffer (50 mM potassium phosphate buffer) were prepared. These vials were maintained at 37°C in a heated water bath.

An aliquot of 95:5 (v/v) acetonitrile:ethanol (extraction buffer), containing a suitable internal standard was added to each sample well of a 96 deep well plate in accordance with a pre prepared sample reference plate map. This plate was referred to as the extraction Plate.

To start the assay a 5 µL aliquot of test compound was added to allocated test wells of the Incubation plate (total incubation volume 550µL - 150mg/mL lung tissue, 0.5µM test compound and were appropriate 100uM on isovanillin). Immediately after compound was added, a 0 min sample aliquot (10 µL) from each incubation well was taken and dispensed into the allocated wells of the extraction plate. Further samples were taken from the incubation plate at pre-defined times e.g. 10, 20, 30, 60, 120, 180, 240 min and dispensed into the extraction plate. After the last sample was taken, the extraction plate was then centrifuged at 3500 rpm for 10 min. A volume of each supernatant was placed into a fresh 96 well plate and diluted with water. Each well was then assayed for test compound, the assumed MZ of the test compounds AO metabolite i.e. +16 of the test compound, isovanillin and internal standard, using LC-MS/MS.

6.4.2 Data analysis, interpretation and reporting

For each compound, a single exponential decay equation was calculated from the time response plot generated from the procedure above. Equation 40 represents a single exponential decay function used to calculate the elimination rate constant k.

Equation 40

$$y = A_0 \cdot e^{-kt}$$

Where A_0 = initial value, k = Elimination rate constant, t = time, e = exponential. This equation should be applicable for most datasets.

For stable compounds displaying a low elimination rate constant there was a minimum value that could be quoted, i.e. at least 15% disappearance of parent was required by

the last time point (e.g. in a 60 min assay, the elimination rate constant must be higher than 0.0027/ min (< -0.0027)) for an absolute value to be quoted). A 15% loss of parent was based on the inherent variability of the LC-MS/MS system, which determined the limit of quantification of the assay.

Regression statistics using a 95% confidence level were generated using an excel data analysis tool, which was calculated to ensure that the elimination rate constant measured was statistically different from zero based on a 95% confidence interval.

A compound was defined as an AO substrate when the turnover of parent compound had been fully inhibited in the presence of the AO inhibitor. Parent turnover continuing in the presence of the AO inhibitor may suggest that the compound could be a substrate for other cytosolic components, or degradation by other incubation conditions. If this occurred, the test compound could be confirmed as an AO substrate.

6.5 Experimental Methods to Measure Solubility in Simulated Lung Fluid (SLF) and Cell Permeability using MDCK Cells

6.5.1 SLF Solubility

Duplicate 1 mg compound samples were accurately weighed into two separate 2 mL glass screw cap vials. The standard vial (A) was dissolved in 1 mL DMSO. The second sample vial (B) had 1 mL of SLF added to it. The composition of SLF was phosphate buffer (pH 6.9) and 0.75 mM lecithin with 1 mg/mL bovine serum albumin (BSA). The sample vials were placed on a Tecan™ robot plate shaker for 4 hours at room temperature, shaking at 900 rpm. A 175 μ L sampling was then taken from each vial and dispensed into a 96-well filter plate, which was then vacuum filtered. The filtrate was quantified by HPLC relative to the standard peak area obtained from the compound standard (A) dissolved in DMSO. If there was no compound precipitation from the SLF sample (B) during the 4 h equilibration time, then the solubility of the compound was reported as 1 mg/mL. If no compound was detected in the SLF filtrate, then the solubility was reported to be less than 1 μ g/mL, which was the standard detection limit of the HPLC system. The standard error of the solubility determination was ± 30 μ g/mL. Compounds that had less than 10 μ g/mL solubility were considered to have low solubility, while compounds that had a measured concentration of over 300 μ g/mL were considered to

have high solubility. Larger molecular weight compounds generally appear to show higher $\mu\text{g/mL}$ solubility using this system, so when comparing the solubility of compounds that the molar concentration was used.

6.5.2 Cell Permeability

The Madin-Darby Canine Kidney (MDCK) cell permeability assay is based on the application of a MDCK cell monolayer between two buffer compartments (donor and acceptor compartments). The cell integrity on the 24-well Millipore filter plate was tested using Lucifer Yellow and fluorescence plate reader. The trans-epithelial electrical resistance (TEER) of the cell monolayers was measured to check the cell monolayer integrity. Elacridar was added to the donor compartment to inhibit the drug efflux transporter P-gp. The concentration of the test compound added to the donor compartment was 3 μM . The system was then equilibrated for 90 min and the concentrations of the compound in the donor and acceptor compartments were measured by LC-MS. The drug transport across the cell monolayers was measured in the apical to basolateral direction. The permeability (LogPapp) was expressed in nm/s. The average standard error of the assay was approximately ± 30 nm/s, however, it can be higher in the low permeability range. The typical permeability values measured by this method range between 3 to 600 nm/s. When permeability was measured as less than 10 nm/s, the compound was classed as low permeability. When the permeability was measured to be above 100 nm/s it was classed as high permeability.

6.6 Experimental Methods for Determining *In Vivo* IV Pharmacokinetics and Lung Retention.

6.6.1 Determining IV Pharmacokinetics in Mice

IV PK was generated using surgically cannulated male mice ($n=3$). The jugular vein was used for drug administration and direct venepuncture of the tail vein used for blood sampling. Compounds were typically dosed as a 1 h infusion at 1 mg/kg at an infusion rate of 5 mL/kg/h, formulated as solutions using 10% w/v kleptose.

Serial blood samples were taken at:

IV: 0.5 h, 1 h (end of infusion), 1.083 h, 1.25 h, 1.5h, 2 h, 4 h, 7 h, 12 h & 24 h.

All blood samples were taken into heparinised containers. Individual aliquots of blood were transferred directly into micronics tubes containing an equal volume of sterile water and stored frozen at -20°C prior to analysis by LC-MS/MS.

Preparation of diluted blood calibration standards:

A calibration line was prepared using a 1 mg/mL stock solution. The stock solution was diluted to 200 µg/mL by diluting 20 µL in 80 µL acetonitrile:water (50:50 by volume).

The 200µg/mL solution was then used to prepare a 2000 ng/mL standard. This was done by adding 2.5 µL of the 200 µg/mL solution to 247.5 µL of diluted blood (equivalent to a concentration of 4000 ng/mL in whole blood). The equivalent blood concentration was used for analysis as this corrects for the sample dilution. Standard curves were prepared for a blood concentration range of 1 to 4000 ng/mL by serial dilution in diluted blood. A final sample volume of 20 µL was used.

Preparation of blood samples for analysis:

All of the 20 µL aliquots standards were all transferred in to micronic tubes for extraction along with a 50 µL aliquot of control matrix which was used as a matrix blank sample.

All diluted blood samples and standards were extracted by protein precipitation by adding 400 µL of 95:5 ACN: Water containing 100 ng/mL of internal standard to each sample. The samples were then mixed on a plate shaker for at least 5 minutes. The samples and standards were centrifuged for at least 10 minutes at 3500rpm and then 20 µL aliquots of each supernatant was removed and transferred to a fresh 96-well plate where 300 µL of water was then added. The samples were then mixed on a plate shaker for at least 5 minutes before being analysed by LC-MS/MS.

The resulting concentration-time data were used to determine various PK parameters such as CL_b , V_{dss} , $T_{1/2}$, C_{max} and AUC using WinNonlin non-compartmental analysis (NCA).

6.6.2 Determining IV Pharmacokinetics in Rats

IV PK was generated using surgically cannulated male Wistar Han rats (n=1 to 3). The femoral vein was used for drug administration and the jugular vein for blood sampling. Compounds were typically dosed as a 1 h infusion at 1 mg/kg at an infusion rate of 5 mL/kg/h, formulated as solutions using 10% w/v kleptose. Rats were individually housed in metabolism cages where urine was collected over 24 h and used to measure the contribution of renal elimination.

Serial blood samples were taken at:

IV: pre-dose, 0.25 h, 0.75 h, 1 h (end of infusion), 1.083 h, 1.25 h, 1.5h, 1.75 h, 2 h, 3 h, 5 h, 8 h, 13 h & 24 h.

All blood samples were taken into heparinised containers. Individual aliquots of blood were transferred directly into micronics tubes containing an equal volume of sterile water and stored frozen at -20°C prior to analysis by LC-MS/MS.

Preparation of diluted blood calibration standards:

A calibration line was prepared using a 1mg/mL stock solution. The stock solution was diluted to 200 µg/mL by diluting 40 µL in 160 µL acetonitrile:water (50:50 by volume).

The 200 µg/mL solution was then used to prepare a 2000 ng/mL standard. This was done by adding 5µL of the 200 µg/mL solution to 495 µL of diluted blood (equivalent to a concentration of 4000 ng/mL in whole blood). The equivalent blood concentration was used for analysis as this corrects for the sample dilution. Standard curves were prepared for a blood concentration range of 1 to 4000 ng/mL by serial dilution in diluted blood. A final sample volume of 50 µL was used.

Preparation of blood samples for analysis:

All of the 50 µL aliquots standards were all transferred in to micronic tubes for extraction along with a 50 µL aliquot of control matrix which was used as a matrix blank sample.

All diluted blood samples and standards were extracted by protein precipitation by adding 250 μL of 95:5 ACN: EtOH containing 100 ng/mL of internal standard to each sample. The samples were then mixed on a plate shaker for at least 5 minutes. The samples and standards were centrifuged for at least 10 minutes at 3500rpm and then 100 μL aliquots of the supernatants was removed and transferred to a fresh 96-well plate where 200 μL of water was then added. The samples were then mixed on a plate shaker for at least 5 minutes before being analysed by LC-MS/MS.

The resulting concentration-time data were used to determine various PK parameters such as CL_b , V_{dss} , $T_{1/2}$, C_{max} and AUC using WinNonLin non-compartmental analysis (NCA)

6.6.3 Determining IV Pharmacokinetics in Minipig

IV PK was generated using male Göttingen minipigs (n=2). Temporary cannula were placed in a hind leg vein (e.g saphenous vein) and was used for drug administration and a temporary cannula was also placed in an ear vein or minimise the use of direct venepuncture for blood sampling. The leg vein cannula was used for blood sampling for later timepoints if required once the cannula had been flushed and enough time had passed to ensure no dosed remained at the site of administration. Compounds were typically dosed as a 10-minute infusion at 1 mg/kg at an infusion rate of 6 mL/kg/h, formulated as solutions using 10% w/v kleptose.

Serial blood samples were taken at:

IV: 0min (pre-dose), 10min (end of infusion), 15min, 40min, 1h, 2 h, 4 h, 7 h, 12 h & 24 h.

All blood samples were taken into heparinised containers. Individual aliquots of blood were transferred directly into micronics tubes containing an equal volume of sterile water and stored frozen at $-20\text{ }^{\circ}\text{C}$ prior to analysis by LC-MS/MS.

Preparation of diluted blood calibration standards:

A calibration line was prepared using a 1 mg/mL stock solution. The stock solution was diluted to 200 µg/mL by diluting 40 µL in 160 µL acetonitrile:water (50:50 by volume).

The 200 µg/mL solution was then used to prepare a 2000 ng/mL standard. This was done by adding 5 µL of the 200 µg/mL solution to 495 µL of diluted blood (equivalent to a concentration of 4000 ng/mL in whole blood). The equivalent blood concentration was used for analysis as this corrects for the sample dilution. Standard curves were prepared for a blood concentration range of 1 to 4000 ng/mL by serial dilution in diluted blood. A final sample volume of 50 µL was used.

Preparation of blood samples for analysis:

All of the 50 µL aliquots standards were all transferred in to micronic tubes for extraction along with a 50 µL aliquot of control matrix which was used as a matrix blank sample. All diluted blood samples and standards were extracted by protein precipitation by adding 250 µL of 95:5 ACN: EtOH containing 100ng/mL of internal standard to each sample. The samples were then mixed on a plate shaker for at least 5 minutes. The samples and standards were centrifuged for at least 10 minutes at 3500 rpm and then 100 µL aliquots of the supernatants was removed and transferred to a fresh 96-well plate where 200 µL of water was then added. The samples were then mixed on a plate shaker for at least 5 minutes before being analysed by LC-MS/MS.

The resulting concentration-time data were used to determine various PK parameters such as CL_b , V_{dss} , $T_{1/2}$, C_{max} and AUC using WinNonLin non-compartmental analysis (NCA)

6.6.4 Determining Lung Exposure in Mice

A lung PK/Exposure study utilised 18 female Balb/C mice n=3/observation to generate a blood and lung PK profile. The mice were placed under light anaesthesia using isoflurane to facilitate intranasal (IN) administration of an IN dose volume sufficient to result in lung delivery of the test compound, before being allowed to recover.

The dose for lung retention studies was typically 1 mg/kg for lung retention studies, with a dose volume of 50 μ L (this dose volume had been determined internally within GSK by imaging techniques, eLNB reference N4373-30): the dose concentration was 0.4 mg/mL. The dose formulation was saline (0.85% NaCl w/v pH6) or 10% w/v kleptose depending on the solubility of the molecule being administered, to ensure the dose was administered as a solution. The compound was administered as a solution to determine the “intrinsic lung retention” by removing low solubility as a factor which would enhance lung retention.

Serial blood samples were taken at 10 min, 30 min, 1, 3, 5, 8 and 12 h after dosing, with terminal blood and lung samples collected (n=3 per time point) at the times indicated above to establish serial blood and composite blood and lung profiles. All blood samples were taken into heparinised containers. Individual aliquots of blood were transferred directly into micronics tubes containing an equal volume of sterile water and stored frozen at -20°C prior to analysis by LC-MS/MS.

Preparation of diluted blood calibration standards:

A calibration line was prepared using a 1mg/mL stock solution. The stock solution was diluted to 200 μ g/mL by diluting 20 μ L in 80 μ L acetonitrile:water (50:50 by volume).

The 200 μ g/mL solution was then used to prepare a 2000 ng/mL standard. This was done by adding 2.5 μ L of the 200 μ g/mL solution to 247.5 μ L of diluted blood (equivalent to a concentration of 4000 ng/mL in whole blood). The equivalent blood concentration was used for analysis as this corrects for the sample dilution. Standard curves were prepared for a blood concentration range of 1 to 4000 ng/mL by serial dilution in diluted blood. A final sample volume of 20 μ L was used.

Preparation of blood samples for analysis:

All of the 20 μ L aliquots standards were all transferred in to micronic tubes for extraction along with a 50 μ L aliquot of control matrix which was used as a matrix blank sample. All diluted blood samples and standards were extracted by protein precipitation by adding 400 μ L of 95:5 ACN: Water containing 100 ng/mL of internal standard to each sample. The samples were then mixed on a plate shaker for at least 5 minutes. The samples and standards were centrifuged for at least 10 minutes at 3500 rpm and then 20 μ L aliquots

of each supernatant was removed and transferred to a fresh 96-well plate where 300 μ L of water was then added. The samples were then mixed on a plate shaker for at least 5 minutes before being analysed by LC-MS/MS.

Preparation of compound standards in tissue homogenate:

A calibration line was prepared using a 1 mg/mL stock solution by taking 8 μ L of the 1 mg/mL stock solution and pipetting directly onto a control mouse lung in a Precellys® homogenising tube containing ceramic beads to which 1 mL of water was added. The lung was then homogenised using a Precellys® 24 for 2x20sec at 6500 rpm, a further 1 mL of water was then added and the sample was mixed. This homogenate now contained the highest standard concentration of 8000 ng/lung and was then used to generate the remaining standard line range by serial dilution across a range of 0.4-8000 ng/lung.

All *in vivo* study lungs were homogenised as detailed above.

A 20 μ L aliquot of homogenate from each standard and *in vivo* sample was transferred to a clean micronic tubes for extraction along with an additional 20 μ L aliquot of blank control matrix to be run as a matrix blank sample. All standards and *in vivo* samples were extracted by protein precipitation by adding 400 μ L of 95:5 ACN:Water containing 100 ng/mL of internal standard to each sample. The samples were then mixed on a plate shaker for at least 5 minutes. The samples and standards in the micronic tubes were then centrifuged for 10 minutes at 3500 rpm. A 20 μ L aliquot of the supernatants was then transferred to a new 96-well plate and 300 μ L of water was added to each sample. The plate was then mixed on a plate shaker for at least 5 minutes before being analysed by LC-MS/MS. The lung concentrations were converted from ng/lung to ng/g using the individual tissue weights.

Concentration-time data were used to determine various PK parameters such as C_{max} and AUC in both blood and lung using WinNonLin non-compartmental analysis.

6.6.5 Details of the Intra-Nasal Dose Technique

The IN dose was administered to mice under light isoflurane-induced anaesthesia. The dose was applied to the external nares (25 μ L each side, 50 μ L in total). Care had to be

taken to avoid application of the dose to the lips or mouth. The animals were returned to holding cages and continuously observed until they had recovered from anaesthesia.

Dosing solutions were stored at room temperature before and after dosing (to limit the risk of precipitation) and kept for dose analysis if required.

The same IN dosing technique was used for PKPD experiments. However, due to animal PD model tolerability, the compounds were only formulated using a simple saline formulation with pH adjustment if required.

6.6.6 Inhalation Studies in Rodents

In vivo inhalation studies are complex due to multiple variables that effect these studies such as respiration rate, location of animals on dosing towers due to different API cloud concentrations (Figure 6.6-1), particle size of the API being dosed and doses are calculated as whole body doses rather than delivered dose.

An important starting point for inhalation studies prepare the API for inhalation and determine API particle size to ensure it is within the respirable range. The API particle size was measured by the Product Development group at GSK to ensure the particle size was in the respirable range of 1-5 μM . The particle size was described as the Mass Median Aerodynamic Diameter (MMAD), which was the average diameter if API particles following micronisation. This value is specific for each batch of micronised compound. The batch of GSK3454697 dose *in vivo* had an MMAD of 2.1 μM . The PK data generated from an *in vivo* inhaled mouse study using GSK3454697 was used to validate the PBPK model.

The MMAD was generated using a device called a cascade impactor, the data generated from the filters in this device indicated 48% of particles on stage 6, with an average of 80% stages 6, 7 & 8. The cascade impactor is a multistage column, containing 9 stages with each stage separated by a filter, drug particles were drawn through the cascade impactor using a vacuum pump. Each filter becomes finer moving along the column: particles moving down the column were captured by the filters separating the larger from the smaller particles. The respirable range is generally considered to be between 1 and 5 μM and are typically captured by stage 6.

A pre-study inhalation dose test was performed before every inhaled *in vivo* study using an aerosol generator, either a Wrights Dust Feeder (WDF) or Capsule Based Aerosol Generator (CBAG) along with the dosing tower to be used during the planned *in vivo* study (Figure 6.6-1 and Figure 6.6-2, respectively). To help set and calibrate the correct dose a pre study run was done with a cascade impactor as described above, which was placed on a port on the dosing tower. The inhalation dose was then calculated based on the flow rate, concentration of API on the different filters along with the respirable rate of the species being dosed. This process would be repeated for each batch of API material. Once a pre-study dose was determined that falls within the target dose range, the same CBAG settings were used for the *in vivo* inhaled mouse study, or the process was repeated to adjust the equipment to achieve the desired target dose.

Once the API and towers have been prepared following pre-study dose runs. Inhaled disposition data was generated using male Balb/C mice (up to n= 33/tower). Animals were placed dosing tubes and connected to the tower ports. Inhalation time was 20 min at a flow rate to achieve the target dose.

Lung samples and composite blood samples (n=3)

IH: 0.25 h (inhalation period) IAD, 0.5 h, 1 h, 2 h, 4 h, 7 h, 12 h & 24 h.

All blood samples were taken into heparinised containers. Individual aliquots of blood were transferred directly into micronics tubes containing an equal volume of sterile water and stored frozen at -20 °C prior to analysis by LC-MS/MS.

Blood and lung samples were extracted, and concentrations of test compound were quantified as described in Section 6.6.4.

Concentration-time data were used to determine various PK parameters such as C_{max} and AUC using WinNonLin non-compartmental analysis

Figure 6.6-1 An Inhalation Tower with a Wrights Dust Feeder (for Aerosol Generation) for Rodent Inhaled Dose Studies

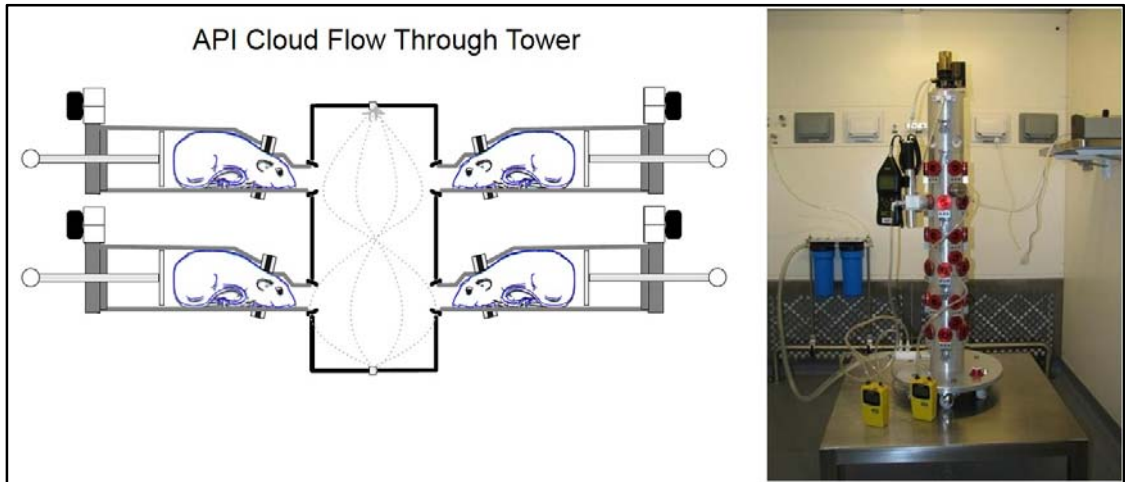


Figure 6.6-1 Shows a picture of a large-scale inhalation dosing tower with a WDF attached used for rodent PK and PKPD studies. The red ports are where the animal holding tubes are attached, the tower can hold up to 33 dosing tubes.

Figure 6.6-2 An Inhalation Tower with a Capsule Based Aerosol Generator (CBAG) used for Low Dose Rodent Inhaled Dose Studies

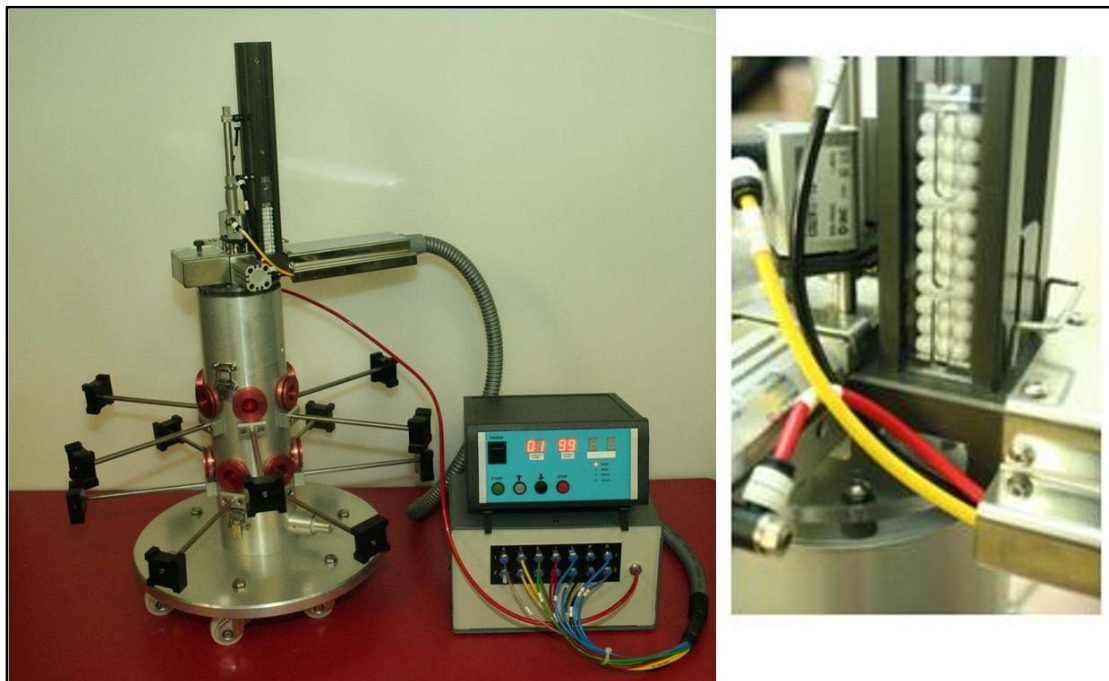


Figure 6.6-2 Figure 6.6-2 Shows a picture of a small-scale inhalation dosing tower with a CBAG attached used for rodent PK and PKPD studies. The red ports are where the animal holding tubes are attached, the tower can hold up to 9 dosing tubes.

6.7 *In Vitro* Enzyme and Cellular Potency Measurements of PAN JAK 1/2/3 Inhibitors

A commercially available kit provided by Perkin-Elmer was used. The LANCE Ultra time-resolved fluorescence resonance energy transfer (TR-FRET) assay uses a proprietary europium chelate donor dye, W-1024m with Ulight, a small molecular weight acceptor dye with a red-shifted fluorescent emission. The kinase assay utilizes the binding of a EU-labelled antiphospho-substrate antibody to the phosphorylated Ulight labelled substrate, which brings donor and acceptor molecules into close proximity. After irradiation of the kinase reaction at 320 or 340 nm, the energy from the EU-donor is transferred to the EU acceptor dye which, in turn, light is emitted at 665 nm. The intensity of the light emission is proportional to the level of Ulight substrate phosphorylation. TR-FRET assay measures the phosphorylation of the tyrosine kinase phosphorylation site

Tyr-1023 based on the synthetic substrate peptide (CAGAGAIETDKEYYTVKD) which has been derived from the JAK-1 phosphorylation site. The kinase assay was performed in 96-well plates using buffer that contained 10 mM MgCl₂, 50 mM/L HEPES (pH7.5) and 1 mM/L dithiotreitol (DTT) and 0.01% bovine serum albumin (BSA). The enzyme reaction contained 50 µM/L of peptide, ATP was added at the apparent K_m for the assay (1.8 µM/L for PAN JAK 1/2/3). Reactions were incubated for 90 min at room temperature and stopped with a detection mixture containing Eu-PT66 Antibody. Plates were then incubated for another 30 min before reading the TR-FRET signal using an excitation setting of 320 nm and emission collection at 665nm and 665 nm.

The cytokine-stimulated pSTAT5 (Signal Transducer and Activator of Transcription) detection assay were carried out using human lung fibroblasts. Cells were pre-treated with the compounds for 30 min at 37°C followed by stimulation with IL-30. The control well contained unstimulated fibroblast cells that were exposed only to buffer.

6.8 Assessment of Unbound Drug Fraction in Blood and Lung Homogenate by Rapid Equilibrium Dialysis (RED)

The unbound fraction of each test compound was determined in blood and lung homogenate, using the RED device for rapid equilibrium dialysis and by LC-MS/MS analysis.

The assay procedure was as follows: a fresh or frozen mouse lung (typical weight 0.2g) was weighed and placed in a 2mL Precellys™ homogenising tubes which were prefilled with ceramic beads. 1mL of buffer was also added (PBS – 100 mM sodium phosphate + 150 mM sodium chloride, pH 6.9 - 7.2) before being homogenised (2 x 20 s at 6500 rpm). The resulting homogenate was further diluted with 0.8 mL PBS buffer to create a 1 in 10 to buffer to tissue ratio.

Fresh blood (from the species required) was collected in hepronised tubes prior to the study and diluted 1:1 (v/v) with PBS (100 mM sodium phosphate + 150 mM sodium chloride, pH 6.9 - 7.2).

A 1 mg/mL DMSO stock solution for each test compound was prepared before being further diluted to 200 µg/mL using acetonitrile:water (50:50 v/v). 10 µL of the 200 µg/mL

solution added to a 1990 μL aliquot of diluted blood result in a nominal starting concentration of $1\mu\text{g/mL}$ containing $<1\%$ organic solvent.

For each compound and species 3 buffer chambers were pre-loaded with the relevant volume of dialysis buffer in line with manufacturers recommendations. The relevant volume of spiked sample matrix in line with manufacturers recommendations was then placed in the 3 corresponding sample chambers of RED insert identified by red ring.

The RED plate was then covered with sealing tape and incubated at 37°C at approximately 100rpm on an orbital shaker for a minimum of 4 hours (no greater than 18 hours).

At the end of the incubation period a sample from each well was transferred and individually matrix matched with either control buffer, diluted blood or lung homogenate in a clean 96-well plate. All samples then underwent precipitation using 95:5 ACN: EtOH containing an internal standard compound. This plate was then centrifuged at 3500 rpm for 10 mins before an aliquot of supernatant was removed and diluted with water for LC-MS/MS analysis. The fraction of compound bound to protein was calculated using the peak area ratio. A correction factor was used to account for the blood dilution or lung homogenate dilution. This methodology has been previously described by Kalvass and Maurer [127].

6.9 Computational and Visualization Tools Applied in the Data Analysis and Evaluation of the Reliability of Various Dose Prediction Methods

Project compounds that are discussed in this project and used as examples for dose estimation did not all have *in vitro* and *in vivo* data available depending on their progression point. In such cases *in silico* calculated data was used from computation models that had been developed and validated by GSK computational chemists. A brief description of these *in silico* models is given below.

6.9.1 *In silico* Volume of Distribution Model (Model not published)

Volume of distribution has been described in Section 4.1.2 is an experimental *in vivo* PK parameter. Therefore, reduce the use of animals *in silico* models can help to give initial estimations to help with compound design at the early stages of a drug discovery program.

The GSK QSAR volume of distribution model was built by computational modellers at GSK using *in vivo* rat data this section gives a general overview of how the model was built indicating what properties were most influential to the model output. V_{dss} data was expressed as L/kg which was converted to a logarithmic scale to Log normalise the data. A dataset of 1178 compounds was divided into training and test sets at the beginning of the model build. Any data that had been reported as less than or higher than values were not included in the model. Once the model was built, a validation set of compounds was used which was also downloaded from the company database; these data had been posted after the model build and was used to further validate the accuracy of the model. The *in silico* model was based on the assumption that the chemical structure and the physicochemical properties of the compounds would relate to the *in vivo* volume of distribution.

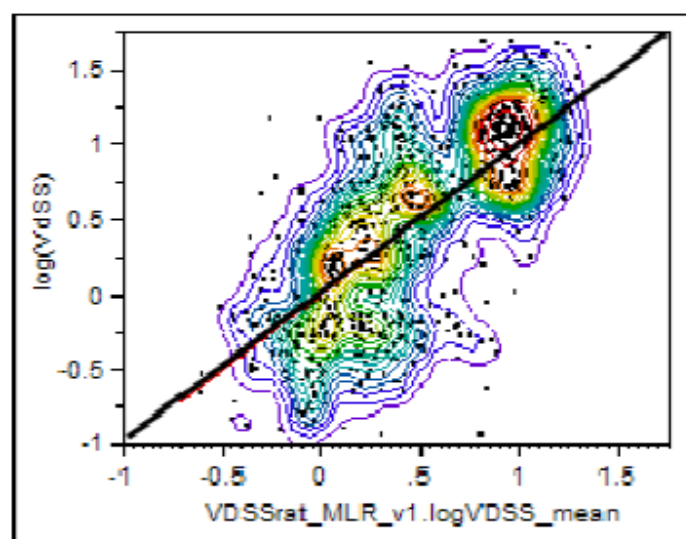
Standard *in silico* physicochemical properties, such as, lipophilicity, log P, log D, polar surface area, molecular weight, H-bond donor and acceptor groups and fragment E-state parameters (topological physical properties) were calculated for each data set. Models were initially built using all of the descriptors, but after a principal component analysis only the first three principal components were used as dependent variables. The models were further refined based on the coefficients and loading plots. Descriptors with minimal influence on the first two principal components were removed. Ultimately, a sufficient number of descriptors were removed to afford the generation of a simple linear regression model (MLR). Using this approach, a QSAR model was generated. The model predictions are illustrated in Figure 6.9-10.

The results show that approximately 50% of the variance in the dataset was described by the model in the training, test and validation sets. Although there is a slight drop off in the predictive ability from the training/test set to the validation set, examination of the root mean square error shows only a small difference, indicating the model prediction error

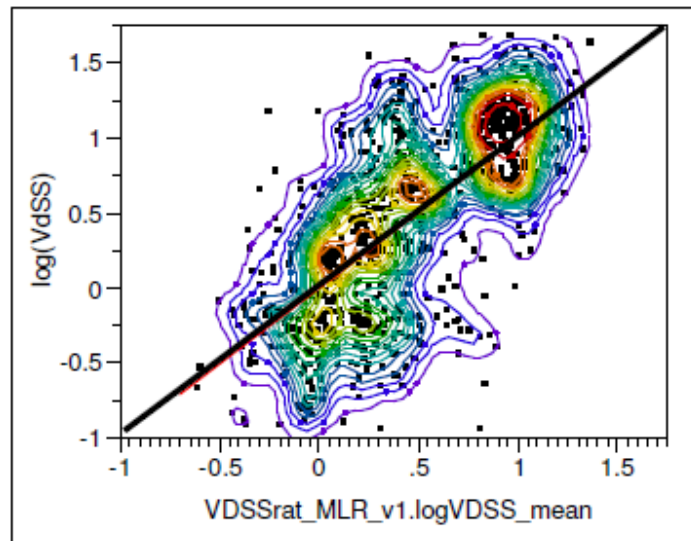
did not change. The statistically significant descriptors in the model correspond to the previous knowledge of structural factors affecting the volume of distribution, such as the ionisation of acids decreases the volume of distribution, while ionisation of bases typically increased volume of distribution. More lipophilic compounds generally have a higher volume of distribution. The E-stat F sum descriptor showed the number of fluorine atoms in a compound, while the NHR2acuc_sum descriptor shows the number of acyclic secondary NH groups (like amine, amide, urea) that significantly influenced the model. The third significant parameter was the basic NH_sum, showing the number of basic NH groups influenced the volume of a compound.

Figure 6.9-1 Plot of observed vs predicted volume of distribution for a) training set; b) test set and c) validation set of compounds.

a)



b)



c)

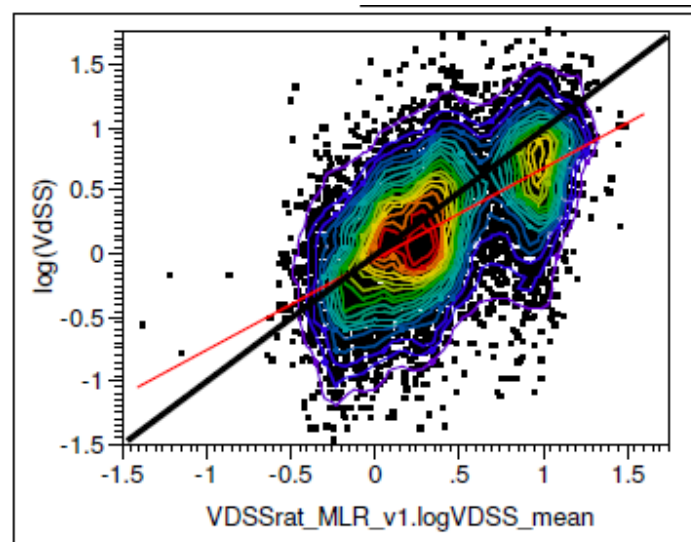


Figure 6.9-1 Red contours represent areas of maximum density while blue areas represent the areas of lowest density.

We can see in Figure 6.9-1 (a, b and c) that visually the model error is quite substantial at 0.7 – 1 Log V_{dSS} unit (L/kg). However, it is still very useful as this data can be used in the early dose estimation equation.

6.9.2 *In silico* Clearance Model (This model has not been published)

The GSK QSAR CL_i model was built by computational modellers at GSK using human *in vitro* microsomal data. This section gives a general overview of how the model was built indicating what properties were most influential to the model output. The continuous intrinsic model is based on physicochemical properties, and E-state descriptors. The model includes the *in silico* prediction of Cytochrome P450 inhibition and smart fragments. The model predicted the clearance value with a 3-fold error (equivalent to a 0.5 log unit error). The model also provided a categorical prediction for clearance. The categorical prediction placed compounds with less than 2 mL/min/g tissue as low clearance, 2 to 10 mL/min/g tissue as medium clearance and over 10 mL/min/g tissue as high clearance. The clearance models were built based on the data of 9,000 compounds, with approximately 3,000 compounds for each clearance category. The model was validated using a set of 18,644 compounds from the GSK database. All values were Log transformed to ensure there was a normal distribution of the data prior to the modelling work.

The correlation was limited experimental and predicted data ($r^2=0.37$). These results show that the model is able to predict 37% of the variance. The prediction error of 0.5 Log units was comparable with the errors obtained in other GSK *in silico* models for CYP P450 inhibition. The statistical characteristics of the model shows how difficult it was to predict the metabolic stability of the compounds using only fragments and simple physicochemical properties. The limited accuracy of this type of model is because it was unable to describe a compound's interaction with multiple enzymes with different specificities using simple physicochemical parameters. It is important to understand that enzyme binding also depends on the 3D structure and this model only used a 2D description of the compounds. In general, clearance increased with increased lipophilicity and size of a compound. Acid and base character and polarity can lower intrinsic clearance. The number of rotatable bonds was observed to increase the clearance in this model, this was associated with inhibition of CYP3A4.

The model was reported to have been applied in 25 GSK projects showing that 25% of measured *in vitro* data was predicted resulting in a correlation coefficient of 0.6. Observed versus predicted CL_{int} is shown in Figure 6.9-2.

Figure 6.9-2 Observed and Predicted Intrinsic Clearance for a Set of Selected Projects. The Colours are Based on “Daylight” Clustering (similarity >0.7).

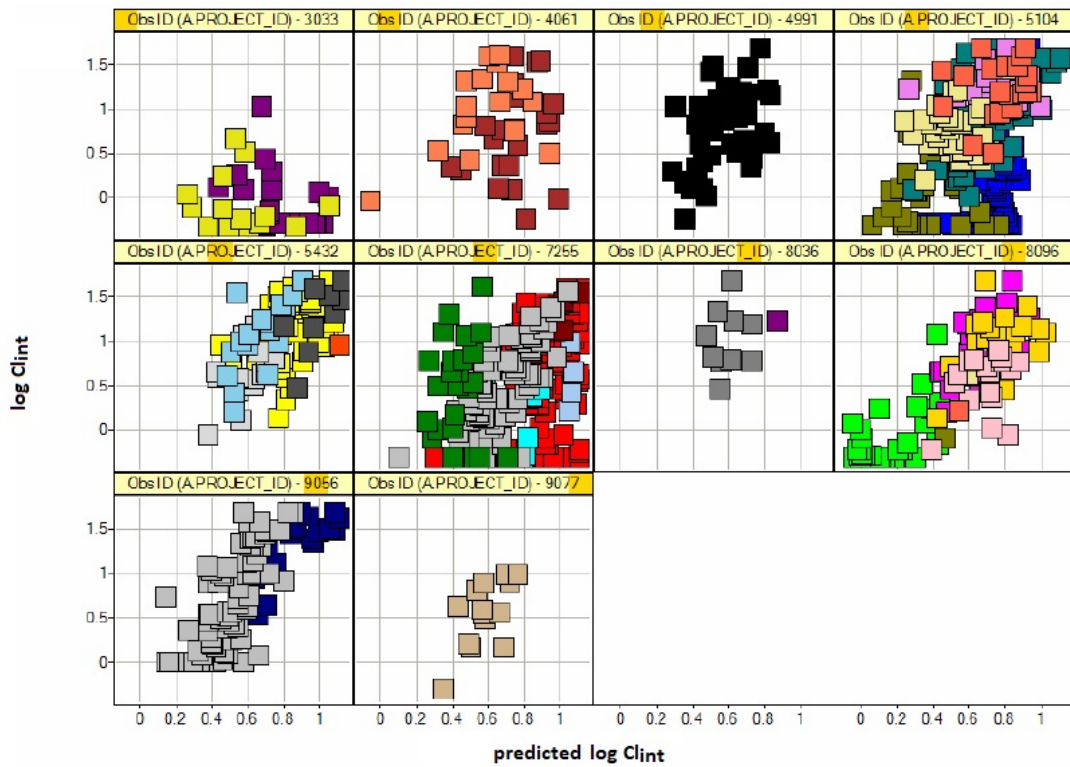


Figure 6.9-2 Colours represent different chemical series within each project

6.10 Physiologically Based Pharmacokinetic Modelling

Physiologically Based Pharmacokinetic (PBPK) models represents an increasingly important and complex method of modelling PK profiles and estimating dose. I have used PBPK in this project to help understand the relationship between concentration and effect for the inhaled JAK program. This section describes the some of the background and concepts used in PKPB modelling.

The PBPK models differ from the classical pharmacokinetic PK models in that they include specific tissues as separate compartments that are involved in exposure, toxicity, biotransformation and clearance and they are connected by the blood flow. The schematic diagram of PBPK models are shown in Figure 6.10-2.

The ACAT model (advanced compartmental absorption and transit model) is a series of differential equations which enables a mathematical description and interpretation of *in vivo* drug behaviour Figure 6.10-1, shows there are a total of nine compartments, where each compartment is further divided into four sub compartments: unreleased, undissolved, dissolved, and enterocyte (pink boxes). Each arrow in Figure 6.10-1 represents a process, and therefore is described mathematically by a differential equation.

The unreleased row of sub compartments is used only for controlled release dosage forms. For controlled release, the drug can be released into solution (dissolved) or as solid particles (undissolved). Undissolved drug undergoes dissolution and only then becomes available for absorption, carrier-mediated transport, and luminal degradation. Undissolved (solid particles) and dissolved (drug in solution) drug undergoes first order transit through the GI tract. The transit of unreleased drug is modified for Gastric Release. An oral drug is eventually excreted from the colon if it is not absorbed before the end of the transit process.

An oral drug is only considered to have been absorbed from the GI tract in the ACAT model when it enters the enterocytes. This definition of absorption is used by the FDA and others in the pharmaceutical industry. Many earlier definitions of “absorption” in the literature often referred to the fraction reaching the portal vein, and some use it to mean to the fraction of drug which reached the systemic circulation (bioavailability). It is

important to distinguish among these definitions, especially when comparing the results of simulations generated by GastroPlus™ to other PBPK software with values reported in literature. To help compare literature values, GastroPlus™ helpfully reports F_a , FD_p (fraction dose reaching portal vein), and F . Drug absorption can be passive process, driven by the concentration gradient across the apical barrier, or it can be a transporter mediated process as a result of uptake and efflux transporters in the enterocytes. It is important to note that when absorbed a drug can also be subject to metabolism in the enterocytes. Once drug crosses the basolateral intestinal barrier, it reaches the portal vein and then the liver. Both arterial and venous blood mix in the liver. First pass extraction and systemic extraction of drug both take place in the liver. Drug escaping metabolism reaches the systemic circulation from where it can distribute to peripheral compartments. The peripheral compartments can then be described by a classic empirical Compartmental PK model, or by numerous physiological tissues in a PBPK model (see Figure 6.10-2). Renal and other forms of elimination can occur from the central compartment.

Compartments and blood flows are described using physiologically meaningful parameters, such as tissue sizes and compositions, which allows for interspecies extrapolation by altering the physiological parameters appropriately [128]. The advantages of PBPK modelling are that factors influencing absorption, distribution, metabolism and excretion can be incorporated into the models in a meaningful way. This mechanistic aspect is supported by physiological parameters influencing absorption such as pH, transit times and differences between species can also be explained. Empirical PK modelling has been used to a great extent for interspecies extrapolation, both among animal models and predicting human PK based on animal data [85]. The PBPK approach has several advantages over other PK modelling approaches. It creates models from physiological, biochemical and anatomical information. It evaluates the mechanisms by which biological processes govern disposition of a wide range of compounds. The development of PBPK modelling is based on the research between blood and tissue concentrations and administered dose and can be used to explain pharmacological action by the presence of the free drug at the site of action. It can be applied in safety evaluation [128].

Initially the PBPK models provided a set of equations for uptake, distribution and elimination of drugs in the body. The simplified equations treated the metabolism,

distribution and elimination processes as first-order, meaning that the rates changed in direct proportion to drug concentration. Later it was realised that saturation of elimination path-ways made it difficult to derive exact solutions to the equations. It was also realised that the blood flow rather than the metabolic capacity of an organ might limit the clearance. This meant that the blood-flow limited the metabolism in an organ and that the elimination rate could not increase indefinitely as the metabolic capacity increased [129]. The PBPK models require physiological, physicochemical and biochemical parameters as input. Over the past 10 years, the capabilities of PBPK models that can simulate PK for humans or preclinical species based on the combination of physicochemical properties and *in vitro* data has advanced significantly. PBPK models can be constructed using program packages such as MATLAB. Powerful commercially available PBPK simulation tools are also available such as GastroPlus™ (Simulations Plus Inc.), SimCyp™ (SimCyp Inc) or PK-SIM™ (Bayer Technology Services).

The current applications of PBPK in the pharmaceutical industry is widespread and it starts with the lead optimisation process or earlier. PBPK modelling can be used in the design of pre-clinical animal experiments. In the lead optimisation stage, the first information generated for NCE's are the *in silico* calculated physicochemical parameters, such as lipophilicity expressed cLogP, pKa, solubility, permeability (P_{eff}) and protein binding. *In vitro* measurements of metabolic stability (measured by microsomes or hepatocytes) are used as inputs, while the physiological parameters for various species are built into the software. Many *in silico* parameters will be followed up with *in vitro* measurements to increase confidence in the models for example plasma protein binding might then be measured to determine if a compound will have sufficient free concentration for therapeutic efficacy [130].

6.10.1 The Advanced CAT (ACAT) model

The original compartmental absorption and transit (CAT) model was developed under the direction of Gordon Amidon at the University of Michigan to estimate the fraction of dose absorbed and the rate of drug absorption for passively transported drugs in immediate release products [131]. The CAT model was a dynamic model designed to simulate and predict how the fraction of an oral drug was absorbed through the human gastrointestinal (GI) tract [131]. The CAT was developed as a dynamic model as it included time in the mathematical coding. GI transit time is a fundamental element of GI absorption and the

CAT model is referred to as a transit model because it describes the flow of a drug through the GI tract.

In the original CAT model, the GI tract was divided into a set of seven small intestinal compartments. The transit of drugs through the seven compartments was described by a set of ordinary differential equations with equal transit times.

This model did not account for the finite rate of dissolution, the pH dependence of solubility of drugs, controlled release, absorption in the stomach or colon, gut metabolism, carrier-mediated transport, exsorption/secretion, pharmacokinetics, or regional changes in such factors as surface area, influx or efflux transporter densities, and other factors within the intestinal tract. For drugs that are absorbed in the colon, the CAT model could be made more accurate by treating the colon as an additional absorbing compartment. In many cases, colonic absorption is a negligible fraction of the total for immediate release formulations; however, many immediate release and most controlled release formulations can have significant colonic absorption, frequently exceeding absorption in the small intestine. Simulations Plus, Inc, developed a new more sophisticated and complex model called the Advanced Compartmental Absorption and Transit model (ACAT) to include all of the effects listed above (see Figure 6.10-1).

Figure 6.10-1 ACAT Model (Taken from the GastroPlus™ User Guide)

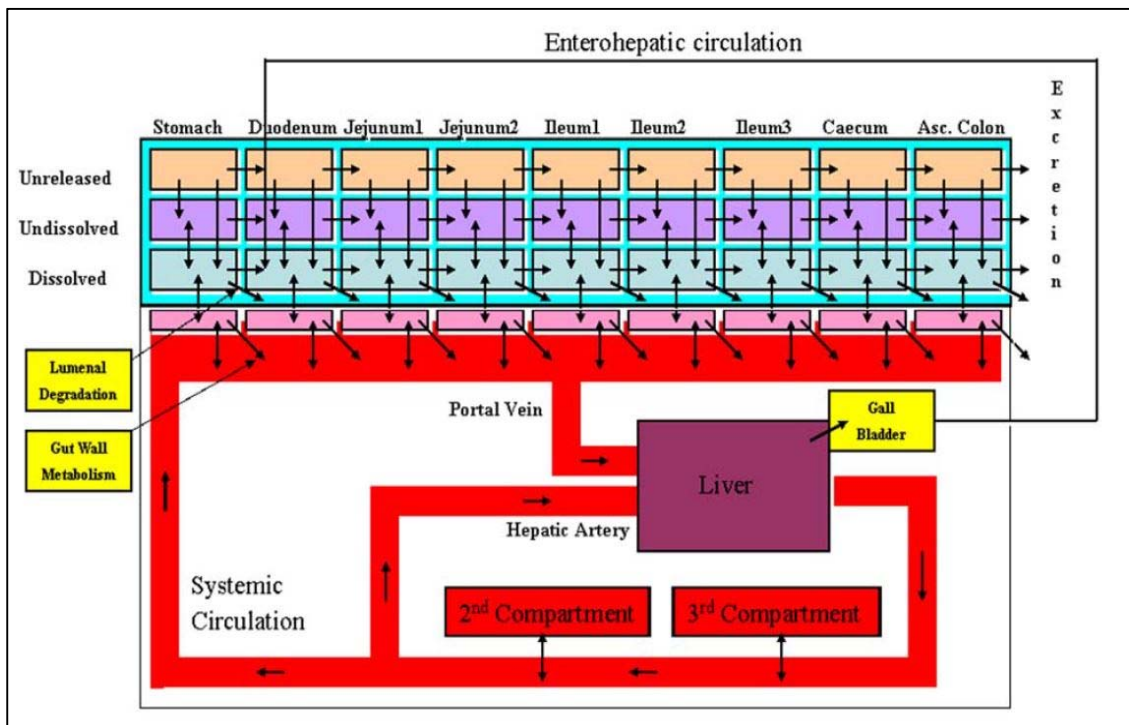


Figure 6.10-1 shows the different compartments and directional flow of the ACAT model. Following the arrows from the stomach illustrates the theoretical paths a drug would follow through the GI tract and potential absorption into the systemic circulation depending on the biopharmaceutical properties of the drug substance being administered.

Figure 6.10-2 The Schematic Illustration of the Principals of the Physiologically Based Pharmacokinetic (PBPK) Modelling Approach for the ACAT Model [132].

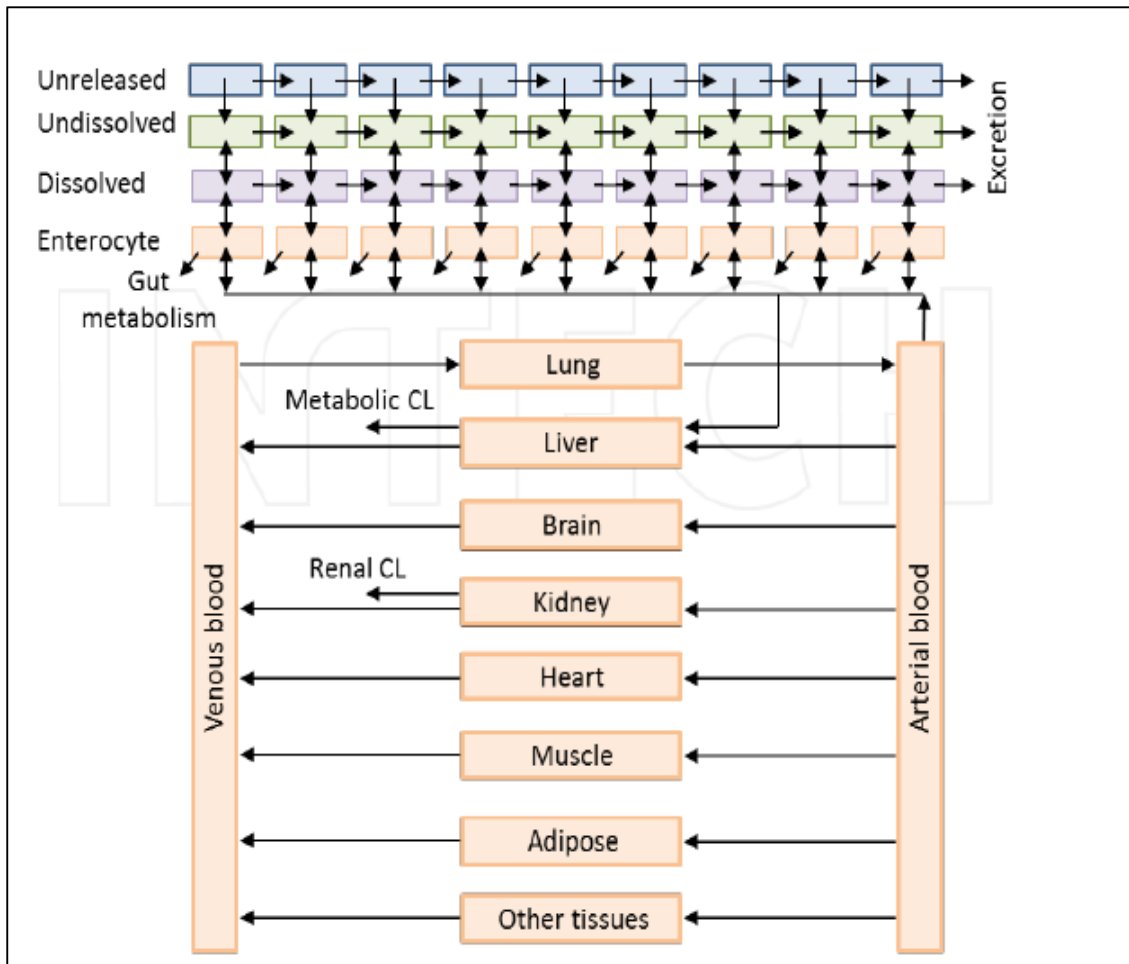


Figure 6.10-2 Shows the ACAT model and its interface with a multi tissue PBPK model

There is also a nasal-pulmonary module available in GastroPlus™. The Nasal-Pulmonary Compartmental Absorption & Transit Model (N-PCAT model) can also be linked to a PBPK model for drugs delivered via either the inhaled or nasal-pulmonary routes in a similar way to the ACAT model for oral drugs as previously described. This new nasal-pulmonary model takes into account the deposition and distribution to the lung and absorption through the lung based on the anatomical and physiological attributes of the lung.

The nasal-pulmonary model can simulate a variety of dosage forms which are currently used in the clinic and describe how they can be distributed in the pulmonary compartments (including the anterior nasal passage) or primarily the nose. This implementation includes up to five compartments: an optional nose (containing the anterior nasal passages), extrathoracic (naso- and oro-pharynx and the larynx), thoracic (trachea and bronchi), bronchiolar (bronchioles and terminal bronchioles) and alveolar-interstitial (respiratory bronchioles, alveolar ducts and sacs and interstitial connective tissue). A schematic diagram of how the different compartments are connected to one another and the rest of the body is shown in Figure 6.10-3.

Figure 6.10-3 Nasal-Pulmonary Compartmental Absorption & Transit Model (N-PCAT Model)

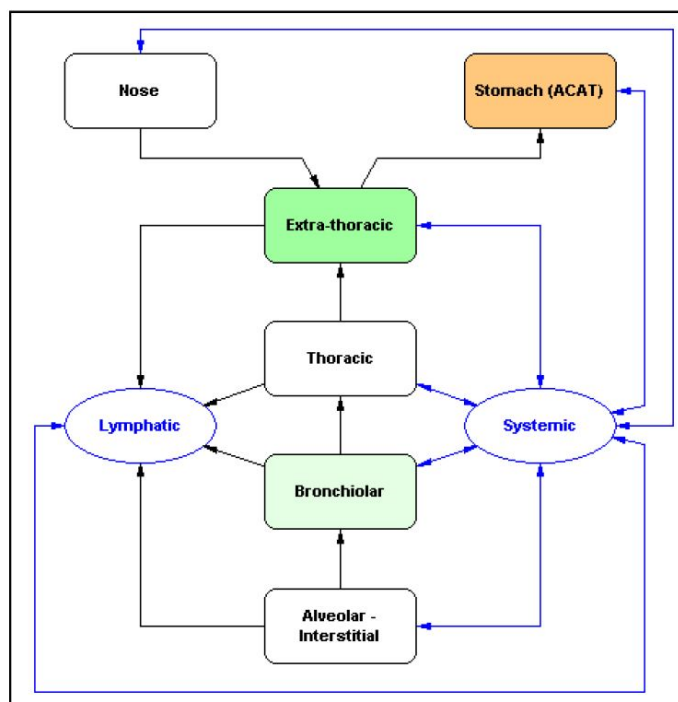


Figure 6.10-3 N-PCAT Model schematic interface showing the main compartments and directional flow of the nasal-pulmonary system.

Figure 6.10-4 shows a more detailed description of the 5 compartments of the pulmonary module described in Figure 6.10-3, which help explain how a solid drug particle moves through the lung once deposited in the nasal-pulmonary system to eventually dissolve

and reach the systemic or lymph systems, or be cleared from the pulmonary system via the mucociliary transfer or escalator.

Figure 6.10-4 A Schematic Illustration of the Principals of Nasal-Pulmonary Compartmental Absorption & Transit Model (N-PCAT Model), Applying Similar Principles to those used for the ACAT model.

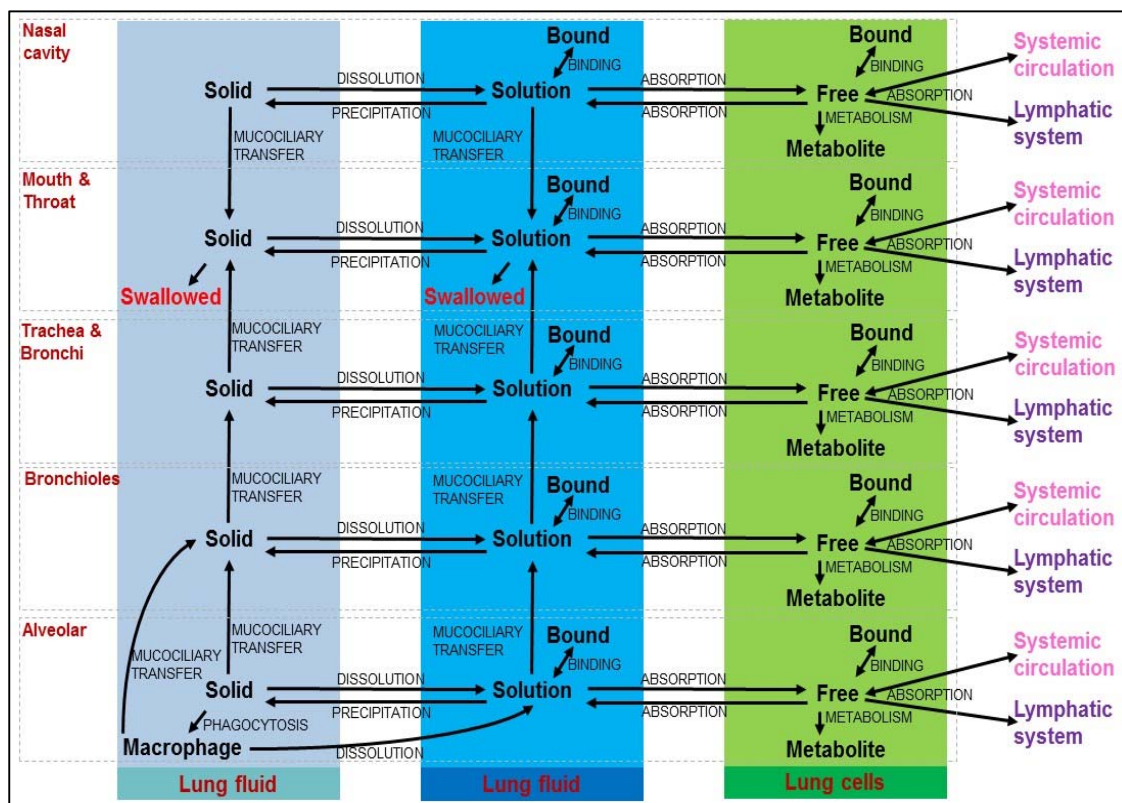


Figure 6.10-4 Shows N-PCAT Model in GastroPlus™

Figure 6.10-5 shows how both the ACAT and N-PCAT models are integrated onto the PBPK functionality of GastroPlus™ to enable PK models to be developed and simulations run to help describe the PK profile of a drug in both pre-clinical species and ultimately to human simulations to predict the exposure and efficacy (PKPD) of a drug.

Figure 6.10-5 The Schematic Illustration of the Principles of the PBPK Modelling Approach Combining the N-PCAT and ACAT Models.

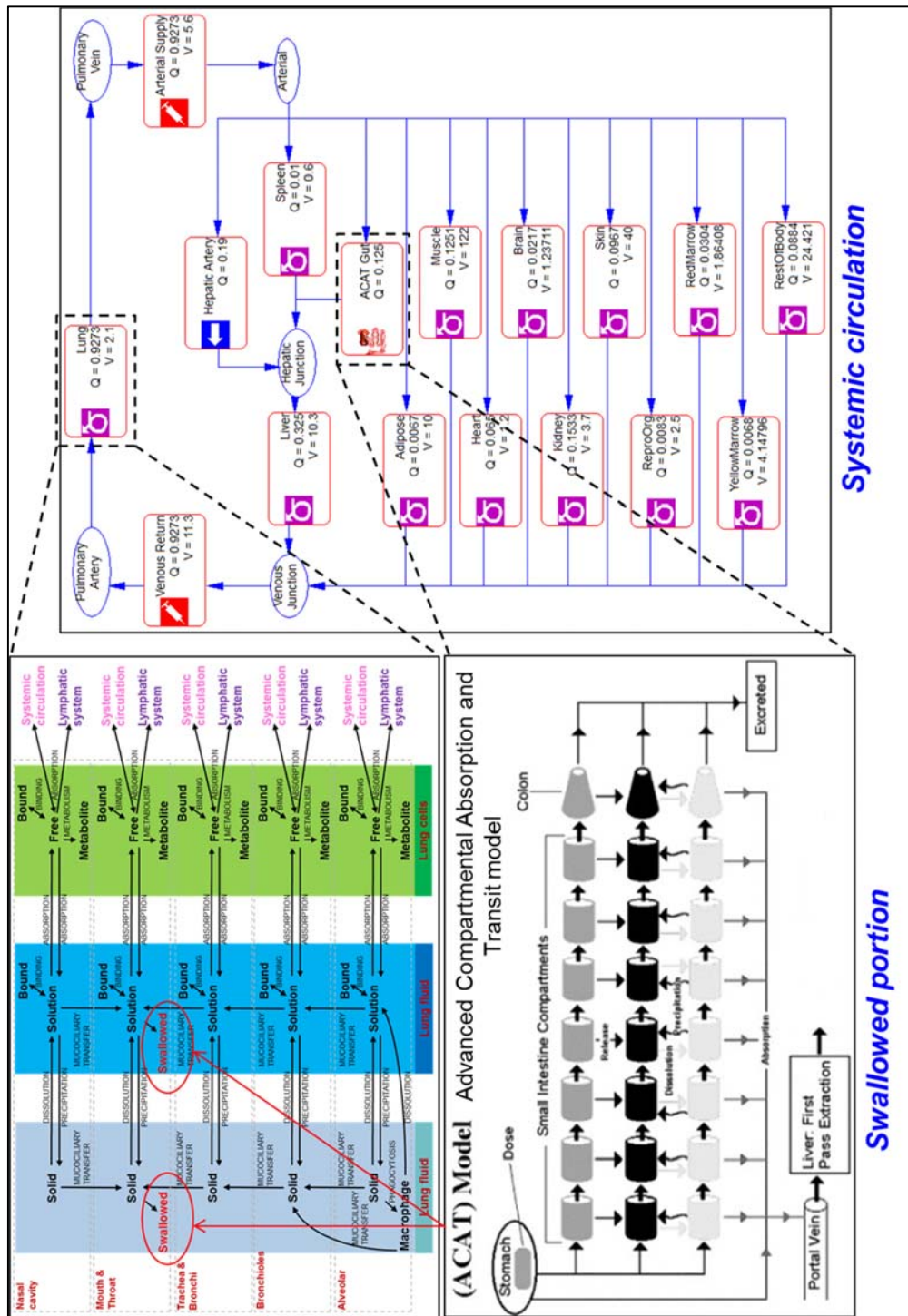


Figure 6.10-5 Shows how both the ACAT and N-PCAT models are integrated in a PBPK model (GastroPlus™). The ACAT and N-PCAT models are shown in greater detail and higher resolution on Figures 6-1-1 and 6-10-4

Figure 6.10-6 The Model Window in GastroPlus™ for Inhaled Drug Deposition, Distribution and Absorption.

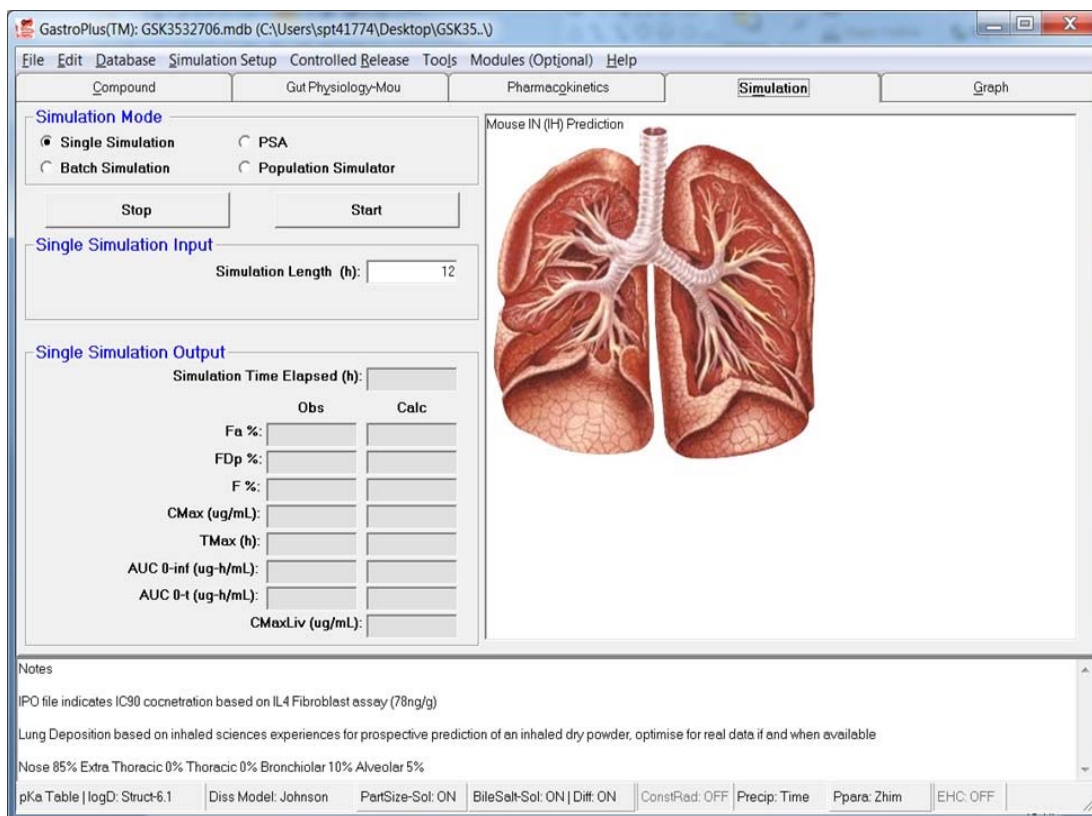


Figure 6.10-6 Nasal-Pulmonary GUI GastroPlus™

GastroPlus™ was used to model and simulate the PK and PK/PD data from the lung retention studies and PKPD studies for the PAN JAK inhibitor program which will be discussed in a later (Section 7.8).

6.10.2 Physiologically Based Pharmacokinetic Modelling using GastroPlus using an Early Lead JAK Inhibitor to Establish Mouse Physiological Settings

For the PBPK analysis the GastroPlus standard physiology parameters are set for multiple species (e.g. mouse, rat, dog, monkey and human). However, for the pulmonary PBPK module of GastroPlus standard lung physiologies are available for mouse, rat and human but they are not as well defined as the GI physiologies. The standard mouse

physiology was the least described and used many of the rat parameters. Therefore, it was important to update the mouse physiology to ensure it would be as representative as possible to enable effective PBPK models to be generated.

The surface area for each lung compartment was reduced by 10-fold, based on alveolar area being 10-fold lower in the mouse than rat [133](p.123). Airway mucus thickness was assumed to be the same as a rat, which was based on rat and human values being similar [133] (p.621). Pulmonary cell thickness was assumed to be the same as a rat based the values being reported in a similar range [133] (p.66). The systemic absorption rate constants (SARC) were set to 0.983/s in the nose and alveolar interstitial (AI) compartments, this value scaled on body weight between rat and mouse. The upper and lower bronchiolar was set to 4.9e-9/s based on similar scaling as the nose and AI compartments. Total lung volume was 0.184mL [134].

The systemic concentration time profile output for GastroPlus is plasma. Therefore, *in vivo* concentration time data generated from whole blood was converted to plasma using Equation 47.

Equation 47

$$f_{up} = f_{ub} \cdot (B/P)$$

f_{up} , is the fraction unbound in plasma, f_{ub} is the fraction unbound in blood, B/P is the blood/plasma ratio

Therefore, if the B:P for a compound was 0.8:1, then the blood concentration would be lower than in plasma due to a compounds higher affinity for whole blood. So, when blood levels are measured from an *in vivo* study then the blood/plasma partition has to be used to convert the concentration to an effective plasma concentration. When compounds were administered to mice via the intranasal (IN) route, they were often dosed as suspensions. To account for this in the dose administered in a PBPK model a mixed multiple dosing (MMD) setting was used. This enabled the dose to be split into dissolved and undissolved fractions based on a compounds solubility when prepared as an IN suspension dose. For example, an MMD used was 0.003mg (ca. 15%) in solution, 0.017mg (ca. 85%) powder. The purpose of this was to ensure a model was able to correctly estimate the deposition and lung retention.

It was noted that the version of GastroPlus™ used had several software bugs. One example was the need to switch between mixed multiple dose input and a standard pulmonary dose to enable model adjustments in the pulmonary module before switching back to the MMD setting to run simulation. To optimise the lung deposition profile the following parameters were used: Final Deposition profile = Nose 50% Extra Thoracic 24.5% Thoracic 0.25% Bronchiolar 0.25% Alveolar 25%. These settings were used to build additional pulmonary PBPK models with only minor adjustments required to correctly predict compound deposition and absorption.

Figure 6.10-7 shows the screen shot from GastroPlus™ for mouse physiology, highlighting the nose and lung compartments which are characterised in the nasal pulmonary module of GastroPlus™.

Figure 6.10-7 Naso-Pulmonary Module Screen Shots for Mouse Physiology

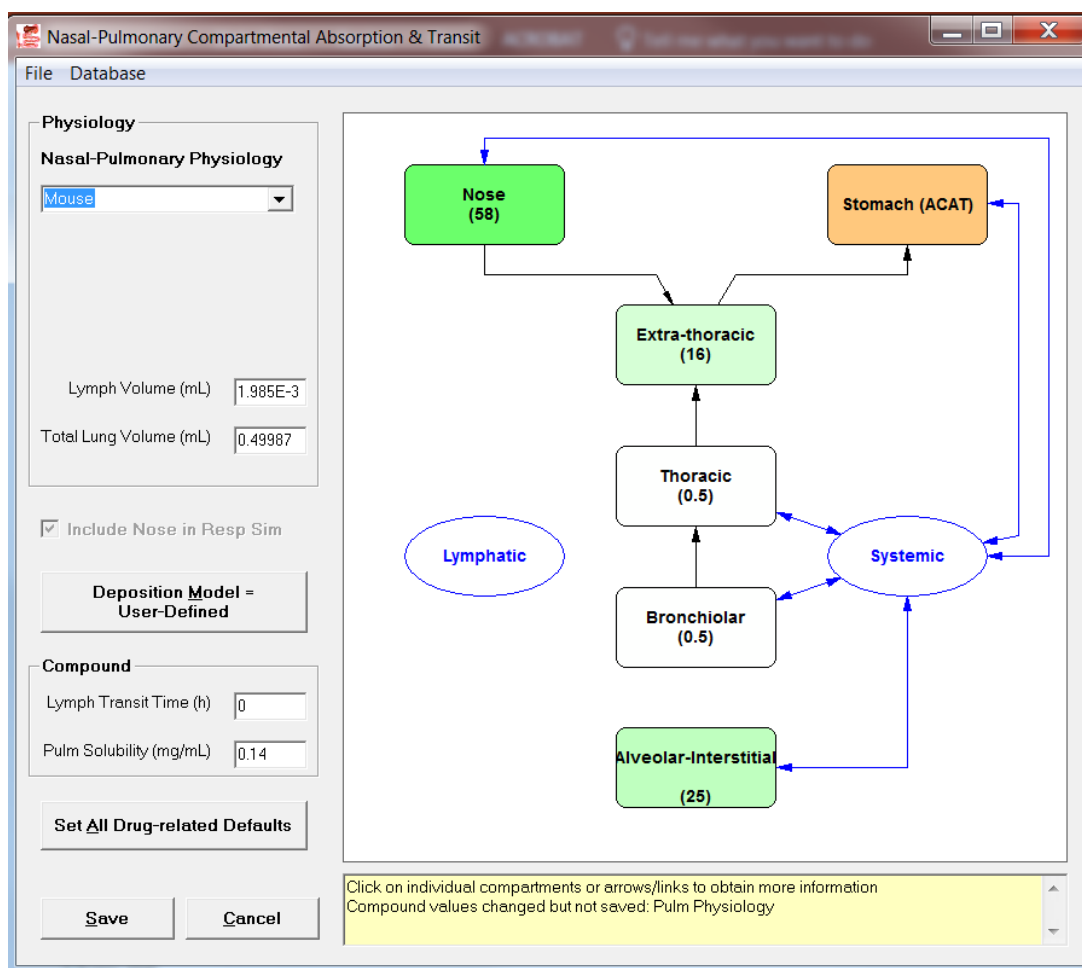


Figure 6.10-7 Shows a schematic of the nose and lung compartments and parameters such as pulmonary solubility and drug deposition applied to the Naso-Pulmonary module of GastroPlus™.

Screen shots from GSK3454697 model as an example. This screenshot is a simple schematic of the main features of the pulmonary module. It is within each component that the pulmonary settings were adjusted as described earlier. It should be noted that permeability, lung tissue and cell binding values are compound specific but physiology which include SARC values, mucus thickness, epithelial thickness and mucociliary transit times should transfer between models. For unbound concentrations in mucus, whole blood binding or PPB binding and for estimating the unbound concentration of the drug in cells the lung tissue binding data were used. Adjustment of deposition profile was required, Figure 6.10-8 shows an example of how this was done for GSK3454697.

Figure 6.10-8 Regional Deposition Profile Settings within GastroPlus

Regional Deposition Calculation

Database Options

Deposition Model:
User-Defined

ICRP 66 Settings
Resting
 Inhalability is Unity

Carrier Information
Carrier mass (mg) 0
Carrier density (g/mL) 1
API CutOff Rad (um) 3
Carrier Size: R=25, D=50
API Size: R=25.00, D=50.00
Compare Fractions

% Deposited in
Nose (ET1) 58
Extra-Thoracic (ET2) 16
Thoracic (BB) 0.5
Bronchiolar (bb) 0.5
Alveolar-Interstitial 25
Exhaled (Custom)
Redistribute Deposition Fractions
% Exhaled = 0.0

OK Cancel

Figure 6.10-8 shows a schematic of the regional disposition used in the Naso-Pulmonary module of GastroPlus™. The species physiology can be selected, and the deposition profile of the drug can be adjusted here.

7 Results and Discussion

7.1 Evaluation of Methods for Dose Prediction at the Early Stages of Lead Optimisation: A Comparison using the Data of Known Drug Molecules

The drug efficiency ($DRUG_{eff}$) concept introduced by Braggio *et al* [27] and described in section 4.2.4, was proposed as a new tool to guide drug discovery program teams, as it relates to the free drug concentration in the target bio-phase relative to the administered dose (Equation 31).

In this analysis, clinical data such as the volume of distribution, clearance, dose, and dosing frequency of 136 marketed drug molecules were obtained from various databases (www.drugbank.ca/drugs and www.Drugs.com) and are listed in Table 7-1 and Table 7-2 together with their *in vitro* pIC_{50} values. The biomimetic albumin and phospholipid binding of these drugs were measured using albumin and immobilised artificial membrane (IAM) HPLC stationary phases as described in references [135] & [136]. The HPLC DE_{max} values were calculated from the measured albumin and phospholipid binding for the known drug molecules listed in Table 7-3, using the sum of the two types of binding as described in the model published by Valko *et al.* [77]. The lipophilicity of the compounds has also been measured by an HPLC method using the Chromatographic Hydrophobicity Index (CHI) approach [137]. The $CHI/LogD$ values have been measured across a pH range of pH 2, pH 7.4 and pH 10.5 to obtain the $CHI/LogD$, $CHI/LogP$, and the acid/base character for each compound as described by Valko *et al.* [138]. Based on the lipophilicity at three pHs, the acid/base character of each drug molecule was determined indicating the presence of positive, negative or no charge. The acid/base classification has been shown on all plots in order to reveal if there are significant trend differences depending on the charge state.

The compounds in Table 7-1 to Table 7-3 have been colour coded to define the acid / base class, which shows the colour key for the acid / base class and matches the legend keys in all graphs where the acid / base class has been defined.

Table 7-1 The Various *In Vivo* ADME Properties for the 136 Marketed Drugs.

Acid/Base Class	Colour Key
Acidic	
Basic	
Neutral	
Weak Acid	
Weak Base	
Amphoteric	
Zwitterionic	
Not Classified	

DRUG	Actual daily dose (mg)	pIC ₅₀	Doses/day	Calculated dose using <i>in vivo</i> data (mg)	pIC ₅₀ expressed from MEC using actual dose	Acid/Base Colour Key
ACETYLSALICYLIC ACID	1200	5.5	4	353.4	4.92	
ALLOPURINOL	300	5.3	1	370.4	5.36	
AMILORIDE (HCl)	5	5.5	1			
CANDESARTAN CILEXETIL	8	10.5	1	<0.1	6.11	
DIAZOXIDE	150	4.7	3	13.5	3.62	
DIFLUNISAL	1000	4.2	2	66.1	3.06	
ETODOLAC	600	6.2	2	7.3	4.26	
FLURBIPROFEN	200	6.2	4			
FUROSEMIDE	80	5	2	243.8	5.48	
GLIBENCLAMIDE	3	5.3	1	138.4	7.07	
GLIMEPIRIDE	1	5.4	1	47.1	7.05	
GLIPIZIDE	3	5.5	1	34.7	6.66	
INDOMETACIN	75	6.5	3	7.1	5.46	
IRBESARTAN	150	9.3	1		5.48	

DRUG	Actual daily dose (mg)	pIC ₅₀	Doses/day	Calculated dose using <i>in vivo</i> data (mg)	pIC ₅₀ expressed from MEC using actual dose	Acid/Base Colour Key
KETOPROFEN	225	7.6	3	0.4	4.92	
MYCOPHENOLIC ACID	1440	8	2	0.3	4.31	
NAPROXEN	1000	5.2	2			
NIMESULIDE	400	4.4	2			
OXAPROZIN	1200	5.7	2			
PIROXICAM	20	6.7	1			
PRAVASTATIN SODIUM	40	8.2	1	1.9	6.84	
PROBENECID	1000	3.8	2	496.8	3.52	
SULFINPYRAZONE	100	3.3	1	3322.1	4.8	
TOLMETIN SODIUM	1800	6.8	3			
ZAFIRLUKAST	40	8.4	2	0.5	6.5	
ACEBUTOLOL (HCl)	400	6.8	2	26.9	5.59	
ALBUTEROL SULFATE	8	7.4	4	3.4	7.03	
AMITRIPTYLINE (HCl)	50	6.2	1	55	6.19	
AMOXAPINE	300	6.5	3			
ARIPIRAZOLE	10	9.7	1	<0.1	6.23	
ATOMOXETINE (HCl)	40	8.7	1	0.2		
BUPROPION (HCl)	300	6.3	1			
CABERGOLINE	0	10	0			
CITALOPRAM (HBr)	20	8.3	1	0.3	6.5	
CLEMASTINE FUMARATE	3	8.6	2			
CLOMIPRAMINE (HCl)	25	7.9	1	1.6	6.68	
CLONIDINE (HCl)	0	8.5	1	0.1	8.02	
DESLORATADINE	5	9.4	1			
DIPHENHYDRAMINE (HCl)	75	8.1	3	0.9	6.19	
DOMPERIDONE	30	9.8	3		6.79	

DRUG	Actual daily dose (mg)	pIC ₅₀	Doses/day	Calculated dose using <i>in vivo</i> data (mg)	pIC ₅₀ expressed from MEC using actual dose	Acid/Base Colour Key
DONEPEZIL (HCl)	5	8.2	1	0.3	6.87	
EBASTINE	60	7.7	3			
FEXOFENADINE (HCl)	60	7.3	2			
FLUOXETINE (HCl)	60	8.6	1			
FLUVOXAMINE MALEATE	50	8.3	1			
GRANISETRON (HCl)	2	9.9	2	<0.1	7.82	
GUANABENZ ACETATE	8	8.2	2			
HALOPERIDOL	2	10	2		7.83	
IMIPRAMINE (HCl)	75	6.6	1	47.2	6.35	
LOXAPINE SUCCINATE	40	8.3	2			
MAPROTILINE (HCl)	75	4.4	3	7219.8	6.37	
MEFLOQUINE (HCl)	1250	4.5	1	218.5	3.71	
METERGOLINE	8	9.4	1			
METOCLOPRAMIDE (HCl)	20	8.4	2	0.3	6.59	
MIANSERIN	60	8.1	2			
MIBEFRADIL (Di HCl)	50	6.2	1	64.5	6.26	
NEOSTIGMINE BROMIDE	15	7.4	1	3.4	6.8	
NORTRIPTYLINE (HCl)	75	9	3	0.1	6.21	
OLANZAPINE	10	7.5	1	3.1	7.01	
PERGOLIDE MESYLATE	0	8.9	1			
PIMOZIDE	8	9.6	2			
PRIMAQUINE PHOSPHATE	15	5.4	1	257	6.66	
PROCHLORPERAZINE MALEATE	15	8.5	3	1	7.26	
PROMETHAZINE (HCl)	50	8.2	2	1.2	6.56	
PROPAFENONE (HCl)	450	5.7	3	502.1	5.75	
PROPRANOLOL (HCl)	160	9.4	2	0.1	5.95	

DRUG	Actual daily dose (mg)	pIC ₅₀	Doses/day	Calculated dose using <i>in vivo</i> data (mg)	pIC ₅₀ expressed from MEC using actual dose	Acid/Base Colour Key
PROTRIPTYLINE (HCl)	15	5.6	3			
QUININE SULFATE	1800	6.3	6	14.2	4.2	
SELEGILINE (HCl)	10	8.1	1	1.4	7.24	
SUMATRIPTAN	75	8.1	3	2.2	6.54	
TAMSULOSIN (HCl)	2	11	2	<0.1	6.86	
VENLAFAXINE (HCl)	75	7.7	2	3.3	6.38	
VERAPAMIL (HCl)	120	6.9	3	47.4	6.5	
ZOLMITRIPTAN	8	8.1	3	0.7	7.07	
BICALUTAMIDE	50	6.1	1			
CAFFEINE	150	4.7	3	227.7	4.92	
CARBAMAZEPINE	800	4.6	1			
CELECOXIB	400	8.5	2	0.3	5.46	
DAPSONE	100	4.8	1	82.7	4.74	
FELBAMATE	1200	3.4	3	2030.1	3.66	
FELODIPINE	5	9.8	1	<0.1	7.59	
FLUTAMIDE	750	5.9	3			
ISRADIPINE	5	6.6	2	111.7	7.95	
LEFLUNOMIDE	100	4.9	1			
LETROZOLE	3	7.9	1	0.1	6.47	
LORAZEPAM	3	8.9	3	<0.1	6.69	
LOVASTATIN	10	9.5	1	<0.1	7.13	
METHYLPREDNISOLONE	4	6.3	1	56.5	7.42	
METOLAZONE	3	5.7	1			
NEVIRAPINE	200	8	1	<0.1	4.26	
NIMODIPINE	120	9.6	4	0.1	6.38	
NISOLDIPINE	20	9.8	1	<0.1	7.13	

DRUG	Actual daily dose (mg)	pIC ₅₀	Doses/day	Calculated dose using <i>in vivo</i> data (mg)	pIC ₅₀ expressed from MEC using actual dose	Acid/Base Colour Key
NITRENDIPINE	20	7.6	2	9.5	7.32	
PENTOXIFYLLINE	800	3.7	2	10000	5.8	
PROCYCLIDINE (HCl)	8	8.6	3		6.18	
ROLIPRAM	1	6.7	1			
SPIRONOLACTONE	100	4.7	1			
THIOTHIXENE (HCl)	6	9.7	3			
VALDECOXIB	10	8.4	1			
ZILEUTON	2400	6.5	2			
BENDROFLUMETHIAZIDE	3	3.4	1			
DIDANOSINE	250	8	2	1.2	5.68	
INDAPAMIDE	1	4.2	1			
PHENYTOIN	90	4.2	1			
ZIDOVUDINE	500	8	5	3.1	5.79	
ABACAVIR	600	7.2	2	12.1	5.46	
ACRIVASTINE	32	8.5	4			
ALOSETRON (HCl)	1	7.3	2	5.9	8.07	
AMINOGLUTETHIMIDE	500	4.9	2			
DIPYRIDAMOLE	200	6.7	2	13.3	5.54	
FENOFIBRATE	145	4.7	1	59	4.35	
KETOCONAZOLE	200	4.7	1			
LAMOTRIGINE	25	4	1	620.6	5.43	
MEBENDAZOLE	200	6.7	2	41.7	6.01	
NICARDIPINE (HCl)	60	5.6	2	639.1	6.61	
PINACIDIL	10	5.9	1			
PRAZOSIN (HCl)	2	8.9	3	0.1	7.74	
RILUZOLE	100	4.4	2			

DRUG	Actual daily dose (mg)	pIC ₅₀	Doses/day	Calculated dose using <i>in vivo</i> data (mg)	pIC ₅₀ expressed from MEC using actual dose	Acid/Base Colour Key
SAQUINAVIR	2000	8.3	2	2	5.3	
TRAZODONE (HCl)	150	6.3	1	13.5	5.2	
TRIAMTERENE	150	5.3	2	3682.5	6.69	
VOGLIBOSE	1	4.6	3			
ZIPRASIDONE (HCl)	40	8.8	2	0.2	6.38	
TELMISARTAN	20	8	1	1.8	7	
ZALCITABINE	2	6.9	3	7.7	7.38	
CETIRIZINE (HCl)	5	8.5	1			
CILOSTAZOL	200	6.7	2			
EFAVIRENZ	600	8.9	1			
FINASTERIDE	5	7.3	1	4.2	7.21	
HYDROCHLOROTHIAZIDE	50	4.7	2			
LANSOPRAZOLE	15	7.1	1	6.7	6.7	
MERCAPTOPYRINE	3	4.8	1	1591.7	7.62	
MIFEPRISTONE	600	8	1			
NADOLOL	40	8.9	1	0.1	6.01	
PIOGLITAZONE (HCl)	15	4.5	1			
ROXITHROMYCIN	450	6.8	3			
SIMVASTATIN	40	8.4	1			

Table 7-2 Literature Data of Known Drug Molecules (www.drugbank.ca/drugs and www.Drugs.com).

DRUG	Clinical Human V_{dss} (L/kg)	Human CL_p (mL/min/kg)	f_{up}	MRT (h)	$T_{1/2}$ (h)	Acid/Base Colour Key
ACETYLSALICYLIC ACID	0.22	12	0.68	0.3	0.3	
ALLOPURINOL	0.58	11	0.97	0.9	0.8	
AMILORIDE (HCl)	5				7.5	
CANDESARTAN CILEXETIL	0.13	0.37	0.01		9	
DIAZOXIDE	0.21	0.06	0.06	58	48	
DIFLUNISAL	0.1	0.1	<0.001	14	10	
ETODOLAC	0.39	0.82	0.01		7.3	
FLURBIPROFEN	0.12		<0.001		5	
FUROSEMIDE	0.12	1.6	0.01	1.3	2.5	
GLIBENCLAMIDE	0.13	1.3	0.01		1.6	
GLIMEPIRIDE	0.19	0.5	0.01	6.3	10	
GLIPIZIDE	0.16	0.56	0.02	4.8	3.3	
INDOMETACIN	0.1	1.3	0.01	1.2	1.4	
IRBESARTAN	0.94	2.3	0.1	6.8	14	
KETOPROFEN	0.13	1.6	0.08	1.4	2.1	
MYCOPHENOLIC ACID	0.77	2	0.02		12	
NAPROXEN			0.01		15	
NIMESULIDE			0.03		2.8	
OXAPROZIN	14		0.01		54.9	
PIROXICAM	0.14		0.06		58	
PRAVASTATIN SODIUM	0.46	14	0.5	0.6	0.8	
PROBENECID	0.13	0.25	0.13	8.7	5.9	
SULFINPYRAZONE	0.12	0.34	0.02	5.9	6.2	
TOLMETIN SODIUM						

DRUG	Clinical Human V_{diss} (L/kg)	Human CL_p (mL/min/kg)	f_{up}	MRT (h)	$T_{1/2}$ (h)	Acid/Base Colour Key
ZAFIRLUKAST	1	4.76	0.01		10	
ACEBUTOLOL (HCl)	1.7	10	0.74	2.8	3.5	
ALBUTEROL SULFATE	1.9	7.8	0.92	4.1	2.4	
AMITRIPTYLINE (HCl)	8.7	6.1	0.07	24	17	
AMOXAPINE						
ARIPIRAZOLE	4.9	0.83	0.01	98	75	
ATOMOXETINE (HCl)	0.85	9.3	0.02	1.5	5.2	
BUPROPION (HCl)			0.16		24	
CABERGOLINE		45.71	0.6		65	
CITALOPRAM (HBr)	12	4.3	0.2	47	33	
CLEMASTINE FUMARATE						
CLOMIPRAMINE (HCl)	13	8.2	0.03	26	26	
CLONIDINE (HCl)	3.3	4	0.56	14	7.6	
DESLORATADINE			0.15		50	
DIPHENHYDRAMINE (HCl)	6.5	9.8	0.19	11	9.3	
DOMPERIDONE	3.4	9.5	0.08	6	7.5	
DONEPEZIL (HCl)	12	2.17	0.04		70	
EBASTINE						
FEXOFENADINE (HCl)			0.35		14.4	
FLUOXETINE (HCl)	32.5		0.06		48	
FLUVOXAMINE MALEATE	25		0.2		15.6	
GRANISETRON (HCl)	3.7	9.1	0.35	6.7	5.2	
GUANABENZ ACETATE			0.1		6	
HALOPERIDOL	17	7.8	0.08	36	35	
IMIPRAMINE (HCl)	12	13	0.08	15	16	
LOXAPINE SUCCINATE					4	
MAPROTYLINE (HCl)	45	14	0.11	54	51	

DRUG	Clinical Human V_{diss} (L/kg)	Human CL_p (mL/min/kg)	f_{up}	MRT (h)	$T_{1/2}$ (h)	Acid/Base Colour Key
MEFLOQUINE (HCl)	20	0.43	0.02		504	
METERGOLINE						
METOCLOPRAMIDE (HCl)	3.2	5.7	0.6	9.4	7.2	
MIANSERIN			0.1		13.5	
MIBEFRADIL (Di HCl)	3.1	4	0.01	13	13	
NEOSTIGMINE BROMIDE	0.74	9.2		1.3	1.3	
NORTRIPTYLINE (HCl)	22	10	0.12	37	30	
OLANZAPINE	14.3	7.14	0.07		37.5	
PERGOLIDE MESYLATE			0.1		27	
PIMOZIDE					29.3	
PRIMAQUINE PHOSPHATE	4	5.8		11	7.1	
PROCHLORPERAZINE MALEATE	22	16		23	9	
PROMETHAZINE (HCl)	14	14	0.09	17	14	
PROPAFENONE (HCl)	2.2	16	0.04	2.2	2.1	
PROPRANOLOL (HCl)	3.1	12	0.13	4.3	3.4	
PROTRIPTYLINE (HCl)	22					
QUININE SULFATE	1.8	1.9	0.3	16	11	
SELEGILINE (HCl)	1.9	20	0.13	1.6	1.3	
SUMATRIPTAN	1.7	19	0.83	1.5	1.7	
TAMSULOSIN (HCl)	0.21	0.62	0.01	5.6	6.8	
VENLAFAXINE (HCl)	4.4	14	0.73	5.2	5	
VERAPAMIL (HCl)	3.7	18	0.09	3.4	2.8	
ZOLMITRIPTAN	1.8	6.7	0.75	4.6	3.6	
BICALUTAMIDE			0.07		144	
CAFFEINE	0.63	1.4	0.64	7.5	4.9	
CARBAMAZEPINE			0.24		17	
CELECOXIB	6.13	6.59	0.03		11	

DRUG	Clinical Human V_{diss} (L/kg)	Human CL_p (mL/min/kg)	f_{up}	MRT (h)	$T_{1/2}$ (h)	Acid/Base Colour Key
DAPSONE	0.83	0.48	0.25	29	22	
FELBAMATE	0.76	0.5	0.7		22	
FELODIPINE	4.4	11	<0.001	6.7	10	
FLUTAMIDE			0.05		6	
ISRADIPINE	1.5	26	0.04	1	3.3	
LEFLUNOMIDE	0.13		0.01		336	
LETROZOLE	1.9	0.57	0.41	59	45	
LORAZEPAM	1.3	1	0.09	22	17	
LOVASTATIN	0.87	7.2	0.04	1.3	1.4	
METHYLPREDNISOLONE	1.2	6.1	0.23	3.5	2.3	
METOLAZONE			0.67		14	
NEVIRAPINE	1.3	0.3	0.32	81	53	
NIMODIPINE	1.1	15	0.02	1.2	1.3	
NISOLDIPINE	5.5	15	<0.001	6.5	11	
NITRENDIPINE	6.1	25	0.02	4.1	8.2	
PENTOXIFYLLINE	1.8	39	0.3	0.8	1.2	
PROCYCLIDINE (HCl)	0.74	0.86		14	12	
ROLIPRAM						
SPIRONOLACTONE			0.1		0	
THIOTHIXENE (HCl)						
VALDECOXIB						
ZILEUTON	1.2		0.07		2.5	
BENDROFLUMETHIAZIDE			0.04		8.5	
DIDANOSINE	0.77	11	0.95	1.2	1.4	
INDAPAMIDE			0.21		14	
PHENYTOIN			0.1		22	
ZIDOVUDINE	1.8	25	0.8	1.2	1.3	

DRUG	Clinical Human V_{diss} (L/kg)	Human CL_p (mL/min/kg)	f_{up}	MRT (h)	$T_{1/2}$ (h)	Acid/Base Colour Key
ABACAVIR	0.84	13	0.5	1.1	1	
ACRIVASTINE					1.5	
ALOSETRON (HCl)	1.1	8.7	0.18	2.1	1.6	
AMINOGLUTETHIMIDE			0.77		12.5	
DIPYRIDAMOLE	1.75	3	0.01		0.7	
FENOFIBRATE	30	0.29	<0.001		20	
KETOCONAZOLE			0.01		2	
LAMOTRIGINE	1.1	0.58	0.45		25	
MEBENDAZOLE	1.2	15	0.09	1.3	1.1	
NICARDIPINE (HCl)	1	11	0.01	1.5	4.1	
PINACIDIL						
PRAZOSIN (HCl)	0.73	4.7	0.06	2.6	2	
RILUZOLE			0.04		12	
SAQUINAVIR	3.6	13	0.03	4.6	13	
TRAZODONE (HCl)	0.52	1.4		6.2	7.3	
TRIAMTERENE	13	63	0.42	3.4	4.3	
VOGLIBOSE						
ZIPRASIDONE (HCl)	1	5.1	<0.001	3.3	3.1	
TELMISARTAN	5.3	8.4	<0.001	11	20	
ZALCITABINE	0.54	5.6		1.6	1.2	
CETIRIZINE (HCl)						
CILOSTAZOL			0.02		12	
EFAVIRENZ			<0.001		47	
FINASTERIDE	0.89	4.7	0.16	3.2	3	
HYDROCHLOROTHIAZIDE			0.32		8	
LANSOPRAZOLE	0.28	4.4	0.02	1.1	1	
MERCAPTOPYRINE	1	15	0.85	1.1	1	

DRUG	Clinical Human V_{diss} (L/kg)	Human CL_p (mL/min/kg)	f_{up}	MRT (h)	$T_{1/2}$ (h)	Acid/Base Colour Key
MIFEPRISTONE			0.02		18	
NADOLOL	1.9	2.9	0.14	11	9.2	
PIOGLITAZONE (HCl)	0.63		0.01		5	
ROXITHROMYCIN			0.04		12	
SIMVASTATIN			0.05		3	

Table 7-3 The Measured *In Vitro* Biomimetic Data of the Investigated Known Drug Molecules.

DRUG	%HSA Binding	LogK (IAM) (converted to LogP scale)	CHI LogD at pH 7.4	CHI LogD at pH 2	CHI LogD at pH 10.5	CHI LogP	HPLC DEmax (%)	HPLC Human VD_{ss} (L/kg)	Acid/Base Colour Key
ACETYLSALICYLIC ACID	66.4		-1.2	1.06	-1.31	1.06			
ALLOPURINOL	19.2	2	-1.64	-1.16	-2.51	-1.16	54.9	1.41	
AMILORIDE (HCl)	38.6	2.56	-0.53	-0.1	-0.18	-0.1	27.3	2.12	
CANDESARTAN CILEXETIL	97.9	3.8	2.65	4.17	2.26	4.17	1.07	0.813	
DIAZOXIDE	77.6	2.05	1.02	1.4	-0.08	1.4	27.3	0.733	
DIFLUNISAL	98.8	2.49	1.21	3.29	1.04	3.29	2.57	0.138	
ETODOLAC	95.6	2.51	1.48	3.06	0.94	3.06	6.52	0.396	
FLURBIPROFEN	98.6	1.99	0.95	3.01	0.93	3.01	4.77	0.095	
FUROSEMIDE	89.7	2.14	0.2	1.59	0.4	1.59	12.4	0.367	
GLIBENCLAMIDE	98.0	2.7	2.07	3.17	1.21	3.17	2.99	0.251	
GLIMEPIRIDE	98.0	2.53	2.29	3.25	1.39	3.25	3.61	0.216	
GLIPIZIDE	95.8	1.83	0.99	2.07	0.52	2.07	12	0.187	
INDOMETACIN	98.6	2.34	1.43	3.3	1	3.33	3.33	0.133	
IRBESARTAN	96.1	2.17	1.21	1.48	0.62	1.48	8.18	0.249	
KETOPROFEN	98.4	2.18	0.7	2.43	0.46	2.43	4.3	0.127	

DRUG	%HSA Binding	LogK (IAM) (converted to LogP scale)	CHI LogD at pH7.4	CHI LogD at pH 2	CHLogD at pH 10.5	CHI LogP	HPLC DEmax (%)	HPLC Human VDss (L/kg)	Acid/Base Colour Key
MYCOPHENOLIC ACID	95.5	1.83	0.81	2.25	-0.31	2.25	12.7	0.2	
NAPROXEN	99.9	1.96	0.63	2.59	0.28	2.59	1.55	0.026	
NIMESULIDE	98.0	2.32	2.5	2.83	0.92	2.83	4.4	0.174	
OXAPROZIN	98.7	2.08	1.24	2.83	1.05	2.83	3.91	0.093	
PIROXICAM	97.3	1.9	0.54	1.12	0.31	1.12	8.14	0.142	
PRAVASTATIN SODIUM	40.3	1.83	0.64	1.34	0.38	1.34	54	0.97	
PROBENECID	95.4	1.81	1.02	2.72	0.84	2.72	13.2	0.199	
SULFINPYRAZONE	97.2	2.11	0.92	2.61	0.69	2.61	6.83	0.181	
TOLMETIN SODIUM	95.0	1.59	0.73	2.34	0.42	2.34	16.6	0.162	
ZAFIRLUKAST	99.1	3.67	2.34	4.12	1.96	4.12	0.789	0.44	
ACEBUTOLOL (HCl)	32.7	1.59	0.32	-0.14	1.2	1.2	72.1	0.806	
ALBUTEROL SULFATE	22.0	1.55	-0.69	-0.99	-0.11	-0.11	81.6	0.843	
AMITRIPTYLINE (HCl)	90.1	6.3	2.65	0.94	5.21	5.21	0.308	37.3	
AMOXAPINE	88.4	6.64	1.93	0.73	3.14	3.14	0.24	58.4	
ARIPIRAZOLE	97.8	6.08	3.74	0.86	4.15	4.15	0.129	9.15	
ATOMOXETINE (HCl)	87.5	5.28	1.76	0.78	5.24	5.24	0.922	15	
BUPROPION (HCl)	73.9	3.21	2.33	0.19	3.34	3.34	9.7	2.66	
CABERGOLINE	83.6	6.41	1.7	-0.36	3.62	3.62	0.366	57.1	
CITALOPRAM (HBr)	72.4	4.85	1.59	0.71	4.32	4.32	2.12	15	
CLEMASTINE FUMARATE	96.0	7.6	3.13	1.24	4.46	4.46	0.048	74.4	
CLOMIPRAMINE (HCl)	94.4	7.6	2.43	1.47	5	5	0.06	95.1	
CLONIDINE (HCl)	37.7	1.96	0.36	-0.73	1.26	1.26	48.9	1.14	
DESLOMATADINE	88.5	6.13	1.32	-0.25	4.03	4.03	0.39	34.3	
DIPHENHYDRAMINE (HCl)	68.7	2.98	1.59	0.6	3.61	3.61	13.3	2.28	
DOMPERIDONE	92.2	3.96	1.37	0.37	2.13	2.13	2.43	2.76	

DRUG	%HSA Binding	LogK (IAM) (converted to LogP scale)	CHI LogD at pH7.4	CHI LogD at pH 2	CHLogD at pH 10.5	CHI LogP	HPLC DEmax (%)	HPLC Human VDss (L/kg)	Acid/Base Colour Key
DONEPEZIL (HCl)	86.1	3.68	1.98	0.5	3.71	3.71	4.45	2.99	
EBASTINE	98.7	6.98	5.02	1.98	6.54	6.54	0.037	15.5	
FEXOFENADINE (HCl)	74.1	2.64	1.17	0.83	1.91	1.91	16.6	1.45	
FLUOXETINE (HCl)	91.2	6.19	2.02	0.92	3.8	3.8	0.305	29.4	
FLUVOXAMINE MALEATE	72.3	5.15	1.98	0.86	3.34	3.34	1.59	20.5	
GRANISETRON (HCl)	69.0	4.34	0.79	-0.01	2.5	2.5	3.57	9.28	
GUANABENZ ACETATE	88.1	4.85	1.02	0.14	1.43	1.43	1.36	9.27	
HALOPERIDOL	90.4	4.6	2.16	0.7	3.5	3.5	1.46	6.04	
IMIPRAMINE (HCl)	86.3	4.23	2.05	0.88	4.6	4.6	2.63	5.31	
LOXAPINE SUCCINATE	92.7	5.28	3.27	0.56	3.79	3.79	0.658	10.4	
MAPROTILINE (HCl)	86.0	6.7	2.03	0.87	4.79	4.79	0.25	69.3	
MEFLOQUINE (HCl)	96.9	1.18	2.18	1.03	4.22	4.22	17.7	0.074	
METERGOLINE	96.0	6.41	2.55	0.95	3.31	3.31	0.149	21.5	
METOCLOPRAMIDE (HCl)	58.9	3.54	0.53	-0.21	1.99	1.99	8.87	4.69	
MIANSERIN	91.9	5.47	3.24	0.6	3.85	3.85	0.595	13.7	
MIBEFRADIL (Di HCl)	93.6	6.3	2.93	0.73	3.99	3.99	0.231	27.3	
NEOSTIGMINE BROMIDE	87.6	1.68	-0.42	-1.17	0.47	0.47	28.1	0.35	
NORTRIPTYLIN (HCl)	86.2	5.66	1.86	0.84	4.74	4.74	0.673	23.5	
OLANZAPINE	86.2	5.06	1.83	-0.77	2.76	2.76	1.2	12.5	
PERGOLIDE MESYLATE	85.2	5.71	2.47	0.54	3.81	3.81	0.672	26.1	
PIMOZIDE	98.6	5.61	3.43	1.1	4.31	4.31	0.142	3.9	
PRIMAQUINE PHOSPHATE	79.2	4.6	1.14	-0.04	4.5	4.5	2.31	10	
PROCHLORPERAZINE MALEATE	96.9	7.67	2.84	0.59	4.51	4.51	0.037	65.2	
PROMETHAZINE (HCl)	92.5	7.2	1.99	0.76	4.18	4.18	0.107	77.8	
PROPAFENONE (HCl)	88.0	4.38	2.23	0.89	3.47	3.47	2.1	5.61	
PROPRANOLOL (HCl)	72.7	4.45	1.35	0.41	3.03	3.03	3.04	9.79	

DRUG	%HSA Binding	LogK (IAM) (converted to LogP scale)	CHI LogD at pH7.4	CHI LogD at pH 2	CHLogD at pH 10.5	CHI LogP	HPLC DEmax (%)	HPLC Human VDss (L/kg)	Acid/Base Colour Key
PROTRIPTYLINE (HCl)	83.8	5.42	1.72	0.81	4.7	4.7	0.929	20.2	
QUININE SULFATE	78.1	5.19	1.04	-0.67	2.09	2.09	1.35	18.8	
SELEGILINE (HCl)	89.6	6.96	1.71	0.43	3.17	3.17	0.17	76.4	
SUMATRIPTAN	28.0	2.68	0	-0.68	1.01	1.01	26.5	2.61	
TAMSULOSIN (HCl)	68.9	2.84	1.37	0.41	2.01	2.01	14.8	1.94	
VENLAFAXINE (HCl)	35.0	3.19	1.27	0.25	3.71	3.71	15.5	4.2	
VERAPAMIL (HCl)	88.1	3.59	2.39	0.96	3.94	3.94	3.93	2.18	
ZOLMITRIPTAN	61.4	2.78	-0.07	-0.58	1.03	1.04	16.3	1.89	
BICALUTAMIDE	96.8	3.21	2.75	2.78	2.8	2.8	2.66	0.646	
CAFFEINE	26.8	1.22	-0.17	-0.16	-0.19	-0.16	108	0.578	
CARBAMAZEPINE	79.9	2.34	1.68	1.68	1.72	1.72	19.7	0.925	
CELECOXIB	97.1	3.9	3.38	3.4	3.5	3.5	1.24	1.16	
DAPSONE	80.6	2.07	0.93	0.74	0.98	0.98	25	0.684	
FELBAMATE	68.7	1.76	1.07	1.11	1.09	1.11	42.3	0.648	
FELODIPINE	95.9	4.45	3.74	3.71	3.71	3.74	0.965	2.8	
FLUTAMIDE	94.3	3.48	3.1	3.16	3.11	3.16	3.11	1.33	
ISRADIPINE	94.4	3.48	3.25	3.21	3.29	3.29	3.05	1.3	
LEFLUNOMIDE	92.6	3.37	3.01	3.11	2.95	3.1	4.07	1.42	
LETROZOLE	59.3	2.42	1.9	2.13	1.94	2.13	25.7	1.47	
LORAZEPAM	91.1	3.16	1.89	1.92	1.97	1.97	5.67	1.33	
LOVASTATIN	95.5	4.09	4.06	4.06	4.26	4.26	1.47	2.1	
METHYLPREDNISOLONE	71.9	2.6	1.54	1.56	1.53	1.56	18.2	1.47	
METOLAZONE	83.8	2.49	1.65	1.67	1.55	1.67	15.2	0.958	
NEVIRAPINE	54.0	1.89	0.93	0.61	1	1	45	0.898	
NIMODIPINE	92.0	3.09	3.08	3.06	3.11	3.11	5.64	1.14	
NISOLDIPINE	91.0	3.16	3.68	3.56	3.71	3.71	5.67	1.33	
NITRENDIPINE	93.9	3.59	3.15	3.15	3.19	3.19	2.88	1.55	

DRUG	%HSA Binding	LogK (IAM) (converted to LogP scale)	CHI LogD at pH7.4	CHI LogD at pH 2	CHLogD at pH 10.5	CHI LogP	HPLC DEmax (%)	HPLC Human VDss (L/kg)	Acid/Base Colour Key
PENTOXIFYLLINE	25.9	1.47	0.53	0.55	0.47	0.55	85.5	0.75	
PROCYCLIDINE (HCI)	86.1	4.49	3.31	3.33	3.22	3.33	1.72	5.7	
ROLIPRAM	79.1	2.17	1.85	1.7	1.71	1.82	23.6	0.791	
SPIRONOLACTONE	86.7	3.02	2.82	2.91	2.97	2.97	8.24	1.49	
THIOTHIXENE (HCI)	97.8	3.93	3.18	3.2	3.22	3.22	1.02	1.01	
VALDECOXIB	94.0	2.91	2.27	2.31	2.28	2.32	5.54	0.761	
ZILEUTON	89.7	2.53	1.43	1.47	1.39	1.49	10.46	0.689	
BENDROFLUMETHIAZIDE	64.4	2.95	2.31	2.31	1.69	2.31	12.7	2.06	
DIDANOSINE	27.5		-0.72	-0.78	-1.66	-0.65			
INDAPAMIDE	75.1	2.6	1.96	1.97	1.47	1.97	17.1	1.38	
PHENYTOIN	83.4	2.51	1.72	1.81	0.43	1.81	15.1	0.987	
ZIDOVUDINE	11.9	1.17	0.12	0.17	-0.39	0.17	127	0.631	
ABACAVIR	31.9	1.77	0.14	-0.62	0.24	0.24	60.9	0.986	
ACRIVASTINE	82.5	2.68	1.42	0.71	1.29	1.42	13.2	1.22	
ALOSETRON (HCI)	75.5	2.68	0.91	0.06	1.11	1.11	15.8	1.48	
AMINOGLUTETHIMIDE	25.9	1.53	0.87	-0.72	0.95	0.95	81	0.808	
DIPYRIDAMOLE	88.2	4.03	2.18	0.76	2.21	2.21	2.93	3.9	
FENOFIBRATE	97.9	4.45	4.76	4.4	5.01	5.01	0.592	1.64	
KETOCONAZOLE	94.6	3.59	2.68	0.47	2.86	2.86	2.69	1.44	
LAMOTRIGINE	59.5	1.99	0.81	-0.11	0.81	0.81	38.5	0.931	
MEBENDAZOLE	92.9	3.07	1.76	1.07	1.68	1.76	5.25	1	
NICARDIPINE (HCI)	95.8	4.23	4	0.86	4.24	4.24	1.21	2.28	
PINACIDIL	58.3	2.44	1.39	0	1.29	1.39	25.4	1.51	
PRAZOSIN (HCI)	85.2	2.47	1.09	0.1	1.29	1.29	14.6	0.884	
RILUZOLE	94.2	3.29	2.29	1.24	2.3	2.3	3.71	1.09	
SAQUINAVIR	95.2	3.77	3.31	1.11	3.39	3.39	2.07	1.57	

DRUG	%HSA Binding	LogK (IAM) (converted to LogP scale)	CHI LogD at pH7.4	CHI LogD at pH 2	CHLogD at pH 10.5	CHI LogP	HPLC DE _{max} (%)	HPLC Human VD _{ss} (L/kg)	Acid/Base Colour Key
TRAZODONE (HCl)	92.0	3.04	2.3	0.4	2.49	2.49	5.81	1.07	
TRIAMTERENE	59.5	2.14	0.48	-0.43	0.47	0.48	33.4	1.09	
VOGLIBOSE	92.8	3.24	2.38	1.35	2.32	2.35	4.53	1.22	
ZIPRASIDONE (HCl)	97.2	4.64	2.89	0.61	3.02	3.02	0.59 6	2.47	
TELMISARTAN	97.1	3.16	1.5	0.6	1.12	1.53	2.55	0.557	
ZALCITABINE	23.6		-1.13	-1.72	-1.59	-1.13			
CETIRIZINE (HCl)									
CILOSTAZOL	89.9	3.02	2.14	2.15	2.61	2.61	6.97	1.24	
EFAVIRENZ	97.3	4.34	3.36	3.47	3.91	3.91	0.77 7	1.76	
FINASTERIDE	88.4	3.34	2.42	2.48	2.68	2.68	5.55	1.89	
HYDROCHLOROTHIAZIDE	45.4	1.62	0.14	-0.01			63.3	0.74	
LANSOPRAZOLE	90.5	2.66	1.71	0.51	1.14	1.79	9.45	0.811	
MERCAPTOPYRINE	41.2		-2.28	-2.38	-1.28	-1.28			
MIFEPRISTONE	95.5	4.2	3.72	0.92	3.5	3.84	1.33	2.34	
NADOLOL	39.7	1.76	-0.11	-0.03	0.92	0.92	58.5	0.923	
PIOGLITAZONE (HCl)	97.9	2.76	2.16	0.5	1.28	2.17	2.97	0.28	
ROXITHROMYCIN	46.6	5.37	1.95				1.88	39.5	
SIMVASTATIN	96.6	4.49	4.35	4.45	5.14	5.14	0.82 3	2.55	

The *in vitro* intrinsic clearance was obtained using human liver microsomes or cryopreserved liver hepatocytes in a similar way to the methodology described by Jacobson *et al.* [139]. The volume of distribution was estimated either using GSK *in silico* rat volume of distribution model as described in section 6.9.1 (which was based on internally sourced *in vivo* rat data and regression analysis using physical property data), or via the published human model by Hollósy *et al.* [65]. These models of the volume of distribution and the HPLC DE_{max} data were estimated from HPLC-based biomimetic measurements of human serum albumin (HSA) binding [136] and Immobilized Artificial Membrane binding (IAM) [135].

The various methods used in this analysis for estimating the clinical dose are listed below in Table 7-4 which shows the different dose estimation methods used to calculate the clinical dose and the data required for each method. The minimum effective concentration (MEC) was calculated from the measured *in vitro* pIC₅₀ (the logarithm of the molar concentration causing a 50% inhibition of the target response) of the compounds. Caution ought to be applied when predicting *in vivo* efficacy by using *in vitro* affinity or potency values since they are often assay specific, which are not likely to translate directly to the *in vivo* situation. In addition to this, competitive inhibitors often require higher levels of target occupancy (>90%) to give a pharmacological effect, which can be observed or considered biologically relevant *in vivo*. The minimum effective concentration (MEC) was calculated using Equation 48 from the literature pIC₅₀ values for the marketed drugs. It should be noted that the compounds represent different target classes, which means that the pIC₅₀ data were obtained from various types of *in vitro* measurements, and that the K_i values were not available for a more systematic and comparable evaluation of the MEC values for the marketed drugs.

Equation 48

$$\text{MEC} = 1000 \cdot \text{mw} \cdot 10^{-1(\text{pIC}_{50})}$$

Where MEC is the minimal effect concentration, mw is the molecular weight of the compound and pIC₅₀ is the concentration causing a 50% inhibition of the target response.

The elimination rate (k_{el}) was calculated from the human total clearance as described in Equation 49

Equation 49

$$k_{el} = [\text{Human Total Clearance (wsm)}] \frac{60}{1000} \cdot 10^{\text{Log } V_{dss}}$$

Where the Human Total Clearance was calculated using the well-stirred model [17], as shown by Equation 50.

Equation 50

$$\text{Human Total Clearance (wsm)} = \frac{(\text{CL}_{int}(\text{ml per min per g})24.5).18}{(\text{CL}_{int}(\text{ml per min per g})24.5)+18}$$

The k_{el} therefore can be calculated using either *in silico* intrinsic clearance estimates or measured *in vitro* intrinsic clearance data.

When drug efficiency was used to express the dose, this method of dose prediction was called HPLC DE_{max}-DP (Drug Efficiency-based Dose Prediction). When albumin (*HSA*) and phospholipid binding (*IAM*) data were available, HPLC DE_{max} was calculated using Equation 51 based on the model described by Valko *et al.* [77]. Equation 52 describes the simplest method for dose prediction and was used when the potency (pIC₅₀) data and the HPLC DE_{max} data were available.

Equation 51

$$\text{HPLC DE}_{\text{max}} = \frac{100}{10^{(0.24 \exp(\text{Logk HSA}) + 0.12 \exp(\text{Logk IAM}) - 0.4)}}$$

In order to express the dose for an average 70 kg human, the dose calculated by Equation 39 was multiplied by 70,000 to give a prediction of clinical dose in mg for an average 70 kg human.

Equation 52

$$\text{Dose} \left(\frac{\text{mg}}{\text{kg}} \right) = \frac{\text{mw} \cdot 10^{-1(\text{pIC}_{50})}}{\text{HPLC DE}_{\text{max}}}$$

The dose values calculated using HPLC DE_{max}-DP (Equation 52) were compared with those calculated by the DMPK-DP method (Equation 38 and Equation 39).

Table 7-4 below shows the different dose estimation methods used to calculate the clinical dose and the data required for each method.

Table 7-4 The Summary of the Various Dose Estimation Methods that were used to Compare the Clinical Dose Estimations for the Known Drugs

Methods / Input needed	pIC ₅₀	Drug Efficiency	Clearance	Volume	Bioavailability
<i>In silico</i> DE-DP	Yes	Yes (<i>in silico</i>)	No	No	No
HPLC DE-DP	Yes	Yes (biomimetic data)	No	No	No
<i>In silico</i> DMPK-DP	Yes	No	Yes (<i>in silico</i>)	Yes (<i>in silico</i>)	Yes (<i>in silico</i>)
<i>In vitro</i> DMPK-DP	Yes	No	Yes (<i>in vitro</i> microsomal clearance)	Yes (<i>in vitro</i> biomimetic data)	Yes (<i>in silico</i> or estimates based on solubility and permeability)
<i>In vivo</i> DMPK-DP	Yes	No	Yes (<i>in vivo</i>)	Yes (<i>in vivo</i>)	Yes (<i>in vivo</i>)

In vivo DMPK-DP refers to rat *in vivo* PK parameters

Firstly, the predicted dose for the Marketed Drugs was investigated using Equation 38 (*In vivo* DMPK-DP), using published clearance and volume of distribution data where available. A value of 3 h⁻¹ for the absorption rate constant was used for all drugs. The assumption made for the absorption rate constant calculation was that the typical rate of absorption is generally fast for an oral drug, resulting in a T_{max} of 1 to 2 hours. A dosing interval three times a day (TID) was used, although for several drugs, different dosing intervals are suggested to provide an efficacious daily dose.

Figure 7.1-1 shows the trend between the predicted and actual daily dose. This single compartment method of dose prediction is the simplest approach when data for the volume of distribution, clearance, and pIC₅₀ values are available [24][25]. At earliest stages of drug discovery, only the *in silico* values for volume of distribution and clearance are available. The *in vitro* clearance data and the HPLC DE_{max} data become available as compounds of interest progress to these assays.

The green line in Figure 7.1-1 is the line of unity. The size of the circle denotes the magnitude of the pIC₅₀ values, while the colour (shape) refers to the acid/base class of

the compounds. It can be seen by reference to the line of unity, that the overall predicted dose is in a similar range as the actual dose, although it is clear from the plot that the correlation is very poor. Compounds with lower *in vitro* potency (smaller pIC₅₀ values indicated by smaller symbols) showed a tendency to predict a higher than actual dose.

Figure 7.1-1 The Actual vs The Estimated Daily Dose for Marketed Drugs using the *In Vivo* DMPK-DP Method (Equation 38).

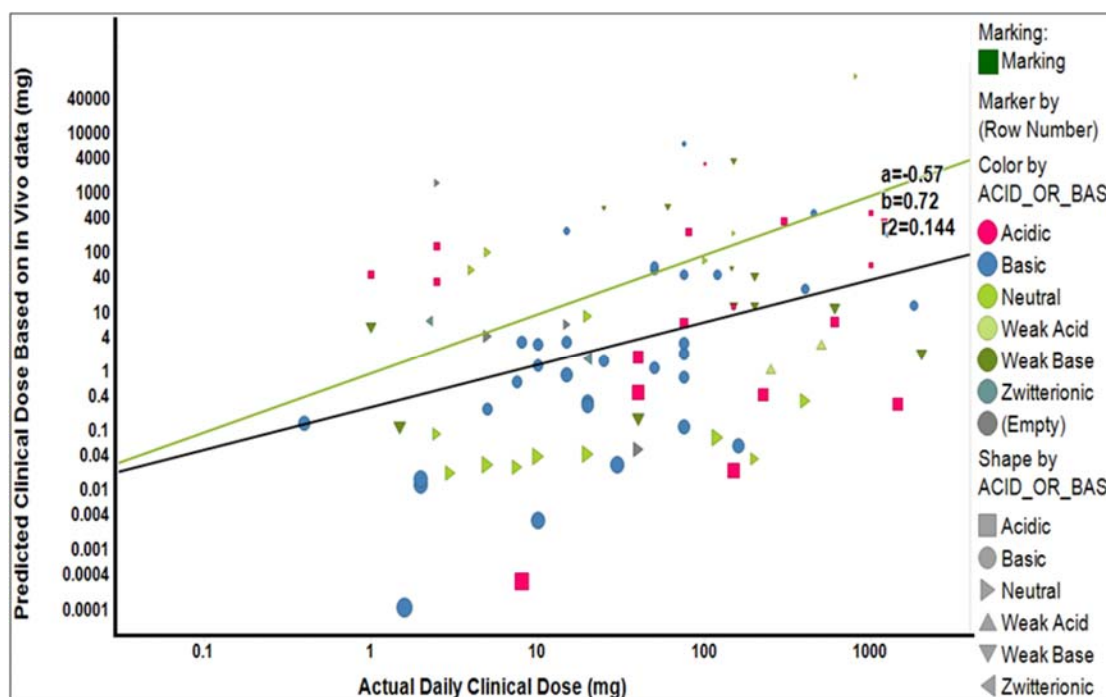


Figure 7.1-1 shows a plot of the predicted clinical dose versus reported clinical dose for marketed compounds. Compounds are marked according to their Acid/Base character. The green line is the line of unity. The size of the data points highlights the difference in potency, the smaller markers refer to a lower pIC₅₀ and the larger markers indicate higher pIC₅₀.

However, for the majority of drugs, the predicted doses were lower than the actual clinical dose. One potential reason for this is that drugs which have strong non-specific binding to lipids and proteins may require a higher clinical dose to achieve the appropriate free concentration available at the site of action (biophase), to deliver clinical efficacy. When the clinical dose was calculated using our *in vitro* method, the assumption was made that the free plasma concentration was the same as the free biophase concentration at steady state, based on the free drug hypothesis. To investigate this hypothesis, the measured

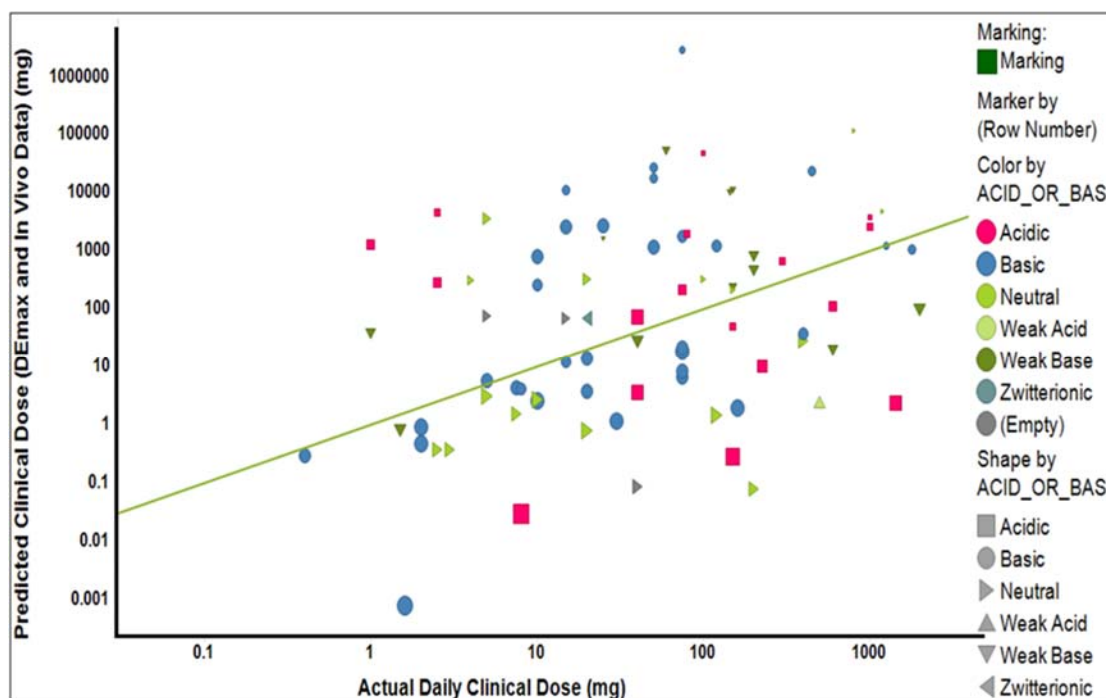
HPLC DE_{max} to refine the MEC value. HPLC DE_{max} assumes the principles of the free drug hypothesis and therefore gives a revised estimation of MEC which may be a more relevant clinical value ($MEC(HPLC DE_{max})$) was incorporated as shown by Equation 53. Using MEC ($HPLC DE_{max}$) to estimate dose using Equation 53 the predicted and the actual doses are spread more evenly around the line of unity, as is shown in Figure 7.1-2.

Equation 53

$$MEC(HPLC DE_{max}) = \frac{HPLC DE_{max}}{100} \cdot MEC$$

Where MEC is the minimal effective concentration

Figure 7.1-2 A Plot of Actual Daily Dose versus Dose Estimated Using MEC ($HPLC DE_{max}$) and *In Vivo* Data in Equation 38 for the Marketed Drugs.



Figures 7.1-2 shows a plot of the predicted clinical dose (MEC adjusted for DE_{max}) versus actual clinical dose

This observation helps to support the incorporation of HPLC DE_{max} to estimate the true biophase concentration in calculating the minimum effective concentration (MEC) from the pIC_{50} values.

Another source of error in the dose prediction method is the estimation of MEC based on pIC_{50} . In their dose prediction analysis, McGinnity *et al.* [24] used the observed plasma concentration in patients after the administered efficacious dose as the MEC, and not the measured *in vitro* pIC_{50} values. In this way, they effectively validated the single compartmental pharmacokinetic model, which is the basis of Equation 38. As previously indicated, the idea that an IC_{50} generated from an *in vitro* assay will translate directly to *in vivo* efficacy is probably unlikely, but it is a useful starting point and a good way to compare compounds.

In order to check this hypothesis, the pIC_{50} values were back calculated from the MEC values using Equation 38 and the actual clinical dose of the marketed drugs. These back calculated pIC_{50} values showed a good inverse correlation with the actual clinical dose as shown in in Figure 7.1-3.

Figure 7.1-3 The Plot of the Actual Clinical Dose and the Calculated pIC_{50} (Clinical MEC) Values of Marketed Drugs.

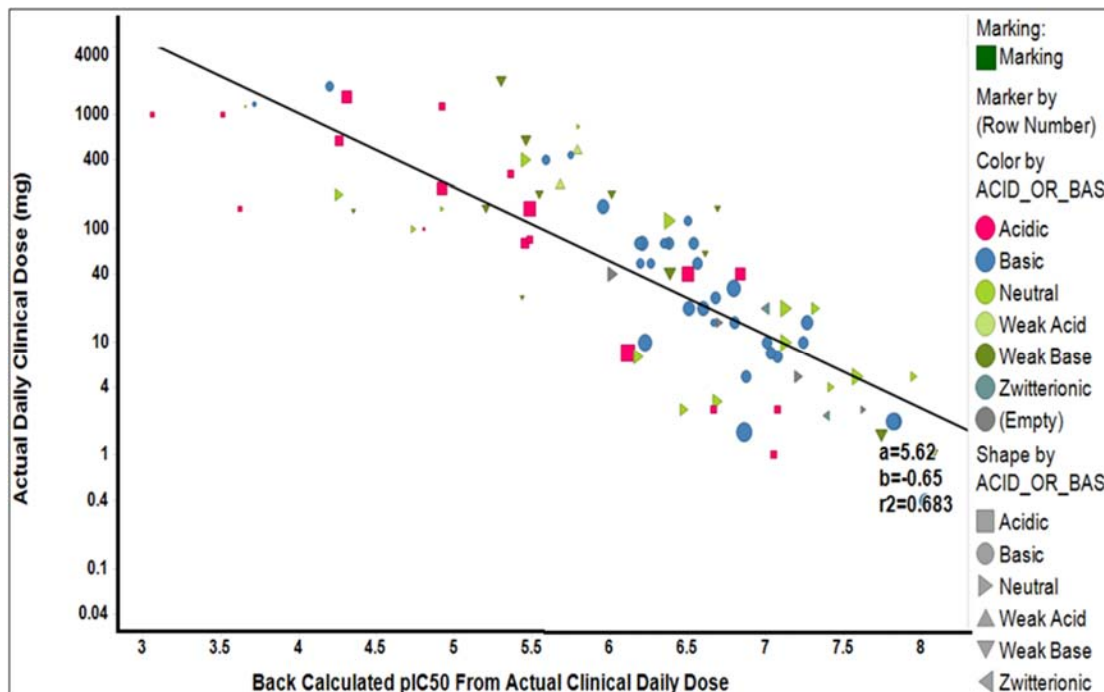


Figure 7.1-3 shows a plot of the actual clinical dose versus the calculated IC_{50} based on clinical plasma concentrations

Unfortunately, the trend between the actual reported *in vitro* pIC_{50} , and the back calculated pIC_{50} is quite poor and therefore suggests that the prediction of the efficacious *in vivo* concentration from *in vitro* potency assays is very difficult. Unfortunately, for drug discovery teams this is typically the only target related affinity value that is available in early drug discovery programs. At a later stage in the drug discovery process, it is likely that *in vivo* data could be included for the estimation of the MEC, which might be considered a more reliable or relevant value for dose prediction. Therefore, the use of a more translatable biophysical value of affinity is encouraged such as K_i , rather than pIC_{50} data. K_i should be considered a more pharmacologically relevant value for MEC that is closer to the clinical target endpoint and assay independent. It is also important to understand the pharmacology behind the efficacy, as the drug target interaction may initiate several biological responses or pathways that may increase or decrease the clinical efficacy. For that reason, the clinical dose may differ significantly from the pre-

clinical or even earlier dose predictions. McGinnity *et al* [24] showed that typically the MEC was 3x higher than the IC₅₀. This observation is also more in line with the idea that most biological systems have a large amount of receptor reserve, and it is therefore likely that for a competitive inhibitor, it would be necessary to inhibit the target protein by at least 90% to give a clinically relevant effect. As the K_i data were not available for the marketed drugs, the comparison of pIC₅₀ data and pK_i data could only be investigated for GSK project compounds where the data was generated and stored in a consistent format.

7.2 Dose Estimation Analysis used for the Pi3Ky Program

Applying dose prediction methods such as drug efficiency analysis to compounds that cover multiple targets assessed in different projects using various assessment methods inevitably introduces significant variability into the data. Using an in-house project focussed on a single target offered the opportunity to evaluate compounds assessed in a more consistent manner.

7.2.1 Comparison of Various Dose Estimation Methods used in the Pi3Ky Program for Intravenous Administration in Acute Lung Injury

As has been described in section 5.2, Pi3Ky kinase is involved in several immunological processes related to the pathology of ALI & ARDS.

The Pi3Ky program involved the development of an intravenous drug for the treatment of an acute disease. Therefore, the bioavailability was fixed at 100%, so F=1 was used in Equation 38 and the absorption rate (k_a) in Equation 38 could also be considered as instantaneous, thus simplifying the dose estimation equation to Equation 39.

Equation 39

$$\text{Dose} \left(\frac{\text{mg}}{\text{kg}} \right) = \frac{24 \cdot \text{MEC} \cdot V_{dss} (\text{Exp}(k_{el} \cdot \tau) - 1)}{F}$$

At the earliest stages of a drug discovery program, typically the only data available for making an early dose prediction are pIC₅₀ and the HPLC based DE_{max} data. *In vitro* intrinsic clearance and an established, in-house *in silico* V_{dss} data (see Section 4.1.2) can

also be used at an early stage in the *In vitro* DMPK-DP method. Figure 7.2-1 shows the plot of the predicted dose using the two methods.

Figure 7.2-1 The Plot of the Predicted Dose for the Pi3Ky Compounds using the DE-DP Method Based on *In Vitro* Potency and the HPLC DE_{max} and the *In Vitro* DMPK-DP Method using *In Vitro* Clearance and Volume of Distribution Data (Equation 37).

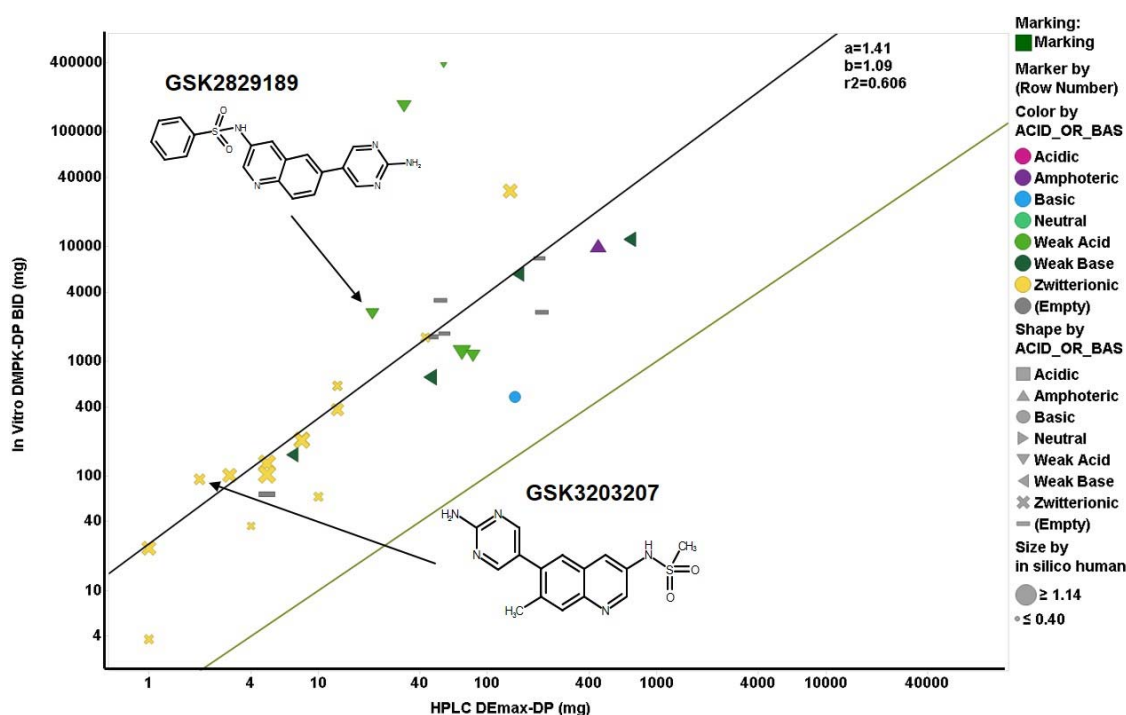


Figure 7.2-1 shows a plot of the *in vitro* DMPK-DP versus the HPLC DE_{max}-DP (DE-DP). The black line is the regression and the green line is the line of unity.

It can be seen that the rank order of the predicted dose is very similar. When the clearance and volume of distribution is included in the *in vitro* DMPK-DP method, the estimated dose values are generally higher. A few compounds with extremely high intrinsic clearance showed the largest discrepancies between the two types of dose prediction. It can also be seen that the DE-DP method provides the best-case scenario for the prediction of dose, as they were lower than the predicted values by the DMPK-DP method. Compounds can be discarded confidently from further studies when the estimated dose by the best-case scenario HPLC DE-DP method is too high or beyond the scope a program team has set for an optimised drug molecule.

Figure 7.2-2 represents the full compound set (1130 compounds) analysed for the Pi3Ky program in this dose prediction analysis. All subsequent plots are based on the same compound set. However, fewer data points will be seen for plots where measured *in vitro* data has been included.

Figure 7.2-2 The Rank Order of Dose Prediction Methods Shows the Original Hit GSK2829189 and the Final Lead Compound GSK3203207 using the *In silico* DMPK-DP and HPLC DE-DP Methods.

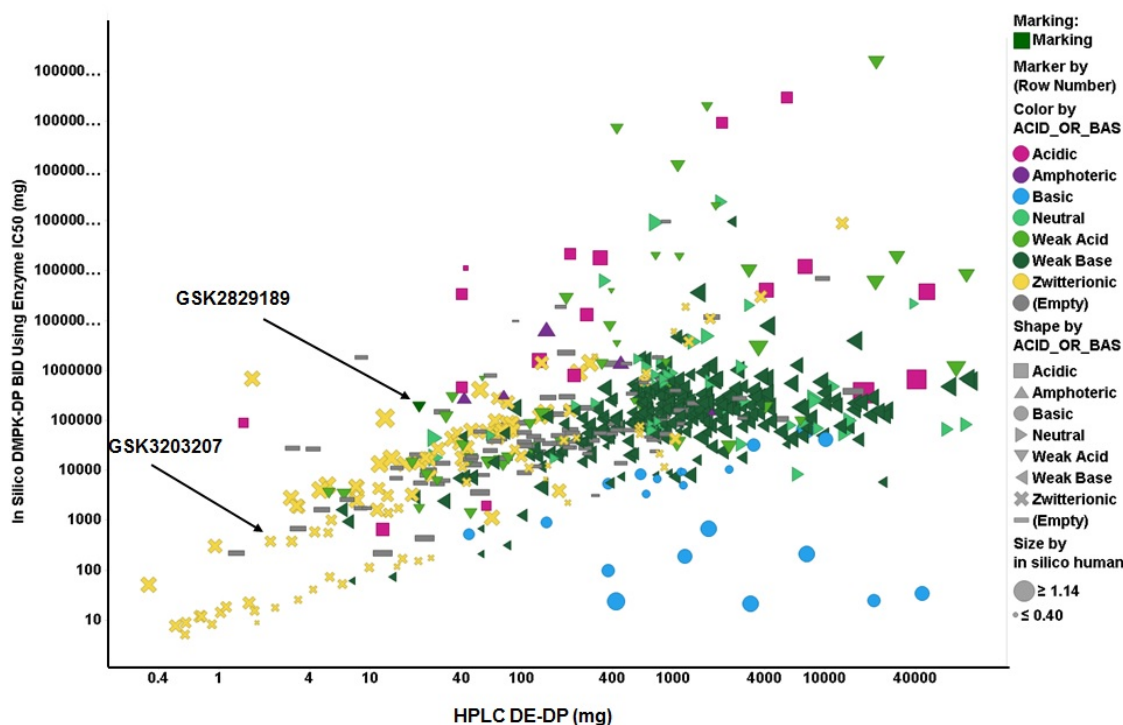


Figure 7.2-2 shows the *in silico* DMPK-DP versus the HPLC DE-DP (DE_{max})

It has been demonstrated that the *in silico* DMPK-DP and *in vitro* DMPK-DP methods predict the rank order of the initial hit GSK2829189 through to the final lead compound GSK3203207 (Figure 7.2-1 and Figure 7.2-2), but the simplest method using the HPLC DE-DP approach where a dose prediction can be generated very early in the screening cascade also predicted the rank order equally well, suggesting that any to these tools can be used for prioritizing compounds. Although the drug efficiency-based dose prediction shows the best-case scenario with the caveat that bioavailability is at maximum and no active transport or permeability barrier exists, it demonstrates that DE_{max} can be used as

a method of dose prediction to help prioritize large numbers of compounds and potentially identify lead-like compounds with minimal data. Table 7-5 and Table 7-6 show the improvement in physicochemical properties and pharmacology of the quinoline series from the initial hit GSK2829189 to the final lead compound GSK3203207; this overall improvement is captured by DE_{max}.

Table 7-5 Summary of Physicochemical Properties for Pi3Ky Hit Compound (GSK2829189) to Lead (GSK3203207)

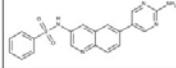
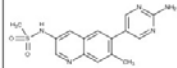
Compound ID	Structure	MW	cLogp	LogD	FaSSIF Solubility (ug/mL)	%HSA	%AGP	CHI IAM	%DE _{max}	PFI	Acid/Base Class
GSK2829189		377.4	2.519	2.09	2	96.6	74.4	25.14	7.79	6.09	Weak Acid
GSK3203207		329.4	1.089	1.27	62	82.2	57.9	18.2	33.3	4.27	Zwitterionic

Table 7-5 show the relative improvement in physicochemical properties from the original hit GSK2829189 to the eventual lead compound GSK3203207

Table 7-6 Summary of *In Vitro* and *In Vivo* Pharmacology for Pi3Ky Hit Compound (GSK2829189) to Lead (GSK3203207)

Compound ID	pIC ₅₀ (Enz)	WB pIC ₅₀	CLi mic r, mp, h (mL/min/g)	CLi hep r, mp, h (mL/min/g)	Rat CL _b (mL/min/kg)	Rat CL _{b,u} (mL/min/kg)	MP CL _b (mL/min/kg)	MP CL _{b,u} (mL/min/kg)	WBB r, mp, h (%)
GSK2829189	8.2	5.3	≤0.5, ≤0.5, ≤0.5	≤0.86, 3.048, 1.16	3	750	13	542	99.6, 97.6, 98.9
GSK3203207	8.7	6.4	≤0.5, ≤0.5, ≤0.5	≤0.86, ≤0.86, ≤0.86	24	244	7.4	55	90.2, 86.5, 87.7

r-rat, mp-minipig & h-human

Table 7-6 show the relative improvement in *In vitro* and *In vivo* pharmacology from the original hit GSK2829189 to the eventual lead compound GSK3203207

7.2.2 Sensitivity analysis, the effect of the potency measured in enzyme assay or in whole blood

In order to assess our dose estimation approaches, a dose sensitivity analysis on various parameters was carried out, such as potency (enzyme and whole blood), volume of distribution (*in vitro* estimates and *in vivo* animal volumes) and clearance (*in silico* and *in vitro*), using compounds from an early discovery lead optimisation program. The aim of this exercise was to demonstrate the impact of the parameters involved in estimating clinical dose and their effect on the compound selection process.

The impact of the *in vitro* potency value on the estimated dose was clearly demonstrated in the case of the marketed drugs. The impact of using whole blood potency instead of the *in vitro* enzyme potency on our predicted dose was also evaluated. Figure 7.2-3 shows the plot of the estimated dose obtained by the enzyme and whole blood (WB) IC₅₀ values. All other parameters in the dose estimation equation remained the same. The compounds shown in Figure 7.2-3 are the same as those plotted in Figure 7.2-2, however, there is less data as WB potency was not measured for all compounds.

Figure 7.2-3 The Plot of the Estimated Dose Obtained When Using the Enzyme and the Whole Blood pIC₅₀ Values.

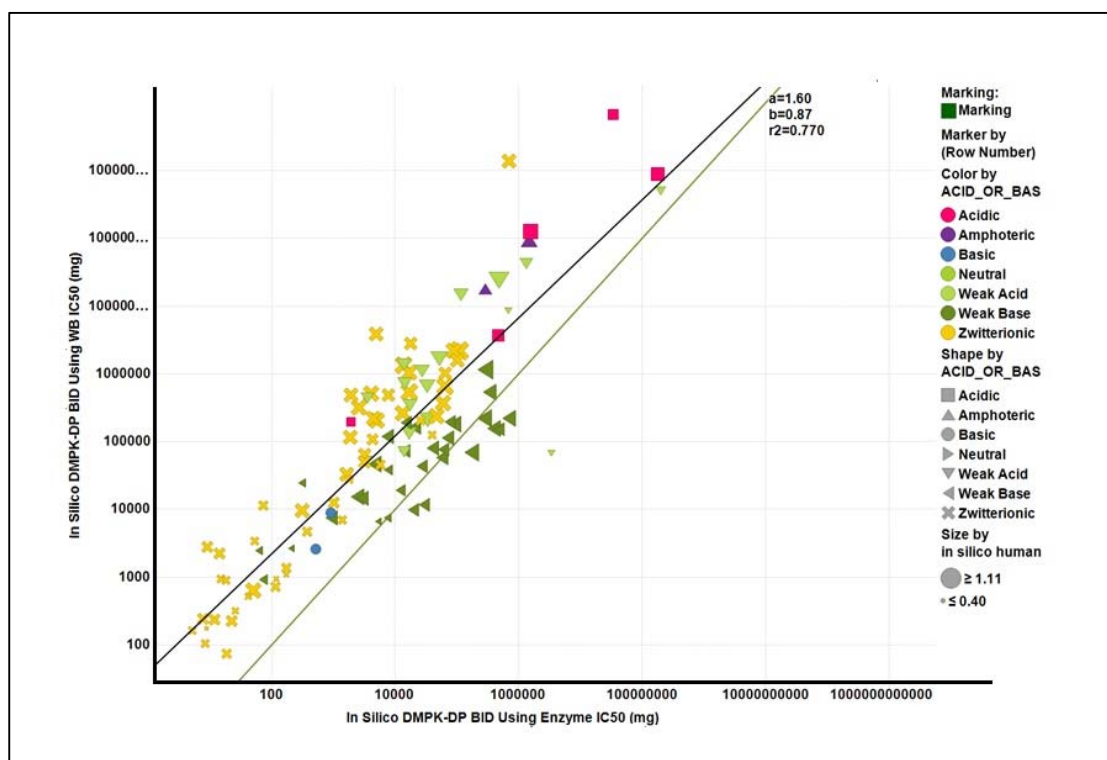


Figure 7.2-3 Shows a plot of the *in silico* DMPK-DP WB (whole blood potency) versus the *in silico* DMPK-DP enzyme potency. The line of unity is green and the regression line is black.

Although the predicted doses show a reasonably good correlation, the differences can be large and the scatter is wide. The whole blood potency using the predicted dose was generally higher than the predicted value using the enzyme potency. This is what would be expected, as cellular derived IC₅₀ is often at least half a log unit lower than an enzyme derived IC₅₀. The question arises as to which potency should be relied upon when calculating dose predictions for large numbers of compounds where the aim is to identify the most interesting compounds for progression. The whole blood potency drop off can be due to multiple reasons, such as differences in assay conditions, which would directly influence the IC₅₀, low permeability, or the high non-specific binding that would reduce the actual free concentration. It is therefore advisable to investigate the reasons for the potency drop off on a compound by compound basis, and to determine if the drop off is consistent across the chemical space being analysed. Therefore, when performing a dose prediction analysis on a large number of compounds, either value can be used when

they have been established and program teams are simply ranking compounds against one another. It is however, important to be consistent with the value being used for each analysis.

7.2.3 Sensitivity Analysis of the Effect of the Errors on Early Estimation of the Volume of distribution and Intrinsic Clearance of the Compounds

The volume of distribution is related to the elimination rate of the compounds in the dose estimation equation, but it may also influence the required efficacious dose depending on where the target is in the plasma or in a tissue compartment [28].

Figure 7.2-4 shows the impact of V_{dss} on the estimation of dose. To assess sensitivity of this parameter on the predicted dose has been illustrated by taking the *in silico* V_{dss} and adding 2 L/kg to it. This has then been plotted against the original *in silico* DMPK-DP dose prediction.

Figure 7.2-4 The Difference in the Estimated Dose Caused by a Small Fixed Increase in V_{dss} Using *In Silico* Estimated V_{dss} in Equation 38, for all Pi3K γ Project Compounds.

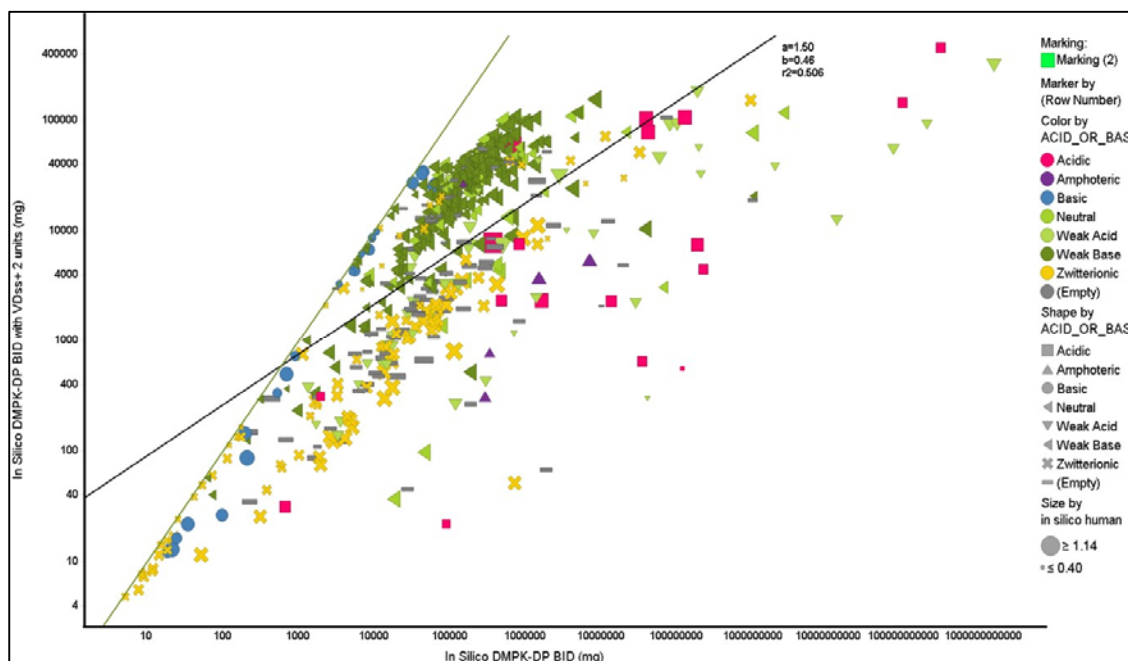


Figure 7.2-4 shows a sensitivity analysis of V_{dss} for the *in silico* DMPK-DP ($V_{dss} + 2$) versus *in silico* DMPK-DP. The line of unity is green and the regression line is black.

The discrepancies between the predicted doses can be large, but it is clear from the plot that the larger the estimated dose the larger these discrepancies can be. It is reassuring that the variability on the dose estimation seems to be smaller when the estimated dose is low. It can also be seen that the acid/base character influenced the sensitivity of the volume of distribution change on the dose estimation. When the volume of distribution is larger, the estimated dose is smaller as shown by all the points being below the line of unity. The correlation between the estimated dose values is around 0.6, but it can also be seen that the change in the volume of distribution did not appear to affect the estimated dose for certain compounds (they are positioned on the line of unity in Figure 7.2-4). There was a trend towards zwitterionic compounds here, although this was not exclusive, and the number of compounds was quite small.

7.2.4 Sensitivity Analysis of the Effect of Errors in the Estimation of Intrinsic Clearance

The impact of clearance on the estimated dose was investigated by increasing the clearance by a small fixed value of 0.5 mL/min/kg for each compound. A small increase was to see how sensitive the dose estimation method was to this parameter across the wide dose range of this analysis, as opposed to an exaggerated increase in clearance which would result in large changes across the analysis. The plot of the originally estimated dose and the estimated dose with the increased clearance can be seen in Figure 7.2-5.

Figure 7.2-5 Plot of the Predicted Dose for the Pi3Ky Compounds Using *In Silico* Clearance and *In Vitro* V_{dss} Data to Predict Dose Using a Small Fixed Increased Clearance (0.5 mL/min/kg) for Each Compound Using Equation 38

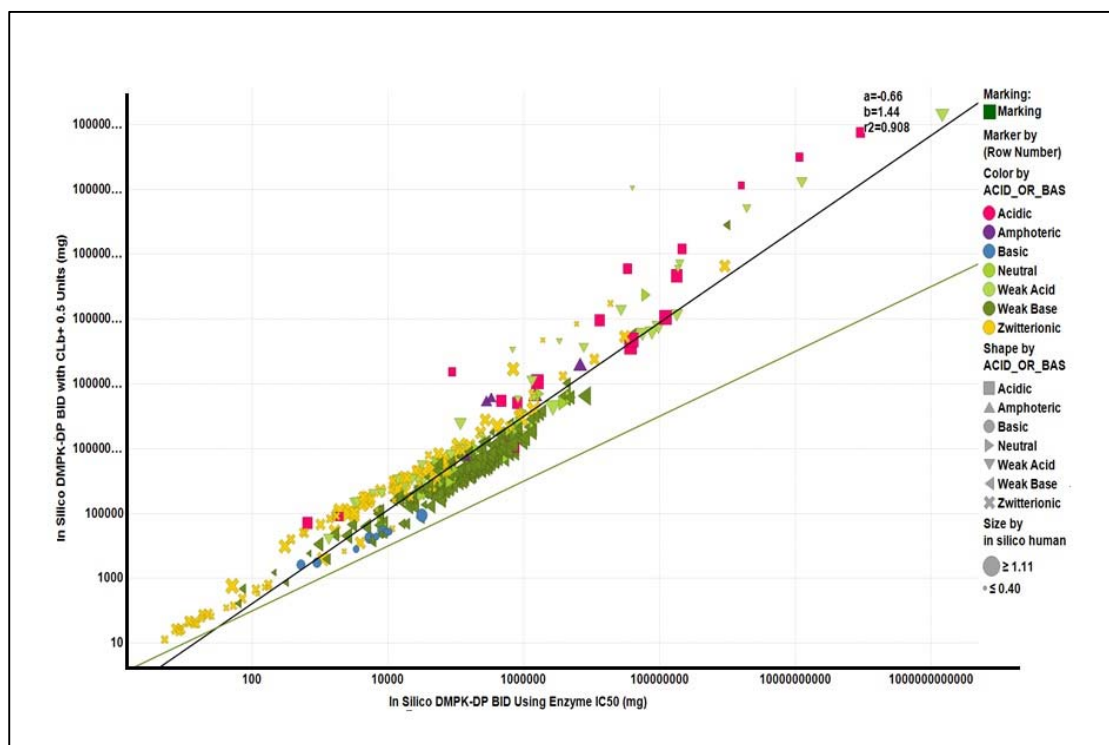


Figure 7.2-5 shows a sensitivity analysis of clearance for the *in silico* DMPK-DP (CL + 0.5) versus *in silico* DMPK-DP. The line of unity is green and the regression line is black.

It can be seen that the predicted dose increased when the clearance was increased. The trend between the two methods of dose estimation is good, and the difference is smaller at the lower dose range estimates. The correlation between the estimated dose by the two method is very good ($r^2 > 0.9$), indicating that the effect of clearance was relatively small and less impactful than the V_{dss} at higher doses.

In order to reveal the effect of the $DRUG_{eff}$ in the dose estimation, the modified MEC was incorporated into the HPLC DE_{max} value as described by Equation 53. The theory is that only a fraction of the available drug will be free at the site of action, which is proportional to the HPLC DE_{max} . As expected, the predicted dose is slightly higher when the drug

efficiency is taken into account. However, the rank order of the compounds is very similar and the correlation between the two types of estimates is high ($r^2=0.87$), as shown in Figure 7.2-6.

Figure 7.2-6 The Plot of the Estimated Dose Using Equation 38 and the Modified Equation 34 by the MEC(HPLC DE_{max}) for the Pi3Ky Project Compounds.

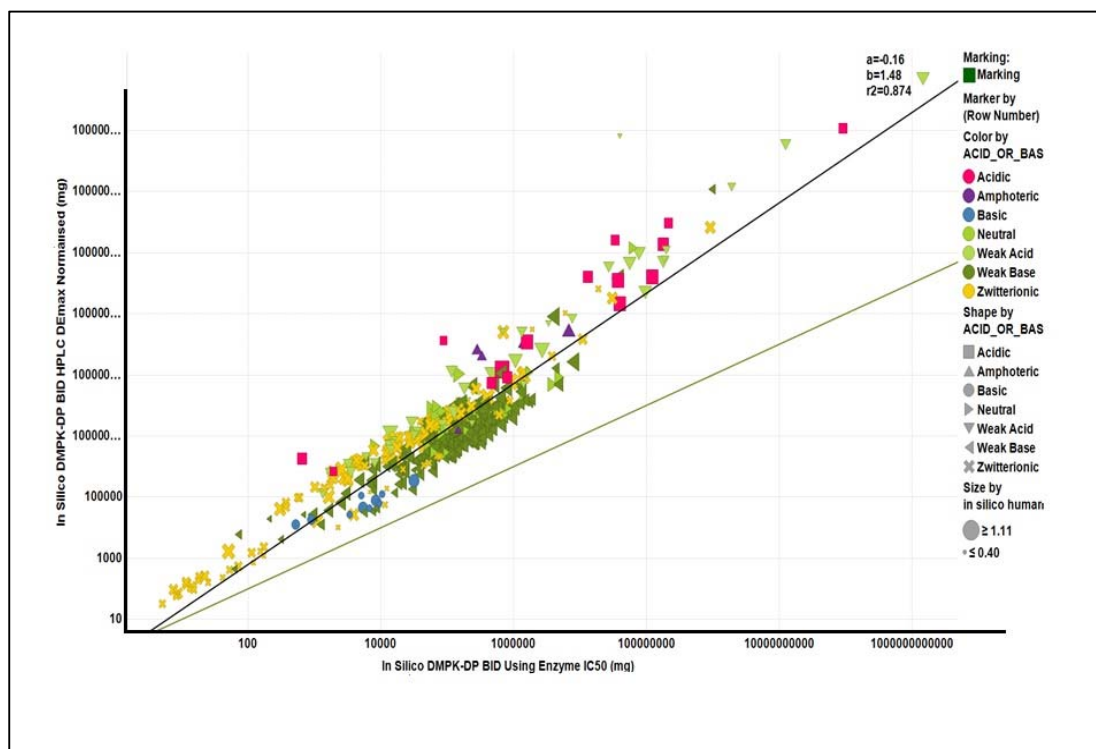


Figure 7.2-7 shows the *in silico* DMPK-DP with HPLC DE_{max} adjusted MEC versus *in silico* DMPK-DP. The line of unity is green and the regression line is black.

It can be seen in Figure 7.2-6 that the difference between the estimated dose values is much greater at the higher estimated dose range. However, at the lower dose range the difference between a 50 mg and a 100 mg clinical dose can be considered significant in respect of the potential side effects and also in the expense of drug manufacture. Therefore, it is suggested to use a modified version of Equation 38, where the MEC values are estimated from the *in vitro* potency and the *in vitro* HPLC DE_{max} as described by Equation 54.

Equation 38 previously shown

$$\text{Dose} \left(\frac{\text{mg}}{\text{kg}} \right) = \frac{\frac{24}{\tau} \cdot \text{MEC} \cdot V_{dss} (k_a - k_{el})}{F \cdot k_a \left(\frac{1}{1 - \exp(-k_{el}\tau)} - \frac{1}{1 - \exp(-k_a\tau)} \right)}$$

Equation 54

$$\text{Dose} \left(\frac{\text{mg}}{\text{kg}} \right) = \frac{\frac{24}{\tau} \cdot \text{MEC} (\text{HPLC DE}_{\text{max}}) \cdot V_{dss} (k_a - k_{el})}{F \cdot k_a \left(\frac{1}{1 - \exp(-k_{el}\tau)} - \frac{1}{1 - \exp(-k_a\tau)} \right)}$$

The investigation of dose calculation procedures for program compounds designed for IV administration was simplified by assuming an instant absorption rate. However, the maximum dose that a patient can receive by this route of administration depends greatly on the solubility of the compound. When a bolus injection is considered, the solubility of the compound should be high enough to enable the dose to dissolve in a maximum of 10 mL of aqueous solvent compatible for IV injections. This means that for a 50 mg dose, the solubility should be above 10 mg/mL, which can be challenging for small drug molecules. When an IV infusion dose is considered, then slightly lower solubility is acceptable as dose concentrations can be reduced.

An additional consideration for ALI patients is the dose volume as oedema is a major symptom of the disease, which means that there are strict limits on the amount of fluids that can be safely administered to patients.

7.3 Aldehyde Oxidase: A Special Case

During the optimisation phase for the quinoline series from the initial hit GSK2829189 to the final lead compound GSK3203207, an issue of drug metabolism was revealed when evaluating unbound blood clearance, which would otherwise have not been evident based on the total clearance. This arose because of the metabolising enzyme aldehyde oxidase (AO), which is becoming increasingly important in drug discovery for molecules with certain N-containing aromatic heterocycles.

Aldehyde Oxidases (AO) are a small group of highly conserved molybdoflavoproteins, along with xanthine oxidoreductase (XOR) [140] whose physiological role is largely unknown from an evolutionary perspective. In the drug discovery process they are emerging as extremely important enzymes, which need to be considered because of profound interspecies variation in their expression and activity toward various substrates of both medicinal and toxicological interest [140]. Historically, AO was generally considered a human specific drug metabolizing enzyme and responsible for a number of drug candidates being negatively impacted in drug development, due to a lack of understanding of AO metabolism and difficulty in predicting high clearance in human [141]. However, there is mounting evidence to show that there are forms of AO expressed in the majority of preclinical species used in drug discovery e.g. mouse, rat, minipig and non-human primate that can be used to help assess the risk of this route of metabolism in human [126,140–143].

Figure 7.3-1 shows there are several genes coding for distinct AO isoforms in different pre-clinical species, although AOX1 is the only active AO isoform expressed in human. Aox1, 3, 4 & 311 are expressed in rodent, and primates generally express an active form of AO similar to human AOX1, as a result primate has often been the pre-clinic species to identify an AO liability risk for human [144]. However, there can be a risk that AO metabolism in pre-clinical species will not translate to human. One such example was carbazeran, which showed good pre-clinical exposure and efficacy, but had poor oral bioavailability due to high clearance in human, which had not been predicted. The high human clearance was due to AO metabolism [145].

Figure 7.3-1 Cross Species Variability in Aldehyde Oxidase Expression [140]

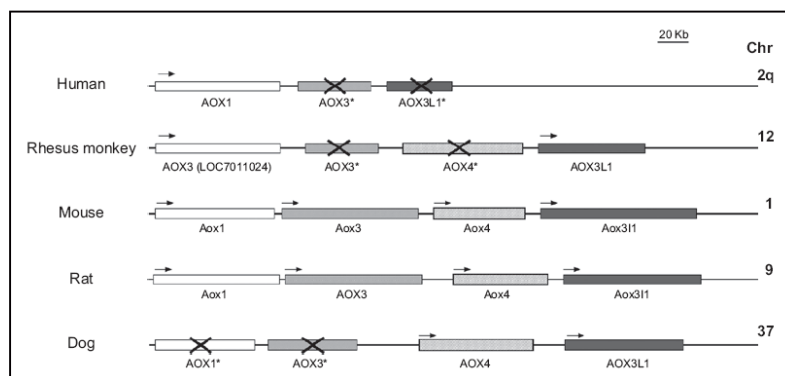


Figure 7.3-1 Different genes responsible for AO expression in human, rhesus monkey, mouse, rat and dog

The physicochemical features of drug molecules are an important aspect of AO metabolism and a good understanding of these can help identify compounds with the potential for AO metabolism by the use of an *in vitro* assay [142].

Figure 7.3-2 Some Common Substrates for AO Metabolism

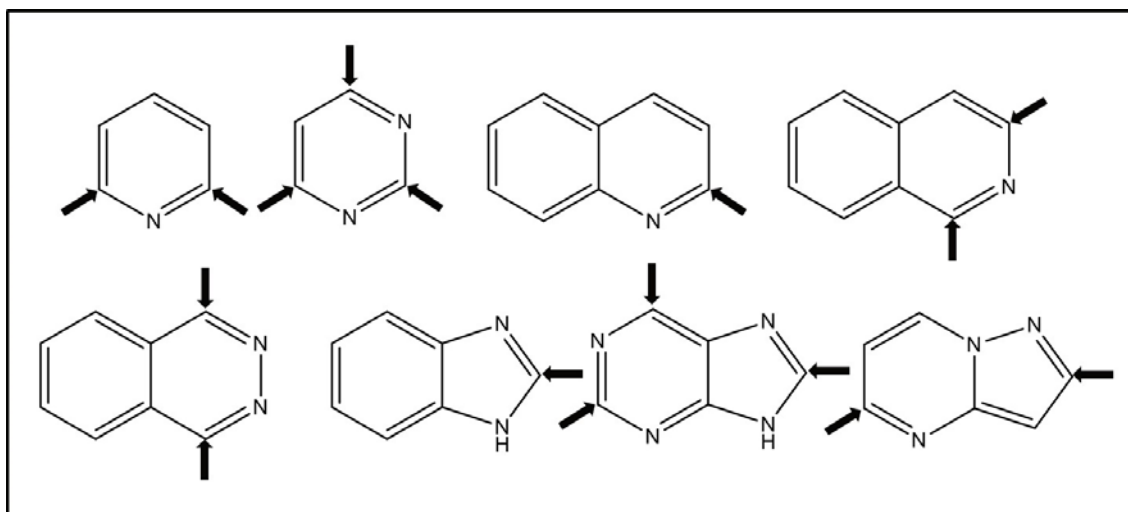


Figure 7.3-2 Shows the potential sites of oxidation due to AO metabolism.

Figure 7.3-3 Understanding Risks Factors for Aldehyde Oxidase Metabolism

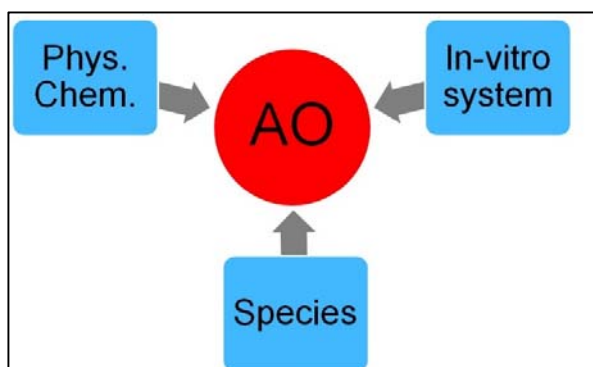


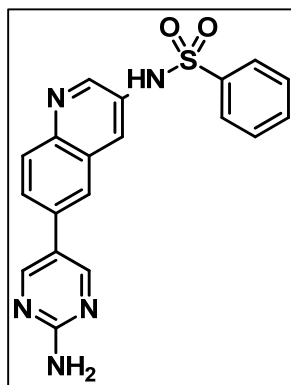
Figure 7.3-3 Shows the main points which need to be considered when assessing AO metabolism

It is important think carefully about template liabilities with respect to functional metabolism during lead optimisation. The drive to improve physicochemical properties of NCE's in recent years has resulted in a trend to replace lipophilic groups such as phenyl rings with aromatic N-heterocycles, which often help to reduce lipophilicity (LogP) and reduce aromatic CYP 450 oxidation. However, these motifs are now known to increases the potential for non-CYP P450 metabolism by enzymes such as AO. It is therefore important to consider profiling early series exemplars of these types of molecule using appropriate *in vitro* metabolising systems, such as liver cytosol, which explicitly express AO. Along with other metabolic transformations, it is necessary to identify, understand and address AO metabolism early in lead optimisation to avoid suboptimal clinical PK later in development, such as the carbazeran example described earlier. If AO metabolism cannot be blocked by modification of the chemical template, then an alternative template should be identified, because unlike generally well understood Phase I and Phase II routes of metabolism, which can be scaled from pre-clinical species to human clearance with reasonable confidence, the AO route of metabolism and scaling of human clearance is not well understood and this route typically results in high rates of clearance in human [145].

7.3.1 The Importance of Considering Unbound Clearance

The initial chemical template starting point for the PI3K γ program was from a quinoline series, and the first compound of significant interest was GSK2829189 (Figure 7.3-4).

Figure 7.3-4 GSK2829189 Structure



It can be seen from the compound structure that the quinoline core has a sulfonamide substituent at the 3-position, and a 2-amino pyrimidine at the 6-position of the quinoline. This compound met the program team's physicochemical criteria of MW <400 and a cLogP <3 along with good target potency (pIC₅₀) against PI3K γ and PI3K δ of 8.2 and 7.2 respectively and low intrinsic clearance across species rat, minipig and human <0.5 mL/min/g. In a rat IV profile generated to assess the *in vivo* PK, GSK2829189 had low *in vivo* blood clearance (CL_b) of 3 mL/min/kg (see Figure 7.3-5) and a volume of distribution of 0.4 L/kg which resulted in a half-life of ca. 3 h.

Figure 7.3-5 GSK2829189 Quinolone Series Lead Compound *In vitro* and *In vivo* Rat PK Profile

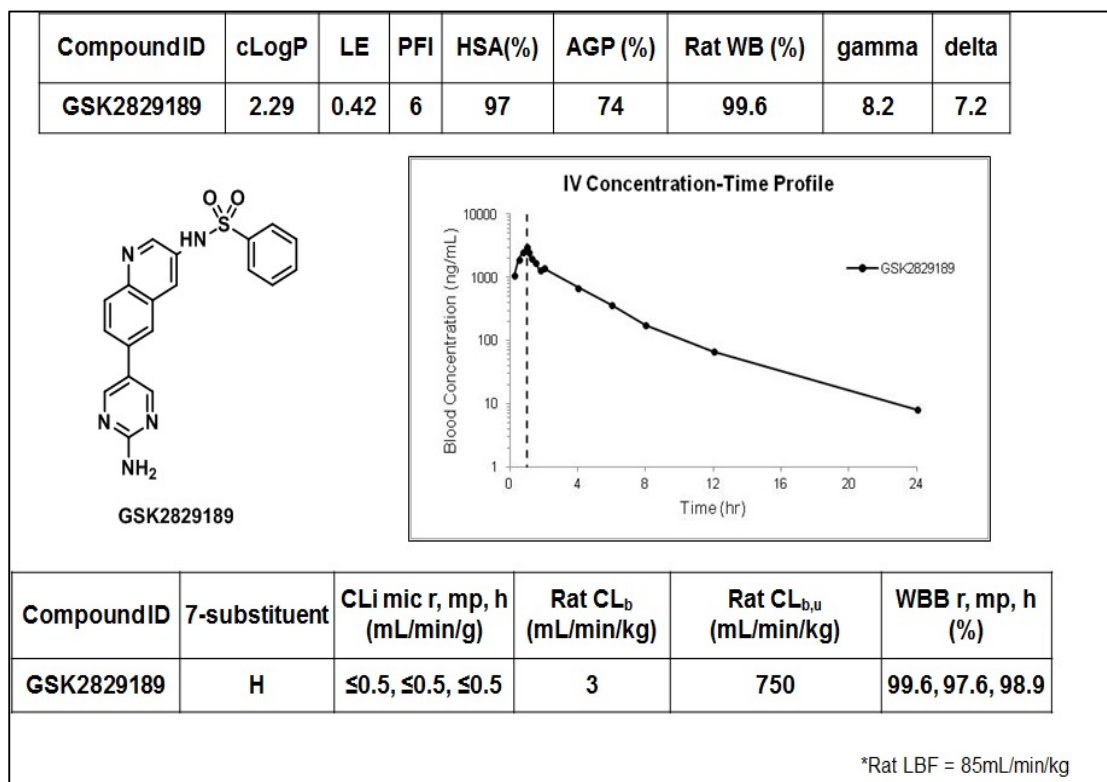


Figure 7.3-5 shows an *in vitro* and *in vivo* summary of the main physicochemical and DMPK data for GSK2829189. Intravenous dose of 1mg/kg.

This was very promising pre-clinical data for an initial hit compound despite two potential sites of AO metabolism at the alpha carbons of the quinoline, and 2-amino pyrimidine. However, based on the *in vitro* CL_i and *in vivo* CL_b, it did not appear that there were any significant risks of any major routes of metabolism for this compound, and as a result there was very little interest in pursuing further metabolism studies despite the risk of AO metabolism in human with this type of template.

Figure 7.3-6 In Vitro and In Vivo Profiles of GSK2829189 and its Non-Phenyl Analogue GSK3180869

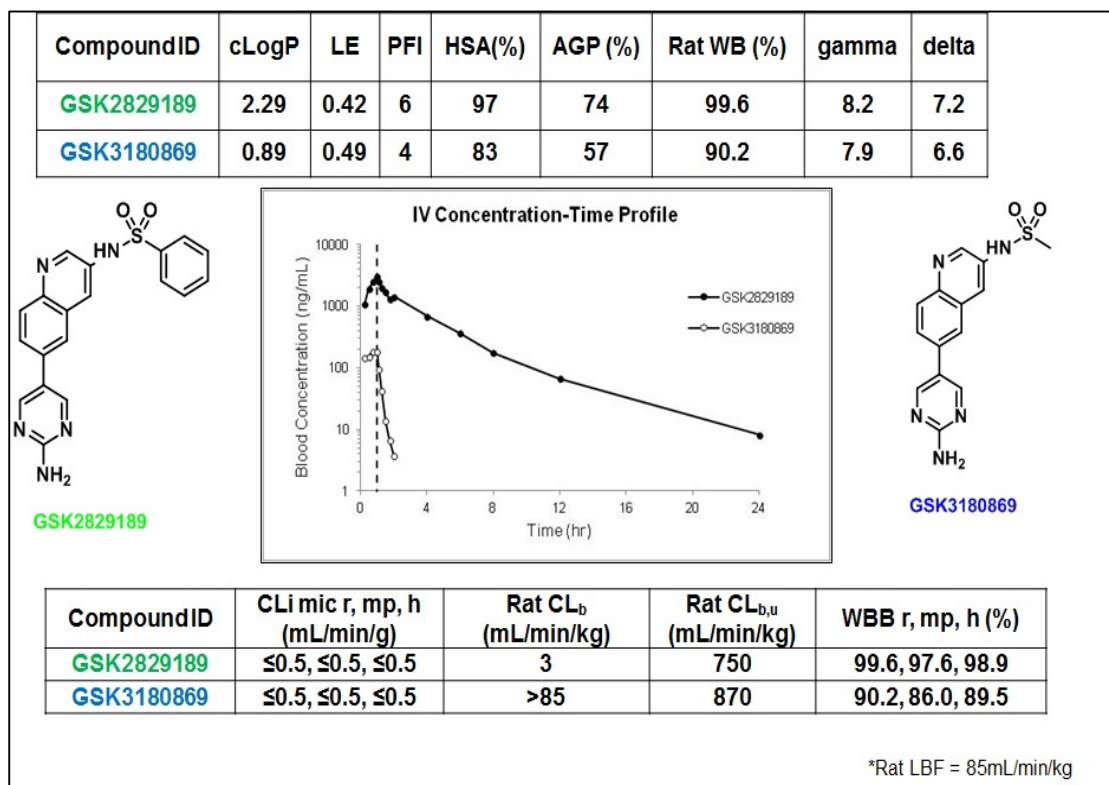


Figure 7.3-6 shows an *in vitro* and *in vivo* summary of the main physicochemical and DMPK data for GSK2829189 and GSK3180869. Intravenous dose of 1mg/kg.

It can be seen from Figure 7.3-6 that there is a large difference in the total blood clearance (CL_b) between the phenyl analogue GSK2829189 and its non-phenyl analogue GSK3180869 3mL/min/kg and >85mL/min/kg (liver blood flow), respectively. This data would suggest there was difference in the route of metabolism or a difference in metabolising enzyme specificity, resulting in very different rates of CL_b. However, if we convert CL_b to unbound blood clearance (CL_{b,u}), it can be seen there is very little difference in the CL_{b,u} between these two analogues see Figure 7.3-6, suggesting a similar rate and possibly route of metabolism. The reason these two analogues now look very similar with respect to the rate of clearance (CL_{b,u}) is that only the free drug is available to be metabolised/cleared.

Figure 7.3-7 Results from Rat and Human *In Vitro* Cytosol AO Assay

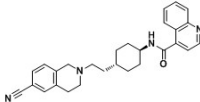
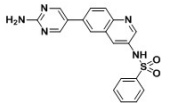
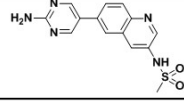
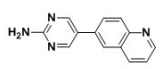
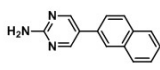
Compound ID	Structure	Species	AO Substrate
SB-277011		Human	Yes
		Rat	No
GSK2829189		Human	Yes
		Rat	Yes
GSK3180869		Human	Yes
		Rat	Yes
GSK1346856		Human	Yes
		Rat	Yes
GSK3184135		Human	Yes
		Rat	Yes

Figure 7.3-7 shows results of an *in vitro* liver cytosolic AO assay for a set of Pi3Kγ compounds. SB-277011 is a known human AO substrate and represents a positive control for the assay.

The *in vitro* cytosol AO assay data illustrated in Figure 7.3-7 shows that both GSK2829189 and its non-phenyl analogue GSK3180869 are both substrates for AO metabolism, along with another analogue GSK1346856 which does not have the sulfonamide group attached to the quinolone. Notably, the naphthyl analogue GSK3184135 is also an AO substrate, which suggested that AO metabolism was not at the quinolone ring but involves the 2-amino pyrimidine (2-AP). Metabolite identification analysis was performed to confirm the site of AO metabolism for each of the compounds listed in Figure 7.3-7 and Figure 7.3-8 shows the metabolite for each compound. It can be seen that AO metabolism resulted in oxidation at either the quinoline and 2-AP, but the site of metabolism was dependant on the substitution of the quinoline at the 3-position. From these analyses it also appeared that AO metabolism in human liver cytosol tended to favour the 2-AP, whereas in rat liver cytosol the quinoline was typically favoured if the quinoline was not sterically hindered by the presence of the sulfonamide group. SB-277011 is a known human AO substrate and used as a positive control: interestingly it is not an AO substrate in rat [144], highlighting the potential problem of using preclinical species to predict human metabolism.

Figure 7.3-8 Metabolite Identification of Pi3Ky Lead Series Compounds

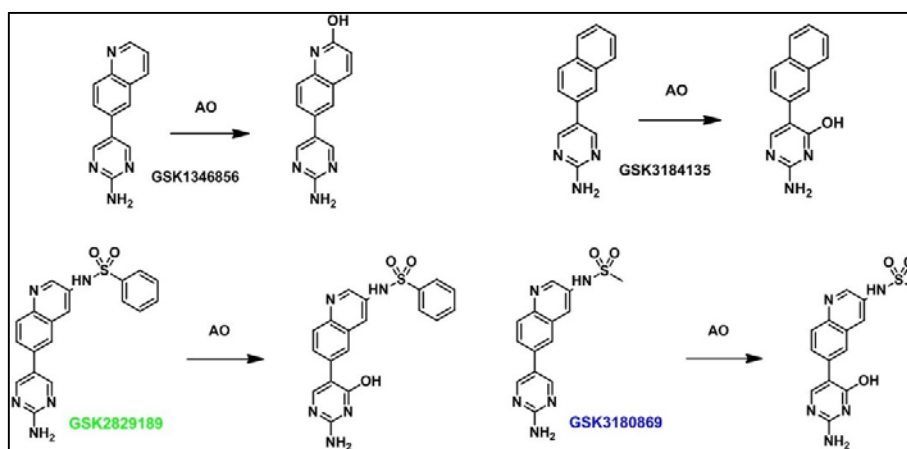


Figure 7.3-8 shows routes of metabolism analysis from the *in vitro* cytosolic AO assay for a set of Pi3Ky compounds in Figure 7.3-7

7.3.1.1 The effect of a “Magic Methyl” group on AO metabolism

Based on the positive AO data and MET ID information (Figure 7.3-8), a methyl was introduced onto the quinoline core at the 7-position which reduced metabolic susceptibility (Figure 7.3-9). The reason the 7-position was initially targeted by the medicinal chemistry team was to sterically hinder access to the 2-amino pyrimidine by AO and reduce susceptibility to nucleophilic attack of the electron deficient carbon atom by AO. From a synthetic perspective, the 7-position was readily accessible, and this position was less likely to negatively impact potency. In practice the 7-methyl substitution blocked the AO metabolism and increased potency by an order of magnitude.

Figure 7.3-9 The Effect of a “Magic Methyl” Group on AO Metabolism

Compound ID	Structure	Species	AO Substrate
GSK2829189		Human	Yes
		Rat	Yes
GSK3203206		Human	No
		Rat	No
GSK3180869		Human	Yes
		Rat	Yes
GSK3203207		Human	No
		Rat	No

Figure 7.3-9 shows results of an *in vitro* liver cytosolic AO assay for Pi3Ky compounds with and without a methyl at the 7 positions of the quinoline ring

Once the effect of the 7-methyl on AO metabolism was shown *in vitro*, a translation to reduce *in vivo* clearance was assessed. GSK2829189 and GSK3180869 along with their 7-methyl analogues GSK3203206 and GSK3203207 were profiled in both rat and minipig *in vivo* PK studies (Figure 7.3-10 and Figure 7.3-11). There is an increase in potency of almost a log unit for the methyl analogues of GSK2829189 and GSK3180869. It was interesting to note that the microsomal stability of GSK3203206 was reduced, indicating there was an increase in P450 or other phase I metabolism by introducing this methyl group, which was likely to the increase in lipophilicity from a relatively high baseline for GSK2829189 of cLogP from 2.5 to 2.7. The microsomal stability was not affected by the methyl group on GSK3203207 where the lipophilicity was only increased from 0.89 to 1.1. The metabolic stability was confirmed for each compound using an *in vitro* hepatocyte assay which have both Phase I and II enzymes (Figure 7.3-11).

It can also be seen that the *in vivo* CL_b for GSK3203206 increased relative to GSK2829189, which was consistent with the increase in *in vitro* clearance, whereas the CL_b for GS3203207 was substantially reduced relative to its non-methyl analogue GSK3180869 (>LBF CL_b). Importantly, the effect on CL_{bu} can be seen with GSK3203207.

This reduction in unbound clearance shows that the lead optimisation to address the AO metabolic liability of the quinoline template was successfully achieved.

Figure 7.3-10 Rat PK With and Without a “Magic Methyl”

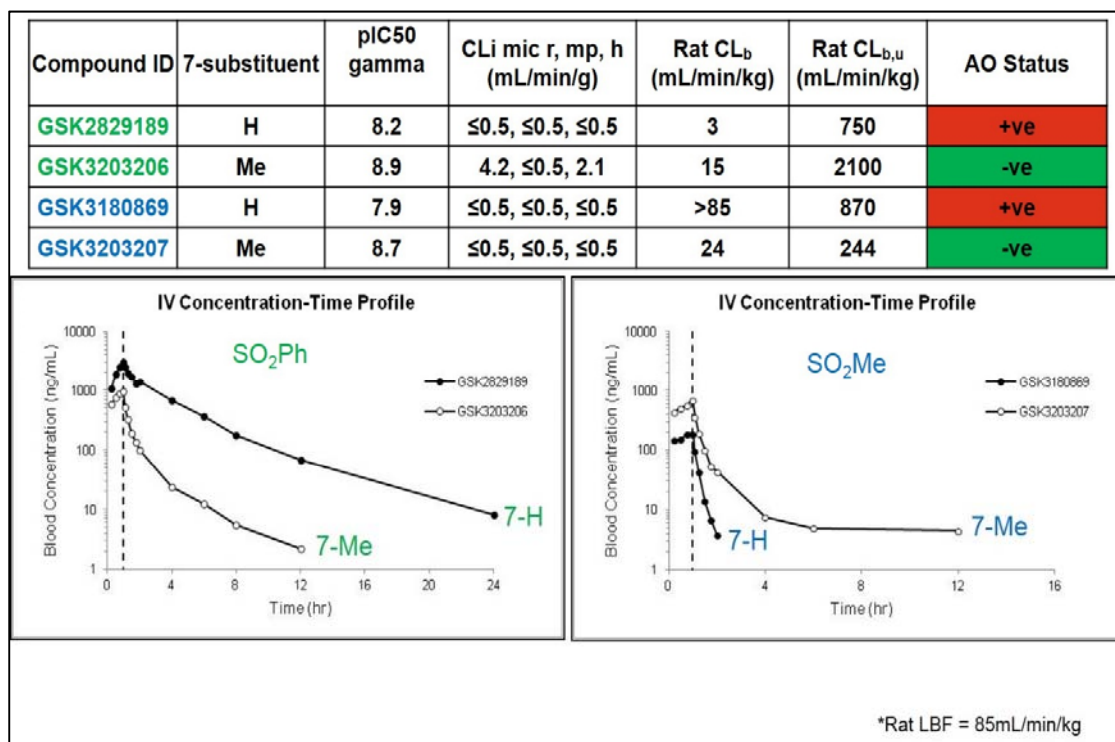


Figure 7.3-10 shows the *in vivo* rat PK profiles for the methyl and non-methyl analogues. Intravenous dose of 1mg/kg

As previously discussed the dog is not a good preclinical PK model where AO metabolism could occur as it does not express an active form of the enzyme. This was discussed earlier in this section and highlighted by the carbazeran example. To increase confidence in the human PK predictions a second preclinical species was selected. The minipig has become the preferred non-rodent species in recent years, however, there is generally limited published PK and metabolism information available for this species. The Pi3Ky program presented an opportunity to investigate AO metabolism and PK in the minipig. This additional workstream resulted in the Pi3K AO substrates and methyl analogues being profiled using *in vitro* minipig microsomes, liver cytosol and hepatocytes, *in vivo* PK profiles were also generated.

Figure 7.3-11 shows the *in vitro* and *in vivo* data generated using the minipig. It can be seen there were some species differences, with minipig *in vitro* and *in vivo* clearance for GSK3203206 being lower than its non-methyl analogue. The minipig also confirmed what had been seen with the rat that GSK3203207 had lower CL_{bu} indicating that the AO liability had been addressed and increasing confidence that the human *in vitro* AO data should translate to human PK. This work which was also part of a larger analysis has also helped establish the minipig as an alternative non-nodent PK species to the dog which does express AO and is a useful second species to predict human PK.

Figure 7.3-11 Minipig an Alternative Pre-Clinical Species to Help Predict Human AO Metabolism

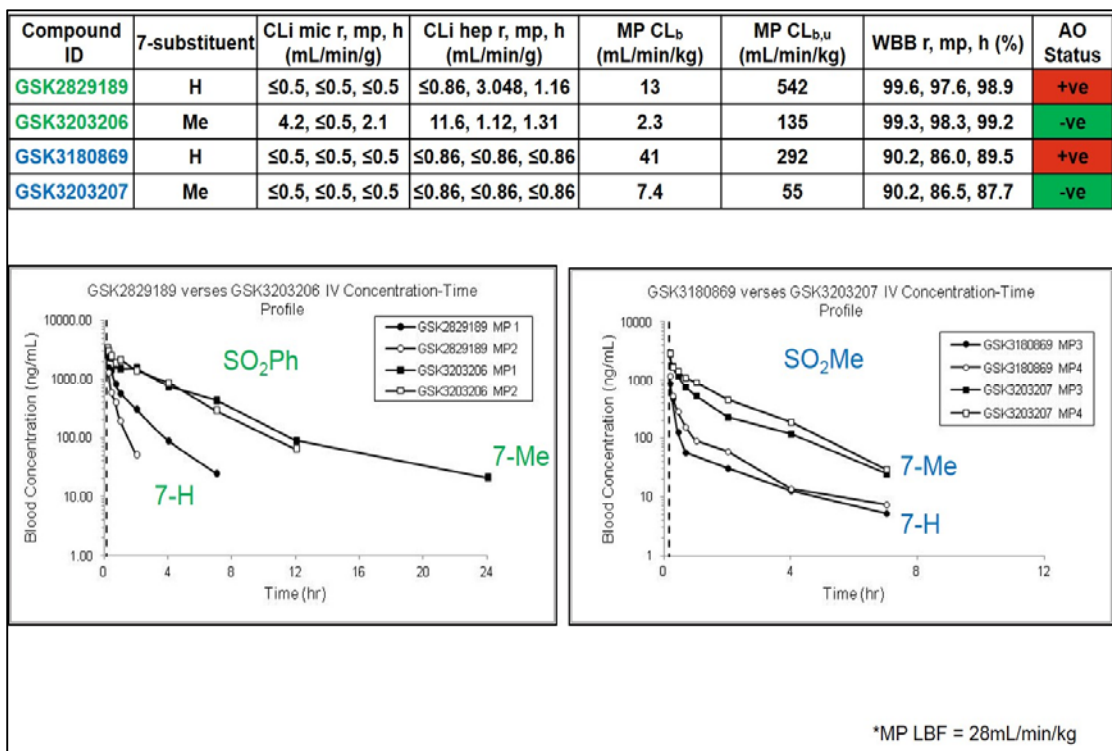


Figure 7.3-11 shows the *in vivo* rat PK profiles for the “magic” methyl and non-methyl analogues of the quinoline series. Intravenous dose of 0.5mg/kg

7.4 Investigation of the Estimated Dose using Various Methods for the Pi3K δ Program for Oral Administration in Asthma

As has been described in section 5.3, Pi3K δ kinase is involved in several processes related to the pathology of asthma. The Pi3K δ program involved the development of an oral drug for the treatment of asthma and COPD, and therefore introduced additional parameters that required consideration when applying dose prediction.

Following on from previous work, I extended my evaluation of the various dose prediction methods that are available for an early oral drug discovery program to an oral therapy, in order to address the following questions:

1. What is the impact of the parameters of potency, volume of distribution and clearance on the predicted dose when we only have *in silico* or *in vitro* estimates for these parameters?
2. How do these parameters affect our decision-making process on compound ranking and progression?
3. How does the estimated dose change when our preliminary input data is subsequently refined?

All of compounds that are registered under the Pi3K δ program code 17951 were retrieved (10th October 2017). The measured physicochemical and biomimetic data were retrieved using the Physchem Summary Table in Helium for excel and the compounds removed that had no *AGP*, *HSA*, *IAM* and HPLC DE_{max} . The *in vitro* potency data named as Pi3KD_TRFRET_SM as well as the cellular potency data (Pi3KDELTA_WB_CYTOSTIM) were retrieved. Altogether a complete dataset for 1509 compounds was available for dose estimation analysis. From the parent smiles / structures, so called “simple physchem properties” were calculated (molecular weight, polar surface area, number of proton donor and acceptor groups and the number of rotatable bonds). The *in silico* rat volume of distribution, intrinsic clearance, and DE_{max} data have been calculated using the derived property server (DPS) associated with the GSK repository database. The measured intrinsic clearance and rat volume of distribution data that were available for a much smaller number of compounds were then retrieved. The data was then merged using Tibco™ Spotfire® program.

The following parameters were also calculated for this analysis as they are required inputs for the complex McGinnity dose estimation method (Equation 38) for oral drugs.

Equation 38

$$\text{Dose} \left(\frac{\text{mg}}{\text{kg}} \right) = \frac{\frac{24}{\tau} \cdot \text{MEC} \cdot V_{dss} \cdot (k_a - k_{el})}{F \cdot k_a \left(\frac{1}{1 - \exp(-k_{el}\tau)} - \frac{1}{1 - \exp(-k_a\tau)} \right)}$$

7.4.1 Absorption Rate

The CLND solubility was multiplied with the measured AMP permeability at pH 7.4. The logarithmic values of the product term were used to classify the compounds into low, medium and high absorption compounds as described in the introduction (section 4.2.3). Based on the estimated absorption categories different absorption rates (k_{ab} or k_a) were used in the complex dose estimation method (Equation 38) [24].

7.4.2 Elimination Rate

The elimination rate (k_{el}) was calculated using Equation 55.

Equation 55

$$k_{el} = \frac{CL}{V_{dss}}$$

The clearance was calculated using the well-stirred model according to Equation 50

Equation 50

$$\text{Human Total Clearance (wsm)} = \frac{(CL_{int}(\text{mL per min per g})24.5) \cdot 18}{(CL_{int}(\text{mL per min per g})24.5) + 18}$$

The CL_{int} value was estimated using the *in silico* model described in section 6.9.2, or measure using an *in vitro* hepatocyte assay as described in section 6.3.

7.4.3 Estimating Clinical Dose from DE_{max} (HPLC DE-DP)

The dose estimation based on the drug efficiency (DE_{max}) concept (HPLC DE-DP) was carried out using Equation 37.

Equation 37 previously shown

$$\text{Dose (mg)} = \frac{\text{mw. } 10^{-1(\text{pIC}_{50})}}{\text{HPLC DE}_{\text{max}}}$$

Where the HPLC DE_{max} was calculated using Equation 34.

The estimated oral dose considering twice a day administration has been calculated using Equation 38 [24], with the input of *in silico* absorption, volume of distribution and clearance. The estimated dose has been named *in silico* DMPK-DP. Using the absorption potential derived from the measured solubility and permeability data, the human volume of distribution was calculated based on the measured *HSA* and *IAM* data, and the *in silico* clearance model data was used. The estimated dose was calculated and is referred to as *in vitro* DMPK-DP. In both cases the dose was estimated using both the enzyme and whole blood cellular potency, as well as incorporating the HPLC DE_{max} into the calculation of MEC, as described by Equation 53. As potency has the greatest impact on the dose, it is important to investigate the observed differences between the enzyme and cellular potency. For the whole blood value, the actual free compound concentration can be different from the incubation concentration that has been applied to the cell, due to solubility, cellular permeability, and the non-specific binding of test compounds. It is also important to consider the target substrate concentrations will be different in a whole cell assay. Therefore, IC₅₀ is not a translatable value across *in vitro* assays. The fundamental relationship between IC₅₀ and K_i was described by Cheng and Prusoff in the 1970's [146], and is a critical concept in pharmacology which is often overlooked. As a result, IC₅₀ is frequently misused or taken as an absolute value which will translatable across *in vitro* and *in vivo* assays. Equation 56 describes the relationship between IC₅₀ and K_i.

Equation 56

$$K_i = \frac{IC_{50}}{1 + \left(\frac{S}{K_m}\right)}$$

K_i is the inhibition constant, IC_{50} is concentration of inhibitor which causes 50% inhibition, K_m is the Michaelis constant for the substrate (S), S is the substrate concentration

The plot of the Pi3K δ enzyme and cellular potency for the compounds is shown in Figure 7.4-1.

Figure 7.4-1 The Plot of the Measured *In Vitro* Enzyme and Whole Blood Pi3K δ Potency of the Compounds

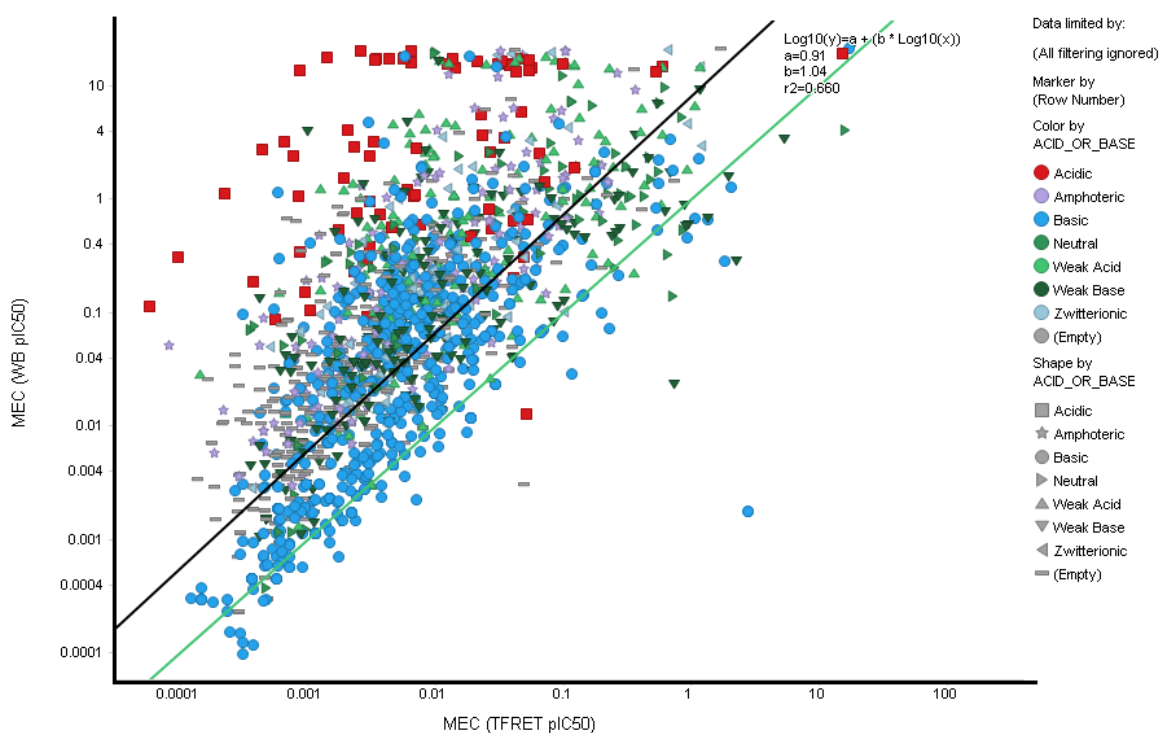


Figure 7.4-1 shows a plot of WB (Whole blood) potency versus enzyme potency. The line of unity is green, and the regression line is black.

Figure 7.4-1 clearly highlights that there are differences between the two types of potency data. A higher concentration of the compounds is needed to achieve the 50% inhibition

(IC_{50}) using the whole blood assay. The acidic compounds (marked as red squares) which typically bind more strongly to serum albumin, show the biggest discrepancy/offset.

The simplest dose estimation that can be carried out very early in the drug discovery process is based only on the measured potency and estimated drug efficiency of the compounds. This has been described earlier as the DE-DP approach using Equation 37. The *in vitro* potency is only considered in this DE-DP calculation equation, as the drug efficiency includes the nonspecific binding of the compounds, which effectively reduces the actual biophase concentration. However, during the whole blood potency assay, other effects of the compounds are also included, as previously indicated. Therefore, it is important to investigate how these processes affect the estimated dose. Figure 7.4-2 shows the plot obtained for the estimated dose (on a logarithmic scale) when the Pi3K δ enzyme and whole blood potency data are used in Equation 37.

Figure 7.4-2 The Plot of the DE-DP Dose Estimation Method using the Pi3Kδ Enzyme and Whole Blood Cellular Potency Data.

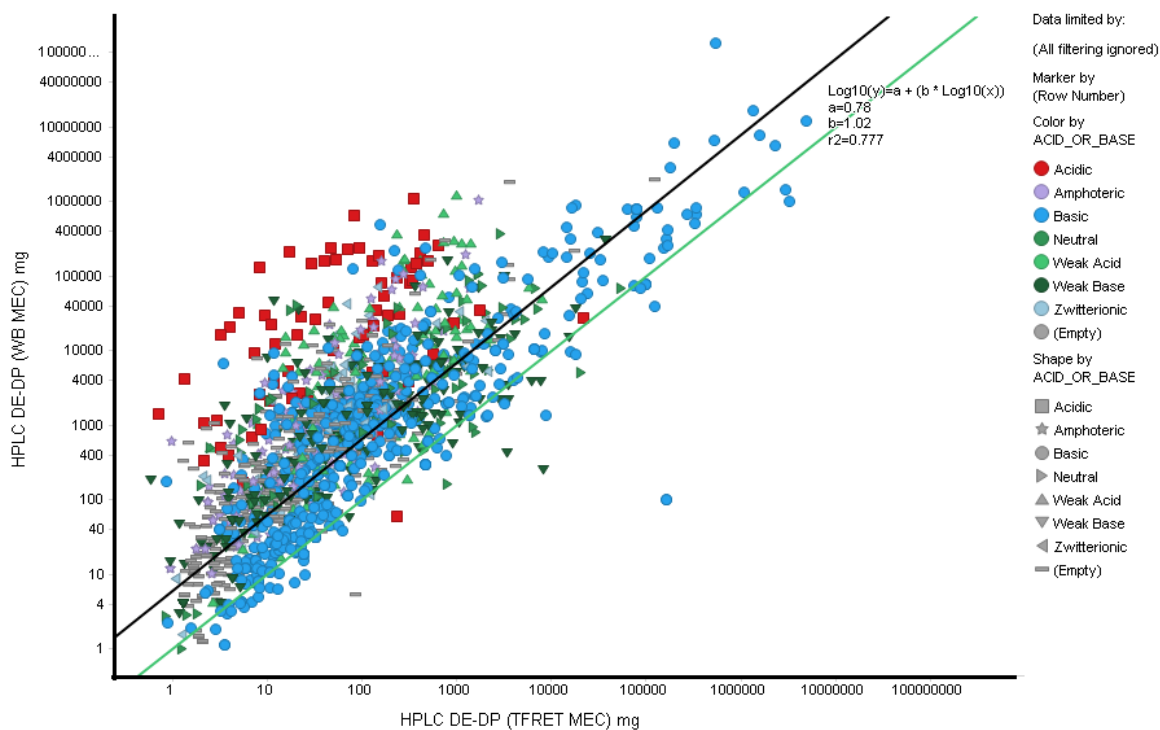


Figure 7.4-2 shows a plot of the predicted dose for HPLC DE-DP (WB) versus HPLC DE-DP enzyme. The line of unity is green and the regression line is black.

It can be seen in Figure 7.4-2 that the estimated dose is higher when the whole blood (WB) potency is used, where a higher concentration is expected to produce the same effect as in the isolated enzyme assay. This is especially evident for the acidic compounds marked as red squares. A similar trend is seen when comparing the enzyme and WB potencies (Figure 7.4-1). The basic compounds have similar upwards shifts in the estimated dose when the whole blood potency is considered, although it is less dramatic than that seen with the acid compounds and is indicative of the nature of the binding to *HSA* over *IAM*. The correlation between the two dose estimates is reasonably good (r^2 above 0.77). This correlation is reassuring and highlights that as long as potency is considered in a consistent manner when analysing compounds, then either value can be used. However, it is important to be mindful that enzyme-based potency values will always represent a best-case scenario, and it is advantageous to switch to a cellular

potency value when possible, particularly when refining dose estimations in the later stages of lead optimisation.

The differences between the estimated dose calculated by applying the different potency data in Equation 38 are compared in the plot of the *in silico* DMPK-DP, which is shown in Figure 7.4-3. The correlation between the two estimated dose values using the whole blood and the enzyme potencies is even higher when the *in silico* DMPK-DP dose prediction is employed. This could be explained by the equation containing absorption and elimination rates, in addition to the volume of distribution, and not only the potency and binding data used in the HPLC DE-DP estimation method. As the other pharmacokinetic inputs were the same in both axis of the dose estimation methods, the observed differences between the applications of the enzyme and whole blood potency are much smaller (the correlation coefficient was above 0.9).

Figure 7.4-3 A Comparison of the Estimated Dose using *In Silico* Inputs in the DMPK-DP Method Using Enzyme Potency and Whole Blood Cellular Potency Data.

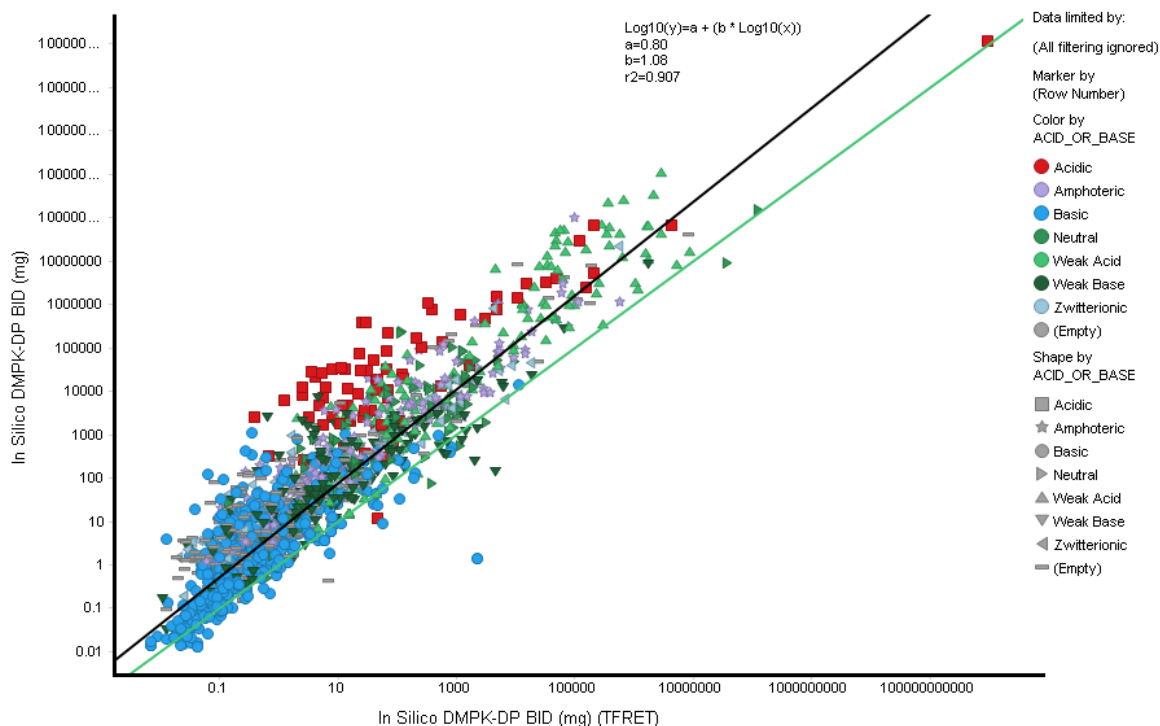


Figure 7.4-3 shows a plot of *in silico* DMPK-DP using WB potency verses *in silico* DMPK-DP using enzyme potency. The line of unity is green and the regression line is black.

Figure 7.4-3 shows the plot of the calculated dose using the *in vitro* DMPK-DP method by Equation 38, with the enzyme potency and whole blood potency data as inputs, and using the *in vitro* volume of distribution, intrinsic clearance measured using hepatocytes, and the absorption rate that was estimated from the measured kinetic solubility and artificial membrane permeability data.

Figure 7.4-4 The Plot of the Estimated Dose using the *In Vitro* DMPK-DP Method with *In Vitro* Inputs of V_{dss} , Intrinsic Clearance and Absorption Rate with Enzyme and Whole Blood Potency Data.

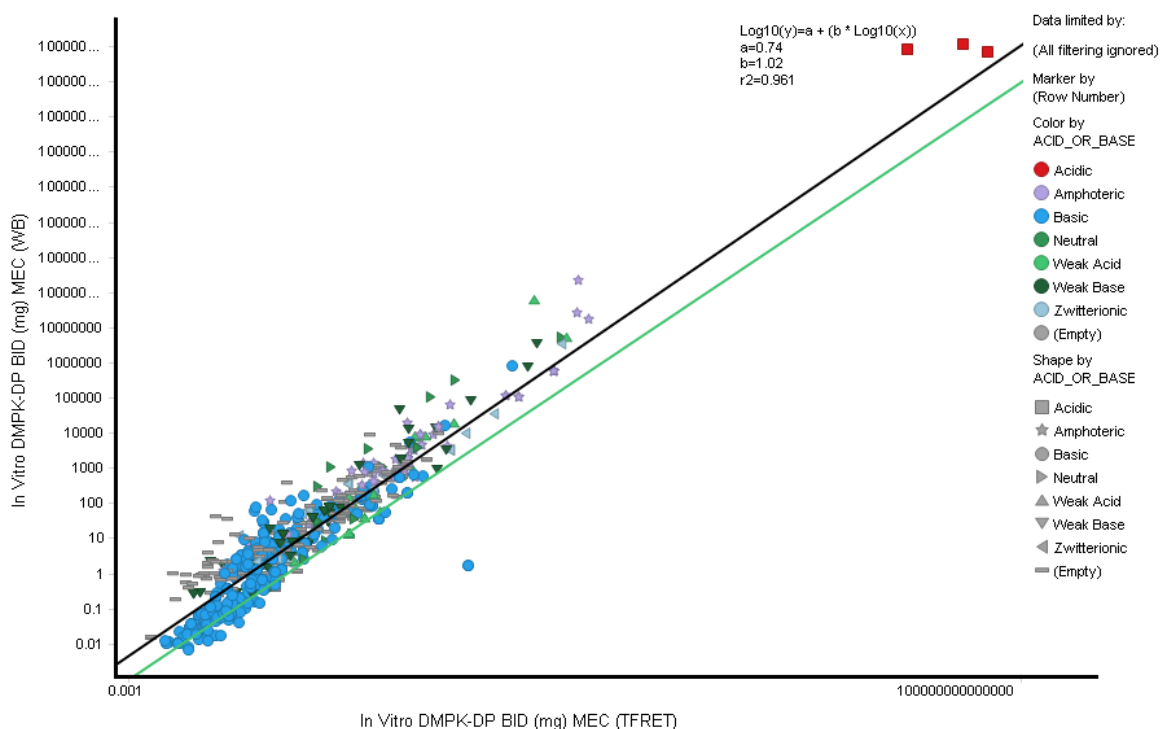


Figure 7.4-4 shows a plot of *in vitro* DMPK-DP using WB potency verses *in vitro* DMPK-DP using enzyme potency. The line of unity is green and the regression line is black.

It can be seen that the impact of the potency data is even smaller when the *in vitro* volume of distribution, clearance and absorption rate data are used in the equation. A substantial factor influencing this is that the majority of the acidic compounds and compounds that showed high potency drop off in the whole blood assay were not submitted for *in vitro* clearance measurements meaning the number of compounds included in the plot is substantially less. From the previous plot shown in Figure 7.4-3, it was clear the acidic compounds showed the biggest discrepancy between the estimated dose between the enzyme and whole blood potency dose estimation data. Clearly, the Pi3Kδ program team deselected the majority of acidic compounds prior to *in vitro* DMPK profiling. Based on this dose estimation analysis, the deselection of these compounds appears to be the correct decision, as the *in vitro* DMPK-DP estimation approach indicates they would represent very high clinical dose compound relative to others within

the lead optimisation process. A pharmacokinetic reason for the high clinical dose estimation is driven by the nature of acidic compound distribution. The VD_{ss} of acid class compounds is typically very low, which is an important observation when considering the HPLC DE-DP dose estimation method.

The difference between the calculated dose when using the *in silico* and *in vitro* input in Equation 38 is shown in Figure 7.4-5. It is interesting to observe that the estimated dose for acidic compounds is much greater when the actual *in vitro* clearance data are used in the dose estimation equation. The explanation for this is the *in silico* clearance, elimination rate, volume were underestimated when compared with the measured *in vitro* data for these parameters.

Figure 7.4-5 The Plot of the DMPK-DP Estimated Dose Method with *In Silico* and *In Vitro* Inputs of V_{dss}, Clearance and Absorption Rate.

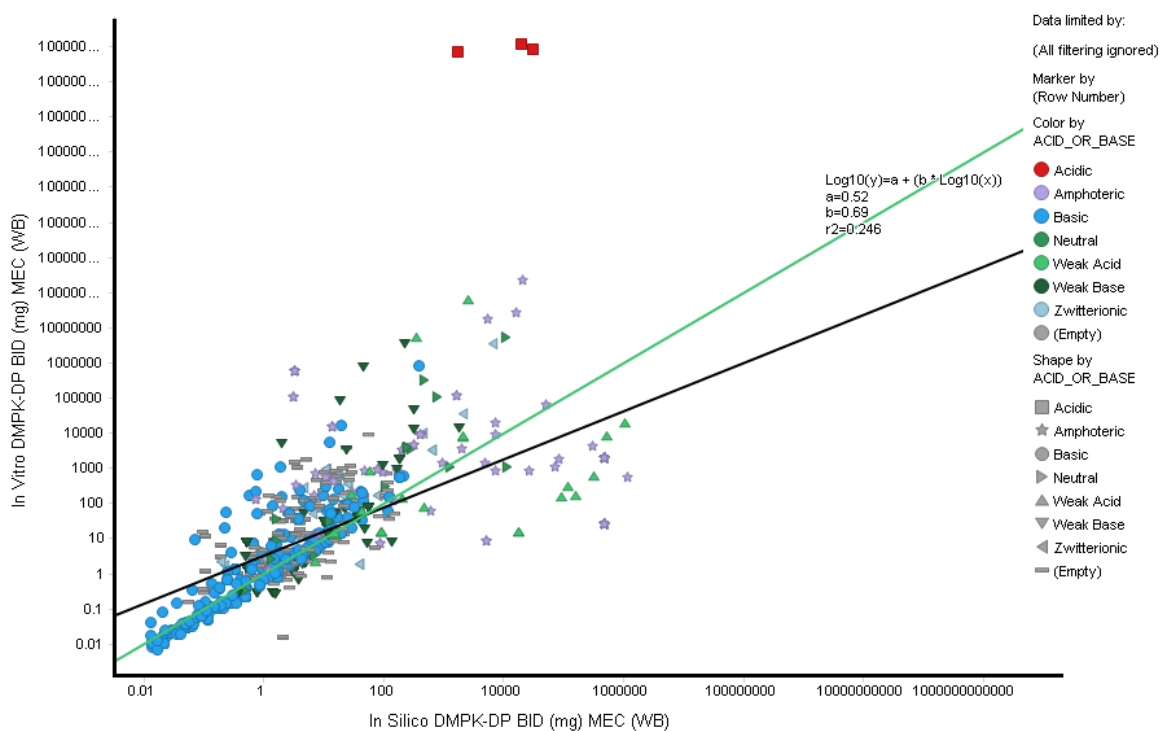


Figure 7.4-5 shows a plot of *in vitro* DMPK-DP using WB potency versus *in silico* DMPK-DP using WB potency. The line of unity is green and the regression line is black.

The estimated dose for the majority of the basic compounds was very similar when the *in silico* and the *in vitro* PK parameters were used in the equation, especially around the low dose range <100mg. The discrepancies are much more significant for compounds for which the estimated dose was very large. It can be concluded from the plot that the error is proportionally larger when the predicted dose is large. However, the rank order is what is really important here, and the high dose compounds can easily be identified by either method.

Figure 7.4-6 shows the trend between the estimated dose using the simple HPLC DE-DP Equation 37 with measured cellular potency and the dose estimated using the *in silico* DMPK-DP method using Equation 38. The discrepancies between the estimated dose values are much larger than expected. However, when used as a ranking tool, it can be seen that both the DE-DP and *in silico* DMPK-DP methods show the progression of an early lead compound for the Pi3K δ program. This can be seen in Figure 7.4-6 where GSK3343837 represents a relatively early lead series compound of interest and GSK3493251 is the eventual candidate molecule from what was referred to as the short hinge series.

Figure 7.4-6 The Plot of the Estimated Dose Using the DE-DP Method Using Whole Blood Potency Data and the *In silico* DMPK-DP Method Using Whole Blood Potency Data. Lead Series Progression Has Also Been Shown With GSK3343837 and GSK3493251.

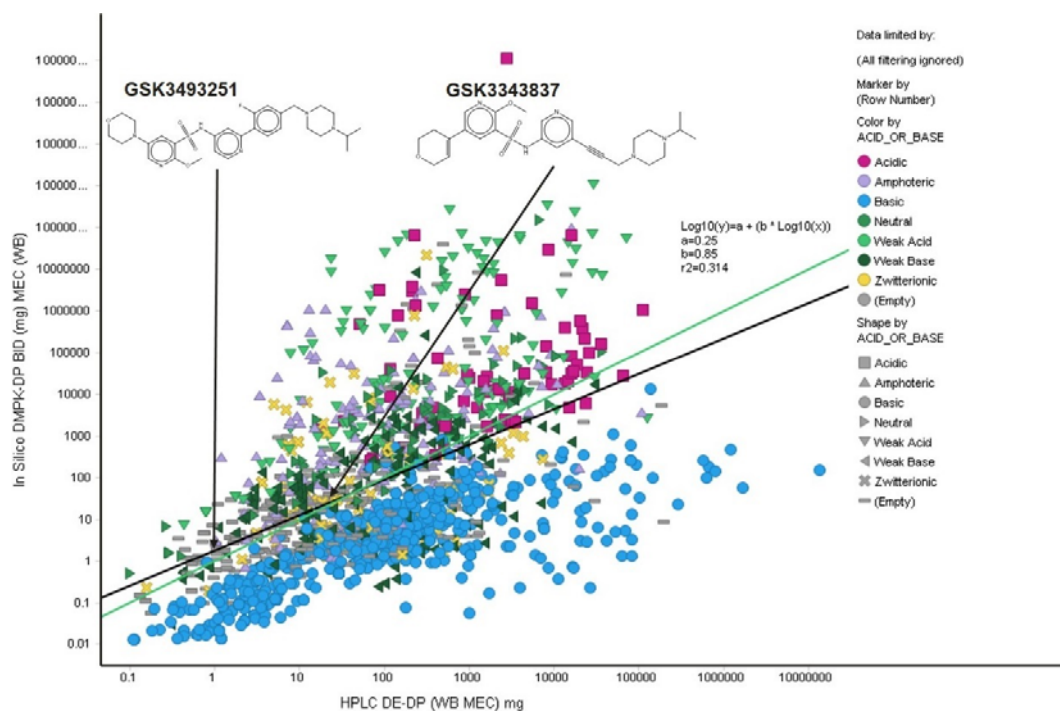


Figure 7.4-6 shows a plot of *in silico* DMPK-DP using WB potency versus HPLC DE-DP using WB potency. The line of unity is green and the regression line is black.

The advantage of using *in silico* data is there are fewer limitations to the number of compounds that can be analysed in the early stages of drug discovery, as there is less reliance on expensively acquired *in vitro* data, such as from *in vitro* clearance assays. However, *in silico* analysis relies on the quality of the *in silico* model or models being used, which need to be both predictive and accurate. When using the *in silico* DMPK-DP based approach, there are several *in silico* models that can be used, including CL, V_{dss} and K_a . Without evidence for the accuracy of the *in silico* DMPK-DP method, it is reasonable to question the validity of this approach for effectively filtering compounds for further progression. To help evaluate whether the *in silico* DMPK-DP predictions are consistent with measured parameters, Figure 7.4-7 shows the comparison of HPLC DE-DP and *in vitro* DMPK-DP. It can be seen that by including measured *in vitro* data in

Equation 38, the same rank order as seen with the *in silico* approach was achieved, which is emphasised by highlighting early lead compound GSK3343837 and the eventual candidate GSK3493251 have the same rank order as in the previous Figure 7.4-6.

Figure 7.4-7 The plot of the estimated dose using the DE-DP method with equation 38 and the whole blood potency data and the *in vitro* DMPK-DP method using equation 31 with *in vitro* measured data input and the whole blood potency.

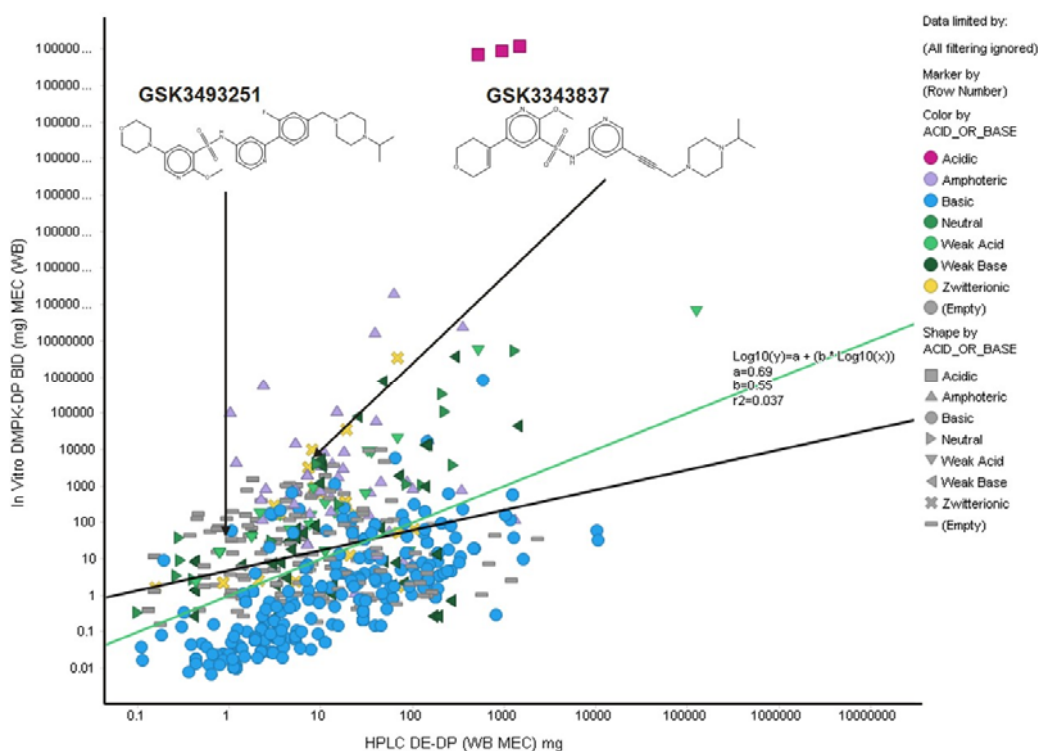


Figure 7.4-7 shows a plot of *in vitro* DMPK-DP using WB potency verses *in vitro* DMPK-DP using WB potency. The line of unity is green and the regression line is black.

When performing this type of early dose prediction analysis, it is important that the dose estimation methodology is used in a pragmatic way, and to recognise that the absolute dose estimation value is not the primary consideration. In a drug discovery setting, the ability to predict the rank order is more important than the absolute accuracy of the dose prediction. This helps guide the selection process to progress compounds or groups of compounds to more expensive, in-depth and labour intensive *in vitro* and *in vivo* assays,

where the output can then be used to further refine the dose estimation approaches and thus improve the accuracy of prediction. By applying this type of approach, the goal of achieving improved physicochemical properties with good ADME properties should be possible.

In Figure 7.4-8, a comparison of *in vitro* DMPK-DP and *in vivo* DMPK-DP has been plotted. It might be considered that *in vivo* data would offer the greatest opportunity to give the most accurate estimation of clinical dose. However, this is open to debate, as the accuracy of scaling *in vivo* preclinical PK data to human is modest, although this has been and continues to be a commonly used method of predicting human pharmacokinetics [147] [148] Figure 7.4-8 shows the dose prediction methods that compare *in vivo* data and *in vitro* data to enable the rank order of compound progression to be identified. GSK3343837, and the eventual candidate GSK3493251 are highlighted

Figure 7.4-8 The Plot of the Estimated Dose Using In vitro DMPK-DP and In vivo DMPK-DP Data with and the Whole Blood Potency Data Using Equation 31.

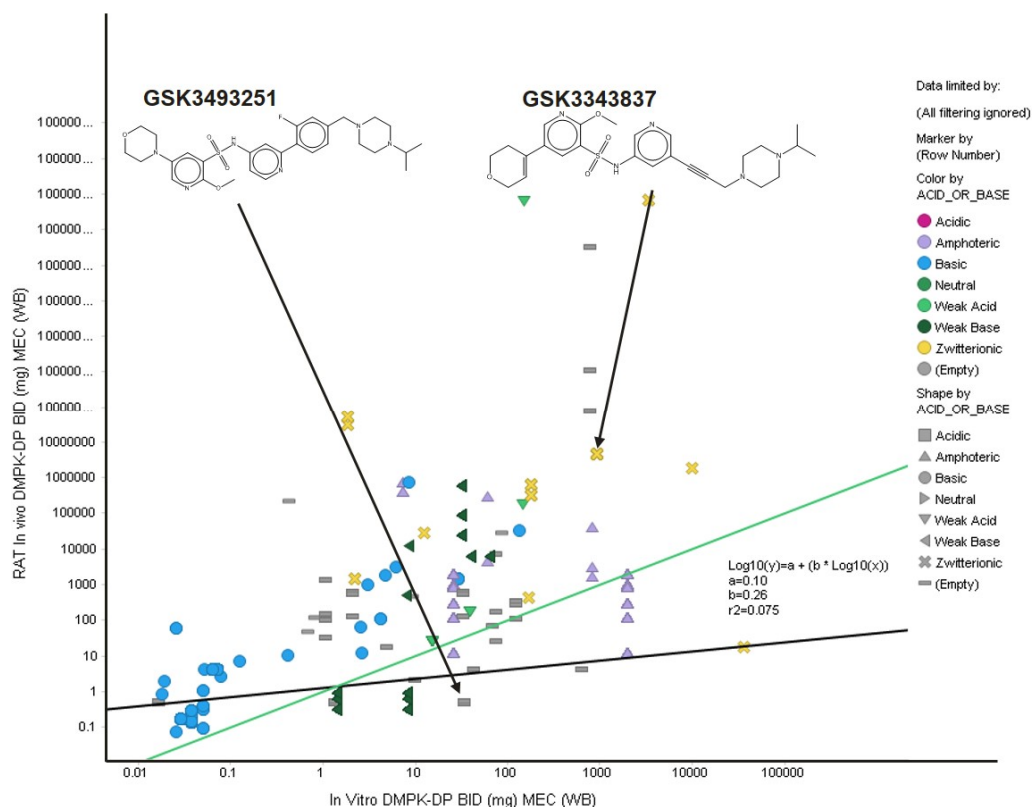


Figure 7.4-8 shows a plot of *in vivo* rat DMPK-DP using WB potency versus *in vitro* DMPK-DP using WB potency. The line of unity is green, and the regression line is black.

An important comparison is between the *in vivo* DMPK-DP and HPLC DE-DP methodology to establish if very early dose estimation can successfully identify the lower dose compounds and reduce the reliance on extensive *in vitro* and *in vivo* testing required for the *in vitro* and *in vivo* DMPK-DP approaches (Figure 7.4-9). Once again, this figure shows how the simplest high throughput HPLC DE-DP method tracks the important trend identifying the progression of the short hinge series, from GSK3343837 to the eventual candidate GSK3493251. This is despite the obvious limitations of the HPLC DE-DP method for estimating dose. This approach enables the identification of compounds with enhanced physicochemical and ADME properties linked to a cluster of chemical space

where a candidate quality molecule may sit. This can be performed with a fraction of the data required for classical dose estimation using the *in vitro* or *in vivo* DMPK-DP methods.

Figure 7.4-9 The plot of the Estimated Dose using the DE-DP Method with Whole Blood Potency Data and the *In vivo* DMPK-DP Method with *In Vitro* Measured Data Inputs and Whole Blood Potency Data

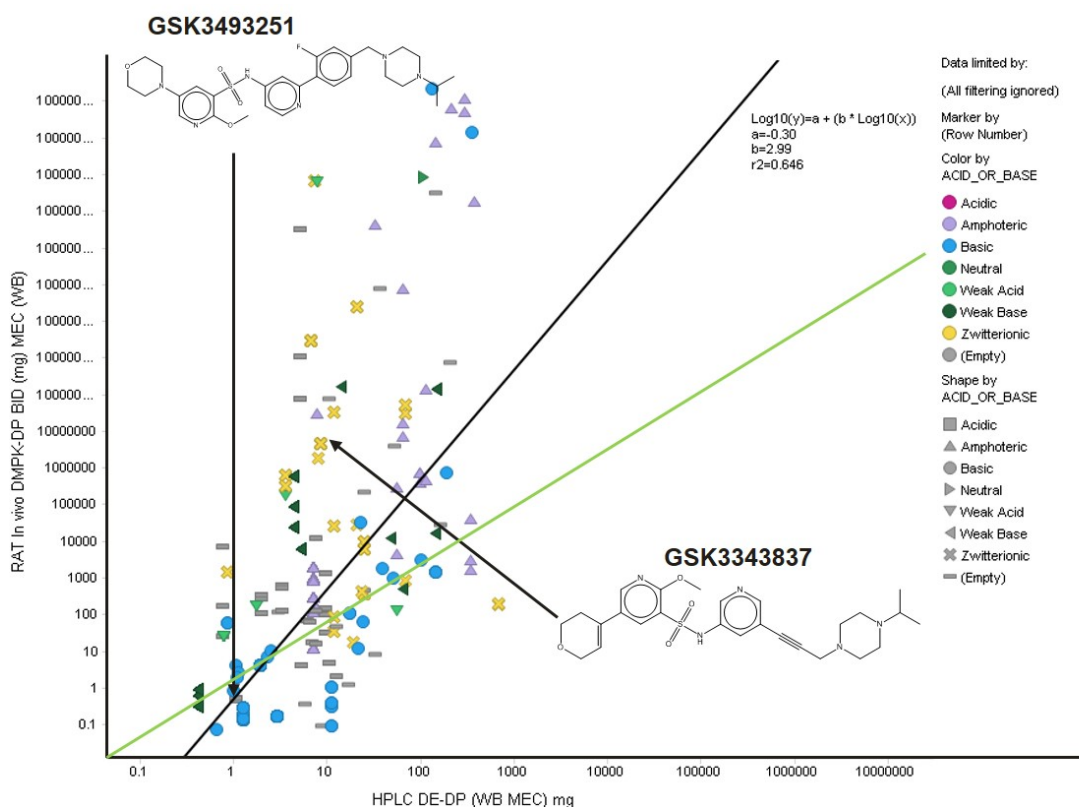


Figure 7.4-9 shows a plot of *in vivo* rat DMPK-DP using WB potency versus HPLC DE-DP using WB potency. The line of unity is green, and the regression line is black.

Table 7-7 shows physicochemical properties of the short hinge sulphonamide series were maintained throughout the lead optimisation process which is captured in the single parameter DE_{max} . The reason for the lower estimated dose for GSK3493251 is the improved potency.

Table 7-7 Summary of Physicochemical Properties for Pi3K δ Hit Compound (GSK3343837) to Lead (GSK33493251)

Compound ID	IC50 Enzyme	IC50 WB	MW	cLogp	LogD	FaSSIF Solubility (ug/mL)	%HSA	%AGP	CHI IAM	DEmax %	PFI	Acid/Base Class	Permeability (nm/s)
GSK3343837A	8.2	7.3	511.6	0.957	1.91	1000	84.2	54.8	23.16	24.2	4.91	Zwitterionic	13
GSK3493251A	9	8.2	584.7	4.478	1.78	1000	83.2	54.5	26.08	21.1	3.78	Zwitterionic	19

Table 7-7 show the maintenance of physicochemical properties from the original hit GSK3343837 to the eventual lead compound GSK3493251, and improvement in the pharmacology was the main difference.

Given that the compounds under development were for oral administration, one final consideration was to assess the importance of including the additional complexity of absorption rate in the McGinnity equation (Equation 38). Does the inclusion of other parameters such as K_a substantially improve the quality of the dose estimation approach? To evaluate this, the K_a parameter was removed, to take us back to the simpler DMPK-DP equation (Equation 39) used in the IV analysis for the Pi3K γ program.

Equation 38 Previously shown

$$\text{Dose} \left(\frac{\text{mg}}{\text{kg}} \right) = \frac{\frac{24}{\tau} \text{MEC} \cdot V_{dss} \cdot (k_a - k_{el})}{F \cdot k_a \left(\frac{1}{1 - \exp(-k_{el} \cdot \tau)} - \frac{1}{1 - \exp(-k_a \cdot \tau)} \right)}$$

Equation 39 Previously shown

$$\text{Dose} \left(\frac{\text{mg}}{\text{kg}} \right) = \frac{\frac{24}{\tau} \text{MEC} \cdot V_{dss} \cdot (\exp(k_{el} \cdot \tau) - 1)}{F}$$

It can be seen in

Figure 7.4-10 where the comparison of *in silico* DMPK-DP without K_a to the HPLC DE-DP is plotted, that there is an almost identical correlation to that seen in Figure 7.4-6, which is a plot of *in silico* DMPK-DP and HPLC DE-DP (the correlation coefficients of these analysis are 0.227 and 0.314, respectively).

Figure 7.4-10 The plot of the Estimated Dose Using the DE-DP Method and the *In Silico* DMPK-DP Method Without K_a .

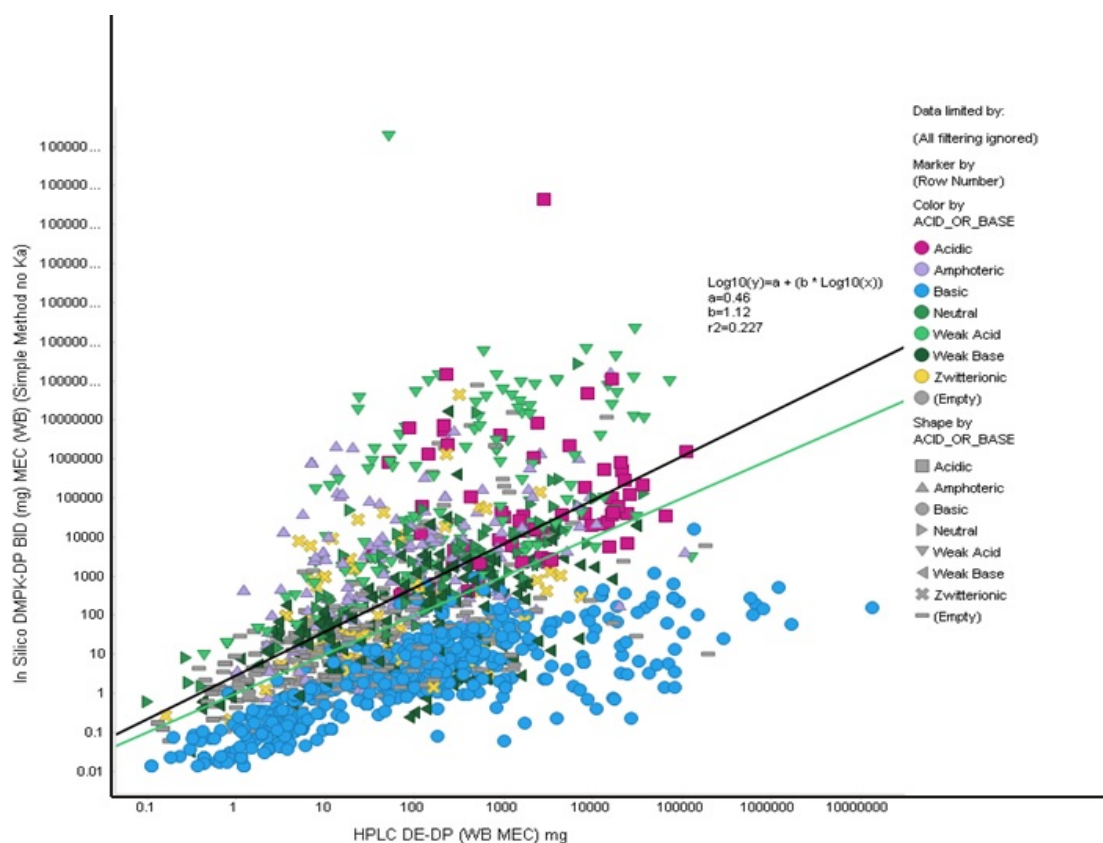


Figure 7.4-10 shows a plot of *in silico* DMPK-DP with no absorption constant (K_a , Equation 39) using WB potency versus HPLC DE-DP using WB potency. The line of unity is green, and the regression line is black.

This analysis shows that the majority of compounds in the low dose range (<100mg) were common to both dose estimation methods with varying degrees of data complexity within the DMPK-DP method. Much larger discrepancies in the magnitude of the dose estimation were observed when the estimated dose was large (above 1000 mg).

The conclusion from this study is that within one program of compounds, the estimated dose shows a good trend regardless of the dose estimation method used. The potency value, clearance and the volume of distribution all have an impact on the estimated dose. The absorption potential appears to be less important, and as such, the simple DMPK-DP Equation 39 could be considered for oral programs with minimal loss of predictivity, although further analysis with other programs is required to confirm this.

Although there is a poor correlation coefficient between the *in silico* clearance and the *in vitro* clearance, the trend in the estimated dose within the series is consistent, and highlighted by the lead (GSK33433837) and candidate (GSK3493251) examples throughout this analysis. This suggests that there is value in using the simple dose estimation method as a tool that can be used to filter and rank large numbers of compounds early in drug discovery to select compounds to progress to more complex and in-depth *in vitro* and ultimately *in vivo* studies.

7.5 Do the Properties of Inhaled/Pulmonary Drugs Differ from Oral Non-CNS and Oral CNS Drugs?

In contrast to oral drugs, the physicochemical properties required for optimal inhaled therapies are less well-defined. To identify the principle descriptors for inhaled drugs, the biomimetic properties of known drugs administered via the inhaled route, JAK inhaled project compounds, oral drugs targeting non-CNS disorders and oral drugs targeting CNS disorders were evaluated. The aim was to determine which physicochemical features clearly define drugs that are delivered by a specific route by selecting examples from what would be typically considered the major small molecule drug classes alongside a set of project compounds from an inhaled lead optimisation program. A major challenge when investigating properties of inhaled drugs is the limited number of marketed drugs in this class. Generally, there is a relatively small number of inhaled drugs approved by the regulatory authorities relative to the oral drug space. An additional challenge for the inhaled space is its domination by inhaled steroids, β agonists and a few muscarinic antagonists. This differs substantially from the oral space where the breadth of biological targets is much more extensive.

When comparing the known properties of oral, inhaled, inhaled JAKi and CNS drugs (Table 7-8), no significant differences could be identified by analysing the box plots for

albumin binding (Log k_{HSA}), *AGP* binding (Log k_{AGP}), cLogP or total polar surface area (tPSA) as can be seen in Figure 7.5-1 to Figure 7.5-7.

Table 7-8 Physicochemical Properties of Known Drugs for Oral, Oral CNS, Inhaled Drug Administration and GSK Inhaled JAK Lead Optimisation Compounds.

Application	Colour Key
CNS	
Inhaled	
JAKi	
Oral/Systemic	

Drug Name	Application	MW	TPSA	cLogP	Log k HSA	Log k AGP	Log k IAM	Colour Key
Venlafaxine	CNS	277.4	32.7	3.27	-0.43	0.03	2.06	
Diflunisal	CNS	250.2	57.5	4.40	1.65	-0.01	1.82	
Tolmetin	CNS	257.3	59.3	2.21	1.08	-0.91	1.17	
Amitriptyline	CNS	277.4	3.2	4.85	0.91	1.05	2.96	
Amoxapine	CNS	313.8	36.9	3.41	0.85	1.06	3.02	
Aripiprazole	CNS	448.4	44.8	5.31	1.46	1.22	2.9	
Cabergoline	CNS	451.6	71.7	4.17	0.68	0.67	2.98	
Citalopram	CNS	324.4	36.3	3.13	0.40	0.44	2.66	
Clomipramine	CNS	314.9	6.5	5.92	1.16	1.18	3.17	
Donepezil	CNS	379.5	38.8	4.60	0.77	0.52	2.33	
Fluoxetine	CNS	309.3	21.3	4.57	0.99	0.99	2.94	
Fluvoxamine	CNS	318.3	56.8	3.32	0.40	0.59	2.73	
Haloperidol	CNS	375.9	40.5	3.85	0.76	0.73	2.46	
Loxapine	CNS	327.8	28.1	3.98	1.05	1.06	2.76	
Maprotiline	CNS	277.4	12.0	4.52	0.77	0.99	3.03	
Mianserin	CNS	264.4	6.5	3.76	1.00	1.01	2.8	
Nortriptyline	CNS	263.4	12.0	4.32	0.77	1.03	2.84	
Olanzapine	CNS	312.4	30.9	3.01	0.77	0.72	2.71	
Pergolide	CNS	314.5	19.0	4.40	0.73	1.04	2.85	
Pimozide	CNS	461.6	41.0	6.40	1.41	1.47	2.83	
Protriptyline	CNS	263.4	12.0	4.87	0.69	1.03	2.79	

Drug Name	Application	MW	TPSA	cLogP	Log k HSA	Log k AGP	Log k IAM	Colour Key
Selegiline	CNS	187.3	3.2	3.02	0.89	1.12	3.07	
Sumatriptan	CNS	295.4	65.2	0.74	-0.42	-0.04	1.92	
Tomoxetine	CNS	255.4	21.3	3.94	0.81	0.74	2.76	
Zolmitriptan	CNS	287.4	57.4	1.29	-0.10	-0.03	1.93	
Carbamazepine	CNS	236.3	46.3	2.38	0.50	0.51	1.75	
Procyclidine	CNS	287.4	23.5	4.59	0.91	0.80	2.57	
Rolipram	CNS	275.3	47.6	1.72	0.56	0.79	1.62	
Phenytoin	CNS	252.3	58.2	2.09	0.68	0.15	1.83	
Lamotrigine	CNS	256.1	90.7	2.53	0.16	-0.33	1.49	
Trazodone	CNS	371.9	45.8	3.85	1.02	0.56	2.09	
Ziprasidone	CNS	412.9	48.5	4.21	1.42	1.09	2.62	
Benzonatate	Inhaled set	603.7	121.4	2.54	0.44	0.32	2.24	
Dextromethorphan	Inhaled set	271.4	12.5	3.95	0.34	0.55	2.8	
Oxolamine	Inhaled set	245.3	42.2	2.39	1.08	0.38	2.37	
Pranlukast	Inhaled set	481.5	123.0	5.07	1.67	0.85	2.38	
Trospium	Inhaled set	392.5	46.5	-1.16	0.18	0.63	2.14	
Umeclidinium	Inhaled set	428.6	29.5	1.60	0.62	0.87	2.55	
Xylometazoline	Inhaled set	244.4	24.4	5.38	0.01	0.51	2.74	
Xylometazoline	Inhaled set	244.4	24.4	5.38	0.02	0.45	2.98	
SB-332235	Inhaled set	410.7	121.5	2.61	1.68	0.72	2.29	
Ramatroban	Inhaled set	416.5	88.4	3.97	1.34	0.16	1.95	
Seratrodast	Inhaled set	354.4	71.4	4.95	1.50	0.58	2.15	
Tranilast	Inhaled set	327.3	84.9	3.99	1.40	0.20	1.81	
Elubrixin	Inhaled set	463.3	110.8	3.32	1.47	0.75	2.65	
GSK1004723	Inhaled set	641.3	50.6	8.61	1.42	1.58	2.82	
GSK240928	Inhaled set	380.4	125.9	2.92	0.49	0.37	1.77	
GSK922892	Inhaled set	381.9	38.1	4.04	0.91	1.04	2.85	
GSK256066	Inhaled set	518.6	131.7	3.80	0.95	0.68	2.2	
Albuterol	Inhaled set	239.3	72.7	0.06	-0.55	-1.22	1.1	
Ambroxol	Inhaled set	378.1	58.3	2.33	0.60	0.73	2.5	
Brompheniramine	Inhaled set	319.2	16.1	3.30	0.68	0.68	2.8	
Butamirate	Inhaled set	307.4	38.8	4.08	-0.09	0.52	2.52	
Cetirizine	Inhaled set	388.9	53.0	2.08	0.85	0.23	2.28	
Chlophedianol	Inhaled set	289.8	23.5	3.63	0.40	0.67	2.63	
Cloperastine	Inhaled set	329.9	12.5	5.38	1.05	1.00	2.92	
Dimethoxanate	Inhaled set	358.5	42.0	4.21	0.74	0.87	2.8	
Ipratropium	Inhaled set	332.5	46.5	-2.19	0.36	0.02	1.67	
Ipratropium	Inhaled set	332.5	46.5	-2.19	-0.55	0.05	1.8	
Mabuterol	Inhaled set	310.7	58.3	2.77	-0.34	0.43	2.43	
GSK1645469	Inhaled set	447.6	71.5	4.32	0.96	0.90	2.74	

Drug Name	Application	MW	TPSA	cLogP	Log k HSA	Log k AGP	Log k IAM	Colour Key
GSK1645469	Inhaled set	447.6	71.5	4.32	1.01	0.91	2.77	
GSK1399686	Inhaled set	821.1	197.1	4.17	0.18	0.43	2.66	
Oxymetazoline	Inhaled set	260.4	44.6	4.61	-0.06	0.45	2.7	
Phenyltoloxamine	Inhaled set	255.4	12.5	4.23	0.80	0.76	2.79	
Pimethixene	Inhaled set	293.4	3.2	4.92	1.21	1.13	3.05	
Promethazine	Inhaled set	284.4	6.5	4.40	0.94	0.97	2.99	
Pyrilamine	Inhaled set	285.4	28.6	3.23	0.44	0.49	2.56	
Tiotropium	Inhaled set	392.5	59.1	-1.71	-0.38	0.51	2.05	
GSK1247150	Inhaled set	655.7	122.7	5.72	1.41	1.04	2.6	
SB-731445	Inhaled set	478.4	100.3	3.85	0.97	0.51	1.9	
GSK1223684	Inhaled set	529.4	113.5	3.47	1.09	0.62	2.07	
GW784568	Inhaled set	526.6	80.7	4.14	1.28	0.89	2.47	
6-Methoxy-3-nitroquinoline	Inhaled set	204.2	67.9	2.18	0.90	-0.10	1.87	
Beclomethasone dipropionate	Inhaled set	521.0	107.0	4.26	1.14	0.85	2.43	
Budesonide	Inhaled set	430.5	93.1	2.91	0.88	0.37	2.19	
Ciclesonide	Inhaled set	540.7	99.1	5.25	1.35	1.01	2.61	
Cyclosporin A	Inhaled set	1202.6	278.8		0.79	0.31	2.18	
Dexamethasone	Inhaled set	392.5	94.8	1.79	0.41	-0.08	1.89	
Fluticasone furoate	Inhaled set	538.6	93.8	4.26	1.23	1.02	2.46	
Fluticasone propionate	Inhaled set	500.6	80.7	3.80	1.01	0.27	2.4	
Ibudilast	Inhaled set	230.3	34.4	3.25	0.99	0.49	2.19	
Isofluprednone	Inhaled set	378.4	94.8	1.27	0.10	-0.13	1.71	
Losmapimod	Inhaled set	383.5	71.1	3.98	0.70	0.21	2.04	
Metaproterenol	Inhaled set	211.3	72.7	0.08	0.28	-1.01	1.42	
Mometasone furoate	Inhaled set	521.4	93.8	4.12	1.28	0.90	2.43	
GSK678361	Inhaled set	410.4	97.1	3.75	0.96	0.48	2.1	
Ozagrel	Inhaled set	228.3	55.1	1.60	0.35	-1.97	0.94	
Procaterol	Inhaled set	290.4	85.4	0.66	-0.59	-0.86	1.56	
GW842470	Inhaled set	458.3	84.2	4.58	1.40	1.26	2.48	
Theophylline	Inhaled set	180.2	72.7	-0.03	-0.42	1.00	0.58	
GW846428	Inhaled set	993.1	357.5		1.03	0.61	2.5	
GW766994	Inhaled set	451.4	96.7	3.08	0.95	0.59	1.87	
Fenoterol	Inhaled set	303.4	93.0	0.98	-0.13	-0.11	2.14	
Formoterol	Inhaled set	344.4	90.8	1.26	-0.12	0.21	2.2	
Formoterol	Inhaled set	344.4	90.8	1.26	-0.04	0.29	2.41	
GSK1367441	Inhaled set	497.0	76.5	3.71	1.01	0.93	2.32	
GSK1000064	Inhaled set	392.4	94.7	4.62	1.23	0.72	2.16	
Oseltamivir	Inhaled set	312.4	90.7	2.13	-0.55	0.05	2.07	

Drug Name	Application	MW	TPSA	cLogP	Log k HSA	Log k AGP	Log k IAM	Colour Key
Terbutaline	Inhaled set	225.3	72.7	0.48	-0.58	-0.88	1.57	
Tiaramide	Inhaled set	355.8	65.8	0.67	-0.13	0.04	1.83	
GSK159802	Inhaled set	521.6	106.6	3.99	1.46	1.30	3.37	
Indacaterol	Inhaled set	392.5	85.4	2.97	1.17	1.03	3.18	
GSK3336961A	JAKi	566.6	126.9	4.38	1.61	0.98	2.93	
GSK3686622A	JAKi	469.5	111.2	3.89	1.27	0.76	2.98	
GSK3733362A	JAKi	526.6	140.3	2.98	1.38	1.10	2.28	
GSK3901000A	JAKi	423.5	88.6	2.36	1.13	0.70	2.48	
GSK3901790A	JAKi	423.5	83.4	2.28	1.18	0.77	2.40	
GSK3896132A	JAKi	437.5	74.6	2.64	1.19	0.76	2.00	
GSK3376417A	JAKi	521.0	100.4	3.67	0.69	0.47	2.06	
GSK3532706A	JAKi	481.9	100.4	3.28	0.97	0.70	2.66	
GSK3780731A	JAKi	395.5	87.3	3.62	1.17	0.85	2.96	
GSK3800430A	JAKi	469.6	93.5	5.01	1.32	0.88	1.22	
GSK3816662A	JAKi	454.5	99.1	3.41	1.30	0.83	2.68	
GSK3859782A	JAKi	568.7	130.9	5.33	1.37	0.93	3.11	
GSK3860551A	JAKi	438.5	79.1	4.49	1.27	0.93	2.54	
GSK3861033A	JAKi	509.6	99.4	3.95	1.22	0.93	2.56	
GSK3863783A	JAKi	415.4	101.2	1.47	0.95	0.52	2.74	
GSK3845209A	JAKi	398.4	94.6	2.19	1.17	0.43	3.18	
GSK3074811A	JAKi	410.8	108.1	2.13	0.75	0.32	1.47	
GSK3454697A	JAKi	489.9	97.2	3.08	0.90	0.33	2.42	
GSK3487568A	JAKi	479.9	100.4	2.88	0.76	0.30	3.12	
GSK3489723A	JAKi	519.9	117.4	2.15	0.59	0.12	2.57	
GSK3515539A	JAKi	450.9	97.1	2.67	0.94	0.42	1.90	
GSK3519625A	JAKi	475.9	117.4	2.71	1.02	0.45	2.53	
GSK3901334A	JAKi	474.6	84.1	3.85	1.49		2.16	
GSK3635481A	JAKi	356.4	104.3	3.28	1.25	0.66	0.50	
GSK3908922A	JAKi	409.5	97.4	2.00	1.18	0.76	1.55	
Montelukast	Oral/Systemic	586.2	70.4	8.47	1.78	1.43	2.5	
Zafirlukast	Oral/Systemic	575.7	115.7	7.09	1.67	0.78	2.4	
Prednisolone	Oral/Systemic	360.4	94.8	1.42	0.07	-0.37	1.68	
Cilostazol	Oral/Systemic	369.5	81.9	3.53	0.91	0.33	2.08	
Efavirenz	Oral/Systemic	315.7	38.3	3.73	1.43	0.98	2.53	
Finasteride	Oral/Systemic	372.5	58.2	3.01	0.85	0.45	2.21	
Lansoprazole	Oral/Systemic	369.4	67.9	2.60	0.94	0.40	1.91	
Mifepristone	Oral/Systemic	429.6	40.5	4.65	1.24	1.03	2.49	
Nadolol	Oral/Systemic	309.4	82.0	0.38	-0.22	-0.16	1.3	
Pioglitazone	Oral/Systemic	356.4	68.3	3.53	1.50	0.51	1.96	
Roxithromycin	Oral/Systemic	837.1	216.9	2.29	-0.07	0.60	2.78	

Drug Name	Application	MW	TPSA	cLogP	Log k HSA	Log k AGP	Log k IAM	Colour Key
Simvastatin	Oral/Systemic	418.6	72.8	4.48	1.34	0.96	2.57	
Telmisartan	Oral/Systemic	514.6	72.9	7.29	1.36	0.68	2.52	
Amiloride	Oral/Systemic	229.6	156.8	0.11	-0.27	-0.13	1.85	
Candesartan cilexetil	Oral/Systemic	610.7	143.3	7.08	1.51	1.12	2.37	
Diazoxide	Oral/Systemic	230.7	58.5	1.20	0.52	-0.68	1.54	
Etodolac	Oral/Systemic	287.4	62.3	3.43	1.25	0.32	1.83	
Flurbiprofen	Oral/Systemic	244.3	37.3	3.75	1.60	-0.05	1.49	
Furosemide	Oral/Systemic	330.7	122.6	1.90	1.09	-1.16	1.6	
Glimepiride	Oral/Systemic	490.6	124.7	3.96	1.51	0.40	1.84	
Glipizide	Oral/Systemic	445.5	130.2	2.57	1.27	0.03	1.36	
Glyburide	Oral/Systemic	494.0	113.6	4.24	1.52	0.39	1.93	
Indomethacin	Oral/Systemic	357.8	68.5	4.18	1.65	0.18	1.7	
Irbesartan	Oral/Systemic	428.5	87.1	6.04	1.30	1.10	1.62	
Ketoprofen	Oral/Systemic	254.3	54.4	2.76	1.57	-0.79	1.63	
Mycophenolic acid	Oral/Systemic	320.3	93.1	2.29	1.24	-0.83	1.36	
Naproxen	Oral/Systemic	230.3	46.5	2.82	1.95	-1.06	1.47	
Nimesulide	Oral/Systemic	308.3	101.2	3.21	1.51	0.09	1.72	
Oxaprozin	Oral/Systemic	293.3	63.3	2.95	1.64	0.51	1.56	
Piroxicam	Oral/Systemic	331.4	99.6	1.89	1.42	0.23	1.42	
Pravastatin	Oral/Systemic	424.5	124.3	2.05	-0.18	-0.54	1.36	
Acebutolol	Oral/Systemic	336.4	87.7	1.71	-0.32	0.63	1.12	
Bupropion	Oral/Systemic	239.7	29.1	3.21	0.44	0.57	2.16	
Clonidine	Oral/Systemic	230.1	36.4	1.43	-0.24	0.15	1.47	
Desloratadine	Oral/Systemic	310.8	24.9	3.83	0.85	1.05	2.93	
Diphenhydramine	Oral/Systemic	255.4	12.5	3.45	0.33	0.60	2.06	
Domperidone	Oral/Systemic	425.9	78.8	4.27	1.02	0.92	2.42	
Ebastine	Oral/Systemic	469.7	29.5	6.94	1.63	1.34	3.12	
Fenofibrate	Oral/Systemic	360.8	52.6	5.23	1.46	1.11	2.58	
Fexofenadine	Oral/Systemic	501.7	81.0	1.96	0.45	0.02	1.9	
Granisetron	Oral/Systemic	312.4	50.2	1.72	0.35	0.52	2.53	
Guanabenz	Oral/Systemic	231.1	74.3	2.98	0.83	0.82	2.66	
Mefloquine	Oral/Systemic	378.3	45.2	3.67	1.38	1.11	0.5	
Metergoline	Oral/Systemic	403.5	46.5	4.69	1.28	1.09	2.98	
Metoclopramide	Oral/Systemic	299.8	67.6	2.23	0.15	0.23	2.28	
Mibefradil	Oral/Systemic	495.6	67.5	6.36	1.10	1.11	2.96	
Neostigmine	Oral/Systemic	223.3	29.5	-2.81	0.82	-0.53	1.22	
Primaquine	Oral/Systemic	259.4	60.2	2.60	0.56	0.81	2.68	
Prochlorperazine	Oral/Systemic	373.9	9.7	4.38	1.37	1.39	3.18	
Promethazine	Oral/Systemic	284.4	6.5	4.40	1.04	0.99	3.11	
Propafenone	Oral/Systemic	341.4	58.6	3.64	0.84	0.92	2.54	

Drug Name	Application	MW	TPSA	cLogP	Log k HSA	Log k AGP	Log k IAM	Colour Key
Propranolol	Oral/Systemic	259.3	41.5	2.75	0.42	0.84	2.56	
Quinidine	Oral/Systemic	324.4	45.6	2.79	0.54	0.85	2.74	
Tamsulosin	Oral/Systemic	408.5	99.9	2.17	0.36	0.60	2	
Verapamil	Oral/Systemic	454.6	64.0	4.47	1.01	0.58	2.48	
Bicalutamide	Oral/Systemic	430.4	107.3	2.71	1.36	0.32	2.16	
Celecoxib	Oral/Systemic	381.4	78.0	4.37	1.41	1.31	2.4	
Dapsone	Oral/Systemic	248.3	86.2	0.89	0.60	0.04	1.55	
Felodipine	Oral/Systemic	384.3	64.6	5.30	1.28	0.91	2.56	
Flutamide	Oral/Systemic	276.2	74.9	3.34	1.15	0.27	2.26	
Isradipine	Oral/Systemic	371.4	103.6	3.92	1.16	1.32	2.26	
Leflunomide	Oral/Systemic	270.2	55.1	2.32	1.02	0.51	2.22	
Letrozole	Oral/Systemic	285.3	78.3	1.43	0.15	-0.60	1.78	
Lovastatin	Oral/Systemic	404.5	72.8	4.08	1.24	0.87	2.46	
Metolazone	Oral/Systemic	365.8	92.5	2.06	0.69	0.57	1.82	
Nevirapine	Oral/Systemic	266.3	58.1	2.65	0.06	-0.15	1.41	
Nimodipine	Oral/Systemic	418.4	119.7	4.00	0.98	0.70	2.03	
Nisoldipine	Oral/Systemic	388.4	110.5	4.58	0.96	0.65	2.14	
Nitrendipine	Oral/Systemic	360.4	110.5	3.73	1.13	0.69	2.3	
Pentoxifylline	Oral/Systemic	278.3	78.9	0.12	-0.46	-1.92	0.97	
Spironolactone	Oral/Systemic	416.6	60.4	0.00	0.78	0.50	2.12	
Valdecoxib	Oral/Systemic	314.4	86.2	1.83	1.13	0.90	2.03	
Zileuton	Oral/Systemic	236.3	66.6	2.48	0.98	0.78	1.88	
Bendroflumethiazide	Oral/Systemic	421.4	118.4	1.73	0.42	0.27	2.05	
Indapamide	Oral/Systemic	365.8	92.5	2.96	0.46	0.42	1.88	
Zidovudine	Oral/Systemic	267.2	133.1	0.04	-0.88	-1.71	0.49	
Abacavir	Oral/Systemic	286.3	101.9	0.81	-0.34	0.02	1.31	
Acrivastin	Oral/Systemic	348.4	53.4	1.46	0.65	0.10	1.92	
Alosetron	Oral/Systemic	294.4	53.9	1.74	0.47	0.51	1.92	
Aminoglutethimide	Oral/Systemic	232.3	72.2	0.77	-0.48	-0.30	1.05	
Clemastine	Oral/Systemic	343.9	12.5	5.45	1.25	1.18	3.19	
Dipyridamole	Oral/Systemic	504.6	145.4	1.49	0.84	0.82	2.44	
Ketoconazole	Oral/Systemic	531.4	69.1	3.64	1.17	0.75	2.31	
Mebendazole	Oral/Systemic	295.3	84.1	3.08	1.07	1.00	2.1	
GSK527886	Oral/Systemic	371.5	74.6	2.70	1.06	0.91	2.17	
Nicardipine	Oral/Systemic	479.5	113.7	5.23	1.25	0.94	2.58	
Pinacidil	Oral/Systemic	245.3	73.1	1.91	0.14	-0.17	1.79	
Prazosin	Oral/Systemic	383.4	107.0	2.03	0.74	0.53	1.81	
Riluzole	Oral/Systemic	234.2	48.1	3.24	1.13	0.37	2.18	
Triamterene	Oral/Systemic	253.3	129.6	1.61	0.16	-0.09	1.6	

Figure 7.5-1 The Box Plot of MW for Marketed Oral, Oral CNS, Inhaled Drugs and Inhaled JAK Project Compounds

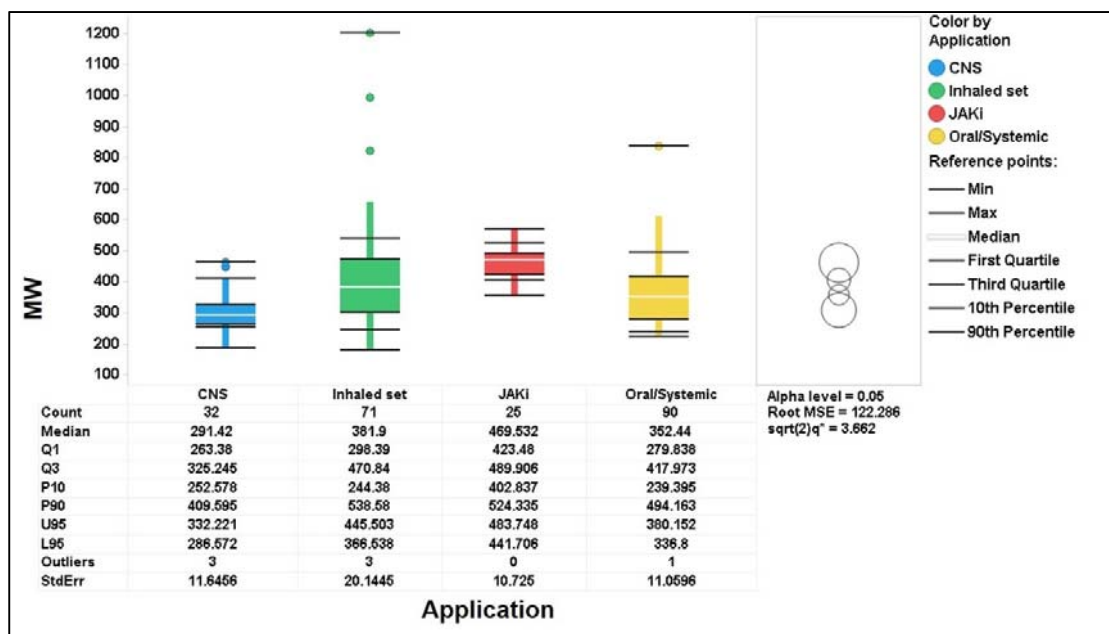


Figure 7.5-1 is a box plot of MW versus different target class molecules (oral, oral CNS, Inhaled, and Inhaled Lead Optimisation JAK program compounds). The righthand panel rings represent a confidence interval (CI) analysis showing statistical analysis between the different classes based on a 95% CI

Figure 7.5-2 The Box Plot of Albumin Binding (*HSA*) for Marketed Oral, Oral CNS, Inhaled Drugs and Inhaled JAK Project Compounds

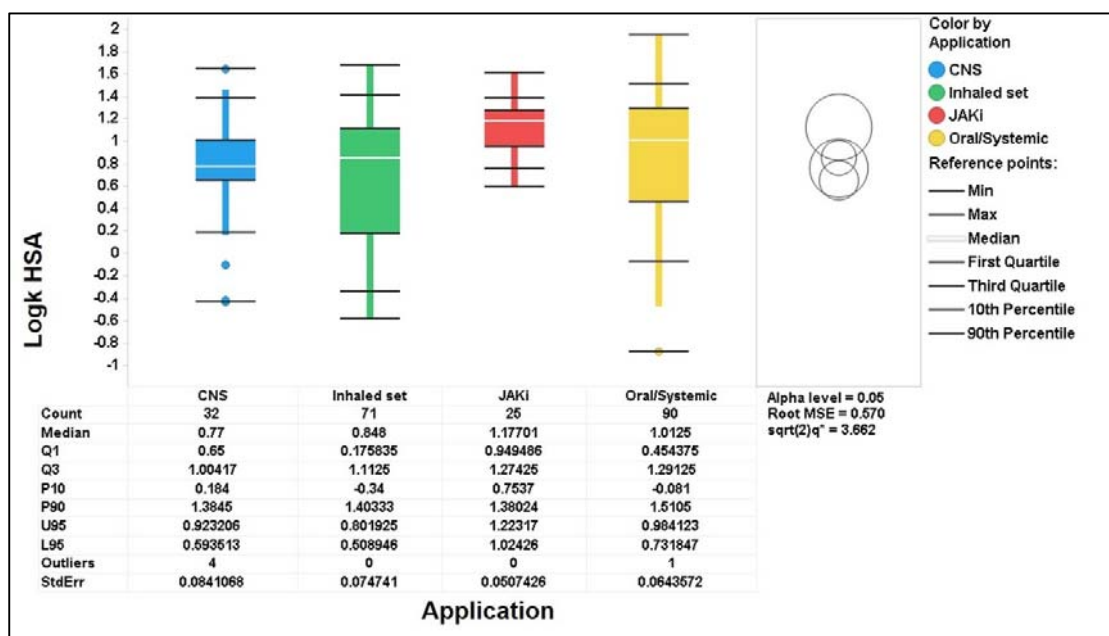


Figure 7.5-2 is a box plot of HSA binding versus different target class molecules (oral, oral CNS, Inhaled, and Inhaled Lead Optimisation JAK program compounds). The righthand panel rings represent a confidence interval (CI) analysis showing statistical analysis between the different classes based on a 95% CI

Figure 7.5-3 The Box Plot of α -1-Acid-Glycoprotein Binding (AGP) for Marketed Oral, Oral CNS, Inhaled Drugs and Inhaled JAK Project Compounds

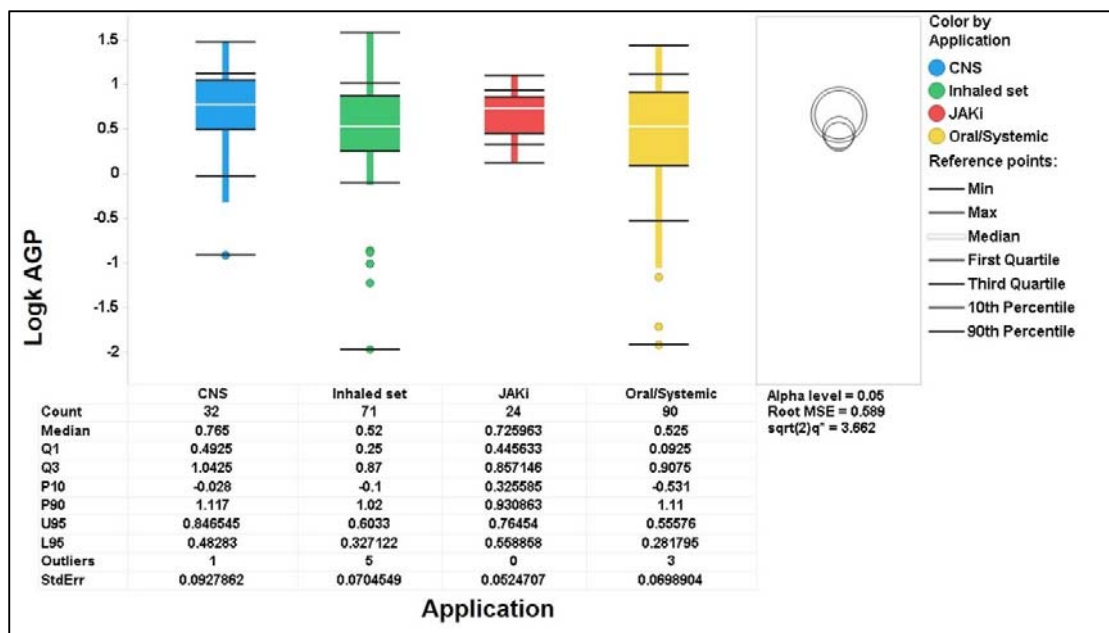


Figure 7.5-3 is a box plot of AGP binding versus different target class molecules (oral, oral CNS, Inhaled, and Inhaled Lead Optimisation JAK program compounds). The righthand panel rings represent a confidence interval (CI) analysis showing statistical analysis between the different classes based on a 95% CI

Figure 7.5-4 The Box Plot of Immobilised Artificial Membrane (IAM) Binding Marketed Oral, Oral CNS, Inhaled Drugs and Inhaled JAK Project Compounds

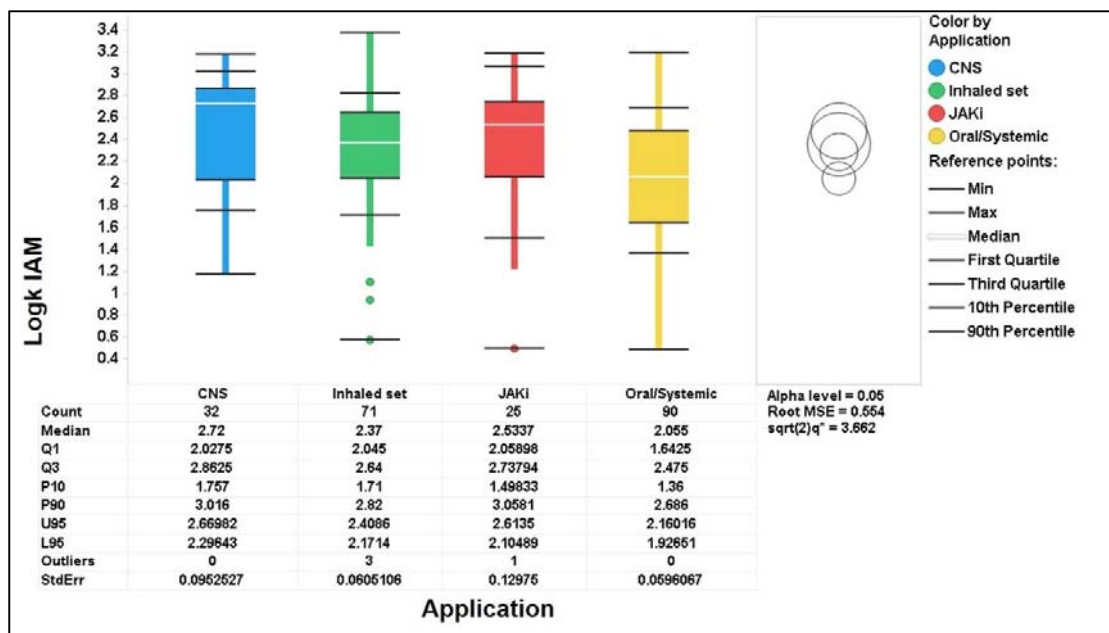


Figure 7.5-4 is a box plot of IAM binding versus different target class molecules (oral, oral CNS, Inhaled, and Inhaled Lead Optimisation JAK program compounds). The righthand panel rings represent a confidence interval (CI) analysis showing statistical analysis between the different classes based on a 95% CI

Figure 7.5-5 The Box Plot of cLogP for Marketed Oral, Oral CNS, Inhaled Drugs and Inhaled JAK Project Compounds

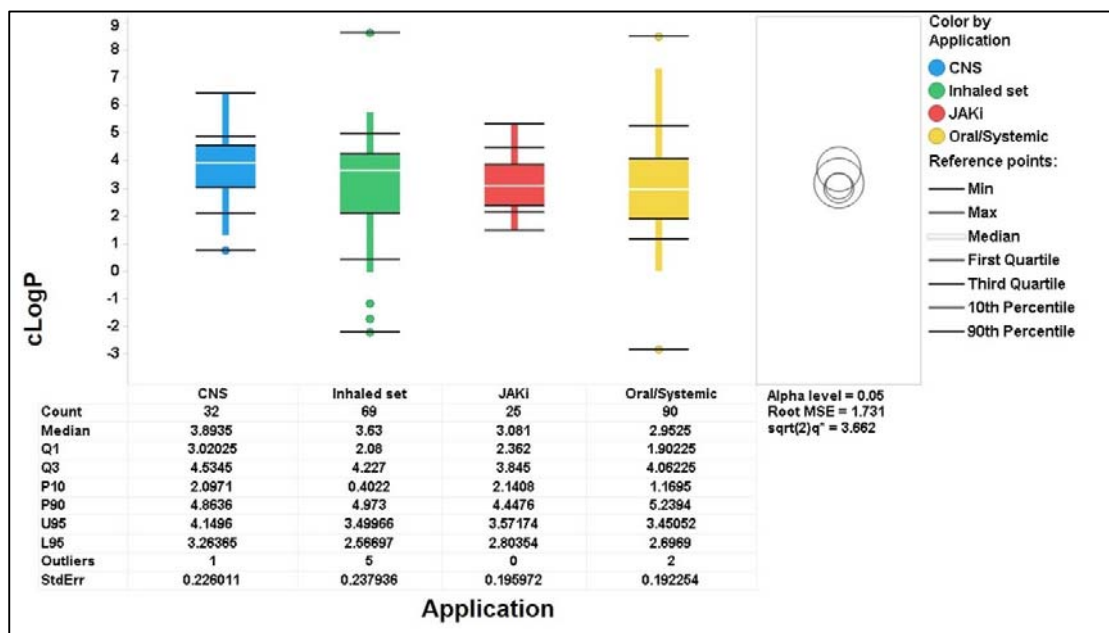


Figure 7.5-5 is a box plot of cLogP binding versus different target class molecules (oral, oral CNS, Inhaled, and Inhaled Lead Optimisation JAK program compounds). The righthand panel rings represent a confidence interval (CI) analysis showing statistical analysis between the different classes based on a 95% CI

Figure 7.5-6 The Box Plot of Total Polar Surface Area (TPSA) for Marketed Oral, Oral CNS, Inhaled Drugs and Inhaled JAK Project Compounds

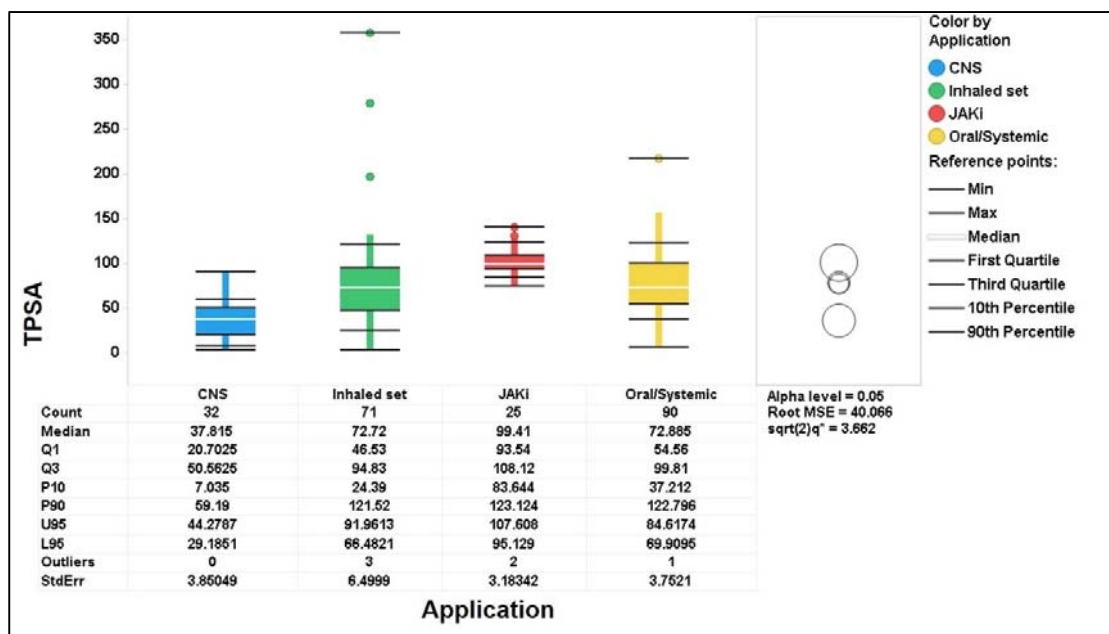


Figure 7.5-6 is a box plot of TPSA binding versus different target class molecules (oral, oral CNS, Inhaled, and Inhaled Lead Optimisation JAK program compounds). The righthand panel rings represent a confidence interval (CI) analysis showing statistical analysis between the different classes based on a 95% CI

Figure 7.5-7 The Box Plot of DE_{max} for Marketed Oral, Oral CNS, Inhaled Drugs and Inhaled JAK Project Compounds

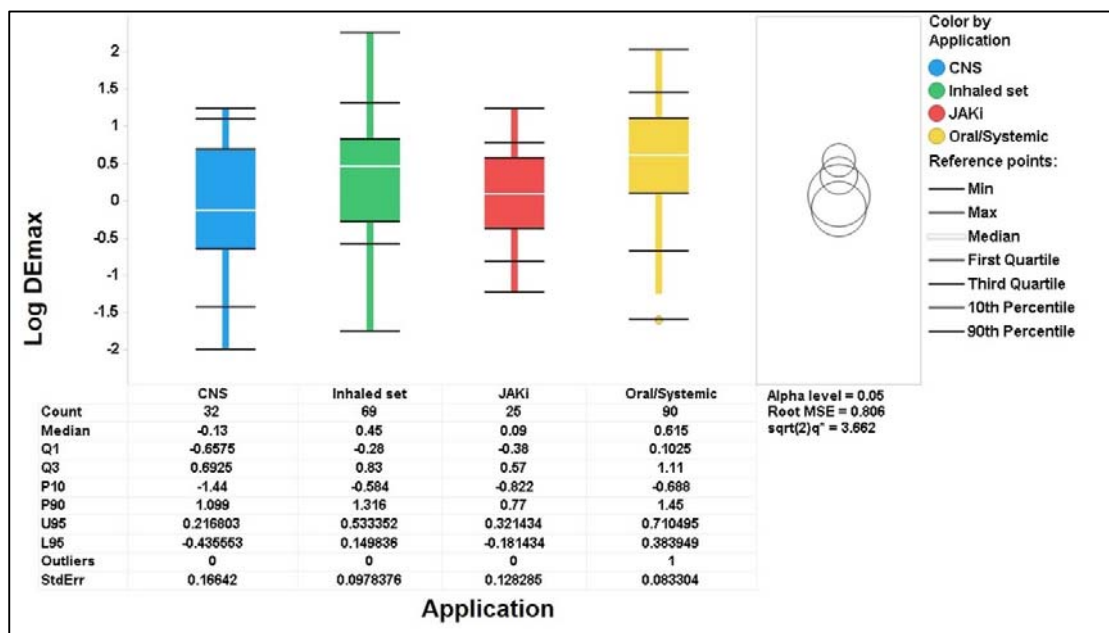


Figure 7.5-7 is a box plot of DE_{max} binding versus different target class molecules (oral, oral CNS, Inhaled, and Inhaled Lead Optimisation JAK program compounds). The righthand panel rings represent a confidence interval (CI) analysis showing statistical analysis between the different classes based on a 95% CI

Figure 7.5-8 The Box Plot of PFI for Marketed Oral, Oral CNS, Inhaled Drugs and Inhaled JAK Project Compounds

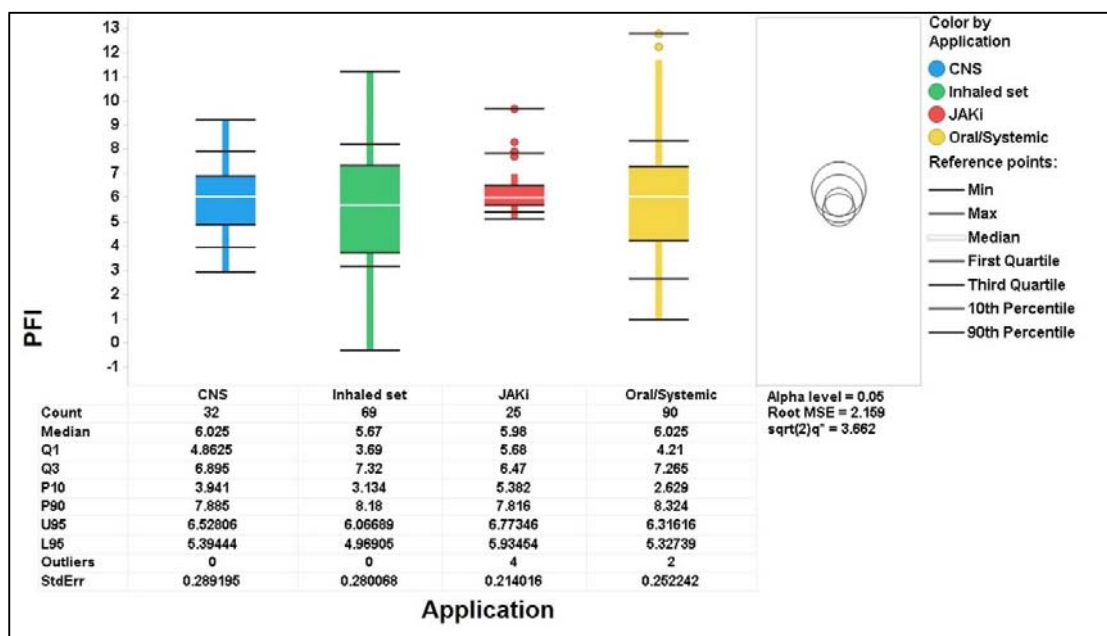


Figure 7.5-8 is a box plot of PFI versus different target class molecules (oral, oral CNS, Inhaled, and Inhaled Lead Optimisation JAK program compounds). The righthand panel rings represent a confidence interval (CI) analysis showing statistical analysis between the different classes based on a 95% CI

Figure 7.5-1 to Figure 7.5-8 show that there very few significant differences in the physicochemical and biomimetic properties of marketed oral, oral CNS and inhaled drugs. The range of certain properties, for example the inhaled JAK project compound also have a slightly higher molecular weight, which suggests that it may be possible to go outside the accepted physicochemical property space for marketed oral drugs (Lipinski's rule of 5) when we consider inhaled administration. There is separation for the TPSA for CNS drugs which underpins the targeting of TPSA of <75 as a design feature of CNS lead optimisation to penetrate the blood brain barrier (BBB). This is due to the tight gap junctions associated with the BBB which helps to protect the CNS from exposure to xenobiotics.

When compared with the JAKi project compounds, some significant differences in the physicochemical and biomimetic properties were more apparent, most notably *HSA* and

IAM binding, which was higher and ultimately determined that the DE_{max} of the JAKi compounds was significantly lower than the other drug classes. An objective for our JAK program team was to develop compounds with lower DE_{max} to improve lung retention, the rationale and approach adopted to achieve this is described in detail in Section 7.6.

7.6 Investigating Lung Retention and Dose in the JAKi Program for Inhaled Administration in Asthma

When targeting the lung/pulmonary system lung retention is believed to be an important characteristic for maintaining efficacy and reducing dosing frequency. Fast-systemic absorption can be a major disadvantage when using the inhaled route of administration as active compound may not be retained in the lung for long enough to maintain efficacious concentrations. This is particularly relevant for antagonist targets where high levels of target engagement are required for efficacy

There are several ways in which lung retention can be modulated, for example through the use of dry powder formulations with a defined particle size to reach deeper in the lung, or aerosol droplets with controlled hydrodynamic diameters [111]. The inherent molecular properties of the active ingredients also play an important role in lung retention. From previous examples of inhaled drugs targeting the lung and in-house studies, it can be concluded that longer lung retention, which does not result in lung toxicity, is promoted when molecules have medium solubility and lipophilicity [105]. Lung toxicity or irritancy is often identified by the presence of foamy macrophages [114], which is an unwanted side effect of delivering poorly soluble compounds to the lung.

The JAKi program was selected to study of a series of compounds being actively developed for the treatment of moderate to severe asthma by inhalation, where the aim was to achieve extended lung exposure only in the lung and minimise systemic exposure and associated adverse pharmacology for the same target. It was during lead optimisation of JAKi program that the potential of DE_{max} as an optimisation parameter for inhaled small molecules was identified.

7.7 JAK Pharmacology in Asthma and COPD

As previously described in section 5.4, small molecules that interact with the JAK pathways have become the focus of interest for many pharmaceutical research groups developing new treatments for immune inflammatory disorders. Therefore, a PAN JAKi an attractive therapeutic target in the lung in order to reduce the chronic inflammation that is associated with asthma [101] as shown in Figure 7.7-1

Figure 7.7-1 The Pharmacological Pathway for JAK Inhibitors for Reducing Chronic Inflammation

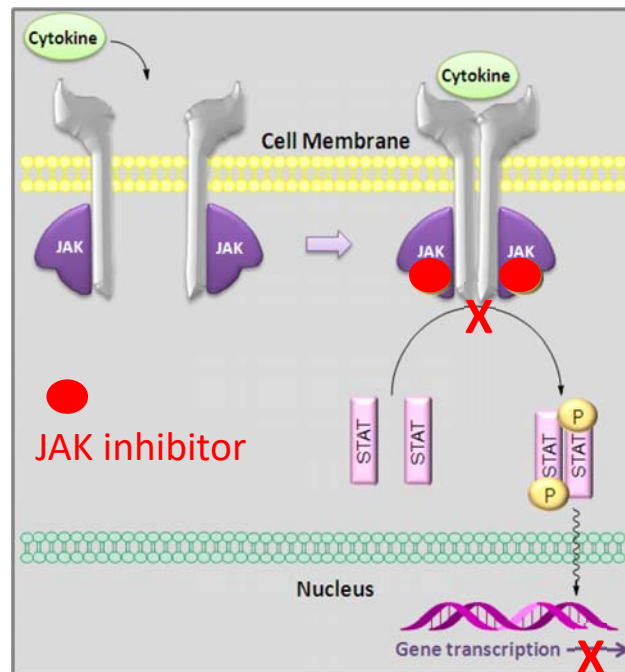


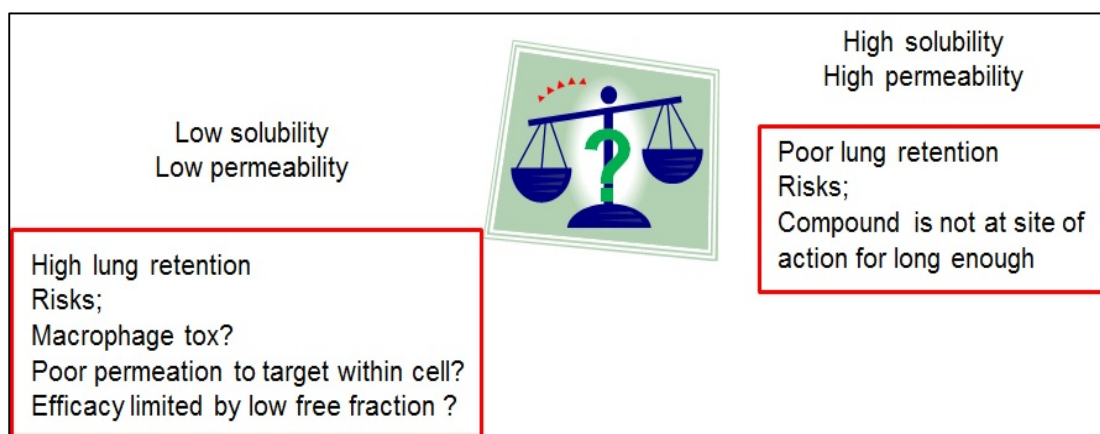
Figure 7.7-1 Schematic showing cytokine binding to resulting in activation of the JAK pathway and STAT proteins

By inhibiting JAK and the phosphorylation of the STAT proteins subsequent gene transcription is inhibited and the production of inflammatory cytokines via this mechanism is blocked. This should then suppress the immune response associated with asthma.

7.7.1 JAK Program Target Product Profile

Based on the physicochemical properties of inhaled drugs described in section 5.4.1, the program team set up a target profile targeting high levels of lung retention which would result in a long duration of action to achieve a once a day dose regimen. The target profile of a candidate compound was set up to have less than 1 mg dose (1 mg represents the maximum deliverable clinical dose for an inhaled dry powder using a preferred delivery device, GSK's Ellipta® device). To achieve this, compounds should be very potent and also at least 100-fold selective against other kinases. Furthermore, for a compound to progress, it should have low or no oral bioavailability and high systemic clearance when it gets into the general circulation in order to avoid systemic pharmacologically related side effects. Data generated by GSK's inhaled sciences group has indicated that compound solubility in simulated lung fluids (SLF) should ideally be higher than 250µg/mL of crystalline material in order to avoid foamy macrophage formation around the solid particles [113]. For reasonably long lung retention, compounds should have medium permeability and solubility [149], as described in section 5.4. Alternatively, in-house data suggested that target permeability could be set to 100 nm/s in an MDCK cell permeability assay and the solubility of the solid material should be 10µg/mL or higher in SLF. As the target is inside the cell, a certain degree of permeability must be maintained, and the solubility cannot be too low to avoid safety related concerns due to toxicity/irritancy. To achieve an inherent physicochemical profile that drives intrinsic lung retention and lung safety, Figure 7.7-2 illustrates the balance required between solubility and permeability.

Figure 7.7-2 Balancing the Solubility and Permeability for Lung Retention



One way to visualise and distinguish compounds with different solubility and permeability properties and the potential for differentiated lung retention profiles is to use a 9 – Box Model (Figure 7.7-3). This visualisation was developed during JAK lead optimisation to simply classify compounds and determine which compounds would be of further interest to profile *in vivo*. Low SLF solubility and MDCK permeability would increase lung residency but increase the risk of lung toxicity with the retention of undissolved compounds. This undissolved compound would be unlikely to engage the target and elicit a pharmacological effect, particularly for intracellular targets. High solubility and permeability would increase the rate of absorption from the lung and reduce the lung residency of a compound and therefore potentially reduce the duration of pharmacological activity. Ideally a balance of these properties is required for the duration of action and safety.

Figure 7.7-3 A 9-Box Model Plot of Solubility and Permeability

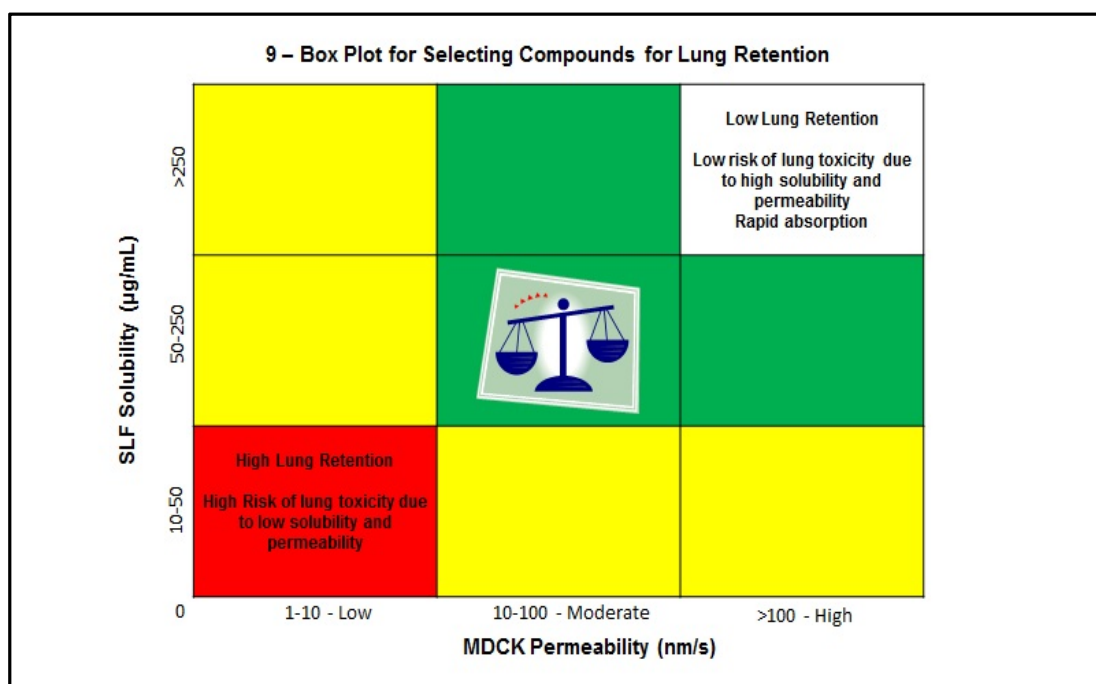


Figure 7.7-3 is a 9-box plot of solubility and permeability used to help select compounds with the desired lung retention profiles

The solubility in simulated lung fluid (SLF) and the MDCK cell membrane permeability of 24 JAK inhibitor compounds were measured and plotted in Figure 7.7-4. Using a 9-box

model with defined ranges for solubility and permeability, the compounds were classified as low, moderate and high for each parameter. The majority of the compounds had medium to high permeability, while the solubility ranged from low to high.

Based on our assumption for long lung retention, we require medium permeability and moderate to high solubility for our compounds. In the plot shown in Figure 7.7-4, the top middle square should capture compounds of interest with the potential of having the right physicochemical profile for an inhaled drug molecule. However, if compounds captured within this square could be differentiated further, the number requiring profiling using *in vivo* lung retention studies could potentially be reduced. To achieve this, a third parameter DE_{max} was added to this visualisation to see if it was possible to differentiate compounds within a single box.

The biomimetic binding properties of human serum albumin (*HSA*), α -1-acid-glycoprotein (*AGP*) and immobilized artificial membrane (*IAM*) have been investigated for their contribution to the modulation of lung retention. Mucus binding has previously been described to correlate well with *AGP* binding [150] and lung tissue binding has also been modelled by the albumin and phospholipid binding measured by the biomimetic HPLC stationary phases [150]. The drug efficiency has been characterised as a sum of the *HSA* and *IAM* binding [55][77] and denoted as HPLC DE_{max} (see section 4.2.4). Here, the biomimetic binding properties *HSA*, *AGP* and *IAM* have been investigated for their contribution to the modulation of lung retention.

In the plot shown in Figure 7.7-4, the size of the markers shows the measured HPLC DE_{max} and allows visualisation of compounds with low and high drug efficiency in association with other physicochemical properties.

Figure 7.7-4 The 9-box Plot Classification of Compounds Based on Solubility and Permeability and DE_{max}

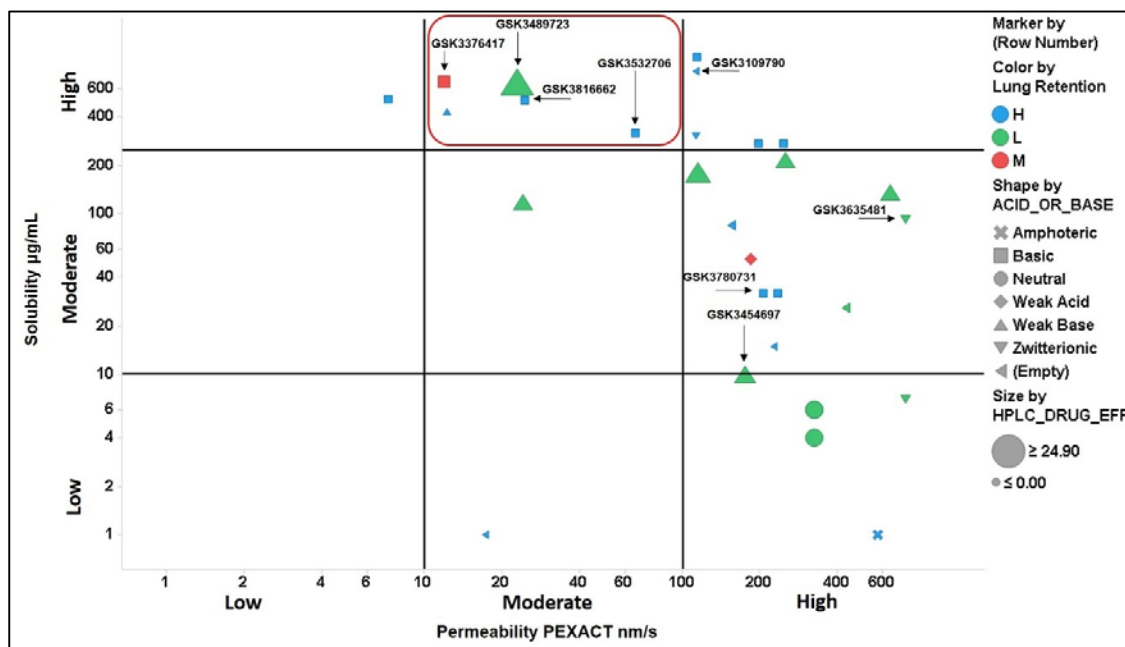


Figure 7.7-4 A 9-box plot of solubility, permeability and DE_{max} .

The derived drug efficiency (HPLC DE_{max}) showed a wide range (<0.1% to 25%) for compounds that were within the same class square based on their solubility and permeability. These compounds also showed large differences in *in vivo* lung retention studies. It can be seen in Figure 7.7-5 which shows that their lung retention profiles are very different and cannot be explained by their solubility and permeability alone (it is important to note that the compounds were administered as solutions to ensure solubility was not a confounding factor). The major difference is in their non-specific binding to proteins and lipids as exemplified by their biomimetic properties and DE_{max} as shown in Table 7-9.

Comparison of for example, GSK3489723 and GSK3532706 (DE_{max} 24.9 and 1.26, respectively) shows that the former is very poorly retained in the lung, dropping to a lung concentration of 15 ng/g after only 90 minutes, whereas the latter has good lung retention with exposure remaining above 100 ng/g for over 8 hours. These two compounds really exemplify the hypothesis linking between DE_{max} and lung retention.

However, the first compound which was profiled *in vivo* which helped to identify the potential link between DE_{max} and lung retention was GSK3376417, its biomimetic binding profile resulted in lower DE_{max} despite its low cLogP, suggesting that a direct relationship between lipophilicity and binding is more complex and it is important to also consider the composition of the biophases in which the targets are located.

Figure 7.7-5 illustrates that compounds with high HPLC DE_{max} (above 5%) have short lung retention regardless of their solubility and permeability. This is due to the low non-specific binding of the compounds to lung tissue. Although a high DE_{max} is in general advantageous because describes global physicochemical properties and distribution of a drug, it also means more rapid absorption of drug from the lung into the systemic circulation.

Table 7-9 also shows the measured and calculated physicochemical and biomimetic properties as well as the potency and drug efficiency index (DEI) values that are the sum of the pIC_{50} and the log HPLC DE_{max} . The objective here was to establish which properties of the compounds play pivotal roles in lung retention. The data demonstrates that all eight compounds are broadly within the typical druggable range for small molecules with respect to their basic physicochemical properties of MW and cLogP (ca. <550 MW and <3.5 respectively). However, GSK3489723 had lipophilicity in the lower range and significantly lower biomimetic binding in all three phases (*HSA*, *AGP* and *IAM*) with the *IAM* binding being much lower together with GSK3454697, which resulted in much higher drug efficiency. Although the potency of GSK3489723 was the lowest, the DEI value, which is described below, was still high (DEI 8) relative to the other compounds because the higher DE_{max} compensates for the low potency.

The DEI is the Drug Efficiency Index and based on the Drug Efficiency concept as described in section 4.2.4, which combines drug efficiency with the potency into a single parameter, as described in Equation 57. which was previously stated in Section 4.2.4.

Equation 57

$$DEI = pIC_{50} + \text{Log}(\%DE_{max})$$

Table 7-9 The Measured and Calculated Physicochemical Properties of Selected JAK Inhibitor Compounds.

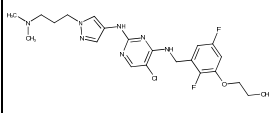
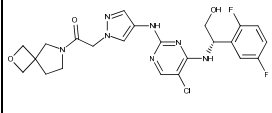
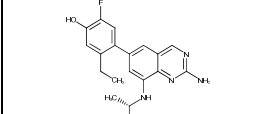
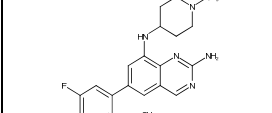
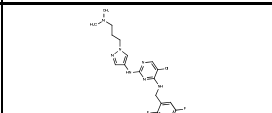
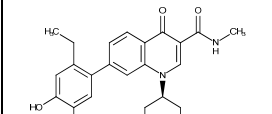
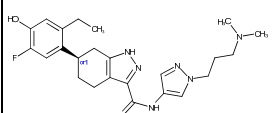
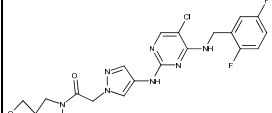
Compound ID	Structure	MW	cLogP	HSA (%)	AGP (%)	CHI IAM	DEmax (%)	Fibroblast pIC50 (IL-13)	DEI
GSK3532706A		482	3.3	91.2	84.1	48.1	1.26	8.0	8.1
GSK3489723A		520	2.2	80.3	57.3	24.8	24.9	6.6	8.0
GSK3635481A		356	3.3	95.6	83.0	40.1	2.52	7.6	8.0
GSK3780731A		395	3.6	94.6	88.5	56.7	0.14	7.8	6.9
GSK3376417A		521	1.9	84.0	75.3	44.2	3.36	6.8	7.3
GSK3901790A		423	2.3	94.8	86.3	53.6	0.29	7.6	7.1
GSK3816662A		455	3.4	96.2	87.9	61.8	0.02	7.3	5.7
GSK3454697A		490	3.5	89.8	68.8	28.1	13.8	7.7	8.8

Table 7-9 shows the measured calculated properties of selected JAK inhibitors with different lung retention profiles.

Table 7-10 The Measured and Calculated Physicochemical Properties of Selected JAK Inhibitor Compounds.

Compound ID	Solubility (µg/mL)	Permeability (nm/s)	DEmax (%)	LTB (%)	HPLC LTB (%)	Predicted Lung Retention	Observed Lung Retention
GSK3532706A	319	66.0	1.26	97.9	97.4	High	High
GSK3489723A	662	23.0	24.9	91.1	81.4	Low	Low
GSK3635481A	92.0	732	2.52	98.7	98.2	High	High
GSK3780731A	32.0	207	0.14	98.3	98.7	High	Low
GSK3376417A	665	12.0	3.36	61.0	92.8	Moderate	Moderate
GSK3901790A	767	113	0.29	99.5	98.5	High	High
GSK3816662A	509	24.5	0.02	95.1	98.9	High	High
GSK3454697A	10.0	181	13.8	95.2	92.8	Low	Low

Table 7-10 shows that reasonably long lung retention can be achieved without decreasing the solubility (below 100 µg/mL) down to a level with the potential to compromise safety by foamy macrophage formation around the solid particle of the inhaled drug.

Figure 7.7-5 Total Lung Concentration Measured After Intra Nasal Dose Administration in Solution to Female BalbC Mice

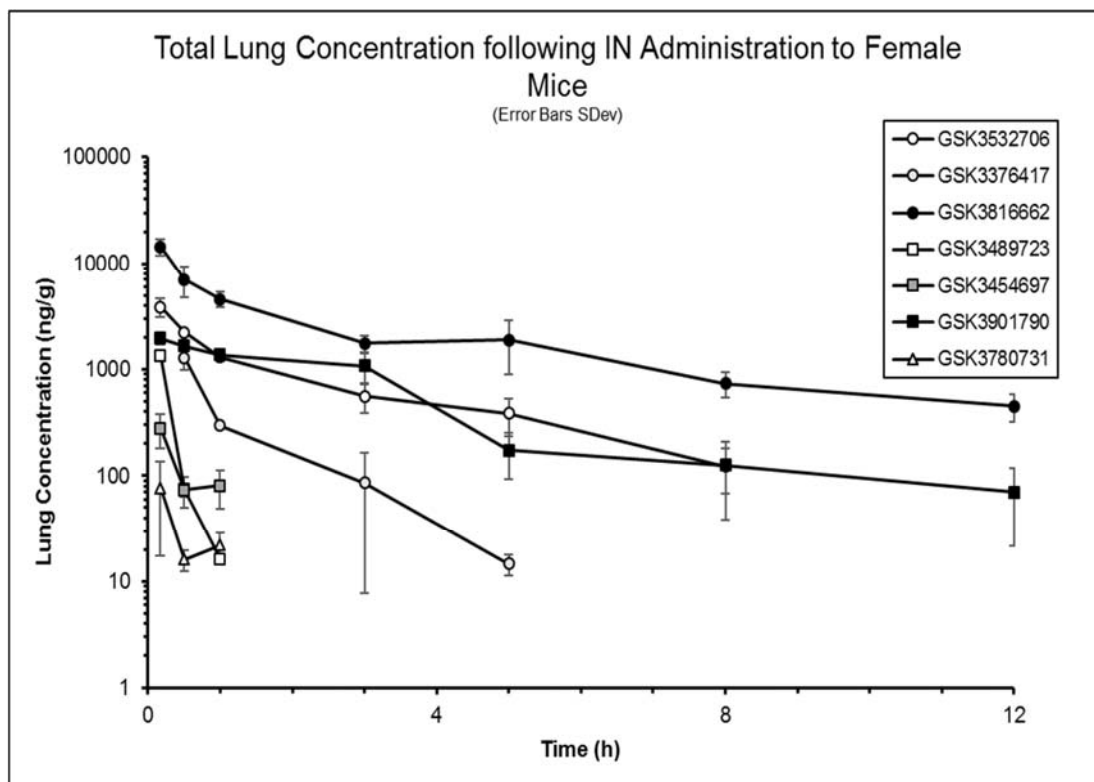


Figure 7.7-5 Shows the lung concentration time profiles of 7 JAKi compounds following IN dosing to mice

With compound solubility removed from the *in vivo* lung retention profiles and all compounds demonstrating a degree of permeability necessary to engage an intracellular target, the major differences between compounds with high “intrinsic” lung retention and low “intrinsic” lung retention were identified as their albumin, α -1-acid-glycoprotein and phospholipid parameters. Although *AGP* is not a component of the DE_{max} equation analysis by Valko *et al* [77], it demonstrates that *IAM* and *AGP* are highly correlated.

Furthermore, lung tissue contains mucus that consists mostly of glycoproteins, which suggests *AGP* binding is significant in order to retain the compound in the airways and on the surface of the alveoli, particularly for positively charged compounds (see Section 4.2.1). Consequently, to achieve long lung retention times, developing

compounds which have lower drug efficiency would appear advantageous, as exemplified by GSK3816662.

Table 7-9 shows that the major difference between high and low “intrinsic” lung retentions is the *AGP* and *IAM* binding, which are much weaker for a compound such as GSK3489723 resulting in much shorter lung retention.

7.7.2 Aldehyde Oxidase Metabolism in the Lung?

Lung metabolism is not typically considered a major risk, due to limited expression of the main metabolizing enzymes (P450's or MOA's), and limited practical evidence that the lung represents a major organ involved in the clearance of small molecules [151]. For inhaled drugs, metabolism external to the lung can be advantageous if it helps to minimise systemic exposure should any adverse pharmacology of the drug be a concern (both on- and off-target). AO metabolism of a drug could therefore be of benefit to increase systemic elimination and improve its therapeutic index (TI). However, there is emerging evidence that AO is expressed in the respiratory tissues, and this may represent a potential risk for maintaining active concentrations of drug within the lung if it is a substrate for this enzyme [143][152].

In Section 7.3 describing the PI3K drug discovery programs, AO metabolism was identified as a potential issue when compounds were being developed to treat diseases of the lung by IV or oral delivery. For compounds being developed for pulmonary delivery in the JAKi program, Table 7-10 illustrates an important caveat when examining the properties that influence lung retention, which is also related to AO metabolism. [151]. GSK3780731 was identified as an outlier in this DE_{max} “intrinsic” lung retention analysis because the DE_{max} was measured to be 0.14%, which should have resulted in good lung retention, however, *in vivo* the lung retention was very low. The reason for this poor prediction of lung retention was because the compound was a substrate for AO metabolism, which was identified during lead optimisation of the quinazoline series. This template contained a potential AO liability [141], but because AO in the lung was considered to have little significance (see Section 7.7.2 [151]) for drugs being developed for administration via the inhaled route, it was considered to be of potential benefit with respect to safety. If an inhaled compound entered the systemic circulation, AO

susceptibility could enhance its clearance and potentially increase the therapeutic index by reducing systemic exposure to JAK inhibition.

Figure 7.7-6 JAK Lead Templates Aldehyde Oxidase Metabolism Risks

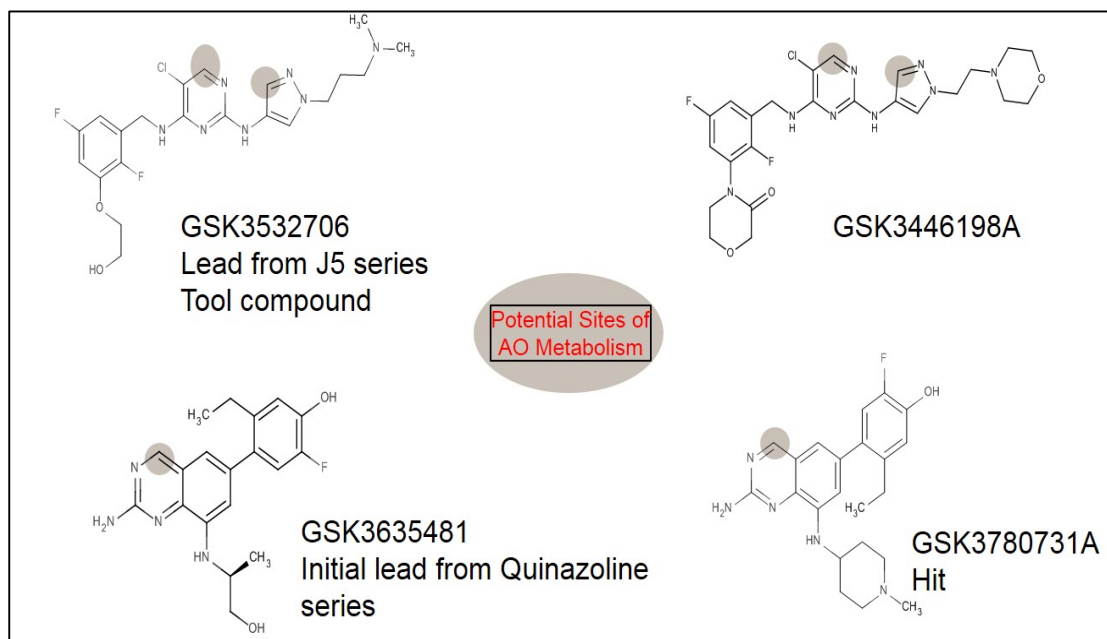


Figure 7.7-6 shows compounds from the J5 and quinazoline series and their potential sites of metabolism by AO

The compounds shown in Figure 7.7-6 are from the J5 and quinazoline series, the potential sites of AO metabolism have been highlighted. The quinazolines but not the J5 series were confirmed as AO substrates using *in vitro* liver cytosolic assays for mouse, rat and human (see Table 7-11).

Table 7-11 Quinazoline AO Metabolism as Identified *In Vitro* using both Mouse, Rat and Human Liver Cytosol Assays

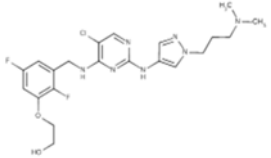
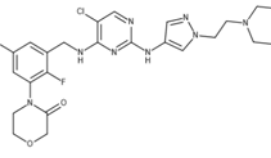
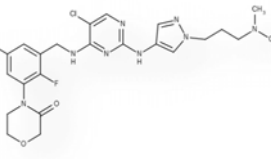
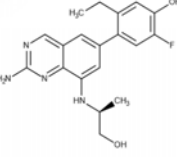
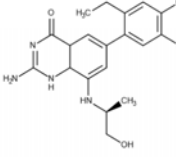
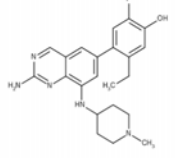
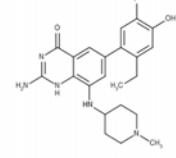
<i>In Vitro</i> Liver Cytosol Assay					
Compound ID	Structure	Metabolite	Mouse	Rat	Human
GSK3532706A		N/A	ND	ND	N
GSK3446198A		N/A	ND	N	N
GSK3376417A		N/A	ND	N	N
GSK3635481A			Y	Y	Y
GSK3780731A			Y	ND	Y

Table 7-11 *In vitro* liver cytosol results in mouse, rat or human for examples compounds from the J5 and quinazoline series. Compounds are shown as AO substrates (Y), non-substrates (N) or not determined (ND)

The absence of any AO-induced metabolism in the J5 series at the α -carbons of the pyrimidine and pyrazole rings was probably limited by either steric hindrance or by the electron withdrawing Cl substituent in the pyrimidine series [153]. Table 7-12 illustrates which tissues express AO in rat and human, with the highest levels in liver and kidney. Notably, AO expression is also evident in pulmonary tissue, albeit at a lower level based on immunostaining.

Table 7-12 Tissues Expressing AO in Rat and Human [125]

Table 1. Summary of aldehyde oxidase distribution in human and rat tissues.

TISSUE	IMMUNOSTAINING	
	Human	Rat
Respiratory tissues		
<i>Throat</i>	-	ND
<i>Lung</i>		
Trachea	±	±~++
Bronchium	++	++
Alveolus	+	+
Urinary tissues		
<i>Kidney</i>		
Glomerulus	-	-
Proximal tubule	+~+++	±
Distal tubule	+~+++	+
Collecting tubule	+~+++	+
<i>Bladder</i>		
Transitional cells	-	ND
<i>Prostate</i>		
Glands	+++	+
Digestive tissues		
<i>Liver</i>		
Pericentral hepatocyte	++	++
Periportal hepatocyte	+	+
Bile duct	++	++

-: no staining; ±: equivocal staining; +: low staining; ++: moderate staining; +++: high staining; ND: not described. Results of tissue distribution of rat aldehyde oxidase are cited from Histochem. Cell Biol. 1996; 105: 71-79 (Moriwaki et al.).

Table 7-12 shows the AO distribution following immunostaining of multiple tissues in rat and human

Figure 7.7-7 Immunostaining of AO in Human Lung Tissue [125]

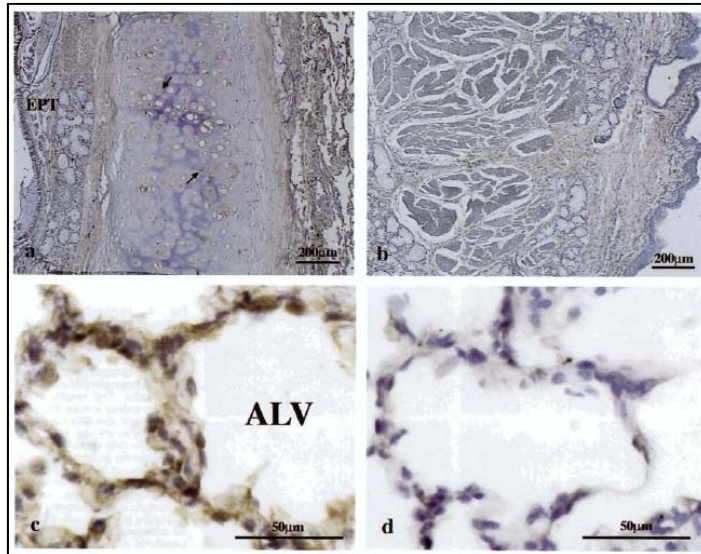


Figure 7.7-7 shows Images of immunochemical staining of AO in the human respiratory system. (a) trachea and bronchium immunostaining in epithelial cells. (c) Immunostaining showing AO expression in the alveoli. (b & d) are control sections treated with normal IgG do not show staining.

Figure 7.7-7 and Table 7-12 show that AO is expressed in respiratory tissues and other organs such as bladder, kidney and liver in both rat and human

Figure 7.7-8 *In Vitro* Stability of GSK3780731 and GSK3635481 in Mouse Lung Homogenate

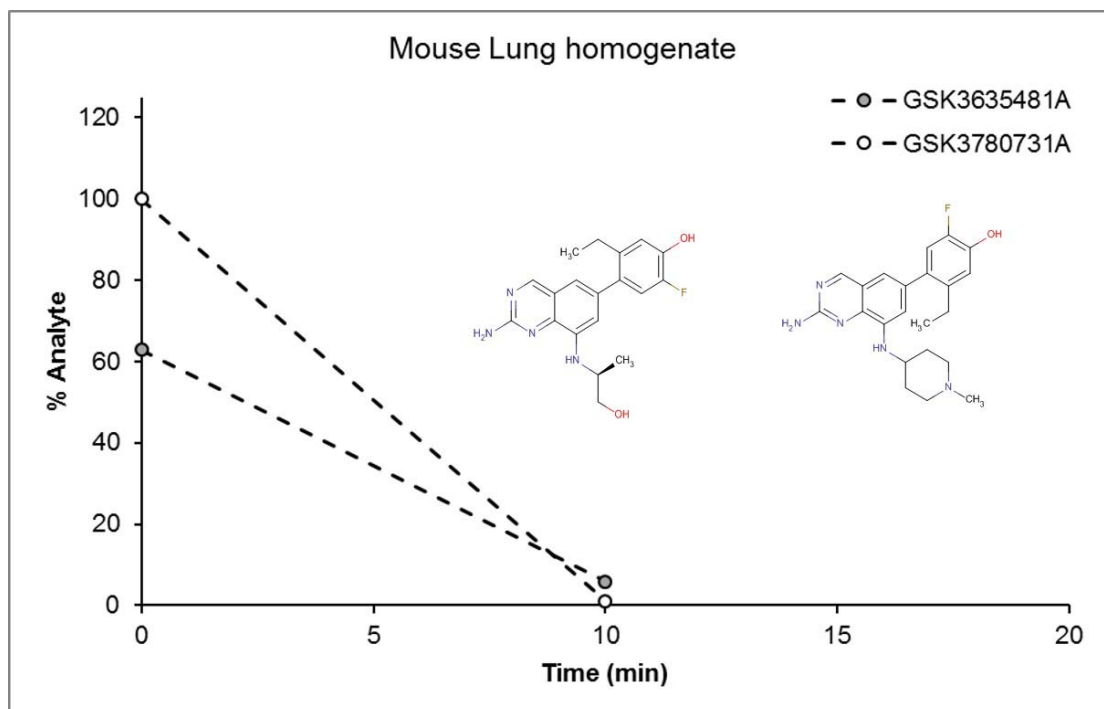


Figure 7.7-8 shows the percentage loss over time of GSK3635481 and GSK3780731 after being incubated in fresh mouse lung homogenate at a concentration of 0.5 μM , 10 μL samples were taken at regular intervals and immediately extracted using protein precipitation. The samples were then analysed by LC-MS/MS.

GSK3780731 and its related analogue GSK3635481 when assessed *in vivo* both demonstrated unexpectedly poor lung exposure (Figure 7.7-5). A lung stability assay showed both were unstable in mouse lung homogenate (Figure 7.7-8) and had a +16 metabolite in liver cytosol in common when analysed by LC-MS/MS indicating a potential AO metabolite.

Figure 7.7-9 Confirming AO Metabolism in Mouse Lung GSK3635481 and GSK3780731.

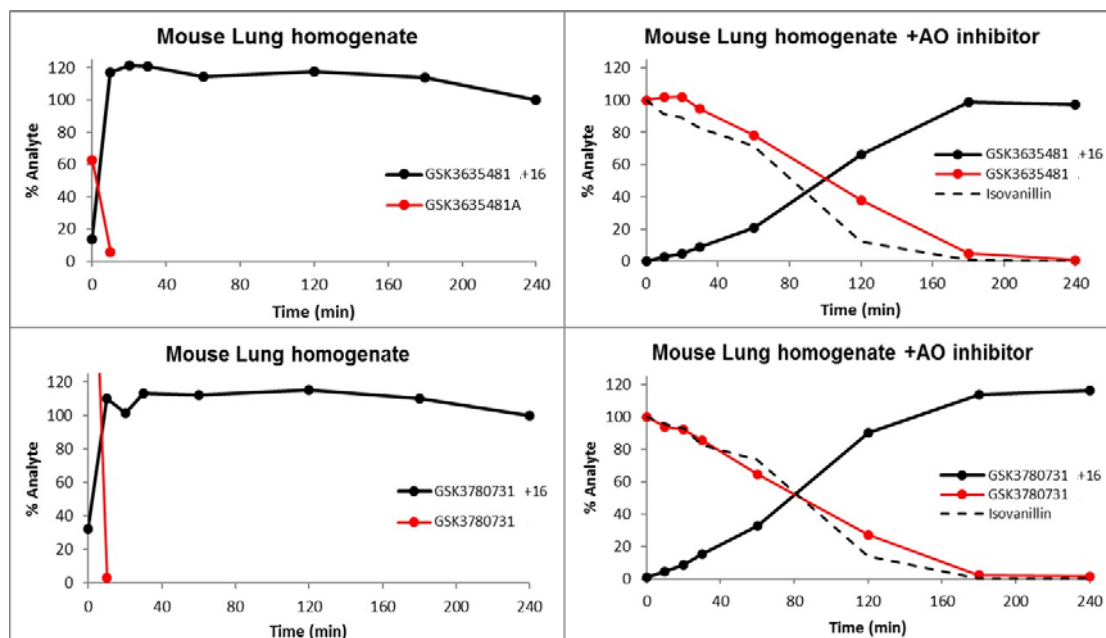


Figure 7.7-9 shows the results of an *in vitro* mouse lung homogenate stability assay. Fresh mouse lung homogenate was incubated with GSK3635481 and GSK3780731 at a concentration of 0.5 μ M and in the presence of an AO inhibitor Isovanillin.

Figure 7.7-9 shows a +16 metabolite was detected for both GSK3635481 and GSK3780731 following incubation of in fresh mouse lung homogenate. Metabolism of both compounds was inhibited in the presence of isovanillin indicating the loss of compound was a result of AO metabolism in the lung [126]. It was also noted that isovanillin was unstable in lung tissue, which was possibly due to the presence of aldehyde dehydrogenase. It can be seen that as the concentration of isovanillin falls so does the concentrations of both GSK3635481 and GSK3780731 and the +16 metabolite was formed in both compounds.

Figure 7.7-10 GSK3635481 *In Vitro* AO Metabolism in Human Lung

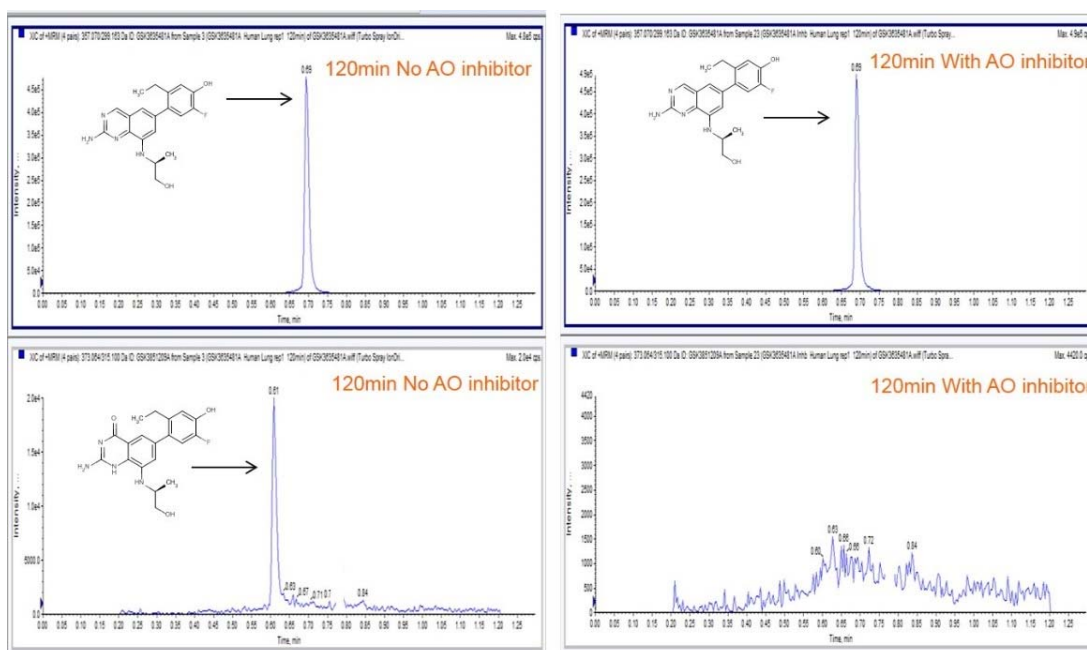


Figure 7.7-10 shows the results of an *in vitro* human lung homogenate stability assay. Human lung tissues which has been stored frozen was thawed and homogenised. GSK3635481 was incubated alone at a concentration of 0.5 μ M and in the presence of an AO inhibitor Isovianillin. A 10 μ L sample were taken at regular time intervals and extracted using protein precipitation. The supernatant was then analysed by LC-MS/MS for parent and the parent +16 metabolite. Only the 120 minute responses are shown in this figure.

Based on an *in vitro* human lung homogenate assay, it does appear that AO metabolism can to occur in human lung tissue. This has not typically been considered previously as the lung is generally considered of little metabolic interest [151]. However, for an inhaled drug where lung exposure and duration of exposure is a fundamental aspect of the project target profile, AO metabolism could impact upon lung exposure and duration of action in human which would require either an increase in the therapeutic dose or the frequency of dosing.

Based on these data from murine models, subsequent experiments using a human lung homogenate assay (Figure 7.7-10) also suggested GSK3635481 was a substrate for AO metabolism in human lung tissue. Taken together, these experiments indicate the importance of cross-validating all parameters being evaluated. For an inhaled drug

where lung exposure and duration of exposure is a fundamental aspect of the project target profile, where retention and efficiency measurements can play an important role in guiding compound optimisation, idiosyncratic factors such as AO metabolism require monitoring.

At the beginning of the project, GSK3780731 was identified as an outlier that was predicted to have good lung retention based on the DE_{max} analysis. However, *in vivo* lung retention studies indicated GSK3780731 had very poor lung retention due to unexpected AO metabolism in the lung.

Further lead optimisation of the quinazoline series enabled the team to identify compounds which were not substrates for AO as shown in Table 7-13. After extensive analysis of this series, it became evident that the 2-position of the bicyclic ring was important in determining binding orientation in the AO enzyme. Using computational techniques, it was possible to build an *in silico* crystal structure model based on a publication by Coelho *et al.* [154]. Based on the description of substrate docking with the enzyme (molybdenum cofactor) it was proposed that an extended functional group at 2-amino position would block the enzyme cofactor (molybdenum) from engaging with the enzyme active site and therefore blocking oxidation of the 4-position on the quinazoline ring by AO (Figure 7.7-11).

Table 7-13 Quinazoline Series Compounds which were Substrates and Non-Substrates for AO

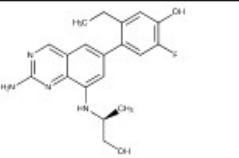
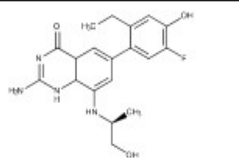
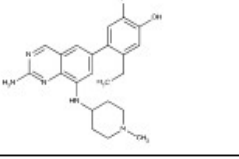
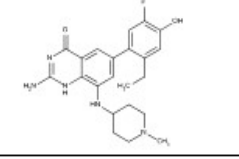
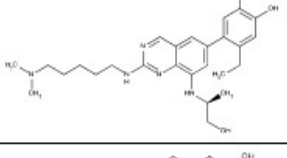
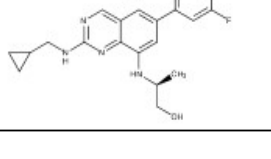
<i>In Vitro</i> Liver Cytosol Assay				
Compound ID	Structure	Metabolite	Mouse	Human
GSK3635481A			Y	Y
GSK3780731A			Y	Y
GSK3800430A		N/A	N	N
GSK3776068A		N/A	ND	N

Table 7-13 shows AO substrates from the quinazoline series with their metabolites and compounds from the same series which were shown not to be AO substrates

Figure 7.7-11 Aldehyde Oxidase Substrate Binding Model

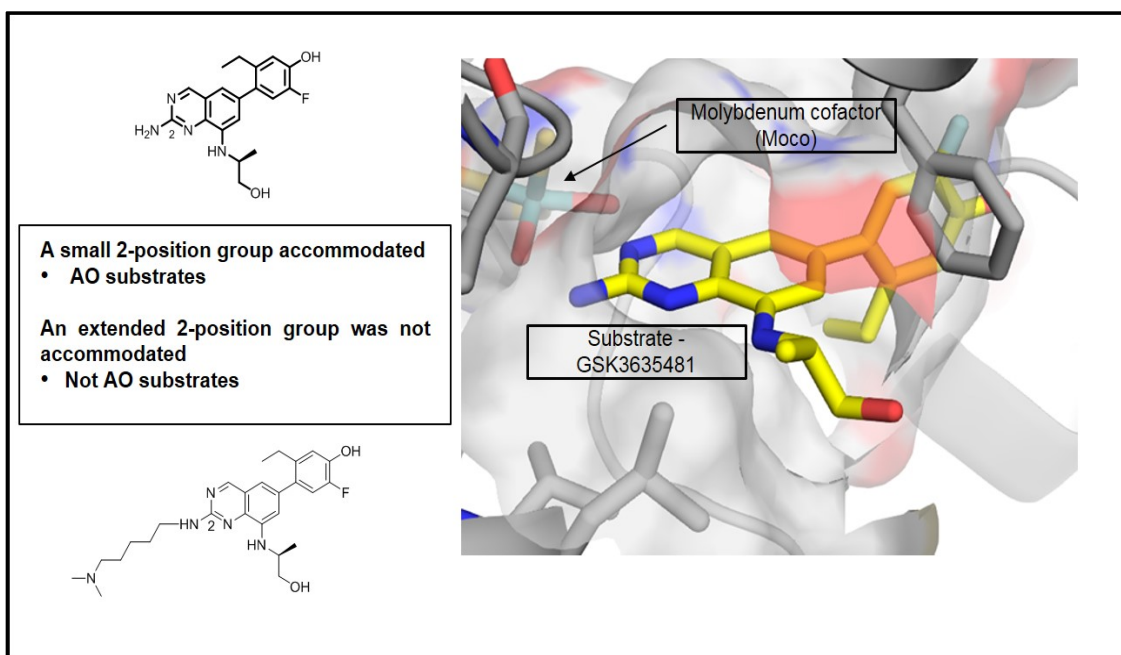


Figure 7.7-11 shows a proposed AO substrate binding model of the active site and enzyme cofactor (Molybdenum cofactor). This work is referenced to the internal communication, Lewell, N59079-33.

7.7.3 Understanding the Pharmacodynamic and Pharmacokinetic (PKPD) Relationship in the JAKi Drug Discovery Project

To demonstrate target engagement and relate compound concentration to effect over time, a multiple time point dose response study was designed to assess the PKPD relationship and to develop a physiological based pharmacokinetic model (PBPK) [155], see section 7.8. The purpose of the PKPD and PBPK modelling was to help put into context the lead optimisation process which utilised DE_{max} to develop and select compounds with improved lung retention by linking target engagement and efficacy to the physicochemical characteristics of the JAKi inhibitors. This type of modelling is ultimately used to understand the concentration effect relationship with the aim of building a more complete understanding of the pharmacology and target engagement, this information can then be used to understand and predict clinical dose of lead compounds which have the potential of being selected for development and progression to clinical studies.

The criteria for JAK inhibitors are different from general inhaled administration such as β -agonists or muscarinic antagonists where the receptor is on the surface of the airways. In this project, an intracellular lung target is involved, raising the importance permeability from the perspective of accessing the target, but also regarding pulmonary absorption from the lung and the unwanted systemic consequences.

To assess whether long lung duration was advantageous for the desired pharmacological activity, PKPD experiments were designed at multiple time points unlike the traditional one-time point (usually at the C_{max}) studies. Figure 7.7-12 and Figure 7.7-13 show the classical and more informative multiple time point longitudinal PD profiles for GSK3532706. However, experiments expressed in this way do not show the fundamental link between PK and PD which is required to fully understand target engagement. GSK3532706 was selected because of its good lung retention profile based on the numerous experimental parameters discussed earlier and was used as a tool compound during the lead optimisation phase of the JAK program in this PKPD, PBPK and PBPK/PD analysis.

Figure 7.7-12 A Classical PD study Design and the Results Obtained for GSK3532706

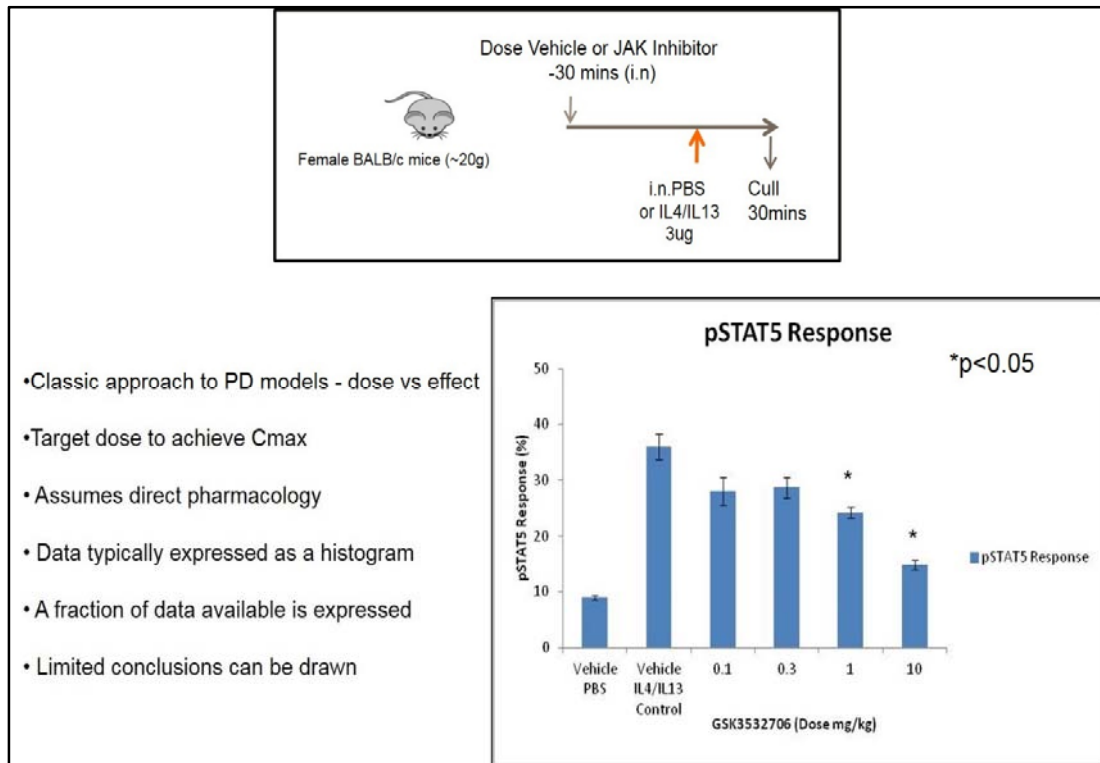


Figure 7.7-12 Shows a classical mouse PD study looking at IL4/13 cytokine induced pSTAT response in the lung using in female BalbC mice, n=6/dose group, vehicle control n=4. The IL4/13 cytokine was given intranasally 30 minutes before the animals were terminated and lungs removed for analysis.

Figure 7.7-13 The PKPD Profile of GSK3532706 using a Longitudinal PKPD Model

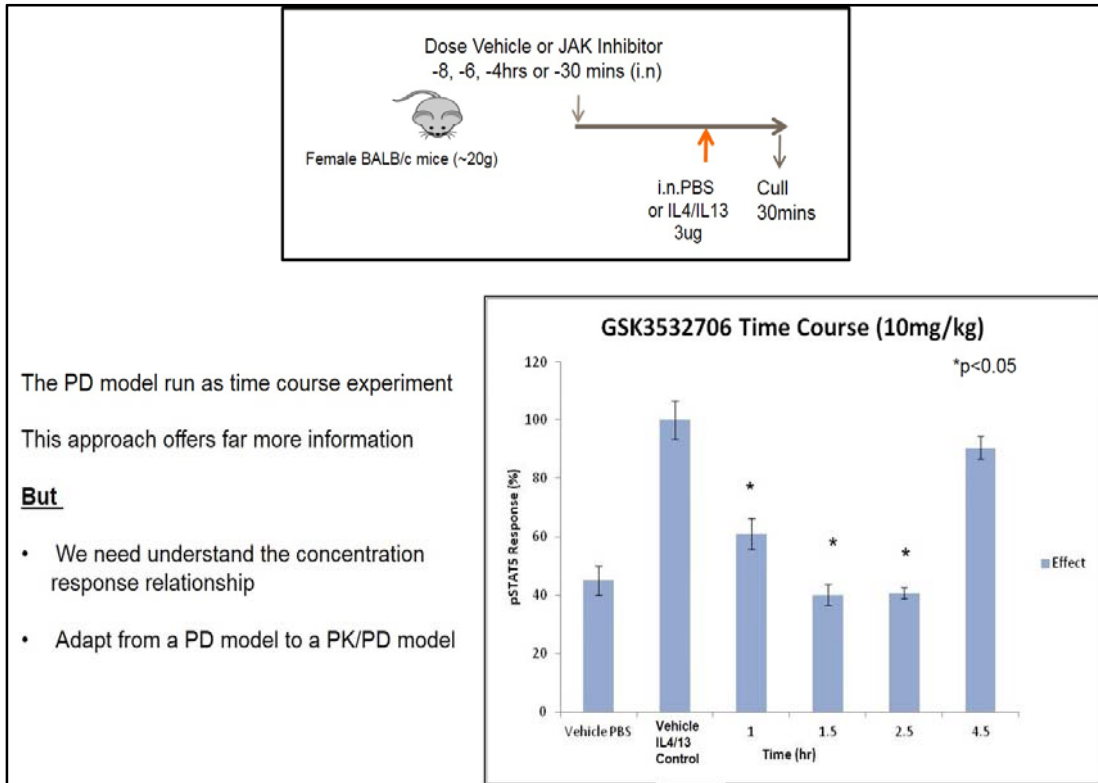


Figure 7.7-13 shows a time course mouse PD study looking at IL4/13 cytokine induced pSTAT response in the lung using in female BalbC mice, n=6/group, vehicle control n=4. The IL4/13 cytokine was given intranasally 30 minutes before the animals were terminated and lungs removed for analysis.

Figure 7.7-14 to Figure 7.7-16 show the total lung, total blood and unbound drug concentration and the observed %pSTAT5 cytokine inhibition, the biomarker for target engagement with JAK as described in Section 5.4. We can see in Figure 7.7-14 and Figure 7.7-15 that higher tissue or blood concentrations of drug results in greater inhibition of cytokine induced pSTAT response.

Figure 7.7-14 The Lung Tissue Concentration Versus %pSTAT Response.

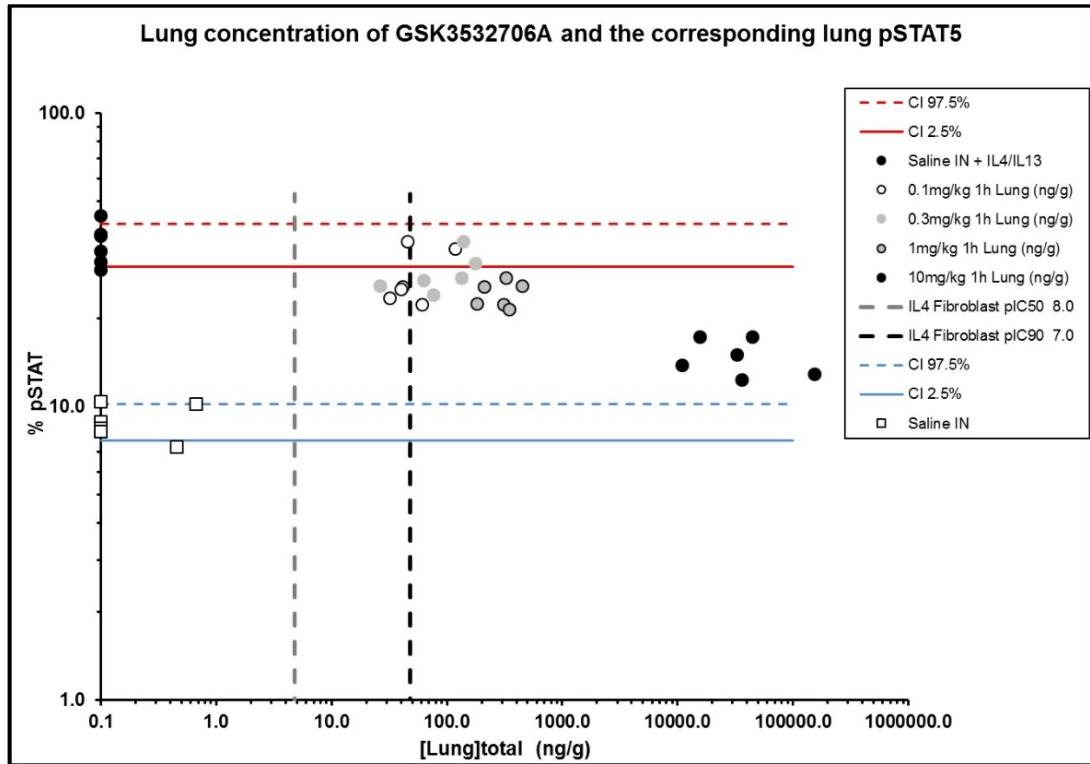


Figure 7.7-14 Shows a PKPD plot showing drug concentration in lung tissue following an intranasal dose over a range of 0.1-10mg/kg versus pSTAT response, following IL4/13 cytokine induction in the lung using female BalbC mice, n=6/dose group. The IL4/13 cytokine was given intranasally 30 minutes before the animals were terminated and lungs removed for analysis. Vertical lines represent the IC₅₀ and IC₉₀ measured *in vitro* using lung fibroblasts.

Figure 7.7-14 shows that the lung tissue concentrations of GSK3532706 do not vary significantly across the dose range (0.1-1mg/kg), however, the blood concentrations from the same experiment in Figure 7.7-15 are clearly separated for each dose group. A more pharmacologically relevant way to express these data was to express the blood concentrations of GSK3532706 as unbound or free blood concentrations as shown in Figure 7.7-16.

Figure 7.7-16 The Unbound Blood Concentration Versus %pSTAT Response.

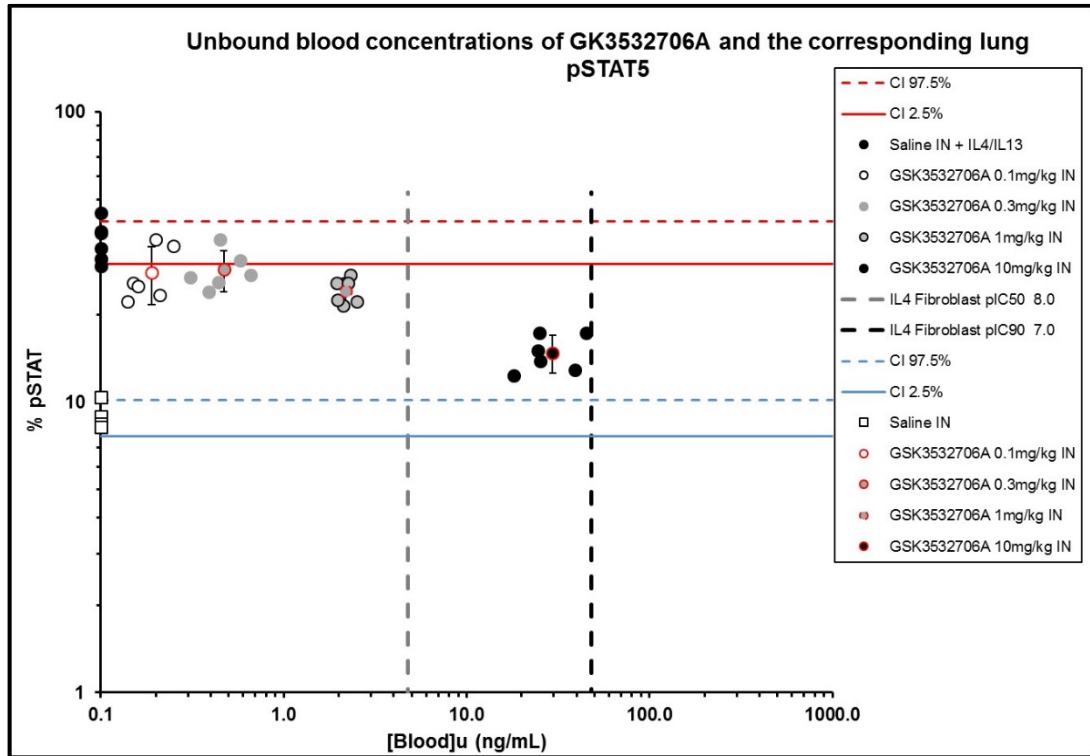


Figure 7.7-16 is a PKPD plot showing unbound drug concentration in blood following an intranasal dose over a range of 0.1-10mg/kg versus pSTAT response, following IL4/13 cytokine induction in the lung using female BalbC mice, n=6/dose group. The IL4/13 cytokine was given intranasally 30 minutes before the animals were terminated and lungs removed for analysis. Vertical lines represent the IC₅₀ and IC₉₀ measured *in vitro* using lung fibroblasts.

It can be seen from Figure 7.7-16 that unbound blood concentration clearly shows separation between each dose group and can now be related to the pharmacological effect, with greater confidence that these concentrations are more directly related to the concentration in the lung. The reason for this is based on the free drug theory, where only the free drug is available to bind to the target receptor of enzyme, the free concentration should be the same or similar in all tissues at steady state and for a drug delivered via the lung the free blood concentration must be in solution and have the opportunity to bind the target of interest (JAK) as it passes through the lung. In addition to this, the lung blood

interface is approximately one cell thick, that the blood concentrations should be very close to the pharmacologically relevant free lung concentrations.

We can see that higher concentrations of the compound in all the three matrices (lung tissue, blood, unbound blood: (Figure 7.7-14, Figure 7.7-15 & Figure 7.7-16) can be related to the pharmacological inhibition that is expressed as pSTAT5 following cytokine induction.

To help build a more robust PKPD profile, GSK3532706 was dosed at 10 mg/kg IN (suspension) in a longitudinal duration of action study, where a lung pSTAT5 profile was measured at 1, 1.5, 2.5 and 4.5 hours post dose of the JAK inhibitor (Figure 7.7-13). The IL4/13 challenge was given 0.5 h before each terminal timepoint due to the transient nature of the pSTAT5 response that would be measured. Robust inhibition of pSTAT5 has been observed at 1, 1.5 and 2.5 h post dose, however, no inhibition was observed at 4.5 hours. This was despite our knowledge that the lung retention PK study had shown good lung retention with concentrations of approximately 200 ng/g of compound in lung at 8 hours post IN dose (dosed from solution, see Figure 7.7-5).

An important factor for the PKPD model is doses administered were typically delivered as suspensions and this affects the lung retention profile. The reason the PD model was dosed as IN suspensions was primarily due to the higher dose concentration being required to deliver a high IN 10 mg/kg dose to the lung (50 µL dose volume), which exceeded the solubility of GSK3532706 and most other compounds subsequently dosed in this model. In addition, the cytokine PD model did not tolerate the PK solubilised formulation necessitating the use of a simple pH adjusted saline formulation. The impact of administering the compound as a suspension resulted in much higher lung retention, which was driven by a slower compound dissolution rate. The problem when determining lung concentration following administration as a suspension or powder is that it is not possible to measure what fraction of the lung concentration is in solution. This is because when the lungs are homogenised for analysis, any undissolved compound is dissolved. This means an unknown fraction of the total lung concentration measured is available to engage the target. The impact of this can be seen in Figure 7.7-17, where there is no obvious separation in lung concentration across the time course of this experiment: increased lung retentions illustrated by data clustering means it is not possible to relate lung concentration to the pharmacological effect. However, in Figure 7.7-18 where

unbound blood has been plotted against the pSTAT response, there is a clear separation between the sample times resulting in a robust PKPD correlation. This is shown by an increase in GSK3532706 blood concentration that reduced pSTAT5 inhibition back to baseline control levels, which was statistically significant based on a 95% confidence interval, with the maximum inhibition being observed between 1.5 and 2.5 hours after administration (Figure 7.7-19).

Figure 7.7-17 A Longitudinal PKPD Plot Showing the Total Lung Concentration of GSK3532706 Versus %pSTAT Response.

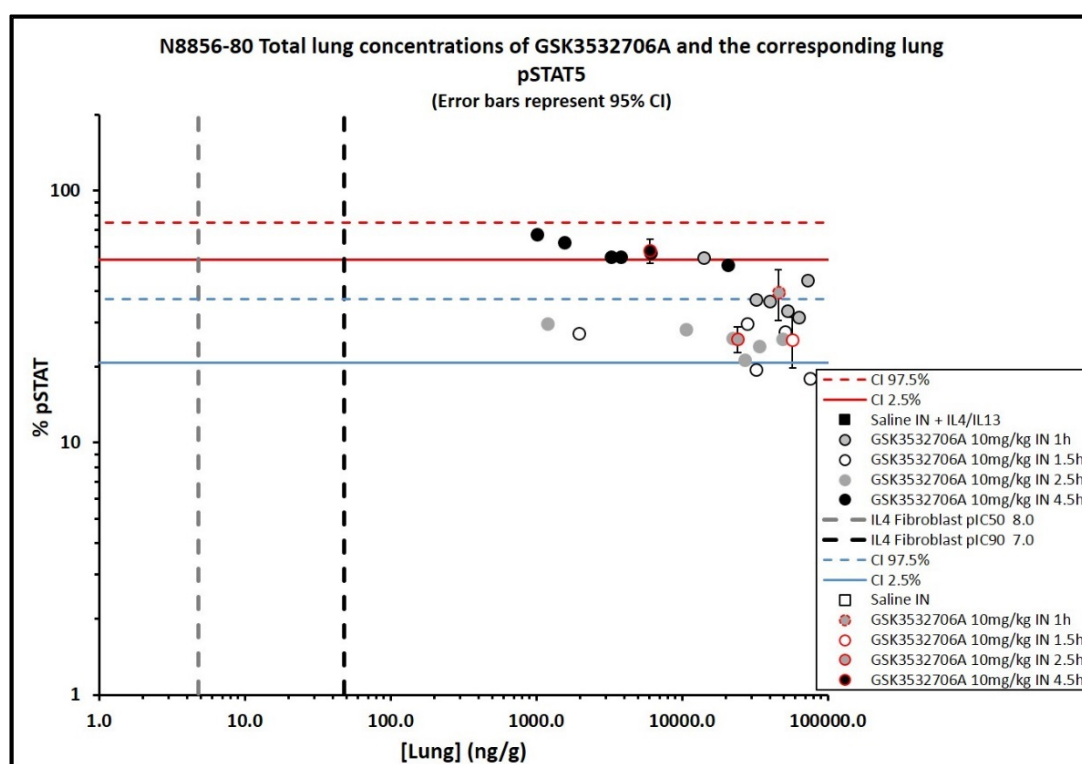


Figure 7.7-17 is a PKPD plot showing total concentration in lung following an intranasal dose of 10mg/kg over a time course of 1 to 4.5 hours versus pSTAT response, following IL4/13 cytokine induction in the lung using female BalbC mice, n=6/dose group. The IL4/13 cytokine was given intranasally 30 minutes before the animals were terminated and lungs removed for analysis. Vertical lines represent the IC₅₀ and IC₉₀ measured *in vitro* using lung fibroblasts.

Figure 7.7-18 A Longitudinal PKPD Plot Showing the Unbound Blood Concentration of GSK3532706 Versus % pSTAT Response

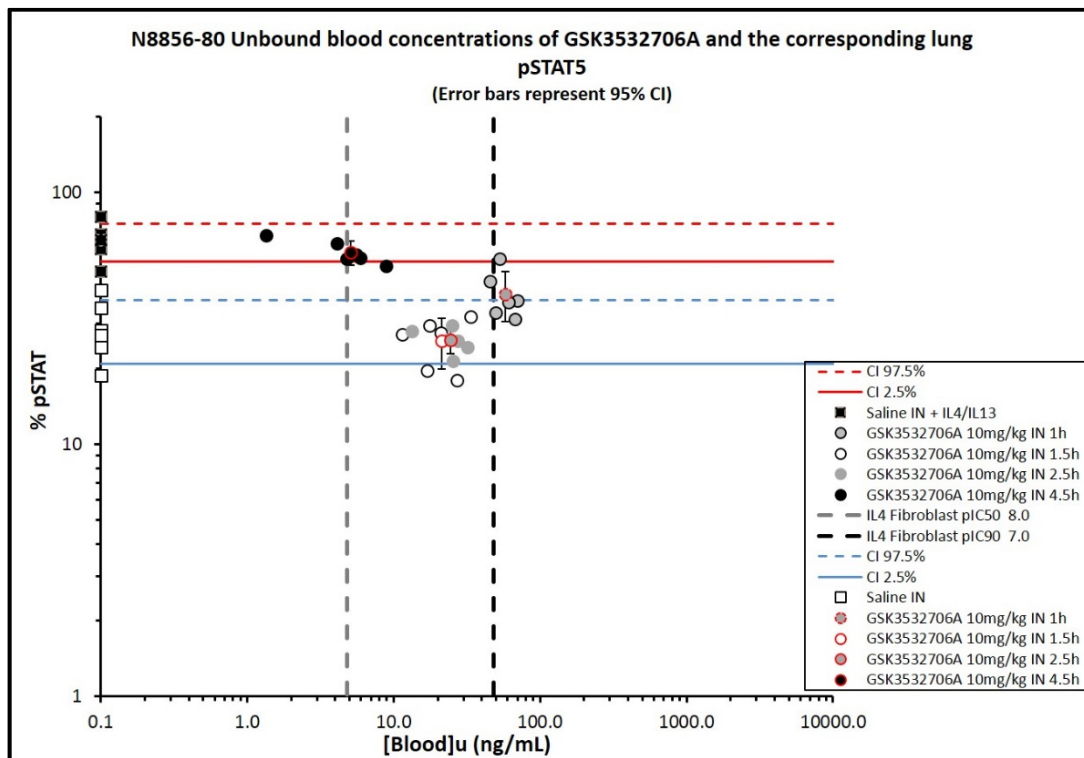


Figure 7.7-18 is a PKPD plot showing unbound drug concentration in blood following an intranasal dose of 10mg/kg over a time course of 1 to 4.5 hours versus pSTAT response, following IL4/13 cytokine induction in the lung using female BalbC mice, n=6/dose group. The IL4/13 cytokine was given intranasally 30 minutes before the animals were terminated and lungs removed for analysis. Vertical lines represent the IC₅₀ and IC₉₀ measured *in vitro* using lung fibroblasts.

Figure 7.7-19 The Blood Concentration of GSK3532706 and %pSTAT5 Response as a Function of Time.

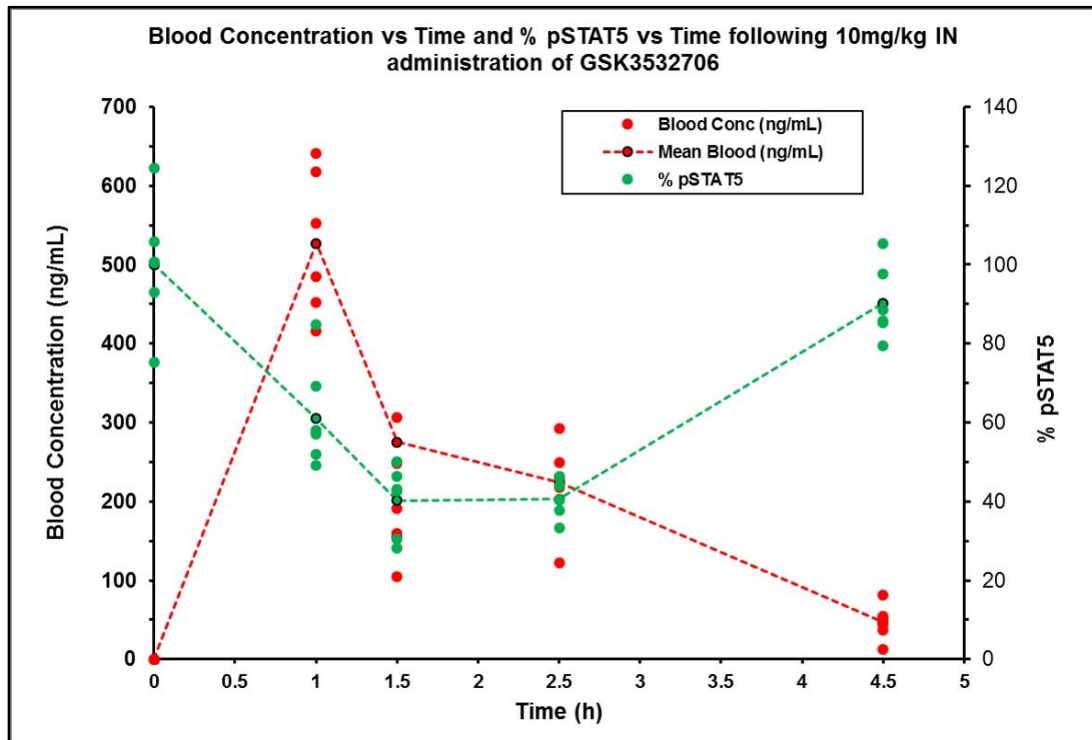


Figure 7.7-19 is a PKPD plot showing unbound drug concentration in blood following an intranasal dose of 10mg/kg and the pSTAT response over a time course of 1 to 4.5 hours, following IL4/13 cytokine induction in the lung using female Balb/C mice, n=6/dose group. The IL4/13 cytokine was given intranasally 30 minutes before the animals were terminated and lungs removed for analysis.

As expected, Figure 7.7-19 shows high blood concentration corresponds with strong inhibition at the 1 h time point, however, after 1.5 and 2.5 hours the blood concentration dropped but the inhibition remained high, indicating a slight offset between the C_{max} and the E_{max} (maximum concentration and maximum effect), which could be attributed to an indirect effect. By plotting the blood concentration and % pSTAT5 inhibition as the measure of the pharmacological activity in Figure 7.7-20, a hysteresis loop was observed, which could be due to an indirect effect, or alternatively to a compound bio-distribution delay with respect to inhibition of the cytokine induced pSTAT response (Figure 7.7-20).

Figure 7.7-20 Hysteresis of % pSTAT5 Inhibition Verse the Blood Concentration of GSK3532706A

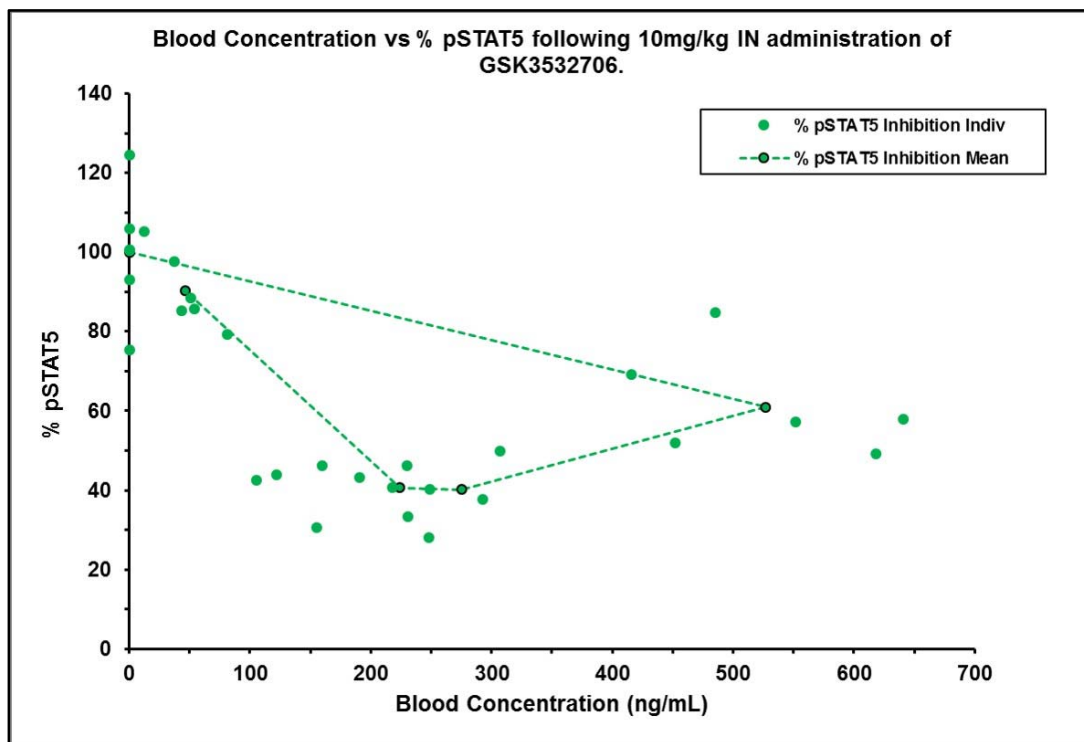


Figure 7.7-20 is a PKPD plot showing a hysteresis loop when the pSTAT response is plotted against drug concentration in blood following an intranasal dose of 10mg/kg observations were taken over a time course of 1 to 4.5 hours, following IL4/13 cytokine induction in the lung using female BalbC mice, n=6/dose group. The IL4/13 cytokine was given intranasally 30 minutes before the animals were terminated and lungs removed for analysis.

Figure 7.7-21 The Temporal Displacement Between the Blood Concentration (Central Compartment) and the Pharmacological Effect Observed in the Lung.

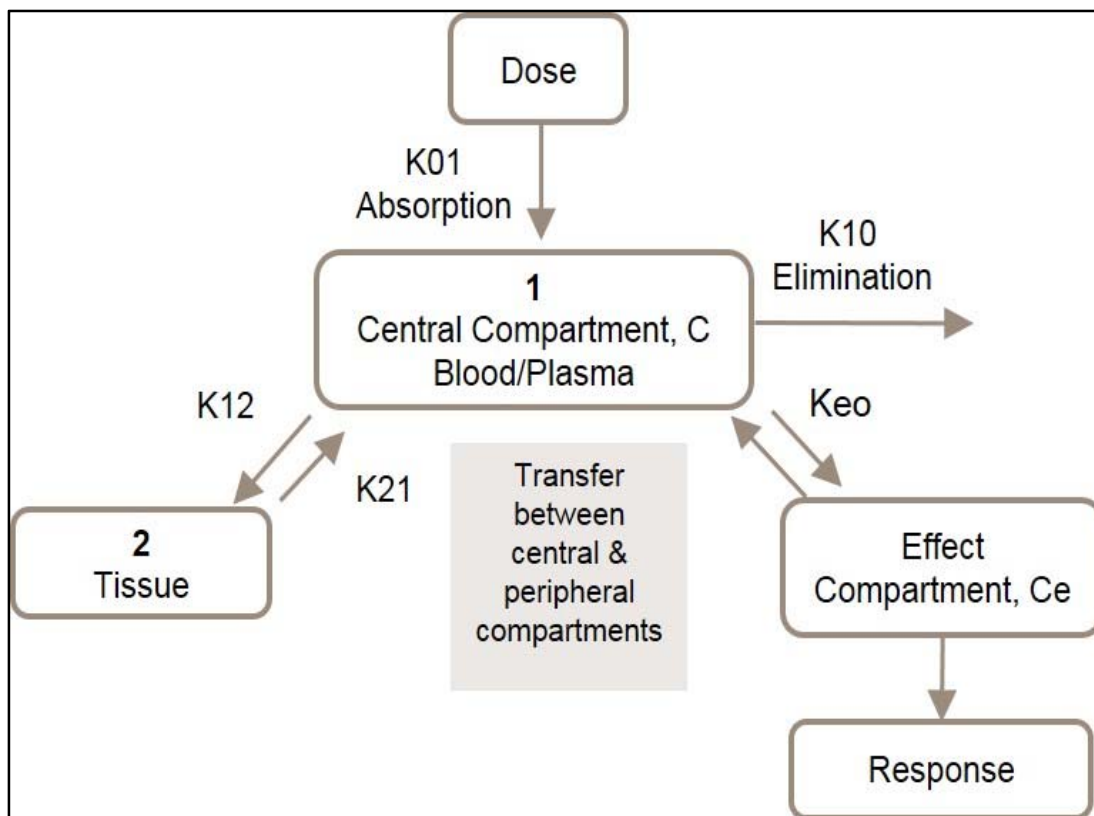


Figure 7.7-21 is a schematic describing an Effect Compartment (Link) PKPD model, where K_{01} is the absorption rate, K_{10} is the elimination rate, $K_{12}/21$ is the transfer rate between the peripheral and central compartments and K_{eo} is the rate constant between the PK compartment and effect compartment

The data shown in Figure 7.7-19 indicates that there is a temporal delay between the drug concentration and effect time courses, this type of delay could be due to several factors such as drug tissue distribution, active metabolites or slow ligand-receptor on / off rates. The reasons for the delay seen in the pSTAT response is most likely due to distribution or slow enzyme kinetics, particularly as there is no evidence to suggest an active metabolite of GSK3532706 is being formed. This type of delayed response can be described by either an Effect Compartment (Link) or Turnover PKPD model, which will be described in later in Section 7.8.

Figure 7.7-21 is a schematic of a Link model. If there is a delay between observed pharmacological effect and the blood/plasma concentration, a plot of the response versus the concentration will result in a hysteresis loop that is seen in the pSTAT PKPD study shown Figure 7.7-20. The Link model is valid where there is an apparent temporal displacement between concentration and response. The purpose of fitting an effect compartment is to estimate the K_{eo} , which is the rate constant describing the delay between the central compartment concentrations (C), the effect compartment concentrations (C_e) and the pharmacodynamics which is described by an E_{max}/I_{max} model for a competitive inhibitor. The E_{max}/I_{max} model is described by Equation 60.

Equation 60

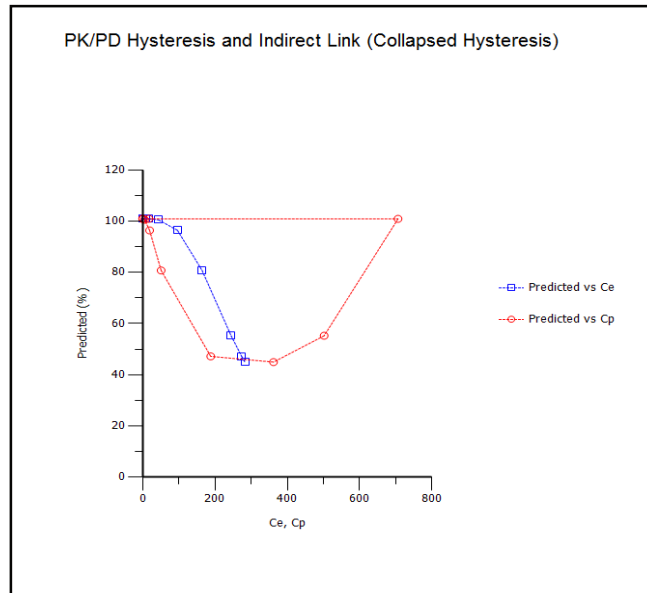
$$E = 1 + \frac{E_{max}.C^N}{EC_{50}+C^N} \quad \text{or} \quad E = E_0 - \frac{I_{max}.C^N}{IC_{50}+C^N}$$

E is the response, E_{max} is the maximum effect, C is the compound concentration, EC_{50} is the half maximal effect of the compound and N is the hill slope. I_{max} is the inhibitory equivalent, either form of the equation can be used.

When an appropriate PK model is fitted to model the blood concentration time course, the K_{eo} can be then be correctly determined, which results in the hysteresis loop collapsing to allow prediction of the effect compartment concentrations. The relationship between the concentration and effect can then be analysed using a simple E_{max}/I_{max} model (Equation 60). The result of this process can be seen in Figure 7.7-22 (Graph B) where the Link model predicts the observed pSTAT.

Figure 7.7-22 The PKPD Data Modelled Using a Link Model

A)



B)

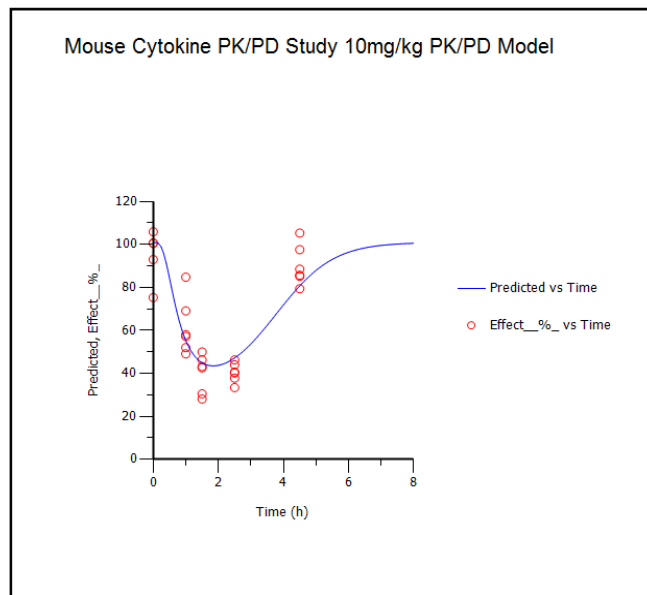


Figure 7.7-22 Graph A. show the PK/PD effect vs blood concentration hysteresis loop and the collapsed hysteresis loop for the effect vs effect concentration. Graph B. shows the predicted pSTAT vs time profile and the experimental observations (red circles).

Figure 7.7-23 shows the simulated blood and effect compartment concentration-time curves and the effect-time curve from the PKPD data in Figure 7.7-18. It can be seen that the effect compartment concentration now inversely correlates (mirrors) with the pSTAT response as you would see for a direct effect.

Figure 7.7-23 Simulated Blood and Effect Compartment Concentration-Time Curves and the Effect-Time Curve

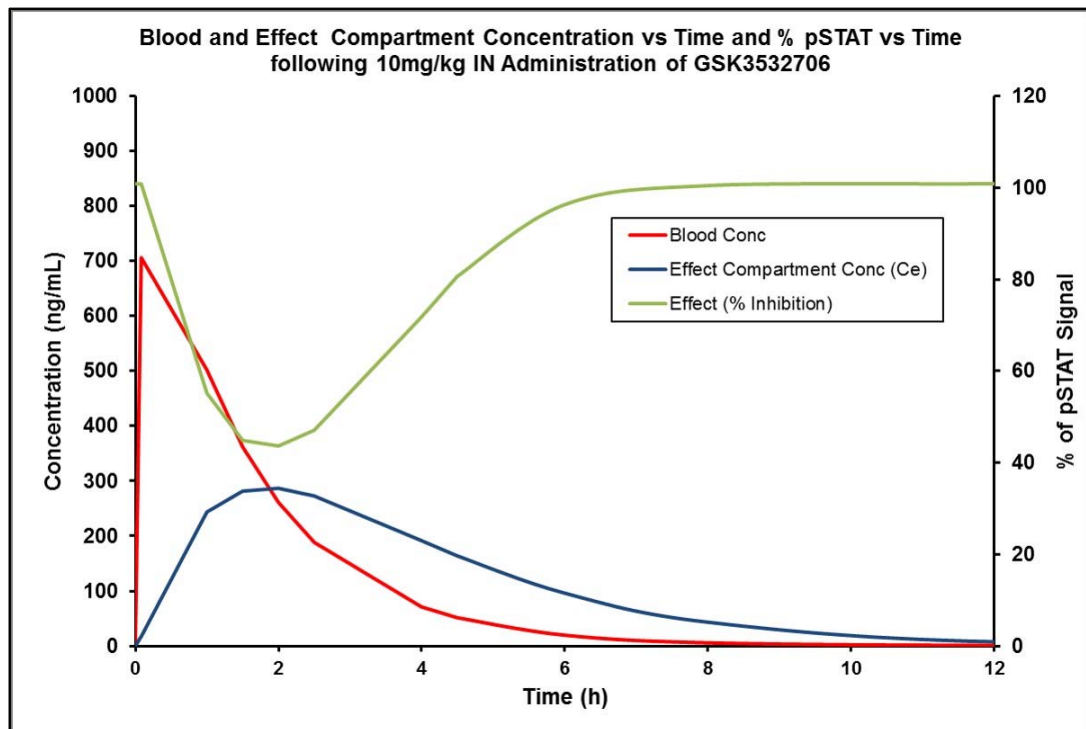


Figure 7.7-23 shows the simulated blood and effect compartment concentration time curves and the effect time curve from the PKPD data in Figure 7.7-18 and modelled using the Link model described in Figure 7.7-21.

Table 7-4 below shows the different dose estimation methods used to calculate the clinical dose and the data required for each method.

Table 7-4Table 7-14 shows the output parameters from the Link model these include I_{max} , IC_{50} , Gamma (Hill slope) and K_{e0} for GSK3532706, these can be used to predict the effect at different doses to avoid further *in vivo* studies or to help refine the design future

in vivo PKPD experiments. These parameters could also be employed in more complex clinical PKPD and dose predictions using appropriate scaling techniques.

Table 7-14 Link Model Output Data for the PKPD Response to GSK3532706

Parameter	Value
E0 (%)	100
I _{max}	98
IC ₅₀ (ng/mL)	233 or [23]u
Gamma	3.4
Keo (1/h)	0.48

Table 7-14 shows the Link model output parameter for GSK3532706. The human *In vitro* fibroblast cell potency was 5 ng/mL.

The Link model built based on the 10mg/kg data for GSK3532706 was then used to predict the pSTAT profile for doses of 3 and 30 mg/kg (Figure 7.7-24). It can be seen from this simulation that a 3mg/kg dose was predicted to have very low pSTAT inhibition, but the 30mg/kg data indicated 100% pSTAT inhibition for an extended period of up to 4 hours with ca. 60% inhibition being maintained for up to 6 to 7 hours. To help validate the Link model, an *in vivo* PKPD study was performed at 30mg/kg: the observed data has been overlaid on the simulated data in Figure 7.7-24. The data shows that the model did predict the 30mg/kg pSTAT profile in terms of E_{max} and duration, no additional model fitting was done, the error bars represent 95% confidence intervals (CI).

Figure 7.7-24 Modelled pSTAT vs Time Profile for a 3, 10 & 30mg/kg IN Doses with Experimental Observations Overlaid

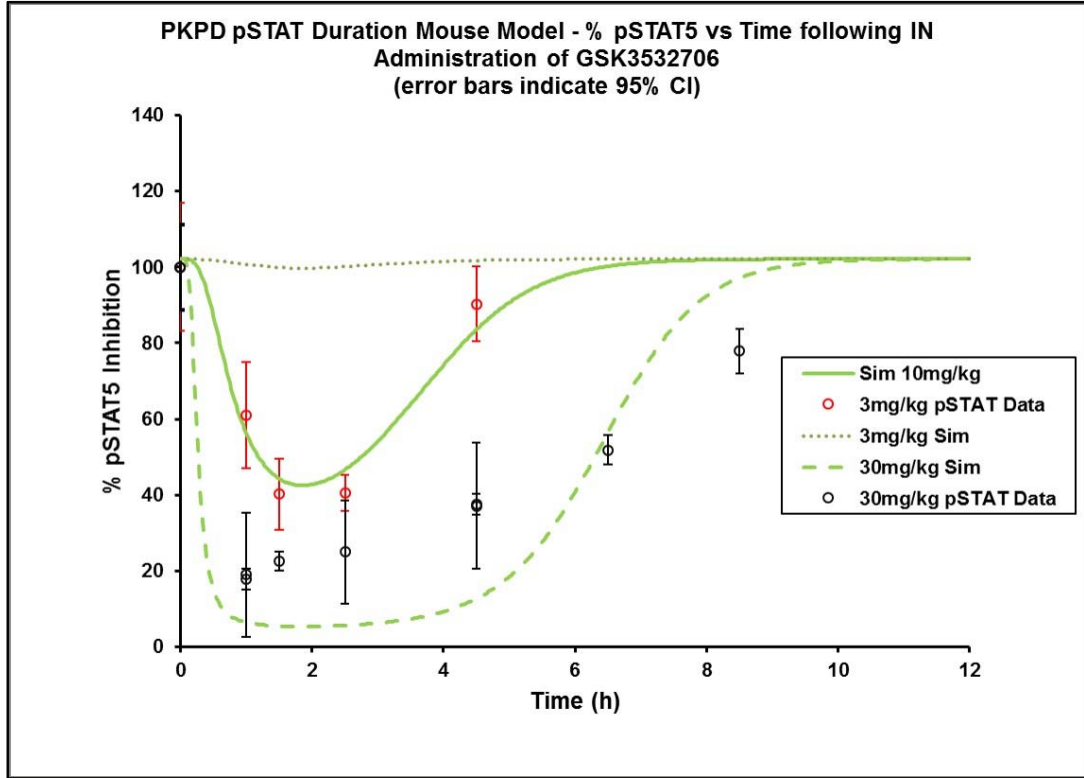


Figure 7.7-24 shows the predicted pSTAT vs time profile for a 3 & 30mg/kg IN dose and the experimental observations (black circles with 95% CI, 30mg/kg only). The predicted data is based on the 10mg/kg Link model.

7.7.4 Confirming Lung Duration is Required for Target Engagement and Cytokine Induced pSTAT5 Inhibition.

The lung retention profiles described in Figure 7.7-5 clearly showed that the tool compound GSK3532706 had an extended lung retention profile up to 8 hours, whereas GSK3489723 was poorly retained, with no quantifiable levels in the lung 1 hour post IN dose (NB these profiles were all generated from solution doses to determine “intrinsic” lung retention). To confirm that lung retention was required for efficacy (TE), a cytokine duration of action PKPD study was performed at 10 mg/kg IN in mice with GSK3489723 (Figure 7.7-25 and Figure 7.7-26).

The unbound blood concentrations are clearly very low for GSK3889723 (Figure 7.7-25) and are below the fibroblast IC_{50} at each timepoint, which was not the case for GSK3532706, where unbound blood concentrations were above the IC_{50} at all efficacious timepoints and above the IC_{90} at 1 hour post dose. Whilst lung concentrations at the earlier timepoints for GSK3889723 were above the fibroblast IC_{50} (Figure 7.7-26), as previously discussed with GSK3532706, they do not truly reflect active compound due to its formulation as a suspension. At these earlier timepoints, the percentage of active drug was low and therefore no efficacy was seen: as the compound dissolved it would be absorbed (removed) from the lung very quickly, therefore TE was not sufficient to inhibit pSTAT.

Comparing the PKPD profiles of GSK3889723 and GSK3532706 retrospectively confirms that the drug efficiency and retention parameters can be used to select compounds for progression through a pulmonary delivery focussed drug discovery project.

Figure 7.7-25 The Measured Unbound Blood Concentration and the %pSTATs Cytokine Inhibition GSK3489723A.

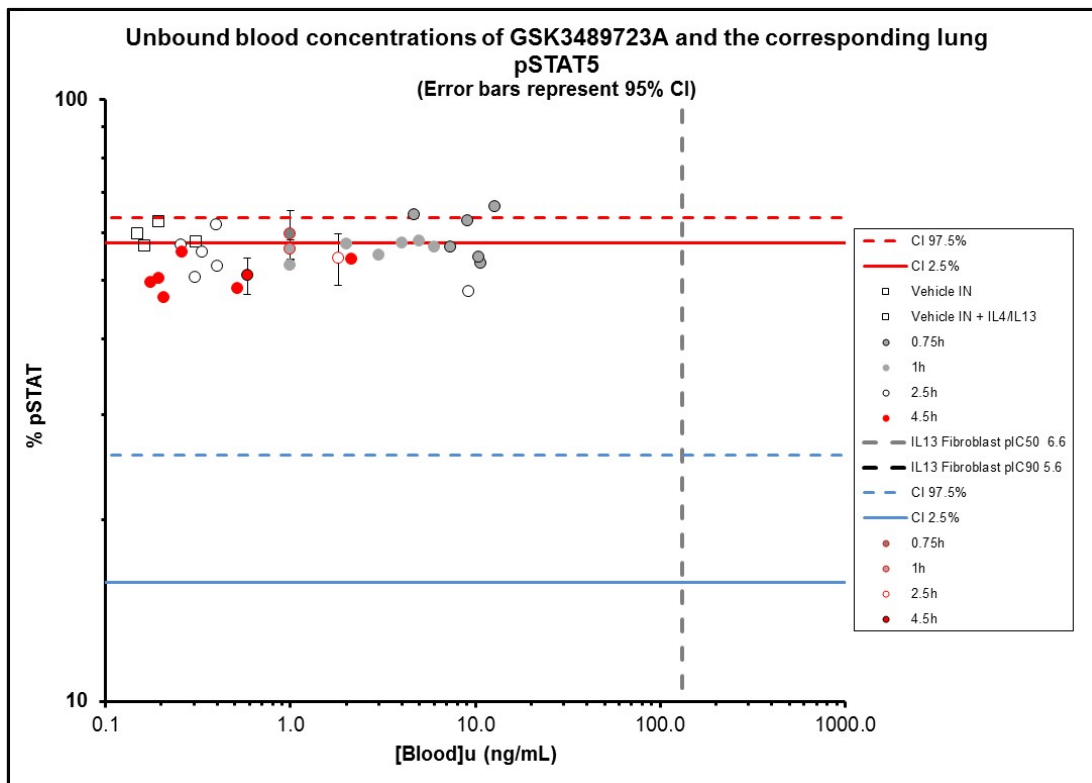


Figure 7.7-25 is a PKPD plot showing unbound drug concentration in blood following an intranasal dose of 10mg/kg over a time course of 1 to 4.5 hours versus pSTAT response, following IL4/13 cytokine induction in the lung using female BalbC mice, n=6/dose group. The IL4/13 cytokine was given intranasally 30 minutes before the animals were terminated and lungs removed for analysis. Vertical lines represent the IC₅₀ and IC₉₀ measured *in vitro* using lung fibroblast cells.

Figure 7.7-26 The Measured Total Lung Concentration and the %pSTATs Cytokine Inhibition GSK3489723A.

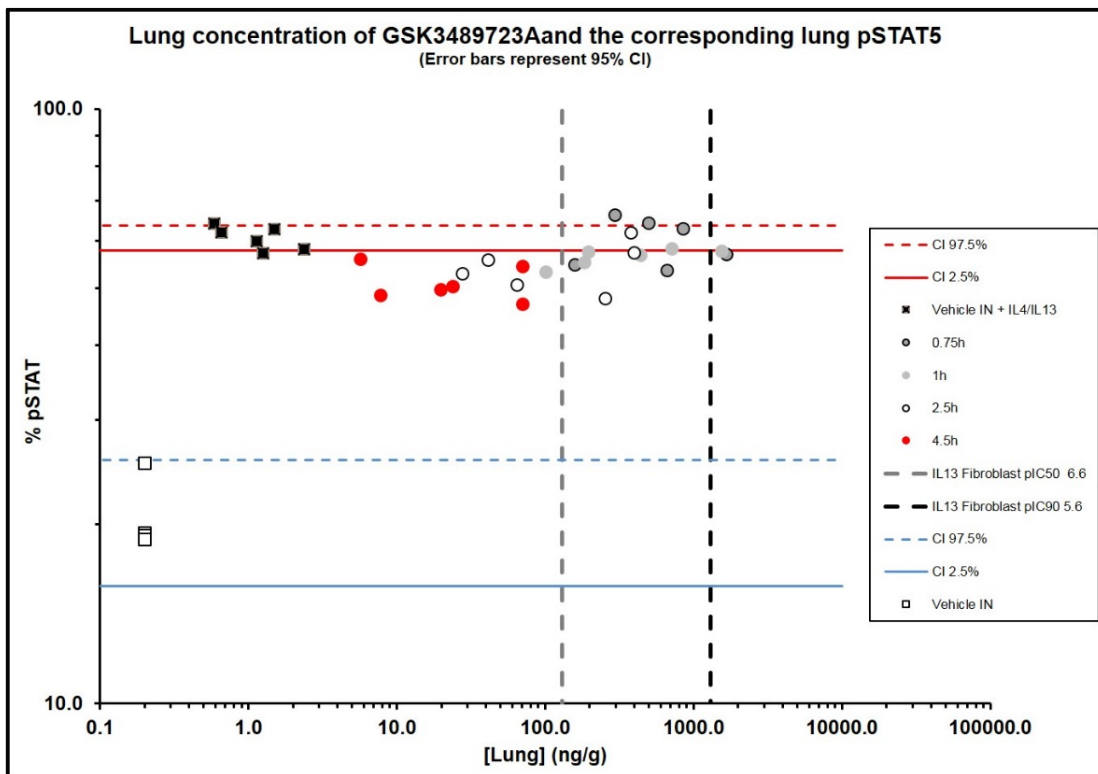


Figure 7.7-26 is a PKPD plot showing drug concentration in lung following an intranasal dose of 10mg/kg over a time course of 1 to 4.5 hours versus pSTAT response, following IL4/13 cytokine induction in the lung using female BalbC mice, n=6/dose group. The IL4/13 cytokine was given intranasally 30 minutes before the animals were terminated and lungs removed for analysis. Vertical lines represent the IC₅₀ and IC₉₀ measured *in vitro* using lung fibroblasts.

7.8 PBPK and PBPKPD Analysis of JAK Inhibitors

An alternative to the empirical PK and PKPD modelling utilised previously and discussed in Section 7.7.3 is PBPK, which utilises the physiological composition of various tissues and estimates a compound's distribution. This PBPK model can then be linked to a PD model to create a dynamic PBPKPD model. Another advantage of PBPK is that it opens up the possibility to look at exposure and potential pharmacology in other compartments, which are not typically accessible from *in vivo* studies or would require large number of animals to generate composite profiles. This PBPK based simulation approach can be

helpful in not only understanding drug efficacy but also safety, which can offer new insight into how program strategy should evolve to improve the therapeutic index of a compound.

Figure 7.8-1 Why Use PBPK?

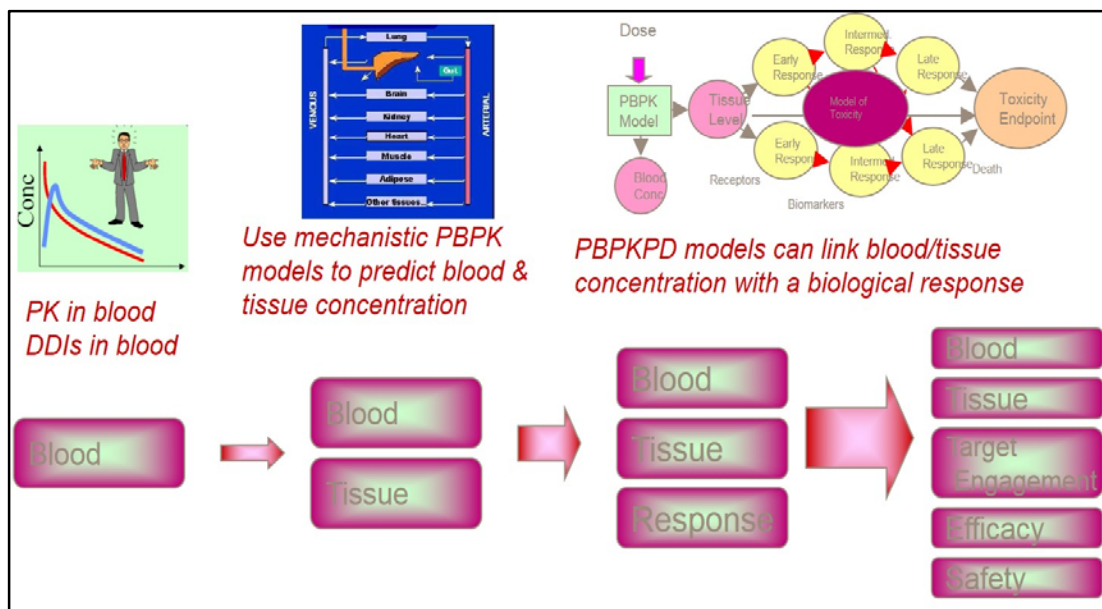


Figure 7.8-1 is a schematic showing the advantages of PBPK over simple PK profiles of the central compartment.

As most drugs exert their pharmacological effect in tissue compartments other than the systemic circulation (blood/plasma), understanding their concentration-time profile and distribution in different biophases is an important factor in drug discovery. However, it is impractical to measure the exposure profiles in many compartments such as lung, liver or brain because of their inaccessibility to repeat sampling. PBPK is a mechanistic tool that can be used to help understand the profile of a drug in multiple compartments in the body in both pre-clinical species and human. By understanding the PK and distribution in multiple compartments, it then becomes possible to link the pharmacological effect to the PK and to link PBPK to PKPD.

7.8.1 Building a PBPK Model Using the Tool Molecule GSK3532706

It is possible to build a PBPK model using minimal measured data: for certain programs such as GastroPlus™, it is possible to build one purely from the structure of a compound. However, *in vitro* and *in vivo* inputs are required to help validate the output from these models, which can then be used to understand the *in vivo* data, or design better *in vivo* studies by predicting future PK and PKPD outcomes.

To build a mouse PBPK model for GSK3532706, *in vitro* CL_i, whole blood binding, lung tissue binding, biomimetic data along with IV and IN *in vivo* data was used. The IV *in vivo* data ensures that the underlying PK model is accurate with respect to CL_b, V_{dss} and half-life.

Figure 7.8-2 Intravenous Mouse Blood and Intranasal Blood and Lung Profiles for GSK3532706

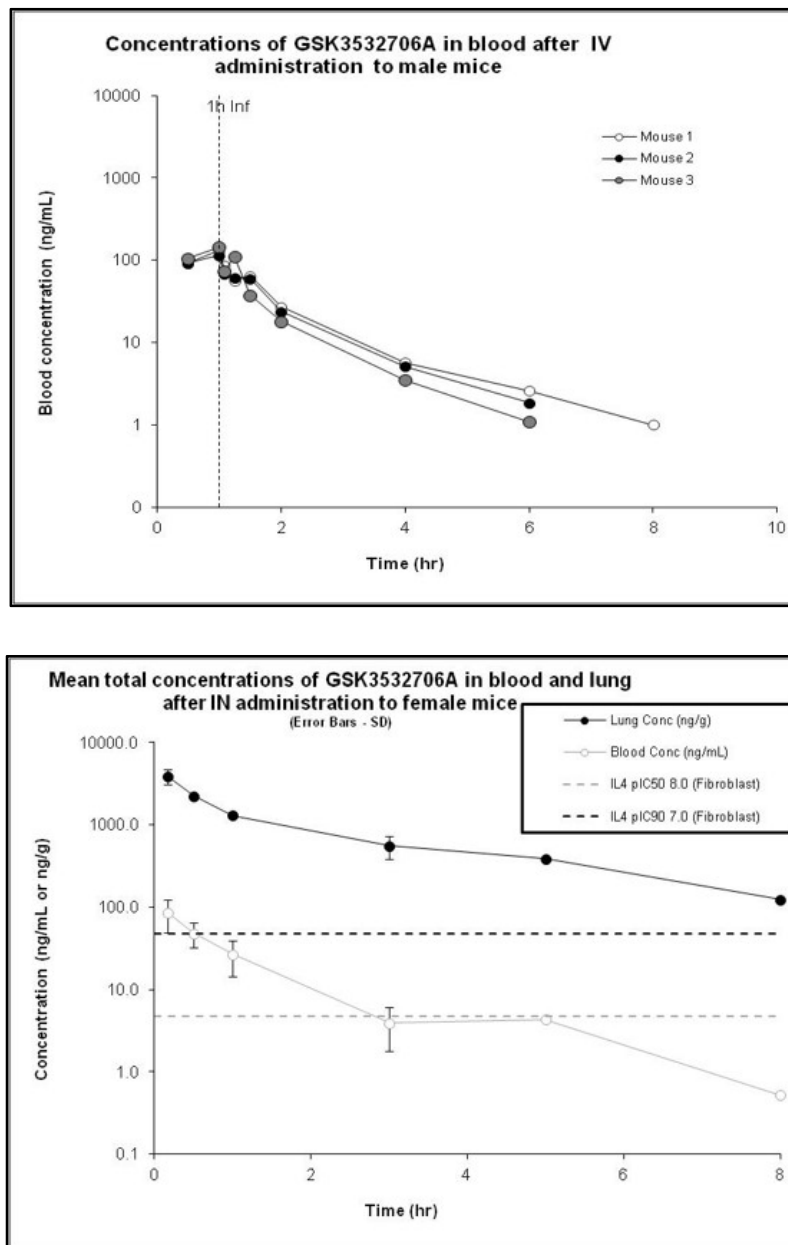


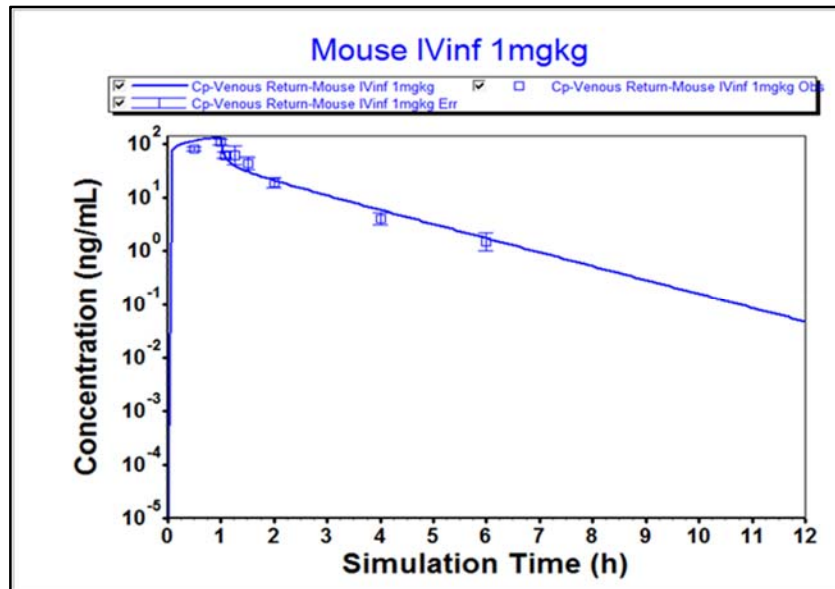
Figure 7.8-2 shows the *in vivo* IVinf blood and IN blood and lung concentration time profiles in Balb/C mice following doses of 1mg/kg

GSK3532706 was dosed to mice as an IV infusion (1 mg/kg) and as an intranasal solution (1 mg/kg). *In vivo* lung and blood concentration profiles are described in the graphs above

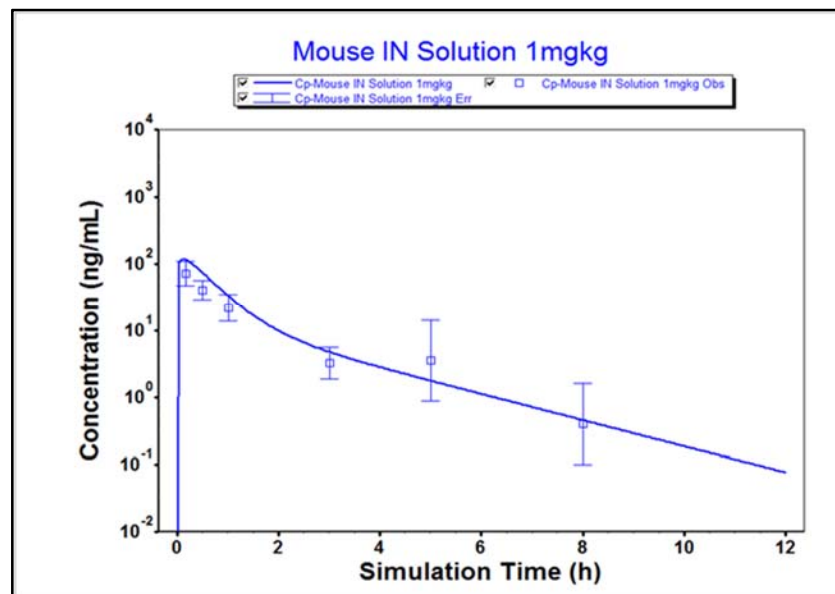
in Figure 7.8-2, Graph A shows the IV infusion blood concentration time profile and Graph B shows the lung and blood concentration profiles following IN dosing. The IV PK characteristics of GSK3532706 were high blood clearance (ca. 126 mL/min/kg or mouse liver blood flow), a large V_{dss} (7.4L/kg), low F (<10%) and good lung retention based on the DE_{max} hypothesis as described earlier in Section 7.6. The IN blood profile shows flip flop kinetics where the absorption rate (K_a) is smaller than the elimination rate (K_e). The effect of this switch in K_a and K_e rates is the downward curve becomes a reflection of actual k_a while the upward part of the curve is the actual representation of k_e . Therefore the "flip-flop" part of curve is the so-called flip-flop kinetics.

Figure 7.8-3 Mouse PBPK Model for GSK3532706, IV Blood/Plasma, IN Blood and IN Lung Profiles

A.



B.



C.

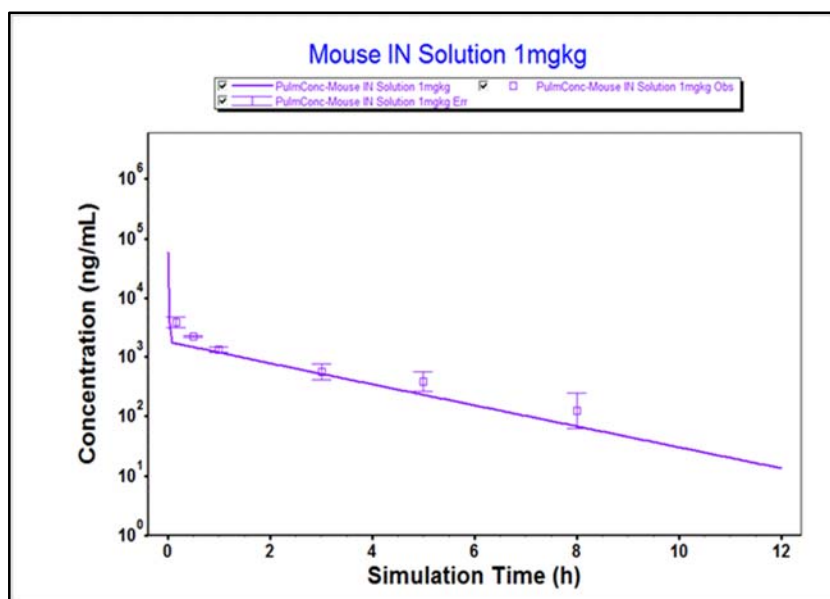
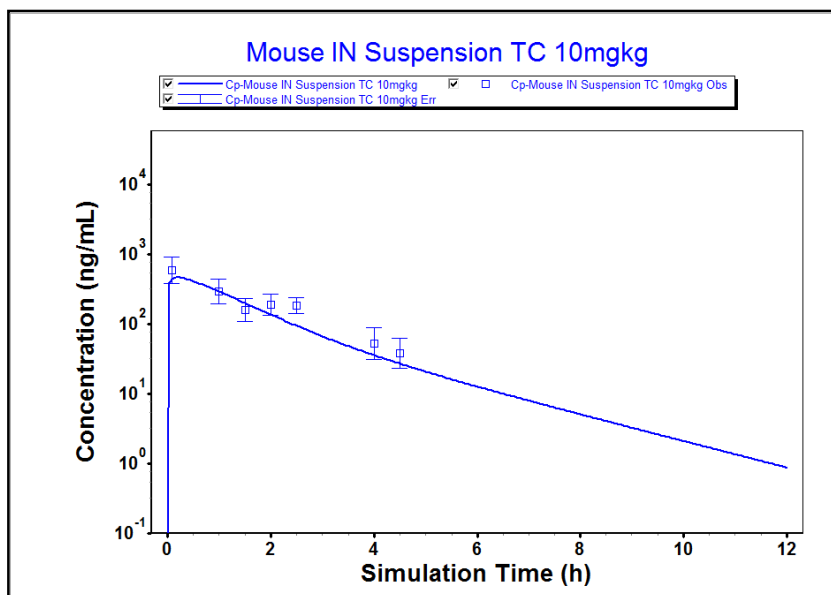


Figure 7.8-3 shows the PBPK model simulation outputs. Graphs A. IVinf plasma concentrations, B. IN Plasma concentrations and C. IN Pulmonary concentrations. The models were developed using mouse PK data from a mouse IV infusion study and an intra nasal lung retention study, where lung and blood profiles were generated from the same study. The model simulations show the model has been parametrised to give a good fit of both the IV plasma and intra nasal lung and plasma *in vivo* profiles. A B:P (Blood:Plasma) ratio of 0.8:1 was used to convert blood to plasma or plasma to blood as required.

The IV data was modelled to establish the underlying pharmacokinetic profile of GSK3532706. *In vitro* and *in silico* physicochemical, *in vitro* intrinsic clearance and *in vivo* data were used to help refine the model, depending on availability of data. The *in vivo* IV blood/plasma profile was well described by the model as can be seen in Figure 7.8-3. The mouse pulmonary physiology as described in Section 6.10.2 was then used to build a model to describe the IN lung and blood concentration time profiles. The *in vivo* IN lung and blood/plasma profiles were also well described by the models.

Figure 7.8-4 GSK3532706 Blood and Lung Profiles after 10mg/kg IN Dose (Suspension)

A.



B.

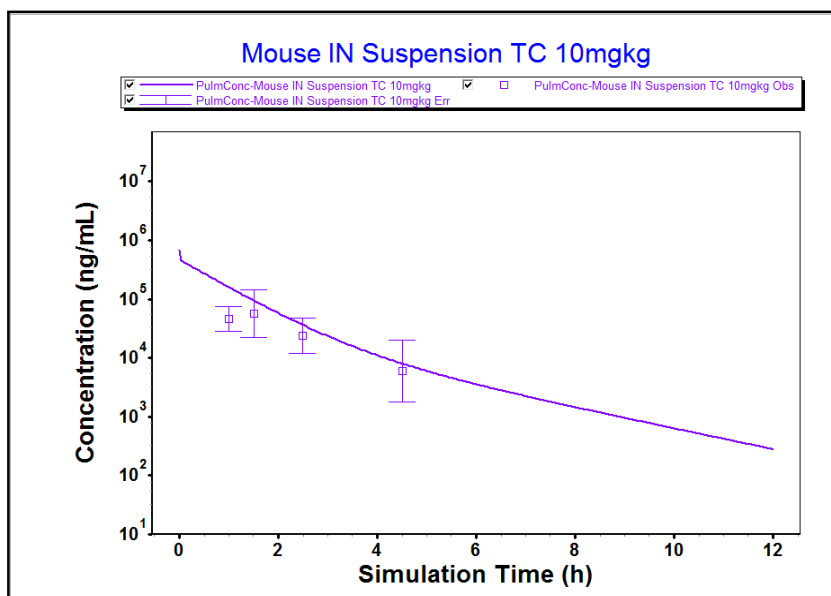


Figure 7.8-4 shows 10mg/kg PBPK simulations using the PBPK model in Figure 7.8-3. Graphs A. IN Plasma concentrations and B. IN Pulmonary concentrations. The experimental *in vivo* data was generated from a 10mg/kg study (suspension dose) using female Balb/C mice n=3/timepoint, the *in vivo* experimental data has been overlaid on the simulations.

As the aqueous solubility of GSK3532706 was in the low to moderate range (ca. 0.400-0.600 mg/mL), doses ≥ 1 mg/kg (0.4 mg/mL) were administered as suspensions. If modelling *in vivo* PK with a PBPK model is to be of value, predicting these suspension doses with reasonable accuracy is necessary. To help account for the fraction of dose which will be dissolved versus undissolved, an input function within GastroPlus™ called mixed multiple dosing (MMD) was used to help model the lung deposition and absorption.

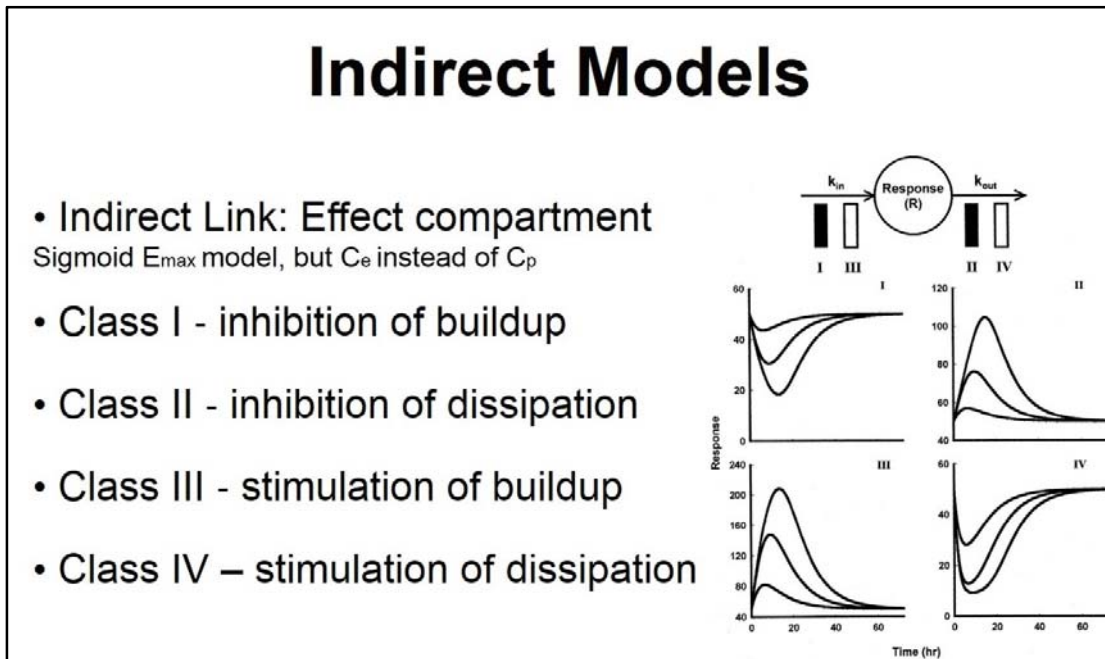
Figure 7.8-4 shows that the blood and lung concentrations for GSK3532706 after a 10 mg/kg IN dose (suspension) were predicted well by the PBPK model: ca. 100,000 ng/g was predicted vs ca. 50,000 ng/g measured in lung 1 hr post dose and ca. 400 ng/mL was predicted vs ca. 500 ng/mL measured in blood 1 hr post dose. Concentrations from IN suspension doses at 3 and 30 mg/kg were also well predicted by the model, as were blood/plasma and lung concentrations from IN doses over a range of 0.1, 0.3 & 1 mg/kg where the dose was typically in solution.

7.8.2 Linking PBPK to PKPD to Build an Integrated PBPKPD Model

As described in Section 7.7.3, PKPD modelling can be performed using direct effect models i.e. where the PD response mirrors the PK exposure profile. Indirect concentration response profiles can be modelled using a Link model which has been discussed and shown in Section 7.7.3 and Figure 7.7-21, which can be used where there is an offset in the peak PK concentration and the PD response. However, an indirect response model or Turnover model can also be used to describe this type of PKPD offset.

Indirect response models have been described in detail by Jusko *et al.* [156]. There are four basic indirect response models which have been characterised by Dayneka *et al.* [157] which describe the indirect PD response after drug administration, and are detailed in Figure 7.8-5. This type of model is based on the effect a drug has on a biological system by either inhibition or stimulation of factors that control the production or loss of a response. The model can help interpret PD effects that are not solely due to biodistribution effects but rather where a drug is affecting the production or loss of a response; the PD response from each model is described in Figure 7.8-5.

Figure 7.8-5 Description of the Different Indirect Response Models and how they Describe the Pharmacodynamic Response of a Drug [157]



A Class I indirect response model using the differential equation shown in Figure 7.8-6 can also be used to describe this offset between compound exposure and PD response for the JAK *in vivo* pSTAT PD model. This model is also semi-mechanistic with respect to the pharmacological processes of the target.

Figure 7.8-6 An Alternative Approach to Explain the Slight Offset of the Blood Concentration (Central Compartment) and the Effect Observed in the Lung.

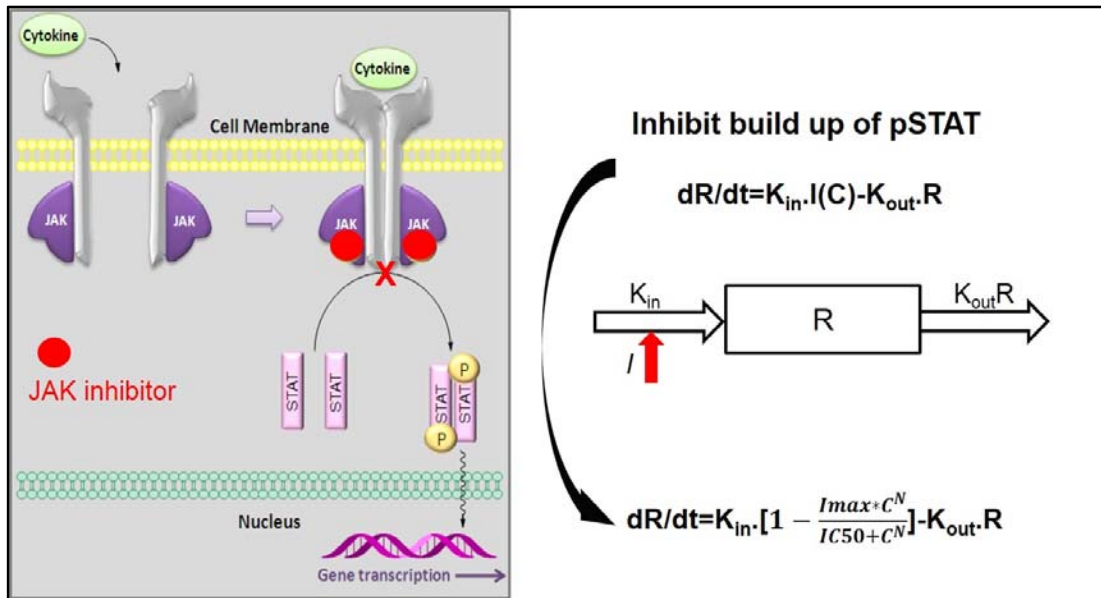
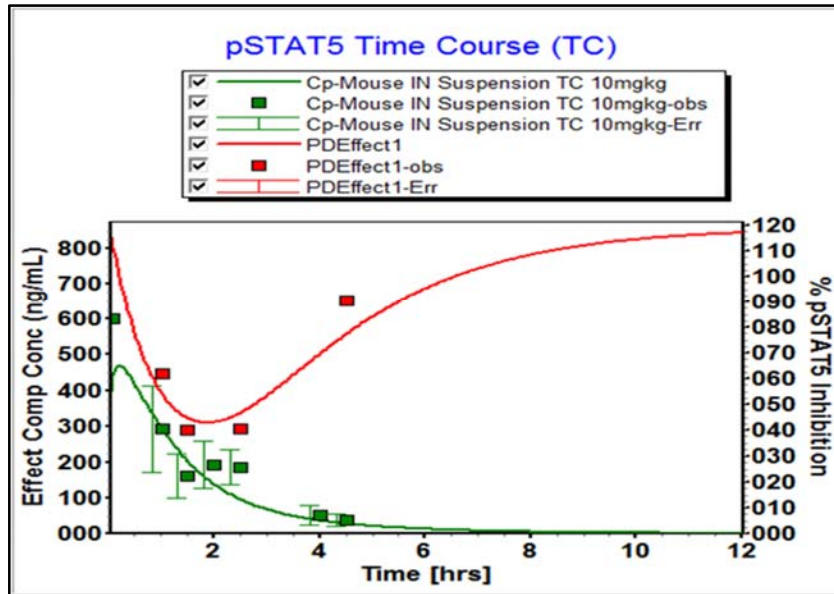


Figure 7.8-6 shows a schematic of the JAK pathway and an inhibitory turnover model with the differential equation which mathematically describes the change in response with time. dR/dt = change in response with time, K_{in} = turnover rate, the rate of input of production, k_{out} = fractional turnover rate or loss, R = response to a drug, $I(C)$ = I_{max} model

Figure 7.8-7 PBPKPD Modelling for GSK3532706 using a Turnover Model

A.



B.

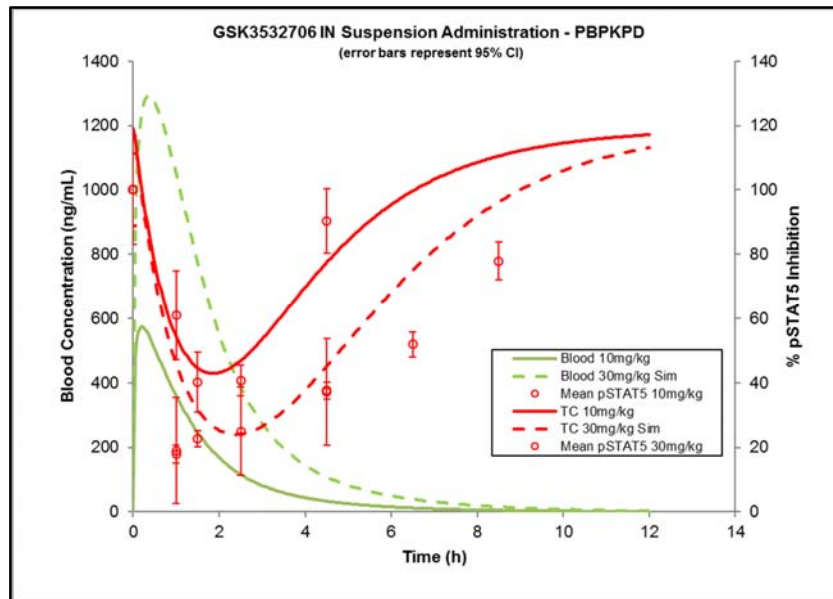


Figure 7.8-7 Graph A shows the model predicts for the observed IN PK and pSTAT inhibition at 10 mg/kg, the predicted IN blood/plasma PK profile is shown by the solid green line and the observed *in vivo* PK concentrations are overlaid as green squares. the predicted pSTAT profile is shown by the solid red line and the observed pSTAT vales are overlaid as red squares. Graph B shows the predicted PKPD profiles for a 30mg/kg IN dose

It can also be seen in Figure 7.8-7 that the pSTAT5 PD response model also fits the experimental data very well, the predicted effect is shown by the red line and the observed data by the square red boxes. The PBPK model had already been established and discussed, see Figure 7.8-4. This then enabled a prospective model of a 30mg/kg IN PKPD profile to be simulated: the resulting PKPD *in vivo* data has been overlaid on the modelled data in Graph B. The *in vivo* data and the model correlate very well without any further optimisation required to fit the data. This model was then used to predict and design more complex *in vivo* PKPD studies such as the 8-Day Cytokine Model and House Dust-Mite Model, which are described in the sections below.

Table 7-15 A Comparison of the Link PKPD and PBPKPD Model Output Parameters

<u>Link Model</u>		<u>Turnover Model</u>	
Parameter	Value	Parameter	Value
E0 (%)	100	Kin (1/h)	133
I _{max}	98	K _{out} (1/h)	1.1
IC ₅₀ (ng/mL)	233 or [23]u	IC ₅₀ (ng/mL)	88 or [8.8]u
Gamma	3.4		
Keo (1/h)	0.48		

Table 7-15 shows a comparison of the output for the Link and indirect PKPD models for GSK3532706 in the mouse pSTAT *in vivo* model

As can be seen from Table 7-15, the IC₅₀'s from this PBPKPD indirect turnover model and the link model are similar to each other. The unbound *in vivo* potency is also similar to the *in vitro* human fibroblast cell data (6 ng/mL) indicating these models show some correlation with human *in vitro* data and could be used to help predict human clinical target engagement.

7.8.3 Developing More Complex 8-Day Cytokine Mouse Model

The 8-Day Cytokine Mouse model which is a pre-clinical model of airway inflammation is described in Figure 7.8-8. This model was used to measure a functional lung eosinophilic response to daily IN repeat administration of IL-4/13 cytokine. After repeated challenge with IL-4/13 to the lungs, there is an activation of inflammatory processes which include the release of IL-5 response in these tissues, which results in the migration of eosinophils to the lung. Eosinophils, along with mast cells are key cells involved in the innate immune response [158]. Lung eosinophils are a classical immunoinflammatory response in allergic asthma and used as a biomarker for compound activity as described in Section 5.4, Figure 5.4-2 and Figure 5.4-3. Although there are other models of airway inflammation which are similar and have been published [159], the 8-day Cytokine Mouse Model was developed as part of the JAK program.

Figure 7.8-8 An 8-Day Cytokine Challenge PKPD Model

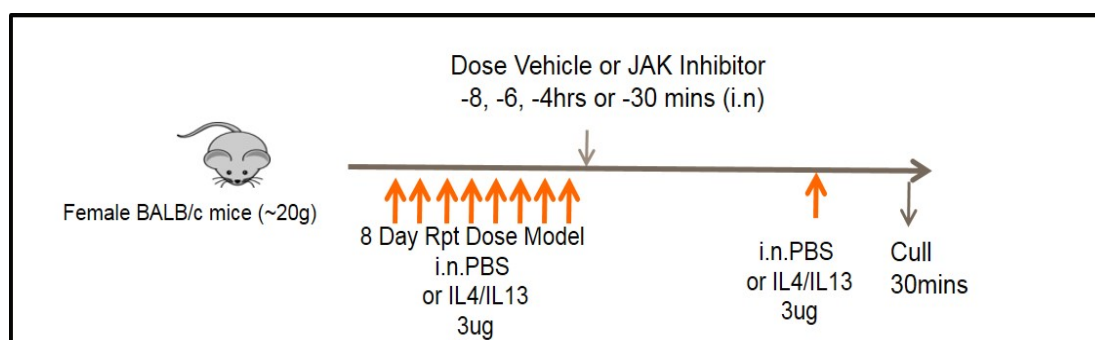


Figure 7.8-8 shows a schematic of the 8-day cytokine challenge mouse model of airway inflammation, the compound dosing regimen and PD endpoints

Figure 7.8-9 The PBPKPD Analysis of the Effect of GSK3532706 in the 8-Day Repeat Cytokine Mouse Model

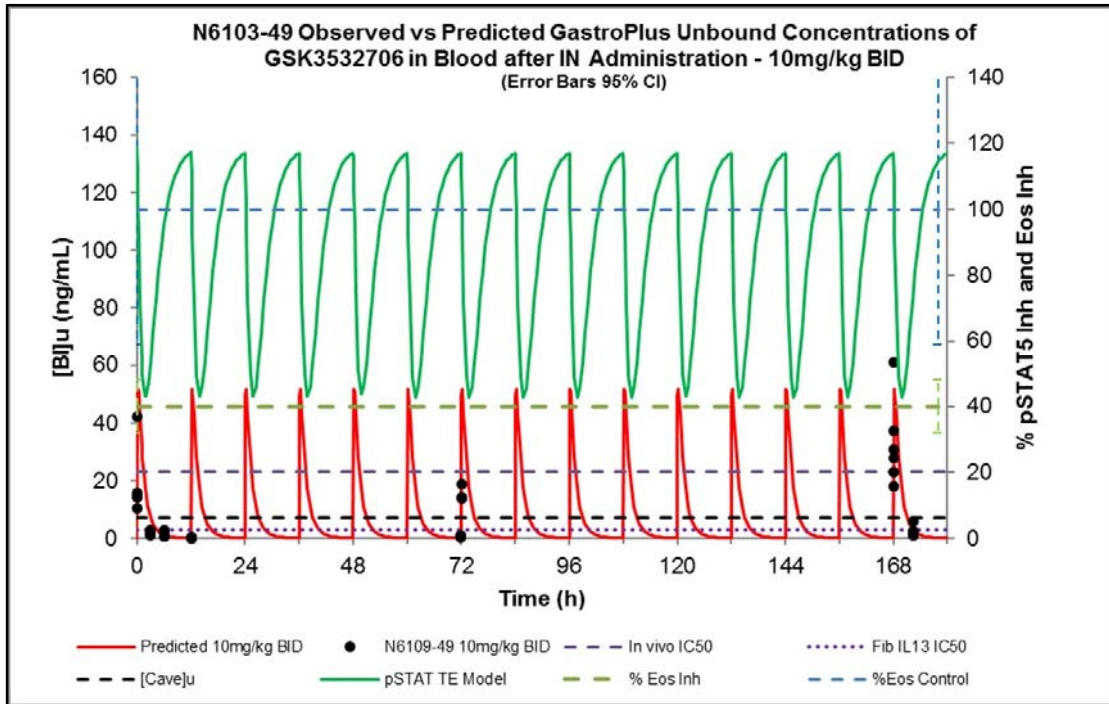


Figure 7.8-9 shows the modelled PBPKPD data for GSK3532706 with observed experimental PK and PD data from the 8-day cytokine mouse model

The data shown in Figure 7.8-9 for GSK3532706 provided confidence in the models' ability to predict the pSTAT5 target engagement response. They were then used to help define a dose level and dosing regimen to maximise unbound lung exposure and associated target engagement in order to produce a functional response that could be measured by inhibition of eosinophils in the lung. Although GSK3532706 was not optimal in terms of lung exposure and retention, it represented the best tool compound within the program to test the efficacy of an inhaled JAK inhibitor in terms of target engagement and functional efficacy.

Figure 7.8-9 shows the predicted outcomes of the PK exposure following repeat dosing of GSK3532706 and its expected effect on target engagement and lung eosinophilia. This figure describes the predicted unbound blood concentration following BID 10 mg/kg intranasal dosing, which was set to achieve maximum target engagement in the lung

without any adverse pharmacology in the animal. The plot has been annotated with various potency markers, which include an *in vivo* IC₅₀ from the pSTAT5 TE model and an *in vitro* whole cell fibroblast IC₅₀. Measured blood concentrations are also overlain with the predicted blood profiles to show how predictive the PK model is. The figure shows that the average concentration (C_{ave}) is above the fibroblast potency for approximately 6 hours of the dosing interval and only above the *in vivo* potency for about 1 hour. The pSTAT5 inhibition profile is taken from the model to show the expected level of target engagement throughout the dosing interval. The eosinophil inhibition was measured on day 8 in lung tissue and indicates a significant effect by up to 60% based on a 95% CI. These data demonstrate that PBPKPD analysis can help predict potential outcomes for a bespoke *in vivo* model and relate these to the *in vivo* PKPD data in terms of target engagement and functional response.

7.8.4 House Dust-Mite (HDM) Mouse *In Vivo* Efficacy Model

A second mouse model (the HDM model; Figure 7.8-10) was used to measure a functional lung eosinophilic response to HDM sensitised and re-challenged mice. The HDM model is an accepted disease relevant model of airway inflammation for compound evaluation in asthma [157]. Asthma is a chronic disease resulting from intermittent or continued aeroallergen exposure leading to airway inflammation [159] and HDM is a known allergen which plays a part in allergic inflammation of the airways. Continuous exposure to HDM elicits severe and persistent eosinophilic airway inflammation in mouse models of airway inflammation [159].

Figure 7.8-10 Schematic of a House Dust-Mite (HDM) Mouse *In Vivo* Efficacy Model

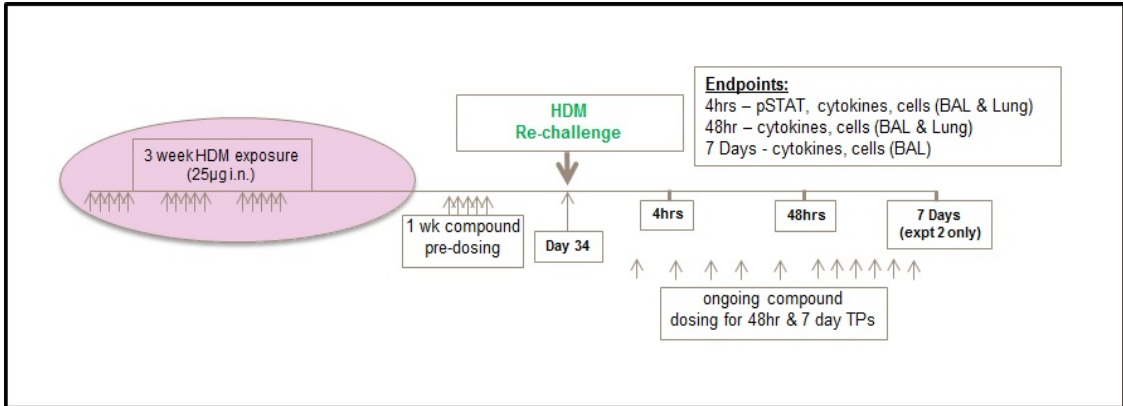


Figure 7.8-10 shows a schematic of the HDM sensitisation period, HDM re-challenge, the compound dosing options and PD endpoints.

After repeated challenge with HDM to the lungs during a 3-week period of sensitisation, there is an activation of inflammatory processes which include the release of IL-5 response in the lungs, which following activation of inflammatory mechanisms as previously described, results in the migration of eosinophils to the lung. Figure 7.8-11 shows a schematic of the proposed events following the HDM sensitisation and re-challenge in a pre-clinical mouse model of airway inflammation. The aim of a JAK inhibitor is to inhibit the inflammatory processes described in Figure 7.8-11 and therefore produce clinical efficacy in moderate to severe asthma where the current standard of care is not effective.

Figure 7.8-11 Proposed Inflammatory Processes of HDM Re-Challenge Model (not published)

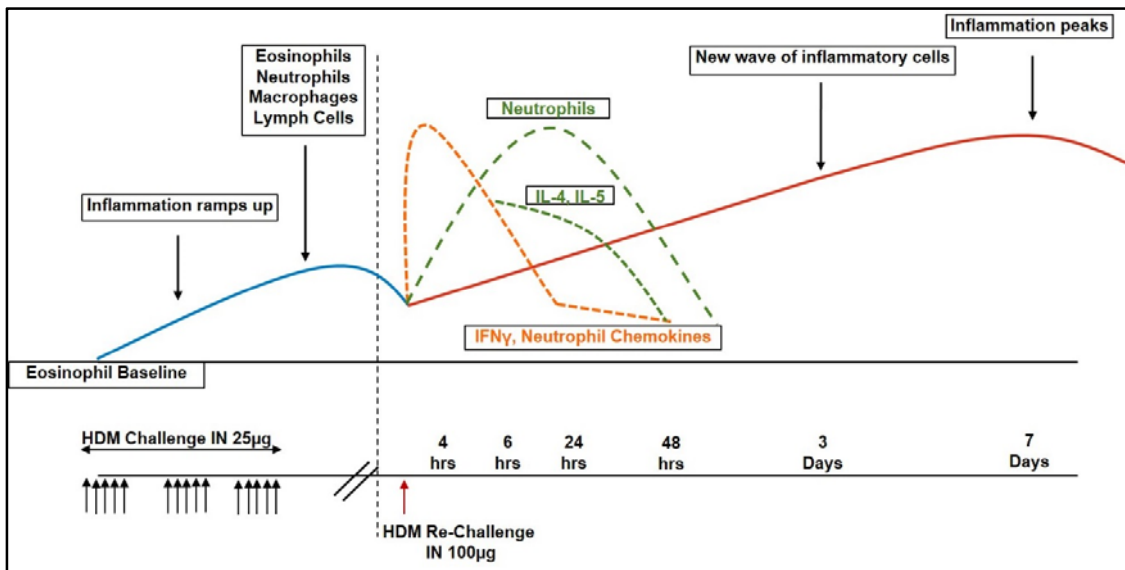


Figure 7.8-11 is a schematic showing the proposed immune inflammatory processes that occur following HDM sensitisation and re-challenge. The schematic is based on *in vivo* HDM model observations but does not represent a quantitative analysis of the inflammatory processes described.

The positive efficacy seen in 8-Day Cytokine model with GSK3532706 allowed progression to the established disease relevant HDM model. The data shown in Figure 7.8-12 shows the predicted outcomes of the PK exposure following repeat dosing of GSK3532706 and its expected effect on target engagement and lung eosinophilia following BID 10 mg/kg intranasal dosing and is annotated with the same potency markers as the 8-Day model. The model appears to generally under predict the C_{max} and blood exposure in this study. C_{ave} is above the fibroblast potency for approximately 6-7 hours of the dosing interval, and only above the *in vivo* potency for about 1 hour, which is similar to the 8-Day Cytokine model duration of exposure.

The predicted pSTAT5 inhibition profile was taken from the PBKPD turnover model (acute challenge IL4/13 PD model) to show the expected level of target engagement, because the PK and potency limitations of this tool molecule rendered full and continuous TE throughout the dosing interval impossible. As with the 8-Day Cytokine model eosinophil inhibition was measured on day 8 in lung tissue, and produced a very similar

eosinophil inhibition (inhibition by up to 60% based on a 95% confidence interval (CI)). Importantly in this experiment, a measure of pSTAT5 was also incorporated in the study protocol, which was taken 4 hours after the HDM re-challenge. The importance of this pSTAT measurement was to give an observed measure of TE (pSTAT) from the *in vivo* model to overlay and compare to the simulated pSTAT profile that was built from the acute Cytokine PD model (Figure 7.8-7). It can be seen from Figure 7.8-12 that there was significant inhibition of pSTAT5 based on a 95% CI and this response overlays the TE model well, despite the data being taken from different models. By connecting concentration of the compound at the site of action (PK) with a measure of target engagement (pSTAT5 inhibition), followed by an associated functional response (eosinophil inhibition), agreement with the Three Pillars validation of efficacy has been accomplished [16]. A repeat of this study was completed to confirm repeatability and robustness the data.

Figure 7.8-12 Effect of GSK3235706 in the Mouse HDM Model Experiment 1

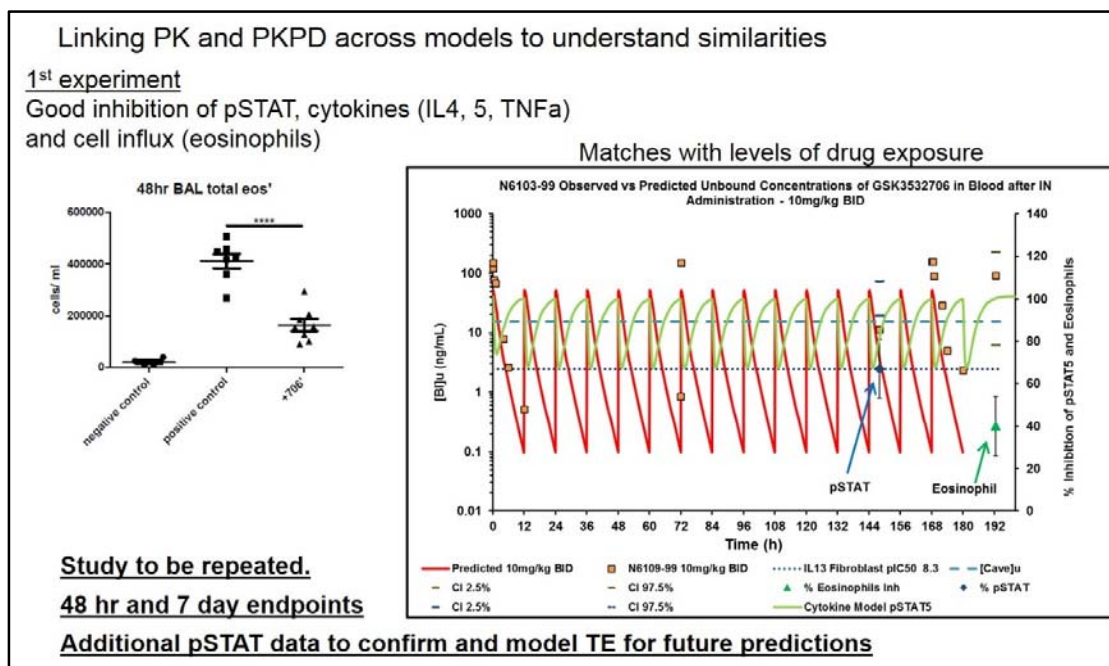


Figure 7.8-12 shows the modelled PBPKPD data for GSK3532706 with observed experimental PK and PD data from the HDM mouse model

Figure 7.8-13 shows the results from the second HDM re-challenge study which was performed to show reproducibility and robustness of the first experiment shown in Figure 7.8-12. It can be seen that in this second study the measured blood exposures are lower than predicted and approximately 10 times lower than observed in the experiment 1. The C_{ave} concentration is only above the fibroblast potency for approximately 3 hours of the dosing interval, and above the *in vivo* potency for <1 hour. Furthermore, when the eosinophil inhibition was measured on day 8, the response is not significantly inhibited based on a 95% confidence interval (CI).

Although it was not possible to give an exact reason for the 10 times lower exposure in experiment two, there are several factors which could have caused or contributed to it. Different batches of crystalline GSK3532706 were used which may have produced differences in dose suspension, which may have impacted up both deposition and dissolution rate. The IN-dosing technique is a potential source of variability due to the use of anaesthesia which effects both the depth and rate of respiration. These are all factors in highlighting why it is important to measure drug concentration in PKPD experiments and not rely on dose alone.

Figure 7.8-13 Effect of GSK3235706 in the Mouse HDM Model Experiment 2. Using PBPKPD Analysis to Understand a Negative Result

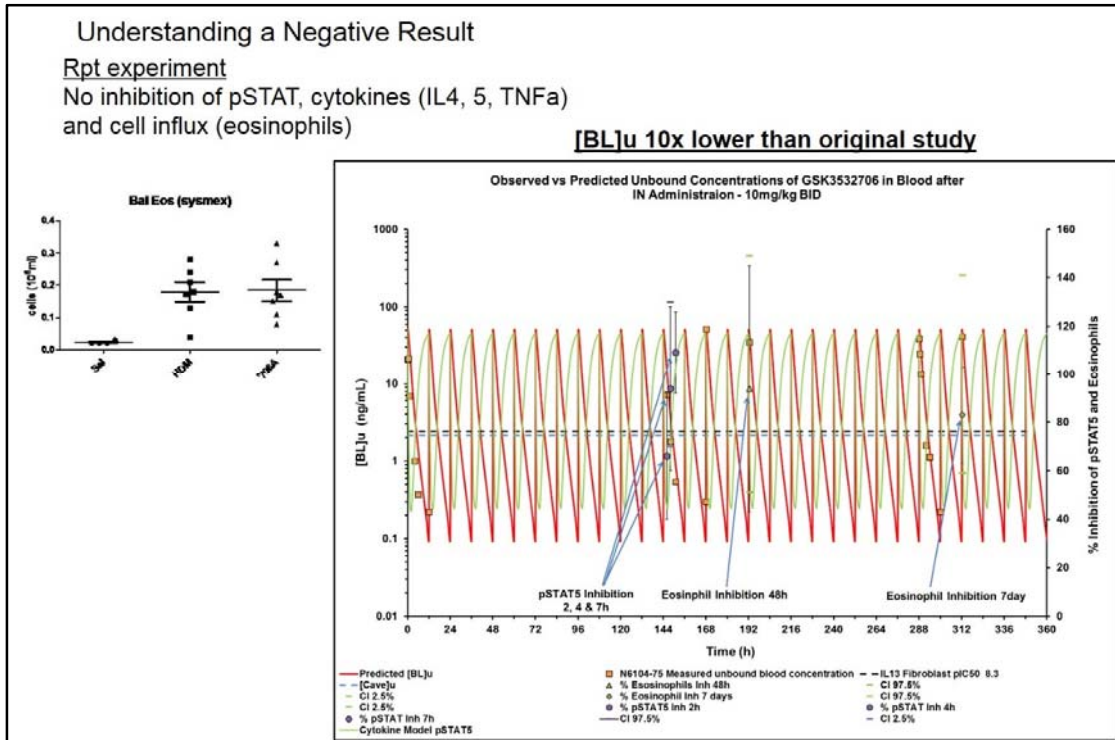


Figure 7.8-13 shows the modelled PBPKPD data for GSK3532706 with observed experimental PK and PD data from the HDM mouse model

Importantly, a measure of pSTAT5 was successfully incorporated into experiment 1 which enabled us to confirm TE and link this to a functional response. In the second experiment, a more extensive pSTAT profile was incorporated into the study protocol providing a pSTAT5 profile with data at 2, 4 and 7 hours after the HDM re-challenge. It can be seen from this pSTAT profile there was no significant inhibition of pSTAT5 at any of the measured timepoints based on a 95% CI (Figure 7.8-14).

Figure 7.8-14 PBPK/PD Analysis Enables us to Understand a Negative Result (2)

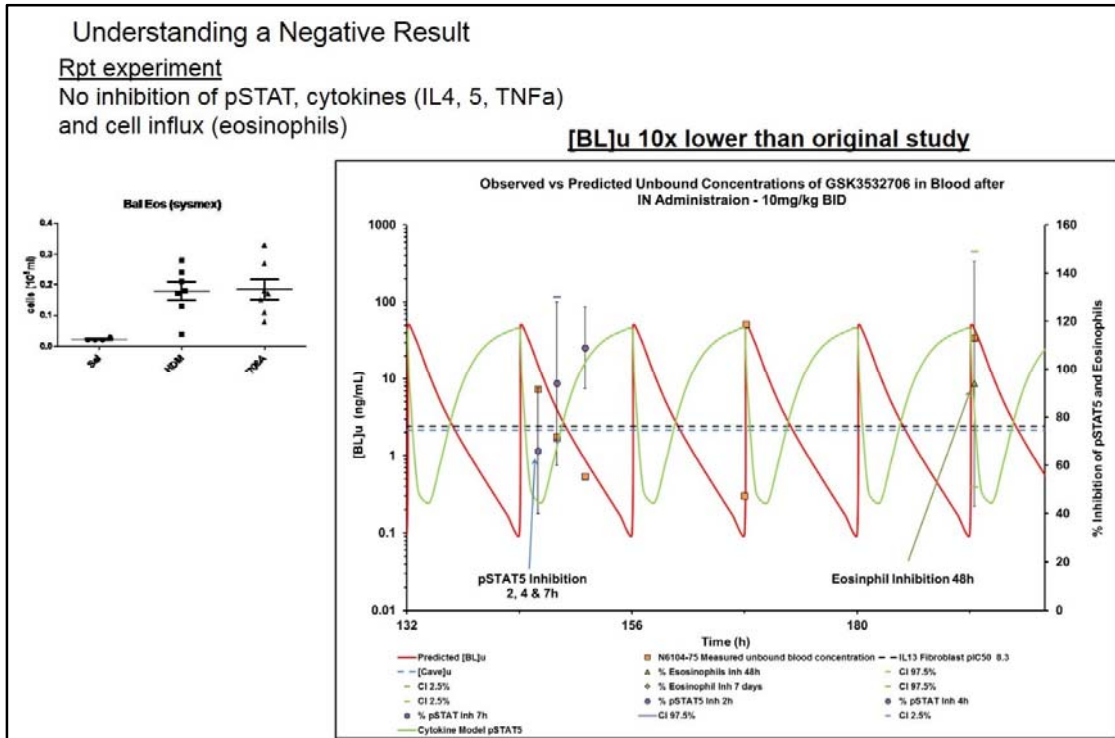


Figure 7.8-14 shows the modelled PBPKPD data for GSK3532706 with observed experimental PK and pSTAT data from the HDM mouse model where TE wasn't achieved

This important result revealed that a lower PK exposure (10x less) did not result in effective TE and thus no functional response (no eosinophil inhibition) was observed. These data highlight the importance of fully understanding the PKPD response (TE) and then linking it to a functional pharmacological endpoint. In this second experiment, none of the Three Pillars conditions were met, but using this framework explained why the negative result occurred. Understanding the reasons for a negative result is more valuable for a program teams development in understanding the target pharmacology and molecule properties required for efficacy than only seeing positive efficacy data.

7.8.5 PBPK Enables us to Dig Deeper into other Compartments of Interest

One of the biggest challenges in PKPD study design is understanding drug concentration at the site of action, which is particularly challenging in Respiratory PKPD models where the biophase of interest is the lung and it is not possible to repeatedly sample from this tissue. Figure 7.8-15 shows that PBPK modelling allows a more comprehensive understanding of the influence of compartments on a compound's profile, providing an opportunity to identify correlations which would be otherwise inaccessible using standard *in vivo* PK analysis. Although it was only possible to build a correlation with TE based on measured blood concentration in these PK/PD analyses, PBPK provides an approximation of concentrations in different lung compartments that can be related to efficacy. These are mathematically derived profiles, but they are representative and physiologically relevant to the compartment being modelled, which have been taken from multiple literature sources by the developers of GastroPlus™.

Figure 7.8-15 Predicting the Exposure of GSK3532706 in different Compartment in the Lung using the Mouse HDM PKPD Model

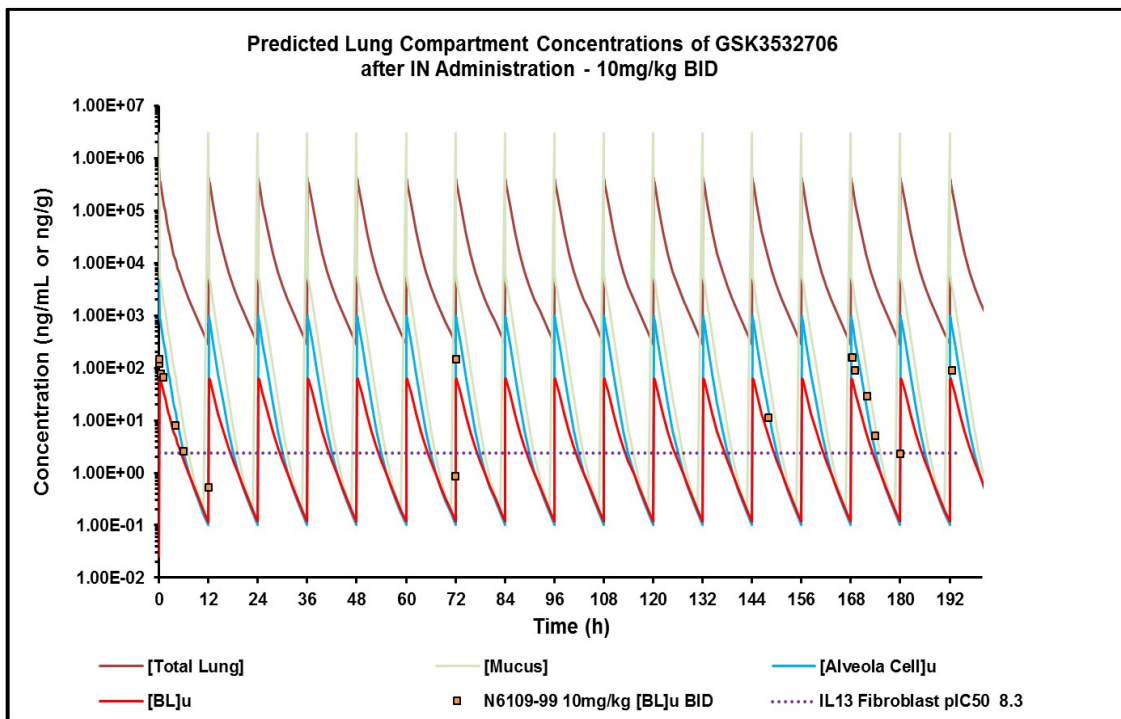


Figure 7.8-15 shows the predicted concentration of GSK3532706 in different lung compartments

Figure 7.8-16 extends the use of the theoretical PBPK exposures to compare the predicted exposure in alveoli cells to the PD response in the HDM model. This is a further example of how PBPKPD modelling opens up the opportunity to explore drug concentration in tissues that would otherwise be inaccessible and compare the concentration to a PD response.

Figure 7.8-16 Predicting the Exposure of GSK3532706 in Alveolar Cells in the Lung using the Mouse HDM PBPKPD Model

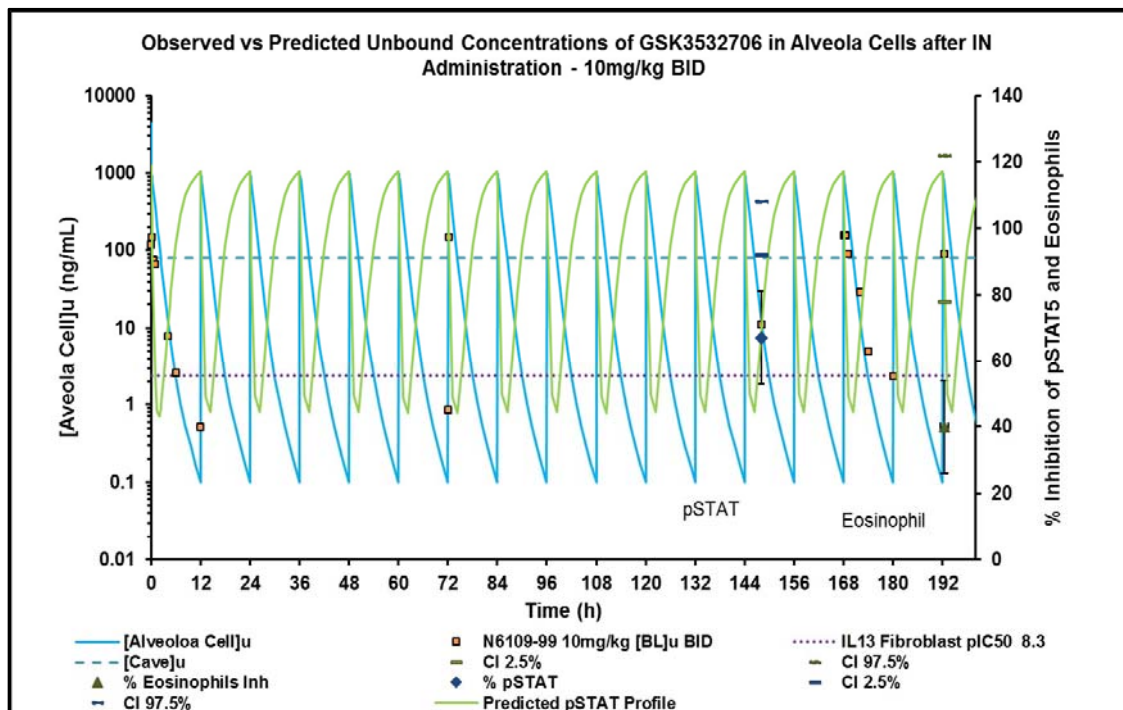


Figure 7.8-16 shows the predicted unbound concentration of GSK3532706 in alveolar cells, the observed unbound blood concentration, the observed and predicted pSTAT profile and the function eosinophil response.

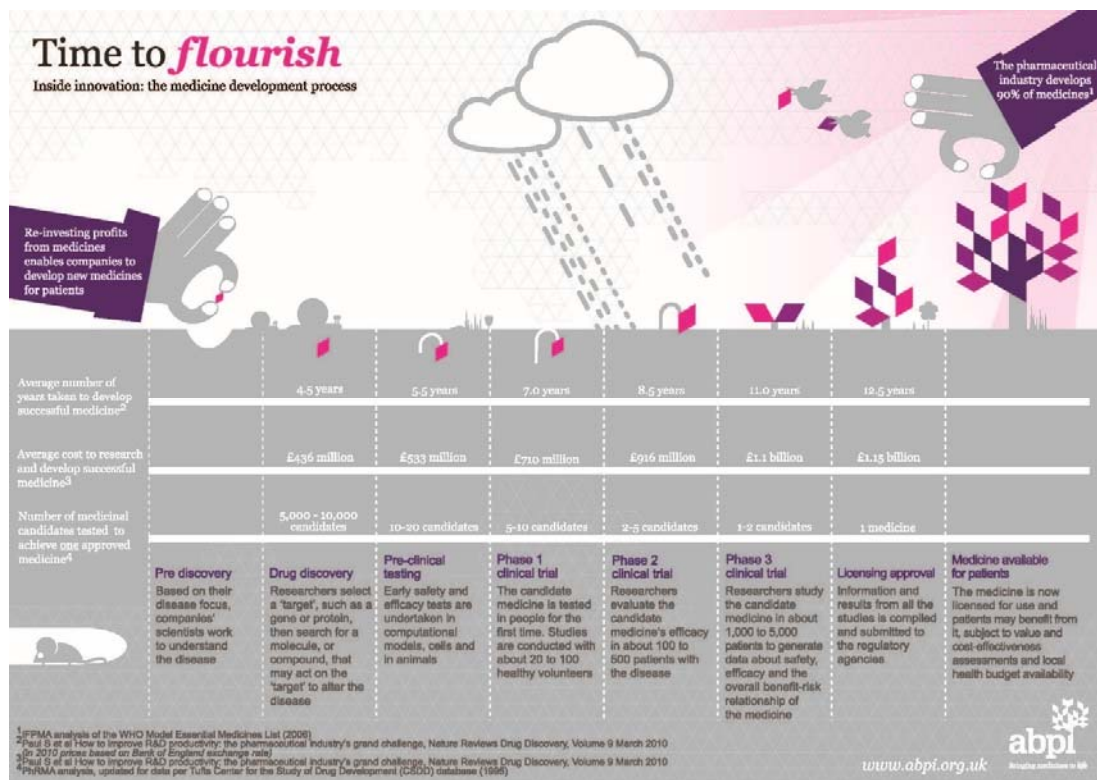
It can be seen from Figure 7.8-16 that the predicted free concentration in alveola cells was very similar to the observed free blood concentration. Based on the lung physiology the alveola space has only a single cell layer separating the air blood interface therefore the free concentration at this interface should be very similar. The observation in this model helps to further validate the use of free blood concentration as a surrogate for free lung concentration to build the PKPD correlation.

8 Concluding Discussion

8.1 Drug Attrition

The journey to discover and develop new medicines is a long and expensive one with many challenges to navigate along the way, and come primarily in the form of safety, efficacy, ADME properties, cost and changes in strategic priorities. The Association of British Pharmaceutical Industries (ABPI) suggest the average drug development cost is reported to be around £1.15 billion and 12 years [160] (Figure 8.1-1). Every year, a dozen or so drugs are approved by the medicine's agencies such as the FDA and EMEA, but to achieve this, thousands of NCE's and drug candidates fall by the wayside. As a drug discovery scientist, I know all too well the highs and lows of working in this field, but being part of a team that could make a breakthrough and deliver a transformative and effective medicine to patients motivates us as research scientists, even when the odds are stacked so heavily against success.

Figure 8.1-1 The Association of British Pharmaceutical Industries (ABPI) – The Medicine Development Process



Drug attrition remains a key challenge for the pharmaceutical industry to overcome, with less than 1% of NCE's and less than 10% of drug candidates tested in clinical studies becoming medicines. Consequently, even small improvements in efficiency will result in substantial savings in both time and money. Failure to achieve clinical approval for new medicines is the primary challenge for the pharmaceutical industry and if we are to address this, we need to embrace it and use the knowledge to improve decision making. Within this context, the key aim of this project was to assess the value of Drug Efficiency in early estimates of likely human therapeutic dose and establish whether it can be used to select compounds with better physicochemical properties. This in turn would lead to compounds having better ADME properties and PKPD efficacy thus improving the quality of drug candidates and ultimately help to reduce drug attrition.

Some success has been achieved with respect to improving the drug discovery/development process by focussing on solubility and permeability through the BCS classification system [10] or Lipinski's Ro5 [4,14], both of which were aimed at

improving small molecule oral absorption and human pharmacokinetics. Another complimentary system to the BCS is the biopharmaceutics drug disposition classification system (BDDCS) proposed by Wu and Benet [13]. The BCS focuses on the pharmaceutical properties of solubility and permeability whilst the BDDCS predicts drug disposition and potential drug-drug interactions in the liver and intestine. This modification was made because Wu and Benet recognised that drugs which have high intestinal permeability are typically eliminated via metabolism, whereas drugs which have low intestinal permeability are eliminated as unchanged drug in the urine or faeces [13].

Our improved understanding of pharmacokinetics and the recognition for the need to focus on ADME/DMPK properties during lead optimisation, and along with safety and efficacy, has helped reduce drug attrition in Phases I and II [161]. However, Figure 8.1-2, highlights that from 2000 to 2010, based on an analysis from four major pharmaceutical companies (AstraZeneca, Eli Lilly, GSK and Pfizer) published in 2015 [161], that the reasons for drug attrition remain largely the same as those reported by Kola et al. [162] a decade earlier. Progress had been made in selecting and progressing compounds with improved clinical pharmacokinetics and bioavailability, but poor PK still remains a significant cause of attrition in Phase I studies. As the purpose of a Phase I study is largely to assess the clinical PK in human, it is probably not surprising that there are a high proportion of terminations at this stage.

Figure 8.1-2 An analysis of the Attrition of Drug Candidates from Four Major Pharmaceutical Companies [161]

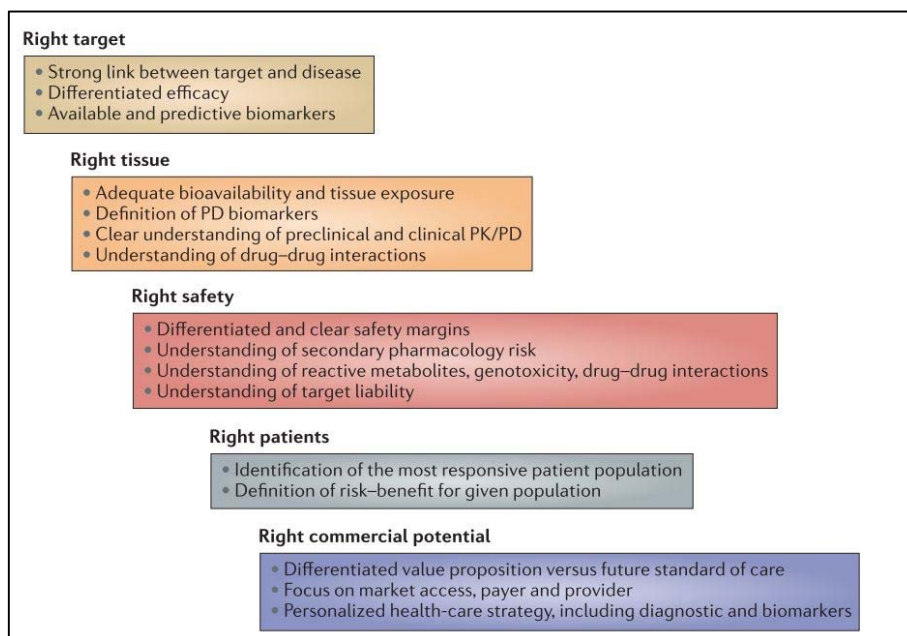
Termination reason	Overall	Period		Phase		
		2000–2005	2006–2010	Candidate nomination	Phase I	Phase II
Clinical safety	68 (11%)	48 (13%)	20 (8%)	5 (1%)	40 (25%)	22 (25%)
Commercial	40 (7%)	23 (6%)	17 (7%)	26 (7%)	10 (6%)	4 (4%)
Efficacy	55 (9%)	45 (11%)	10 (4%)	10 (3%)	14 (9%)	31 (35%)
Formulation	9 (1%)	4 (1%)	5 (2%)	8 (2%)	1 (0.6%)	0
Non-clinical toxicology	240 (40%)	144 (40%)	96 (40%)	211 (59%)	21 (13%)	7 (8%)
Patent issue	1 (0.2%)	0	1 (0.4%)	1 (0.3%)	0	0
Pharmacokinetics or bioavailability	29 (5%)	19 (5%)	10 (4%)	3 (0.8%)	25 (16%)	1 (1%)
Rationalization of company portfolio	124 (21%)	46 (13%)	78 (32%)	75 (21%)	29 (18%)	19 (21%)
Regulatory	2 (0.3%)	2 (0.6%)	0	1 (0.3%)	1 (0.6%)	0
Scientific	33 (5%)	28 (8%)	5 (2%)	13 (4%)	15 (10%)	5 (6%)
Technical	3 (1%)	3 (1%)	0	2 (0.6%)	1 (0.6%)	0
Other	1 (0.2%)	0	1 (0.4%)	1 (0.3%)	0	0
Total	605	362	243	356	157	89

*Table entries for each column indicate the total number and the percentage in parentheses.

One of the most surprising reasons for attrition is portfolio rationalisation, which raises questions as to why this figure is so high. Simplistically, it could be poor target selection or validation, or poor judgement and short term thinking by senior management and shareholders around the level of commitment the drug discovery process requires. This then leads to a search for “quick win projects” which rarely exist, in an industry where history shows that a long-term commitment is required to develop an effective medicine (Figure 8.1-1).

An interesting review by Cook *et al.* from AstraZeneca (AZ) [163] discusses a five dimensional framework based on a retrospective analysis of their 2005-2010 AZ portfolio, which is similar to the Three Pillars concept by Pfizer and describes the five R's: the right target, the right patient, the right tissue, the right safety and the right commercial potential (Figure 8.1-3).

Figure 8.1-3 Lessons Learned from the Fate of AstraZeneca’s Drug Pipeline: A Five-Dimensional Framework [163]



It expands on the Three Pillars and adds greater granularity to the pharmacological descriptors which are important to establish confidence in the biological target with respect to the disease and the molecule being developed. They also considered the commercial aspect of the drug being developed: was the target and molecule a first-in-class, an improvement to the standard-of-care and would health care providers be prepared to pay for this “new” medicine.

The right target, right tissue essentially focuses in on the pharmacology of the target and its link to the disease of interest, the ability to deliver the molecule to the site of action (PK), and the link between pharmacology and concentration at the site of action (PKPD), all to reduce attrition. The importance of establishing a clear link between PK, PKPD and a functional response was shown in with the HDM mouse *in vivo* efficacy model in Section 7.8.4.

8.2 Lipophilicity

It has often been suggested by drug discovery scientists who have analysed physicochemical properties looking for trends or correlations with ADME properties, that in the vast majority of cases, LogP is the parameter which is consistently highlighted above all others. This is despite the introduction of several other parameters or approaches such as LE, LLE, BEI, PFI etc., which have been devised to help identify molecules with optimal or improved physicochemical properties. It should be noted that all of these approaches have their own individual merits, but it appears that logP or lipophilicity/hydrophobicity dominates ADME properties and generally describes the overall picture of small molecules very well.

Of course, there are subtleties of how the measure of lipophilicity can be used and expressed to characterise small molecules in drug discovery. The typical measures are LogP or LogD and the simplicity of how they can be measured and how the number can be easily interpreted highlights its importance in the key areas of drug design, and make a very compelling argument for why it is such a relevant parameter to focus on in drug design.

In recent years there has been greater focus on LogD, given the impact of ionisation on the lipophilicity of acids and bases at physiological pH (pH7.4). For ionisable molecules there can be substantial differences in the LogD of a molecule from its neutral form to that at physiological pH. The influence of charge can be advantageous to a medicinal chemist when highlighting their molecules improved physicochemical properties over molecules from the same or similar series or those of a competitor. It is also important to note that a charged species can still bind to proteins, so acids will favour albumin and bases will favour phospholipids. Importantly, this behaviour is not captured in a classical octanol/water system. In addition to this, further caution should be used when considering LogD as a measure of lipophilicity, as pH is not constant in a physiological system. It is for this reason that LogP and LogD should always both be considered, when assessing a molecule's properties: LogP because it represents the intrinsic properties of a molecule and LogD because it can take into account the impact of environment.

Although LogP represents an extremely important parameter to help describe the properties of a molecule, there is a need to understand that the binding and distribution

of a molecule are not only influenced by lipophilicity. It is too broad a statement to suggest that all ADME properties relate back to lipophilicity and oversimplifies the challenge of designing small molecules that have the potential to become successful medicines. This is where understanding the nature of how a compound distributes is important, and to understand this we need to think beyond general terms like LogP to develop a greater understanding of the intrinsic properties of small molecules. This can be achieved by adopting the use of Drug Efficiency, or more specifically DE_{max} .

8.3 Drug Efficiency

Why is DE_{max} an important consideration alongside LogP, and is it different? DE_{max} is different and offers greater insight into the nature of how a molecule interacts with a physiological system because of how it is calculated. DE_{max} is the inverse term of the unbound V_{dss} , and *in vitro* V_{dss} and unbound V_{dss} can be calculated from biomimetic HPLC methods that employ HSA and IAM stationary phases, which are two highly relevant components of physiological systems and have clear relevance in the way a drug distributes [55]. The combination of HSA and IAM effectively forms the basis of a simplistic PBPK system. The reason this analogy is important is because PBPK software essentially involves a series of complex volume of distribution calculators, which calculate multi-compartment partition coefficients to work out the overall V_{dss} for a compound.

The focus on Drug Efficiency and early dose estimation in this project should be considered as a complementary approach to the Three Pillars analysis as well as aspects of the five-dimension framework [16][163]. Using DE_{max} as a complementary parameter to help improve the selection of NCE's can help ensure there is an improvement in the quality of the physicochemical properties at the centre of compound design, and help facilitate an improvement in ADME properties [19].

The importance of balancing the physicochemical properties of small molecules has been the focus of numerous publications since the seminal analysis by Lipinski and the rule of 5 in the mid 1990's [4] and the theoretical basis of the BCS which was described by Amidon [10], both of which link the importance of solubility with permeability when designing orally available small molecules. The analyses I have performed with different compound libraries described in Section 6.10 suggests that including DE_{max} as an additional global DMPK parameter to the early stage drug discovery selection process

can help with compound development during hit-to-lead optimisation. This has been demonstrated for both the Pi3K γ and Pi3K δ programs with their early hit-to-lead compounds (Table 7-5 and Table 7-7).

8.4 Dose Estimation of Systemically Delivered Compounds

Various dose estimation procedures have been investigated that require different input parameters. I have studied the recently developed simple approach to estimate the dose, using only the potency and drug efficiency of the compounds, which is referred to as the drug efficiency-based dose prediction (HPLC DE-DP). I have investigated the estimated dose using the HPLC DE-DP method applying the HPLC based DE_{max} values and various potency values, such as *in vitro* and cellular potency of Pi3K γ and Pi3K δ program compounds. While the *in vitro* and cellular potency showed wider discrepancies due to the different mechanisms involved, the predicted dose using the DE-DP method showed reasonably good agreement with a shift towards higher doses when the cellular potency values are used in the prediction (Figure 7.2-3 and Figure 7.4-4). This was not a major surprise, as cellular based systems typically result in slightly lower potencies, compared to enzyme systems. The reason for this is a combination of the physicochemical properties of the molecule, such as solubility, lipophilicity and permeability, and the pharmacology of a cellular system due to the difference in concentration of the target substrate. For example, ATP levels in an enzyme system are typically added at the K_m of the enzyme, but in a cellular system the ATP levels will be 100 times greater than the K_m, which will result in a lower measure of IC₅₀ as described by the Cheng-Prusoff correction [146].

The HPLC DE-DP methodology is available for medicinal chemists to assess a compound that has been proposed as a next iteration before they actually make it by assuming a good *in vitro* potency (pIC₅₀ 8 to 9) based on previous SAR of related compounds and by using an *in silico* calculated DE_{max}, which is available within GSK via an Excel Helium based tool using the derived property server (DPS). The *in silico* calculated DE_{max} and *in vitro* DE_{max} correlate very well because the *in silico* model was built using the measured HSA and IAM data stored in the GSK database. Using this *in silico* approach is a good way to quickly check the potential of a new series or set of compounds being considered prior to synthesis, as the retrospective analysis I have performed with the two Pi3K inhibitor series has shown. Although a degree of caution

should always be taken when using predicted data, it allows medicinal chemists valuable insight into the potential of new molecules or arrays of molecules prior to synthesis which could help save time and guide optimisation. When the compounds are synthesised, the albumin and phospholipid binding can be measured using biomimetic HPLC stationary phases in a high-throughput manner, and is available for medicinal chemists at the same time as the *in vitro* potency data. It should be noted that this dose prediction method provides the best-case scenario because it is a static system i.e. it does not include dynamic elements such as clearance or absorption/bioavailability of the compounds. The estimated dose refers to the steady-state plasma concentration assuming 100% bioavailability. Depending on the clearance and volume, the predicted dose may be required more frequently (high clearance compounds and/or low volume of distribution).

In early stage drug discovery programs, it is common that input parameters to guide the decision-making process towards compound selection and development are not available. Therefore, I have investigated the effect of the errors in the *in silico* prediction of these input parameters for the dose estimation equations. The impact of potency, clearance, volume of distribution and absorption were assessed using the DMPK-DP based dose estimation approach.

8.4.1 Potency

As previously discussed, the impact of pharmacology was assessed in terms of potency in an enzyme system or cellular system, which had systematic differences due to the assay formats highlighted above. The result was that the whole blood potency using the predicted dose was generally higher than the predicted value using the enzyme potency. This was to be expected, as cellular derived IC_{50} is often at least half a log unit lower than an enzyme derived IC_{50} and is why the biophysical measure of affinity (K_i) is preferable, although it may not be as widely available because of the way HTS potency screens are setup.

8.4.2 Volume of Distribution

The impact of V_{dss} on dose prediction using the DMPK-DP method was explored using compounds from the Pi3Ky program. It was apparent that discrepancies between the

predicted doses can be large when V_{dss} is increased, for example the largest variability is seen when the dose estimation was high (Figure 7.2-4), although this is an area of chemical space which is not of interest. It was far more reassuring to see that the variability in the dose estimation was smaller when the estimated dose was low, which is the preferred area of chemical space in which program teams are most interested (Figure 7.2-4). It was also evident that the acid/base character appeared to influence the sensitivity of the V_{dss} on dose estimation (Figure 7.2-4); this is not surprising given that acids tend to bind to plasma proteins but bases typically bind to phospholipids. When the V_{dss} was larger, the estimated dose was generally smaller, which is due to the change in shape of the PK profile and the impact V_{dss} has on dosing frequency by typically increasing the half-life. This can be both of benefit and concern: a higher V_{dss} has the potential to increase duration of action, but it can also increase the risk of adverse pharmacology in non-target related tissues, so the on-target and off-target pharmacology could be more difficult to balance.

8.4.3 Clearance

It should be of very little surprise that an increase in clearance will result in an increase in the dose (Figure 7.2-5), and a reduction in clearance will reduce the dose. However, it is fundamentally important that the free clearance (or more correctly referred to as the intrinsic clearance, CL_{int}) is considered rather than the total clearance in lead optimisation, which is because it is the free clearance that will affect the free concentration. Therefore, to improve the efficiency of a drug *in vivo*, it is important to reduce the free clearance (CL_{int}) [70]. The only caveat to focussing on reducing the CL_{int} , is that the *in vitro* assays used to measure it typically cannot generate a quantifiable value below 0.5 mL/min/g liver. When this *in vitro* value is scaled to *in vivo* using the well-stirred model (WSM), this equates to approximately 20% liver blood flow for a rat, and 40% for human. As the lower limit of quantification for human is close to 50% liver blood flow, it is clear to see how difficult it is to be confident that an optimised molecule will have low *in vivo* human CL_{int} (free clearance) based on *in vitro* data alone.

Clearance is a PK parameter which most scientists developing new medicines can relate to. Clearance is simply a mathematical description of the rate of removal of drug from the body. However, the key effect of clearance is on the magnitude of the dose; its influence on the frequency of dosing is less significant, unlike V_{dss} . This is highlighted by the sensitivity analysis in Section 7.2.4, where the trend between the two methods of dose estimation is good, with the correlation coefficient being very high ($r^2 > 0.9$) (see Figure 7.2-5) and confirms that the effect of clearance was relatively small and less impactful than the V_{dss} at higher doses.

8.4.4 Absorption

As the complexity of the dose prediction method was increased with the application to the oral Pi3K δ program, Equation 39 was replaced with

Equation 38 to include an absorption rate. The absorption rate (K_a) is not a parameter that is readily available in drug discovery for dose prediction and a standardised value is often applied based on preclinical *in vivo* observations. This type of approach is not possible for early discovery compounds where *in vivo* data is not available and therefore an estimation of absorption was generated based on an early measure of solubility (CLND) multiplied by the early permeability estimate (AMP) at pH 7.4. The value was classified as low, moderate or high for each compound and applied to Equation 38. The overall conclusion when comparing the simple DMPK-DP Equation 39 with the more complex DMPK-DP Equation 38 was that this derived K_a parameter added only a very limited improvement in the dose prediction when the two methods were compared (r^2 0.314 Figure 7.4-6 and r^2 0.227

Figure 7.4-10).

We can therefore conclude that there is little value in adding a derived value for K_a to the DMPK-DP estimation approach, and the simple methodology using Equation 40 is just as effective when performing early dose estimations. Importantly the HPLC DE-DP method still gives the same rank order of initial hit-to-lead and can be used without the need to generate more complex data in the early stages of drug discovery.

The overall conclusion is that HPLC DE-DP can be used to identify the chemical space associated with lower dose compounds or early leads with a good physicochemical

property profile to direct optimisation of the overall pharmacology and ADME characteristics into a lead and onwards. Retrospective analyses of other drug discovery program databases should help support this approach and coupled with its application to live lead optimisation programs, the methodology could be evaluated in real-time scenarios. Throughout the analysis, the HPLC DE-DP approach showed the same trend towards a reduction in dose from early hits to the candidate molecule for both the Pi3K γ and Pi3K δ programs when compared to the more complex *in silico*, *in vitro* and *in vivo* DMPK-DP methods.

8.4.5 Aldehyde Oxidase and Unbound Clearance

Whilst it is extremely valuable to have models or parameter estimations such as DE_{max} to enable discovery scientists to gain valuable insight around whether a series of compounds has the potential to be developed to drug-like endpoint, it is important that they do not to rely on models or data in isolation from their drug discovery knowledge and experience if good decision making is to be promoted.

AO metabolism is one such example, where drug discovery experience, and in particular DMPK knowledge and awareness, was critical to the recognition of how data can be misleading, particularly when outliers in a series become apparent. The example of GSK2829189 in the Pi3K γ program illustrates this, where experience of certain chemical features presenting a higher risk of metabolism [145] allowed data misinterpretation to be avoided.

The isoquinoline core of the initial hit/lead template GSK2829189 represented a potential point of metabolism [141][164] and by simply taking into account only the low total *in vivo* clearance in rat for GSK2829189 (3 mL/min/kg), a metabolic liability would have been missed and a risk in lead optimisation overlooked. It was only as a result of understanding the structural features of the template that the α -carbon of the quinoline ring represented a potential substrate for AO metabolism. The underlying metabolic liability was further exemplified by comparing the unbound *in vivo* clearance (CL_{bu}) in rat of GSK2829189 and a close analogue GSK3180869, which had high *total* clearance in rat (ca. liver blood flow clearance) but similar intrinsic *in vivo* clearance (CL_{bu}): their structural similarities (isoquinoline core) suggested they were likely to have the same metabolic liability. Profiling both compounds in an *in vitro* cytosolic liver assay demonstrated that they were

substrates for AO with the same routes and similar rates of metabolism. By understanding that only unbound drug was available for metabolism and therefore cleared *in vivo*, the risks within the GSK2829189 template were recognised, and the site of AO metabolism could be blocked by the introduction of the “magic methyl” group (Figure 7.3-9).

8.5 DE_{max} and Inhaled Delivery Compounds

Traditionally, the approach to designing inhaled drugs with extended lung retention profiles has been to reduce solubility or permeability. However, the reduced solubility approach often led to an increased risk of lung toxicity, which manifested itself in the form of foamy macrophages [113]. Reducing permeability also carried the risk of compounds being unable to access intracellular targets, which is of particular importance when many current pulmonary drug targets are kinases. A key aim of this analysis was to identify alternative technologies in addition to solubility and permeability to aid the selection of compounds with extended lung retention profiles. We have shown that compounds falling into the same solubility and permeability class can be further differentiated by the HPLC DE_{max} values toward this end.

The results from the JAK inhaled delivery project have shown for the first time that it is possible to increase lung retention for compounds that have good solubility and permeability by decreasing the DE_{max} via an increase in non-specific binding to tissue components, such as albumin, glycoprotein and phospholipids. Whilst the DE_{max} of compounds with extended lung retention ranged from 0.02-1.26% (Table 7-9) indicated higher *HSA* and *IAM* binding, binding to *AGP*, another important protein present in the lung that is not directly captured in the DE_{max} model, was also monitored. These higher binding values resulted in greater lung tissue binding *in vivo* and extended the “intrinsic” lung retention. Despite the higher tissue binding for these high lung retention compounds, the free fraction in lung tissue was still >1%. It is important to maintain a free fraction to ensure sufficient free concentration can be reached to achieve target engagement for efficacy. Compounds with much higher DE_{max} values, ranging from >3.36 to 24.9% (Table 7-8) correlated with a higher free fraction in lung tissue, and as a result low “intrinsic” lung retention.

These results demonstrate the importance of using biomimetic HPLC measurements in inhaled delivery programs in order to optimise lead chemical series by selecting

compounds with non-specific binding to albumin, glycoprotein and phospholipids. Compounds with a higher probability of having “intrinsic” lung properties can be identified much earlier in the screening cascade, which could then progress to *in vivo* studies to confirm an extended lung retention profile and reduce the number of animal experiments.

It should be acknowledged that increasing lung tissue binding could result in the free concentrations of drug being too low to achieve levels of target engagement required for robust efficacy. At this point it is important to reflect on what determines the free concentration *in vivo*. Under sink conditions the magnitude of the free concentration will be determined by the binding of the compound to proteins but the free concentration in a dynamic system will ultimately be determined by the rate of removal of the unbound drug. In the lung this will be mostly through absorption into the systemic circulation. The higher binding serves to provide a depot of drug and prolong the $T_{1/2}$ in the lung.

Inhaled delivery has the unique potential to achieve temporal high local concentration in lung tissue. From this analysis we can see that the free fraction does not fall below 1%, even for high “intrinsic” lung retention compounds and is therefore sufficient, given an appropriate level of potency relative to the biological target of interest, to generate a response, potency is the other key factor as most inhaled medicines have very high affinity for their target. When delivering an inhaled drug to the target, its effect in the lung requires an extended lung retention to achieve duration of action. The HPLC DE_{max} values for compounds with “intrinsic” lung retention, should ideally be over the range of ca. 0.1 to 3%. Compounds that have a high HPLC DE_{max} (>5%) are absorbed from the lung very quickly into the central compartment/systemic circulation, where their fate will be determined by their systemic pharmacokinetic properties. If the biological target of interest is in the central compartment (systemic), or a combination of the lung and the central compartment, a higher drug efficiency for inhaled drugs targeting the whole body and not just locally in the lung could be an advantage. This could provide an alternative route of administration that offers rapid and efficient bioavailability to the systemic circulation when oral delivery has been discounted as an option for other ADMET reasons.

By identifying the link between DE_{max} and “intrinsic” lung retention, this approach offers lead optimisation scientists a simple parameter based on physiologically relevant *in vitro* binding data that is relatively high throughput very early in the screening cascade. DE_{max}

has a further advantage over early solubility screening because it is not affected by the physical form of the molecule and dependant on formulation, and cellular permeability screening, which involves a low throughput assay that can be very costly to measure for large numbers of compounds.

8.5.1 Aldehyde Oxidase in the Lung – Implications for Drug Discovery in Inhaled Delivery Programs

As with the Pi3Kγ program, an unexpected but very interesting observation within the JAK program was identified with respect to AO metabolism. In this case, it was metabolism in the lung when profiling GSK3780731, a compound selected for progression to an *in vivo* mouse model of lung retention based on its DE_{max}. The DE_{max} was low, implying increased *in vivo* lung retention. GSK3780731 had already demonstrated good cellular potency *in vitro* and therefore was of significant interest to the program team. The potential AO liability in its quinazoline core was identified and the compound was subsequently profiled in a human, rat and mouse *in vitro* liver cytosol assay and shown to be an AO substrate. Other analogues with the template were tested in the same assay and were also shown to be AO substrates, indicating clearly that there was a template liability. However, the JAK program was employing inhaled delivery to maximise lung exposure and minimise systemic exposure to reduce on-target systemic pharmacology and increase the therapeutic index. The AO liability in the liver was therefore considered a potential benefit for an inhaled drug, as the higher systemic elimination could further increase its safety. This would in essence produce a “soft” drug with a high rate of metabolism once it was absorbed into the systemic circulation [165]. The lung itself is generally considered to be of limited metabolic interest, so metabolism of inhaled compounds is generally not a concern [151].

It was therefore a surprise to find that when GSK3780731 was administered *in vivo* to determine its lung retention profile, no compound was detected following a 1mg/kg intranasal (IN) dose. The subsequent analysis determined that the compound was rapidly metabolised in mouse lung as a consequence of AO metabolism (Section 7.7.2). Further analysis identified that GSK3780731 was metabolised in minipig and a +16 metabolite in human lung tissue was observed, which although at low intensity, was sufficient to cause concern for the development of an inhaled compound. Given that extended lung retention and duration of action were principal goals for the program, any potential metabolism that

would reduce them presented a substantial risk to the efficacy and once daily dose envisaged by the TPP. Even with a low possibility of AO lung metabolism in human, the cost of drug development made this potential drug development risk too high to allow compounds which were AO substrates to progress.

This observation that the lung appeared to express AO in a pre-clinical mouse model to a level that resulted in extensive metabolism of a small molecule has resulted in a strategic change in how we develop inhaled small molecules within GSK. It highlighted the importance of having a strong DMPK focus when developing new chemical entities and the need to ensure data is correctly interpreted to enable program teams to make the right adjustments to program strategy and maximise the chances of achieving project goals. As the pharmaceutical industry continues its drive to externalise more and more resources to help control costs, it is important that integrated scientific knowledge and expertise is not lost as a result, as this could lead to a false economy.

8.5.2 PKPD and PBPKPD Modelling and Simulation in the Inhaled Delivery Project

An effective PKPD program strategy requires the integration of *in vitro* and *in vivo* concentration-time, response-time and concentration-response relationships to ultimately link this information to a disease or disease state (Figure 8.5-1) [166]. PK characteristics are both important and linked to the magnitude and duration of the pharmacological response for a given target. An integrated PKPD approach helps to focus program questions around what PD properties are required or need to be improved for a compound to maximise target engagement and the pharmacological response.

Figure 8.5-1 Integrated PKPD

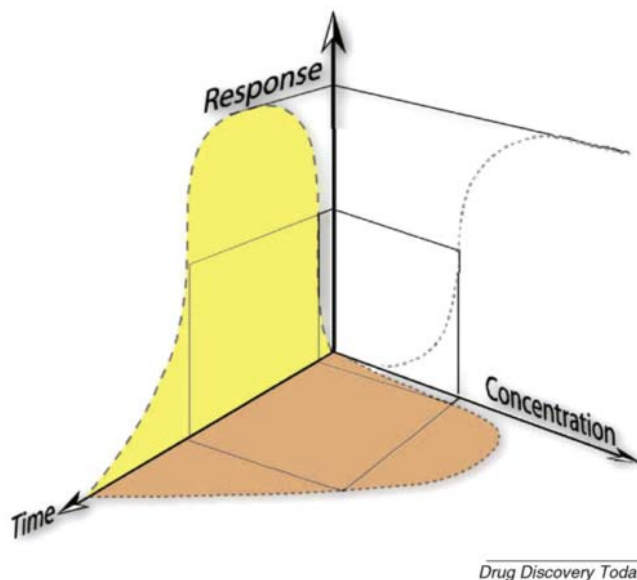


Figure 8.5-1 shows the relationships between concentration response, concentration time and response time [166].

As already discussed, DE_{max} can be used to help select compounds with intrinsic lung retention and therefore a greater chance of achieving lung concentrations which result in pharmacological activity. The use of “classic empirical” PKPD analysis during the lead optimisation phase of the JAK program helped to characterise an indirect concentration-response relationship and to predict the response for future *in vivo* PD studies. Figure 8.5-2 shows a schematic of the JAK biology which was characterised by using an acute *in vivo* mouse cytokine model. The model was designed and validated as a means to measure target engagement as part of the JAK project, as it was specific to the biology of the JAK program. Whereby the induction of a pSTAT response was induced by IL4/13 which are cytokines that are known to be important mediators of the immune response following allergen challenge in asthma. This approach of using an *in vivo* model which was target specific was consistent with pillars one and two of the Three Pillars concepts. The output from these *in vivo* target engagement studies was modelled using both link and indirect PKPD analysis as shown in Figure 8.5-2. Both models were applied to explore the hysteresis that was observed between the PK (peak compound concentration in the blood) and PD response (peak pSTAT response measured in the lung), which could have been due to two different effects: a slight time delay in the biological response

following compound engaging with the target, or most likely because the PK and PD were measured in different biophases. A combination of both could also apply. The important factor in this PKPD analysis was to recognise the offset between PK and PD response, identify if a hysteresis was present and then apply an appropriate PKPD model to ensure the model could then predict future outcomes with a reasonable degree of confidence which the results in Sections 7.7.3 and 7.8.2 have shown.

This meant the PKPD models could subsequently be used to refine the design of future PKPD studies by helping to select dose, dose regimens, sampling times and sample size distribution design in the next set of PKPD studies. The aim here was to establish and validate these models against *in vivo* data to then help with clinical dose predictions in combination with PK scaling techniques for the candidate molecule for potential use in clinical trials.

Figure 8.5-2 PKPD Models Used to Describe JAK PD Effect – Link and Indirect Models

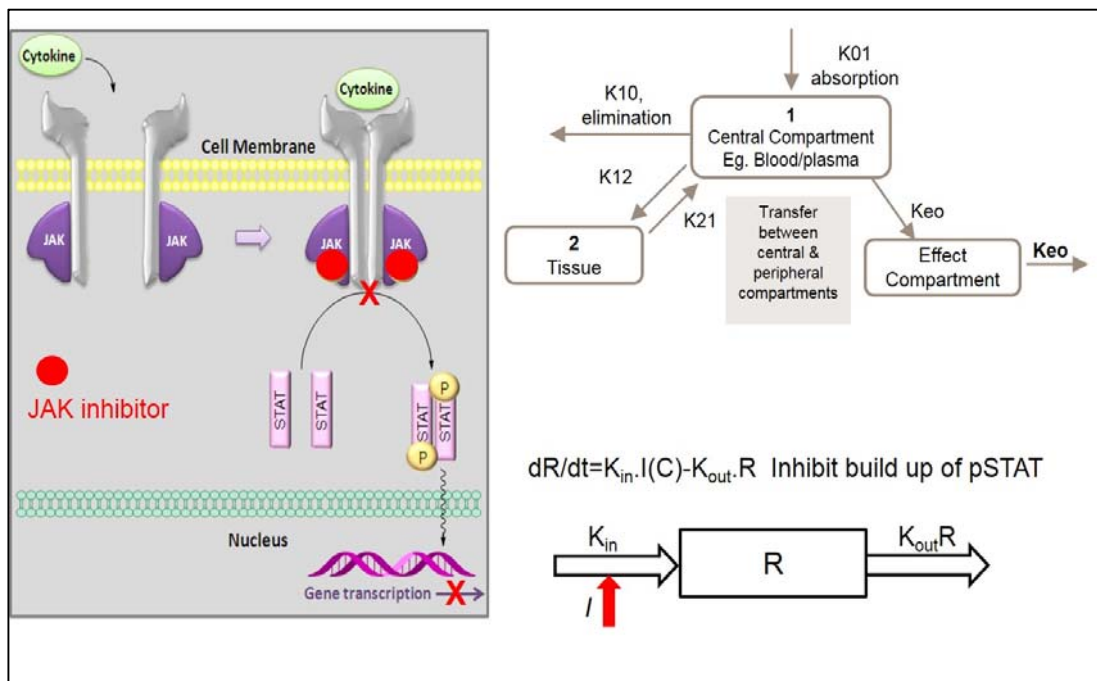


Figure 8.5-2 shows the different PKPD models used to model the JAK pharmacology

Building a robust relationship between the concentration of drug and its pharmacological response is always a challenge, and with inhaled programs there is the added complexity of understanding the concentration-response in a relatively inaccessible tissue. An additional problem is that the dosing volumes to the lung are often quite small, for example an intranasal dose volume to a mouse for pulmonary delivery is only 50 μL . This small dose volume often means a high dose concentration and can result in many compounds being dosed as suspensions if they have solubility issues. Consequently, if terminal lung samples are taken to quantify the lung concentration from an *in vivo* PD study, the concentration measured in the lung tissue will be a mixture of dissolved and undissolved compound. This effectively means a proportion of the compound delivered is dependent on dissolution rate, and therefore can only engage with the target once this process has occurred. It is therefore very difficult to ascertain what the active concentration is, and the associated concentration-response relationship that relates to the level of target engagement is likely to be lower than expected due to the proportion of undissolved and therefore inactive drug in the lung.

To overcome this problem, I reanalysed the mouse cytokine PKPD model data by relating the unbound blood concentration of GSK3532706 to the cytokine induced pSTAT response in the lung to establish a more accurate concentration-response relationship. This was based on the assumption that the concentration of the compound measured in blood had to have been in solution to be absorbed from the lungs, and therefore would have had the chance to bind to the biological target (JAK). By assessing the unbound concentration rather than the total, this would be more representative of the free concentration in the lung based on the free drug theory [129]. By focussing on the free concentration of drug this meant the exposure was proportionally lower relative to the WBB/PPB of the compound, but it meant the pharmacologically active blood concentration was more comparable to *in vitro* measures of potency which was one criteria being used in lead optimisation and selection of future compounds. Even if steady-state conditions were not achieved in the lung, it is reasonable to assume that the unbound blood concentration will be more representative of the active lung concentration, although this in itself could still be a conservative estimate of the true value. The more realistic concentration-response relationship established by this approach was used to relate *in vitro* to *in vivo* potency to direct subsequent lead optimisation and clinical dose prediction strategies.

To gain a deeper understanding of the PKPD relationship in the JAK program, PBPK and PBPKPD modelling was also used to analyse the compound distribution and concentration-time profiles with respect to the different biophases of the tissue compartments remote from the systemic circulation (blood/plasma) and where most drugs actually exert their pharmacological effect. Although it is often impractical to measure the concentration-time profiles in many compartments within the body because of their inaccessibility to repeat sampling, PBPK models can represent these tissue and organ spaces with their physical volumes as show in Figure 8.5-3. By understanding the PK and distribution in multiple compartments, it then becomes possible to link the pharmacological effect to the PK in the primary biophase of interest e.g. blood, lung or lung compartment by linking the PBPK model to a PKPD model. This approach can give greater understanding of the pharmacologically active concentration and therefore the dose required to achieve this concentration. A PBPK model also allows consideration of exposure in compartments/organs where there may be a safety or toxicity (e.g spleen, liver or accumulation in adipose) this type of analysis is particularly relevant to an inhaled delivery program where systemic distribution needs to be avoided because of potential target related pharmacology outside of the lung. The JAKi program was actively trying to avoid systemic exposure to avoid more general immunosuppression which could increase the risk of viral infections in patients.

Figure 8.5-3 An Example of a Physiology Based Model

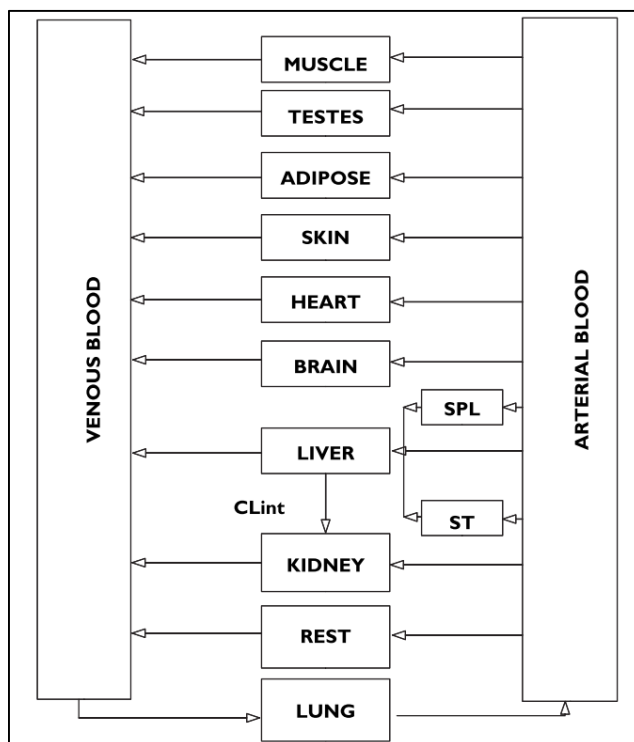


Figure 8.5-3 is a schematic of a Physiologically Based Pharmacokinetic model. The compartments represent tissues and organs, the arrows represent the blood supply; ST is the stomach; SPL is the splanchnic organs; and CL_{int} is the intrinsic hepatic clearance. [167]

PBPK modelling for the JAK program not only enabled robust predictions of lung and blood/plasma concentration profiles for GSK3532706, but also allowed the prediction of compound concentrations in other tissues such as unbound alveolar cell concentrations and mucus concentrations. This information was then used to further link concentration to effect, and design future pre-clinical studies to maximise exposure in those tissues. Once the PBPK model has been built and validated with *in vivo* data, the model can be linked to a relevant PD model as previously described with the empirical PKPD modelling in Section 7.8.2.

Having evaluated and established the PKPD relationship for GSK3532706, to finally address the Three Pillars requirements of demonstrating: (1) drug concentration in the relevant biophase (2) target engagement and (3) a related pharmacological response, a HDM mouse model was used to measure a functional lung eosinophilic response to HDM

sensitised and re-challenged mice, which is an accepted disease relevant model of airway inflammation for compound evaluation in asthma. Figure 7.8-12 shows the outcomes (actual and predicted) of the PK exposure following repeat dosing of GSK3532706 and its effect on target engagement and lung eosinophilia following intranasal dosing. Significant inhibition of pSTAT5 was evident based on a 95% CI and this response was related to the target engagement model. Agreement with the Three Pillars validation of efficacy for tool compound GSK3532706 was therefore achieved: (1) connecting concentration of the compound at the site of action (PK) with (2) a measure of target engagement (pSTAT5 inhibition), followed by (3) an associated functional response (eosinophil inhibition).

In conclusion, in the JAK inhibitor program we have shown for the first time that it is possible to increase lung retention for compounds by decreasing the DE_{max} , which helped to direct selection and development of compounds with a higher probability of having “intrinsic” lung properties, an extended lung retention profile and reduce the number of animal experiments. Pulmonary PBPK models have been developed to predict lung and blood drug concentrations *in vivo* following intranasal and inhaled administration. These PKPD and PBPK models had an impact on further *in vivo* study design and dose regimens for target validation and functional *in vivo* studies in an active drug discovery program. Integration of PBPK and PKPD approaches to establish a PBPKPD model helped to refine the PD study design and compound profiles. Finally, PBPK and PKPD methodology has been established that can be used to help predict the clinical dose of lead and candidate molecules emerging from this program. Now this approach has been established it can and is beginning to be applied to other inhaled programs within GSK.

8.6 Summary of key findings of this work within the GSK Respiratory Therapeutic Area

Systemic Programs

- DE_{max} was both conceived and applied to discovery programs within GSK
- DE_{max} is a valuable tool for predicting the dose for systemically delivered compounds
- The DE_{max} and HPLC DE-DP approach consistently identified the progression path from early hits to lead/candidate molecules in the Pi3K γ and Pi3K δ drug discovery programs
- It is important to consider the unbound *in vivo* clearance when optimising *in vivo* PK
- AO metabolism can be easily overlooked in pre-clinical *in vitro* and *in vivo* PK profiling, which has important implications when the drive towards more polar molecules often involves introducing aromatic nitrogens in modern drug design

Inhaled Programs

- DE_{max} is an emerging concept for inhaled drug design where there are few design guides available for inhaled drug design, unlike oral drugs
- DE_{max} has been used to help identify compounds with extended lung retention
- A lung retention link has been established for duration of target engagement with the JAK program
- The application of DE_{max} to inhaled drug design is currently a unique approach used by GSK inhaled drug discovery teams
- Innovative approaches to data visualisation have now been embedded within Respiratory DMPK for PKPD analysis.
- This was the first application of inhaled PKPD modelling in the Respiratory TA at GSK.
- This was also the first application of inhaled PBPKPD in a lead optimisation program at GSK
- AO metabolism was a previously unknown risk in the lung

- The Three Pillars framework was successfully applied to an inhaled target in lead optimisation for the first time at GSK.

9 Future Work

Following on from this project there are several areas of research that could be either initiated or expanded using the techniques and practices highlighted in this study.

These could include:

- The investigation and expansion of research into factors influencing lung permeability
- The influence of ionisation on absorption has been extensively studied for oral drugs, but not for the lung
- Establish whether permeability, solubility and DE_{max} studies could form the basis for a pulmonary equivalent of the BCS for oral drugs
- Continue to apply DE_{max} to other inhaled projects to gain a greater understanding of its influence and value when designing small molecules with extended lung retention. This is now happening at GSK for other inhaled programs within the Respiratory TA at GSK.
- Continue to develop new pulmonary PBPK and PBPKPD models to continue to help understand this challenging route of administration and predict the effective clinical dose.

10 Appendix

10.1 List of Tables

Table 2-1 Percentage of Compounds with MWT (Inc. Salt) above 500 [4]	26
Table 3-1 Drug Withdrawals in the United States between 1980-2006 [26].....	32
Table 4-1 The Most Common Phase I and II Reactions	50
Table 4-2 Percentages of Compounds Achieving Defined Target Values in Various Developability Assays Categorised by PFI or iPFI Bins [8].....	62
Table 4-3 Example Solubility and Lipophilicity for a Theoretical Base Showing the Independence of the Product Term from pH. See Data Plot in Figure 4.2-7	78
Table 6-1 Typical calibration data for the HSA binding measurements using an HSA column.....	104
Table 6-2 Excel Calculations for the HSA Binding from the Gradient Retention Time Obtained on the ChiralPak-HSA Column.	105
Table 6-3 The Calibration set of Compounds used for Obtaining the <i>IAM</i> Binding Parameter <i>CHI (IAM)</i>	106
Table 6-4 The Chromatographic Hydrophobicity Index Values for the Calibration [45]	109
Table 7-1 The Various <i>In Vivo</i> ADME Properties for the 136 Marketed Drugs.	156
Table 7-2 Literature Data of Known Drug Molecules (www.drugbank.ca/drugs and www.Drugs.com).....	162
Table 7-3 The Measured <i>In Vitro</i> Biomimetic Data of the Investigated Known Drug Molecules.	167
Table 7-4 The Summary of the Various Dose Estimation Methods that were used to Compare the Clinical Dose Estimations for the Known Drugs.....	175
Table 7-5 Summary of Physicochemical Properties for Pi3K γ Hit Compound (GSK2829189) to Lead (GSK3203207).....	183
Table 7-6 Summary of <i>In Vitro</i> and <i>In Vivo</i> Pharmacology for Pi3K γ Hit Compound (GSK2829189) to Lead (GSK3203207).....	183
Table 7-7 Summary of Physicochemical Properties for Pi3K δ Hit Compound (GSK3343837) to Lead (GSK33493251)	219
Table 7-8 Physicochemical Properties of Known Drugs for Oral, Oral CNS, Inhaled Drug Administration and GSK Inhaled JAK Lead Optimisation Compounds.	223

Table 7-9 The Measured and Calculated Physicochemical Properties of Selected JAK Inhibitor Compounds.....	244
Table 7-10 The Measured and Calculated Physicochemical Properties of Selected JAK Inhibitor Compounds.....	246
Table 7-11 Quinazoline AO Metabolism as Identified <i>In Vitro</i> using both Mouse, Rat and Human Liver Cytosol Assays.....	250
Table 7-12 Tissues Expressing AO in Rat and Human [125].....	251
Table 7-13 Quinazoline Series Compounds which were Substrates and Non-Substrates for AO.....	257
Table 7-14 Link Model Output Data for the PKPD Response to GSK3532706.....	274
Table 7-15 A Comparison of the Link PKPD and PBPKPD Model Output Parameters.....	290
Table 11-1 Table Marketed Drugs with all Structures with Application and Acid / Base Class.....	344

10.2 List of Figures

Figure 2.2-1 The Biopharmaceutical Classification System Model [11].	22
Figure 2.2-2 Metabolism and Transporter Effects of Solubility and Permeability	23
Figure 2.2-3 Lipinski's Rule of 5 Highlighting the Importance of Lipophilicity [4].	25
Figure 2.2-4 Trends in Molecular Mass and cLogP in Approved Compounds [9].	27
Figure 2.2-5 Changes in Physical Properties of Patented Compounds by Target Over Time [14].	28
Figure 2.2-6 Three Pillars Concept as a Confidence Matrix [12].	30
Figure 2.2-7 PKPD and Human Clinical Dose Estimation Matrix Used at GSK	31
Figure 2.2-1 PhD Project Plan	34
Figure 2.2-1 Basic Definition of ADME	36
Figure 2.2-2 Process of Absorption of a Drug from the GI Tract	38
Figure 2.2-3 Physiological Body Fluid Volumes for Human [28].	44
Figure 2.2-4 The Schematic Illustration Free Drug Partitioning Between the Plasma and Tissue Compartments.	45
Figure 2.2-5 A Physiological Schematic Describing Volume of Distribution Illustration of a Drug's Partitioning Between the Plasma and Tissue Compartments	46
Figure 2.2-6 Description of Volume Terms from Concentration-Time Curve	47
Figure 2.2-7 Physiological Schematic of the Hepatobiliary System and Upper GI Tract	51
Figure 2.2-8 Physiological Schematic of the Renal System	52
Figure 2.2-9 Hepatobiliary Uptake	53
Figure 4.2-1 Plot of Measured and Calculated ChromLogD Values for Mixed Project Compounds. Source Data Downloaded from GSK Corporate Database April 2018	61
Figure 4.2-2 Common Stationary Phase Proteins which are Commercially Available	63
Figure 4.2-3 The Similarity of the Phosphatidylcholine Membrane Bilayer and the Immobilized Artificial Membrane (IAM) Stationary Phase.	66
Figure 4.2-4 The Logk (IAM) Values of the Acetophenone Homologues up to Octanophenone as a Function of their LogP Values [45].	68
Figure 4.2-5 The Plot of the Logk (HSA) Values for the Acetophenone Homologues as a Function their LogP Values [45].	69
Figure 4.2-6 The Plot of the HSA and IAM Binding of 2000 Cross Project Compounds. This Data was Downloaded from the GSK Database in March 2018.	71

Figure 4.2-7 A Theoretical Plot Showing the Independence of the Product Term of Lipophilicity and Solubility (LogD*S) from pH. Adapted from Reference [74].....	77
Figure 4.2-9 The DRUG _{eff} Definition – Dose and Effect (PKPD)	79
Figure 4.2-10 The Plot of <i>In Vivo</i> and <i>In Vitro</i> Log DRUG _{eff max} for 115 Known Drug Molecules. Shape and Colour are According to the Target Class the Drugs Belong [77]	81
Figure 4.2-11 Agreement Between <i>In Vitro</i> DEI _{max} (pXC50+Log DRUG _{eff max}) and LLE (pXC50 – cLogP) [77]	83
Figure 4.3-1 DMPK Dose Prediction (DMPK-DP) and DE _{max} Dose Prediction (DE-DP) Schematic.....	88
Figure 5.2-1 Neutrophil Fate and Function in ALI (ARDS).....	92
Figure 5.3-1 Cells Involved in Atopic Asthma which are Targets of Current Therapies.	94
Figure 5.4-1 Cytokine Binding and JAK Signalling.....	95
Figure 5.4-2 Consequences of JAK Activation.....	96
Figure 5.4-3 Mechanisms of Allergic Inflammation in Asthma (adapted from [102]).....	97
Figure 5.4-4 The Illustration of Epithelial Cells in Different Parts of the Lung	100
Figure 6.2-1 An Example Chromatogram of Known Drugs using Immobilized Human Serum Albumin (ChiralPak-HSA) HPLC Column.	104
Figure 6.2-2 Calibration Plot for the Gradient Retention Times and HSA Binding for the Calibration Set of Compounds (GSK data).	105
Figure 6.2-3 A Typical Chromatogram of the IAM Calibration Set of Compounds (Paracetamol, Acetanilide Acetophenone, Propiophenone, Butyrophenone, Valerophenone, Hexanophenone, Heptanophenone and Octanophenone)	107
Figure 6.2-4 A Typical Calibration Plot used to Calculate CHI IAM Values from the Measured Gradient Retention Times of Drug Discovery Compounds.....	108
Figure 6.2-5 A Typical uHPLC Chromatogram.....	110
Figure 6.2-6 Calibration Plots for the CHI Determination on C-18 Reversed Phase Columns at Three Different Starting Mobile Phase pH: a) pH2.6; b) pH7.4; c) pH10.5	111
Figure 6.3-1 The Schematic Illustration and Calculation of Hepatic Extraction Ratio. .	114
Figure 6.3-2 The Schematic Illustration of Various Liver Models used to Estimate the <i>In Vivo</i> Hepatic Clearance from <i>In Vitro</i> Microsomal Stability Data [31].	118
Figure 6.6-1 An Inhalation Tower with a Wrights Dust Feeder (for Aerosol Generation) for Rodent Inhaled Dose Studies	132

Figure 6.6-2 An Inhalation Tower with a Capsule Based Aerosol Generator (CBAG) used for Low Dose Rodent Inhaled Dose Studies	133
Figure 6.9-1 Plot of observed vs predicted volume of distribution for a) training set; b) test set and c) validation set of compounds.	137
Figure 6.9-2 Observed and Predicted Intrinsic Clearance for a Set of Selected Projects. The Colours are Based on “Daylight” Clustering (similarity >0.7).....	140
Figure 6.10-1 ACAT Model (Taken from the GastroPlus™ User Guide).....	145
Figure 6.10-2 The Schematic Illustration of the Principals of the Physiologically Based Pharmacokinetic (PBPK) Modelling Approach for the ACAT Model [132].....	146
Figure 6.10-3 Nasal-Pulmonary Compartmental Absorption & Transit Model (N-PCAT Model).....	147
Figure 6.10-4 A Schematic Illustration of the Principals of Nasal-Pulmonary Compartmental Absorption & Transit Model (N-PCAT Model), Applying Similar Principles to those used for the ACAT model.	148
Figure 6.10-5 The Schematic Illustration of the Principles of the PBPK Modelling Approach Combining the N-PCAT and ACAT Models.....	149
Figure 6.10-6 The Model Window in GastroPlus™ for Inhaled Drug Deposition, Distribution and Absorption.....	150
Figure 6.10-7 Naso-Pulmonary Module Screen Shots for Mouse Physiology	153
Figure 6.10-8 Regional Deposition Profile Settings within GastroPlus.....	154
Figure 7.1-1 The Actual vs The Estimated Daily Dose for Marketed Drugs using the <i>In Vivo</i> DMPK-DP Method (Equation 38).	176
Figure 7.1-2 A Plot of Actual Daily Dose verses Dose Estimated Using MEC (HPLC DE _{max}) and <i>In Vivo</i> Data in Equation 38 for the Marketed Drugs.....	177
Figure 7.1-3 The Plot of the Actual Clinical Dose and the Calculated pIC ₅₀ (Clinical MEC) Values of Marketed Drugs.	179
Figure 7.2-1 The Plot of the Predicted Dose for the Pi3Ky Compounds using the DE-DP Method Based on <i>In Vitro</i> Potency and the HPLC DE _{max} and the <i>In Vitro</i> DMPK-DP Method using <i>In Vitro</i> Clearance and Volume of Distribution Data (Equation 37).	181
Figure 7.2-2 The Rank Order of Dose Prediction Methods Shows the Original Hit GSK2829189 and the Final Lead Compound GSK3203207 using the <i>In silico</i> DMPK-DP and HPLC DE-DP Methods.	182
Figure 7.2-3 The Plot of the Estimated Dose Obtained When Using the Enzyme and the Whole Blood pIC ₅₀ Values.	185

Figure 7.2-4 The Difference in the Estimated Dose Caused by a Small Fixed Increase in V_{dss} Using <i>In Silico</i> Estimated V_{dss} in Equation 38, for all Pi3Ky Project Compounds. .	187
Figure 7.2-5 Plot of the Predicted Dose for the Pi3Ky Compounds Using <i>In Silico</i> Clearance and <i>In Vitro</i> V_{dss} Data to Predict Dose Using a Small Fixed Increased Clearance (0.5 mL/min/kg) for Each Compound Using Equation 38.	189
Figure 7.2-6 The Plot of the Estimated Dose Using Equation 38 and the Modified Equation 34 by the MEC(HPLC DE_{max}) for the Pi3Ky Project Compounds.	190
Figure 7.3-1 Cross Species Variability in Aldehyde Oxidase Expression [140]	193
Figure 7.3-2 Some Common Substrates for AO Metabolism.....	193
Figure 7.3-3 Understanding Risks Factors for Aldehyde Oxidase Metabolism	194
Figure 7.3-4 GSK2829189 Structure	195
Figure 7.3-5 GSK2829189 Quinolone Series Lead Compound <i>In vitro</i> and <i>In vivo</i> Rat PK Profile	196
Figure 7.3-6 In Vitro and In Vivo Profiles of GSK2829189 and its Non-Phenyl Analogue GSK3180869.....	197
Figure 7.3-7 Results from Rat and Human <i>In Vitro</i> Cytosol AO Assay	198
Figure 7.3-8 Metabolite Identification of Pi3Ky Lead Series Compounds	199
Figure 7.3-9 The Effect of a “Magic Methyl” Group on AO Metabolism.....	200
Figure 7.3-10 Rat PK With and Without a “Magic Methyl”	201
Figure 7.3-11 Minipig an Alternative Pre-Clinical Species to Help Predict Human AO Metabolism	202
Figure 7.4-1 The Plot of the Measured <i>In Vitro</i> Enzyme and Whole Blood Pi3K δ Potency of the Compounds.....	206
Figure 7.4-2 The Plot of the DE-DP Dose Estimation Method using the Pi3K δ Enzyme and Whole Blood Cellular Potency Data.	208
Figure 7.4-3 A Comparison of the Estimated Dose using <i>In Silico</i> Inputs in the DMPK-DP Method Using Enzyme Potency and Whole Blood Cellular Potency Data.	210
Figure 7.4-4 The Plot of the Estimated Dose using the <i>In Vitro</i> DMPK-DP Method with <i>In Vitro</i> Inputs of V_{dss} , Intrinsic Clearance and Absorption Rate with Enzyme and Whole Blood Potency Data.	211
Figure 7.4-5 The Plot of the DMPK-DP Estimated Dose Method with <i>In Silico</i> and <i>In Vitro</i> Inputs of V_{dss} , Clearance and Absorption Rate.	212
Figure 7.4-6 The Plot of the Estimated Dose Using the DE-DP Method Using Whole Blood Potency Data and the <i>In silico</i> DMPK-DP Method Using Whole Blood Potency Data. Lead Series Progression Has Also Been Shown With GSK3343837 and GSK3493251.....	214

Figure 7.4-7 The plot of the estimated dose using the DE-DP method with equation 38 and the whole blood potency data and the <i>in vitro</i> DMPK-DP method using equation 31 with <i>in vitro</i> measured data input and the whole blood potency.	215
Figure 7.4-8 The plot of the estimated dose using In vitro DMPK-DP and In vivo DMPK-DP data with and the whole blood potency data using equation 31.	217
Figure 7.4-9 The plot of the Estimated Dose using the DE-DP Method with Whole Blood Potency Data and the <i>In vivo</i> DMPK-DP Method with <i>In Vitro</i> Measured Data Inputs and Whole Blood Potency Data	218
Figure 7.4-10 The plot of the Estimated Dose Using the DE-DP Method and the <i>In Silico</i> DMPK-DP Method Without K_a	220
Figure 7.5-1 The Box Plot of MW for Marketed Oral, Oral CNS, Inhaled Drugs and Inhaled JAK Project Compounds.....	229
Figure 7.5-2 The Box Plot of Albumin Binding (<i>HSA</i>) for Marketed Oral, Oral CNS, Inhaled Drugs and Inhaled JAK Project Compounds.....	230
Figure 7.5-3 The Box Plot of α -1-Acid-Glycoprotein Binding (<i>AGP</i>) for Marketed Oral, Oral CNS, Inhaled Drugs and Inhaled JAK Project Compounds	231
Figure 7.5-4 The Box Plot of Immobilised Artificial Membrane (<i>IAM</i>) Binding Marketed Oral, Oral CNS, Inhaled Drugs and Inhaled JAK Project Compounds.....	232
Figure 7.5-5 The Box Plot of cLogP for Marketed Oral, Oral CNS, Inhaled Drugs and Inhaled JAK Project Compounds.....	233
Figure 7.5-6 The Box Plot of Total Polar Surface Area (TPSA) for Marketed Oral, Oral CNS, Inhaled Drugs and Inhaled JAK Project Compounds	234
Figure 7.5-7 The Box Plot of DE_{max} for Marketed Oral, Oral CNS, Inhaled Drugs and Inhaled JAK Project Compounds.....	235
Figure 7.5-8 The Box Plot of PFI for Marketed Oral, Oral CNS, Inhaled Drugs and Inhaled JAK Project Compounds.....	236
Figure 7.7-1 The Pharmacological Pathway for JAK Inhibitors for Reducing Chronic Inflammation.....	238
Figure 7.7-2 Balancing the Solubility and Permeability for Lung Retention	239
Figure 7.7-3 A 9-Box Model Plot of Solubility and Permeability	240
Figure 7.7-4 The 9-box Plot Classification of Compounds Based on Solubility and Permeability and DE_{max}	242
Figure 7.7-5 Total Lung Concentration Measured After Intra Nasal Dose Administration in Solution to Female BalbC Mice.....	247
Figure 7.7-6 JAK Lead Templates Aldehyde Oxidase Metabolism Risks	249

Figure 7.7-7 Immunostaining of AO in Human Lung Tissue [125].....	252
Figure 7.7-8 <i>In Vitro</i> Stability of GSK3780731 and GSK3635481 in Mouse Lung Homogenate.....	253
Figure 7.7-9 Confirming AO Metabolism in Mouse Lung GSK3635481 and GSK3780731.	254
Figure 7.7-10 GSK3635481 <i>In Vitro</i> AO Metabolism in Human Lung	255
Figure 7.7-11 Aldehyde Oxidase Substrate Binding Model	258
Figure 7.7-12 A Classical PD study Design and the Results Obtained for GSK3532706	260
Figure 7.7-13 The PKPD Profile of GSK3532706 using a Longitudinal PKPD Model ..	261
Figure 7.7-14 The Lung Tissue Concentration Versus %pSTAT Response.	262
Figure 7.7-15 The Blood Concentration Versus %pSTAT Response.....	263
Figure 7.7-16 The Unbound Blood Concentration Versus %pSTAT Response.....	264
Figure 7.7-17 A Longitudinal PKPD Plot Showing the Total Lung Concentration of GSK3532706 Versus %pSTAT Response.....	266
Figure 7.7-18 A Longitudinal PKPD Plot Showing the Unbound Blood Concentration of GSK3532706 Versus % pSTAT Response	267
Figure 7.7-19 The Blood Concentration of GSK3532706 and %pSTAT5 Response as a Function of Time.	268
Figure 7.7-20 Hysteresis of % pSTAT5 Inhibition Verse the Blood Concentration of GSK3532706A	269
Figure 7.7-21 The Temporal Displacement Between the Blood Concentration (Central Compartment) and the Pharmacological Effect Observed in the Lung.	270
Figure 7.7-22 The PKPD Data Modelled Using a Link Model.....	272
Figure 7.7-23 Simulated Blood and Effect Compartment Concentration-Time Curves and the Effect-Time Curve	273
Figure 7.7-24 Modelled pSTAT vs Time Profile for a 3, 10 & 30mg/kg IN Doses with Experimental Observations Overlaid	275
Figure 7.7-25 The Measured Unbound Blood Concentration and the %pSTATs Cytokine Inhibition GSK3489723A.....	277
Figure 7.7-26 The Measured Total Lung Concentration and the %pSTATs Cytokine Inhibition GSK3489723A.....	278
Figure 7.8-1 Why Use PBPK?	279
Figure 7.8-2 Intravenous Mouse Blood and Intranasal Blood and Lung Profiles for GSK3532706.....	281

Figure 7.8-3 Mouse PBPK Model for GSK3532706, IV Blood/Plasma, IN Blood and IN Lung Profiles	283
Figure 7.8-4 GSK3532706 Blood and Lung Profiles after 10mg/kg IN Dose (Suspension)	285
Figure 7.8-5 Description of the Different Indirect Response Models and how they Describe the Pharmacodynamic Response of a Drug [157].....	287
Figure 7.8-6 An Alternative Approach to Explain the Slight Offset of the Blood Concentration (Central Compartment) and the Effect Observed in the Lung.....	288
Figure 7.8-7 PBPKPD Modelling for GSK3532706 using a Turnover Model	289
Figure 7.8-8 An 8-Day Cytokine Challenge PKPD Model.....	291
Figure 7.8-9 The PBPKPD Analysis of the Effect of GSK3532706 in the 8-Day Repeat Cytokine Mouse Model	292
Figure 7.8-10 Schematic of a House Dust-Mite (HDM) Mouse <i>In Vivo</i> Efficacy Model	294
Figure 7.8-11 Proposed Inflammatory Processes of HDM Re-Challenge Model (not published).....	295
Figure 7.8-12 Effect of GSK3235706 in the Mouse HDM Model Experiment 1	296
Figure 7.8-13 Effect of GSK3235706 in the Mouse HDM Model Experiment 2. Using PBPKPD Analysis to Understand a Negative Result	298
Figure 7.8-14 PBPK/PD Analysis Enables us to Understand a Negative Result (2)....	299
Figure 7.8-15 Predicting the Exposure of GSK3532706 in different Compartment in the Lung using the Mouse HDM PKPD Model	301
Figure 7.8-16 Predicting the Exposure of GSK3532706 in Alveolar Cells in the Lung using the Mouse HDM PBPKPD Model	302
Figure 8.1-1 The Association of British Pharmaceutical Industries (ABPI) – The Medicine Development Process.....	304
Figure 8.1-2 An analysis of the Attrition of Drug Candidates from Four Major Pharmaceutical Companies [161].....	306
Figure 8.1-3 Lessons Learned from the Fate of AstraZeneca’s Drug Pipeline: A Five-Dimensional Framework [163].....	307
Figure 8.5-1 Integrated PKPD	319
Figure 8.5-2 PKPD Models Used to Describe JAK PD Effect – Link and Indirect Models	320
Figure 8.5-3 An Example of a Physiology Based Model.....	323

10.3 List of Equations and Reference Number

Equation 1	39
Equation 2	39
Equation 3	40
Equation 4	42
Equation 5	47
Equation 6	48
Equation 7	48
Equation 8	49
Equation 9	49
Equation 10	55
Equation 11	57
Equation 12	57
Equation 13	58
Equation 14	59
Equation 15	59
Equation 16	60
Equation 17	60
Equation 18	63
Equation 19	64
Equation 20	67
Equation 21	67
Equation 22	67
Equation 23	67
Equation 24	68
Equation 25	72
Equation 26	73
Equation 27	73
Equation 28	74
Equation 29	75
Equation 30	75
Equation 31	78
Equation 32	79
Equation 33	80

Equation 34	80
Equation 35	83
Equation 36	83
Equation 37	84
Equation 38	86
Equation 39	86
Equation 40	115
Equation 41	115
Equation 42	116
Equation 43	116
Equation 44	117
Equation 45	119
Equation 46	119
Equation 47	151
Equation 48	173
Equation 49	173
Equation 50	173
Equation 51	174
Equation 52	174
Equation 53	177
Equation 54	191
Equation 55	204
Equation 56	206
Equation 57	243
Equation 58	245
Equation 59	245
Equation 60	271

$$F = F_g \cdot F_a \cdot F_h \quad \text{Equation 1}$$

$$F_h = (1 - E) \quad \text{Equation 2}$$

$$J = -D \frac{d\phi}{dx} \quad \text{Equation 3}$$

$$CL = V_{dss} \cdot Kel \quad \text{Equation 4}$$

$$V_{dc} = \frac{\text{Dose}}{C_0} \quad \text{Equation 5}$$

$$V_{dss} = \text{Dose} \cdot \frac{\text{AUMC}}{(\text{AUC})^2} = CL \cdot \text{MRT} \quad \text{Equation 6}$$

$$V_{d\beta} = \frac{CL}{Kel} \quad \text{Equation 7}$$

$$V_{dss} = V_p + V_t \cdot \left(\frac{f_{up}}{f_{ut}} \right) \quad \text{Equation 8}$$

$$V_{dss} = V_p + V_t \cdot K_p \quad \text{Equation 9}$$

$$\text{Log} D_{pH} = \text{Log} \left(P \cdot 10^{\text{ch}(pK_a - pH)} + D_{\text{fully ionised form}} \right) - \text{Log} (1 + 10^{\text{ch}(pK_a - pH)}) \quad \text{Equation 10}$$

$$k = \frac{t_R - t_0}{t_0} \quad \text{Equation 11}$$

$$\text{Log} K = \text{Log} k + \text{Log} \left(\frac{V_s}{V_m} \right) \quad \text{Equation 12}$$

$$\text{Log} k = a \cdot \phi + b \quad \text{Equation 13}$$

$$\varphi = \text{CHI} = a \cdot t_R + b \quad \text{Equation 14}$$

$$\text{CHI} \log D = 0.054 \text{CHI} - 1.467 \quad \text{Equation 15}$$

$$\text{Chrom} \log D = 0.0857 \text{CHI} - 2 \quad \text{Equation 16}$$

$$\text{PFI} = \text{Chrom} \log D + \text{Number of Aromatic Rings} \quad \text{Equation 17}$$

$$\% \text{HSA bound} = 100 \cdot \frac{k}{1+k} \quad \text{Equation 18}$$

$$\log k (\text{HSA}) = \log \frac{\% \text{HSA bound}}{100 - \% \text{HSA bound}} - \log [\text{HSA}] \quad \text{Equation 19}$$

$$\log P = 0.047 \text{CHI} + 0.36 \text{HBC} - 1.10 \quad \text{Equation 20}$$

$$\log P = 0.054 \text{CHI} + 1.32 \text{A} - 1.88 \quad \text{Equation 21}$$

$$\log k \text{ IAM} = 0.046 \text{CHI IAM} + 0.42 \quad \text{Equation 22}$$

$$\log K \text{ IAM} = 0.29 * e^{\log k \text{ IAM}} + 0.7 \quad \text{Equation 23}$$

$$\log K (\text{HSA}) = e^{\log k \text{ HSA}} \quad \text{Equation 24}$$

$$\log V_{dss} (\text{HUMAN}) = 0.44 \log K (\text{IAM}) - 0.22 \log K (\text{HSA}) - 0.66 \quad \text{Equation 25}$$

$$\log V_{dss} (\text{RAT}) = 0.27 \log K (\text{IAM}) - 0.29 \log K (\text{HSA}) - 0.30 \quad \text{Equation 26}$$

$$\log V_{dssu} = 0.43 \log K (\text{IAM}) + 0.23 \log K (\text{HSA}) - 0.72 \quad \text{Equation 27}$$

$$\log f_{ut} = -0.52 \log K (\text{IAM}) - 0.66 \log K (\text{HSA}) + 0.55 \quad \text{Equation 28}$$

$$F_{abs} = f(P_w, P_{aq}, S_0, X, F_{non}, V_L) \quad \text{Equation 29}$$

$$AP = \text{Log} \left(P \cdot F_{non} \cdot \frac{S_0 \cdot V_L}{X} \right) \quad \text{Equation 30}$$

$$DRUG_{eff} = \frac{\text{Free Bio-phase Concentration}}{\text{Dose}} \cdot 100 \quad \text{Equation 31}$$

$$V_{du} = \frac{\text{Dose}}{\text{Unbound Concentration}} \quad \text{Equation 32}$$

$$DRUG_{eff} = \frac{100}{V_{du}} \quad \text{Equation 33}$$

$$\text{Log (in vitro } DRUG_{effmax}) = 2 - (0.23 \text{Log}K(\text{HSA}) + 0.43 \text{Log}K(\text{IAM}) - 0.72) \quad \text{Equation 34}$$

$$DEI = pIC_{50} + \text{Log}(DE_{max}\%) \quad \text{Equation 35}$$

$$LLE = pIC_{50} - \text{Log}P \quad \text{Equation 36}$$

Equation 36

$$\text{Dose} = \frac{\text{free bio-phase conc}}{DRUG_{eff}} \quad \text{Equation 37}$$

$$\text{Dose} \left(\frac{\text{mg}}{\text{kg}} \right) = \frac{\frac{24}{\tau} * MEC * V_{ss} * (k_a - k_{el})}{F * k_a \left(\frac{1}{1 - \exp(-k_{el}\tau)} - \frac{1}{1 - \exp(-k_a\tau)} \right)} \quad \text{Equation 38}$$

$$\text{Dose} \left(\frac{\text{mg}}{\text{kg}} \right) = \frac{\frac{24}{\tau} * MEC * V_{ss} * (\exp(k_{el}\tau) - 1)}{F} \quad \text{Equation 39}$$

$$y = A_0 \cdot e^{-kt} \quad \text{Equation 40}$$

$$CL_{int} \left(\frac{\mu L}{mg} \text{ protein} \right) = \frac{\frac{Ln2}{k}}{\text{Assay Protein Concentration}} \quad \text{Equation 41}$$

$$CL_{int} (\text{mL/min})/\text{g liver} = CL_{int} (\mu\text{L/min/mg}) \cdot SF \left(\frac{\text{g}}{\text{kg}} \right) \quad \text{Equation 42}$$

$$CL_{int} \left(\frac{\mu L}{\text{million}} \text{ cells} \right) = \frac{\frac{Ln2}{k}}{\text{Assay Cell Density}} \quad \text{Equation 43}$$

$$CL_{int} (\text{mL/min})/\text{g liver} = CL_{int} (\mu\text{L/min/million cells}) \cdot SF \left(\text{million} \frac{\text{cells}}{\text{g}} \right) \quad \text{Equation 44}$$

$$CL_h (\text{WSM non res}) = \frac{(CL_{int} \cdot SF) \cdot Q_h}{(CL_{int} \cdot SF) + Q_h} \quad \text{Equation 45}$$

$$CL_h (\text{WSM res}) = \frac{\left(\frac{CL_{int} \cdot SF \cdot f_{ub}}{f_{uinc}} \right) \cdot Q_h}{\left(\frac{CL_{int} \cdot SF \cdot f_{ub}}{f_{uinc}} \right) + Q_h} \quad \text{Equation 46}$$

$$f_{up} = f_{ub} \cdot (B/P) \quad \text{Equation 47}$$

$$\text{MEC} = 1000 \cdot \text{mw} \cdot 10^{-1(\text{pIC50})} \quad \text{Equation 48}$$

$$k_{el} = [\text{Human Total Clearance(wsm)}] \frac{60}{1000} \cdot 10^{\text{Log } V_{dss}} \quad \text{Equation 49}$$

$$\text{Human Total Clearance (wsm)} = \frac{(CL_{int} (\text{mL per min per g})^{24.5})^{.18}}{(CL_{int} (\text{mL per min per g})^{24.5}) + 18} \quad \text{Equation 50}$$

$$\text{HPLC DE}_{\max} = \frac{100}{10^{(0.24 \exp(\text{Logk HSA}) + 0.12 \exp(\text{Logk IAM}) - 0.4)}} \quad \text{Equation 51}$$

$$\text{Dose} \left(\frac{\text{mg}}{\text{kg}} \right) = \frac{\text{mw} \cdot 10^{-1(\text{pIC}_{50})}}{\text{HPLC DE}_{\text{max}}} \quad \text{Equation 52}$$

$$\text{MEC}(\text{HPLC DE}_{\text{max}}) = \frac{\text{HPLC DE}_{\text{max}}}{100} \cdot \text{MEC} \quad \text{Equation 53}$$

$$\text{Dose} \left(\frac{\text{mg}}{\text{kg}} \right) = \frac{\frac{24}{\tau} \cdot \text{MEC}(\text{HPLC DE}_{\text{max}}) \cdot V_{\text{dss}}(k_a - k_{\text{el}})}{F \cdot k_a \left(\frac{1}{1 - \exp(-k_{\text{el}}\tau)} - \frac{1}{1 - \exp(-k_a\tau)} \right)} \quad \text{Equation 54}$$

$$k_{\text{el}} = \frac{\text{CL}}{V_d} \quad \text{Equation 55}$$

$$K_i = \frac{\text{IC}_{50}}{1 + \left(\frac{S}{\text{KM}} \right)} \quad \text{Equation 56}$$

$$\text{DEI} = \text{pIC}_{50} + \text{Log}(\text{DE}_{\text{max}}\%) \quad \text{Equation 57}$$

$$\text{Log } k (\text{HPLC LTB}) = 0.73 \text{Log } k \text{ HSA} + 1.13 \text{Log } k \text{ AGP} + 0.077 \quad \text{Equation 58}$$

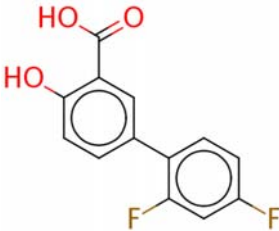
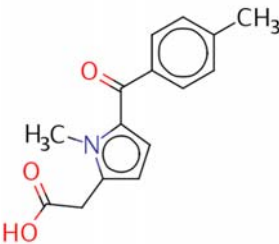
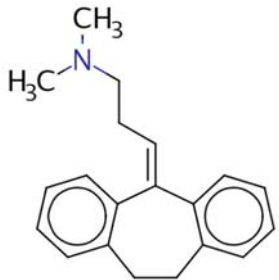
$$\text{Bound} = \frac{100 \cdot 10^{\text{Log } k}}{1 + 10^{\text{Log } k}} \quad \text{Equation 59}$$

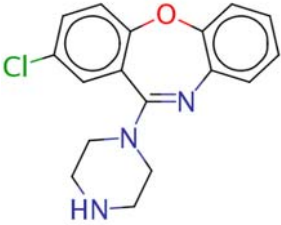
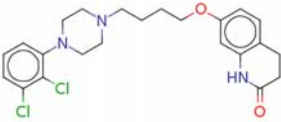
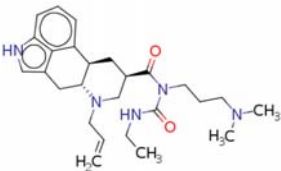
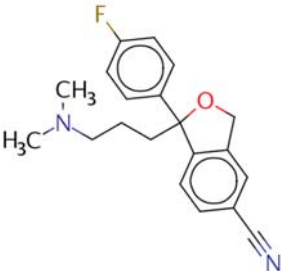
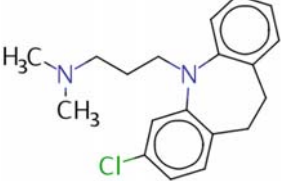
$$E = 1 + \frac{\text{E}_{\text{max}} \cdot C^N}{\text{EC}_{50} + C^N} \quad \text{or} \quad E = E_0 - \frac{\text{I}_{\text{max}} \cdot C^N}{\text{IC}_{50} + C^N} \quad \text{Equation 60}$$

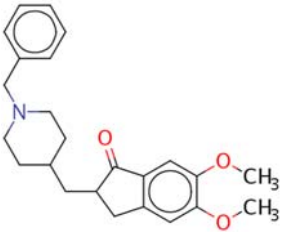
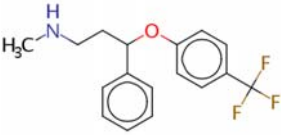
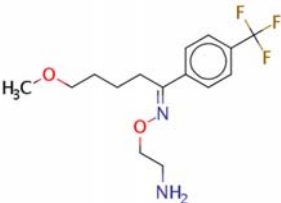
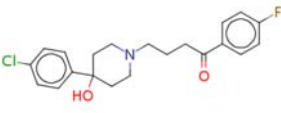
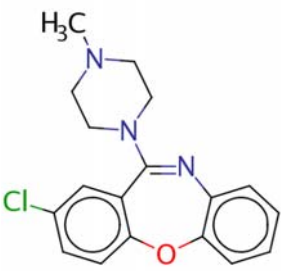
11 Appendix II

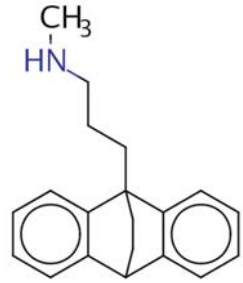
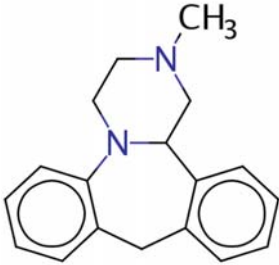
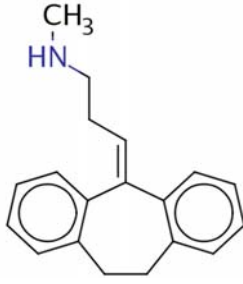
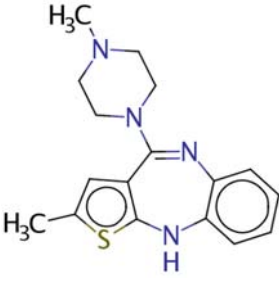

Table 11-1 Table Marketed Drugs with all Structures with Application and Acid / Base Class

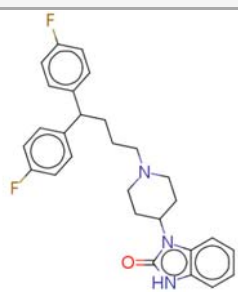
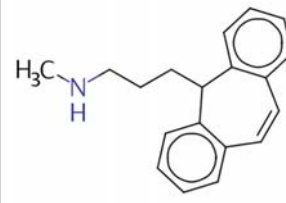
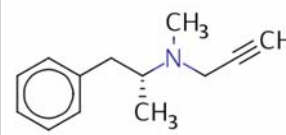
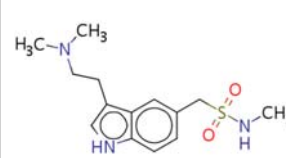
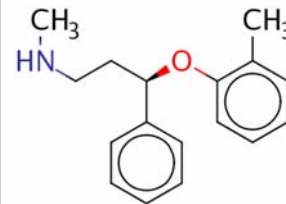
Application	Colour Key
CNS	
Inhaled	
JAKi	
Oral/Systemic	

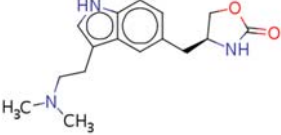
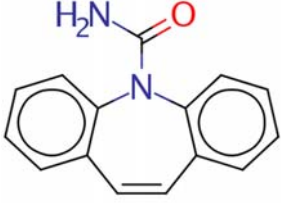
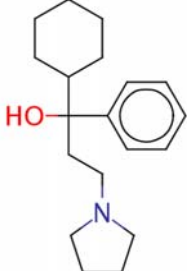
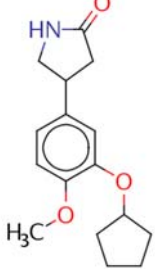
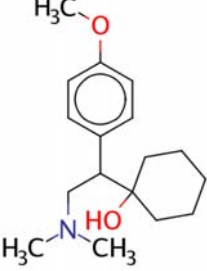
Drug Name	Parent Compound	Application	Acid/Base Class	STRUCTURE
Diflunisal	GI235401	CNS	Acidic	
Tolmetin	SB-213421	CNS	Acidic	
Amitriptyline	CCI11220	CNS	Basic	

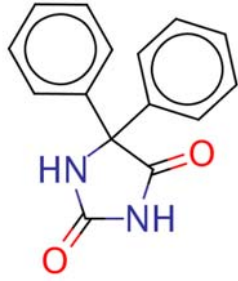
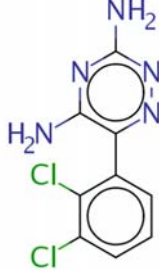
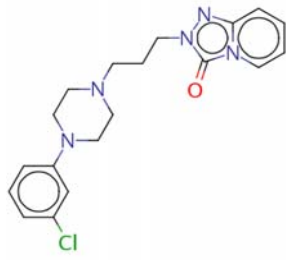
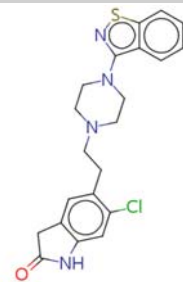
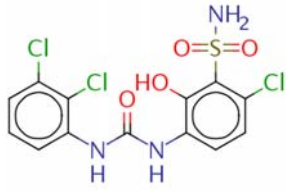
Drug Name	Parent Compound	Application	Acid/Base Class	STRUCTURE
Amoxapine	GF120454	CNS	Basic	
Aripiprazole	SB-731710	CNS	Basic	
Cabergoline	GSK574550	CNS	Basic	
Citalopram	GR60414	CNS	Basic	
Clomipramine	CCI22861	CNS	Basic	

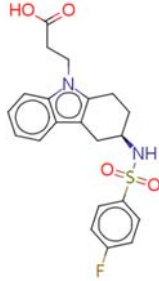
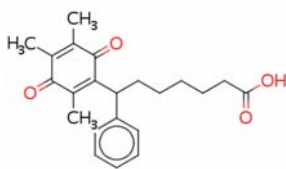
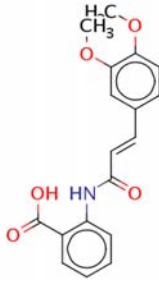
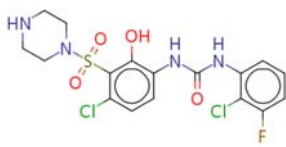
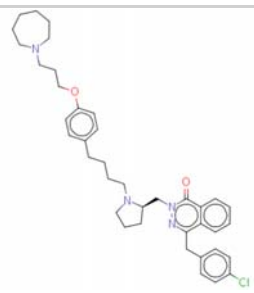
Drug Name	Parent Compound	Application	Acid/Base Class	STRUCTURE
Donepezil	GR220235	CNS	Basic	
Fluoxetine	GR61267	CNS	Basic	
Fluvoxamine	GW367767	CNS	Basic	
Haloperidol	CCI3748	CNS	Basic	
Loxapine	GR41691	CNS	Basic	

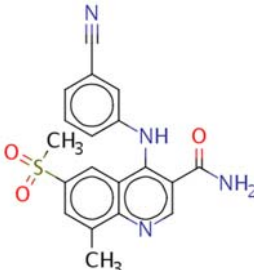
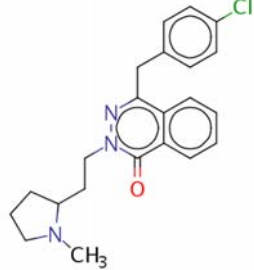
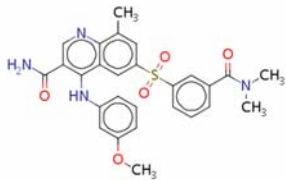
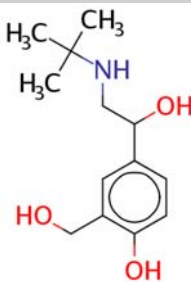
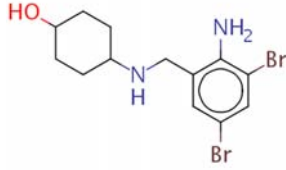
Drug Name	Parent Compound	Application	Acid/Base Class	STRUCTURE
Maprotiline	GI201081	CNS	Basic	
Mianserin	GR119163	CNS	Basic	
Nortriptyline	GR84804	CNS	Basic	
Olanzapine	GR189721	CNS	Basic	
Pergolide	GR55895	CNS	Basic	

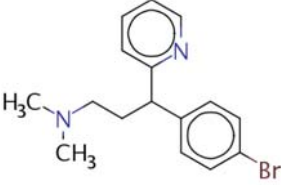
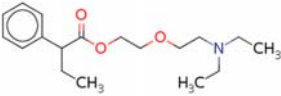
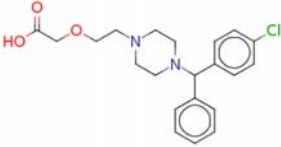
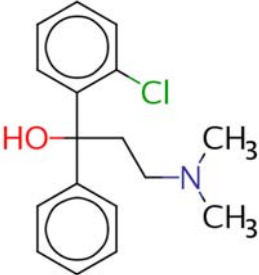
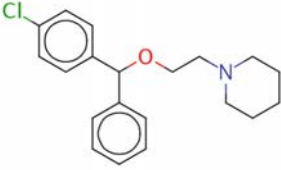
Drug Name	Parent Compound	Application	Acid/Base Class	STRUCTURE
Pimozide	GR30676	CNS	Basic	
Protriptyline	GR230212	CNS	Basic	
Selegiline	GR35846	CNS	Basic	
Sumatriptan	GR43175	CNS	Basic	
Tomoxetine	GW769340	CNS	Basic	

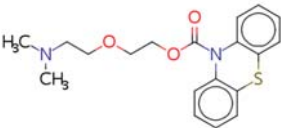
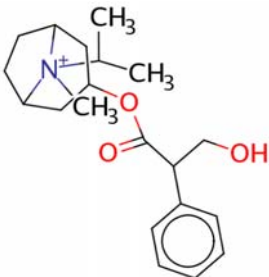
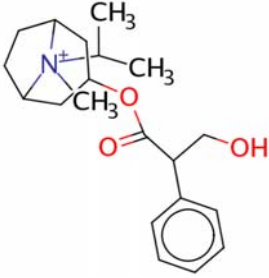
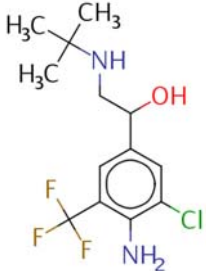
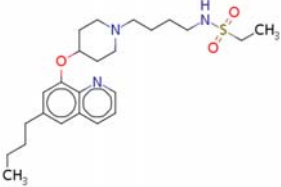
Drug Name	Parent Compound	Application	Acid/Base Class	STRUCTURE
Zolmitriptan	GR183544	CNS	Basic	
Carbamazepine	GR84641	CNS	Neutral	
Procyclidine	GR35842	CNS	Base	
Rolipram	GI115674	CNS	Neutral	
Venlafaxine	SB-416332	CNS	Base	

Drug Name	Parent Compound	Application	Acid/Base Class	STRUCTURE
Phenytoin	CCI23818	CNS	Weak Acid	
Lamotrigine	GI267119	CNS	Weak Base	
Trazodone	AH8919	CNS	Weak Base	
Ziprasidone	SB-254628	CNS	Weak Base	
6-Chloro-3-[[[2,3-dichlorophenyl]carbamoyl]amino]-2-hydroxybenzenesulfonamide	SB-332235	Inhaled set	Acidic	

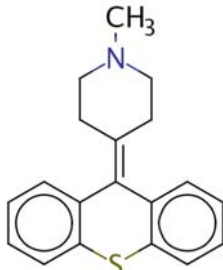
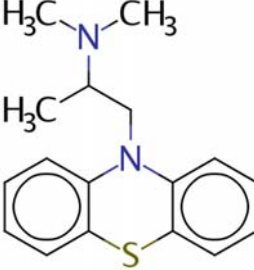
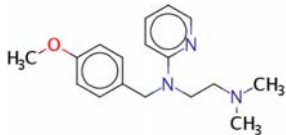
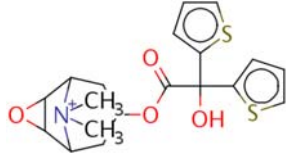
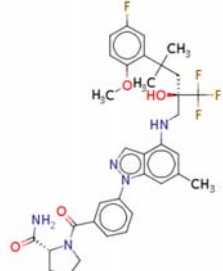
Drug Name	Parent Compound	Application	Acid/Base Class	STRUCTURE
Ramatroban	GSK603598	Inhaled set	Acidic	
Seratrodast	GW615523	Inhaled set	Acidic	
Tranilast	GSK2286993	Inhaled set	Acidic	
Elubrixin	SB-656933	Inhaled set	Amphoteric	
2-[[[1-(4-{4-[3-(Azepan-1-yl)propoxy]phenyl}butyl)pyrrolidin-2-yl]methyl]-4-(4-chlorobenzyl)phthalazin-1(2H)-one	GSK1004723	Inhaled set	Basic	

Drug Name	Parent Compound	Application	Acid/Base Class	STRUCTURE
4-(3-Cyanoanilino)-8-methyl-6-(methylsulfonyl)quinoline-3-carboxamide	GSK240928	Inhaled set	Basic	
4-(4-Chlorobenzyl)-2-[2-(1-methylpyrrolidin-2-yl)ethyl]phthalazin-1(2H)-one	GSK922892	Inhaled set	Basic	
6-[[3-(Dimethylcarbamoyl)phenyl]sulfonyl]-4-(3-methoxyanilino)-8-methylquinoline-3-carboxamide	GSK256066	Inhaled set	Basic	
Albuterol	AH3365	Inhaled set	Basic	
Ambroxol	GF119847	Inhaled set	Basic	

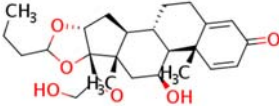
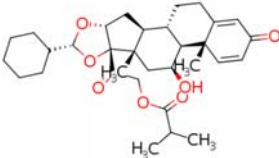
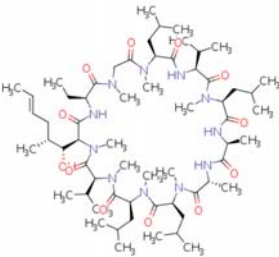
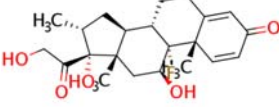

Drug Name	Parent Compound	Application	Acid/Base Class	STRUCTURE
Brompheniramine	GF120370	Inhaled set	Basic	
Butamirate	GW613152	Inhaled set	Basic	
Cetirizine	GR99941	Inhaled set	Basic	
Chlophedianol	GI177616	Inhaled set	Basic	
Cloperastine	SB-408309	Inhaled set	Basic	

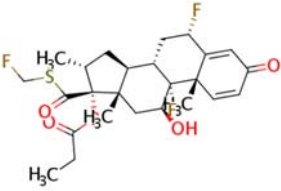
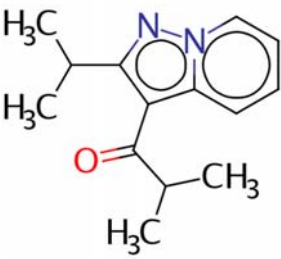
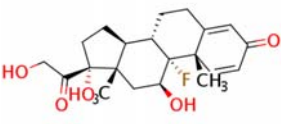
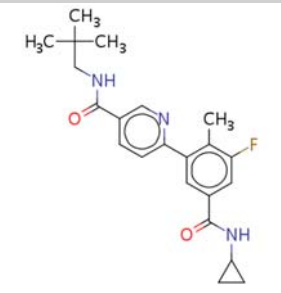
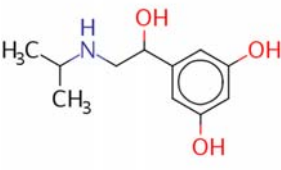
Drug Name	Parent Compound	Application	Acid/Base Class	STRUCTURE
Dimethoxanate	SKF-7497	Inhaled set	Basic	
Ipratropium	AH14211	Inhaled set	Basic	
Ipratropium	SB-452594	Inhaled set	Basic	
Mabuterol	GSK2286999	Inhaled set	Basic	
N-(4-{4-[(6-Butylquinolin-8-yl)oxy]piperidin-1-yl}butyl)ethanesulfonamide	GSK1645469	Inhaled set	Basic	

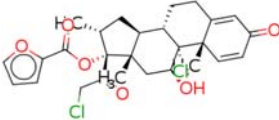
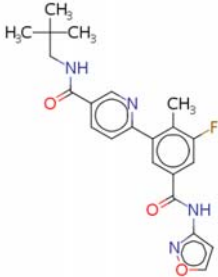
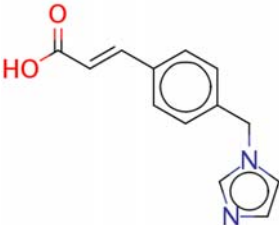
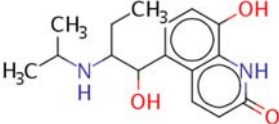

Drug Name	Parent Compound	Application	Acid/Base Class	STRUCTURE
N-(4-{4-[(6-Butylquinolin-8-yl)oxy]piperidin-1-yl}butyl)ethanesulfonamide	GSK1645469	Inhaled set	Basic	
N-[3-(2-Ethyl-3,4,10,11,13-pentahydroxy-3,5,8,10,12,14-hexamethyl-15-oxo-1-oxa-6-azacyclopentadecan-6-yl)propyl]-9-fluoro-11-hydroxy-16-methyl-3-oxoandrosta-1,4-diene-17-carboxamide	GSK1399686	Inhaled set	Basic	
Oxymetazoline	AH1105	Inhaled set	Basic	
Phenyltoloxamine	SKF-6639	Inhaled set	Basic	

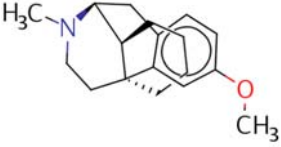
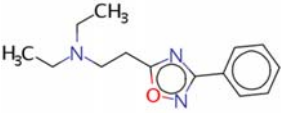
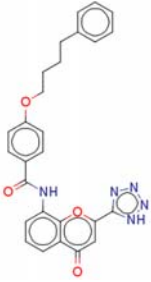
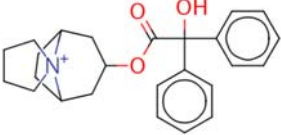
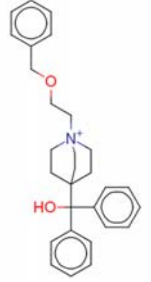
Drug Name	Parent Compound	Application	Acid/Base Class	STRUCTURE
Pimethixene	SKF-34226	Inhaled set	Basic	
Promethazine	CCI3993	Inhaled set	Basic	
Pyrilamine	AH7521	Inhaled set	Basic	
Tiotropium	GW696257	Inhaled set	Basic	
1-[3-(4-([4-(5-Fluoro-2-methoxyphenyl)-2-hydroxy-4-methyl-2-(trifluoromethyl)pentyl]amino)-6-methyl-1H-indazol-1-yl)benzoyl]prolinamide	GSK1247150	Inhaled set	Neutral	

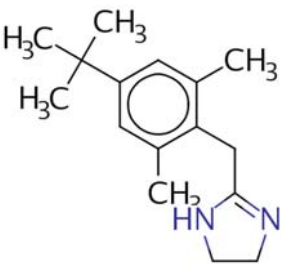
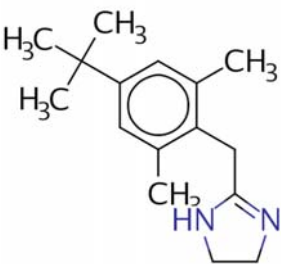
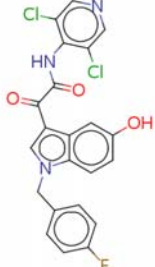

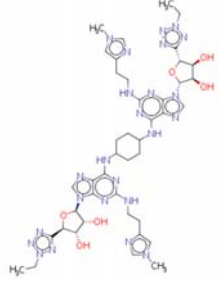
Drug Name	Parent Compound	Application	Acid/Base Class	STRUCTURE
4-(2,4-Difluorophenyl)-2-[(1,3-dihydroxypropan-2-yl)amino]-8-(2,4,6-trifluorophenyl)pyrido[2,3-d]pyrimidin-7(8H)-one	SB-731445	Inhaled set	Neutral	
5-Amino-N-(2-[[[2,6-difluorobenzoyl](ethyl)amino]methyl]-3,3,3-trifluoro-2-hydroxypropyl)-1-(4-fluorophenyl)-1H-pyrazole-4-carboxamide	GSK1223684	Inhaled set	Neutral	
6,9-Difluoro-17-[[[(fluoromethyl)thio]carbonyl]-11-hydroxy-16-methyl-3-oxoandrosta-1,4-dien-17-yl 1-methylcyclopropanecarboxylate	GW784568	Inhaled set	Neutral	
6-Methoxy-3-nitroquinoline	GSK1160274	Inhaled set	Neutral	
Beclomethasone dipropionate	AH15270	Inhaled set	Neutral	

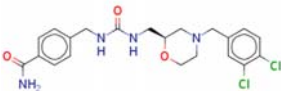
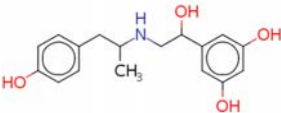
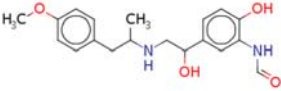
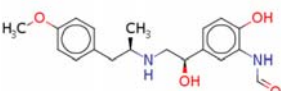
Drug Name	Parent Compound	Application	Acid/Base Class	STRUCTURE
Budesonide	GR160288	Inhaled set	Neutral	 The chemical structure of Budesonide is a corticosteroid with a complex polycyclic core. It features a methyl group at C-13, a hydroxyl group at C-14, and a butyrate ester group at C-21. The A-ring has a ketone at C-3 and a double bond between C-4 and C-5.
Ciclesonide	GW834917	Inhaled set	Neutral	 The chemical structure of Ciclesonide is a corticosteroid with a complex polycyclic core. It features a methyl group at C-13, a hydroxyl group at C-14, and a cyclohexane ring at C-21. The A-ring has a ketone at C-3 and a double bond between C-4 and C-5.
Cyclosporin A	GR92424	Inhaled set	Neutral	 The chemical structure of Cyclosporin A is a cyclic heptadecapeptide. It consists of 11 amino acid residues linked by amide bonds, forming a large macrocyclic ring. The residues include valine, leucine, phenylalanine, proline, threonine, isoleucine, methionine, and others.
Dexamethasone	CCI847	Inhaled set	Neutral	 The chemical structure of Dexamethasone is a corticosteroid with a complex polycyclic core. It features a methyl group at C-13, a hydroxyl group at C-14, and a methyl ester group at C-21. The A-ring has a ketone at C-3 and a double bond between C-4 and C-5.
Fluticasone furoate	GW685698	Inhaled set	Neutral	 The chemical structure of Fluticasone furoate is a corticosteroid with a complex polycyclic core. It features a methyl group at C-13, a hydroxyl group at C-14, and a furoate ester group at C-21. The A-ring has a ketone at C-3 and a double bond between C-4 and C-5.

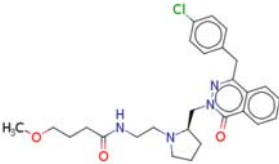
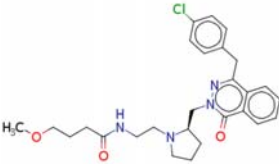
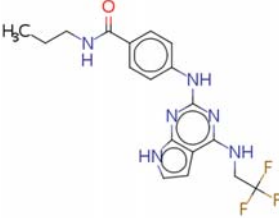
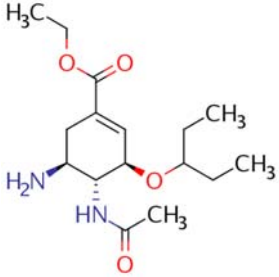
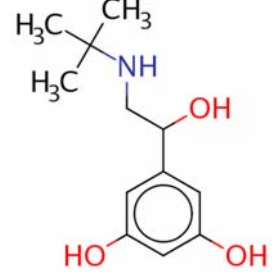
Drug Name	Parent Compound	Application	Acid/Base Class	STRUCTURE
Fluticasone propionate	CCI18781	Inhaled set	Neutral	 The structure shows a complex steroid nucleus with a propionate ester group at C-17, a fluorine atom at C-21, and a 2-(2-fluorophenyl)ethyl side chain at C-3. Stereochemistry is indicated with wedges and dashes.
Ibudilast	GW308612	Inhaled set	Neutral	 The structure features a benzimidazole ring system substituted with two methyl groups at the 2-position, a 2-methylpropanoyl group at the 5-position, and a 2-methylpropanoyl group at the 7-position.
Isofluprednone	CCI3677	Inhaled set	Neutral	 The structure is a steroid with a propionic acid group at C-17, a fluorine atom at C-21, and a 2-(2-fluorophenyl)ethyl side chain at C-3. Stereochemistry is indicated with wedges and dashes.
Losmapimod	GW856553	Inhaled set	Neutral	 The structure consists of a pyridine ring substituted with a tert-butylamino group at the 2-position, a 4-(cyclopropylamino)phenyl group at the 3-position, and a 2-fluorophenyl group at the 5-position.
Metaproterenol	GR270868	Inhaled set	Base	 The structure shows a benzene ring with three hydroxyl groups at the 3, 4, and 5 positions, and a 1-(2-methylpropyl)amino group at the 1 position.

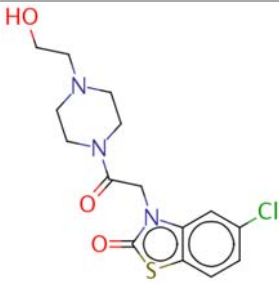
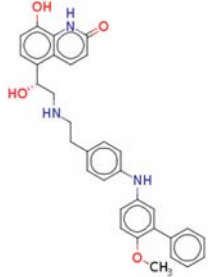
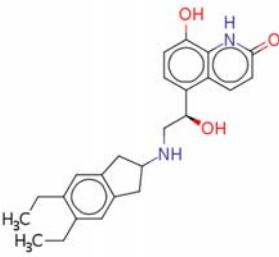
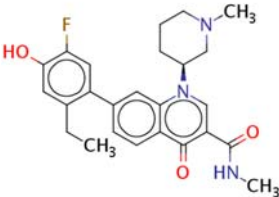
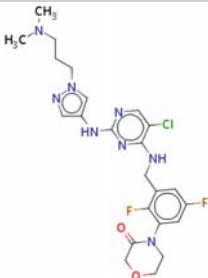
Drug Name	Parent Compound	Application	Acid/Base Class	STRUCTURE
Mometasone furoate	GR226838	Inhaled set	Neutral	
N-(2,2-Dimethylpropyl)-6-[3-fluoro-2-methyl-5-(1,2-oxazol-3-ylcarbamoyl)phenyl]nicotinamide	GSK678361	Inhaled set	Neutral	
Ozagrel	GW311465	Inhaled set	Base	
Procaterol	GR32561	Inhaled set	Neutral	
Benzonatate	SKF-5459	Inhaled set	Not Classified	

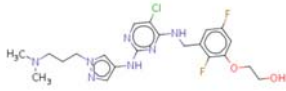
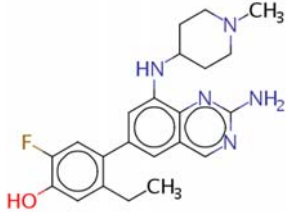
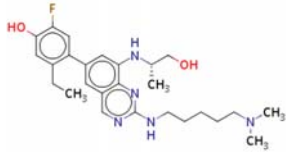
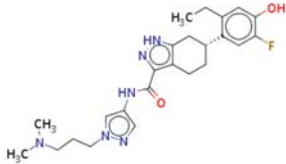
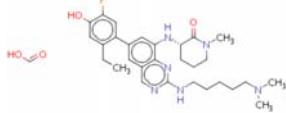
Drug Name	Parent Compound	Application	Acid/Base Class	STRUCTURE
Dextromethorphan	GR87911	Inhaled set	Acid	
Oxolamine	SKF-9976	Inhaled set	Base	
Pranlukast	SB-205312	Inhaled set	Acid	
Trospium	GW335683	Inhaled set	Not Classified	
Umeclidinium	GSK573719	Inhaled set	Not Classified	

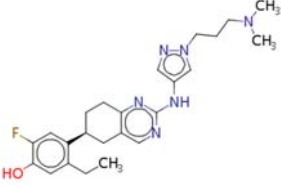
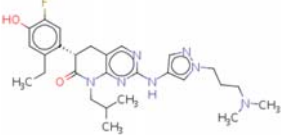
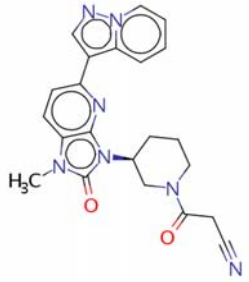
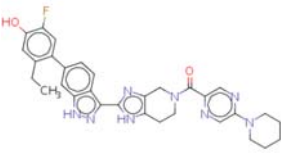
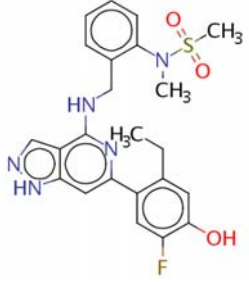
Drug Name	Parent Compound	Application	Acid/Base Class	STRUCTURE
Xylometazoline	SKF-26013	Inhaled set	Base	
Xylometazoline	CCI23820	Inhaled set	Base	
N-(3,5-Dichloropyridin-4-yl)-2-[1-(4-fluorobenzyl)-5-hydroxy-1H-indol-3-yl]-2-oxoacetamide	GW842470	Inhaled set	Weak Acid	
Theophylline	CCI4079	Inhaled set	Weak Acid	
2-(2-Ethyl-2H-tetrazol-5-yl)-5-[6-({4-[(9-[5-(2-ethyl-2H-tetrazol-5-yl)-3,4-dihydroxytetrahydrofuran-2-yl]-2-[[2-(1-methyl-1H-imidazol-4-yl)ethyl]amino]-9H-purin-6-yl)amino]cyclohexyl}ami	GW846428	Inhaled set	Weak Base	

Drug Name	Parent Compound	Application	Acid/Base Class	STRUCTURE
no)-2-{{2-(1-methyl-1H-imidazol-4-yl)ethyl}amino}-9H-purin-9-yl}tetrahydrofuran-3,4-diol				
4-{{[[[4-(3,4-Dichlorobenzyl)morpholin-2-yl]methyl}carbonyl]amino]methyl}benzamide	GW766994	Inhaled set	Weak Base	
Fenoterol	GR123442	Inhaled set	Weak Base	
Formoterol	GR96676	Inhaled set	Weak Base	
Formoterol	GW577790	Inhaled set	Weak Base	

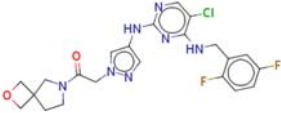
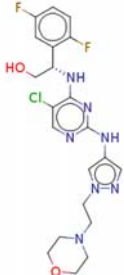
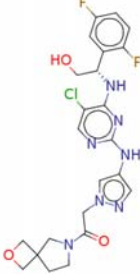
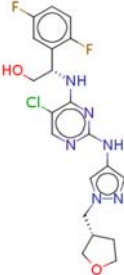
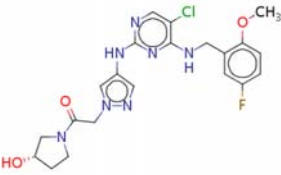
Drug Name	Parent Compound	Application	Acid/Base Class	STRUCTURE
N-[2-(2-[[4-(4-Chlorobenzyl)-1-oxophthalazin-2(1H-yl)methyl]pyrrolidin-1-yl)ethyl]-4-methoxybutanamide	GSK1367441	Inhaled set	Weak Base	
N-[2-(2-[[4-(4-Chlorobenzyl)-1-oxophthalazin-2(1H-yl)methyl]pyrrolidin-1-yl)ethyl]-4-methoxybutanamide	GSK1367441	Inhaled set	Weak Base	
N-Propyl-4-((4-[(2,2,2-trifluoroethyl)amino]-7H-pyrrolo[2,3-d]pyrimidin-2-yl)amino)benzamide	GSK1000064	Inhaled set	Weak Base	
Oseltamivir	GW396512	Inhaled set	Weak Base	
Terbutaline	SKF-51066	Inhaled set	Weak Base	

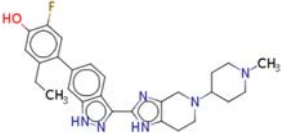

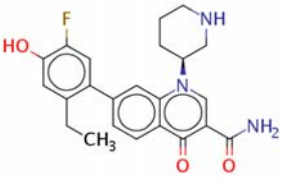
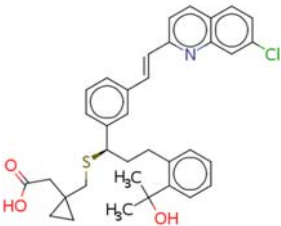
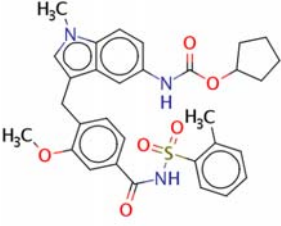
Drug Name	Parent Compound	Application	Acid/Base Class	STRUCTURE
Tiamide	SKF-81296	Inhaled set	Weak Base	
8-Hydroxy-5-{1-hydroxy-2-[(2-{4-[(6-methoxybiphenyl]-3-yl)amino]phenyl)ethyl]amino]ethyl}quinolin-2(1H)-one	GSK159802	Inhaled set	Zwitterionic	
Indacaterol	GW872435	Inhaled set	Zwitterionic	
GSK3896132A	GSK3896132A	JAKi	Amphoteric	
GSK3376417A	GSK3376417A	JAKi	Basic	

Drug Name	Parent Compound	Application	Acid/Base Class	STRUCTURE
GSK3532706A	GSK3532706A	JAKi	Basic	
GSK3780731A	GSK3780731A	JAKi	Basic	
GSK3800430A	GSK3800430A	JAKi	Basic	
GSK3816662A	GSK3816662A	JAKi	Basic	
GSK3859782A	GSK3859782A	JAKi	Basic	

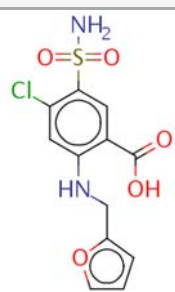
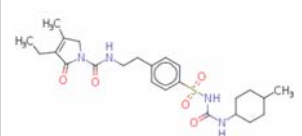
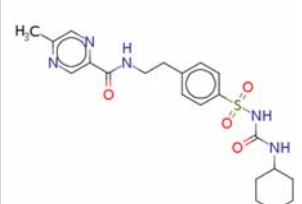
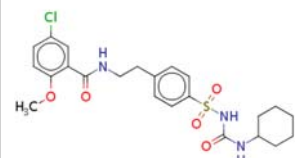
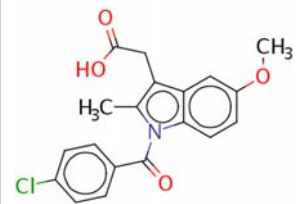
Drug Name	Parent Compound	Application	Acid/Base Class	STRUCTURE
GSK3860551A	GSK3860551A	JAKi	Basic	
GSK3861033A	GSK3861033A	JAKi	Basic	
GSK3863783A	GSK3863783A	JAKi	Neutral	
GSK3336961A	GSK3336961A	JAKi	Not Classified	
GSK3686622A	GSK3686622A	JAKi	Not Classified	


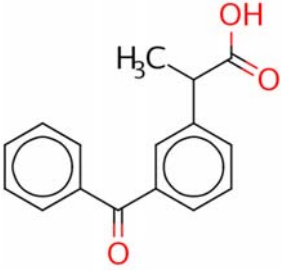
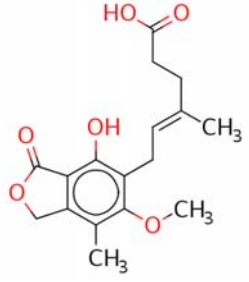
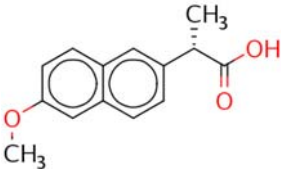
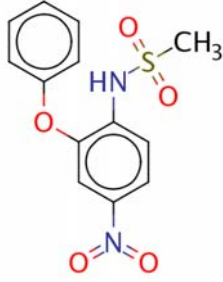
Drug Name	Parent Compound	Application	Acid/Base Class	STRUCTURE
GSK3733362A	GSK3733362A	JAKi	Not Classified	
GSK3901000A	GSK3901000A	JAKi	Base	
GSK3901790A	GSK3901790A	JAKi	Not Classified	
GSK3845209A	GSK3845209A	JAKi	Weak Acid	
GSK3074811A	GSK3074811A	JAKi	Weak Base	

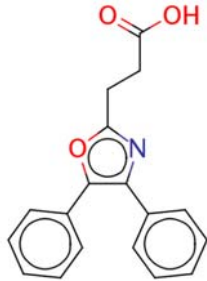
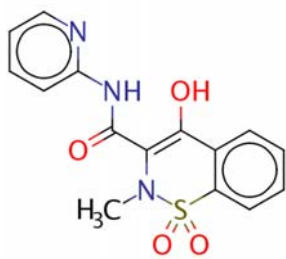
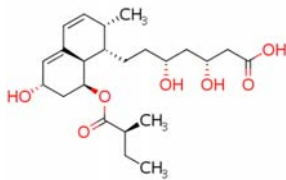
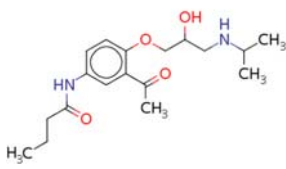
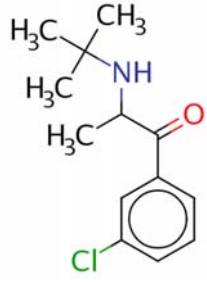
Drug Name	Parent Compound	Application	Acid/Base Class	STRUCTURE
GSK3454697A	GSK3454697A	JAKi	Weak Base	
GSK3487568A	GSK3487568A	JAKi	Weak Base	
GSK3489723A	GSK3489723A	JAKi	Weak Base	
GSK3515539A	GSK3515539A	JAKi	Weak Base	
GSK3519625A	GSK3519625A	JAKi	Weak Base	

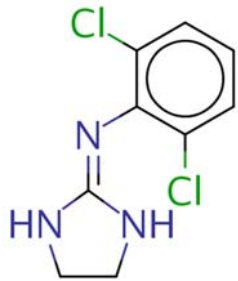
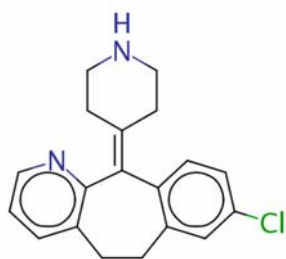
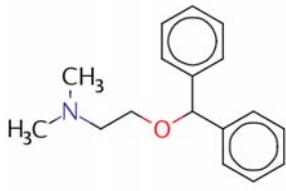
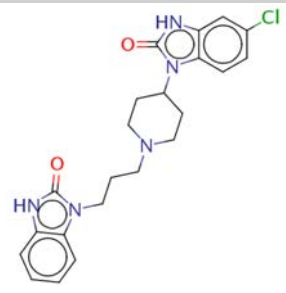
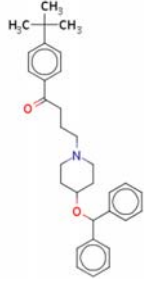
Drug Name	Parent Compound	Application	Acid/Base Class	STRUCTURE
GSK3901334A	GSK3901334A	JAKi	Weak Base	
GSK3635481A	GSK3635481A	JAKi	Zwitterionic	
GSK3908922A	GSK3908922A	JAKi	Zwitterionic	
Montelukast	GW483100	Oral/Systemic	Acidic	
Zafirlukast	GR138714	Oral/Systemic	Acidic	

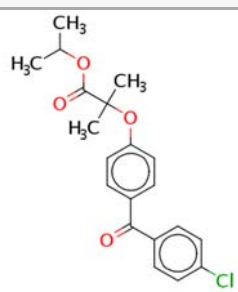
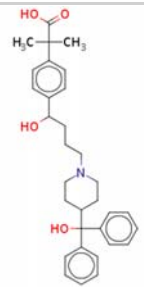
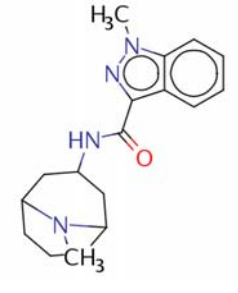
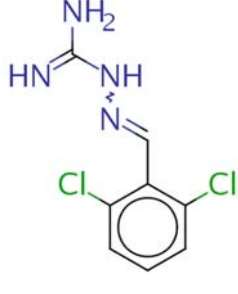
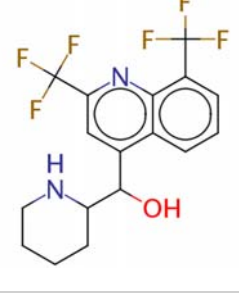
Drug Name	Parent Compound	Application	Acid/Base Class	STRUCTURE
Amiloride	GR77494	Oral/Systemic	Base	
Candesartan cilexetil	GW615775	Oral/Systemic	Acidic	
Diazoxide	CCI6817	Oral/Systemic	Acidic	
Etodolac	GW289865	Oral/Systemic	Acidic	
Flurbiprofen	GR62550	Oral/Systemic	Acidic	

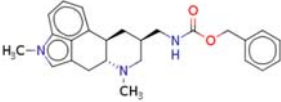
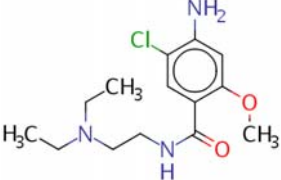
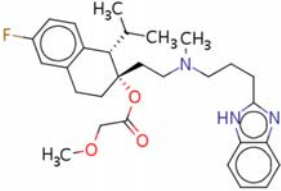
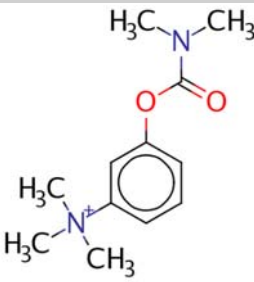
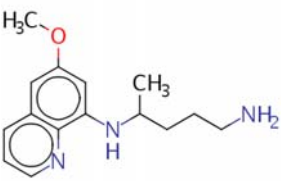
Drug Name	Parent Compound	Application	Acid/Base Class	STRUCTURE
Furosemide	GR118989	Oral/Systemic	Acidic	
Glimepiride	GW425329	Oral/Systemic	Acidic	
Glipizide	GR231784	Oral/Systemic	Acidic	
Glyburide	GR94296	Oral/Systemic	Acidic	
Indomethacin	CCI120	Oral/Systemic	Acidic	

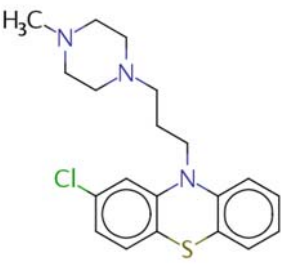
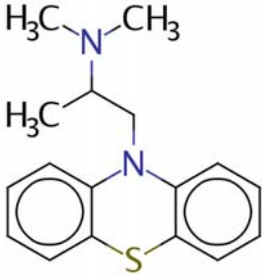
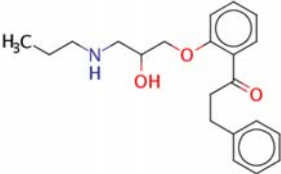
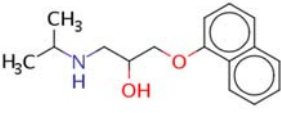
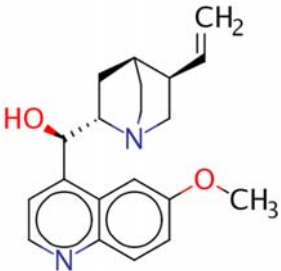
Drug Name	Parent Compound	Application	Acid/Base Class	STRUCTURE
Irbesartan	GW622791	Oral/Systemic	Acidic	
Ketoprofen	AH5057	Oral/Systemic	Acidic	
Mycophenolic acid	GR60857	Oral/Systemic	Acidic	
Naproxen	CCI23760	Oral/Systemic	Acidic	
Nimesulide	GR87272	Oral/Systemic	Acidic	

Drug Name	Parent Compound	Application	Acid/Base Class	STRUCTURE
Oxaprozin	GSK275458	Oral/Systemic	Acidic	
Piroxicam	GR33000	Oral/Systemic	Acidic	
Pravastatin	GR70487	Oral/Systemic	Acidic	
Acebutolol	GR192446	Oral/Systemic	Basic	
Bupropion	GR67205	Oral/Systemic	Basic	

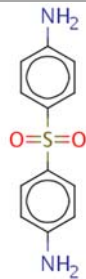
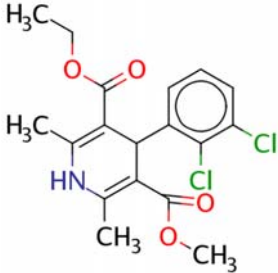
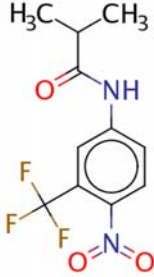
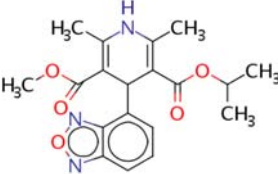
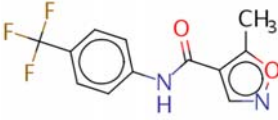
Drug Name	Parent Compound	Application	Acid/Base Class	STRUCTURE
Clonidine	GR63987	Oral/Systemic	Basic	
Desloratadine	GW787034	Oral/Systemic	Basic	
Diphenhydramine	CCI3839	Oral/Systemic	Basic	
Domperidone	GR61265	Oral/Systemic	Basic	
Ebastine	SKF-95914	Oral/Systemic	Basic	

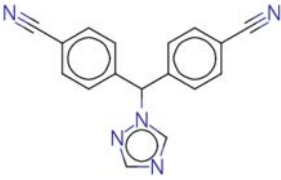
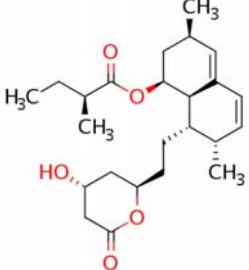
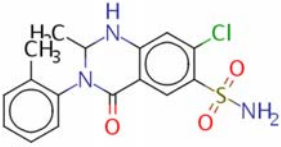
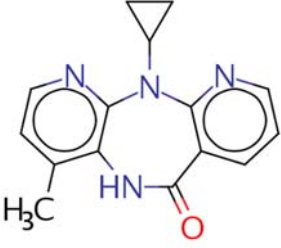
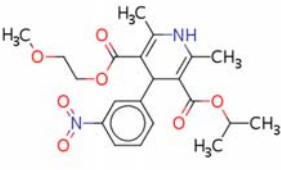
Drug Name	Parent Compound	Application	Acid/Base Class	STRUCTURE
Fenofibrate	GF145020	Oral/Systemic	Basic	
Fexofenadine	GW300671	Oral/Systemic	Basic	
Granisetron	GR75205	Oral/Systemic	Basic	
Guanabenz	GI121045	Oral/Systemic	Basic	
Mefloquine	GW335366	Oral/Systemic	Basic	

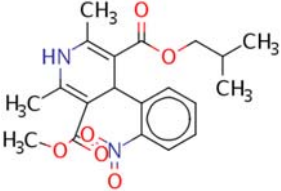

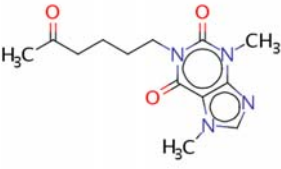
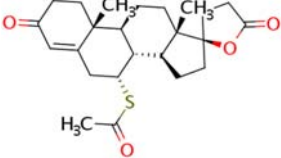
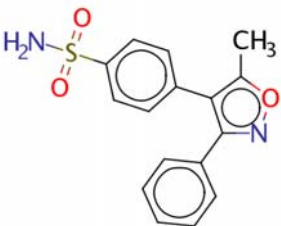
Drug Name	Parent Compound	Application	Acid/Base Class	STRUCTURE
Metergoline	GR61317	Oral/Systemic	Basic	
Metoclopramide	GR34950	Oral/Systemic	Basic	
Mibefradil	GI146356	Oral/Systemic	Basic	
Neostigmine	GR73226	Oral/Systemic	Basic	
Primaquine	CCI4308	Oral/Systemic	Basic	

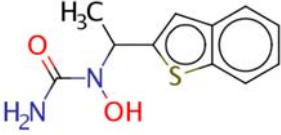
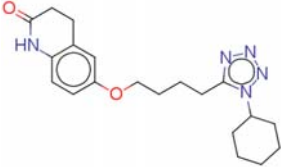
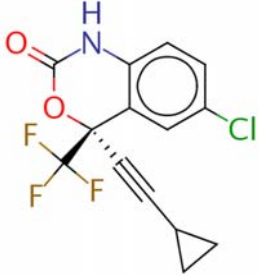
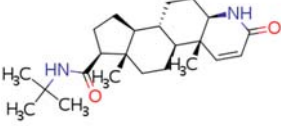
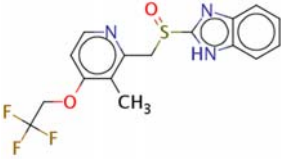
Drug Name	Parent Compound	Application	Acid/Base Class	STRUCTURE
Prochlorperazine	GR32696	Oral/Systemic	Basic	
Promethazine	CCI3993	Oral/Systemic	Basic	
Propafenone	GF119411	Oral/Systemic	Basic	
Propranolol	CCI4001	Oral/Systemic	Basic	
Quinidine	GR36768	Oral/Systemic	Basic	

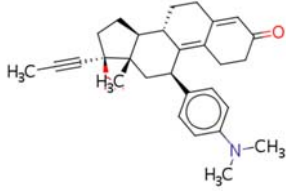
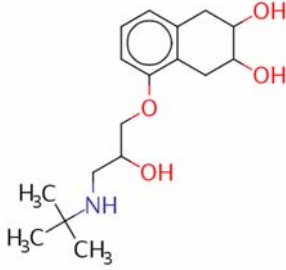
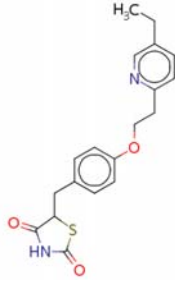
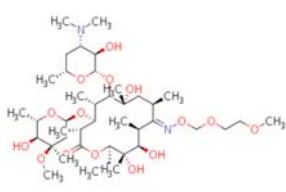
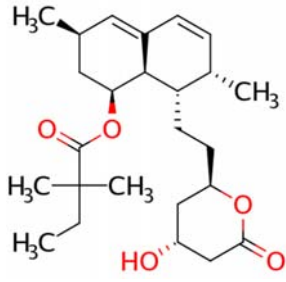
Drug Name	Parent Compound	Application	Acid/Base Class	STRUCTURE
Tamsulosin	GI138525	Oral/Systemic	Basic	
Verapamil	CCI20557	Oral/Systemic	Basic	
Prednisolone	CCI22	Oral/Systemic	Neutral	
Bicalutamide	GW703803	Oral/Systemic	Neutral	
Celecoxib	GW388185	Oral/Systemic	Acid	

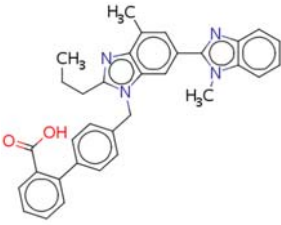
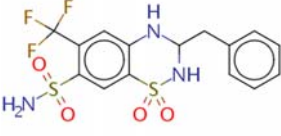
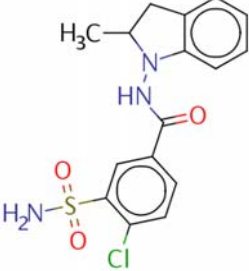
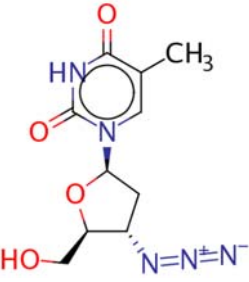
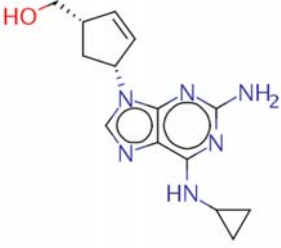
Drug Name	Parent Compound	Application	Acid/Base Class	STRUCTURE
Dapsone	AH23463	Oral/Systemic	Neutral	
Felodipine	GR64334	Oral/Systemic	Neutral	
Flutamide	AH14524	Oral/Systemic	Neutral	
Isradipine	GI116108	Oral/Systemic	Neutral	
Leflunomide	GI99296	Oral/Systemic	Neutral	

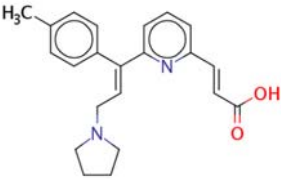
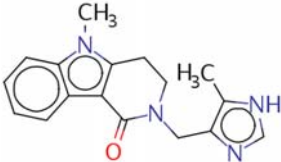
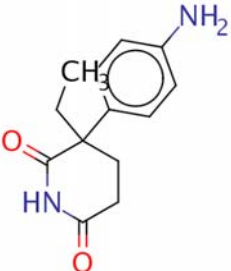
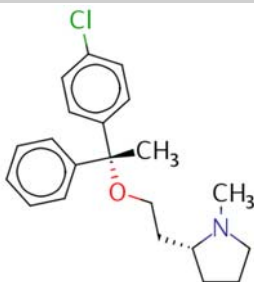
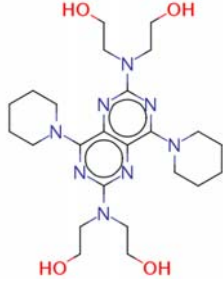
Drug Name	Parent Compound	Application	Acid/Base Class	STRUCTURE
Letrozole	GR119497	Oral/Systemic	Neutral	
Lovastatin	GR78367	Oral/Systemic	Neutral	
Metolazone	GF120403	Oral/Systemic	Neutral	
Nevirapine	GR152114	Oral/Systemic	Neutral	
Nimodipine	GR33914	Oral/Systemic	Neutral	

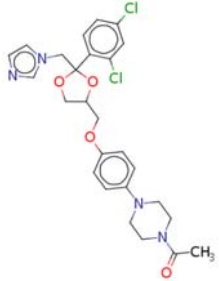
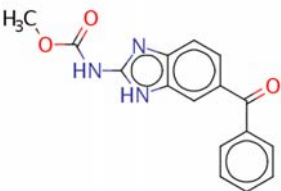
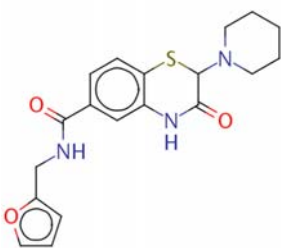
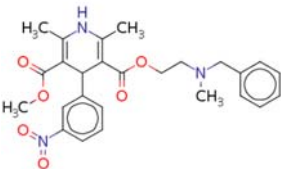
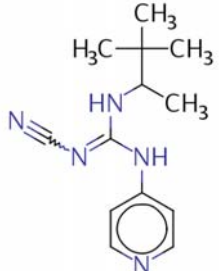
Drug Name	Parent Compound	Application	Acid/Base Class	STRUCTURE
Nisoldipine	GR33913	Oral/Systemic	Neutral	 <p>The structure of Nisoldipine is a dihydropyridine derivative. It features a central dihydropyridine ring with a methyl group at the 2-position, a methyl group at the 4-position, and a methyl group at the 5-position. The 3-position is substituted with a 4-nitrophenyl group. The 4-position is also substituted with a methyl group and a methyl ester group. The 5-position is substituted with a methyl group and a methyl ester group.</p>
Nitrendipine	GR38393	Oral/Systemic	Neutral	 <p>The structure of Nitrendipine is a dihydropyridine derivative. It features a central dihydropyridine ring with a methyl group at the 2-position, a methyl group at the 4-position, and a methyl group at the 5-position. The 3-position is substituted with a methyl group and a methyl ester group. The 4-position is substituted with a methyl group and a methyl ester group. The 5-position is substituted with a methyl group and a methyl ester group.</p>
Pentoxifylline	GR91295	Oral/Systemic	Neutral	 <p>The structure of Pentoxifylline is a xanthine derivative. It features a central xanthine ring system with a methyl group at the 3-position, a methyl group at the 7-position, and a methyl group at the 9-position. The 2-position is substituted with a methyl group and a methyl ester group. The 4-position is substituted with a methyl group and a methyl ester group. The 6-position is substituted with a methyl group and a methyl ester group.</p>
Spirolactone	CCI9371	Oral/Systemic	Neutral	 <p>The structure of Spirolactone is a spirocyclic compound. It features a central spirocyclic ring system with a methyl group at the 2-position, a methyl group at the 4-position, and a methyl group at the 6-position. The 3-position is substituted with a methyl group and a methyl ester group. The 5-position is substituted with a methyl group and a methyl ester group. The 7-position is substituted with a methyl group and a methyl ester group.</p>
Valdecoxib	GW560108	Oral/Systemic	Neutral	 <p>The structure of Valdecoxib is a cyclo-oxygenase inhibitor. It features a central cyclo-oxygenase inhibitor ring system with a methyl group at the 2-position, a methyl group at the 4-position, and a methyl group at the 6-position. The 3-position is substituted with a methyl group and a methyl ester group. The 5-position is substituted with a methyl group and a methyl ester group. The 7-position is substituted with a methyl group and a methyl ester group.</p>

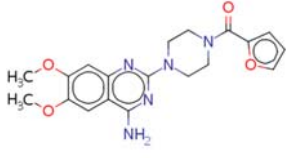

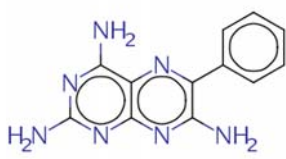
Drug Name	Parent Compound	Application	Acid/Base Class	STRUCTURE
Zileuton	GR104104	Oral/Systemic	Neutral	
Cilostazol	GSK518332	Oral/Systemic	Not Classified	
Efavirenz	GW410886	Oral/Systemic	Not Classified	
Finasteride	GR89244	Oral/Systemic	Not Classified	
Lansoprazole	GW585829	Oral/Systemic	Not Classified	

Drug Name	Parent Compound	Application	Acid/Base Class	STRUCTURE
Mifepristone	GI202328	Oral/Systemic	Not Classified	
Nadolol	GR90871	Oral/Systemic	Not Classified	
Pioglitazone	GR126777	Oral/Systemic	Not Classified	
Roxithromycin	GW622788	Oral/Systemic	Not Classified	
Simvastatin	GF207280	Oral/Systemic	Not Classified	

Drug Name	Parent Compound	Application	Acid/Base Class	STRUCTURE
Telmisartan	GW467678	Oral/Systemic	Not Classified	
Bendroflumethiazide	CCI22819	Oral/Systemic	Weak Acid	
Indapamide	GF113815	Oral/Systemic	Weak Acid	
Zidovudine	GR63367	Oral/Systemic	Weak Acid	
Abacavir	GI265235	Oral/Systemic	Weak Base	

Drug Name	Parent Compound	Application	Acid/Base Class	STRUCTURE
Acrivastin	GW313734	Oral/Systemic	Weak Base	
Alosetron	GR68755	Oral/Systemic	Weak Base	
Aminoglutethimide	GR73674	Oral/Systemic	Weak Base	
Clemastine	GF127680	Oral/Systemic	Weak Base	
Dipyridamole	CCI11224	Oral/Systemic	Weak Base	

Drug Name	Parent Compound	Application	Acid/Base Class	STRUCTURE
Ketoconazole	GR33859	Oral/Systemic	Weak Base	
Mebendazole	GF133426	Oral/Systemic	Weak Base	
N-(2-Furylmethyl)-3-oxo-2-(piperidin-1-yl)-3,4-dihydro-2H-1,4-benzothiazine-6-carboxamide	GSK527886	Oral/Systemic	Weak Base	
Nicardipine	GR38392	Oral/Systemic	Weak Base	
Pinacidil	GR94365	Oral/Systemic	Weak Base	

Drug Name	Parent Compound	Application	Acid/Base Class	STRUCTURE
Prazosin	AH16682	Oral/Systemic	Weak Base	
Riluzole	GR91291	Oral/Systemic	Weak Base	
Triamterene	SKF-8542	Oral/Systemic	Weak Base	

12 Reference

- [1] K.P. Mishra, L. Ganju, M. Sairam, P.K. Banerjee, R.C. Sawhney, A review of high throughput technology for the screening of natural products., *Biomed. Pharmacother.* 62 (2008) 94–8. doi:10.1016/j.biopha.2007.06.012.
- [2] R.A.E. Carr, M. Congreve, C.W. Murray, D.C. Rees, Fragment-based lead discovery: leads by design., *Drug Discov. Today.* 10 (2005) 987–92. doi:10.1016/S1359-6446(05)03511-7.
- [3] M.M. Hann, T.I. Oprea, Pursuing the leadlikeness concept in pharmaceutical research, *Curr. Opin. Chem. Biol.* 8 (2004) 255–263. doi:10.1016/j.cbpa.2004.04.003.
- [4] C.A. Lipinski, F. Lombardo, B.W. Dominy, P.J. Feeney, Experimental and computational approaches to estimate solubility and permeability in drug discovery and development settings, *Adv. Drug Deliv. Rev.* 64 (2012) 4–17. doi:10.1016/j.addr.2012.09.019.
- [5] S. Fox, S. Farr-Jones, L. Sopchak, A. Boggs, H.W. Nicely, R. Khoury, M. Biros, High-throughput screening: update on practices and success., *J. Biomol. Screen.* 11 (2006) 864–9. doi:10.1177/1087057106292473.
- [6] R. Lahana, Who wants to be irrational?, *Drug Discov. Today.* 8 (2003) 655–656. doi:10.1016/S1359-6446(03)02734-X.
- [7] R. Macarron, M.N. Banks, D. Bojanic, D.J. Burns, D.A. Cirovic, T. Garyantes, D.V.S. Green, R.P. Hertzberg, W.P. Janzen, J.W. Paslay, U. Schopfer, G.S. Sittampalam, Impact of high-throughput screening in biomedical research., *Nat. Rev. Drug Discov.* 10 (2011) 188–95. doi:10.1038/nrd3368.
- [8] R.J. Young, D.V.S. Green, C.N. Luscombe, A.P. Hill, Getting physical in drug discovery II: The impact of chromatographic hydrophobicity measurements and aromaticity, *Drug Discov. Today.* 16 (2011) 822–830. doi:10.1016/j.drudis.2011.06.001.
- [9] P.D. Leeson, B. Springthorpe, The influence of drug-like concepts on decision-making in medicinal chemistry, *Nat. Rev. Drug Discov.* 6 (2007) 881–890.

doi:10.1038/nrd2445.

- [10] G.L. Amidon, H. Lennernäs, V.P. Shah, J.R. Crison, A theoretical basis for a biopharmaceutic drug classification: the correlation of in vitro drug product dissolution and in vivo bioavailability., *Pharm. Res.* 12 (1995) 413–20. <http://www.ncbi.nlm.nih.gov/pubmed/7617530> (accessed July 11, 2018).
- [11] D.D.S. Particle Sciences, *Biopharmaceutical Classification System and Formulation Development*, 9 (2011) 1–2. www.mendeley.com/research-papers/biopharmaceutical-classification-system-formulation-development/?utm_source=desktop&utm_medium=1.18&utm_campaign=open_catalog&userDocumentId=%7B6cb3f9b8-429a-4570-a1b0-d14940af7972%7D.
- [12] C.Y. Wu, L.Z. Benet, Predicting drug disposition via application of BCS: Transport/absorption/ elimination interplay and development of a biopharmaceutics drug disposition classification system, *Pharm. Res.* 22 (2005) 11–23. doi:10.1007/s11095-004-9004-4.
- [13] L.Z. Benet, The role of BCS (biopharmaceutics classification system) and BDDCS (biopharmaceutics drug disposition classification system) in drug development., *J. Pharm. Sci.* 102 (2013) 34–42. doi:10.1002/jps.23359.
- [14] C.A. Lipinski, Lead- and drug-like compounds: The rule-of-five revolution, *Drug Discov. Today Technol.* 1 (2004) 337–341. doi:10.1016/j.ddtec.2004.11.007.
- [15] J.D. Hughes, J. Blagg, D.A. Price, S. Bailey, G.A. DeCrescenzo, R. V. Devraj, E. Ellsworth, Y.M. Fobian, M.E. Gibbs, R.W. Gilles, N. Greene, E. Huang, T. Krieger-Burke, J. Loesel, T. Wager, L. Whiteley, Y. Zhang, Physiochemical drug properties associated with in vivo toxicological outcomes, *Bioorganic Med. Chem. Lett.* 18 (2008) 4872–4875. doi:10.1016/j.bmcl.2008.07.071.
- [16] P. Morgan, P.H. Van Der Graaf, J. Arrowsmith, D.E. Feltner, K.S. Drummond, C.D. Wegner, S.D.A. Street, Can the flow of medicines be improved? Fundamental pharmacokinetic and pharmacological principles toward improving Phase II survival., *Drug Discov. Today*. 17 (2012) 419–24. doi:10.1016/j.drudis.2011.12.020.
- [17] M.P. Gleeson, Generation of a set of simple, interpretable ADMET rules of thumb, *J. Med. Chem.* 51 (2008) 817–834. doi:10.1021/jm701122q.

- [18] P.D. Leeson, J.R. Empfield, Reducing the Risk of Drug Attrition Associated with Physicochemical Properties, Edition Ed, Elsevier Inc., 2010. doi:10.1016/S0065-7743(10)45024-1.
- [19] M.P. Gleeson, A. Hersey, D. Montanari, J. Overington, Probing the links between in vitro potency, ADMET and physicochemical parameters, *Nat. Rev. Drug Discov.* 10 (2011) 197–208. doi:10.1038/nrd3367.
- [20] J.A. Arnott, S.L. Planey, The influence of lipophilicity in drug discovery and design, *Expert Opin. Drug Discov.* 7 (2012) 863–875. doi:10.1517/17460441.2012.714363.
- [21] T.H. Keller, A. Pichota, Z. Yin, A practical view of “druggability,” *Curr. Opin. Chem. Biol.* 10 (2006) 357–361. doi:10.1016/j.cbpa.2006.06.014.
- [22] M. Hann, B. Hudson, X. Lewell, R. Lively, L. Miller, N. Ramsden, Strategic Pooling of Compounds for High-Throughput Screening, *J. Chem. Inf. Model.* 39 (1999) 897–902. doi:10.1021/ci990423o.
- [23] P.D. Leeson, S. a. St-Gallay, The influence of the “organizational factor” on compound quality in drug discovery, *Nat. Rev. Drug Discov.* 10 (2011) 749–765. doi:10.1038/nrd3552.
- [24] D.F. McGinnity, J. Collington, R.P. Austin, R.J. Riley, Evaluation of human pharmacokinetics, therapeutic dose and exposure predictions using marketed oral drugs, *Curr Drug Metab.* 8 (2007) 463–479. doi:10.2174/138920007780866799.
- [25] K.H. Grime, P. Barton, D.F. McGinnity, Application of In Silico , In Vitro and Preclinical Pharmacokinetic Data for the Effective and Efficient Prediction of Human Pharmacokinetics, (2013).
- [26] D.A. Smith, E.F. Schmid, Drug withdrawals and the lessons within., *Curr. Opin. Drug Discov. Devel.* 9 (2006) 38–46. <http://www.ncbi.nlm.nih.gov/pubmed/16445116>.
- [27] S. Braggio, D. Montanari, T. Rossi, E. Ratti, Drug efficiency: a new concept to guide lead optimization programs towards the selection of better clinical candidates, *Expert Opin. Drug Discov.* 5 (2010) 609–618. doi:10.1517/17460441.2010.490553.

- [28] D.A. Smith, K. Beaumont, T.S. Maurer, L. Di, Volume of Distribution in Drug Design, *J. Med. Chem.* 58 (2015) 5691–5698. doi:10.1021/acs.jmedchem.5b00201.
- [29] H.M. Materia, Hepato-Biliary System, (n.d.) 1–40. <https://www.youtube.com/watch?v=BsiNDAFYeTs> (accessed December 18, 2018).
- [30] N.K. Hopson, J. L. and Wessells, *Essentials of Biology*, McGraw-Hill Publishing Company, 1990, n.d.
- [31] L. Liu, K.S. Pang, An integrated approach to model hepatic drug clearance, *Eur. J. Pharm. Sci.* 29 (2006) 215–230. doi:10.1016/J.EJPS.2006.05.007.
- [32] D.C. Rees, M. Congreve, C.W. Murray, R. Carr, Fragment-based lead discovery, *Nat. Rev. Drug Discov.* 3 (2004) 660–672. doi:10.1038/nrd1467.
- [33] C. Hansch, T. Fujita, ρ - σ - π Analysis. A Method for the Correlation of Biological Activity and Chemical Structure, *J. Am. Chem. Soc.* 86 (1964) 1616–1626. doi:10.1021/ja01062a035.
- [34] A.L. Hopkins, G.M. Keserü, P.D. Leeson, D.C. Rees, C.H. Reynolds, The role of ligand efficiency metrics in drug discovery, *Nat. Rev. Drug Discov.* 13 (2014) 105–121. doi:10.1038/nrd4163.
- [35] L. Ayouni, G. Cazorla, D. Chaillou, B. Herbreteau, S. Rudaz, P. Lantéri, P.-A. Carrupt, Fast Determination of Lipophilicity by HPLC, *Chromatographia.* 62 (2005) 251–255. doi:10.1365/s10337-005-0608-6.
- [36] S. Gocan, G. Cimpan, J. Comer, Lipophilicity measurements by liquid chromatography., *Adv. Chromatogr.* 44 (2006) 79–176.
- [37] C. Giaginis, A. Tsantili-Kakoulidou, Current State of the Art in HPLC Methodology for Lipophilicity Assessment of Basic Drugs. A Review, *J. Liq. Chromatogr. Relat. Technol.* 31 (2007) 79–96. doi:10.1080/10826070701665626.
- [38] K. Valkó, C. Bevan, D. Reynolds, Chromatographic Hydrophobicity Index by Fast-Gradient RP-HPLC: A High-Throughput Alternative to log P/log D., *Anal. Chem.* 69 (1997) 2022–9. doi:10.1021/ac961242d.

- [39] K. Valkó, L.R. Snyder, J.L. Glajch, Retention in reversed-phase liquid chromatography as a function of mobile-phase composition, *J. Chromatogr. A.* 656 (1993) 501–520. doi:10.1016/0021-9673(93)80816-Q.
- [40] M. Harnisch, H.J. Möckel, G. Schulze, Relationship between log P_{ow} , shake-flask values and capacity factors derived from reversed-phase high-performance liquid chromatography for n-alkylbenzenes and some oecd reference substances, *J. Chromatogr. A.* 282 (1983) 315–332. doi:10.1016/S0021-9673(00)91610-8.
- [41] K. Valkó, P. Slégel, New chromatographic hydrophobicity index ($\phi\{symbol\}0$) based on the slope and the intercept of the log k' versus organic phase concentration plot, *J. Chromatogr. A.* 631 (1993) 49–61. doi:10.1016/0021-9673(93)80506-4.
- [42] K. Valko, C.M.C.M. Du, C.D.C.D. Bevan, D.P.D.P. Reynolds, M.H.M.H. Abraham, Rapid-Gradient HPLC Method for Measuring Drug Interactions with Immobilized Artificial Membrane: Comparison with Other Lipophilicity Measures, *J. Pharm. Sci.* 89 (2000) 1085–1096. doi:10.1002/1520-6017(200008)89:8<1085::AID-JPS13>3.0.CO;2-N.
- [43] Y. Henchoz, D. Guillarme, S. Rudaz, J.-L.L. Veuthey, P.-A.A. Carrupt, High-throughput log P determination by ultraperformance liquid chromatography: A convenient tool for medicinal chemists, *J. Med. Chem.* 51 (2008) 396–399. doi:10.1021/jm7014809.
- [44] Valko, *Separation Methods in Drug Synthesis and Purification*, Elsevier, 2000.
- [45] K.L. Valkó, Lipophilicity and biomimetic properties measured by HPLC to support drug discovery, *J. Pharm. Biomed. Anal.* 130 (2016) 35–54. doi:10.1016/J.JPBA.2016.04.009.
- [46] F. Lovering, J. Bikker, C. Humblet, Escape from flatland: increasing saturation as an approach to improving clinical success., *J. Med. Chem.* 52 (2009) 6752–6. doi:10.1021/jm901241e.
- [47] G.L. Trainor, The importance of plasma protein binding in drug discovery, *Expert Opin. Drug Discov.* 2 (2007) 51–64. doi:10.1517/17460441.2.1.51.
- [48] M.J. Banker, T.H. Clark, J. a Williams, Development and validation of a 96-well

- equilibrium dialysis apparatus for measuring plasma protein binding., *J. Pharm. Sci.* 92 (2003) 967–74. doi:10.1002/jps.10332.
- [49] J. Barré, J.M. Chamouard, G. Houin, J.P. Tillement, Equilibrium dialysis, ultrafiltration, and ultracentrifugation compared for determining the plasma-protein-binding characteristics of valproic acid, *Clin. Chem.* 31 (1985) 60–64.
- [50] Z.H. Israili, P.G. Dayton, Human alpha-1-glycoprotein and its interactions with drugs., *Drug Metab. Rev.* 33 (2001) 161–235. doi:10.1081/DMR-100104402.
- [51] H. Fuchs, J.-P. Tillement, S. Urien, A. Greischel, W. Roth, Concentration-dependent plasma protein binding of the novel dipeptidyl peptidase 4 inhibitor BI 1356 due to saturable binding to its target in plasma of mice, rats and humans, *J. Pharm. Pharmacol.* 61 (2009) 55–62. doi:10.1211/jpp.61.01.0008.
- [52] T. Edeki, B. Dillon-Moore, N. He, Comparison of Plasma Protein Binding of Basic Drugs in Black and White Individuals., *Am. J. Ther.* 3 (1996) 611–615.
- [53] P.A. McDonnell, G.W. Caldwell, J.A. Masucci, Using capillary electrophoresis/frontal analysis to screen drugs interacting with human serum proteins., *Electrophoresis.* 19 (1998) 448–54. doi:10.1002/elps.1150190315.
- [54] C. Pidgeon, S. Ong, H. Liu, X. Qiu, M. Pidgeon, A.H. Dantzig, J. Munroe, W.J. Hornback, J.S. Kasher, IAM chromatography: an in vitro screen for predicting drug membrane permeability, *J. Med. Chem.* 38 (1995) 590–594. doi:10.1021/jm00004a004.
- [55] K.L. Valko, S.P. Teague, C. Pidgeon, In vitro membrane binding and protein binding (IAM MB/PB technology) to estimate in vivo distribution: applications in early drug discovery, *ADMET DMPK.* 5 (2017) 14. doi:10.5599/admet.5.1.373.
- [56] K. Valko, C.M.M. Du, C. Bevan, D.P.P. Reynolds, M.H.H. Abraham, Rapid method for the estimation of octanol/water partition coefficient (Log P_{oct}) from gradient RP-HPLC retention and a hydrogen bond acidity term ($\sum \alpha^2 H$), *Curr. Med. Chem.* 8 (2001) 1137–1146.
- [57] F. Hollósy, K. Valkó, A. Hersey, S. Nunhuck, G. Kéri, C. Bevan, Estimation of Volume of Distribution in Humans from High Throughput HPLC-Based Measurements of Human Serum Albumin Binding and Immobilized Artificial

- Membrane Partitioning, *J. Med. Chem.* 49 (2006) 6958–6971. doi:10.1021/jm050957i.
- [58] F. Barbato, The use of immobilised artificial membrane (IAM) chromatography for determination of lipophilicity, *Curr. Comput. Aided. Drug Des.* 2 (2006) 341–352. doi:10.2174/157340906778992319.
- [59] F. Barbato, G. di Martino, L. Grumetto, M.I. La Rotonda, Can protonated beta-blockers interact with biomembranes stronger than neutral isolipophilic compounds? A chromatographic study on three different phospholipid stationary phases (IAM-HPLC)., *Eur. J. Pharm. Sci.* 25 (2005) 379–86. doi:10.1016/j.ejps.2005.03.011.
- [60] J. Li, J. Sun, S. Cui, Z. He, Quantitative structure-retention relationship studies using immobilized artificial membrane chromatography I: amended linear solvation energy relationships with the introduction of a molecular electronic factor., *J. Chromatogr. A.* 1132 (2006) 174–82. doi:10.1016/j.chroma.2006.07.073.
- [61] D. Vrakas, C. Giaginis, A. Tsantili-Kakoulidou, Different retention behavior of structurally diverse basic and neutral drugs in immobilized artificial membrane and reversed-phase high performance liquid chromatography: Comparison with octanol-water partitioning, *J. Chromatogr. A.* 1116 (2006) 158–164. doi:10.1016/j.chroma.2006.03.058.
- [62] C. Ottiger, H. Wunderli-Allenspach, Immobilized Artificial Membrane (IAM)-HPLC for Partition Studies of Neutral and Ionized Acids and Bases in Comparison with the Liposomal Partition System, *Pharm. Res.* 16 (n.d.) 643–650. doi:10.1023/A:1018808104653.
- [63] J. Li, J. Sun, Z. He, Quantitative structure-retention relationship studies with immobilized artificial membrane chromatography. II: Partial least squares regression, *J. Chromatogr. A.* 1140 (2007) 174–179. doi:10.1016/j.chroma.2006.11.091.
- [64] L.R. Barbato, F. Interactions of nonsteroidal antiinflammatory drugs with phospholipids: Comparison between octanol/buffer partition coefficients and chromatographic indexes on immobilized artificial membranes, *J Pharm Sci.* 86 (1997) 225–229. doi:10.1021/js960233h.

- [65] F. Hollosy, K. Valko, A. Hersey, S. Nunhuck, G. Keri, C. Bevan, F. Hollósy, K. Valkó, A. Hersey, S. Nunhuck, G. Kéri, C. Bevan, Estimation of Volume of Distribution in Humans from HPLC Measurements of Human Serum Albumin Binding and Immobilized Artificial Membrane Partitioning, *J. Med. Chem.* 49 (2006) 6958–6971. doi:10.1021/jm050957i.
- [66] F. Lombardo, R.S. Obach, M.Y. Shalaeva, F. Gao, Prediction of human volume of distribution values for neutral and basic drugs. 2. Extended data set and leave-class-out statistics., *J. Med. Chem.* 47 (2004) 1242–50. doi:10.1021/jm030408h.
- [67] F. Lombardo, R.S. Obach, M.Y. Shalaeva, F. Gao, Prediction of volume of distribution values in humans for neutral and basic drugs using physicochemical measurements and plasma protein binding data, *J. Med. Chem.* 45 (2002) 2867–2876. doi:10.1021/jm0200409.
- [68] D. Kell, P. Dobson, The cellular uptake of pharmaceutical drugs is mainly carrier-mediated and is thus an issue not so much of biophysics but of systems biology, *Syst. Chem.* (2009) 149–168.
- [69] B.B. BRODIE, H. KURZ, L.S. SCHANKER, The importance of dissociation constant and lipid-solubility in influencing the passage of drugs into the cerebrospinal fluid., *J. Pharmacol. Exp. Ther.* 130 (1960) 20–5.
- [70] D.A. Smith, L. Di, E.H. Kerns, The effect of plasma protein binding on in vivo efficacy: misconceptions in drug discovery, *Nat. Rev. Drug Discov.* 9 (2010) 929–939. doi:10.1038/nrd3287.
- [71] S. Øie, T.N. Tozer, Effect of Altered Plasma Protein Binding on Apparent Volume of Distribution, *J. Pharm. Sci.* 68 (1979) 1203–1205. doi:10.1002/jps.2600680948.
- [72] K.L.K.L. Valkó, S.B.S.B. Nunhuck, A.P.A.P. Hill, Estimating unbound volume of distribution and tissue binding by in vitro HPLC-based human serum albumin and immobilised artificial membrane-binding measurements., *J. Pharm. Sci.* 100 (2011) 849–62. doi:10.1002/jps.22323.
- [73] J.B. Dressman, G.L. Amidon, D. Fleisher, Absorption Potential: Estimating the Fraction Absorbed for Orally Administered Compounds, *J. Pharm. Sci.* 74 (1985) 588–589. doi:10.1002/jps.2600740523.

- [74] N. Ni, T. Sanghvi, S.H. Yalkowsky, Independence of the Product of Solubility and Distribution Coefficient of pH, *Pharm. Res.* 19 (2002) 1862–1866. doi:10.1023/A:1021449709716.
- [75] D. Gonzalez, S. Schmidt, H. Derendorf, Importance of relating efficacy measures to unbound drug concentrations for anti-infective agents., *Clin. Microbiol. Rev.* 26 (2013) 274–88. doi:10.1128/CMR.00092-12.
- [76] X. Liu, O. Vilenski, J. Kwan, S. Apparsundaram, R. Weikert, Unbound brain concentration determines receptor occupancy: a correlation of drug concentration and brain serotonin and dopamine reuptake transporter occupancy for eighteen compounds in rats., *Drug Metab. Dispos.* 37 (2009) 1548–56. doi:10.1124/dmd.109.026674.
- [77] K. Valko, E. Chiarparin, S. Nunhuck, D. Montanari, In Vitro Measurement of Drug Efficiency Index to Aid Early Lead Optimization, *J. Pharm. Sci.* 101 (2012) 4155–4169. doi:10.1002/jps.23305.
- [78] D. Montanari, E. Chiarparin, M.P. Gleeson, S. Braggio, R. Longhi, K. Valko, T. Rossi, Application of drug efficiency index in drug discovery: a strategy towards low therapeutic dose, *Expert Opin. Drug Discov.* 6 (2011) 913–920. doi:10.1517/17460441.2011.602968.
- [79] K.M. Wasan, D.R. Brocks, S.D. Lee, K. Sachs-Barrable, S.J. Thornton, Impact of lipoproteins on the biological activity and disposition of hydrophobic drugs: implications for drug discovery., *Nat. Rev. Drug Discov.* 7 (2008) 84–99. doi:10.1038/nrd2353.
- [80] T.T. Wager, B.L. Kormos, J.T. Brady, Y. Will, M.D. Aleo, D.B. Stedman, M. Kuhn, R.Y. Chandrasekaran, Improving the odds of success in drug discovery: Choosing the best compounds for in vivo toxicology studies, *J. Med. Chem.* 56 (2013) 9771–9779. doi:10.1021/jm401485p.
- [81] T.T. Wager, B.L. Kormos, J.T. Brady, Y. Will, M.D. Aleo, D.B. Stedman, M. Kuhn, R.Y. Chandrasekaran, Improving the Odds of Success in Drug Discovery: Choosing the Best Compounds for in Vivo Toxicology Studies, *J. Med. Chem.* 56 (2013) 9771–9779. doi:10.1021/jm401485p.
- [82] I. Mahmood, J.D. Balian, The pharmacokinetic principles behind scaling from

- preclinical results to phase I protocols, *Clin. Pharmacokinet.* 36 (1999) 1–11. doi:10.2165/00003088-199936010-00001.
- [83] I. Mahmood, Prediction of Clearance, Volume of Distribution and Half-life by Allometric Scaling and by use of Plasma Concentrations Predicted from Pharmacokinetic Constants: a Comparative Study, *J. Pharm. Pharmacol.* 51 (1999) 905–910. doi:10.1211/0022357991773320.
- [84] J. Mordenti, Man versus beast: pharmacokinetic scaling in mammals., *J. Pharm. Sci.* 75 (1986) 1028–1040. doi:10.1002/jps.2600751104.
- [85] H.M. Jones, N. Parrott, K. Jorga, T. Lavé, A novel strategy for physiologically based predictions of human pharmacokinetics, *Clin. Pharmacokinet.* 45 (2006) 511–542. doi:10.2165/00003088-200645050-00006.
- [86] F.-P. Theil, T.W. Guentert, S. Haddad, P. Poulin, Utility of physiologically based pharmacokinetic models to drug development and rational drug discovery candidate selection., *Toxicol. Lett.* 138 (2003) 29–49. doi:10.1016/S0378-4274(02)00374-0.
- [87] C. Chen, X. Fang, Y. Wang, Y. Li, D. Wang, X. Zhao, C. Bai, X. Wang, Preventive and therapeutic effects of phosphoinositide 3-kinase inhibitors on acute lung injury, *Chest.* 140 (2011) 391–400. doi:10.1378/chest.10-3060.
- [88] E.J. Yoo, C.A. Ojiaku, K. Sunder, R.A. Panettieri, Jr., Phosphoinositide 3-Kinase in Asthma: Novel Roles and Therapeutic Approaches., *Am. J. Respir. Cell Mol. Biol.* 56 (2017) 700–707. doi:10.1165/rcmb.2016-0308TR.
- [89] D.I. Kim, S.R. Kim, H.J. Kim, S.J. Lee, H.B. Lee, S.J. Park, M.J. Im, Y.C. Lee, PI3K- γ inhibition ameliorates acute lung injury through regulation of I κ B α /NF- κ B pathway and innate immune responses, *J. Clin. Immunol.* 32 (2012) 340–351. doi:10.1007/s10875-011-9628-1.
- [90] K.J.S. Martin, M.J. Muessel, C.E. Pullar, G.B. Willars, A.J. Wardlaw, The Role of Phosphoinositide 3-Kinases in Neutrophil Migration in 3D Collagen Gels, *PLoS One.* 10 (2015) e0116250. doi:10.1371/journal.pone.0116250.
- [91] L.P. Sousa, F. Lopes, D.M. Silva, L.P. Tavares, A.T. Vieira, B.M. Rezende, A.F. Carmo, R.C. Russo, C.C. Garcia, C.A. Bonjardim, A.L. Alessandri, A.G. Rossi, V.

- Pinho, M.M. Teixeira, PDE4 inhibition drives resolution of neutrophilic inflammation by inducing apoptosis in a PKA-PI3K/Akt-dependent and NF- κ B-independent manner, *J. Leukoc. Biol.* 87 (2010) 895–904. doi:10.1189/jlb.0809540.
- [92] S. Chollet-Martin, P. Montravers, C. Gibert, C. Elbim, J.M. Desmots, J.Y. Fagon, M.A. Gougerot-Pocidaló, Subpopulation of Hyperresponsive Polymorphonuclear Neutrophils in Patients with Adult Respiratory Distress Syndrome: Role of Cytokine Production, *Am. Rev. Respir. Dis.* 146 (1992) 990–996. doi:10.1164/ajrccm/146.4.990.
- [93] J.E. Weiland, W.B. Davis, J.F. Holter, J.R. Mohammed, P.M. Dorinsky, J.E. Gadek, Lung neutrophils in the adult respiratory distress syndrome. Clinical and pathophysiologic significance., *Am. Rev. Respir. Dis.* 133 (1986) 218–25. doi:10.1164/arrd.1986.133.2.218.
- [94] K.P. Steinberg, J.A. Milberg, T.R. Martin, R.J. Maunder, B.A. Cockrill, L.D. Hudson, Evolution of bronchoalveolar cell populations in the adult respiratory distress syndrome., *Am. J. Respir. Crit. Care Med.* 150 (1994) 113–22. doi:10.1164/ajrccm.150.1.8025736.
- [95] A.-K. Stark, S. Sriskantharajah, E.M. Hessel, K. Okkenhaug, PI3K inhibitors in inflammation, autoimmunity and cancer, *Curr. Opin. Pharmacol.* 23 (2015) 82–91. doi:10.1016/J.COPH.2015.05.017.
- [96] S.J. PARK, K.H. MIN, Y.C. LEE, Phosphoinositide 3-kinase δ inhibitor as a novel therapeutic agent in asthma, *Respiology.* 13 (2008) 764–771. doi:10.1111/j.1440-1843.2008.01369.x.
- [97] M. Takeda, W. Ito, M. Tanabe, S. Ueki, J. Kihara, H. Kato, T. Tanigai, H. Kayaba, T. Sasaki, J. Chihara, The pathophysiological roles of PI3Ks and therapeutic potential of selective inhibitors in allergic inflammation., *Int. Arch. Allergy Immunol.* 152 Suppl (2010) 90–5. doi:10.1159/000312132.
- [98] T. Southworth, J. Plumb, V. Gupta, J. Pearson, I. Ramis, M.D. Lehner, M. Miralpeix, D. Singh, Anti-inflammatory potential of PI3K δ and JAK inhibitors in asthma patients, *Respir. Res.* 17 (2016) 124. doi:10.1186/s12931-016-0436-2.
- [99] A.-K. Stark, A. Chandra, K. Chakraborty, R. Alam, V. Carbonaro, J. Clark, S. Sriskantharajah, G. Bradley, A.G. Richter, E. Banham-Hall, M.R. Clatworthy, S.

- Nejentsev, J.N. Hamblin, E.M. Hessel, A.M. Condliffe, K. Okkenhaug, PI3K δ hyper-activation promotes development of B cells that exacerbate *Streptococcus pneumoniae* infection in an antibody-independent manner, *Nat. Commun.* 9 (2018) 3174. doi:10.1038/s41467-018-05674-8.
- [100] J.D. Clark, M.E. Flanagan, J.-B. Telliez, Discovery and Development of Janus Kinase (JAK) Inhibitors for Inflammatory Diseases, *J. Med. Chem.* 57 (2014) 5023–5038. doi:10.1021/jm401490p.
- [101] Q. Yang, P. Modi, T. Newcomb, C. Qu??va, V. Gandhi, Idelalisib: First-in-class PI3K delta inhibitor for the treatment of chronic lymphocytic leukemia, small lymphocytic leukemia, and follicular lymphoma, *Clin. Cancer Res.* 21 (2015) 1537–1542. doi:10.1158/1078-0432.CCR-14-2034.
- [102] N.G. Papadopoulos, I. Agache, S. Bavbek, B.M. Biló, F. Braido, V. Cardona, A. Custovic, J. deMonchy, P. Demoly, P. Eigenmann, J. Gayraud, C. Grattan, E. Heffler, P.W. Hellings, M. Jutel, E. Knol, J. Lötval, A. Muraro, L.K. Poulsen, G. Roberts, P. Schmid-Grendelmeier, C. Skevaki, M. Triggiani, R. vanRee, T. Werfel, B. Flood, S. Palkonen, R. Savli, P. Allegri, I. Annesi-Maesano, F. Annunziato, D. Antolin-Amerigo, C. Apfelbacher, M. Blanca, E. Bogacka, P. Bonadonna, M. Bonini, O. Boyman, K. Brockow, P. Burney, J. Buters, I. Butiene, M. Calderon, L. Cardell, J.-C. Caubet, S. Celenk, E. Cichocka-Jarosz, C. Cingi, M. Couto, N. deJong, S. Del Giacco, N. Douladiris, F. Fassio, J.-L. Fauquert, J. Fernandez, M. Rivas, M. Ferrer, C. Flohr, J. Gardner, J. Genuneit, P. Gevaert, A. Groblewska, E. Hamelmann, H. Hoffmann, K. Hoffmann-Sommergruber, L. Hovhannisyán, V. Hox, F.L. Jahnsen, Ö. Kalayci, A. Kalpaklioglu, J. Kleine-Tebbe, G. Konstantinou, M. Kurowski, S. Lau, R. Lauener, A. Lauerma, K. Logan, A. Magnan, J. Makowska, H. Makrinioti, P. Mangina, F. Manole, A. Mari, A. Mazon, C. Mills, E. Mingomataj, B. Niggemann, G. Nilsson, M. Ollert, L. O'Mahony, S. O'Neil, G. Pala, A. Papi, G. Passalacqua, M. Perkin, O. Pfaar, C. Pitsios, S. Quirce, U. Raap, M. Raulf-Heimsoth, C. Rhyner, P. Robson-Ansley, R. Alves, Z. Roje, C. Rondon, O. Rudzeviciene, F. Ruëff, M. Rukhadze, G. Rumi, C. Sackesen, A.F. Santos, A. Santucci, C. Scharf, C. Schmidt-Weber, B. Schnyder, J. Schwarze, G. Senna, S. Sergejeva, S. Seys, A. Siracusa, I. Skypala, M. Sokolowska, F. Spertini, R. Spiewak, A. Sprickelman, G. Sturm, I. Swoboda, I. Terreehorst, E. Toskala, C. Traidl-Hoffmann, C. Venter, B. Vlieg-Boerstra, P. Whitacker, M. Worm, P.

- Xepapadaki, C.A. Akdis, Research needs in allergy: an EAACI position paper, in collaboration with EFA, *Clin. Transl. Allergy*. 2 (2012) 21. doi:10.1186/2045-7022-2-21.
- [103] I.M. Keith, E.B. Olson, N.M. Wilson, C.R. Jefcoate, Immunological identification and effects of 3-methylcholanthrene and phenobarbital on rat pulmonary cytochrome P-450., *Cancer Res*. 47 (1987) 1878–82.
- [104] A. Tronde, B. Nordén, H. Marchner, A. Wendel, H. Lennernäs, U.H. Bengtsson, Pulmonary Absorption Rate and Bioavailability of Drugs in Vivo in Rats: Structure–Absorption Relationships and Physicochemical Profiling of Inhaled Drugs, *J. Pharm. Sci.* 92 (2003) 1216–1233. doi:10.1002/jps.10386.
- [105] C.D. Edwards, C. Luscombe, P. Eddershaw, E.M. Hessel, Development of a Novel Quantitative Structure-Activity Relationship Model to Accurately Predict Pulmonary Absorption and Replace Routine Use of the Isolated Perfused Respiring Rat Lung Model, *Pharm. Res.* 33 (2016) 2604–2616. doi:10.1007/s11095-016-1983-4.
- [106] J.S. Patton, C.S. Fishburn, J.G. Weers, The Lungs as a Portal of Entry for Systemic Drug Delivery, *Proc. Am. Thorac. Soc.* 1 (2004) 338–344. doi:10.1513/pats.200409-049TA.
- [107] S. Endter, U. Becker, N. Daum, H. Huwer, C.-M. Lehr, M. Gumbleton, C. Ehrhardt, P-glycoprotein (MDR1) functional activity in human alveolar epithelial cell monolayers, *Cell Tissue Res*. 328 (2007) 77–84. doi:10.1007/s00441-006-0346-6.
- [108] E.R. Weibel, Morphometry of the human lung: the state of the art after two decades., *Bull. Eur. Physiopathol. Respir.* 15 (1979) 999–1013. <http://www.ncbi.nlm.nih.gov/pubmed/389332>.
- [109] S. Ganesan, A.T. Comstock, U.S. Sajjan, Barrier function of airway tract epithelium., *Tissue Barriers*. 1 (2013) e24997. doi:10.4161/tisb.24997.
- [110] J.C. Hogg, Response of the lung to inhaled particles., *Med. J. Aust.* 142 (1985) 675–8.
- [111] J.S. Patton, P.R. Byron, Inhaling medicines: delivering drugs to the body through the lungs, *Nat. Rev. Drug Discov.* 6 (2007) 67–74. doi:10.1038/nrd2153.

- [112] M. Geiser, M. Casaulta, B. Kupferschmid, H. Schulz, M. Semmler-Behnke, W. Kreyling, The Role of Macrophages in the Clearance of Inhaled Ultrafine Titanium Dioxide Particles, *Am. J. Respir. Cell Mol. Biol.* 38 (2008) 371–376. doi:10.1165/rcmb.2007-0138OC.
- [113] D.J. Lewis, T.C. Williams, S.L. Beck, Foamy macrophage responses in the rat lung following exposure to inhaled pharmaceuticals: A simple, pragmatic approach for inhaled drug development, *J. Appl. Toxicol.* 34 (2014) 319–331. doi:10.1002/jat.2950.
- [114] B. Forbes, B. Asgharian, L.A. Dailey, D. Ferguson, P. Gerde, M. Gumbleton, L. Gustavsson, C. Hardy, D. Hassall, R. Jones, R. Lock, J. Maas, T. McGovern, G.R. Pitcairn, G. Somers, R.K. Wolff, Challenges in inhaled product development and opportunities for open innovation, *Adv. Drug Deliv. Rev.* 63 (2011) 69–87. doi:10.1016/j.addr.2010.11.004.
- [115] B. Forbes, R. O'Lone, P.P. Allen, A. Cahn, C. Clarke, M. Collinge, L.A. Dailey, L.E. Donnelly, J. Dybowski, D. Hassall, D. Hildebrand, R. Jones, J. Kilgour, J. Klapwijk, C.C. Maier, T. McGovern, K. Nikula, J.D. Parry, M.D. Reed, I. Robinson, L. Tomlinson, A. Wolfreys, Challenges for inhaled drug discovery and development: Induced alveolar macrophage responses, *Adv. Drug Deliv. Rev.* 71 (2014) 15–33. doi:10.1016/J.ADDR.2014.02.001.
- [116] J.S. Patton, J.D. Brain, L. a Davies, J. Fiegel, M. Gumbleton, K.-J. Kim, M. Sakagami, R. Vanbever, C. Ehrhardt, The particle has landed--characterizing the fate of inhaled pharmaceuticals., *J. Aerosol Med. Pulm. Drug Deliv.* 23 Suppl 2 (2010) S71-87. doi:10.1089/jamp.2010.0836.
- [117] H. Marchner, A. Wendel, H. Lennerna, A.N.N. Tronde, B.O. Norde, U.H. Bengtsson, Pulmonary Absorption Rate and Bioavailability of Drugs In Vivo in Rats : Structure – Absorption Relationships and Physicochemical Profiling of Inhaled Drugs, 92 (2003) 1216–1233.
- [118] D.F. Price, C.N. Luscombe, P.J. Eddershaw, C.D. Edwards, M. Gumbleton, The Differential Absorption of a Series of P-Glycoprotein Substrates in Isolated Perfused Lungs from Mdr1a/1b Genetic Knockout Mice can be Attributed to Distinct Physico-Chemical Properties: an Insight into Predicting Transporter-Mediated, Pulmonary Speci, *Pharm. Res.* (2017) 1–19. doi:10.1007/s11095-017-

2220-5.

- [119] T.J. Ritchie, C.N. Luscombe, S.J.F. Macdonald, Analysis of the calculated physicochemical properties of respiratory drugs: Can we design for inhaled drugs yet?, *J. Chem. Inf. Model.* 49 (2009) 1025–1032. doi:10.1021/ci800429e.
- [120] T.J. Ritchie, C.N. Luscombe, S.J.F. Macdonald, T.J. Ritchie, C.N. Luscombe, S.J.F. Macdonald, Analysis of the Calculated Physicochemical Properties of Respiratory Drugs: Can We Design for Inhaled Drugs Yet? Analysis of the Calculated Physicochemical Properties of Respiratory Drugs: Can We Design for Inhaled Drugs Yet ?, (2009) 1025–1032. doi:10.1021/ci800429e.
- [121] A. Kestranek, A. Chervenak, J. Longenberger, S. Placko, Chemiluminescent nitrogen detection (CLND) to measure kinetic aqueous solubility, *Curr. Protoc. Chem. Biol.* 5 (2013). doi:10.1002/9780470559277.ch130145.
- [122] D.F. Veber, S.R. Johnson, H. Cheng, B.R. Smith, K.W. Ward, K.D. Kopple, Molecular Properties That Influence the Oral Bioavailability of Drug Candidates, *J. Med. Chem.* 45 (2002) 2615–2623. doi:10.1021/jm020017n.
- [123] R.S. Obach, Prediction of human clearance of twenty-nine drugs from hepatic microsomal intrinsic clearance data: An examination of in vitro half-life approach and nonspecific binding to microsomes, *Drug Metab. Dispos.* 27 (1999) 1350–1359. doi:10.1124/dmd.30.7.831.
- [124] R.L. Walsky, R.S. Obach, R. Gallegos, V. Uttamsingh, C.Q. Xia, G.T. Miwa, S.K. Balani, L.-S. Gan, VALIDATED ASSAYS FOR HUMAN CYTOCHROME P450 ACTIVITIES, *Drug Metab. Dispos.* 32 (2004) 647–660. doi:10.1124/dmd.32.6.647.
- [125] Y. Moriwaki, T. Yamamoto, S. Takahashi, Z. Tsutsumi, T. Hada, Widespread cellular distribution of aldehyde oxidase in human tissues found by immunohistochemistry staining., *Histol. Histopathol.* 16 (2001) 745–753. <http://www.ncbi.nlm.nih.gov/pubmed/11510964> (accessed February 15, 2017).
- [126] C. Beedham, S.E. Bruce, D.J. Critchley, Y. Al-Tayib, D.J. Rance, Species variation in hepatic aldehyde oxidase activity., *Eur. J. Drug Metab. Pharmacokinet.* 12 (n.d.) 307–10. <http://www.ncbi.nlm.nih.gov/pubmed/3130251> (accessed April 6, 2018).
- [127] J.C. Kalvass, T.S. Maurer, Influence of nonspecific brain and plasma binding on

- CNS exposure: Implications for rational drug discovery, *Biopharm. Drug Dispos.* 23 (2002) 327–338. doi:10.1002/bdd.325.
- [128] M. B., H.J. Clewell III, T. Lave, M. E., Physiologically Based Pharmacokinetic Modeling: A Tool for Understanding ADMET Properties and Extrapolating to Human, in: *New Insights into Toxic. Drug Test.*, InTech, 2013. doi:10.5772/54965.
- [129] T. Bohnert, L. Gan, Plasma protein binding: From discovery to development, *J. Pharm. Sci.* 102 (2013) 2953–2994. doi:10.1002/jps.23614.
- [130] I. Poggesi, Predicting human pharmacokinetics from preclinical data., *Curr. Opin. Drug Discov. Devel.* 7 (2004) 100–111.
- [131] L.X. Yu, G.L. Amidon, A compartmental absorption and transit model for estimating oral drug absorption, *Int. J. Pharm.* 186 (1999) 119–125. doi:10.1016/S0378-5173(99)00147-7.
- [132] N. Gobeau, R. Stringer, S. De Buck, T. Tuntland, B. Faller, Evaluation of the GastroPlus™ Advanced Compartmental and Transit (ACAT) Model in Early Discovery, *Pharm. Res.* 33 (2016) 2126–2139. doi:10.1007/s11095-016-1951-z.
- [133] R.A. Parent, A. Studholme, Comparative biology of the normal lung, n.d.
- [134] B. Davies, T. Morris, Physiological parameters in laboratory animals and humans, *Pharm. Res.* 10 (1993) 1093–1095. doi:10.1023/A:1018943613122.
- [135] K. Valko, C.M. Du, C.D. Bevan, D.P. Reynolds, M.H. Abraham, Rapid-gradient HPLC method for measuring drug interactions with immobilized artificial membrane: Comparison with other lipophilicity measures, *J. Pharm. Sci.* 89 (2000) 1085–1096. doi:10.1002/1520-6017(200008)89:8<1085::AID-JPS13>3.0.CO;2-N.
- [136] K. Valko, S. Nunhuck, C. Bevan, M.H.M.H. Abraham, D.P.D.P. Reynolds, Fast Gradient HPLC Method to Determine Compounds Binding to Human Serum Albumin. Relationships with Octanol/Water and Immobilized Artificial Membrane Lipophilicity, *J. Pharm. Sci.* 92 (2003) 2236–2248. doi:10.1002/jps.10494.
- [137] K. Valkó, Chromatographic hydrophobicity index by fast-gradient RP-HPLC: A high-throughput alternative to log P/log D, *Anal. Chem.* 69 (1997) 2022–2029.
- [138] K. Valko, C.C.M.M. Du, C. Bevan, D.D.P.P. Reynolds, M.H.H.M. Abraham, Rapid

method for the estimation of octanol/water partition coefficient (Log Poct) from gradient RP-HPLC retention and a hydrogen bond acidity term ($\sum\alpha_2H$), *Curr. Med. Chem.* 8 (2001) 1137–1146. doi:10.2174/0929867013372643.

- [139] L. Jacobson, B. Middleton, J. Holmgren, S. Eirefelt, M. Fröjd, A. Blomgren, L. Gustavsson, An optimized automated assay for determination of metabolic stability using hepatocytes: assay validation, variance component analysis, and in vivo relevance., *Assay Drug Dev. Technol.* 5 (2007) 403–15. doi:10.1089/adt.2007.059.
- [140] E. Garattini, M. Terao, Increasing recognition of the importance of aldehyde oxidase in drug development and discovery., *Drug Metab. Rev.* 43 (2011) 374–386. doi:10.3109/03602532.2011.560606.
- [141] D.C. Pryde, D. Dalvie, Q. Hu, P. Jones, R.S. Obach, T.D. Tran, Aldehyde oxidase: An enzyme of emerging importance in drug discovery, *J. Med. Chem.* 53 (2010) 8441–8460. doi:10.1021/jm100888d.
- [142] D.C. Pryde, T.D. Tran, P. Jones, J. Duckworth, M. Howard, I. Gardner, R. Hyland, R. Webster, T. Wenham, S. Bagal, K. Omoto, R.P. Schneider, J. Lin, Medicinal chemistry approaches to avoid aldehyde oxidase metabolism, *Bioorganic Med. Chem. Lett.* 22 (2012) 2856–2860. doi:10.1016/j.bmcl.2012.02.069.
- [143] E. Garattini, M. Fratelli, M. Terao, Mammalian aldehyde oxidases: Genetics, evolution and biochemistry, *Cell. Mol. Life Sci.* 65 (2008) 1019–1048. doi:10.1007/s00018-007-7398-y.
- [144] N.E. Austin, S.J. Baldwin, L. Cutler, N. Deeks, P.J. Kelly, M. Nash, C.E. Shardlow, G. Stemp, K. Thewlis, A. Ayrton, P. Jeffrey, Pharmacokinetics of the novel, high-affinity and selective dopamine D3 receptor antagonist SB-277011 in rat, dog and monkey: in vitro/in vivo correlation and the role of aldehyde oxidase, *Xenobiotica.* 31 (2001) 677–686. doi:10.1080/00498250110056531.
- [145] B. Kaye, J.L. Offerman, J.L. Reid, H.L. Elliott, W.S. Hillis, A species difference in the presystemic metabolism of carbazeran in dog and man, *Xenobiotica.* 14 (1984) 935–945. doi:10.3109/00498258409151492.
- [146] C. Yung-Chi, W.H. Prusoff, Relationship between the inhibition constant (KI) and the concentration of inhibitor which causes 50 per cent inhibition (I50) of an

- enzymatic reaction, *Biochem. Pharmacol.* 22 (1973) 3099–3108. doi:10.1016/0006-2952(73)90196-2.
- [147] I. Mahmood, J.D. Balian, Interspecies scaling : predicting clearance of drugs in humans . Three different approaches ?, 26 (1996) 887–895.
- [148] R.S. Obach, J.G. Baxter, T.E. Liston, B.M. Silber, B.C. Jones, F.M.A.C. Intyre, D.J. Rance, P. Wastall, The Prediction of Human Pharmacokinetic Parameters from Preclinical and In Vitro Metabolism Data, 283 (1997) 46–58.
- [149] C. Ehrhardt, P. Bäckman, W. Couet, C. Edwards, B. Forbes, M. Fridén, M. Gumbleton, K.I. Hosoya, Y. Kato, T. Nakanishi, M. Takano, T. Terasaki, R. Yumoto, Current Progress Toward a Better Understanding of Drug Disposition Within the Lungs: Summary Proceedings of the First Workshop on Drug Transporters in the Lungs, *J. Pharm. Sci.* 106 (2017) 2234–2244. doi:10.1016/j.xphs.2017.04.011.
- [150] K. Valkó, Physicochemical and biomimetic properties in drug discovery : chromatographic techniques for lead optimization, in: Wiley Hoboken NJ, 2014: p. 450.
- [151] G.I. Somers, N. Lindsay, B.M. Lowdon, A.E. Jones, C. Freathy, S. Ho, A.J.M. Woodrooffe, M.K. Bayliss, G.R. Manchee, A comparison of the expression and metabolizing activities of phase I and II enzymes in freshly isolated human lung parenchymal cells and cryopreserved human hepatocytes., *Drug Metab. Dispos.* 35 (2007) 1797–805. doi:10.1124/dmd.107.015966.
- [152] D. Dalvie, C. Xiang, P. Kang, S. Zhou, Interspecies variation in the metabolism of zoniporide by aldehyde oxidase, *Xenobiotica.* 43 (2013) 1–10. doi:10.3109/00498254.2012.727499.
- [153] R.A. Torres, K.R. Korzekwa, D.R. McMasters, C.M. Fandozzi, J.P. Jones, Use of density functional calculations to predict the regioselectivity of drugs and molecules metabolized by aldehyde oxidase, *J. Med. Chem.* 50 (2007) 4642–4647. doi:10.1021/jm0703690.
- [154] C. Coelho, A. Foti, T. Hartmann, T. Santos-Silva, S. Leimkühler, M.J. Romão, Structural insights into xenobiotic and inhibitor binding to human aldehyde oxidase., *Nat. Chem. Biol.* 11 (2015) 779–83. doi:10.1038/nchembio.1895.

- [155] J.E. Sager, J. Yu, I. Ragueneau-Majlessi, N. Isoherranen, Physiologically Based Pharmacokinetic (PBPK) Modeling and Simulation Approaches: A Systematic Review of Published Models, Applications, and Model Verification., *Drug Metab. Dispos.* 43 (2015) 1823–37. doi:10.1124/dmd.115.065920.
- [156] D.E. Mager, E. Wyska, W.J. Jusko, Diversity of mechanism-based pharmacodynamic models., *Drug Metab. Dispos.* 31 (2003) 510–8. doi:10.1124/DMD.31.5.510.
- [157] N.L. Dayneka, V. Garg, W.J. Jusko, Comparison of four basic models of indirect pharmacodynamic responses., *J. Pharmacokinet. Biopharm.* 21 (1993) 457–78. <http://www.ncbi.nlm.nih.gov/pubmed/8133465> (accessed September 18, 2018).
- [158] A. Kotsimbos, Q. Hamid, IL-5 and IL-5 receptor in asthma, *Mem. Inst. Oswaldo Cruz.* 92 (1997) 75–91. doi:10.1590/S0074-02761997000800012.
- [159] N. Debeuf, E. Haspeslagh, M. van Helden, H. Hammad, B.N. Lambrecht, Mouse Models of Asthma, in: *Curr. Protoc. Mouse Biol.*, John Wiley & Sons, Inc., Hoboken, NJ, USA, 2016: pp. 169–184. doi:10.1002/cpmo.4.
- [160] I. Torjesen, Drug development: the journey of a medicine from lab to shelf, *Pharm. J.* (2015). <https://www.pharmaceutical-journal.com/publications/tomorrows-pharmacist/drug-development-the-journey-of-a-medicine-from-lab-to-shelf/20068196.article>.
- [161] M.J. Waring, J. Arrowsmith, A.R. Leach, P.D. Leeson, S. Mandrell, R.M. Owen, G. Pairaudeau, W.D. Pennie, S.D. Pickett, J. Wang, O. Wallace, A. Weir, An analysis of the attrition of drug candidates from four major pharmaceutical companies, *Nat. Rev. Drug Discov.* 14 (2015) 475–486. doi:10.1038/nrd4609.
- [162] I. Kola, J. Landis, Can the pharmaceutical industry reduce attrition rates?, *Nat. Rev. Drug Discov.* 3 (2004) 711–716. doi:10.1038/nrd1470.
- [163] D. Cook, D. Brown, R. Alexander, R. March, P. Morgan, G. Satterthwaite, M.N. Pangalos, Lessons learned from the fate of AstraZeneca’s drug pipeline: a five-dimensional framework., *Nat. Rev. Drug Discov.* 13 (2014) 419–31. doi:10.1038/nrd4309.
- [164] E. Garattini, M. Terao, The role of aldehyde oxidase in drug metabolism, *Expert*

Opin. Drug Metab. Toxicol. 8 (2012) 487–503.
doi:10.1517/17425255.2012.663352.

- [165] P. Buchwald, N. Bodor, Recent advances in the design and development of soft drugs., *Pharmazie*. 69 (2014) 403–13. doi:10.1691/ph.2014.3911R.
- [166] J. Gabrielsson, H. Dolgos, P.-G. Gillberg, U. Bredberg, B. Benthem, G. Duker, Early integration of pharmacokinetic and dynamic reasoning is essential for optimal development of lead compounds: strategic considerations, *Drug Discov. Today*. 14 (2009) 358–372. doi:10.1016/J.DRUDIS.2008.12.011.
- [167] L. Aarons, Physiologically based pharmacokinetic modelling: a sound mechanistic basis is needed., *Br. J. Clin. Pharmacol.* 60 (2005) 581–3. doi:10.1111/j.1365-2125.2005.02560.x.

13 Published Work

13.1 How to identify and eliminate compounds with a risk of high clinical dose during the early phase of lead optimisation in drug discovery

European Journal of Pharmaceutical Sciences 110 (2017) 37–50



Contents lists available at ScienceDirect
European Journal of Pharmaceutical Sciences

journal homepage: www.elsevier.com/locate/ejps



How to identify and eliminate compounds with a risk of high clinical dose during the early phase of lead optimisation in drug discovery



Simon Teague^{a,*}, Klara Valko^b

^a GlaxoSmithKline Medicine Research Centre, Stevenage, Hertfordshire, UK

^b Research Department of Pharmaceutical and Biological Chemistry, UCL School of Pharmacy, London, UK

ARTICLE INFO

Article history:
Received 24 November 2016
Received in revised form 8 February 2017
Accepted 9 February 2017
Available online 12 February 2017

Keywords:
Dose estimation
Drug efficiency
PK parameters
Free concentration
Minimal effective concentration

ABSTRACT

An alternative approach has been developed to estimate the clinical dose of new drug molecules at an early stage in the drug discovery process. This approach has been compared to traditional methods using the clinical dose as indicated on the drug label of 136 marketed drugs. At the early stages of drug discovery only *in silico* predictions or some initial *in vitro* screening data are normally available, typically parameters such as affinity/potency (pXC50) from isolated enzymes or receptors, measured albumin and phospholipid binding using biomimetic HPLC measurements, and *in vitro* clearance using P450 enzymes or liver microsomes. The combination of the biomimetic HPLC phospholipid and protein binding provides a drug efficiency max parameter described previously (HPLC DE_{max}), and *in vitro* potency makes it possible to estimate a clinical dose that would result in an efficacious steady state free concentration at the site of action. The influence of the potential discrepancies between the *in vitro* and a later stage *in vivo* DE_{max}, the whole blood potency, volume of distribution and clearance on the dose estimation has been investigated, using data from a GSK programme profiled during lead optimisation. It was found that drug potency had the greatest influence on estimating the clinical dose. When the estimated dose is low, the impact of other parameters such as the volume of distribution and clearance was much less significant and typically did not affect compound ranking.

© 2017 Elsevier B.V. All rights reserved.

1. Introduction

When designing a new drug molecule the ultimate goal for the research team is to achieve the maximum safe and effective biological response with the smallest possible amount of drug administered (Tam, 2013). The low dose helps to reduce the potential risk of toxicity (Hughes et al., 2008; Wager et al., 2013) and the risk of potentially unwanted secondary pharmacology. Therefore, the ability to predict human clinical dose with a reasonable degree of confidence, and use this information when progressing new chemical entities as early as possible during lead optimisation is important (McGinnity et al., 2007; Page, 2016). The most common approach to reducing the clinical dose is to design highly potent and selective compounds that engage the target at very low blood or tissue concentrations, normally in the low nanomolar range. However, this alone does not guarantee a low dose, if the drug molecule cannot reach the site of action at the required concentration due to poor absorption, a sub-optimal pharmacokinetic profile (high clearance, poor distribution profile).

Targeting a low dose and exposure is important to avoid adverse effects. The study of Wager et al. (2013) showed that the occurrence of *in*

vivo toxicity correlated with the exposure. They found that if the total human efficacious concentration was <250 nM and the free drug concentration was <40 nM, the failure rate of exploratory compounds due to animal toxicity was reduced significantly. The drug efficiency (DRUG_{eff}) concept introduced by Braggio et al. (2010), was proposed as a new tool to guide drug discovery program teams, as it relates to the free drug concentration in the target bio-phase relative to the administered dose (Fig. 1 and Eq. (1)).

$$\text{DRUG}_{\text{eff}} = \frac{\text{free biophase conc}}{\text{Dose}} \quad (1)$$

From *in vitro* potency measurements, we can estimate the efficacious concentration of the compound that sufficiently engages the target to produce a certain response. Under *in vitro* assay conditions, DRUG_{eff} is typically >99%, with any non-specific binding having only a marginal impact on the free concentration. However, at this stage, it is very difficult to estimate the dose that will be required to produce an equivalent efficacious free bio-phase concentration *in vivo*. Valko et al. (2012) described how it is possible to estimate the maximum DRUG_{eff} *in vitro* by measuring a compound's non-specific binding to phospholipids and albumin type of proteins. The DRUG_{eff,max} would be achieved when oral absorption is 100%, and there are no permeability barriers or

* Corresponding author.
E-mail address: Simon.P.Teague@gsk.com (S. Teague).

13.2 *In vitro* membrane binding and protein binding (IAM MB/PB technology) to estimate *in vivo* distribution: applications in early drug discovery

ADMET & DMPK 5(1) (2017) 14-38; doi: 10.5599/admet.5.1.373

ADMET

Open Access : ISSN : 1848-7718

<http://www.pub.lapchem.org/ojs/index.php/admet/index>

Original scientific paper

***In vitro* membrane binding and protein binding (IAM MB/PB technology) to estimate *in vivo* distribution: applications in early drug discovery**

Klara Valko^{*1}, Simon Teague², and Charles Pidgeon³

¹Bio-Mimetic Chromatography, Unit 5B Business & Technology Centre, Stevenage, SG1 2DX Hertfordshire United Kingdom

²GlaxoSmithKline, Stevenage, United Kingdom

³Independent Researcher, affiliate of Regis Technologies Inc, Morton Grove, IL 60052 USA

*Corresponding Author: E-mail: Klara_Valko@bio-mimetic-chromatography.com; Tel.: +44-7521989558;

Received: February 07, 2017; Revised: March 14, 2017; Published: March 25, 2017

Abstract

The drug discovery process can be accelerated by chromatographic profiling of the analogs to model *in vivo* distribution and the major non-specific binding. A balanced potency and chromatographically determined membrane and protein binding (IAM MB/PB) data enable selecting drug discovery compounds for further analysis that have the highest probability to show the desired *in vivo* distribution behavior for efficacy and reduced chance for toxicity. Although the basic principles of the technology have already appeared in numerous publications, the lack of standardized procedures limited its widespread applications especially in academia and small drug discovery biotech companies. In this paper, the standardized procedures are described that has been trademarked as Regis IAM MB/PB Technology®. Comparison between the Drug Efficiency Index (DEI=spIC50-logVdu+2) and generally used Ligand Lipophilicity Efficiency (LLE) has been made, demonstrating the advantage of measured IAM and HSA binding over calculated log P. The power of the proposed chromatographic technology is demonstrated using the data of marketed drugs.

Keywords

Drug efficiency; Biomimetic properties by HPLC; unbound volume of distribution; *in vivo* distribution

Introduction

Medicinal chemists face multi-factorial challenge problems when designing drug molecules that can reduce the impact or cure a pathological condition; drug discovery scientists seek the smallest possible dose with minimal side effects [1-4]. Screening cascades often generate vast quantities of primarily *in-vitro* data, and in some cases, *in vivo* data on compounds that form a decision on which compounds are selected for further progression. This paper documents an alternative screening triage which can help to avoid the problem of analysing too much discovery data when choosing lead compounds to pursue.

Chemical structure design of discovery molecules usually focuses on elucidating the structure – activity relationships after identifying the target enzyme/receptor followed by the development of a potency screening method. The active molecules are then tested for a variety of assays for affinity and

doi: 10.5599/admet.5.1.373

14

13.3 Physicochemical and biomimetic properties of molecules that affect lung retention after inhaled administration

Publication placed on hold please see note below.

ADMET & DMPK X(Y) (20xx) pp-pp; doi: <http://dx.doi.org/10.5599/admet.0000.000>

ADMET

Open Access : ISSN : 1848-7718

<http://www.pub.iapchem.org/ojs/index.php/admet/index>

Original scientific paper, Review, Feature article, Short communications, Note (Type of Paper)

Physicochemical and biomimetic properties of molecules that affect lung retention after inhaled administration

Simon Teague¹, Simon MacKay², Diane M Coe¹, Michael D Barker¹, Shenaz Bunally¹ and Klara Valko³

¹Glaxo SmithKline Medicine Research Centre, Stevenage, Herts SG1 2NY, United Kingdom

²University of Strathclyde, Glasgow, G1 1XU, United Kingdom

³Bio-Mimetic Chromatography Ltd, Stevenage, Herts, SG1 2DX, United Kingdom

*Corresponding Author: E-mail: simon.p.teague@gsk.com; Tel.: +1-111-111-1111; Fax: +1-111-111-1112

Received: MMMM DD, YYYY; Revised: MMMM DD, YYYY; Published: MMMM DD, YYYY

Abstract

Solubility and permeability of inhaled drugs are known to affect lung retention. Low solubility compounds however, have safety concerns due to their potential induce foamy macrophage formation following lung dosing. Very low permeability also has the potential to increase lung retention and for intracellular targets this can limit the ability of compounds to access the cell and limit target engagement. In this paper, an alternative approach is described on how to select compounds with extended lung retention by increasing the non-specific binding of compounds to lung tissue components, such as albumin, glycoprotein and phospholipids, whilst still maintaining an effective free lung concentration. HPLC measurements using biomimetic stationary phases such as human serum albumin (HSA), α -1-acid glycoprotein (AGP), and Immobilized Artificial Membrane (IAM) provide a method to estimate lung tissue binding and drug efficiency, which can then be directly related to lung retention. Lung retention was measured for a set of small molecules JAK inhibitors, which all had similar solubility and permeability, but different intrinsic lung retention. It was found that compounds with drug efficiencies (DE_{max}) of around 1%, had extended lung exposure which could be maintained for up to 8-12 hours. Introducing DE_{max} as an additional parameter has shown that biomimetic binding can provide further information to help identify and differentiate between compounds which have greater potential for "intrinsic" lung retention but fall into a similar solubility and permeability class.

Keywords

Asthma, Biomimetic, COPD, Drug Efficiency, DE_{max} , Foamy Macrophages, Inhaled, Intrinsic, Lung Retention, Permeability, Solubility

Introduction

Inhaled administration is especially advantageous for topical treatment of various lung diseases, particularly when treating inflammatory lung disorders such as asthma and Chronic Obstructive Pulmonary Disease (COPD). From a drug development perspective, for a once daily dosage regime to succeed, drugs utilising the treat these conditions via inhaled route require pulmonary delivery, it is now recognised that to ensure

doi: 10.5599/admet.0000.0000

1

Note: Prior to submission to the ADMET journal this manuscript was not approved for release by GSK Respiratory Senior Management. The reason for this was due to

concerns about publishing a strategically important concept which could be used by our competitor in the area.